Shtykov (Ed.)
**Nanoanalytics**

## Also of interest

*Innovations in Nanoscience and Nanotechnology.*
*Nano-sized Materials Application*
Van de Voorde (Ed.), 2018
ISBN 978-3-11-054720-7, e-ISBN 978-3-11-054722-1

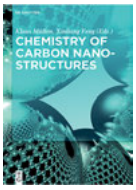


*Chemistry of Carbon Nanostructures.*
Müllen, Feng (Eds.), 2017
ISBN 978-3-11-028450-8, e-ISBN 978-3-11-054722-1

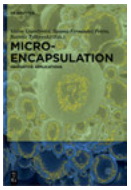


*Microencapsulation.*
*Innovative Applications*
Giamberini, Fernandez Prieto, Tylkowski (Eds.), 2015
ISBN 978-3-11-033187-5, e-ISBN 978-3-11-033199-8

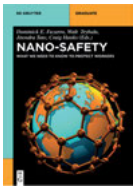


*Nano-Safety.*
*What We Need to Know to Protect Workers*
Fazarro, Trybula, Tate, Hanks (Eds.), 2017
ISBN 978-3-11-037375-2, e-ISBN 978-3-11-037376-9

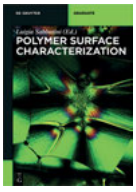


*Polymer Surface Characterization.*
Sabbatini (Ed.), 2014
ISBN 978-3-11-027508-7, e-ISBN 978-3-11-028811-7

*Physical Sciences Reviews.*
e-ISSN 2365-659X

# Nanoanalytics

Nanoobjects and Nanotechnologies
in Analytical Chemistry

Edited by
Sergei Shtykov

DE GRUYTER

**Editor**
Prof. Dr. Sergei Shtykov
Saratov State University
Institute of Chemistry
Department of Analytical Chemistry
and Chemical Ecology
Astrakhanskaya Street 83
410012 Saratov
Russia
shtykovsn@mail.ru

ISBN 978-3-11-054006-2
e-ISBN (PDF) 978-3-11-054201-1
e-ISBN (EPUB) 978-3-11-054024-6

**Library of Congress Cataloging-in-Publication Data**
A CIP catalog record for this book has been applied for at the Library of Congress.

**Bibliographic information published by the Deutsche Nationalbibliothek**
The Deutsche Nationalbibliothek lists this publication in the Deutsche Nationalbibliografie; detailed bibliographic data are available on the Internet at http://dnb.dnb.de.

© 2018 Walter de Gruyter GmbH, Berlin/Boston
Typesetting: Konvertus, Haarlem
Printing and binding: CPI books GmbH, Leck
Cover image: Brookhaven National Laboratory/Science Photo Library
♾ Printed on acid-free paper
Printed in Germany

www.degruyter.com

# Preface

In the last two decades, nanoscience and nanotechnology have found widespread application in various fields of study relating to the properties of inorganic, organic and biological objects on the nanoscale. Analytical chemistry takes advantage of the new possibilities and phenomena offered by nanoscience and nanotechnology and apply them for two purposes: to solve classical analytical problems arising in different methods of separation, preconcentration and analysis, and to develop new methods of nanoobjects analysis and characterization. So far this new area of analytical chemistry has no agreed-upon name or consensus on its definition. Therefore, Chapter 1 of this book proposes and justifies the use of the term "Nanoanalytics", its concept and definition. The aim of this chapter is to share and discuss with professional analysts and other specialists involved in the area of nanoanalytics an integrated view on this area of analytical chemistry to find new possibilities for development of chemical analysis. Toward the aim, this chapter is mainly focused on the many faces of nanoobjects and nanotechnologies used as tools for nanoanalytics. It is proposed to subdivide the nanoobjects into two groups: solid (hard) and liquid (soft) ones. The solid 0D-3D nanoobjects (nanoparticles) are characterized by unusual quantum-sized, surface-to-volume ratio, shape and composition effects with highly enhanced analytical characteristics based on unique spectroscopic, electrochemical, sorption or magnetic properties of nanosized matter. Liquid nanoobjects can exist only in liquid medium and contrary to solid ones are equilibrium and thermodynamically stable systems. Their characteristic features that are valuable for analysis are based on local microenvironment effect, compartmentalizing and distance effects that enhance the reactivity, stability, decrease hydration of reactants, change the chemical reaction pathway and rate, increase electron and energy transfer due to solubilization and inclusion effects as well as change dynamically the sorbent surface properties. Nanoanalytics deals with different nanotechnologies that in turn can be also subdivided into two groups. First one includes measuring physical technologies that are applied to characterization of the particle sizes as well as chemical composition in order to find their relation to the amplification of the analytical signal when using nanoobjects. A design of new analytical instruments based on new approaches can also be fit into this group. The second group includes synthetic technologies for development of new kind of nanoobjects or modification of their surface to get new analytical possibilities. It should be noted that nanoanalytics is both an actor in the development of the nanoobjects and nanotechnologies, and simultaneously a user of the resulting nanostructures, technologies and devices. The combination of these tools helps to apply new driving forces to improve different classical analytical methods and to create new types of analytical procedures. In addition, the roles of nanoanalytics in solving cell imagine and theranostics problems as well as problems of nanometrology are discussed. Nanoanalytics is highly multidisciplinary field, ranging from chemistry, physics,

https://doi.org/10.1515/9783110542011-202

and biology to medicine and engineering. Thus, it is crucial to integrate researchers who are experts in the mentioned fields to make possible and foster communication between them to generate novel approaches in nanoanalytics.

The book also contains eleven reviews containing up-to-date information on a wide range of developments and applications of solid and liquid nanoobjects in various methods of analysis, separation and preconcentration of organic, inorganic and biological substances. So Chapters 2, 3, 4, 5 represent reviews that are devoted to the use of nanoobjects and nanotechnologies in spectrometric (molecular absorption and luminescence) methods of analysis. Chapter 2 is written by biologist and physicists who have extensive experience in applying of gold nanoparticles in bioassay. Chapter 3 describes the use of different kinds of nanoparticles (gold, silver, quantum and carbon dots, lanthanide chelates, etc) to enhancement of absorption and luminescence signals for application in rapid immunotests. Chapter 4 provides information on the use of nanofilms (produced by self-assembled monolayers, layer-by-layer or Langmuir-Blodgett technique) as sensitive layers of chemical and biochemical sensors. Chapter 5 focuses on the application of excitation electron energy transfer in liquid and solid nanoobjects for luminescent analysis of organic, pharmaceutical and bioorganic substances.

The Chapters 6, 7, and 8 are reviews devoted to advantageous of the use of nanomaterials in electrochemical analysis. Chapter 6 reviews the specific properties of different nanomaterials (high adsorptive capacity, catalytic activity, excess of surface Gibbs free energy) that influence on the kinetics and thermodynamics of the electrode processes and their use in chemical and biochemical sensors. Chapter 7 is devoted to the application of carbon nanomaterials and surfactants as electrode surface modifiers in organic electroanalysis. In Chapter 8 the development of electrochemical DNA sensors and aptasensors based on nanoparticles different in nature, size, shape, and preparation protocols has been considered with particular emphasis to the mechanism of their influence on signal readout and way of implementation in the biosensor assembly.

The last part of the monograph consists of four chapters that review recent progress in the use of nanoobjects in separation and preconcentration methods. Chapter 9 describes of modern trends in the field of molecular imprinted polymers that are representatives of nanoporous materials used as the selective sorbents in solid-phase extraction but also in creation of various types of sensors. Chapter 10 talks about carbon nanotubes that are the widely used in analytical chemistry for sorption, separation and preconcentration of metal ions, radioisotopes, and organic substances owing to high sorption capacity, completeness of analyte extraction–reextraction stages, and their easy modifications. Advances in application of microemulsions for extraction and concentration of hydrophobic target compounds and metals ions from various food, pharmaceutical, ecological, and other objects which can then be analyzed by high performance liquid chromatography (HPLC) are the topic of Chapter 11. Finally, Chapter 12 gives a review of application surfactant micelles in thin

layer chromatography and HPLC that allow the modification of mobile and stationary phases in dynamic mode.

Nanoanalytics is the first book of its kind and will be of interest to researchers, students and all specialists in Chemistry, Physics, Biology, Material, Life and Environmental Sciences, as well as those who are involved in the development of analytical methods and procedures based on nanoobjects and nanotechnologies or analysis of nanomaterials.

Sergei Shtykov
*Saratov, December 2017*

# Contents

**Preface —— V**

**List of contributing authors —— XV**

Part I: **Nanoanalytics: Concepts, Elements, and Peculiarities**

S. N. Shtykov

**1 Nanoanalytics: Definitions, Classification, History, and Primary Advances —— 3**

1.1 Introduction —— **3**

1.2 Brief historical overview —— **7**

1.3 The concept of nanoanalytics —— **11**

1.4 Nanoobjects as tools for nanoanalytics —— **13**

1.4.1 Definition, classification, and fundamental properties of nanoobjects —— **13**

1.4.2 Liquid nanoobjects —— **15**

1.4.3 Solid nanoobjects (nanomaterials) —— **22**

1.5 Nanotechnologies as tools for nanoanalytics —— **27**

1.6 Nanoanalysis and nanometrology —— **31**

1.6.1 Definitions and elements —— **31**

1.6.2 Analysis of chemical composition of nanoobjects —— **32**

1.6.3 Imaging of bioobjects and theranostics —— **36**

1.6.4 Nanometrology in nanoanalytics —— **37**

1.7 Conclusions —— **40**

References —— **42**

Part II: **Application in Spectrometric Methods**

L. A. Dykman, N. G. Khlebtsov and S. Y. Shchyogolev

**2 Gold Nanoparticles in Bioanalytical Techniques —— 55**

2.1 Introduction —— **55**

2.2 Homophase techniques —— **58**

2.3 Dot blot immunoassay —— **60**

2.4 Immunochromatographic assays —— **64**

2.5 Plasmonic biosensors —— **66**

2.6 Conclusions —— **70**

References —— **71**

I. Y. Goryacheva
**3 Extinction and Emission of Nanoparticles for Application in Rapid Immunotests — 87**
3.1 Introduction — **87**
3.2 Extinction of nanoparticles — **88**
3.2.1 Colloidal gold — **88**
3.2.2 Colloidal carbon — **91**
3.2.3 "Colloidal" dyes — **92**
3.3 Emission of nanoparticles — **92**
3.3.1 Fluorescence dyes — **93**
3.3.2 Lanthanide chelates — **94**
3.3.3 Quantum dots — **94**
3.3.4 Nanoparticles with infrared luminescence — **96**
3.3.5 Up converting phosphors — **97**
3.3.6 Nanoparticles with long-lived luminescence — **98**
3.4 Conclusions — **99**
References — **99**

T. Yu. Rusanova
**4 Nanofilms as Sensitive Layers of Chemical and Biochemical Sensors — 107**
4.1 Introduction — **107**
4.2 Nanofilm types and techniques of their preparation — **108**
4.2.1 Self-assembled monolayers — **108**
4.2.2 LbL technique — **110**
4.2.3 LB films — **112**
4.3 Nanofilms' sensor application — **113**
4.3.1 SAM — **113**
4.3.2 LbL technique — **114**
4.3.3 LB films — **117**
4.4 Conclusions — **121**
References — **121**

T. D. Smirnova, S. N. Shtykov and E. A. Zhelobitskaya
**5 Energy Transfer in Liquid and Solid Nanoobjects: Application in Luminescent Analysis — 131**
5.1 Introduction — **131**
5.2 Nanoobjects involved in ET — **133**
5.3 Application of FRET in analysis — **135**
5.3.1 FRET in micellar solutions — **135**
5.3.2 FRET with protein participation — **136**
5.3.3 FRET with nanomaterials' participation — **136**

5.3.3.1 Quantum dots — **136**
5.3.3.2 Nanoparticles based on Au, Ag, Au–Ag, and graphene — **140**
5.4 The lanthanide chelates' ET application — **146**
5.4.1 Liquid micellar nanosystems — **146**
5.4.2 ET in binuclear complexes of heteronanoparticles — **152**
5.5 Conclusions — **153**
References — **154**

## Part III: **Application in Electroanalysis**

Kh. Brainina, N. Stozhko, M. Bukharinova and E. Vikulova
**6 Nanomaterials: Electrochemical Properties and Application in Sensors — 165**
6.1 Introduction — **165**
6.2 Properties of nanoparticles — **166**
6.3 Theoretical and experimental approaches to nanoscale material study — **167**
6.4 Macro- to micro- and to nanoscale transition — **171**
6.5 Nanostructures in chemical monitoring — **177**
6.5.1 Nanomaterials as transducers and catalysts in electrochemical sensors — **177**
6.5.2 Nanomaterials in electrochemical sensors for antioxidant detection — **189**
6.5.3 Nanomaterials in electrochemical immunoassay — **196**
6.5.4 Nanomaterials – transducers and adsorbents in electrochemical immunosensors — **196**
6.5.5 Nanomaterials as analyte transporters — **201**
6.5.6 Nanomaterials as labels in electrochemical immunosensors — **202**
6.6 Conclusions — **206**
References — **207**

G. Ziyatdinova and H. Budnikov
**7 Carbon Nanomaterials and Surfactants as Electrode Surface Modifiers in Organic Electroanalysis — 223**
7.1 Introduction — **223**
7.2 Carbon nanomaterial-based electrodes — **224**
7.2.1 Graphene — **224**
7.2.2 Fullerenes — **228**
7.2.3 Carbon nanotubes — **229**
7.3 Surfactant-modified electrodes for the organic electroanalysis — **232**

7.4 Analytical possibilities of the electrodes with co-immobilized carbon nanomaterials and surfactants — **238**
7.5 Conclusions — **242**
References — **243**

G. Evtugyn, A. Porfireva, H. Budnikov and T. Hianik
**8 Nanomaterials in the Assembly of Electrochemical DNA Sensors — 253**
8.1 Introduction — **253**
8.2 DNA sensors: Recognition elements and signal transduction — **255**
8.2.1 Biochemical elements applied in the DNA sensors assemblies — **255**
8.2.2 Measurement of the signal of electrochemical DNA sensors — **258**
8.3 DNA sensors based on metal nanoparticles — **262**
8.3.1 Au nanoparticles — **262**
8.3.2 Other metal nanoparticles — **269**
8.4 DNA sensors based on carbonaceous materials — **271**
8.4.1 Carbon nanotubes — **271**
8.4.2 Graphene-based DNA sensors — **281**
8.5 Conclusions — **288**
References — **289**

Part IV: **Application in Sorption and Separation Methods**

S. G. Dmitrienko and V. V. Apyari
**9 Molecularly Imprinted Polymers: Synthesis, Properties, and Application in Analysis of Real Samples — 303**
9.1 Introduction — **303**
9.2 The principle of molecular imprinting — **304**
9.2.1 Covalent and noncovalent approach — **304**
9.2.2 Selecting the template and the reagents — **306**
9.3 Methods for synthesis of MIPs — **308**
9.3.1 Radical bulk polymerization — **308**
9.3.2 Synthesis of spherical microparticles — **309**
9.3.3 Synthesis of nanoscale imprinted materials — **312**
9.3.4 Other methods — **314**
9.4 Sorption properties of MIPs and selectivity of processes with their participation — **315**
9.5 Application in the analysis of real samples — **320**
9.6 Conclusions — **326**
References — **328**

S. Grazhulene and A. Red'kin
**10 Sorbents Based on Carbon Nanotubes — 343**
10.1 Introduction — **343**
10.2 Synthesis, properties of CNTs, and methods of their study — **344**
10.2.1 History of CNTs — **344**
10.2.2 Synthesis, functionalization, and characterization of CNTs — **346**
10.2.2.1 Methods of synthesis — **346**
10.2.2.2 Modification and functionalization — **350**
10.2.2.3 Methods of characterization — **353**
10.3 Sorption properties of CNTs — **356**
10.3.1 Sorption of metals from aqueous solutions — **356**
10.3.2 Sorption of organic substances — **362**
10.3.3 Comparison of CNTs with other sorbents — **364**
10.4 CNTs for chemical analysis — **366**
10.4.1 Concentration and determination of metals — **366**
10.4.2 On-line preconcentration and speciation analysis — **368**
10.4.3 Piezosensors — **369**
10.4.4 Other applications of CNTs — **372**
10.5 Conclusions — **375**
References — **378**

A. V. Pirogov
**11 Application of Microemulsions for Extraction and Preconcentration of Hydrophobic Target Compounds — 389**
11.1 Introduction — **389**
11.2 Microemulsions: structure and classification — **389**
11.3 Preparation and decomposition of microemulsions — **393**
11.4 Application of micellar and microemulsion media for extraction of target compounds — **396**
11.4.1 Extraction and preconcentration of organic substances — **396**
11.4.2 Extraction and preconcentration of metals — **398**
11.4.3 Extraction and preconcentration of PAHs — **402**
11.5 Conclusions — **405**
References — **406**

E. G. Sumina
**12 Surfactant Micelles in Liquid Chromatography — 411**
12.1 Introduction — **411**
12.2 General characteristics of the method — **413**
12.3 Features of mobile and stationary phases in MLC — **415**
12.3.1 Mobile phases — **415**

12.3.2 Stationary phases — **420**
12.4 Retention models in MLC — **423**
12.5 Application of MLC in analysis — **427**
12.6 Conclusions — **434**
References — **435**

**Index — 442**

# List of contributing authors

**Vladimir Apyari**
Lomonosov Moscow State University
Department of Chemistry
Analytical Chemistry Division
Leninskie Gory 1/3
119991 Moscow
Russia
apyari@mail.ru

**Anna Brainina**
Ural State University of Economics
62, 8 Marta St
620144 Ekaterinburg
Russia
baz@usue.ru

**Herman Budnikov**
Kazan Federal University
Analytical Department
A.M. Butlerov' Chemistry Institute
18 Kremlevskaya Street
420008 Kazan
Russia
Herman.Budnikov@kpfu.ru

**M. Bukharinova**
Ural State University of Economics
62, 8 Marta St
620144 Ekaterinburg
Russia
mbuharinova@mail.ru

**Stanislava Dmitrienko**
Lomonosov Moscow State University
Department of Chemistry
Analytical Chemistry Division
Leninskie Gory 1/3
119991 Moscow
Russia
dmitrienko@analyt.chem.msu.ru

**Lev Dykman**
Russian Academy of Sciences
Institute of Biochemistry and Physiology of
Plants and Microorganisms
13 Prospekt Entuziastov
410049 Saratov
Russia
dykman_l@ibppm.ru

**Gennady Evtugyn**
Kazan Federal University
Analytical Chemistry Department
A.M. Butlerov' Chemistry Institute
18 Kremlevskaya Street
420008 Kazan
Russia
gevtugyn@mail.ru

**Irina Goryacheva**
Saratov State University
Institute of Chemistry
83 Astrakhanskaya St
410012 Saratov
Russia
goryachevaiy@mail.ru

**Svetlana Grazhulene**
Russian Academy of Sciences
Institute of Microelectronics Technology and
High Purity Materials
Academician Osipyan St 6
142432 Chernogolovka
Russia
grazhulene@mail.ru

**Tibor Hianik**
Comenius University
Department of Nuclear Physics and Biophysics
Mlynska dolina F1
842 48 Bratislava
Slovakia
Tibor.Hianik@fmph.uniba.sk

**Nikolai Khlebtsov**
Russian Academy of Sciences
Institute of Biochemistry and Physiology of Plants and Microorganisms
13 Prospekt Entuziastov
410049 Saratov
Russia
khlebtsov@ibppm.ru

**Andrey Pirogov**
Lomonosov Moscow State University
Department of Chemistry
Analytical Chemistry Division
Leninskie Gory 1/3
119991 Moscow
Russia
pirogov@analyt.chem.msu.ru

**Anna Porfireva**
Kazan Federal University
Analytical Department
A.M.Butlerov' Chemistry Institute
18 Kremlevskaya Street
420008 Kazan
Russia
porfireva-a@inbox.ru

**Anna Porfireva**
Kazan Federal University
Analytical Chemistry Department
A.M. Butlerov' Chemistry Institute
18 Kremlevskaya Street
420008 Kazan
Russia
porfireva-a@inbox.ru

**A. N. Red'kin**
Russian Academy of Sciences
Institute of Microelectronics Technology and High Purity Materials
Academician Osipyan St 6
142432 Chernogolovka
Russia
arcadii@iptm.ru

**Tatyana Rusanova**
Saratov State University
Institute of Chemistry
83 Astrakhanskaya St
410012 Saratov
Russia
tatyanarys@yandex.ru

**Sergei Shchyogolev**
Russian Academy of Sciences
Institute of Biochemistry and Physiology of Plants and Microorganisms
13 Prospekt Entuziastov
410049 Saratov
Russia
s_shegolev@rambler.ru

**Sergei Shtykov**
Saratov State University
Institute of Chemistry
83 Astrakhanskaya St
410012 Saratov
Russia
shtykovsn@mail.ru

**Tatyana Smirnova**
Saratov State University
Institute of Chemistry
83 Astrakhanskaya St
410012 Saratov
Russia
smirnovatd@mail.ru

**Natalia Stozhko**
Ural State University of Economics
62, 8 Marta St
620144 Ekaterinburg
Russia
sny@usue.ru

**Elena Sumina**
Saratov State University
Institute of Chemistry
83 Astrakhanskaya St
410012 Saratov
Russia
suminaeg@yandex.ru

**Ekaterina Vikulova**
Faculty of Chemistry
Adam Mickiewicz University
Umultowska 89b
61-614 Poznan
Poland
viekat@yandex.ru

**Elena Zhelobitskaya**
Saratov State University
Institute of Chemistry
83 Astrakhanskaya St
410012 Saratov
Russia
elen3444046@mail.ru

**Guzel Ziyatdinova**
Kazan Federal University
Analytical Department
A.M. Butlerov' Chemistry Institute
18 Kremlevskaya Street
420008 Kazan
Russia
ziyatdinovag@mail.ru

# Part I: **Nanoanalytics: Concepts, Elements, and Peculiarities**

S. N. Shtykov

# 1 Nanoanalytics: Definitions, Classification, History, and Primary Advances

## 1.1 Introduction

The last decade of twentieth century and the beginning of twenty-first century have witnessed a *new paradigm* in the scientific community. This paradigm is based on the unique properties of nanosized samples of different substances and combines the previously disembodied data observed by physicists, chemists, biologists, and material scientists. It was also brought about by an advent of new instrumental methods such as scanning tunneling microscopy (STM), atomic force microscopy (AFM), scanning electron microscopy (SEM), transmission electron microscopy (TEM), and several other methods, the potential of which helped to form a new interdisciplinary research field – *nanoscience* – and its practical implementation – *nanotechnology*. Implementation of these methods allowed researchers not only to visualize and directly produce nanosized objects but also to control them.

It should be noted that "nanotechnologies" gained a more widespread, although not necessarily justified recognition than "nanoscience" did. By the end of twentieth century, nanotechnologies became a blanket term used to describe a large area of science dedicated to studying nanostructures and involved in their application phenomena, measurements of nanosized objects, as well as practical implementation of this knowledge in various fields of science and technology. Nevertheless, today "nanoscience" and "nanotechnologies" received international recognition as separate terms with their own meanings. This is evidenced by publication of a number of monographs such as UNESCO encyclopedia entitled "Nanoscience and Nanotechnologies" [1], "Nanoscience and Nanotechnologies in Engineering" [2], and "Nanoscience" [3]. All these publications clearly differentiate "nanoscience" and "nanotechnologies."

The response of scientific community to emergent nanoscience and nanotechnologies is very diverse. Some consider these concepts a "novel," revolutionary trend but also carefully admit that nanoscience and nanotechnologies have yet to leave the academic laboratory level and that it is still not clear how fast can advances of nanoscience be transformed into real industrial nanotechnological applications [4]. Other researchers believe that nanoscience is not yet a scientific discipline on its own, and may never become one, because it is not yet evident that the Laws of Nature are particularly special between 1 and 100 nm [5]. Therefore, one may conclude that nanoscience *is merely a collection of fragments of traditional classic disciplines – physics, chemistry and biology* – which describe the properties of nanoobjects using quantum chemistry and surface science, or those currently existing terms and definitions have

https://doi.org/10.1515/9783110542011-001

*social* but not scientific value. The purpose of these definitions is to convince the society that there is a certain threshold in objects size, which distinguishes nanoobjects from micro- and macro-objects. At the same time, the definitions do not provide the fundamental reasons that can be used to *explain* the existence of such a boundary, given a variety of anomalies exhibited by nanoobjects whose size varies from 1 to 100 nm.

Currently, "nano-words" are broadly used by people from all layers of society, including scientists, engineers, physicians, ecologists, military officers, politicians, and economists. Their use increases dramatically and pervades common language. Analysis of the reports presented at the world largest conference on analytical chemistry in Pittsburgh distinguishes more than 30 different terms using "nano-" as a prefix. The most common "nano-words" are collected and systematized in Tab. 1.1.

In addition, in nanotechnologies, there is a wide range of terms describing properties and phenomena typical for nanoobjects, including size effect, self-assembly, self-organization, surface plasmon resonance (SPR), superparamagnetism, and smart materials. Another field closely related to nanotechnologies is originated from various metering and visualization techniques such as electron microscopy (TEM, SEM) and multiple variations of scanning probe microscopy, the most famous of which are STM, AFM, magnetic force microscopy (MFM), and near-field scanning optical microscopy (NSOM), which find a wide application in nanoobjects research.

Popularity of this research field resulted in creation of national nanotechnology development programs adopted in more than 55 countries. The first of such programs was the National Nanotechnology Initiative in United States, which was proposed in 1998 and finally implemented in 2001. However, only a few people fully understand the significance and capabilities as well as positive and negative aspects of current achievements of nanoscience and nanotechnology, especially their potential. There are numerous assumptions and false information (hoaxes), regarding capabilities, positive and negative effects, and ethics of nanoscience and nanotechnology application, both in society (spread by mass media) and among scientific community; at the same time, business, science, and society are united in their attitudes to maximizing the profit from such applications. Nanoscience and nanotechnologies, in particular, became a sort of icon for the idea of "breakthrough to the future."

The illusion of fast and easy synthesis of nanomaterials and achievement of their practical application led to first successes in several countries, in the first instance, in United States, Germany and Japan, where hundreds if not thousands of companies already made money off nanotechnologies. At the same time, a few people note that the last decade of the twentieth century was marked by large-scale fundamental studies of the unexplained properties of nanosized and nanostructural objects, which, in turn, led to foundation of the basic nanoscience. And only after that, in the twenty-first century, as the amount of data on nanosized

**Tab. 1.1:** Examples of words with "nano" prefix

| General terms | Objects | | | Measurement Units |
|---|---|---|---|---|
| | Shape | Nature | Functions | |
| Nanoscience | Nanotube | Nanoobject | Nanoreactor | Nanodimension |
| Nanochemistry | Nanowire | Nanostructure | Nanoelectrode | Nanoscale |
| Nanophysics | Nanofiber | Nanomaterial | Nanobalance | Nanosize |
| Nanobiology | Nanobelt | Nanocrystal | Nanomembrane | Nanometer |
| Nanomedicine | Nanorod | Nanocolloid | Nanoseparation | Nanogram |
| Nanotechnology | Nanotubulene | Nanosuspension | Nanoprobe | Nanoliter |
| Nanoelectronics | Nanowhiskers | Nanodispersion | Nanosensor | Nanovolume |
| Nanophotonics | Nanosphere | Nanocomposite | Nanobiosensor | Nanoidentation |
| Nanospectroscopy | Nanocapsule | Nanofluid | Nanotweezers | Nanometrology |
| Nanoelectrochemistry | Nanolayer | Nanopowder | Nanotemplate | |
| Nanolithography | Nanofilm | Nanoclusters | Nanochannel | |
| Nanotribology | Nanosheet | Nanopaper | Nanobarcode | |
| Nanodevices | Nanoring | Nanoribbon | NEMS | |
| Nanoindustry | Nanorose | Nanosome | Nanoencapsulation | |
| Nanobusiness | Nanoshell | Nanoceramics | Nnaoactuators | |
| Nanopharmacology | Nano-onion | Nanoglass | Nanorobot | |
| Nanobiotechnology | Nano-dot | Nanocarbon | Nanodrugs | |
| Nanoeducation | | Nanodiamons | Nanotoxicity | |
| Nanomarket | | Nanogold | Nanoflow | |
| Nanoparticle | | Nanosilver | Nanopores | |
| | | Nanomagnetite | Nano-HPLC | |
| | | Nanohardness | Nano-SCF | |
| | | Nanofiller | Nanoelectrospray | |
| | | | Nanoionics | |
| | | | Nanobattery | |
| | | | Nanoglue | |
| | | | Nanocars | |
| | | | Nanothermometer | |
| | | | Nanoink | |
| | | | Nanomaterial-based vectors | |

NEMS nanoelectro-mechanical systems
HPLC high-performance liquid chromatography
SCF Supercritical Fluid

compounds and their change patterns increased, first real nanotechnologies started to emerge.

So, the question is arisen: which of the current scientific fields can be surely classified as nanotechnology? According to experts' opinions, they include [1–9]:

– nanoelectronics and spintronics, where the size of individual device elements does vary between 50 and 100 nm;

- nanobiotechnologies and medical (pharmaceutical) technologies in which nano- and microcapsules are used to transport therapeutic agents to and inside the organs affected by a disease; over the last 5 years such technologies have been incorporated into a new field of science called theranostics;
- production of nanomaterials;
- production of metering equipment and devices for nanotechnology;
- production of fuel cells that convert chemical energy into electricity using nanoparticles (NPs);
- car industry and automotive remediation based on catalytic properties of NPs;
- cosmetics industry using NPs for preparing lotions, creams, or shampoos;
- textile industry using NPs to produce stain-repellent and gas-filtering fabrics.

It should be noted that some of the nanotechnologies evolved from previously established microtechnologies; the most prominent example of such phenomenon is nanoelectronics, which is the next logical downscaling step after microelectronics. Novel or "revolutionary" nanotechnologies include production of fullerenes, quantum dots, and carbon nanotubes, various types of metal and metal oxide NPs (gold, silver, magnetite, etc.), and especially, emergence of types of scanning probe or electron microscopy, which is capable of separating and identifying single atoms on the surface of nanoobjects.

At first, professional analytical chemists did not pay attention to nanotechnologies as much as physicists, material scientists conducting synthesis of inorganic materials, or even biologists did. However, analytical chemistry is an interdisciplinary science, so that it could not ignore an appearance of new spectral or other physicochemical phenomena. Likewise, opportunities provided by application of nanoobjects and nanotechnologies in chemical analysis should not be neglected, especially due to unique capabilities of nanomaterials, including detection of mind-bogglingly small quantities (femto-, atto-, or even zeptomoles!) of inorganic, organic, and biological substances using chemical sensors. Physicists, in their turn, developed different types of "probes" to measure the size and even to make a conclusion about the nature of atoms or molecules comprising the sized nanoobject. We speak here about atomic, molecular, or magnetic force microscopy; STM; and electron (TEM, SEM) microscopy or spectroscopy. It should be particularly pointed out that in the near future a great qualitative advance of mankind life can be anticipated as a combination of four basic technologies of the twenty-first century: Nano-, Bio-, Info-, and Cogno-technologies abbreviated as NBIC.

Similar to physicists, while acquiring new materials and technologies, material scientists and biologists (probably unwittingly) overtook analytical chemists in developing novel approaches for chemical analysis. Therefore, if analytical chemists want to keep the pace (we believe they do), they have to cooperate with nanoscience and nanotechnology experts and try to gain a better understanding of fundamental capabilities of new methods not only to detect but also to concentrate, separate, and determine different compounds. This will help them to see in a new light already

well-established methods and approaches and to propose new ones, which cannot be foreseen by specialists from other fields because of their specific background and vision. This remark is especially true for metrology, particularly its part dealing with the development of different fields of nanometrology and their application for nanoanalytical chemistry. Creation of standards (Certified Reference Materials [CRM]) for nanomaterials and nanoobjects is equally important. The key role of analytical chemists for these nanometrology problems, which exactly tasks, is obvious.

## 1.2 Brief historical overview

Nanotechnologies did not emerge suddenly in the last decade of the last century but stemmed from a gradual evolution (and perfection) of several high-temperature techniques used in the production of glass and luster potteries over ages [9–15]. As it is evident from these publications, chemical synthesis of metallic NPs incorporated into glass or luster glaze used for covering dishes, potteries, and decorations has been performed since ancient times, probably from the bronze age [10]. Usually, such techniques were discovered accidentally by various craftsmen during Ancient and medieval periods. Data provided by modern electronic and scanning microscopy investigations of many antique artifacts with an unusual coloration proves the presence of metallic NPs, as has clearly been shown in a special issue of the *Journal of Nano Research* in 2009 [14].

One of the first examples of such nanotechnology is "Egyptian blue," an inorganic material with tremendous cultural significance [1, 9–14]. This term refers to a complex mixture of primary $CaCuSi_4O_{10}$ and $SiO_2$ (both glass and quartz), which has the distinction of being the first synthetically produced pigment in human history. Historical and archeological evidence indicates that it was being manufactured since as early as the third millennium B.C. Egyptian blue was used extensively for decorative purposes in Ancient Egypt, Mesopotamia, Greece, and Roman Empire. It was shown by modern investigations that Egyptian blue consists of both nanosheets (<10 nm thick) and nanoplatelets (>10 nm thick) of $CaCuSi_4O_{10}$. In some cases, the thickness of such sheets is close to 1 nm.

The second well-known and famous example of using nanotechnology is the glass Lycurgus Cup (4th century A.D., Rome), which is kept in the British Museum (Fig. 1.1). The most remarkable feature of this cup relies on its dichroism. It contains gold and silver alloyed NPs (with sizes varying from 5 to 60 nm), which are distributed in such a way as to make the glass looking wine-red when viewed in the transmitted light, but green in the reflected light [1, 10, 11].

Other well-known examples of nanotechnology are stained glass windows of many medieval European cathedrals, for example, Cassius Purple. Several Christian cathedrals built between the fourth and twelfth centuries in Rome and then in

seventeenth century in other parts of Europe are decorated by ruby glass or Cassius Purple containing gold NPs [10–14].

**Fig. 1.1:** The Lycurgus Cup, illuminated from outside (left) or from inside (right). Trustees of the British Museum.

Damascus steel swords from the Middle East were made between 300 and 1700 A.D. and are known for their impressive strength, shatter resistance, and exceptionally sharp cutting edge. It was established that the steel blades contain oriented nanoscale wire- and-tube-like carbon structures that almost certainly enhanced the material's properties [15]. A further example of nanotechnology is silver photography, in which the specificity of very small nanosized particles resulted of photochemical reaction was used from the nineteenth century [9, 16].

Francesco Selmi (Italy, 1843) was the first to investigate systematically colloids by studying aqueous colloidal solutions of sulfur, Prussian blue, and casein. He concluded that these solutions are not true solutions but suspensions of small particles in water [17]. One of the first scientific experiments in the field of nanotechnology was carried out by Michael Faraday (England, 1857), who prepared stable solutions of red colloidal gold and investigated some of their optical properties [18]. Fifty years later, Gustav Mie proposed a theory that explained these unusual optical properties [19, 20].

Works published in 1861 by British chemist Thomas Graham have actually led to foundation of a new independent field of science – colloid chemistry that studies dispersed matter and surface phenomena in disperse systems. Graham [21] summarized all existing research data, introduced new concepts, such as "colloid," "sol," and "gel," and described several features characteristic to colloidal matters.

Colloid chemistry was advanced further by Russian chemists – I. Borschov (1869), P. von Weimarn (1904), A. Dumansky (1904), and P. Rehbinder (1928), who systematically studied surfactant solutions, as well as their European and American colleagues – H. Schulze, W. Hardy, (1883), R. Zsigmondy and R. Siedentopf (1903), A. Einstein and M. Smoluchowski (1906, theory of Brownian movement of colloid particles), J. McBain (1913), I. Langmuir (1916), T. Svedberg (1919, development of ultracentrifugation technique), W. Ostwald, and many others [17, 22–24].

At the turn of twentieth century, biological colloid particles similar to their inorganic counterparts were also discovered. In 1892, D. Ivanovsky discovered the first biological colloid particle – Tobacco mosaic disease virus (https://en.wikipedia.org/wiki/Dmitri_Ivanovsky), and in 1901 W. Reed found the yellow fever virus, which was the first human virus discovered. Later, it was established that the size of this virus ranged from 40 to 80 nm [22–24].

It should be noted that until 1903, when R. Zsigmondy and R. Siedentopf developed their optical ultramicroscope with a resolution of up to 5 nm, "colloid particles" were defined as particles, which are invisible in ordinary optical microscopes with a resolution of up to 300 nm. However, the lack of capability to observe such particles did not prevent P. von Weimarn from stating the fundamental principle of universality of colloid or ultradisperse state of matter, which gains new characteristic physical and chemical properties. Other singular examples in colloid chemistry development are foundation of the first laboratory dedicated to the related research by A. Dumansky and systematic studies of surfactant micelles by P. Rehbinder in 1930–50s [22–24].

It is also interesting to note systematic studies of properties and forms of surfactant micelles conducted at the beginning of the twentieth century by J. McBain. A new step of studying colloids and interfaces began in 1916 when I. Langmuir described his method of production and study of monolayers (two-dimensional nanoobjects) at phase interface. Later Langmuir and his student, K. Blodgett, developed a technique for transferring monolayers from water surface onto a solid support. Another prominent achievement was made in 1931 when E. Ruska and M. Knoll developed the first electron microscope. Therefore, one can consider colloid chemistry, which subject is to study colloid (ultradisperse) state of matter, that is, the nanosized objects, as a predecessor of contemporary nanoscience, as was stated by A.I. Rusanov. The reader interested in a more detailed historical evidence of development of nanoscience and nanotechnologies is referred to refs. [17, 22–24].

Nonetheless, it is generally accepted that the nanotechnology era began with the famous lecture of R. Feynman given at the meeting of American Physical Society in 1959. He was the first one to raise the question whether there are any fundamental restrictions on manipulations with certain atoms or groups of atoms [25]. Fifteen years later, in 1974, Taniguchi [26] for the first time introduced the term "nanotechnology".

The next event that played a very important role in nanotechnology formation was the development of scanning tunnel microscope by G. Binnig and H. Rohrer in 1981, followed by the development of atomic force microscope by G. Binnig in 1986. After these powerful sizing tools became available, the era of scanning probe microscopy was started, which currently has over 30 different variations [27]. As a result, nowadays scientists are able not only to visualize nanoobjects but also to manipulate them.

For quite a long time, such studies were conducted intuitively in separate laboratories and were not considered as a part of a single scientific field. Specific interest in nanotechnologies became expressed by both scientists and the public only after Drexler [28] published his book in 1989, in which he demonstrated in popular terms

the fantastic capabilities of nanoworld for humanity, both of positive and negative effects. For example, Drexler discussed the possibility of engineering nanorobots and said that their fast self-replication would lead to formation of so-called "grey goo," which may eventually wipe out the humanity from the Earth.

Among other events important for stimulating the development and formation of a new nanotechnological paradigm are the discovery of fullerenes by R. Smalley, H. Kroto, and R. Curl (1986) [29] and carbon nanotubes (CNTs) by Iijima in 1991 [30]; production of the first CNT-based field-effect transistor in 1998 [31]; production of graphene by A.K. Geim and K.S. Novoselov in 2004 (Nobel prize award, 2010) [32]; and the development of graphene-based sensor capable of sensing a single molecule of adsorbed gas, in 2007 [33]. The year of 2007 was also marked by the development of transmission electron microscope, with a definition of 0.05 nm and fast-acting scanning tunnel microscope, which allows online tracking nano-level processes [1, 2, 23].

Significant advances in the application of nanomaterials and nanotechnologies for *chemical analysis* were made by Mirkin [34], who used modified gold NPs for detecting biomolecules, and by Alivisatos [35] and Nie [36], who implemented semiconductor quantum dots. During the past 15 years, dozens of reviews, tens of monographs, and more than 3,000 research papers were published, which provided examples on various applications of solid nanoobjects – metallic; metal oxide; chalcogenide; and other NPs, nanotubes, nanofilms, and nanoporous materials – for different types of analysis, including separation and enrichment steps. However, these studies, as mentioned above, were mostly conducted separately by different research groups of physicists, chemists, biologists, and material scientists and never considered to be within the frames of a single research field. This is likely the main reason why "nanoanalytics" term has emerged only 10 years ago, that is, much later than the majority of other "nano-" terms and has not gained widespread recognition [37]. For this very reason, this term is absent in dictionaries and glossaries of nanotechnological terms [8, 38–40] and has so few Internet references. Moreover, the nanoanalytics term was initially used (and still used) by physicists to designate the laboratories and research methods in use, such as STM, AFM, TEM, and X-ray diffraction (XRD) methods, with the purpose to investigate the morphology, size, interphase boundaries, and, to an extent, chemical composition of nanoobject surface [41].

Since 2007 "nanoanalytics" has started to be also used by analytical chemists to define the field of science concerned with the application of nanoobjects in various traditional methods of separation and identification of compounds, as well as chemical sensors [37]. Scientometric analysis shows that "nanoanalytics" is still rarely used and has no certain definition even among scientists specializing in analytical chemistry. Some define nanoanalytics as analysis of chemical composition of NPs, and others as chemical analysis of surface, nanofilms, and interphase boundaries; still others mean sizing and characterization of nanoobjects morphology, while yet others think of application of nanoobjects for the purpose of chemical analysis and sometimes of using the nanovolumes of analyzed liquid media [42–45]. Among the aforementioned goals,

precise evaluation of *physical size* of nanoobjects is the most difficult task as it requires using standards and conducting precise image processing, which resulting in development of *nanometrology*. However, metrology was always an important part of analytical chemistry. Thus, there are still many problems for analytical chemists to solve.

Concept development and classificatory generalization have to be interesting both for scientists involved in that field and for state and business bodies funding such research, as well as for education institutions with chemical analysis and nanotechnologies disciplines.

This chapter is dedicated to a brief description of the concepts and primary topics of nanoanalytics, nanoobjects, and nanotechnologies, as well as certain metrological aspects of its constituent parts. With this objective, the author intends to provide a certain narrative logic and systemize all primary fields of nanoanalytics development without merely listing the most interesting experimental facts. At the same time, the proposed classification shall be supported by exciting general and specific examples of analytical techniques that are already practiced by scientists worldwide. It is important to mark the goalposts for nanoanalytics development and establish its place in contemporary analytical chemistry. Also in author's opinion, it is necessary to account for discrepancies between the specialists on the role of nanotechnology in analytical chemistry, as some believe in limitless possibilities and revolutionary nature of nanotechnologies, whereas others are skeptical about their possibilities for improving analysis; there are yet some who critically consider that everything with the prefix "nano" is merely another "bubble."

Concepts proposed in this chapter are based on the analysis of numerous reports on nanoobjects and nanotechnologies application for chemical analysis published during the last decade [42–51]. At the same time, the author understands the importance of comprehending or even listing all aspects of such diverse and interdisciplinary area of analytical chemistry. This notion is supported by the famous statement of A. Einstein that "no problem can be solved from the same *level of* consciousness that created it." Nanoanalytics serves as a proof of that statement as it cannot be developed merely by professional analytical chemists but also by chemists, specializing in other fields, as well as by physicists, material scientists, biologists, metrologists, and mathematicians. The main purpose of this chapter is to share with the analysts and other specialists working in the area of nanoanalytics, an integrated view on its subject to find new possibilities from nanoscience and nanotechnology for nanoanalytics development.

## 1.3 The concept of nanoanalytics

The absence of consensus among various specialists on opinion regarding the term of "nanoanalytics" can be eliminated if the concept of nanoanalytics after discussion becomes generally accepted. Such concept shall not only unite the abovementioned views on this area of analytical chemistry but also enlarge the wide world of

nanoscale objects and nanotechnological data used in chemical analysis, that is, to extend the nanoanalytics scope of application. Generalization of scarce literature sources, which use the term, and a large number of experimental papers allowed to distinguish several branches that constitute the subject of nanoanalytics as shown in the following schematic (Fig. 1.2).

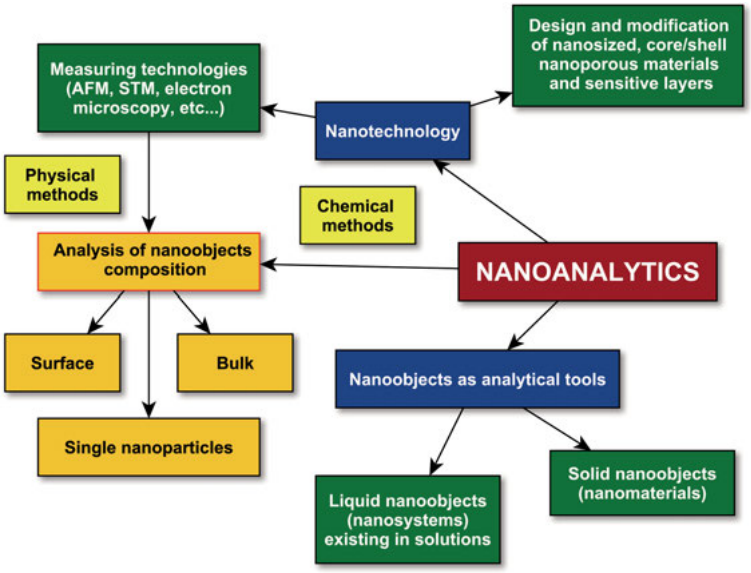


**Fig. 1.2:** The proposed concept of nanoanalytics.

As a result, nanoanalytics can be defined as follows: *Nanoanalytics is an area of analytical chemistry that develops the principles and methods of application of nanotechnologies and specific properties of nanosized objects in chemical analysis*. This version of the definition and corresponding concept have been formed and discussed throughout the term of nearly 10 years at various analytical chemistry conferences in Russia and other countries [46–51].

According to this concept, nanoanalytics consists of three primary branches:

- application of various types of *nanotechnologies* in analytical chemistry: chemical one that includes the synthesis and modification of nanomaterials for subsequent chemical analysis as well as sampling and physical one including measurement (evaluation) of size, shape, and morphology of nanoobjects in order to find their relation to analytical signal;
- application of various *nanoobjects* as tools for chemical analysis, which can be used to modify sensitivity and selectivity of analytical signal;
- *chemical analysis* of nanoobjects themselves via chemical and physical methods and corresponding metrological problems.

Let us discuss each of these three branches consecutively in accordance with definitions of some other *nano-* terms.

## 1.4 Nanoobjects as tools for nanoanalytics

As we can see from the schematic (Fig. 1.2), *one of branches of nanoanalytics* involves utilization of solid and liquid nanoobjects for analysis, separation, and preconcentration (enrichment) techniques as *means of tools for* solving traditional analytical problems, particularly, increase in sensitivity and selectivity of analytical determinations.

### 1.4.1 Definition, classification, and fundamental properties of nanoobjects

Consistent use of terminology is especially important in new fields of scientific activity like nanoscience, nanotechnology, or nanoanalytics to ensure common understanding of concepts and tools among different stakeholders, such as science experts, regulatory authorities, industry, and consumers. This situation in the field of "nano" requires the ongoing global discussion on the meaning of some important key terms in this field. Up to the present time, the information about main "nano" terms has become so numerous and diverse that its systematization is due for this field. Everybody understands that "nano," of course, means "billionth of" something, usually size, but a question arises: what is the boundary at which properties become unusual? What is the boundary that can separate nanoobjects from atoms and molecules on one side and from bulk material on another? Therefore, many people, especially scientists, question themselves – "what is nano?" "Is nano a bubble?" [52]. Distrust for everything new is increasing because every day we hear about a bubble in a national economy or a housing market. So, bubbles are ubiquitous, and everybody can ask: "Are nanoscience and nanotechnology bubbles, and if so, how can we avoid such a violent collapse?"

If someone believes that nano-effect is a real phenomenon, then the next question follows: "To be nano or not to be nano?" [53]. In other words, can we distinguish nanoobject with unusual properties (and in what field of physics, chemistry, or biology they can be applied for?) between nanoobjects with bulk properties? In the case of positive answer, other questions can arise, such as "What can nano do?" [54] and "What are the products of nanotechnology?" [55]. Nevertheless, in spite of many questions, during the last two decades the era of nano has had a tremendous positive impact on scientific research and in some extent on the technology level across the global world. Therefore, many developed countries have created nano-dedicated

research programs, research fellowships, networks, special institutes, and educational initiatives that aim to understand and leverage nanoscale discoveries [56].

In this part of the chapter, we shall become acquainted with tools that nanoscience and nanotechnology employ in their practice, that is, *nanoobjects*. First of all, we need to provide our *definition of nanoobject* using chemical concepts and describe their nature compared with atoms, molecules, and phases specific for macro-objects. According to ISO 80004-1-2015, "nanoobject" is a discrete piece of material with one, two, or three external dimensions in the nanoscale, that is, with length range approximately from 1 to 100 nm. This is physical description of nanoobject without regard for chemical nature and aggregate state. It is evident only that nanoobjects fall in between phases and atoms, which have diametrically opposite properties from thermodynamics standpoint [57–59]. Phases are macroscopic objects and only *internal* energy matters for them. On the opposite, in the case of atoms (molecules) only *external* energy matters, while their internal energy is considered constant. The specific feature of nanoobjects is that both internal and external *are equally important* for understanding their properties.

Examples of external energy manifestation include NPs' gaseous phase in the air or osmotic pressure of liquids. The internal energy of the system changes as a result of such processes as breakage or heating (both of solid and liquid NPs). Therefore, an important question arises – what model better describes the structure of nanoobjects? Are they small phases or very large molecules? The author of papers [57–59] believes that chemical approach shall have priority, that is, first we need to evaluate the internal energy and then (when it is not considered a constant) we can apply the phase approach. This may help us to consider both crystalline and amorphous nanoobjects as *supramolecules*; if a certain amount of such molecules have similar nature but growing size, they can be considered *homologues* (e.g., fullerenes C60, C70, ..., 140, 260, etc. or a series of magnetic NPs with varying magic numbers), while molecules with different structures can be considered *isomers* [59]. Such approach may lead to formation of a strict thermodynamic NPs theory, which utilizes the concept of chemical potential [57]. As a result, the formula was proposed showing the possibility of the particle size boundary below which the stable existence of NPs becomes impossible due to their spontaneous dissolution.

On the other hand, nanosized objects can be considered as a transition territory (area) of matter from laws of classical mechanics to laws of quantum mechanics, that is, nanoobjects means quantum-sized structure.

A few words shall be said about nanoobjects terminology. Such terms as *nanoobject*, *nanostructure*, and *nanosystem* can be considered in some extent as equivalents as they have mostly the same meaning as indicators of objects size and complexity. *Nanoparticle* has a narrower definition and cannot be applied, for example, to nanosized films or nanoporous materials. At the same time, *nanostructure* and *nanostructured object* are not equivalent terms as the latter may include not only nano- but also micro- or macrosized bulk parts.

In the twenty-first century, the era of nanotechnologies thrusts *solid nanoobjects*, which can be produced both in solution and by simple solid phase dispersion, into the spotlight. However, it was aptly noted that some nanoobjects may be created as a result of spontaneous association of molecules or ions in the solution forming so-called liquid nanoobjects [57–59]. The most graphic example of such nanoobjects are the well-known micelles, microemulsions, or vesicles, which form in liquid media as a result of self-organization (self-assembly) of surfactant molecules or ions. This category of nanoobjects includes many biological (proteins, RNA, DNA) and some synthetic compounds with high molecular mass and their complexes with surfactants.

Surfactant micelles are typical nanostructures both in size (3–10 nm) and in nature. Unlike solid nanoobjects, micelles do not act as nucleating seeds for new phases, that is, they exist only in nanosized state and form truly balanced and stable nanostructured systems. Thus, the majority of nanoobjects can be separated on the grounds of their phase into two groups – *solid* and *liquid*. Both of these groups find widespread application as tools of nanoanalytics, which (in addition to nanotechnologies) separate this field from classical analytical chemistry. Therefore, let us further discuss the properties of liquid and solid nanoobjects and spheres of their application for chemical analysis.

### 1.4.2 Liquid nanoobjects

*Liquid* nanoobjects (nanosystems, nanostructures) include micelles and microemulsions (enclosed monolayers) and vesicles (enclosed bilayers) formed by diphilic surfactant molecules and also their complexes with macromolecular substances [57, 59]. Micelles and microemulsions are considered as the most *typical examples of nanostructures* for both their size (which may vary from three to tens of nm) and their unique characteristics and properties. Unlike solid molecular aggregates, which act as nucleating seeds for new phases and form an unstable equilibrium with the solution or vesicles, which posses only kinetic stability, micelles are an example of truly equilibrium and thermodynamically stable nanostructures. They can exist even in oversaturated solution, which only reinforces the concept of their inability to act as nucleating seeds for new macroscopic phases [57]. Thus, the term “nanostructure” gains its true meaning when applied for micelles as they have *no macroscopic counterparts* and may exist *only in nanosized state* [57, 59]. This statement is true for both direct and reverse micelles and oil/water or water/oil microemulsions existing in polar water or non-polar solvents, respectively. In addition to micellar objects, the second type of liquid nanoobjects (nanostructures) includes receptor molecules like cyclodextrins, calixarenes, cyclopeptides, etc.

The studies of distinctive features of organized media containing both types of liquid nanoobjects, which can be used for chemical analysis reached their peak

during 1980–90s. A prerequisite of their application in analytical chemistry was the emergence of the following problems during the beginning of 1980s, which resulted from well-known restrictions of contemporary molecular spectrometry, separation, and preconcentration techniques [60–62]:

- the need for close proximity and localized preconcentration of analyte and reagent in very dilute solutions within detection threshold ($10^{-8}$–$10^{-18}$ M) when chemical reaction could not be executed; this resulted in significant improvement of detection sensitivity and decreased the detection limits for many compounds;
- the need for overcoming incompatibility of simultaneous detection of hydrophilic and hydrophobic components of analytical reaction in aqueous solution or implementation of interaction between analyte and reagent molecules with vastly different solubility;
- the need for increased efficiency of intra- and intermolecular electronic excitation energy transfer and electron transfer in order to increase the sensitivity of methods, which utilize their effects;
- implementation of potential simultaneous separation of hydrophilic and hydrophobic components of analyzed mixture via chromatography and capillary electrophoresis;
- radical change the surface properties of sorbents in dynamic mode to facilitate substance concentration and separation.

Thus, we can establish two groups of molecules that form nanostructures in the solution by the means of liquid nanoobjects formation [60–62]:

- media containing *organized micellar systems* that form their own nano-pseudophase;
- media containing *receptor molecules* that have an internal three-dimensional cavity and function in a "guest–host" manner.

The term *micellar systems* originated from the name of the simplest representatives of this type of organized system – surfactant micelles. Examples of micellar systems include both direct and reverse micelles, microemulsions (water/oil and oil/water), vesicles, liposomes, Langmuir–Blodgett films, and liquid crystals, which form spontaneously as a result of association of diphilic molecules or surfactant ions (Fig. 1.3).

*Receptor molecules* (cyclodextrins, calixarenes, cyclophanes, cyclopeptides, cavitands, carcerands, etc.) (Fig. 1.4) form rigid three-dimensional cavities in their environments and act as "hosts" (receptors) for "guests" (substrates) – solubilized organic reagents or analytes. Sometimes, they are called supermolecules and corresponding solutions are called pre-organized media [63, 64].

In order to make a single group for solutions containing micellar systems or receptor molecules, a general term – *microheterogeneous* (actually, nanoheterogeneous) *organized media* – was proposed in the early 1980s. These media include transparent optically isotropic solutions, which have various supra- or supermolecular

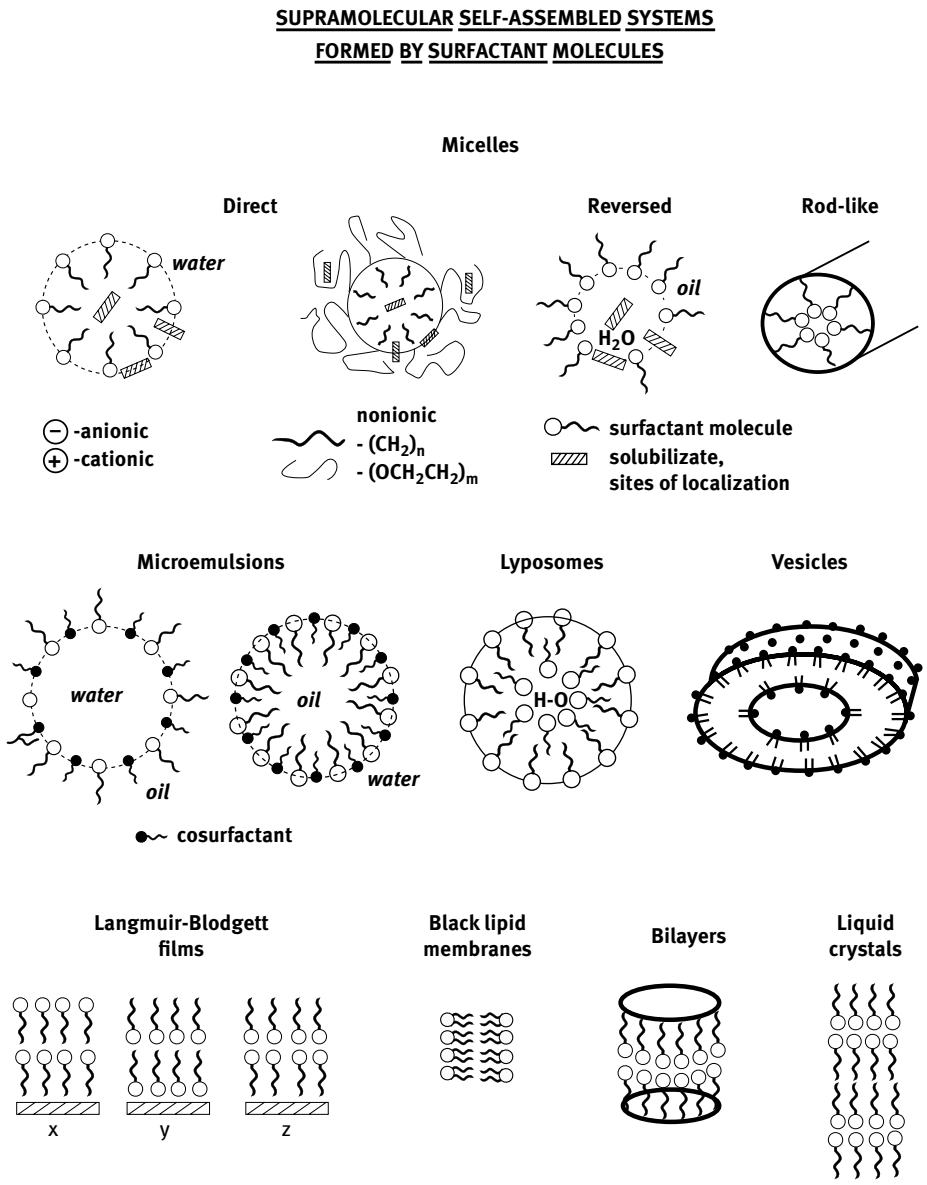


**Fig. 1.3:** The examples of liquid micellar self-assembled nanosystems.

nanosystems dispersed in the bulk of solvent (aqueous or non-aqueous dispersion medium) with each of such nanosystems forming their own nano-pseudophase. Every single micellar nano-pseudophase actually serves as example of *nanoreactor* present in the bulk of solvent [60–62, 65]. Existence of the nano-pseudophase can be easily proved via changes in the color of solubilized molecular probes – special dyes or indicators, which colors (spectra) vary in the media with different polarities [65–67].

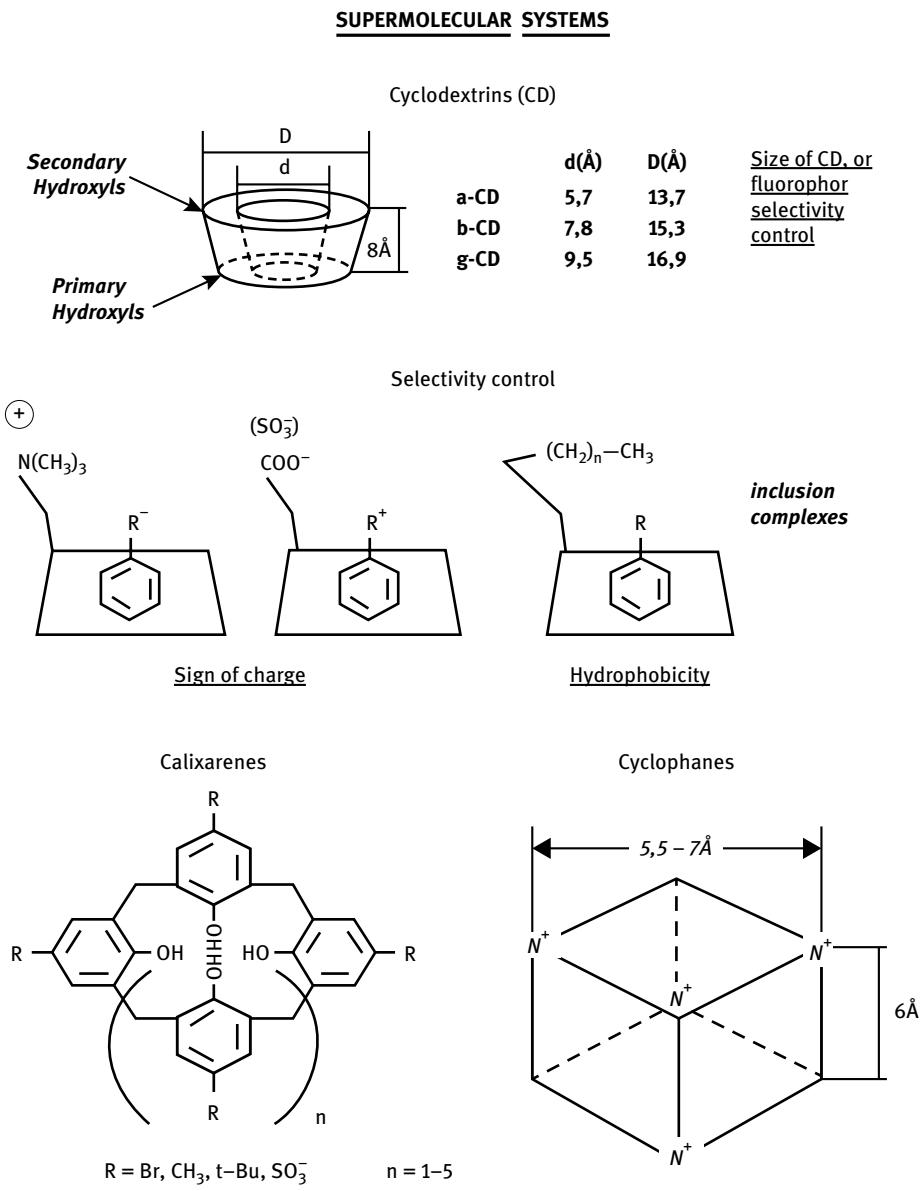


**Fig. 1.4:** The examples of supermolecular systems.

By this means *liquid organized media are homogeneous at a macroscale* (look like as single macrophase), *but they also are microheterogeneous at a nanoscale* [61, 62, 68].

In fact, liquid nanoobjects (nanoreactors) and derived from them organized media serve as examples the achievements of nanochemistry and principles of

supramolecular chemistry that have found a wide application in nanoanalytics because of self-assembly (supramolecular) effect and thermodynamic stability in solution [63, 64, 69].

Micellar nanosystems have some specific features, which separate them from solid NPs [60–62]:

- they form by self-assembly (via supramolecular interaction) of diphilic molecules and ions with their size varying from 3 to 100 nm;
- they have no macroscopic counterparts and do not act as seeds for new phases;
- they are equilibriums and stable systems; the mass action law is applicable for them;
- their solubility increases with increase of their size;
- they form abruptly, contain molecules with polar and non-polar fragments, and have a developed surface, while ionic nanosystems have high surface electrostatic potential (SEP) up to 100 mV on several $nm^2$;
- they are capable of spontaneous solubilization (act as co-solvents) of other substances at their surface or in their core by self-assembly effect, so they can act as nanoreactors;
- they can change the physicochemical, spectroscopic and electrochemical properties of reacting compounds and the analytical system as a whole, as well as direction of chemical reaction that is a result of changing of medium properties in the microenvironment of substances due to surface potential influence or donor–acceptor and hydrophobic interactions.

Enormous variety of diphilic surfactant molecules and receptor molecules serve as a basis for the most important advantage of liquid nanostructures – the possibility of *controlling* their composition and properties in the solution. This resulted in significant improvement of analytical signal characteristics (sensitivity, reproducibility) for various methods of analysis as well as selectivity of analytical determination and processes [60–62, 68, 69]. It should be noted that such control over properties of liquid nanoobjects has several aspects, which helps to regulate the properties of liquid nanoobjects in the following ways:

1. By way of direct choose the *type* of organized nanosystem (direct or reverse micelles, microemulsions [oil/water or water/oil], cyclodextrins);
2. By way of direct choose the nature of surfactant or receptor molecules, which form the abovementioned organized nanosystems, for example:

- the nature of hydrophilic group of surfactant (cation, anion, length of oxyethylene (oxypropylene) chain);
- the nature of hydrophobic group (aliphatic or aromatic);
- hydrophilic–lipophilic balance between surfactant and analyte molecules;
- ratio between the sizes of cavity (or functional group charges) of receptor and analyte molecules.

3. By way of regulation of organized nanosystem properties through changing the following factors:
- the charge density and surface potential of the micelle;
- the hydration and hydrophobic properties of micelles phase boundary;
- the micropolarity and microviscosity of micelles nano-pseudophase;
- the size and aggregation number of micelles and microemulsions;
- the distance between reacting agents solubilized in micelle [67];
- the degree of electron excitation energy transfer, electron transfer, and substrate exchange kinetics for micelle–solvent system;
- the concentration of oxygen and other gases inside the micelle.

Primary factors establishing the ability of liquid nanoobjects for making significant changes to properties and reactivity of analytical reaction components are as follows [60, 61]:
- the ability to solubilize (dissolve) compounds with low solubility in the solvent forming the dispersion medium, which results in local changes of medium properties in microenvironments of analytical reaction components;
- the ability to bring close together and to concentrate the components of an analytical reaction, even though they are considerably different in hydrophobicity, in the nanophase of an organized system;
- the multicenter and multifunctional (electrostatic, donor – acceptor, van der Waals, and hydrophobic) interactions of the components or parts of a nanophase with a solubilized substrate; among these interactions, the hydrophobic interaction plays a predominant role;
- the pronounced oriented sorption and cavity effect, in which the nature and geometric compatibility between the host and the guest are the decisive factors in the binding of a substrate analyte;
- the considerable microheterogeneity of a medium within nanoreactor in a direction from the water (bulk solvent) interface to the center, which manifests itself in dramatic changes in the dielectric constant, microviscosity, micropolarity, microacidity, and other physicochemical properties of the medium and solubilized analyte itself.

It should be noted that not only formation of micellar nanoreactor but also solubilization of analytical reaction components within them performed by self-assembly principles, that is, both processes have supramolecular nature typical for live organisms [60–62, 68–70]. Similar self-assembly occurs during formation of inclusion complexes, resulting from interactions between analytes and receptor molecules.

Liquid nanoobjects are used in analytic chemistry since the end of 1970s. They helped not just to improve metrological characteristics of spectrometric, electrochemical, chromatographic, extraction, and other analytical separation and preconcentration

techniques but also to developed new variations of such methods as described in several reviews and books on the subject [60–62, 68–92]. These new variations include room temperature phosphorescence (RTP) and sensitized RTP of luminophors in micelles, microemulsions and cyclodextrins, which allow one to eliminate the use of liquid nitrogen to obtain a low temperature necessary for phosphorescence method [74–80]. Another example is sensitized fluorescence of some lanthanide chelates, which helped to develop highly sensitive methods for metal ions as well as many toxic substances, antibiotics, pesticides, and other organic compounds determination [81–83].

Some of the examples of liquid nanoobjects application for separation and preconcentration techniques are micellar liquid chromatography, micellar (cyclodextrin) electrokinetic chromatography, micellar extraction, micellar ultrafiltration, and several other methods, which made a significant impact into development of separation and collection techniques [68, 70, 85–92]. Figure 1.5 shows a generalized schematic illustrating the widespread application of different organized liquid nanoobjects for various analysis, separation, and preconcentration techniques.

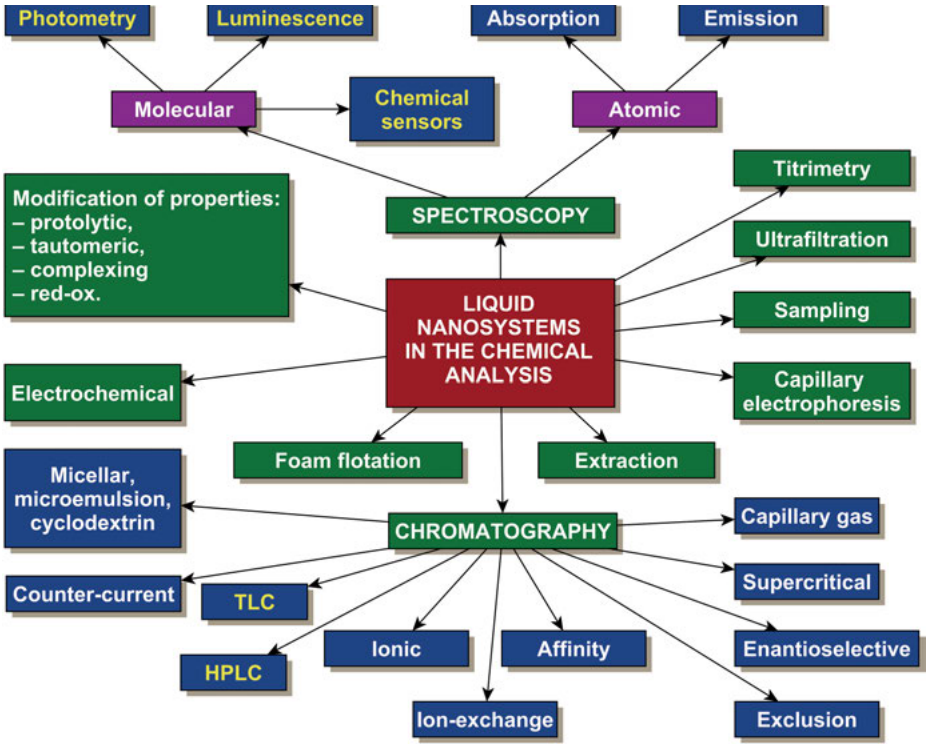


**Fig. 1.5:** Application of liquid micellar nanoobjects in chemical analysis.

The number of studies dedicated to application of liquid nanosystem for analysis reached its peak during late 1980s and early 1990s. Currently, surfactant molecules and their self-assembly process are used for functionalization, modification, and surface protection of solid nanoobjects, particularly various NPs (gold, silver, quantum dots, carbon nanotubes, magnetic NPs); thus, these two "nano" approaches to analytical methods improvement can be used simultaneously.

### 1.4.3 Solid nanoobjects (nanomaterials)

One of the definitions of *materials* states that they are substances or mixtures that can (after sufficient processing) be turned to products with specifically required features. This definition distinguishes materials from raw materials (substances). Thus, the concept of *materials* is mostly associated with solid compounds, which can be used to develop some devices or their components. *Nanomaterials* currently do not have any particular definitions either in different countries or in various state or international organizations [1, 2, 38–40, 42, 44, 93–98]. Sometimes this term is substituted with more narrow one *nanostructured materials* or even *nanoparticles*. In our opinion s*olid nanoobjects* is a more general term, which can include nanomaterials, NPs, and most nanostructured materials within nanometer range including nanoporous objects and films.

Generalization of existing concepts allows to define the solid nanoobjects (nanomaterials) as "objects (materials) with *qualitatively new properties, functional and operational characteristics* which size or structural elements do not exceed 100 nm in at least one dimension" [1–4, 6–8, 38–40, 44, 50, 51, 53, 69]. From this point of view, the properties of nanoobjects are more important than their size [47–51, 53]. The most important parameters determining the properties of nanomaterials are the *nature* of compounds along with *size* and *shape* of nanoobjects. For these reasons, the nanoscale phenomena play a role but rare and exclusive one [7].

There are multiple several classifications and terms describing nanomaterials of various size and shapes; however, they are not always clearly defined and consistent. For example, the 7th International Conference (2004) list of terms was proposed; however, these terms were based on different structural and morphological principles, and thus they should not have been combined into a single classification. The list goes as follows:

- NPs (nanoobjects with complex geometric shape, which have no usual counterparts being shaped as, for example, roses, nails, clams, brushes, rings, etc.);
- nanotubes (carbon, metal, oxide, organic);
- nanofibers (nanowires, nanorods, nanoribbons);
- nanocrystals (size may vary from 5 to 100 nm, number of atoms may vary from $10^3$ to $10^8$ atoms);
- nanoclusters (particles with organized structure, which size varies from 1 to 5 nm and may contain up to 1000 atoms);

- nanoporous structures (porous silicon, sol and gel materials and films [membranes] with molecular imprints, which properties are derived from the nature of material and pore size);
- nanofilms (Langmuir–Blodgett, polyelectrolytes, graphene-based sheets);
- nanocomposites – arrays of nanoobjects with varying chemical composition.

The most simple and easy to understand classification, unfortunately lacking any fundamental basis, is nanoobjects' classification by their *geometric shape* into NPs with unclear geometric shape (brushes, snowflakes, roses) and particles with clearly defined geometric shape (spheres, prisms, cubes, tubes, ribbons, rods, fibers, wires, rings).

Other classifications take into consideration the *object structure* (clusters, crystals, nanostructured or nanoporous materials) or *material nature* (inorganic – carbonaceous, oxide, chalcogenic or metallic – organic–inorganic hybrid or composition materials). Gleiter [99] proposed to divide all nanomaterials into three classes, which take into account their physical dimensionality: NPs; nanolayers, nanofilms, and surface structures; and three-dimensional nanostructured materials.

One of the proposed criteria is that the assignment of substance to nanoobject or nanostructured material can be significant impact of its size or nanosized structural elements on discussed properties. In such a situation, it is certainly possible that some properties of material are specific for nanoobjects, while others are not; thus, the material may not be classified as a nanoobject or nanostructured material.

The most fundamental fact from the scientific point of view is the classification that strictly divides various types of nanoobjects on the basis of their dimensionality. This classification mostly accounts for spatial anisotropy and divides NPs into zero- (0D), one- (1D), two- (2D), and three- (3D) dimensional particles [1–4, 6–8, 13, 42, 44, 69, 93]. In turn, 0D particles are called quantum dots, 1D quantum wires, and 2D quantum wells.

*Zero-dimensional* nanoobjects are objects in which three dimensions (length, breadth, and height) are nanoscale and are less than or equal to the so-called "critical" diameter (length), that is, they are fully confined in 3D space. The value of the diameter does not have any certain meaning because it is dictated by a critical characteristic of some physical phenomena (free path length of electrons and phonons, length of de Broglie wave, length of external electromagnetic and acoustical waves, correlation length, penetration length, diffusion length, magnetic domain, etc.) giving rise to quantum-size effects. Examples of such objects are semiconductor NPs (so-called quantum dots, QD), metal (Au, Ag, Cu) NPs, or carbon QD with size up to 10, 40–50, or 1–3 nm, respectively. Thus, 0D objects include clusters of various materials, which size usually rarely exceeds 5–10 nm and the number of atoms or molecules is less than 1,000–5,000; this group includes fullerenes, carbon, and quantum dots, and many other nanostructures.

*One-dimensional* nanoobjects are solid nanoobjects (nanostructures) with one dimension significantly exceeding two others, which may range from 1 to 100 nm. If

length-to-diameter ratio is greater than 1,000, these nanoobjects are called nanowires or nanofibers. Such objects also include wire-like nanocrystals – whiskers – whose thickness ranges from 20 to 40 nm. If width and thickness of such whiskers differ, then such objects are called nanobelts. In addition, there is a whole class of tubular nanoobjects – nanotubes. When the length of nanoobjects is greater than their diameter by 10 times or less, such objects are called nanorods. The most famous examples of 1D nanostructures are carbon nanotubes. In addition to carbon, such objects can be formed by Si, Ge, Se, Au, Ag, Fe, Ni, Cu, as well as oxides (MgO, $Al_2O_3$, $Ga_2O_3$, $SnO_2$, $SiO_2$, $TiO_2$), nitrides (BN, AlN, InN, GaN, $Si_3N_4$), chalcogenides (ZnS, ZnSe, PbS, CdTe), complex oxides formed by several elements, and protein molecules.

*Two-dimensional nanoobjects* are nanoscale only for one dimension – width that may not exceed 100 nm. These objects include various films formed by metals, non-metals, oxides, and other compounds, which exhibit conductor, semiconductor, dielectric, and magnetic properties. Synthesis and practical application of these objects began several decades ago. They were produced using both physical and chemical methods such as precipitation from gaseous or liquid phase. Most famous physical methods include molecular beam epitaxy, pulsed laser deposition, and cathode sputtering by direct current. Chemical methods include chemical vapor deposition (CVD) from gas phase and chemical precipitation from solution via spin-coating, dip-coating, or spray coating. Nanofilms of organic and biomolecules are produced via Langmuir–Blodgett or Langmuir–Schaefer technique.

Recently, the list of two-dimensional objects was extended by graphene monolayers and their derivatives such as graphane, graphene oxide, and graphene fluoride (fluorographene) [100]. In addition, graphene-like hexagonal silicone sheets and graphene-like binary phases such as GeC and SnC or boronitrene (white graphene), B–C–N triple systems as well as graphene-like $A^{II}B^{VI}$ phases (ZnO, BeO) and metal carbides have been produced.

*Three-dimensional* nanoobjects (nanostructures), as stated by IUPAC, are three-dimensional arrays of nanoobjects and nanocomposite materials. They may include as constituents the 0D, 1D, and 2D or nanoporous structures.

The most distinctive features of solid nanoobjects or nanomaterials are their *unique optical, electrical, magnetic, mechanical or catalytic properties*, which are not inherent in bulk objects. As is the case of traditional bulk materials, nanomaterials can have various *composition and functions* (organic and inorganic compounds, metals, semiconductors, dielectrics, magnetic and catalytic materials) and *shape* (spherical NPs, rods, wires, belts, tubes, cubes, triangular prisms, and porous materials). Due to their highly developed and active surface, NPs can be *easily functionalized* by physical, chemical, and biological means, which serve as a basis for potentially limitless variety of functional nano-sized devices with practical applications, including chemical analysis.

As said above, NPs act as an intermediate between phases and atoms, which thermodynamics describe from completely opposite positions – for phases, only internal energy matters, while for atoms – only external energy does [57–59]. *For nanoparticles,*

*both energies are relevant*. Therefore, abovementioned unique properties of NPs are caused by two factors: *surface* (high surface-to-bulk atoms ratio) and *quantum-sized* effects. The latter are especially significant when dimensions of solid NPs are comparable with *correlation radius of a physical phenomenon* (free path length of electrons and phonons, size of magnetic domain or excitons, etc.) [1–4, 6–8, 13, 69, 101, 102].

Thus, generalization of solid nanoobjects' properties results in distinguishing the following characteristic features of nanoobjects [48–51]:

1. Solid nanoobjects (nanomaterials, nanostructures, NPs) occupy an *intermediate* position between phases and atoms, which are described by opposite thermodynamic concepts – in the case of phases only internal energy is taken into account, while in the case of atoms only external energy is considered significant. For solid nanoobjects, both kinds of energies are equally important. These nanoobjects can be considered polymers or supramolecules.
2. Solid nanoobjects can be produced by dispersion of macrophase (top-down) or by self-assembling (down-top) of atoms (molecules); they act as *nuclei for new phases*. There is a size boundary below which the nanoobject cannot exist in solution.
3. Very high ratio of surface atoms to bulk ones: for NPs which size is close to 3 nm, the ratio is about 50%, and for particles which size varies between 1.5 and 2 nm, this ratio is almost 80% (!). This results in their greatly enhanced catalytic activity for chemical and biochemical reactions.
4. Quantum-sized effects: they are especially great when the sizes of nanoobjects are comparable with correlation radius of physical phenomenon (the length of free pass of electrons and photons, the size of exciton or magnetic domain, etc.). "Internal atoms" form a continuous energy zone and energy levels of "surface" atoms are discrete and clearly expressed.
5. The defects of crystal structure are small or absent leading to high durability of nanoobjects. For example, carbon nanotubes have tensile strength that is 10 times greater than steel.

Application of nanomaterials for improvement of analytical determination characteristics was the primary topic of special issues of *Analytical and Bioanalytical Chemistry* in 2010 and 2011 [103, 104]. They contained several general reviews dedicated to application of various types of nanomaterials in various methods of chemical analysis [42, 46, 69, 98, 105–108]. Other reviews considered application of solid nanoobjects for sample preparation [109, 110], separation and preconcentration techniques [111–114].

Nanoobjects application in various spectroscopic methods of analysis is based on their unique optical properties including absorption, emission, and diffraction of electromagnetic radiation by different nanoobjects. These properties include surface plasmonic resonance (SPR) and surface-enhanced Raman scattering (SERS). It has been established that SPR effect for 2D objects and local SPR characteristic for 0D NPs increase the molar absorption coefficient of light by 1 to 5 orders of magnitude (up to $10^6$–$10^{10}$) (!), thus allowing one to determine femto- and attograms of analytes. Similar

anomalous increase of analytical signal intensity is observed when giant Raman scattering (SERS) is applied; in this case, signal intensity may increase by 4 to 12 (!) orders of magnitude. The results obtained were published in the monograph [115] and a series of reviews [116–121] and shall be discussed further in subsequent chapters of this book. Another effect is caused by application of unique quantum dots (both semiconductor [122–124] and carbon [125, 126]) fluorescence parameters for chemical analysis.

Solid nanoobjects are widely used in environmental analysis [127], foodstuff analysis [128], medicine and clinical diagnostics [129, 130], bioanalysis and biodiagnostics [118, 131–133], explosives detection [134], living cell sensors [135, 136], and as primary components of various sensors [44, 127, 130, 137–140].

Nanomaterials, especially carbon nanotubes (CNTs), found widespread application in electrochemical analysis including electrochemical sensors [46, 141–147]. In addition to CNT, graphene [100, 148–151] and carbon dots [152, 153] also became a popular choice for electrochemical and other types of chemical analysis during the last 5 years. The scope of nanomaterials application for analysis is shown in Fig. 1.6.

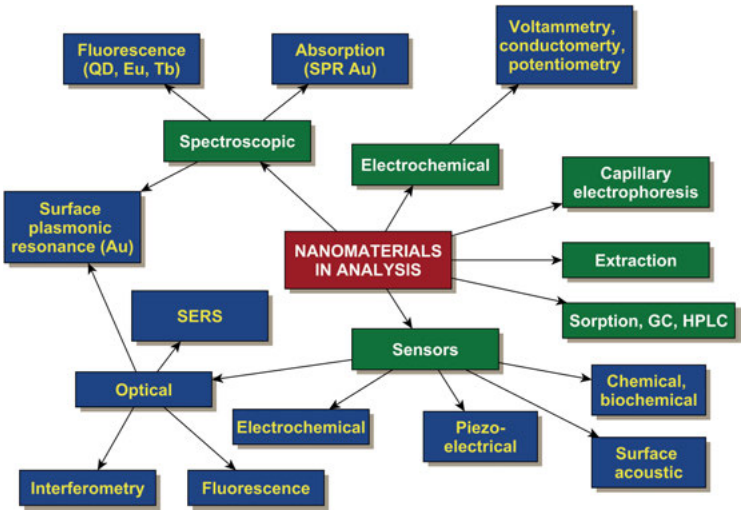


**Fig. 1.6:** Application of solid nanoobjects in chemical analysis.

As we can see, in addition to abovementioned techniques, nanomaterials are used for extraction, sorption, and capillary electrophoresis [154, 155]. Magnetic NPs are widely used for separation and preconcentration of organic, bioorganic, and inorganic substances as they allow decreasing the time required to separate sorbent from matrix solution down to tens of seconds [156–160]. For now, the number of studies on solid nanoobjects application is less than that for liquid nanoobjects and organized media, but it is growing rapidly. It should also be noted that theoretical and practical study on the subject began nearly 25 years later than those for liquid nanoobjects.

## 1.5 Nanotechnologies as tools for nanoanalytics

While a definition of the term "nanomaterial" has been intensely debated during the last 15 years, less focus has been put on a definition of "nanotechnology" [161]. At the same time, the proposed concept (see Fig. 1.2) clearly shows that nanotechnologies are also an integral part and tool of nanoanalytics; thus, it is important to define the elements of this term when applied to nanoanalytics. The reason is that if you can't define a term, you can't evaluate its elements and importance in the field intend for. Thus, let us first review some general definitions of this term and then the types of nanotechnologies inherent in nanoanalytics.

As was the case for nanomaterials, academic and nanotechnological communities of various countries as well as official international societies provide various definitions of nanotechnologies, that is, the meaning of this word is not yet well established [2, 8, 23, 38–40, 69, 95, 97, 102]. Some authors try to provide a comparative analysis of various definitions of "nanotechnologies" accepted in different countries and international organizations [8, 38–40, 47–51, 97, 102, 162, 163]. It is evident that nanotechnology often has *different meaning in different fields of science* (chemistry, physics, biology, medicine, or materials science) or pursues different goals. Therefore, it may appear that there is no single perceive of nanotechnology and this term broadly refers to the fields mentioned above.

Nevertheless, the definitions of nanotechnology shall have a fundamental base and shall not conceptually differ. Balzani [164] argues that first of all it is important to understand that "technology" has a quite different meaning from an apparently similar word "technique". *Technique* is a *method* of doing or performing, with skill acquired by experience, something that has already been established. *Technology can be defined as the ability of making advantage of the progress of science to create novel opportunities for practical applications*. Therefore, technology is a driving force for the progress that provides a lot of novel materials, devices, and methods capable of improving the quality of industry and human life, and, in our case, developing analytical chemistry. In general terms, Balzani considers "nanotechnology" as a "technology concerning objects of nanometer dimensions."

A comparative analysis of tens currently accepted definitions of "nanotechnology" shows that they differ by the extent of generalization and can be classified into several groups. One group of definitions describes nanotechnologies as "*manipulation* of individual atoms, molecules and nanosized objects to develop, produce and apply physical, chemical or biological materials, structures, devices or systems which size varies from 1 to 100 nm" [38]. More general definition proposed in [165] states that nanotechnology is "application of scientific knowledge to *manipulate* and *control* nanoscale matter to utilize size- and structure-dependent properties and phenomena distinct from those associated with individual atoms or molecules or bulk materials." The same but more concise definition is published in Wikipedia: "Nanotechnology is *manipulation* of matter on an atomic, molecular,

and supramolecular scale" [166] or "Nanotechnology manipulates individual atoms and molecules to produce materials for applications at the submicroscopic level" [167]. The keywords for this group of definitions are "*manipulation … to produce…*" of atoms, molecules, nanosized objects, or simply objects. This definition fits the initial concepts of Feynman [25] and Drexler [28] but is poorly suitable for practical application.

Authors of another group of definitions regard nanotechnologies as a *collection of methods and techniques* that can be used for controlled production of materials, devices, and technological systems operation of which is based on components that are not more than 100 nm in size [38]. The keywords here are *a collection of methods and techniques* and *production of materials*. As can be seen later, the both of aforementioned types of definitions are rather broad and do not always correlate with practical actions specific for nanotechnologies in nanoanalytics.

Online "nanodictionary" includes more than 15 definitions of the term *nanotechnologies*, such as: "*Nanotechnologies* are design, characterization, production and application of structures, devices and systems by controlling shape and size at nanometer scale". These definitions contain a third group of keywords related only to practical results [168]. This group is also the first that contains the word "application."

The fourth group of definitions combines properly the terms "nanoscience" and "nanotechnologies." An example of such broad definition is provided in the program of National Nanotechnology Initiative (United States): "Nanotechnology is science, engineering, and technology conducted at the nanoscale which is about 1 to 100 nanometers" [169]. Another example is a definition provided in [102]: "Nanotechnologies are a group of fundamental and applied studies and designs aimed at researching the specific behavior of substances and controlling their properties within 1 to 100 nm range … ." Finally, the nanotechnologies are identified with nanoscience: "Nanotechnology can be defined as the science of manipulating matter at the nanometer scale in order to discover new properties and possibly produce new products" [170].

In essence, one should consider that definitions of "nanotechnologies" provided by various national and international organizations are merely *working* definitions. As such, they reflect specifics of particular programs and projects they were formulated for, that is, they vary depending on the sphere of application, the scope of problem they are intended for and the authority level of such organization. Nevertheless, generalization of all variations of "nanotechnology" definition helps in a broad sense to reveal three primary components of this term [102]:

- fundamental research and studies of properties and characteristic features of nanosized or nanostructured compounds, which form the basis of nanoscience;
- variety of laboratory and industrial methods, techniques, and technologies applicable for any nanosized objects;
- nanoindustry and its products.

It should be noted that formulating the definition of "nanotechnologies" is very important not just for any particular science or institution but also for potential investors who may fund research in that field of science. A consistent definition of "nanotechnologies" is appealed to determine the boundaries of the area to be considered and to exclude unnecessary.

In accordance with concept (Fig. 1.2) nanotechnologies used in nanoanalytics can be divided into *several* groups. The first group includes *metering* physical nanotechnologies purpose of which is establishing physical dimensions of NPs and their size-based distribution and characterization of surface morphology and interphase boundaries down to single atoms. This group includes various forms of scanning tunneling, atomic, and molecular force microscopy, that is, probing microscopy as well as TEM, dynamic light scattering, and other similar methods [50, 69]. As this kind of equipment is designed for nanoobjects *characterization*, it is multifunctional and can also be used to determine *chemical composition of nanomaterials*; thus its application for such tasks surely lies within competence of nanoanalytics [41, 69].

Thus, combinations of electron and probing microscopy with different variations of X-ray spectroscopy, such as dispersive X-ray (EDX) spectroscopy and electron energy-loss spectroscopy (EELS) are considered standard nanoanalytical tools today [167, 171]. These combinations are the basis for chemical speciation analysis within localized nanoareas and subsequent visualization of spatial distributions of specific chemical states (speciation) with high spatial resolution, so called *spectrum imaging*.

Characterization of nanoobjects using the combination of aforementioned and other similar methods allows performing *complex research* providing data about size, shape, structure, surface area, sign, and magnitude of its electrostatic potentials, electric charge, chemical composition, and concentration of various nanoobjects. The basis and justification for vital assignment (connection) of physical measurement and chemical analysis of nanoobjects to development of nanoanalytics is that physicochemical properties of nanoobjects and, therefore, unique metrological characteristics of analysis significantly depend on their 3D morphology (size, shape, surface topography), surrounding medium and spatial microenvironment.

This direction of nanoanalytics also includes development of new types of nanoanalytical tools by nanoengineering methods (*using* various lithography techniques such as photolithography, e-beam, and laser lithography), for example, NEMS and some forms of optical, electrochemical, and other types of sensors or devices, such as nanoscales [167, 170]. A special feature of this direction is that nanoanalytics serves both as developer of these structures and methods and as important user of the resulting devices as new tools for analysis. Intensive development of this direction can be attributed to considerable joined efforts by various physicists and chemists; however, physicists still play a more active role. Recently, there have been studies dedicated to identification of various ions at the surface of crystalline lattice as well as other molecules that utilize new variations of field probing methods [43].

Second group of nanotechnologies is fundamentally different from the first one as it is *chemical* in nature and includes *methods of synthesis, construction and modification* of various solid nanoobjects (nanomaterials or sensitive nanolayers of electrochemical, piezoelectric, optical and chemical sensors, specific nanoprobes or sorbents) to improve analytical and metrological characteristics of determination of various inorganic and organic compounds using traditional methods of chemical analysis [1, 2, 44, 46, 50, 69, 167, 170]. Materials developed by nanotechnologies can have homogeneous or hybrid ("core-shell") chemical composition; they can be as independent tools for analysis or act as nanoobjects placed within the macroscopic matrix of optical, piezoelectric, or electrochemical sensors. They can be both completely inorganic (metals, oxides, chalcogenides) and have attached organic molecules that improve selectivity of analysis or merely solubility of NPs in water. The most prospective for synthesis and modification of nanoobjects are *supramolecular chemical* methods based on self-assembling effects.

Let us consider several examples of successful application of different types of nanotechnologies for chemical analysis. Sol–gel nanotechnology, which can develop chemical and biochemical nanomaterials with required nanopore sizes, has been used for quite a long time [44, 69, 172, 173]. They are essentially chemical and biological variations of nanotechnologies, that is, they are a subject of studies for both *nanochemistry* and *nanobiotechnology* as they utilize well-known chemical and biochemical reactions and processes for nanoobjects instead of traditional macroscopic objects. These reactions may have specific features caused by distinctive reactivity of atoms and molecules at the nanosized surface or kinetics of undergoing processes, but generally the pattern of synthesis remains consistent. This field of studies mostly attracts analytical chemists, specialists in organic and inorganic synthesis, biochemist, and, to a lesser degree, physicists.

Other well-known examples of nanotechnologies used for chemical analysis include the Langmuir–Blodgett technique [44, 174, 175] proposed at the dawn of twentieth century, layer-by-layer self-assembling technique [44, 176–178] proposed in 1997–98, production of self-assembling monolayers such as alkylthiols [178, 179] that are further used to obtain nanosized films with variable layer width for chemical sensors [44]. Physicists have been successfully using various forms of lithography as well as molecular-beam and gas epitaxy to produce nanosized coating with required configuration for quite a long time.

Other types of nanotechnologies used for analysis are utilization of nanotubes, nanoribbons, and nanorods as nanoelectrodes and nano-"bar codes" or modification of electrodes by NPs [46, 167, 170], production of nanoporous materials and nanofilters for separation of gaseous and liquid compounds via molecular imprinting technique. More details about these applications shall be provided in respective chapters of this monograph. All the more so as listing and describing all types of nanotechnologies utilized by analytical chemists has never been the point of this section.

## 1.6 Nanoanalysis and nanometrology

### 1.6.1 Definitions and elements

The term "nanoanalysis," like "nanoanalytics," does not have a common definition, which reveals the subject of research. At the same time, in contrast to "nanoanalytics," it is used rather often in various papers, conference proceedings, and commercial advertising of analytical equipment. Some researchers suppose that the term "nanoanalysis" refers to techniques used for "determining the atomic structures of materials" especially crystals [180]. In special dictionary, we can find two kinds of nanoanalysis. One for "physics" defined as "the analysis of a surface or material at the nanometer level," while second for "chemistry" defined as "the analysis of nanogram amounts of material" [181]. However, such dichotomy is not convenient for everybody, and even both definitions do not embrace all fields of modern nanoanalysis.

Another definition is presented in [38]: "Nanoanalysis is an area of chemical analysis aligned to determination of chemical composition of individual nanoobjects and (or) local chemical analysis with nanometer dimensionality." This definition pursues only "chemical" targets and excludes physical characterization of nanoobjects related to analytical signal as well as analysis of biological nanoobjects like single cell characterization.

In our opinion, the terms "nanoanalysis" and "nanoanalytics" are as related to each other like traditional "analysis" and "analytical chemistry" or "analytics" are. If we define that "Nanoanalytics is an area of analytical chemistry that develops the principles and methods of application of nanotechnologies and specific properties of nanosized objects in chemical analysis," then we in general can define "Nanoanalysis as a tool (or service) of nanoanalytics."

At the same time, the term "Nanoanalysis" compared with common term "analysis" possesses a significant specificity owing to unique nature and properties and, therefore, possibilities of nanoobjects and nanotechnologies. This specificity presumes that nanoanalysis involves not only qualitative and quantitative determination of chemical composition but also *measures and evaluates dimensions and form or morphology of nanoobjects* as these parameters can also influence analytical signal due to size-related and quantum-sized effects. Bioobjects nanoanalysis, as a consequence, shall involve *visualization* (detection) of nano- and microscale areas, for example, separate cell parts. It may also include a *proof of drug delivery to a target organ and its subsequent transformation*, that is, *theranostics*.

Moreover, traditional procedures of common analysis in many cases can also change radically and bring new problems for both analyst and consumer. One problem is that we cannot see the nanoobject when we are sampling and analyzing it and we cannot analyze and control the chemical composition of *any* particular (0-, 1-, 2-, or

3D) NP in a nanopowder or nanocomposite material. In turn, nanoanalysis divides *chemical* analysis of nanoobjects or nanostructured objects into two variations, that is, analysis of single NPs and general analysis of the nanopowder (nanomaterial) as a whole or local analysis. In both cases, a new problem related to standards or reference materials as well as metrological aspects of chemical determination arises. Development of standards for nanomaterials and nanoobjects (NPs) is important for both cases.

Another problem specific for nanoobjects is *physical* measurement of their size and morphology as these characteristics define chemical, physical, optical, magnetic, electrochemical, and catalytic properties of such objects. The purpose of this part of the chapter is to share peculiarities of nanoanalysis with other analysts and involved researchers. It is especially important because an interesting opinion on the subject of nanoanalysis was expressed by Valcárcel scientific group [98].

### 1.6.2 Analysis of chemical composition of nanoobjects

Methods used for analysis of chemical composition of nanoobjects can be divided into two conventional groups: first group involves chemical analysis of single NP or nanopowder, while second one involves analysis of chemical composition of local nanosized areas of various surfaces and interphase boundaries (local analysis).

**Local surface and interface analysis.** Development of surface analysis methods has been stimulated by growing needs of semiconductor and electronics industry since as early as 1980s. Therefore, let us review some examples of contemporary capabilities for utilizing new variations of such methods. Methods utilized for local chemical composition analysis of surfaces and interphase boundaries can be divided into four groups based on the nature of interaction between electromagnetic emission and compound, that is, on the nature of *probe* used for analysis. Such probes include electrons, photons, ions, and force fields [182]. Each group of methods consists of dozens of different variations; however, no more than 15–20 of such methods are used in practice. These methods allow describing multiple properties of nanomaterial surfaces, such as their topology, morphology, elemental composition of primary and additional components of nanomaterial, chemical bond structure, and geometry and electron structure of the material.

One of the most rapidly evolving methods are hybrid ones, which are capable of simultaneous characterization of dimensions, shape and morphology of particles and surfaces as well as their chemical composition. With any instrument used for nanoanalysis, there is a limit to the resolution of nanoobject or local area on the surface. This is true when the instrument works directly with electromagnetic radiation such as infrared, ultraviolet or visible light, or X-rays, and also when the instrument employs high-speed subatomic particles such as electrons or ions. However, it is impossible to observe objects, which diameters are less than wavelength of incident

radiation. In general, as the wavelength becomes shorter, the required particle or wave energy increases. This stimulates scientists involved with nanoanalysis to seek ever-more-powerful machines with which to observe samples.

A fine illustration of such approach is provided in a review [183] that describes advances in theory and application of electron microscopy (EM) and scanning microanalysis, including theoretical aspects of electron beam – solid interactions, instrumentation, and methodology of particular techniques and image analysis, sample preparation, and some typical applications. Various electron–specimen interactions generate significant structural and analytical information in the form of emitted electrons and/or photons and internally produced signals such as elastically and inelastically scattered electrons, Auger electrons (AE), X-rays, and cathodoluminescence (CL), which can be analyzed in different operating modes. Inelastic interactions form the basis for all chemical analytical techniques like energy-dispersive and wavelength-dispersive X-ray spectroscopy, EELS, energy-filtering TEM (EFTEM), AE spectroscopy, and CL spectroscopy [183]. It was shown that application of multivariate curve resolution technique enhances resolution of spectral imaging by scanning TEM (STEM) and EELS or EFTEM that allows one to provide a 2D spatial distribution map of different elements speciation [171].

Recent advances in nanoanalysis of surface and edges of graphene as the most popular nanomaterial using scanning probe techniques were reviewed in [184]. It should be noted that contemporary studies have shifted from homogeneous to composite materials, from almost perfect single-crystal surfaces to surfaces with functionalized "active sites," and from thin-film materials to promising 2D materials with thickness of one or several atomic layers [185]. In this case, the most promising nanoanalytical method is surface-enhanced Raman spectroscopy (SERS) that strongly relies on optical resonance properties of some metal nanostructures, largely owing to excitation of SPR. Based on similar mechanisms, many other variations of SERS including two important ones – tip-enhanced Raman spectroscopy (TERS) and shell-isolated NP-enhanced Raman spectroscopy (SHINERS) – as well as ultraviolet SERS, near-infrared SERS, and surface-enhanced nonlinear Raman spectroscopy have been developed for a wide range of applications. The abovementioned techniques can be collectively described as plasmon-enhanced Raman spectroscopy [185]. It was shown that besides Au, Ag, and Cu, there are other plasmonic materials such as Al, Ga, In, Sn, Tl, Pb, and Bi, which can be used for ultraviolet plasmonics [186]; Al:ZnO, Ga:ZnO, and n-type semiconductors, including n-GaAs, n-InP, and n-Si, for near-infrared plasmonics; III–V or IV–IV semiconductors for mid-infrared plasmonics [187], and Sn:$In_2O_3$ and graphene for terahertz plasmonics [188].

Currently, there is no doubt that surface characterization and interfacial chemistry in *biological systems* is one of the most challenging problems of surface and interface analysis [189]. Techniques with nanoscale lateral resolution, such as standard AFM, STM, and SEM, typically provide no chemical information. At the same time,

there is no single analytical method that can do this. The analyst has to use a collection of complementary techniques of molecular analysis, each with their special advantages. Many of these techniques such as nanoscale fluorescence imaging [190], TERS [191], secondary ion mass spectrometry (SIMS) [192], and others have been described in a special issue of *Current Opinion in Chemical Biology* [189]. Near-field fluorescence spectroscopy, near-field Raman spectroscopy, and near-field laser ablation mass spectrometry are also powerful analytical methods that can be used for characterization of thin molecular films and biological samples whose lengths vary from 20 to 200 nm [193].

The AFM potentialities for detecting and visualizing separate biomolecules and emerging their surface topography with accuracy of 1 nm for width and 0.1 nm for height as well as the possibility of local activation and manipulation of such molecules directly in buffer solution has been discussed in [194]. There are examples of gas molecules [195] and picomoles of oligonucleotide detection were described [196]. According to authors of [194], an array of two or even hundreds of cantilevers conjugated with a diode array has a great potential for utilization in biological nanoanalysis. The other capabilities of TERS, for example, chemical reaction mechanisms, evaluation of components distribution, and identification and localization of specific molecular structures at the nanometer scale have been analyzed [197, 198]. Capabilities of nanobiophotonics as a new tool of biological system and cell nanoanalysis were reviewed in [119]. The potential of resonance optical antenna [199] and scanning electrochemical microscopy [200] as a nanoanalysis tool has also been evaluated.

**Chemical analysis, sizing, and size distribution of single NPs.** In 2011 the European Commission introduced new regulations on how nanomaterials should be defined [201]. According to these regulations, a more complete characterization of NPs includes not just mass and size determinations, but also determination of particle number concentrations and, of course, chemical composition of NPs.

Mass spectrometry (MS) has gained much importance in recent years as a powerful tool for reliable analytical characterization of NPs. MS can offer invaluable elemental and molecular information on the composition, structure, and chemical state of NPs and their bioconjugation to target biomolecules and can be used to quantify them. This fact is important for nano- and environmental sciences, nanobiotechnology, nanomedicine, toxicology, etc. In order to find more reliable methods of sample introduction, two different modes of NP suspension analysis via inductively coupled plasma mass spectrometry (ICP-MS) were investigated and compared – pneumatic nebulization of single particle (SP-ICP-MS) and microdroplet generation (MDG-ICP-MS) [202].

Efforts to couple effective online separation techniques with ICP-MS for evaluation of NPs mainly focused on characterizing NPs size distribution offer another growing field of nanoanalysis. In particular, detection by SP-ICP-MS coupled with a proper separation technique offers a bright future for these applications [203–206].

Determination of elemental composition can be achieved both after acidic decomposition of NPs, which concentration does not exceed 1 $\mu g\ L^{-1}$, and directly which is the case of aluminum, titanium, cerium and zinc oxides, or gold and silver NPs. It is important to note that high sensitivity of ICP-MS also allows finding micro-contaminants within NPs after their microwave-assisted acidic decomposition, for example, finding trace metals in carbon nanotubes. This ability was used by ISO to develop a standard for determination of CNT elemental impurities [207].

A novel method for separation and quantitative characterization of NPs in aqueous suspension was established by coupling thin layer chromatography (TLC) with laser ablation inductively coupled plasma mass spectrometry (LA-ICP-MS) [208]. Gold NPs (AuNPs) of various sizes were used as the model system. It was demonstrated that TLC not only allowed separation of AuNPs from ionic gold species by using acetyl acetone/butyl alcohol/triethylamine (6:3:1, v/v) as the mobile phase, but also achieved separation of differently sized gold NPs (13, 34, and 47 nm) by using phosphate buffer (0.2 M, pH = 6.8), Triton X-114 (0.4 %, w/v), and ethylenediaminetetraacetic acid (10 mM) as the mobile phase.

Another example of SP-ICP-MS coupling with separation method is online preconcentration by capillary electrophoresis (CE-SP-ICP-MS), which features 5 $\mu s$ time resolution (100 % duty cycle) to separate and quantify mixtures of silver NPs (AgNPs) as described for the first time in [209]. Field-flow fractionation (FFF) and SP-ICP-MS are even better examples of this approach [210, 211].

Three emerging techniques have been compared including hydrodynamic chromatography (HDC), asymmetric flow FFF (AF4), and SP-ICP-MS. The pretreatment procedure of centrifugation was evaluated. HDC can estimate the AgNP sizes, which were consistent with the results obtained from DLS. AF4 can also determine the size of AgNPs but with lower recoveries, which could result from interactions between AgNPs and working membrane. For SP-ICP-MS, both the particle size and concentrations can be determined with high AgNP recoveries. The particle size found by SP-ICP-MS also corresponds with the TEM observation. Therefore, HDC and SP-ICP-MS are recommended for environmental analysis of samples after their pretreatment as established in [212]. Very interesting information concerning application of surface chemical analysis for characterization of NPs (3D structures instead of above-described 2D local surface analysis) is reviewed in [213], which briefly summarizes the kind of information that can be obtained from NP analysis via Auger electron spectroscopy, X-ray photoelectron spectroscopy (XPS), time-of-flight SIMS, and low-energy ion scattering including STM and AFM.

Many other applications of ICP-MS for chemical analysis, including NPs size determination and distribution were published in reviews [214–216] and original papers [217–219] over the last 5 years. Recent publications describe methods of detection and separation of NPs in various media, for example, metal and oxide NPs in food and water [212, 220, 221], biological tissues [222], silver NPs in blood plasma [223], and cerium (IV) NPs in plants [224]. It is interesting to note that ICP-MS techniques

used for NPs detection, counting, and size determination are very expensive but also simple and available to all researchers molecular spectrophotometric methods can be applied for this purpose [225, 226].

Combination of ICP-MS with data provided by spectrophotometry, luminescent spectrometry, X-ray diffraction, or transmitting electron microscopy can be used to provide full characterization of NPs. Information about grafted ligands can be obtained by combining ICP-MS with electrospray MS and MALDI. Chemical composition of NPs can be found by using SIMS in combination with glow discharge, XPS Raman–Fourier spectroscopy, and other methods, which potentialities were described in special issues of *Analytical and Bioanalytical Chemistry* (numbers 1 and 3) [103]. In conclusion, it should be noted that analysis of chemical composition of nanoobjects is a very important and prospective field of studies as resulting knowledge can be used to create standard materials and improve reproducibility of peculiar physical effects and analytical signals. The problem of creation of standard samples of nanomaterials and development of metrological standards is still relevant as it has yet to receive much attention from scientific community [227].

### 1.6.3 Imaging of bioobjects and theranostics

Over the last decade nanoanalytical methods devoted to chemical imaging of small areas of biological tissues or single cells for medicine and biology have been a subject of intensive research dedicated to improve their spatial resolution, sensitivity, selectivity, and accuracy [228]. Nanoobjects are the most promising *multifunctional platform* for delivery, therapeutic and diagnostic applications based on contrast imaging and sensing. This leads to development of new direction in nanomedicine named theranostics that is defined as a combination of aforementioned functions in one platform. Wide variety of both liquid and solid nanoobjects are used in theranostics [229–232]: micelles, liposomes, vesicles, polymeric nanostructures, peptides, proteins, ribonucleic acid (RNA), carbon dots and nanotubes, nanodiamonds, graphene as well as the other inorganic materials such as mesoporous silica NPs, superparamagnetic iron oxides (SPIONs), quantum dots (QDs), plasmonic NPs, gold nanoclusters, and upconverting NPs. In most theranostics applications, different kinds of contrast agents are attached to functionalized NPs that may have targeting moieties for magnetic resonance, radiolabels, fluorescent, SPR or SERS imaging, different kinds of computer tomography, optical techniques, nano- and microengineered implants, etc. As mentioned above, many of these nanoscale objects have unique size- and shape-dependent optical, electronic, and magnetic properties that serve as the basis for their application in theranostics. It should be noted that control over interactions between NPs and biosystems is essential for the effective utilization of these materials in biology and medicine.

There is much work to be done in all areas of nanomedicine and theranostics where the help of analytical chemist is required. Optical imaging involves inexpensive

and highly sensitive absorption, luminescence (bioluminescence), and scattering-based spectroscopic methods that use UV, IR, and visible light [231]. Fluorescence provides analytical signal for analytes with concentration of $10^{-9}$–$10^{-12}$ M and bioluminescent probes can push detection limit down to $10^{-15}$–$10^{-18}$ M. Core/shell functionalized quantum dots or rare earth element complexes are often used as luminescent probes that have great potential in the form of multiplexing or fluorescence resonance energy transfer imaging mode [230, 233].

Gold NPs possess many advantageous features for their utilization as a delivery platform such as stability, easy modification, and biocompatibility. Their imaging properties are based on SPR that can be used in photoacoustics, photothermal ablation, or SERS effect [234, 235]. The main disadvantage of this approach is that gold is expensive. Carbon nanotubes, modified silica NPs [236, 237], are also used in theranostics as well as iron oxides, especially biocompatible and inexpensive magnetite NPs (MNPs). The superparamagnetism of MNPs allows them to be used as magnetic resonance imaging (MRI) contrast agents [238, 239]. External magnetic field can be used for tissue targeting and drug delivery.

Different directions in future theranostics that can revolutionize personalized medicine are discussed in [231]. Nanomedicine and theranostics as a subtype of nanoanalytics lie within interdisciplinary field. Therefore, success in nanoanalytics that combine efforts of biologists, physicists, engineers, and medics can serve as one of foundations for theranostics development.

### 1.6.4 Nanometrology in nanoanalytics

One of the greatest problems in nanomaterials science is determining the best way to characterize increasing number of complex nanostructures and nanoobjects developed by chemists, physicists, and material scientists [240]. Without generally accepted methods of characterization, both reproducibility and quality control are rendered impossible, and application of such irreproducible materials will be a complicated problem. One reason for this situation is that nanoscale materials are often fabricated or synthesized in different ways and by different specialists (chemists, biologists, physicists, or material engineers) that use different processes and methods (different top-down, down-top or e.g. bacteria-based approach).

Nanomaterials may have different dimensions, size distribution, composition, and structural hierarchies; they may be amorphous, composite (mixed or core/shell), or polycrystalline. Another problem is that nanoscale materials may be formed as thin films, dry powders, or solution-dispersed materials. The products of nanotechnology besides nanomaterials include bionanosystems, nanosystems for target drug delivery, procedures for chemical composition analysis, electronic devices, sensors, etc. Common characterization methods are neither obvious nor applicable to all different classes of nanomaterials [240]. It is important to recognize that there is great

difference in metrological requirements associated with transition from micro- to nanoscale [241]. For example, interferometry using visible light with a wavelength of a few hundred nanometers is ideal for examining microstructures but cannot be applied when dimensions are two or three orders smaller. Moreover, in comparison of measurement results, consideration should be given to the nanoobjects composition change with time, handling, and environmental conditions [242]. Therefore, the time between analysis and application is important and some types of consistency or verification process can also be important. A record of sample provenance information for a set of particles can play a useful role in identifying some of the sources and decreasing the extent of particle variability and the lack of reproducibility observed by many researchers.

It is obvious that due to wide variety of nanomaterials, one single characterization method is not applicable for all cases. On the contrary, characterization of certain properties can be reliably provided using similar methodologies. For example, structural properties of nanomaterials can be characterized by TEM, SEM, STM, AFM, XRD, ICP-MS, elemental analysis, etc. as standard techniques. It is often typical that for one nanoobject there is not only one "size," but different methods will produce different "types" of sizes [243]. Standardization of nanotechnology has been accelerated not only to promote industrial application of nanotechnology but also to bring about social acceptance of nanotechnology [240, 241, 244].

Therefore, a pressing need for nanomaterial science community is to consolidate and agree on the methods of characterization and minimal levels of nanomaterials analytical data. As a result, many national, European, and international organizations have been developing standards associated with synthesis, studies, and application of nanomaterials. Established specific committees on nanotechnology have also been developing regulations on protection of human health and environment from production and application of chemicals and consumer products that use nanomaterials. For this reason, in 2004 ISO picked up the challenge of making standards in nanotechnology field and initiated a technical committee (TC) on nanotechnologies (TC 229), which was established in May 2005 [245, 246]. One year later, TC 229 implemented a collaboration with IEC TC 113 (Nanotechnology Standardization for Electrical and Electronic Products and Systems) in the form of Joint Working Groups (JWG) JWG1 and JWG2. Both committees actively cooperate with each other and similar national organizations. By now, 37 countries participate in TC 229 activities and 14 countries have the observer status; their joint efforts resulted in developed by now 57 published standards and 37 standards under development [245].

Furthermore, in 2005–2006, several major standards development organizations also established technical committees (TCs) focused on nanotechnology: European Committee on Standardization CEN TC 352, American Society for Testing and Materials (ASTM) International E56, American National Standards Institute (ANSI), Organization for Economic Cooperation and Development (OECD) with Working party on Manufactured Nanomaterials (WPNM) as well as such Committees in Germany, Great

Britain, Japan, Russia, China, and many other countries. The combined efforts of these Committees have produced a large body of standards concerning terminology; physicochemical and biological measurements; and the environmental, health, and safety of nanomaterials and nanotechnologies. However, as CEN and ISO collaborate on nanotechnology standardization and ISO has the lead in most working groups, ISO has been the focus here [247]. The Working Groups and Task groups that form the basis for ISO/TC 229 are outlined in Tab. 1.2.

**Tab. 1.2:** The structure of ISO TC 229 Nanotechnologies [245]

| Type of group | Title |
|---|---|
| ISO/TC 229/CAG | Chairman Advisory Group |
| ISO/TC 229/JWG 1 | Terminology and nomenclature<br>28 participants from 17 countries |
| ISO/TC 229/JWG 2 | Measurement and characterization |
| ISO/TC 229/TG 2 | Consumer and societal dimensions of nanotechnologies |
| ISO/TC 229/TG 3 | Nanotechnologies and sustainability |
| ISO/TC 229/WG 3 | Health, safety, and environmental aspects of nanotechnologies |
| ISO/TC 229/WG 4 | Material specifications |
| ISO/TC 229/WG 5 | Products and applications |

A first step in standard development is review of project application sent by a national organization or ISO members by a majority of committee members. In the case of a positive review, the authors of application are given 6 months to prepare a draft of project, which is then reviewed by Committee for 12 months; during this time all its members and observers provide their commentaries, and the draft has to be approved by 2/3 of its members. During the next year, the ISO standard has to be approved by 2/3 of ISO constituent members, 9 more months is required to approve the project, and 3 months is needed to publish it. Thus, the whole procedure takes 3 years and the standard is reviewed every 5 years.

The primary goal of created TC 229 is promotion of standardization of nanotechnologies, scientific research and industrial production of nanomaterials and nanosystems. Their priorities include the following tasks: development of terms and definitions; development of metrology guidelines and new testing and measuring methods; development of standard nanomaterial samples to measure size, composition, structure, and properties; process modeling; developing health and safety regulations and establishing environmental impact. Each of these tasks is accomplished by corresponding work groups supervised by separate countries [241, 244, 247]. In addition to development of official methods, several groups of scientists also develop alternative, usually rather simple methods of NP characterization [213, 225–227, 248–250] as well as standard materials [251].

However, regardless of the concept presented above, nanoanalytics consist of several very different sections; thus, metrological problems characteristics for these

sections and their complexity also differ. It should be noted that in the case of liquid nanoobjects that form nanoheterogenous organized media used in chemical analysis, metrological approaches shall be the same as those used for ordinary homogenous solutions. In this case, nanoobjects only serve as nanoreactors that change the medium in microenvironment of analyte, while analytical signal is measured in normal macroscopic conditions. Reproducibility of dimensions of such nanoreactors that form spontaneously in the solution with a constant (maintained) surfactant concentration lies within the limits of error of corresponding method of analysis and does not significantly influence reproducibility of analytical signal and results of analysis. In some cases, metrological characteristics can even improve due to solubilization of analytical reagents in micelles leading to decrease of their aggregation, that is, dispersion into single molecules.

Much more complex problems arise from using solid nanomaterials for analysis, as their size and especially surface modification greatly depend on synthesis conditions, handling, and storage conditions and do not have required reproducibility. This is caused by different experimental conditions in this field of studies as well as ongoing process determining stabilization and protection conditions of NP aggregations as well as time and thermal instability of their nanosized state caused by high surface energy. Almost all approaches to increasing stability of solid NPs in solutions are based on charging their surface by adsorbing organic ions with low or high molecular weight, for example, surfactants or polymer polyelectrolytes; however, this problem is not completely solved yet. Another problem related to this one is the necessity of standardization of such materials both in their size and homogeneity of chemical composition; this problem does not have a fast and simple solution.

The most complex problems are related to nanoobjects geometry measurement as it requires developing theory, methods, and tools for measuring nanoscale parameters of such objects as well as creation of corresponding standard instruments, standard samples for comparison and finding correlation between these standards and macroscopic ones. If we can find a general solution to all of these problems, we can form a basis for uniformity of measurements and observe an increase in their quality for nanometrology purposes.

## 1.7 Conclusions

The last decade of twentieth century and the beginning of twenty-first century have witnessed a new paradigm in the scientific community. This paradigm is based on the unique properties of nanosized samples of different substances and combines the previously disembodied data observed by physicists, chemists, biologists, and material scientists. It also was brought about by an advent of new instrumental methods

such as STM, AFM, SEM, TEM, and several other methods, the potential of which helped to form a new interdisciplinary research field – nanoscience – and its practical implementation – nanotechnology. The response of scientific community to emergent nanoscience and nanotechnologies is very diverse. Some consider these concepts a "novel," revolutionary trend; other researchers believe that nanoscience is not yet a scientific discipline on its own because it is not yet evident that the Laws of Nature are particularly special between 1 and 100 nm. Nevertheless, nanoscience and nanotechnologies, in particular, became a sort of icon for the idea of "breakthrough to the future."

Significant advances in the application of nanomaterials and nanotechnologies for chemical analysis were made by different research groups of physicists, chemists, biologists, and material scientists and never considered to be within the frames of a single research field that can be denoted as "Nanoanalytics." Therefore, professional analytical chemists, at first, did not pay attention to nanoobjects and nanotechnologies as aforementioned scientists did. However, analytical chemistry is an interdisciplinary science, so that it could not ignore an appearance of new possibilities and phenomena that put at disposal nanoscience and nanotechnology. Scientometric analysis shows that "nanoanalytics" is still rarely used and has no certain definition even among scientists specializing in analytical chemistry. The absence of consensus among various specialists involved in chemical analysis on opinion regarding the term of "nanoanalytics" can be eliminated if the concept of nanoanalytics after discussion becomes generally accepted. Such concept bringing to analysts shall not only unite the abovementioned views on this new area of analytical chemistry but also enlarge the wide world of nanoscale objects and nanotechnological data used in chemical analysis, that is, to extend the nanoanalytics scope of application.

In this chapter, an attempt at brief description of the concepts and primary topics of nanoanalytics, nanoobjects, nanotechnologies, their current definitions, as well as certain metrological aspects of its constituent parts were performed. With this objective, the author intends to provide a certain narrative logic and systemize all primary fields of nanoanalytics development without merely listing the most interesting experimental facts. At the same time, the proposed classification is supported by exciting general and specific examples of analytical techniques that are already practiced by scientists worldwide. It is important to mark the goalposts for nanoanalytics development and establish its place in contemporary analytical chemistry. Also in author's opinion, it is necessary to account for discrepancies between the specialists on the role of nanoscience and nanotechnology in analytical chemistry, as some believe in limitless possibilities and revolutionary nature of nanotechnologies.

**Acknowledgments:** The work was supported by Russian Foundation for Basic Research (grant No. 15-03-99704).

## References


[1] Nanoscience and nanotechnologies. In: Awadelkarim OO, Bai Ch, Kapitsa SP., ed. *Encyclopedia of Life Support Systems (EOLSS), UNESCO*. Moscow, Magister-Press Publishing House, 2009. 991 pp. (Translation into Russian) http://www.eolss.net/outlinecomponents/nanoscience-and-nanotechnologies.aspx

[2] Varadan VK, Pillai AS, Mukherji D, Dwivedi M, Chen L. *Nanoscience and Nanotechnology in Engineering*. Singapore, World Scientific Publishing Co. Pte. Ltd, 2010.

[3] Schaefer H-E. *Nanoscience*. Heidelberg, Springer-Verlag, 2010.

[4] Whitesides GM. Nanoscience, nanotechnology, and chemistry. *Small* 2005, 1, 172–9.

[5] Mulvaney P, Weiss PS. Have nanoscience and nanotechnology delivered? *ACS Nano* 2016, 10, 7225–6.

[6] Kagan CR, Fernandez LE, Gogotsi Y, Hammond PT, Hersam MC, Nel AE, et al. Nano day: Celebrating the next decade of nanoscience and nanotechnology. *ACS Nano* 2016, 10, 9093–103.

[7] Chidsey CED. Nanoscience: The role of "Making" new forms of matter. Proc. France/Stanford Meeting, Avignon, 12/2006. stanford.edu/dept/france-stanford/Conferences/.../Chidsey.pdf

[8] Алфимов МВ, Гохберг ЛМ, Фурсов КС. Нанотехнологии: определения и классификация. Рос. *нанотехнол*. 2010, 5(no.7–8), 8–15. (Alfimov MV, Gokhberg LM, Fursov KS. Nanotechnologies: Definitions and classification. Nanotechnol in Russia 2010, 5, 8–15.) Original source in Russian.

[9] Schaming D, Remita H. Nanotechnology: From the ancient time to nowadays. *Found Chem Springer Science + Business Media Dordrecht* 2015.

[10] Colomban P. The use of metal nanoparticles to produce yellow, red and iridescent colour, from Bronze Age to present times in lustre pottery and glass: Solid state chemistry, spectroscopy and nanostructure. *J Nano Res* 2009, 8, 109–32.

[11] Johnson-McDaniel D, Barrett CA, Sharafi A, Salguero TT. Nanoscience of an ancient pigment. *JACS* 2013, 135, 1677–9.

[12] Berke H. The invention of blue and purple pigments in ancient times. *Chem Soc Rev* 2007, 36, 15–30.

[13] Psaro R, Guidotti M, Sgobba M. Nanosystems. In: Bertini I, ed. *Inorganic and Bioorganic Chemistry, Encyclopedia of Life Support Systems* (EOLSS), e-book, UNESCO, EOLSS Publishers, Oxford, UK, 2006. http://www.eolss.net/ebooks/.../C06/E6-100-14-00.pdf

[14] *J Nano Res* 2009, 8, 1–157.

[15] Reibold M, Paufler P, Levin AA, Kochmann W, Pätzke N, Meyer DC. Carbon nanotubes in an ancient Damascus sabre. *Nature* 2006, 444, 286.

[16] Belloni J. The role of silver clusters in photography. *C R Phys* 2002, 3, 381–390.

[17] Jirgensons B, Straumanis ME. *A Short Textbook of Colloid Chemistry,* 2nd Ed. Pergamon Press Ltd, 1962.

[18] Faraday M. Experimental relations of gold (and other metals) to light. *Philos Trans R. Soc Lond* 1857, 147, 145–81.

[19] Mie G. Beiträge zur Optik trüber Medien, speziell kolloidaler Metallösungen. *Annalen der Physik* 1908, 330(3), 377–445.

[20] Hergert W, Wriedt T. eds. *The Mie Theory. Springer Series in Optical Sciences*. Berlin, Heidelberg, Springer-Verlag, 2012.

[21] Graham T. Liquid diffusion applied to analysis. *Phil Trans Rog Soc London, Ser A* 1861, 151, 183–224. On the properties of silicic acid and other analogous colloidal substances. *J Chem Soc* 1864, 17, 318–27.

[22] Khamraev MS. From the history of development of classic colloid chemistry. *Austrian J Techn Natur Sci* 2016, 3–4, 153–8.

[23] Киреев В. Нанотехнологии: история возникновения и развития. *Наноиндустрия* 2008, 2, 2–5. (Kireev V. Nanotechnology: a history of beginnings and development. Nanoindustry 2008, 2, 2–5). Original source in Russian.
[24] Shchukin ED, Pertsov AV, Amelina EA, Zelenev AS. *Colloid and Surface Chemistry*. Amsterdam, Elsevier Science BV, 2001.
[25] Feynman RP. There's plenty of room at the bottom. *Eng Sci* 1960, 23(5), 22–36.
[26] Taniguchi N. On the basic concept of ''nano-technology''. In: Proceedings of Intern. Conf. on Production Engineering. Tokyo, Part II, Jap Soc Precision Eng,1974.
[27] Binnig G, Rohrer H. "Scanning tunneling microscopy" IBM. *J Res Develop* 1986, 30(4), 355–69.
[28] Drexler KE. *Engines of Creation. The Coming Era of Nanotechnology*. N.Y., Anchor books Double Day, 1986.
[29] Kroto HW, Heath JR, O'Brien SC, Curl RF, Smalley RE. $C_{60}$: Buckminsterfullerene. *Nature* 1985, 318, 162–3.
[30] Iijima S. Helical microtubules of graphitic carbon. *Nature* 1991, 354, 56–8.
[31] Tans SJ, Verschueren ARM. Dekker C. Room-temperature transistor based on a single carbon nanotube. *Nature* 1998, 393, 49–52.
[32] Novoselov KS, Geim AK, Morozov S, Jiang D, Zhang Y, Dubonos SV, Grigorieva IV, Firsov AA. Electric Field Effect in Atomically Thin Carbon Films. Science 2004, 306, 666–9.
[33] Schedini F, Geim AK, Morozov SV, Hill EW, Blake P, Katsnelson MI, et al. Detection of individual gas molecules adsorbed on graphene. *Nature Mater*. 2007, 6, 652–5.
[34] Elghanian R, Storhoff JJ, Mucic RC, Letsinger RL, Mirkin CA. Selective colorimetric detection of polynucleotides based on the distance-dependent optical properties of gold nanoparticles. *Science* 1997, 277(5329), 1078–81.
[35] Bruchez JrM, Moronne M, Gin P, Weiss S, Alivisatos AP. Semiconductor nanocrystals as fluorescent biological labels. *Science* 1998, 281, 2013–6.
[36] Chan WCW, Nie S. Quantum dot bioconjugates for ultrasensitive nonisotopic detection. *Science* 1998, 281, 2016–8.
[37] Proc. 10th Anal. Russian-German-Ukrainian Symp. (ARGUS'2007-Nanoanalytics). Shtykov S.N. ed. Saratov, Nauchnaya Kniga, 2007.
[38] Нанотехнологии, метрология, стандартизация и сертификация в терминах и определениях / Под ред. М.В. Ковальчука, П.А. Тодуа. М.: *Техносфера*, 2009. Nanotechnologies, metrology, standardization and certification in terms and definitions. Ed. by MV. Kovalchuk and PA. Todua, Moscow, Technosphera, 2009. Original source in Russian.
[39] Словарь нанотехнологических и связанных с нанотехнологиями терминов / Под ред. С.В. Калюжного. М.: ФИЗМАТЛИТ, 2010. 528 с. Vocabulary of nanotechnological and related with nanotechnology terms. Kalyuzhny SV. ed. Moscow, Fizmatlit, 2010. Original source in Russian
[40] http://www.nanodic.com
[41] http://www.nanoanalytics.com; http://mathur.uni-koeln.de/905.html
[42] Valcarcel M, Simonet BM, Cardenas S. Analytical nanoscience and nanotechnology today and tomorrow. *Anal Bioanal Chem* 2008, 391, 1881–87.
[43] Fuchs. H. Nanoanalytics – probing matter at the atomic scale. *Abstr. Euroanalysis XV*. Innsbruck, Austria. 6–10 September 2009. P. 3.
[44] Shtykov SN, Rusanova TYu. Nanomaterials and nanotechnologies in chemical and biochemical sensors: capabilities and applications. *Rus J General Chem* 2008, 78(12), 2521–31.
[45] Zolotov YA. Nanoanalytics. *J Anal Chem* 2010, 65, 1207–08.
[46] Budnikov HC, Shirokova VI. Term "Nano" in electroanalysis: a trendy prefix or a new stage of its development? *J Anal Chem* 2013, 68, 663–70.
[47] Shtykov SN. About conception of nanoanalytics. Abstr. XIX Mendeleev Congress on General and Applied Chemistry. *Volgograd* 2011, 4, 301. Original source in Russian http://sci.isuct.ru/images/stories/conf/mendeleev2011/abstracts_4_ru.pdf.

[48] Shtykov SN. Nanoanalytics: a concept, elements and peculiarities. *Euroanalysis XVII: Book of Abstr*. 25–29 August 2013. Warsaw, Poland. S-4-O4 Abstr. ID 0143. P. 102.
[49] Штыков СН. Современное состояние и перспективы наноаналитики Второй съезд аналитиков России: Тез. докл. 23–27 сент. 2013. Москва, 2013, 177. Shtykov SN. Current status and prospects of nanoanalytics. Abstr. Second Congress of Russian Analysts. Moscow, 2013, 177. Original source in Russian http://www.wssanalytchem.org/car2013/doc/Abstracts-CRusAn2013.pdf.
[50] Shtykov SN. Nanoanalytics: concept and metrology problems. *Vestnik Lobachevsky State Univ of Nizhni Novgorod* 2013, 5, 55–60. Original source in Russian.
[51] Shtykov S. Nanoanalytics – a reply of analytical chemistry to the era of nanotechnology. *Anal Bioanal Tech* 2014, 5(4), 35.
[52] Möhwald H, Weiss PS. Is nano a bubble? *ACS Nano* 2015, 9, 9427–8.
[53] Joachim C. To be nano or not to be nano? *Nature Mater* 2005, 4, 107–9.
[54] Weiss PS. What can nano do? *ACS Nano* 2013, 7, 9507–8.
[55] Weiss PS. Where are the products of nanotechnology? *ACS Nano* 2015, 9, 3397–8.
[56] Mulvaney P, Weiss PS. Have nanoscience and nanotechnology delivered? *ACS Nano* 2016, 10, 7225–6.
[57] Rusanov AI. Striking world of nanostructures. *Rus J Gen Chem* 2002, 72, 495–511.
[58] Rusanov AI. Surface thermodynamics revisited. *Surf Sci Rep* 2005, 58, 111–239.
[59] Русанов АИ. Нанотермодинамика – химический подход. *Рос хим журн*. 2006, 50(2), 145–51. Rusanov AI. Nanothermodynamics – a chemical approach. Rus Khim J 2006, 50(2), 145–51. Original source in Russian.
[60] Shtykov SN. Surfactants in analysis: progress and development trends. *J Anal Chem* 2000, 55, 608–614.
[61] Shtykov SN. Chemical analysis in nanoreactors: main concepts and applications. *J Anal Chem* 2002, 57, 859–868.
[62] Штыков СН. *Природа*. 2009, 7, 12–20. Shtykov SN. Organized media – a world of liquid nanosystems. Priroda (Nature) 2009, 7, 12–20. Original source in Russian.
[63] Lehn J-M. *Supramolecular Chemistry: Concepts and Perspectives*. Weinheim, Wiley-VCH Verlag GmbH, 1995.
[64] Steed JW, Atwood JL. *Supramolecular Chemistry*. Chichester, John Wiley & Sons, Ltd., 2003.
[65] Reichardt Ch. *Solvents and Solvent Effects in Organic Chemistry*. Weinheim, Wiley-VCH Verlag GmbH, 2003.
[66] Reichardt Ch. Pyridinium-N-phenolate betaine dyes as empirical indicators of solvent polarity: some new findings. *Pure Appl Chem* 2008, 80, 1415–32.
[67] Behera GB, Mishra BK, Behera PK, Panda M. Fluorescent probes for structural and distance effect studies in micelles, reversed micelles and microemulsions. *Adv Colloid Interface Sci* 1999, 82, 1–42.
[68] Savvin SB, Chernova RK, Shtykov SN. *Surface-Active Substances – Analytical Reagents*. Moscow, Nauka (Science), 1991. Original source in Russian.
[69] Shtykov SN. Concept and elements of nanoanalytics. In: Shtykov SN, ed. *Nanoobjects and Nanotechnologies in the Chemical Analysis*. Moscow, Nauka (Science), 2015, 11–41. Original source in Russian.
[70] Pramauro E, Pelizzetti E. *Surfactants in Analytical Chemistry. Application of Organized Amphiphilic Media*. Amsterdam, Elsevier, 1996.
[71] McIntire GL. Micelles in analytical chemistry. *Crit Rev Anal Chem* 1990, 21, 257–78.
[72] Savvin SB, Shtykov SN, Mikhailova AV. Organic reagents in spectrophotometric methods of analysis. *Russ Chem Rev* 2006, 75, 380–9.
[73] Pramauro E, Prevot AB. Solubilization in micellar systems. Analytical and environmental applications. *Pure Appl Chem* 1995, 67, 551–9.

[74] Memon N, Balouch A, Hinze WL. Fluorescence in organized assemblies. In: *Encyclopedia of Analytical Chemistry*. Meyers RA, ed. New York, John Wiley & Sons, Ltd., 2008, 10364–447.
[75] Rodriguez JJS, Halko R, Rodriguez JRB, Aaron JJ. Environmental analysis based on luminescence in organized supramolecular systems. *Anal Bioanal Chem* 2006, 385, 525–45.
[76] Alarfaj NA, El-Tohamy MF. Applications of micelle enhancement in luminescence-based analysis. *Luminescence* 2015, 30, 3–11.
[77] Shtykov SN, Goryacheva IYu. Luminescent analytical spectroscopy in microheterogeneous supra- and supermolecular self-assembled organized media. *Optics Spectrosc* 1997, 83, 645–50.
[78] Goryacheva I, Shtykov S, Melnikov G, Fedorenko E. Analysis of polycyclic aromatic hydrocarbons by sensitized room temperature phosphorescence. *Environ Chem Lett* 2003, 1, 82–5.
[79] Melnikov G, Shtykov S, Goryacheva I. Sensitized room temperature phosphorescence of pyrene in sodium dodecylsulphate micelles with triphaflavine as energy donor. *Anal Chim Acta* 2001, 439, 81–6.
[80] Kuijt J, Ariese F, Brinkman UATh. Gooijer C Room temperature phosphorescence in the liquid state as a tool in analytical chemistry. *Anal Chim Acta* 2003, 488, 135–71.
[81] Smirnova TD, Shtykov SN, Zhelobitskaya EA, Safarova MI. Determination of flunixin by sensitized terbium fluorescence in the presence of surfactant micelles. *J Anal Chem* 2017, 72, 562–6.
[82] Shtykov SN, Smirnova TD, Molchanova YuV. Synergistic effects in the europium(III)–thenoyltrifluoroacetone–1,10-phenanthroline system in micelles of block copolymers of nonionic surfactants and their analytical applications. *J Anal Chem* 2001, 56, 920–4.
[83] Lis S, Elbanowski M, Makowska B, Hnatejko Z. Energy transfer in solution of lanthanide complex. *J Photochem Photobiol A Chem* 2002, 150, 233–47.
[84] Lin J-M, Yamada M. Microheterogeneous systems of micelles and microemulsions as reaction media in chemiluminescent analysis. *Trends Anal Chem* 2003, 22, 99–107.
[85] Goryacheva IYu, Shtykov SN, Loginov AS, Panteleeva IV. Preconcentration and fluorimetric determination of polycyclic aromatic hydrocarbons based on the acid-induced cloud-point extraction with sodium dodecylsulphate. *Anal Bioanal Chem* 2005, 382, 1413–8.
[86] Ojeda CB, Rojas FS. Separation and preconcentration by a cloud point extraction procedure for determination of metals: an overview *Anal Bioanal Chem* 2009, 394, 759–82.
[87] Ferrera ZS, Sanz CP, Santana CM, Rodriguez JJS. Use of micellar systems in extraction and preconcentration of organic pollutants in environmental samples. *Trends Anal Chem* 2004, 22, 469–79.
[88] Berthod A, García-Álvarez-Coque C. *Micellar Liquid Chromatography*. NY, USA, CRC Press, 2000.
[89] Ruiz-Ángel MJ, García-Álvarez-Coque MC, Berthod A. New insights and recent developments in micellar liquid chromatography. *Separ Purif Rev* 2009, 38, 45–96.
[90] Sumina EG, Shtykov SN, Tyurina NV. Surfactants in thin-layer chromatography. *J Anal Chem* 2003, 58, 720–30.
[91] Khaledi MG. Micelles as separation media in high-performance liquid chromatography and high-performance capillary electrophoresis: overview and perspective *J Chromatogr A* 1997, 780, 3–40.
[92] Basova EM, Ivanov VM, Shpigun OA. Micellar liquid chromatography. *Rus Chem Rev* 1999, 68, 983–1000.
[93] Tiwari JN, Tiwari RN, Kim KS. Zero-dimensional, one-dimensional, two-dimensional and three-dimensional nanostructured materials for advanced electrochemical energy devices. *Progr Mater Sci* 2012, 57, 724–803.
[94] Schmid G. *Nanoparticles. From Theory to Application*. 2nd Ed. Weinheim, WILEY-VCH Verlag GmbH & Co. KGaA, 2010.

[95] Pokropivny V, Lohmus R, Hussainova I, Pokropivny A, Vlassov S. *Introduction in Nanomaterials and Nanotechnology*. Tartu, Tartu University Press, 2007.
[96] Ozin GA, Arsenault AC. *Nanochemistry: A Chemical Approach to Nanomaterials*. Cambridge, RSC Publ, 2005.
[97] http://www.nanodic.com/Nanotechnology
[98] López-Lorente AI, Valcárcel M. The third way in analytical nanoscience and nanotechnology: involvement of nanotools and nanoanalytes in the same analytical process. *Trends Anal Chem* 2016, 75, 1–9.
[99] Gleiter H. Nanostructured materials: basic concepts and microstructure. *Acta Mater* 2000, 48, 1–29.
[100] Ivanovskii AL. Graphene-based and graphene-like materials. *Rus Chem Rev* 2012, 81, 571–605.
[101] Елисеев АА, Лукашин АВ. *Функциональные наноматериалы* М, ФИЗМАТЛИТ, 2010. Eliseev AA, Lukashin AV. *Functional Nanomaterials*. Moscow, FIZMATLIT, 2010. Original source in Russian.
[102] Головин ЮИ, Наномир без формул М. *БИНОМ. Лаборатория знаний*, 2012. Golovin YuI. Nanoworld Without Formulas. Moscow, BINOM. Laboratory of Knowledge, 2012. Original source in Russian.
[103] *Anal Bioanal Chem* 2010, 396, Nos. 1, 3.
[104] *Anal Bioanal Chem* 2011, 399, 1–147.
[105] Valentini F, Palleschi G. Nanomaterials and analytical chemistry. *Anal Lett* 2008, 41, 479–520.
[106] Zamborini FP, Bao L, Dasari R. Nanoparticles in measurement science. *Anal Chem* 2012, 84, 541–76.
[107] He L, Toh Ch-S. Recent advances in analytical chemistry – a material approach. *Anal Chim Acta* 2006, 556, 1–15.
[108] Chaudhuri RG, Paria S. Core/Shell nanoparticles: classes, properties, synthesis mechanisms, characterization, and applications. *Chem Rev* 2012, 112, 2373–2433.
[109] Lucena R, Simonet BM, Cardenas S, Valcarcel M. Potential of nanoparticles in sample preparation. *J Chromatogr A* 2011, 1218, 620–37.
[110] Pyrzynska K. Use of nanomaterials in sample preparation. *Trends Anal Chem* 2013, 43, 100–8.
[111] Guihen E, Glennon JD. Nanoparticles in separation science – recent developments. *Anal Lett* 2003, 36, 3309–36.
[112] Nesterenko EP, Nesterenko PN, Connolly D, He X, Floris P, Duff E, et al. Nano-particle modified stationary phases for high-performance liquid chromatography. *Analyst* 2013, 138, 4229–54.
[113] Kaur A, Gupta U. A review on applications of nanoparticles for the preconcentration of environmental pollutants. *J Mater Chem* 2009, 19, 8279–89.
[114] Pyrzynska K. Nanomaterials in extraction techniques. In: Hussain ChM, Kharisov B. eds. *Adv Environ Anal: Appl Nanomater,* Vol. 1 RSC 2017, 284–305.
[115] Дыкман ЛА, Богатырев ВА, Щёголев СЮ, Хлебцов НГ. Золотые наночастицы: синтез, свойства, биомедицинское применение. М: Наука, 2008. Dykman LA, Bogatyrev VA, Schogolev SYu, Khlebtsov NG. *Gold Nanoparticles: Synthesis, Properties, Biomedical Application*. Moscow, Nauka (Science), 2008. Original source in Russian.
[116] Khlebtsov NG, Bogatyrev VA, Dykman LA, Khlebtsov B, Staroverov S, Shirokov A, et al. Analytical and theranostic applications of gold nanoparticles and multifunctional nanocomposites. *Theranostics* 2013, 3, 167–80.
[117] Panfilova E, Shirokov A, Khlebtsov B, Matora L, Khlebtsov N. Multiplexed dot immunoassay using Ag nanocubes, Au/Ag alloy nanoparticles, and Au/Ag nanoboxes. *Nano Res* 2012, 5, 124–34.
[118] Saha K, Agasti SS, Kim Ch, Li X, Rotello VM. Gold nanoparticles in chemical and biological sensing. *Chem Rev* 2012, 112, 2739–79.

[119] Huser T. Nano-Biophotonics: new tools for chemical nano-analytics. *Curr Opin Chem Biol* 2008, 12, 497–504.
[120] Petryaeva E, Krull UJ. Localized surface plasmon resonance: nanostructures, bioassays and biosensing – a review. *Anal Chim Acta* 2011, 706, 8–24.
[121] Fan M, Andrade GFS, Brolo AG. A review on the fabrication of substrates for surface enhanced Raman spectroscopy and their applications in analytical chemistry. *Anal Chim Acta* 2011, 693, 7–25.
[122] Frigerio C, Ribeiro DSM, Rodrigues SSM, Abreu VLRG, Barbosa JAC. Prior JAV, et al. Application of quantum dots as analytical tools in automated chemical analysis: a review. *Anal Chim Acta* 2012, 735, 9–22.
[123] Algar WR, Susumu K, Delehanty JB, Medintz IL. Semiconductor quantum dots in bioanalysis: crossing the valley of death. *Anal Chem* 2011, 83, 8826–37.
[124] Costa-Fernandez JM, Pereiro R, Sanz-Medel A. The use of luminescent quantum dots for optical sensing. *Trends Anal Chem* 2006, 25, 207–18.
[125] Lim SY, Wei Shen W, Zhiqiang Gao Z. Carbon quantum dots and their applications. *Chem Soc Rev* 2015, 44, 362–81.
[126] Wang H, Gao P, Wang Y, Guo J, Zhang K-Q, Du D, et al. Fluorescently tuned nitrogen-doped carbon dots from carbon source with different content of carboxyl groups. *APL Mater* 2015, 3, 086102.
[127] Riu J, Maroto A, Rius FX. Nanosensors in environmental analysis. *Talanta* 2006, 69, 288–301.
[128] Valdes MG, Valdes Gonzalez AC, Calzon JAG, Diaz-Garcia ME. Analytical nanotechnology for food analysis. *Microchim Acta* 2009, 166, 1–19.
[129] Jain KK. Applications of nanobiotechnology in clinical diagnostics. *Clin Chem* 2007, 53, 2002–9.
[130] Chamorro-Garcia A, Merkoçi A. Nanobiosensors in diagnostics. *Nanobiomed* 2016, 3, 1–26.
[131] Gómez-Hens A, Fernández-Romero JM, Aguilar-Caballos MP. Nanostructures as analytical tools in bioassays. *Trends Anal Chem* 2008, 27, 394–406.
[132] Chen J, Andler SM, Goddard JM, Nugen SR, Rotello VM. Integrating recognition elements with nanomaterials for bacteria sensing. *Chem Soc Rev* 2017, 46, 1272–83.
[133] Smith BR, Gambhir SS. Nanomaterials for in vivo imaging. *Chem Rev* 2017, 117, 901–86.
[134] Senesac L, Thundat TG. Nanosensors for trace explosive detection. *Mater Today* 2008, 11, 28–36.
[135] Vo-Dinh T. Nanosensing at the single cell level. *Spectrochim Acta Pt B* 2008, 63, 95–103.
[136] Vo-Dinh T, Zhang Y. Single-cell monitoring using fiberoptic nanosensors. *Rev Nanomed Nanobiotechnol* 2011, 3, 79–85.
[137] Shi J, Zhu Y, Zhang X, Baeyens WRG, Garcia-Campaña AM. Recent developments in nanomaterial optical sensors. *Trends Anal Chem* 2004, 23, 351–60.
[138] Guo Sh, Dong Sh. Biomolecule-nanoparticle hybrids for electrochemical biosensors. *Trends Anal Chem* 2009, 28, 96–109.
[139] Van Staden R-IS, van Staden JF, Balasoiu S-C, Vasile O-R. Micro- and nanosensors, recent developments and features: a minireview. *Anal Lett* 2010, 43, 1111–8.
[140] Morales-Narvaez E, Golmohammadi H, Naghdi T, Yousefi H, Kostiv U, Horák D, et al. Nanopaper as an optical sensing platform. *ACS Nano* 2015, 28, 7296–305.
[141] Scida K, Stege PW, Haby G, Messina GA, García CD. Recent applications of carbon-based nanomaterials in analytical chemistry: critical review. *Anal Chim Acta* 2011, 691, 6–17.
[142] Pumera M, Sánchez S,Ichinose I, Tang J. Electrochemical nanobiosensors. *Sens Actuat B* 2007, 123 1195–1205.
[143] Welch CM. Compton RG. The use of nanoparticles in electroanalysis: a review. *Anal Bioanal Chem* 2006, 384, 601–19.
[144] Oyama M. Recent nanoarchitectures in metal nanoparticle-modified electrodes for electroanalysis. *Anal Sci* 2010, 26, 1–12.

[145] Oja SM, Wood M, Zhang B. Nanoscale electrochemistry. *Anal Chem* 2013, 85, 473–86.
[146] Ziyatdinova G, Kozlova E, Ziganshina E, Budnikov H. Surfactant/carbon nanofibers-modified electrode for the determination of vanillin. *Monat Chem* 2016, 147, 191–200.
[147] Zhang T, Mubeen S, Myung NV, Deshusses MA. Recent progress in carbon nanotube-based gas sensors. *Nanotechnol* 2008, 19, 332001–14.
[148] Chang J, Zhou G, Christensen ER, Heideman R, Chen J. Graphene-based sensors for detection of heavy metals in water: a review. *Anal Bioanal Chem* 2014, 406, 3957–75.
[149] Shao Y, Wang J, Wu H, Liu J, Aksay IA, Lin Y. Graphene based electrochemical sensors and biosensors: a review. *Electroanal* 2010, 22, 1027–36.
[150] Nguyen BH, Nguyen VH. Promising applications of graphene and graphene-based nanostructures. *Adv Nat Sci: Nanosci Nanotechnol* 2016, 7, 023002.
[151] Hernaez M, Zamarreño CR, Melendi-Espina S, Bird LR, Mayes AG, Arregui FJ. Optical fibre sensors using graphene-based materials: a review. *Sensors* 2017, 17, 155–78.
[152] Song J, Li J, Guo Z, Liu W, Ma Q, Feng F, et al. A novel fluorescent sensor based on sulfur and nitrogen co-doped carbon dots with excellent stability for selective detection of doxycycline in raw milk. *RSC Adv* 2017, 7, 12827–34.
[153] Lu Sh, Wu D, Li G, Lv Zh, Chen Z, Chen L, et al. Carbon dots-based ratiometric nanosensors for highly sensitive and selective detection of mercury(II) ions and glutathione. *RSC Adv* 2016, 6, 103169–77.
[154] Valcarcel M, Cardenas S, Simonet BM, Moliner-Martınez Y, Lucena R. Carbon nanostructures as sorbent materials in analytical processes. *Trends Anal Chem* 2008, 27, 34–43.
[155] Li H, Ding GS, Chen J, Tang AN. Amphiphilic silica nanoparticles as pseudostationary phase for capillary electrophoresis separation. *J Chromatogr A*. 2010, 1217, 7448–54.
[156] Xie L, Jiang R, Zhu F, Liu H, Ouyang G. Application of functionalized magnetic nanoparticles in sample preparation. *Anal Bioanal Chem* 2014, 406, 377–99.
[157] Herrero-Latorre C, Barciela-García J, García-Martín S, Pena-Crecente RM, Otarola-Jimenez J. Magnetic solid-phase extraction using carbon nanotubes as sorbents: a review. *Anal Chim Acta* 2015, 892, 10–26.
[158] Wierucka M, Biziuk M. Application of magnetic nanoparticles for magnetic solid-phase extraction in preparing biological, environmental and food samples. *Trends Anal Chem* 2014, 59, 50–8.
[159] Šafařikova M, Šafařik I. Magnetic solid-phase extraction. *J Magn Magn Mater* 1999, 194, 108–112.
[160] Kaur R, Hasan A, Iqbal N, Alam S, Saini MK, Raza SK. Synthesis and surface engineering of magnetic nanoparticles for environmental cleanup and pesticide residue analysis: a review. *J Sep Sci* 2014, 37, 1805–25.
[161] https://ec.europa.eu/jrc/sites/jrcsh/files/jrc_reference_report_201007_ nanomaterials.pdf
[162] www.ea-aw.de/fileadmin/downloads/Graue_Reihe/ GR_35_Nanotechnology_112003.pdf
[163] Lövestam G, Rauscher H, Roebben G, Klüttgen BS, Gibson N, Jean-Philippe Putaud J-P, et al. Considerations on a definition of nanomaterial for regulatory purposes. JRC Ref Rep Eur Commission. Luxembourg, Publ Office of the Eur Union 2010.
[164] Balzani V. Nanoscience and nanotechnology: a personal view of a chemist. *Small* 2005, 1, 278–83.
[165] ISO TC 229 (ISO/DTS 80004-1).
[166] https://en.wikipedia.org/wiki/Nanotechnology
[167] Adams F, Barbante C. Nanotechnology and analytical chemistry. In: *Chemical Imaging Analysis. Comprehensive Analytical Chemistry*. Barcelo D., ed. Vol 69, Chapter 4. Amsterdam, Elsevier, 2015, 125–57.
[168] Nanoscience and nanotechnologies: opportunities and uncertainties. Royal Society and Royal Academy of Engineering. July 2004. Retrieved 13 May 2011. http://www.nanotec.org.uk/finalReport.htm Accessed 07.06.2017

[169] www.nano.gov/nanotech-101/what/definition Accessed 07.06.2017
[170] Nanotechnology: delivering on the promise. Vol 1. In: Cheng HN, Doemeni L, Geraci CL, Schmidt DG. eds. *ACS Symp Series 1220*. Washington, DC, Amer Chem Soc, 2016.
[171] Muto Sh, Yoshida T, Tatsumi K. Diagnostic nano-analysis of materials properties by multivariate curve resolution applied to spectrum images by S/TEM-EELS. *Mater Trans* 2009, 50, 964–69.
[172] Malgras V, Ji Q, Kamachi Y, Mori T, Shieh F-K, Wu KC-W, et al. Templated synthesis for nanoarchitectured porous materials. *Bull Chem Soc Jpn* 2015, 88, 1171–200.
[173] Qiu X, Yu H, Karunakaran M, Pradeep N, Nunes SP, Peinemann K-V. Selective separation of similarly sized proteins with tunable nanoporous block copolymer membranes. *ACS Nano* 2013, 7, 768–76.
[174] Ariga K, Yamauchi Y, Mori T, Hill JP. 25th anniversary article: What can be done with the Langmuir-Blodgett method? Recent developments and its critical role in materials science. *Adv Mater* 2013, 25, 6477–512.
[175] Wales DJ, Kitchen JA. Surface-based molecular self-assembly: Langmuir-Blodgett films of amphiphilic Ln(III) complexes. *Chem Central J* 2016, 10, 72–9.
[176] Decher G. Fuzzy Nanoassemblies: toward layered polymeric multicomposites. *Science* 1997, 277, 1232–7.
[177] Ariga K, Yamauchi Y, Rydzek G, Ji Q, Yonamine Y, Wu KC-W, et al. Layer-by-layer nanoarchitectonics: invention, innovation, and evolution. *Chem Lett* 2014, 43, 36–68.
[178] Schreiber F. Structure and growth of self-assembling monolayers. *Progr Surf Sci* 2000, 65, 151–257.
[179] Love JC, Estroff LA, Kriebel JK, Nuzzo RG, Whitesides GM. Self-assembled monolayers of thiolates on metals as a form of nanotechnology. *Chem Rev* 2005, 105, 1103–69.
[180] http://whatis.techtarget.com/definition/nanoanalysis
[181] http://www.yourdictionary.com/nanoanalysis
[182] Kellner R, Mermet J-M, Otto M, Valcarcel M, Widmer HM. *Analytical Chemistry: A Modern Approach to Analytical Science*, 2nd Ed. Weinheim, Wiley-VCH, 2004.
[183] Oleshko VP, Gijbels R, Amelinckx S. Electron microscopy, nanoscopy, and scanning micro- and nanoanalysis. In: Meyers RA, ed. *Encyclopedia of Analytical Chemistry*. RAMTECH, Inc Larkspur, CA, USA, John Wiley & Sons, Ltd., 2013, 1–44.
[184] Connolly MR, Smith CG. Nanoanalysis of graphene layers using scanning probe techniques. *Phil Trans R Soc A* 2010, 368, 5379–89.
[185] Ding S-Y, Yi J, Li J-F, Ren B, Wu D-Y, Panneerselvam R, et al. Nanostructure-based plasmon-enhanced Raman spectroscopy for surface analysis of materials. *Nature Rev Mater* 2016, 1, 16021.
[186] McMahon JM, Schatz GC, Gray SK. Plasmonics in the ultraviolet with the poor metals Al, Ga, In, Sn, Tl, Pb, and Bi. *PhysChemChemPhys* 2013, 15, 5415–23.
[187] Zhong Y, Malagari SD, Hamilton T, Wasserman D. Review of mid-infrared plasmonic materials. *J Nanophotonics* 2015, 9, 093791.
[188] Grigorenko AN, Polini M, Novoselov KS. Graphene plasmonics. *Nat Photonics* 2012, 6, 749–58.
[189] Alexander MR, Gilmore IS. Analytical techniques: surface and interfacial characterization. *Curr Opinion Chem Biol* 2011, 15, 664–66.
[190] Klenerman D, Korchev YE, Davis SJ. Imaging and characterisation of the surface of live cells. *Curr Opinion Chem Biol* 2011, 15, 696–703.
[191] Deckert-Gaudig T, Deckert V. Nanoscale structural analysis using tip-enhanced Raman spectroscopy. *Curr Opinion Chem Biol* 2011, 15, 719–24.
[192] Fletcher JS, Vickerman JC, Winograd N. Label free biochemical 2D and 3D imaging using secondary ion mass spectrometry. *Curr Opinion Chem Biol* 2011, 15, 733–40.
[193] Schmid T, Schmitz TA, Setz PD, Yeo B-S, Zhang W, Zenobi R. Methods for molecular nanoanalysis. *Chimia* 2006, 60, 783–8.

[194] Frederix PLTM, Akiuama T, Staufer U, Gerber Ch, Fotiadis D, Muller DJ, et al. Atomic force bio-analytics. *Curr Opinion Chem. Biol* 2003, 7, 641–7.
[195] Lang H, Hegner M, Meyer E, Gerber C. Nanomechanics from atomic resolution to molecular recognition based on atomic force microscopy technology. *Nanotechnol* 2002, 13, R29–36.
[196] Arntz Y, Seelig J, Lang H, Zhang J, Hunziker P, Ramseyer J, et al. Label-free protein assay based on a nanomechanical cantilever array. *Nanotechnol* 2003, 14, 86–90.
[197] Deckert-Gaudig T, Deckert V. Tip-enhanced Raman scattering (TERS) and high resolution bio nano-analysis – a comparison. *PhysChemChemPhys* 2010, 12, 12040–9.
[198] Deckert-Gaudig T, Taguchi A, Kawata S, Deckert V. Tip-enhanced Raman spectroscopy – from early developments to recent advances. *Chem Soc Rev* 2017, 46, 4077–110.
[199] Hecht B, Mühlschlegel P, Farahani JN, Eisler H-J, Pohl DW, Martin OJF, et al. Prospects of resonant optical antennas for nano-analysis. *Chimia* 2006, 60, 765–69.
[200] Ufheil J, Hess C, Borgwarth K, Heinze J. Nanostructuring and nanoanalysis by scanning electrochemical microscopy (SECM). *PhysChemChemPhys* 2005, 7, 3185–90.
[201] European Commission. Commission recommendation of 18 October 2011 on the definition of nanomaterial (2011/696/EU), Official Journal, 2011. https://ec.europa.eu/research/industrial_technologies/pdf/policy/commission-recommendation-on-the-definition-of-nanomater-18102011_en.pdf
[202] Gschwind S, de Lourdes Aja Montes M, Günther D. Comparison of sp-ICP-MS and MDG-ICP-MS for the determination of particle number concentration. *Anal Bioanal Chem* 2015, 407, 4035–44.
[203] Costa-Fernández JM, Menéndez-Miranda M, Bouzas-Ramos D, Encinar JR, Sanz-Medel A. Mass spectrometry for the characterization and quantification of engineered inorganic nanoparticles. *Trends Anal Chem* 2016, 84, A, 139–48.
[204] Bustos ARM, Winchester MR. Single-particle-ICP-MS advances. *Anal Bioanal Chem* 2016, 408, 5051–2.
[205] Bustos ARM, Encinar JR, Sanz-Medel A. Mass spectrometry for the characterisation of nanoparticles. *Anal Bioanal Chem* 2013, 405, 5637–43.
[206] Fabricius A-L, Duester L, Meermann B, Ternes TA. ICP-MS-based characterization of inorganic nanoparticles – sample preparation and off-line fractionation strategies. *Anal Bioanal Chem* 2014, 406, 467–79.
[207] ISO/TS-13278:2011. Determination of elemental impurities in samples of carbon nanotubes using inductively coupled plasma mass spectrometry.
[208] Yan N, Zhu Z, Jin L, Guo W, Gan Y, Hu S. Quantitative characterization of gold nanoparticles by coupling thin layer chromatography with laser ablation inductively coupled plasma mass spectrometry. *Anal Chem* 2015, 87, 6079–87.
[209] Mozhayeva D, Strenge I, Engelhard C. Implementation of online preconcentration and microsecond time resolution to capillary electrophoresis single particle inductively coupled plasma mass spectrometry (CE-SP-ICP-MS) and its application in silver nanoparticle analysis. *Anal Chem* 2017, 89, 7152–9.
[210] Meermann B, Laborda F. Analysis of nanomaterials by field-flow fractionation and single particle ICP-MS. *J Anal At Spectrom* 2015, 30, 1226–8.
[211] Mitrano DM, Barber A, Bednar A, Westerhoff P, Higginsd CP, Ranville JF. Silver nanoparticle characterization using single particle ICP-MS (SP-ICP-MS) and asymmetrical flow field flow fractionation ICP-MS (AF4-ICP-MS). *J Anal At Spectrom* 2012, 27, 1131–42.
[212] Chang YJ, Shih YH, Su CH, Ho HC. Comparison of three analytical methods to measure the size of silver nanoparticles in real environmental water and wastewater samples. *J Hazard Mater* 2017, 322 A, 95–104.

[213] Baer DR, Gaspar DJ, Nachimuthu P, Techane SD, Castner DG. Application of surface chemical analysis tools for characterization of nanoparticles. *Anal Bioanal Chem* 2010, 396, 983–1002.
[214] Laborda F, Bolea E, Jiménez-Lamana J. Single particle inductively coupled plasma mass spectrometry: a powerful tool for nanoanalysis. *Anal Chem* 2014, 86, 2270–8.
[215] Wang W, Tao N. Detection, counting, and imaging of single nanoparticles. *Anal Chem* 2014, 86, 2–14.
[216] Timerbaev AR. Role of mass spectrometry in the development and medical implementation of metal-based nanoparticles. *J Anal Chem* 2016, 70, 1031–46.
[217] Pace HE, Rogers NJ, Jarolimek C, Coleman VA, Higgins CP, Ranville JF. Determining transport efficiency for the purpose of counting and sizing nanoparticles via single particle inductively coupled plasma mass spectrometry. *Anal Chem* 2011, 83, 9361–9.
[218] Benešová I, Dlabková K, Zelenák F, Vaculovič T, Kanický V, Preisler J. Direct analysis of gold nanoparticles from dried droplets using substrate-assisted laser desorption single particle-ICPMS. *Anal Chem* 2016, 88, 2576–82.
[219] Lamsal RP, Jerkiewicz G, Beauchemin D. Flow injection single particle inductively coupled plasma mass spectrometry: an original simple approach for the characterization of metal-based nanoparticles. *Anal Chem* 2016, 88, 10552–8.
[220] Peters R, Herrera-Rivera Z, Undas A, van der Lee M, Marvin H, Bouwmeester H, et al. Single particle ICP-MS combined with a data evaluation tool as a routine technique for the analysis of nanoparticles in complex matrices. *J Anal At Spectrom*, 2015, 30, 1274–85.
[221] Donovan AR, Adams CD, Ma Y, Stephan C, Eichholz T, Shi H. Detection of zinc oxide and cerium dioxide nanoparticles during drinking water treatment by rapid single particle ICP-MS methods. *Anal Bioanal Chem* 2016, 408, 5137–45.
[222] Su C-K, Sun Y-C. Considerations of inductively coupled plasma mass spectrometry techniques for characterizing the dissolution of metal-based nanomaterials in biological tissues. *J Anal At Spectrom* 2015, 30, 1689–705.
[223] Roman M, Rigo C, Castillo-Michel H, Munivrana I, Vindigni V, Micetic I, et al. Hydrodynamic chromatography coupled to single-particle ICP-MS for the simultaneous characterization of AgNPs and determination of dissolved Ag in plasma and blood of burn patients. *Anal Bioanal Chem* 2016, 408, 5109–24.
[224] Dan Y, Ma X, Zhang W, Liu K, Stephan C, Shi H. Single particle ICP-MS method development for the determination of plant uptake and accumulation of CeO2 nanoparticles. *Anal Bioanal Chem* 2016, 408, 5157–67.
[225] Haiss W, Thanh NTK, Aveyard J, Fernig DG. Determination of size and concentration of gold nanoparticles from UV-Vis spectra. *Anal Chem* 2007, 79, 4215–22.
[226] Khlebtsov NG. Determination of size and concentration of gold nanoparticles from extinction spectra. *Anal Chem* 2008, 80, 6620–5.
[227] Ichimura Sh. Current activities of ISO TC229/WG2 on purity evaluation and quality assurance standards for carbon nanotubes. *Anal Bioanal Chem* 2010, 396, 963–71.
[228] Wu B, Becker JS. Imagine of elements and molecules in biological tissues and cells in the low-micrometer and nanometer range. *Intern J Mass Spectrom* 2011, 307, 112–22.
[229] Mout R, Moyano DF, Rana S, Rotello VM. Surface functionalization of nanoparticles for nanomedicine. *Chem Soc Rev* 2012, 41, 2539–44.
[230] Prabhu P, Patravale V. The upcoming field of theranostic nanomedicine: an overview. *J Biomed Nanotechnol* 2012, 8, 859–82.
[231] Crawley N, Thompson M. Theranostics in the growing field of personalized medicine: an analytical chemistry perspective. *Anal Chem* 2014, 86, 130–60.
[232] Pelaz B, Alexiou C, Alvarez-Puebla RA, et al. Diverse applications of nanomedicine. *ACS Nano* 2017, 11, 2313–81.

[233] Bagalkot V, Zhang L., Levy-Nissenbaum E., Jon S., Kantoff PW, Langer R, et al. Quantum dot-aptamer conjugates for synchronous cancer imaging, therapy, and sensing of drug delivery based on bi-fluorescence resonance energy transfer. *Nano Lett* 2007, 7, 3065–70.
[234] Matteini P, Cottat M, Tavanti F, Panfilova E, Scuderi M, Nicotra G, et al. Site-selective surface-enhanced Raman detection of proteins. *ACS Nano* 2017, 11, 918–26.
[235] Dykman LA, Khlebtsov NG, Multifunctional gold-based nanocomposites for theranostics. *Biomater* 2016, 108, 13–34.
[236] Schwartz JA, Shetty AM, Price RE, Stafford RJ, Wang JC, Uthamanthil R.K, et al. Feasibility study of particle-assisted laser ablation of brain tumors in orthotopic canine model. *Cancer Res* 2009, 69, 1659–67.
[237] Carniato F, Muñoz-Úbeda M, Tei L, Botta M. Selective functionalization of mesoporous silica nanoparticles with ibuprofen and Gd(III) chelates: a new probe for potential theranostic applications. *Dalton Trans* 2015, 44, 17927–31.
[238] Hajba L, Guttman A. The use of magnetic nanoparticles in cancer theranostics: toward handheld diagnostic devices. *Biotechnol Adv* 2016, 34, 354–61.
[239] Godage OS, Bucharskaya AB, Navolokin NA, Maslyakova GN, German SV, Gorin DA. The magnetite nanoparticles in theranostics applications. *J Nanomed Res* 2017 5(3), 00119.
[240] Mulvaney P, Parak WJ, Caruso F, Weiss PS. Standardizing Nanomaterials. *ACS Nano* 2016, 10, 9763–4.
[241] Bogue R. Nanometrology: a critical discipline for the twenty-first century. *Sensor Rev* 2007, 27, 189–96.
[242] Baer DR, Munusamy P, Thrall BD. Provenance information as a tool for addressing engineered nanoparticle reproducibility challenges. *Biointerphases* 2016, 11, 04B401–9.
[243] Sperling RA, Liedl T, Duhr S, Kudera S, Zanella M, Lin C-AJ, et al. Size determination of (bio-) conjugated water-soluble colloidal nanoparticles: a comparison of different techniques. *J Phys Chem C* 2007, 111, 11552–9.
[244] Bard D, Mark D, Möhlmann C. Current Standardization for nanotechnology. *J Physics: Conf. Series* 2009, 170, 012036.
[245] https://www.iso.org/committee/381983.html
[246] Benko H. ISO Technical Committee 229 Nanotechnologies. In: Mansfield E, Kaiser DL, Fujita D, Van de Voorde M. eds. *Metrology and Standardization of Nanotechnology: Protocols and Industrial Innovations*. Weinheim, Germany, Wiley-VCH Verlag, GmbH & Co. KGaA, 2017, 259–68.
[247] Forsberg E-M. The Role of ISO in the Governance of Nanotechnology. Oslo, Work Research Institute, 2010. https:// hioaresponsibleinnovation.files.wordpress.com/2017/02/
[248] Brar SK, Verma M. Measurement of nanoparticles by light-scattering techniques. *Trends Anal Chem* 2011, 30, 4–17.
[249] Allmaier G, Maißer A, Laschober C, Messner P, Szymanski WW. Parallel differential mobility analysis for electrostatic characterization and manipulation of nanoparticles and viruses. *Trends Anal Chem* 2011, 30, 123–32.
[250] Thunemann AF, Rolf S, Knappe P, Weidner S. In situ analysis of a bimodal size distribution of superparamagnetic nanoparticles. *Anal Chem* 2009, 81, 296–301.
[251] Linsinger TPJ, Roebben G, Solans C, Ramsch R. Reference materials for measuring the size of nanoparticles. *Trends Anal Chem* 2011, 30, 18–27.

# Part II: **Application in Spectrometric Methods**

L. A. Dykman, N. G. Khlebtsov and S. Y. Shchyogolev

# 2 Gold Nanoparticles in Bioanalytical Techniques

## 2.1 Introduction

Gold is one of the first metals discovered by humans, and the history of its study and application is estimated to be a minimum of several thousand years. The first information on colloidal gold (CG) can be found in tracts by Chinese, Arabic, and Indian scientists who obtained CG as early as in the fifth and fourth centuries B.C. and used it, in particular, for medical purposes (the Chinese "gold solution" and the Indian "liquid gold"). In the Middle Ages, alchemists in Europe actively studied and used CG. Probably, wonderful color changes that accompany condensation of gold atoms prepared by reduction of salt solutions led alchemists to believe in transformations of elements, CG being considered as a panacea. Specifically, Paracelsus wrote about the therapeutic properties of *quinta essentia auri*, which he obtained through reduction of auric chloride with alcohol or oil plant extracts. He used "potable gold" to treat some mental disorders and syphilis. Paracelsus once proclaimed that chemistry is for making medicines, not for making gold out of metals: "Many have said of Alchemy, that it is for the making of gold and silver. For me such is not the aim, but to consider only what virtue and power may lie in medicines." His contemporary Giovanni Andrea applied *aurum potabile* to the treatment of lepra, ulcer, epilepsy, and diarrhea. The first book on CG preserved to our days was published by philosopher and doctor of medicine Francisco Antonii in 1618 [1]. It contains information on the preparation of CG and on its medical applications, including practical suggestions. From the seventeenth century, CG was used for the production of red (ruby) glasses, decoration on porcelain (purple of Cassius), and silk coloration [2]. In 1633, alchemist de Planis-Campy [3], surgeon to the King of France Louis XIII, recommended his "elixir of longevity" – an aqueous CG solution – as a means of life prolongation. In 1712, Heicher [4] published a complete summary of gold's medicinal uses, which describes the solutions and the gold stabilization with boiled starch, which is an example of stabilization of CG with ligands.

The beginning of scientific research on CG dates back to the mid-nineteenth century, when Faraday [5] published an article devoted to methods of synthesis and properties of CG. In this article, Faraday described, for the first time, aggregation of CG in the presence of electrolytes, the protective effect of gelatin and other high-molecular-mass compounds and the properties of thin films of CG. CG solutions prepared by Faraday are still stored in the Royal Institution of Great Britain in London.

In 1898, Zsigmondy [6] published the fundamental paper on the properties of CG. He was the first to describe methods of synthesis of CG with different particle sizes with the use of hydrogen peroxide, formaldehyde, and white phosphorus as reducing

https://doi.org/10.1515/9783110542011-002

agents and report on important physicochemical (including optical) properties of gold sols. Zsigmondy used CG as the main experimental object when inventing (in collaboration with Siedentopf) an ultramicroscope. In 1925, Zsigmondy was awarded the Nobel Prize in Chemistry "for his demonstration of the heterogeneous nature of colloid solutions and for the methods he used, which have since become fundamental in modern colloid chemistry."

Studies by the Nobel Prize laureate Svedberg [7] on the preparation, analysis of mechanisms of CG formation, and sedimentation properties of CG (with the use of the ultracentrifuge he had invented) are also among classical studies. Svedberg investigated the kinetics of reduction of gold halides and formulated the main concepts about the mechanism of formation (chemical condensation) of CG particles.

CG in color analytical reactions toward spinal-fluid and blood-serum proteins has been used since the first half of the twentieth century [8].

Methods of synthesis of CG (and other metal colloids) can be arbitrarily divided into the following two large groups: dispersion methods (metal dispersion) and condensation methods (reduction of the corresponding metal salts). Dispersion methods for the preparation of CG are based on destruction of the crystal lattice of metallic gold in high-voltage electric field [9] or laser ablation [10]. If an electric arc is created in a liquid between two gold electrodes under electric field, its blazing leads to the mass transfer between electrodes accompanied by the CG formation. The yield and shape of gold particles formed under electric current depend not only on the voltage between electrodes and the current strength, but also on the presence of electrolytes in solution. The use of direct current leads to the formation of nonuniform gold particles. The addition of even very small amounts of alkalis or chlorides and the use of high-frequency alternating current for dispersion substantially improve the quality of gold hydrosols.

Condensation methods are more commonly employed than dispersion methods. CG is most often prepared by reduction of gold halides (e. g., of $HAuCl_4$) with the use of chemical reducing agents and/or irradiation (ultrasonic and UV irradiation, pulse or laser radiolysis). Various organic and inorganic compounds (more than 100) serve as chemical reducing agents. At present, the most popular colloidal synthesis protocols involve the citrate reduction of $HAuCl_4$, as suggested by Borowskaja [11], Turkevich et al. [12], and Frens [13], to produce relatively monodisperse particles with controlled average equivolume diameters of 10–100 nm.

Despite the centuries-old history, a "revolution in immunochemistry," associated with the use of gold nanoparticles (GNPs) in biological research, took place in 1971, when British investigators Faulk and Taylor [14] published an article titled "An immunocolloid method for the electron microscope." In that article, they described a technique for conjugating antibodies to CG for direct electron microscopic visualization of *Salmonella* surface antigens, representing the first time that a CG conjugate as an immunochemical marker. From this point on, the use of CG

biospecific conjugates in various fields of biology and medicine became very active. There has been a wealth of reports dealing with the application of functionalized GNPs (conjugates with recognizing biomacromolecules, for example, antibodies, lectins, enzymes, or aptamers) [15, 16] to the studies of biochemists, microbiologists, immunologists, cytologists, physiologists, morphologists, and many other specialist researchers.

Functionalization of GNPs with surface molecules is aimed at fabricating multifunctional nanoparticle (NP) bioconjugates possessing various modalities, such as active biosensing, enhanced imaging contrast, drug delivery, and tumor targeting. At present, bioconjugation chemistry, recently reviewed comprehensively by Sapsford et al. [17], can be considered a separate specific branch of nanobiotechnology. Sapsford et al.'s review is based on 2,081 literature sources and covers a broad range of particle types (including GNPs) and a great variety of functionalization technologies. For more detailed information, we point readers to this section; what follows is a description of only some general principles.

The range of uses of GNPs in current medical and biological research is extremely broad. In particular, it includes genomics; biosensorics; immunoassay; clinical chemistry; detection and photothermolysis of microorganisms and cancer cells; targeted delivery of drugs, peptides, DNA, and antigens; and optical bioimaging and monitoring of cells and tissues with the use of state-of-the-art nanophotonic recording systems. It has been proposed that GNPs be used in practically all medical application, including diagnostics, therapy, prophylaxis, and hygiene [18, 19]. Such a broad range of application is based on the use of the unique physical and chemical properties of GNPs. Specifically, the optical properties of GNPs are determined by their plasmon resonance, which is associated with the collective excitation of conduction electrons and is localized in a wide region (form visible to infrared, depending on particle size, shape, and structure) [20].

In the past few years, hybrid NP systems have attracted significant interest, as they combine different nanomaterials in a single multifunctional nanostructure that exhibits the modalities of its component modules [21]. Theranostics, an emerging trend in nanomedicine, is capable of combining all the above advanced properties into a single nanostructure with simultaneous diagnostic and therapeutic functions, which can be physically and chemically tailored for a particular organ, disease, or patient [22, 23]. The first time that the term "theranostics" appeared in the literature was in 2002 [24, 25]. In 2010, Lukianova-Hleb et al. [26] presented a complete concept of theranostics. Theranostics is closely related to the fabrication and application of multifunctional NPs, which combine therapeutic and diagnostic possibilities within a single structure [27, 28].

This chapter summarizes data on bioanalytical use of GNPs, their applications in homophase and solid-phase analytical techniques. A special section is devoted to applications of GNPs in plasmonic biosensors.

## 2.2 Homophase techniques

Beginning in 1980s, CG conjugates to recognizing biomacromolecules were coming into use in various analytical methods in clinical diagnostics. In 1980, Leuvering et al. [29] put forward a new immunoanalysis method that they called sol particle immunoassay (SPIA). This method is based on two principles: (1) the sol color and absorption spectrum change little when biopolymers are adsorbed on individual particles [30]; (2) when particles move closer to each other by distances smaller than 0.1 of their diameter, the red color of the sol changes to purple or gray and the absorption spectrum broadens and red-shifts [31]. This change in the absorption spectrum can easily be detected spectrophotometrically or visually (Fig. 2.1a, b [32–35]).

The authors employed on optimized variation of SPIA (by using larger gold particles and monoclonal antibodies to various antigen sites) to detect human chorionic gonadotropin [36]. Subsequently, the assay was used for the immunoanalysis of *Shistosoma* [37] and *Rubella* [38] antigens; estimation of immunoglobulins [39, 40], thrombin (by using aptamers) [41], glucose [42], ATP [43], alpha-fetoprotein [44], C-reactive protein [45], lysozyme [46], fecal calprotectin [47], fibronectin [48], and selenoprotein P [49]; direct detection of cancerous cells [50] and antigens [51]; detection of *Leptospira* [52], bacteriophage [53], and influenza A virus [54]; detection of Alzheimer's disease markers [55]; determination of protease activity [56]; and other uses [57–61]. The simultaneous use of antibody conjugates of gold nanorods and nanospheres for the detection of tumor antigens was described by Liu et al. [62]. Wang et al. [63] provided data on the detection of hepatitis B virus in blood by using gold nanorods conjugated to specific antibodies.

All SPIA versions proved to be easy to implement and demonstrated high sensitivity and specificity. However, investigators came up against the fact that antigen–antibody reaction on sol particles does not necessarily lead to system destabilization (aggregation). Sometimes, despite the obvious complementarily of the pair, changes in solution color (and, correspondingly, in absorption spectra) were either absent or slight. Dykman et al. [64] proposed a model for the formation of a second protein layer on gold particles without loss of sol aggregative stability. The spectral changes arising from biopolymer adsorption on the surface of metallic particles are comparatively small [65] (Fig. 2.1c, d). However, even such minor changes in absorption spectra, resulting from a change in the structure of the biopolymer layer (specifically, its average refractive index) near the GNP surface, could be recorded and used for assay in biological application, as demonstrated by Englebienne et al. [34, 66].

For increasing the sensitivity of the analytic reaction, new techniques for recording interaction are used, including photothermal spectroscopy [67], laser-based double beam absorption spectroscopy [68], hyper-Rayleigh scattering [69], differential light-scattering spectroscopy [70], and dynamic light scattering [71]. In addition, the vibrational spectroscopy method – surface-enhanced infrared absorption spectroscopy [72–74] and surface-enhanced Raman spectroscopy (SERS) [75–79] – have been proposed for use in recording SPIA results.

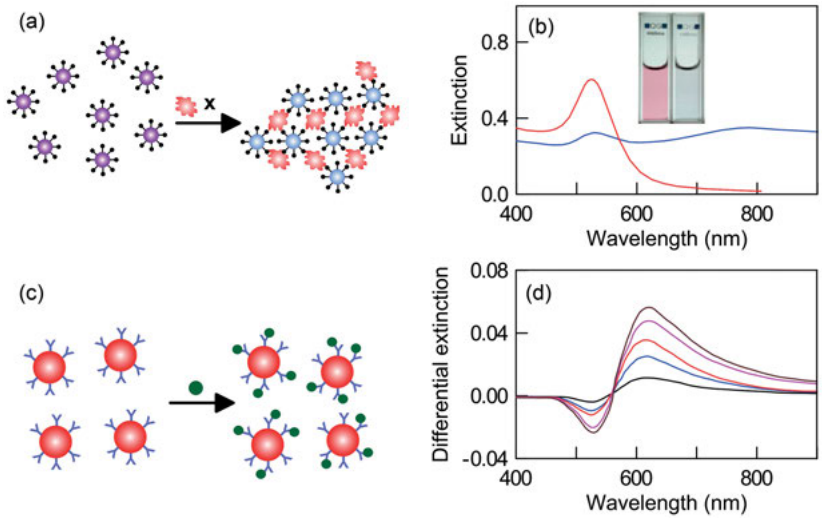


**Fig. 2.1:** Sol particle immunoassay. (a) Scheme for the aggregation of conjugates as a result of binding by target molecules and (b) the corresponding changes in the spectra and in sol color. (c) Scheme for the formation of a secondary layer without conjugate aggregation and (d) the corresponding differential extinction spectra at 600 nm. Reprinted with permission from [18]. Copyright 2012 Royal Society of Chemistry.

The ability of gold particles interacting with proteins to aggregate with a solution color change served as a basis for the development of a method for the colorimetric determination of proteins [80]. A new version of gold aggregation assay using microplates and enzyme-linked immunosorbent assay (ELISA) reader, with CG-conjugated trypsin as a specific agent for proteins, was advanced by Dykman et al. [81].

A new version of gold aggregation assay was advanced by Mirkin et al. [82] for the colorimetric detection of DNA. Currently, the colorimetric detection of DNA includes two strategies: (1) the use of GNPs conjugated to thiol-modified ssDNA [82–86] or aptamers [87]; (2) the use of unmodified GNPs [88–90]. The first strategy is based on the aggregation of conjugates of 10- to 30-nm GNPs with thiol-modified ssDNA probes after the addition of target polynucleotides to the system. It used two types of probes complementary to two terminal target sites. Hybridization of the targets and probes leads to the formation of GNP aggregates, which is accompanied by a change in the absorption spectrum of the solution and can readily be detected visually, photometrically [91], or by the method of dynamic light scattering [86, 92]. Within the limits of the first strategy, Sato et al. [93] used a diagnostic system based on the aggregation of GNPs modified with probes of one type, with DNA targets added to the solution under high ionic force condition. Contrary to their data, Baptista et al. [85, 94] devised a detection method based on the increased conjugate stability after the addition of complementary targets even at high ionic force (2 M NaCl), and they observed aggregation for noncomplementary targets. The apparent contradictions

between the two approaches were explained by Song et al. [95], be the difference in surface functionalization density.

The second strategy [89] is based on the fact that at high ionic force, ssDNA protects unmodified GNPs against aggregation, whereas the formation of duplex during hybridization cannot stabilize the system. This approach was employed to detect hepatitis C virus RNA [96]. Recently, Xia et al. [97] described a new version of the second strategy that uses ssDNA, unmodified GNPs, and a cationic polyelectrolyte. The same approach proved suitable for detection of a wide range of targets, including peptides, amino acids, pesticides, antibiotics, and heavy metals. As distinct from techniques employing usual GNPs, He et al. [90] proposed a method for detecting HIV-1 U5 virus DNA by using nanorods stabilized with cetyltrimethylammonium bromide (CTAB) and light scattering with a detection limit of 100 pM. In an optimized version using absorption spectroscopy [98], the detection limit was lowered to 0.1 pM. Recently, it is also possible to use CTAB-coated positively charged GNPs in combination with spectroscopic and dynamic scattering methods [99].

The above-listed versions of the method of sol particle aggregation at the cost of the hybridization reaction have been used for the detection of the DNA of *Mycobacterium* [85, 100, 101], *Staphylococcus* [102], *Streptococcus* [103], *Chlamydiae* [104], *Serratia* [105], *Bacillus* [106], *Salmonella* [107], and *Acinetobacter* [108] in clinical samples.

## 2.3 Dot blot immunoassay

At the early stages of immunoassay development, preference was given to liquid-phase techniques in with bound antibodies were precipitated or unbound antigen was removed by adsorption with dextran-coated activated charcoal. Currently, the most popular techniques are solid-phase ones (first used for protein radioimmunoassay) because they permit the analysis to be considerably simplified and the background signal to be reduced. The most widespread solid-phase carriers are polystyrene plates and nitrocellulose membranes.

The solid-phase immunoassays are based on adsorption of antigens onto a solid substrate followed by binding of adsorbed target molecules with biospecific labels. In the membrane version, the solid-phase immunoassay can be called "dot-immunoassay" as usually a drop of analyte is deposited into center of a 5 × 5-mm delineate square and the reaction outcome looks like a colored dot. The simplicity of analyses and the saving of antigens and reagents allow one to implement the solid-phase immunoassays in laboratory, field, or even domestic circumstances to detect proteins (Western blotting), DNA (Southern blotting), or RNA (Northern blotting).

Membrane immunoassays (dot and blot assays) commonly employ radioactive isotopes ($^{125}$I, $^{14}$C, $^{3}$H) and enzymes (peroxidase, alkaline phosphatase, etc.) as labels. In 1984, four independent reports were published [109–112], in which CG was proposed for use as a label in solid-phase immunoassay. The use of GNP conjugates in

solid-phase assay is based on the fact that the intense red coloration of a gold-containing marker allows the results of a reaction run on a solid carrier to be determined visually. Immunogold methods in dot-blot assay outperform other techniques (e. g., enzyme immunoassay) in sensitivity (Tab. 2.1), rapidity, and low cost [113–115]. After an appropriate immunochemical reaction is run, the sizes of GNPs can be increased by enhancement with salts of silver [116] or gold (autometallography) [117], considerably expanding the application limits of the method. An optimized solid-phase assay using a densitometry system afforded a lineal detection range of 1 pM to 1 μM [118] with detection limit of 100 aM, which was lowered to 100 zM by silver enhancement. His use of state-of-the-art instrumental detection methods, such as photothermal deflection of the laser beam, caused by heating of the local environment near absorbing particles by heating laser impulses [119], also ensures a very broad detection range (up to three orders of magnitude to the extent of several individual particles in a dot spot).

**Tab. 2.1:** Sensitivity limits for immunodot/blot methods on nitrocellulose filters by using various labels (according to [113])

| Label | Sensitivity limit (pg of protein/fraction) |
|---|---|
| $^{125}$I | 5 |
| Horseradish peroxidase | 10 |
| Alkaline phosphatase | 1 |
| CG | 1 |
| CG + silver | 0.1 |
| Fluorescein isothiocyanate | 1,000 |

In specific staining, a membrane with applied material under study is incubated in a solution of antibodies (or other biospecific probes) labeled with CG [120]. As probes, "gold" dot or blot assay uses immunoglobulins, Fab and scFv antibody fragments, staphylococcal protein A, lectins, enzymes, avidin, aptamers, and other probes. Sometimes, several labels are used simultaneously (e. g., CG and peroxidase or alkaline phosphatase) for detection of multiple antigens on a membrane [121, 122].

CG in membrane assay have been used for the diagnosis of parasitic diseases [123–128], viral diseases [129–132], fungal diseases [133, 134], tuberculosis [135–137], melioidosis [138], syphilis [139], brucellosis [140], shigellosis [141], *E. coli* infections [142], salmonellosis [143, 144], yersiniosis [145, 146], and early pregnancy [147]; blood group determination [148]; dot blot hybridization [149]; detection of diphtheria toxin [150], ferritin [151], thrombin [152], β-amyloid peptide [153], tumor-associated antigens [154], and antibiotics [155]; diagnosis of myocardial infarction [156] and hepatitis B [157]; and other purposes.

The immunodot assay is one of the simplest methods for analyzing membrane-immobilized antigens. In some cases, it permits determination quantity of antigen. Most commonly, the immunodot assay is employed to study soluble antigens [158]. However, there have been several reports in which corpuscular antigens (whole

bacterial cells) were used as a research object in dot assays with enzyme labels [159]. Bogatyrev et al. [160, 161] were the first to perform a dot assay of whole bacterial cells, with the reaction products being visualized with immunogold markers ("cell gold immunoblotting"), with a view to serotyping nitrogen-fixing soil microorganisms of the genus *Azospirillum*. Subsequently, this method was applied for the rapid diagnosis of enteric infections [162] and for the study of surface physicochemical properties of microorganisms [163]. Gas et al. [164] used a dot assay with GNPs to detect whole cells of the toxic phytoplankton *Alexandrium minutum*.

Khlebtsov et al. [165, 166] first presented experimental results for the use of gold nanoshells (GNSs) as biospecific labels in dot assay. In the experiments, three types of GNSs were examined that had silica core diameters of 100, 140, and 180 nm and a gold shell thickness of about 15 nm. The biospecific pair was normal rabbit serum (target molecules) and sheep antirabbit immunoglobulins (recognizing molecules). When the authors used a standard protocol for a nitrocellulose-membrane dot assay, with 15-nm CG as labels, the minimum detectable quantity of rabbit IgG was 15 ng. Replacing CG conjugates with GNSs increased the assay sensitivity to 0.2 ng for 180/15-nm gold nanoshells and to 0.4 ng for 100/15-nm and 140/15-nm nanoshells (Fig. 2.2). Such a noticeable increase in sensitivity with nanoshells, as compared with nanospheres, can be explained by the different optical properties of the particles [167].

By using multicolor composite GNPs (Ag nanocubes, Au–Ag alloy NPs, and Au–Ag nanocages), was recently developed a multiplexed variant of immunodot assay [168]. As in usual immunodot assay, the multiplexed variant is based on the staining of analyte drops on a nitrocellulose membrane strip by using multicolor NPs conjugated with biospecific probing molecules. Depending on the Ag–Au conversion ratio, the particle plasmon resonance was tuned from 450 to 700 nm and the suspension color changed from yellow to blue (Fig. 2.3).

The particles of yellow, red, and blue suspensions were functionalized with chicken, rat, and mouse IgG molecular probes, respectively. The multiplex capability of the assay is illustrated by a proof-of-concept experiment on simultaneous one-step determination of target molecules (rabbit antichicken, antirat, and antimouse antibodies) with a mixture of fabricated conjugates. Under naked eye examination, no cross-colored spots or nonspecific bioconjugate adsorption was observed, and the low detection limit was about 20 fmol [168].

A very promising direction is the use of CG to analyze large arrays of antigens in micromatrices (immunochips) [169, 170]. These enable an analyte to be detected in 384 samples simultaneously at a concentration of 60–70 ng/L or, with account taken of the microliter amounts of sample and detecting immunogold marker, with a detection limit of lower than 1 pg. One area with prospects is the development of commercially available, handheld, sensitive readers for evaluation of quantitative results and the integration into systems designed to optimize the performance of the overall assay from sample to answer [171–173].

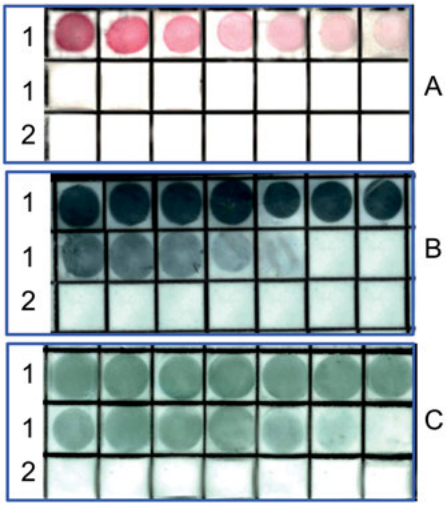


**Fig. 2.2:** Dot assay of normal rabbit serum (1) by using suspensions of conjugates of 15-nm GNPs (A) and $SiO_2$/Au nanoshells (100- and 180-nm silica core diameters and 15-nm gold shell, B and C, respectively) with sheep antirabbit antibodies. The amount of IgG in the first square of the top row was 1 μg, decreasing from left to right in accordance with twofold dilutions. The lower rows (2) correspond to the application of 10 μg of bovine serum albumin to each square as a negative control. The detected analyte quantity was 15 ng for 15-nm GNPs and 0.4 and 0.2 ng for 100/15- and 180/15-nm nanoshells, respectively. Reprinted with permission from [18]. Copyright 2012 Royal Society of Chemistry.

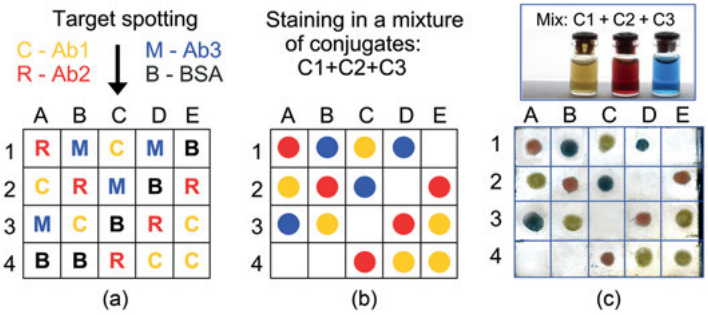


**Fig. 2.3:** Scheme for the multiplexed dot immunoassay (a, b) and its experimental verification (c). At the first step (panel a), antichicken rabbit antibodies Ab1 were spotted in squares A2, B3, C1, D4, and E3; antirat rabbit antibodies Ab2 were spotted in squares A1, B2, C4, D3, and E2; antimouse rabbit antibodies Ab3 were spotted in squares A3, B1, C2, and D1; and for negative control, BSA was spotted in squares A4, B4, C3, D2, and E1. The concentration of all analytes was 100 μg/mL. After staining in a mixture of conjugates (C1 + C2 + C3), the expected spot colors are shown in panel b. The experimental panel c confirms the expected assay results. Reprinted with permission from [168]. Copyright 2012 Springer.

## 2.4 Immunochromatographic assays

In 1990, several companies began to manufacture immunochromatographic test system for instrument-free handheld diagnostics. Owing to their high specificity and sensitivity, these strip tests have found a wide utility in the detection of narcotics and toxins, and in screening for highly dangerous infections and urogenital diseases [174–181]. Methods have been developed for the diagnosis of tuberculosis [182, 183], helicobacteriosis [184], staphylococcal infection [185, 186], hepatitis B [187], shigellosis [188, 189], diphtheria [190], pseudorabies [191], botulism [192], chlamydiosis [193], *E. coli* infections [194], prostatitis [195, 196], and early pregnancy [197]; for DNA hybridization [198]; for the detection of pesticides [199, 200], aflatoxin [201, 202], fumonisin [203], hexoestrol [204], and antibiotics [205–207] in environmental constituents; and other purposes.

The immunochromatographic assay is based on eluent movement along the membrane (lateral diffusion), giving rise to specific immune complexes at different membrane sires; the complexes are visualized as colored bands. As labels, these systems use enzymes, colored latexes, but mostly GNPs [208–210].

The sample being examined migrates along the test strip at the cost of capillary forces. If the sample contains the sought-for substance or immunochemically related compounds, there occurs a reaction with colloidal-gold-labeled specific antibodies at the instant the sample passes through the absorbing device. The reaction is accompanied by the formation of antigen–antibody complex. The colloidal preparation enters into a competitive binding reaction with the antigen immobilized in the test zone (as a rule, the detection of low-molecular-weight compounds employs conjugates of haptens with protein carrier for immobilization). If the antigen concentration in the sample exceeds the threshold level, the conjugate does not possess free valences for interaction in the test zone and the colored band corresponding to the formation of the complex is not revealed. When the sample does not contain the sought-for substance or when the concentration of that substance is lower than the threshold level, the antigen immobilized in the test zone of the strip reacts with the antibodies on the surface of CG, which leads to the development of a colored band.

When the liquid front moves on, the gold particles with immobilized antibodies that have not reacted with the antigen in the strip test zone bund to antispecific antibodies in the control zone of the test strip. The appearance of a colored band in the control zone confirms that the test was done correctly and that the system's components are diagnostically active. A negative test result – the appearance of two colored bands (in the test zone and in the control zone) – indicates that the antigen is absent from the sample or that its concentration is lower than the threshold level. A positive test result – the appearance of one colored band in the control zone – indicates that antigen concentration exceeds the threshold level (Fig. 2.4).

Studies have shown that such assay systems are highly stable, their results are reproducible, and they correlate with alternative methods. Densitometric

characterization of the dissimilarity degree for the bands detected yields values ranging from 5 % to 8 %, allowing reliable visual determination of the analysis results. These assays are very simple and convenient to use.

In summary, being effective diagnostic tools, rapid tests allow qualitative and quantitative determination, in a matter of minutes, of antigens, antibodies, hormones, and other diagnostically important substances in humans and animals. Rapid tests are highly sensitive and accurate, as they can detect more than 100 diseases (including tuberculosis, syphilis, gonorrhea, chlamydiosis, and various types of viral hepatitis) and the whole gamut of narcotic substances used, with the reliability of detection being high. An important advantage of these tests is their use in diagnostics *in vitro*, which does not require a patient's presence.

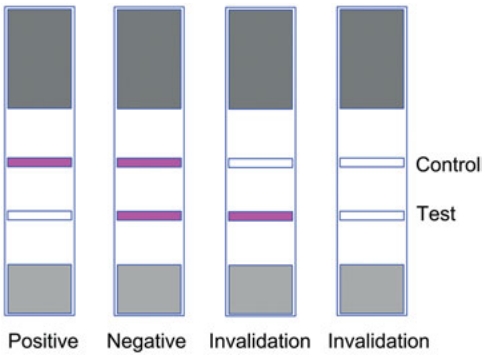


**Fig. 2.4:** Results of an immunochromatographic assay: positive, negative, and invalid determination because of the absent coloration in the control zone. Reprinted with permission from [18]. Copyright 2012 Royal Society of Chemistry.

However, immunochromatographic test strips are not devoid of weak points, related to reliability, sensitivity, and cost-effectiveness. Reliability and sensitivity depend, first, on the quality of monoclonal antibodies used in a test and, second, on the antigen concentration in a biomaterial. The quality of monoclonal antibodies depends on the methods of their preparation, purification, and fixation on a carrier. The antigen concentration depends on the disease state and the biomaterial quantity. For increasing the analysis sensitivity, it has been proposed to employ the silver enhancement procedure [211] or GNRs [212] or GNSts [213] as labels. Several studies demonstrate the novel application of an artificial non-immunoglobulin structures (aptamers, DARPins) as the new line of a visible detector using a rapid diagnostic test with characteristics that have the potential to be superior to those that utilize antibody-based tests [214, 215]. In addition, semiquantitative and quantitative instrumental formats of immunochromatographic analysis have been developed that use special readers for recording the intensity of a label's signal in the test zone of a test strip [216–219].

## 2.5 Plasmonic biosensors

In recent years, gold and silver NPs and their composites have been widely utilized as effective optical detectors of biospecific interactions [220]. In particular, the resonant optical properties of nanometer-sized metallic particles have been successfully used for the development of biochips and biosensors. There are many types of sensors, viz. colorimetric, refractometric, electrochemical, piezoelectric, and certain others [221, 222]. Such devices are of much interest in biology (determination of nucleic acid, protein, and metabolite content), medicine (screening of drugs, analysis of antibodies and antigens, diagnosis of infection), and chemistry (rapid environmental monitoring, assays of solutions and disperse systems). Of particular significance is the detection of specified nucleic acid (gene) sequences and the construction of new materials, which is based on the formation of 3D ordered structures during hybridization in solutions of complementary oligonucleotides that are covalently attached to metallic NPs [223].

The detection of biospecific interaction that is based on a change in the optical properties of the NP-carrier system can be assigned to biosensoric, a comparatively new domain of science. The biosensor is constituted either by the system itself in its entirety or by an individual marker particle (an elementary sensor). Among the localized plasmon resonance biosensors, CG occupies a special place, because it can serve both as a label in a nanosensing device and as a tool in molecular biological studies, which is used *in vitro, in situ*, and *in vivo*.

For more than 10 years, biospecific interactions have been studied in systems in which GNPs are represented as ordered structures: self-assembling (thin films) [224] or as part of polymer matrices [225]. Such structures have been actively used for detection of biomolecules and infectious agents, development of DNA chips, and other purposes. In this case, investigators directly realize the possibility in principle of using the sharp enhancement of the optical signal from the probe (GNPs conjugated to biospecific macromolecules) resulting from the strengthening of the exciting local field in the aggregate formed from gold nanoclusters. Currently, biosensors are built with novel, unique technologies, including monolayer self-assembly of metallic particles [226–229], nanolithography [230], vacuum evaporation [231], and others. It is of fundamental importance to note that the optical response of NPs or their aggregates (especially ordered ones) in substantially influenced by particle size and shape [232], interparticle distance [233, 234], and the properties of the particles' local dielectric environment [235, 236], which enables the "tuning" of sensors to be controlled. These properties of metallic clusters served as a basis for creation of new promising (localized) surface plasmon resonance biosensing systems [(L)SPR biosensors] based on the transformation of biospecific interactions into an optical signal. The theory behind the creation of such systems and their use in practice have been considered in the numerous books and reviews [237–269].

In experimental work with SPR biosensors, three stages can be singled out [238]: (1) one of the reagents (target-recognizing molecules) is covalently attached to the sensor surface. (2) The other reagent (target molecules) is added at a definite concentration to the sensor surface along with the flow of the buffer. The process of complex formation is then recorded. (3) The sensor is regenerated (dissociation of the formed complexes).

As this takes place, the following conditions should be met:

- reagent immobilization on the substrate should not lead a critical change in the conformation of native molecules;
- the relatively small difference between the refractive indices of most biological macromolecules forces one to use a high local concentration of binding sites on the sensor surface (10–100 μM);
- the reagent being added should be vigorously agitated to achieve effective binding to the immobilized molecules, and unbound reagent should be promptly removed from the sensor surface to avoid nonspecific sorption.

Apart from that, the sensitivity, stability, and resolution of a sensor depend directly on the characteristics of the optical system being used for recording. The most popular sensor system of this type is BIAcore™ [270–272]. The measurement principle of the planar, prismatic, or mirror biosensors is similar to the principle of the method of frustrated total internal reflection, traditionally employed to measure the thickness and refractive index of ultrathin organic films on metallic (reflecting) surfaces [221]. The excitation of the plasmon resonance in a planar gold layer occurs when polarized light is incident on the surface at a certain angle. At the metal/dielectric interface, electromagnetic fields are excited that run along the interface and are localized near it at the cost of an exponential decrease in amplitude perpendicularly to the dielectric with a typical attenuation length of up to 200 nm (the effect of total internal reflection, Fig. 2.5). The reflection coefficient at a certain angle and light wavelength depends on the dielectric properties of the thin layer at the interface, which are ultimately determined by the concentration of target molecules in the layer.

GNP-based biosensor are used not only in immunoassay [273–275] but also for the supersensitive detection of nucleotide sequences [82, 223, 276, 277]. In their pioneering works, Raschke et al. [278] and McFarland et al. [279] obtained record-high sensitivity of such sensors in the zeptomolar range, and they showed the possibility of detecting spectra of resonance scattering from individual particles. This opens up the way to the recording of intermolecular interactions at the level of individual molecules [251, 280]. To make the response stronger, investigators often use avidin–biotin, barnase–barstar, and other systems [281]. In addition, GNPs are applied in other analytical methods (various versions of chromatography, electrophoresis, and mass spectrometry) [282].

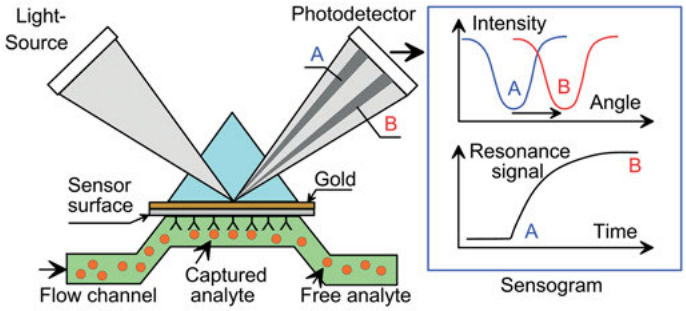


**Fig. 2.5:** Typical setup for analyte detection in a BIAcore-type SPR biosensor. The instrument detects changes in the local refractive index near a thin gold layer coated by a sensor surface with probing molecules. SPR is observed as a minimum in the reflected light intensity at an angle dependent on the mass of captured analyte. The minimum SPR angle shifts from A to B when the analyte binds to the sensor surface. The sensogram is a plot of resonance angle versus time that allows for real-time monitoring of an association/dissociation cycle. Reprinted with permission from [18]. Copyright 2012 Royal Society of Chemistry.

SPR and LSPR biosensors were compared in side-by-side experiments by Yonzon et al. [283] for concanavilin A binding to monosaccharides and by Svedendahl et al. [284] for biotin–streptavidin binding. It was found that both techniques demonstrate similar performance. As the bulk refractive index sensitivity is known to be higher for SPR, the above similarity was attributed to the long decay length of propagating plasmons, compared with the localized ones. The overall comparison of SPR and LSPR sensors can be found in [251, 255].

Future development of low-cost SPR and LSPR biomedical sensors needs increasing the detection sensitivity and creating substrates that can operate in biological fluids and can be easy to functionalize with probing molecules, to clean, and to reuse [285, 286].

A special class of plasmonic sensors is based on SERS nanoplatforms that can be divided into two main subclasses. The first includes top-down approaches, in which a metal layer is controllably deposited on a parent rough or nanoscale arranged surface. Well-known examples are SERS substrates fabricated by use of nanosphere lithography [287] or "film-over-spheres" platforms [288]. The second consists in the bottom-up formation of metal NP aggregates or self-assembled NP structures. Thanks to the recent progress in metal NP synthesis, the published examples of bottom-up SERS substrates include assemblies made of noble metal nanospheres [289], nanorods [290–292], nanostars [293–295], and other NP types. For improving the reproducibility of self-assembling processes, parent microstructures such as micron-sized pillars [296], elastomeric templates [297, 298], and colloidal silica crystals

[299, 300] have been proposed. Quite recently, a novel type of multilayered SERS probes with embedded Raman reporters has been proposed (see, e. g. [301, 302] and references therein). Such SERS multilayered structures, also called nanomatryoshkas (NMs) have great potential for analytical applications owing to several advantages: (1) Raman molecules are protected from desorption, subjected to a strongly enhanced electromagnetic field in the gap and their SERS response does not depend on the environmental conditions; (2) owing to bright and uniform spectral pattern, NMs provide a linear correlation between probe concentration and SERS intensity and allow for a real-time *in vivo* imaging and high throughput sensing with short integration times; (3) NM probes can be multiplexed by incorporating different Raman molecules into multilayered NMs.

An important analytical task is a rapid, simple, and sensitive detection of pesticides [303, 304]. From this point of view, SERS seems very promising due to the fingerprint nature of SERS spectra, low-spectrum accumulation time, and accessibility of cheap and portable Raman devices. But many pesticides usually have very small Raman cross sections and a low affinity for gold or silver surfaces. For example, in the first pesticide study, Alak and Vo-Dinh [305] demonstrated that an accidentally spilled pesticide can be detected in soil samples only when present at a high concentration (1.25 % by weight). More recent studies have focused on the development of SERS substrates and their testing with simple pesticide solutions [306–310], but only few were aimed at real-life detection. For example, Shende et al. [311] conducted rapid SERS detection of 50 parts-per-billion of Chlorpyrifos-methyl artificially added to orange juice. The overall time of analysis was about 12 min, including the time taken by solvent and solid-phase extraction.

In our work [312], we employed a simple wet-chemical approach to fabricate centimeter-scale gold nanoisland films (NIFs) with tunable morphology of islands, strong electromagnetic coupling between them, and with excellent reproducibility. The optimized NIFs demonstrated the Raman scattering enhancement factor of $3 \times 10^8$, as found by use of 1,4-aminothiophenol Raman reporters. In principle, such enhancement factors are large enough to enable the detection of single-molecule responses. Variations in SERS response were as low as 6 % in point-to-point and batch-to-batch measurements. As the large-area NIFs are easy and cheap to make, they can be helpful in label-free immunoassays, biosensing, and fast detection of pesticides. As an example, thiram fungicide concentrations at least 100-fold lower than the levels currently permissible in farming were fast detected on apple peels. Specifically, the NIF-based label-free SERS technology detected thiram on apple peel down to level of 5 ng/cm$^2$ (Fig. 2.6), which is almost one order lower than that reported previously [310].

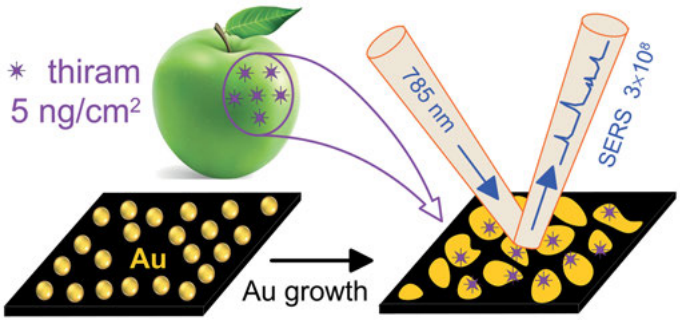


**Fig. 2.6:** Schematic illustration of the gold NIF fabrication through overgrowth of gold seeds and SERS detection of thiram fungicide in apple peals with sensitivity 5 ng/cm$^2$. Reprinted with permission from [312]. Copyright 2015 American Chemical Society.

## 2.6 Conclusions

GNP conjugates have found numerous applications in analytical research based on both state-of-the-art instrumental methods and simple solid-phase or homophase techniques (dot assay, immunochromatography, etc.). The following two examples are illustrative: (1) by using GNP–antibody conjugates, it is possible to detect a prostate-specific antigen with a sensitivity that is millionfold greater than that in the ELISA [313]. (2) The sharp dependence of the color of the system on interparticle distances enables mutant DNAs to be detected visually in a test known as the Northwestern spot test [83]. Along with the literature examples of clinical diagnostics of cancer, Alzheimer's disease, AIDS, hepatitis, tuberculosis, diabetes, and other diseases, new diagnostic application of GNPs should be expected. Progress in this direction will be determined by success achieved in increasing the sensitivity of analytical tests with retention of the simplicity of detection. The limitations of homophasic methods with visual detection are due to the need to use a large number (on the order of $10^{10}$ [314]) of NPs. Even at the minimal ratio between target molecules and particles (1:1), the detection limit will be on the order of 0.01 pM, which is considerably (millionfold) higher than the quantity of target molecules that needs to be detected, for example, in typical biopsy samples [314]. Thus, sensitivity can be improved either by enhancing the signal (polymerase chain reaction, autometallography, etc.) or by using sensitive instrumental methods. For instance, single-particle instrumental methods [280] have a single-molecule detection limit that is attainable in principle. Specifically, the SERS is a trend technique to detect very low concentrations of solutes (see, e. g., the recent review and reports by Liz-Marzán and coworkers [315–317] regarding SERS detection of biological molecules). However, the topical problem is to create multiplex sensitive tests that do not require equipment and can be performed by the end used under non-laboratory conditions. An example of the prototype of such devices is Pro Strips™,

which can simultaneously detect five threads: antrax, ricin toxin, botulinum toxin, *Yersinia pestis* (plague), and staphylococcal enterotoxin B. The physical basis of the new tests may be associated with the dependence of the plasmon resonance wavelength on the local dielectric environment or on the interparticle distance.

**Acknowledgments:** This research was supported by a grant from the Russian Scientific Foundation 15-14-00002.

## References

[1] Antonii F. *Panacea Aurea-Auro Potabile*. Hamburg, Bibliopolio Frobeniano, 1618.
[2] Antonio Neri RP. *L'arte Vetraria*. Firenze, Nella Stamperia de'Giunti, 1612.
[3] de Planis-Campy D. *Traicté de la vraye, unique, grande, et universelle médecine des anciens dite des recens, or potable*. Paris, François Targa, 1633.
[4] Heicher HH. *Aurum Potabile, Oder Gold-Tinctur*. Breslau, Lepzig, J. Herbord Klossen, 1712.
[5] Faraday M. Experimental relations of gold (and others metals) to light. *Phil Trans Royal Soc (Lond)* 1857, 147, 145–81.
[6] Zsigmondy R. Ueber wassrige Lösungen metallischen Goldes. *Ann Chem* 1898, 301, 29–54.
[7] Svedberg T. *Die Methoden zur Herstellung kolloider Lösungen anorganischer Stoffe*. Dresden, Theodor Steinkopff, 1909.
[8] Lange C. Die Ausflockung kolloidalen Goldes durch Zerebrospinalflüssigkeit bei luetischen Affektionen des Zentralnervensystems. *Ztschr f Chemotherap* 1912, 1, 44–78.
[9] Bredig G. Darstellung colloidaler Metallösungen durch elektrische Zerstäubung. *Z angew Chem* 1898, 11, 951–4.
[10] Kabashin AV, Delaporte P, Perreira A, et al. Nanofabrication with pulsed lasers. *Nanoscale Res Lett* 2010, 5, 454–63.
[11] Borowskaja DP. Zur Methodik der Goldsolbereitung. *Ztschr f Immunitatsforsch u exper Therap* 1934, 82, 178–82.
[12] Turkevich J, Stevenson PC, Hillier J. A study of the nucleation and growth processes in the synthesis of colloidal gold. *Discuss Faraday Soc* 1951, 11, 55–75.
[13] Frens G. Controlled nucleation for the regulation of the particle size in monodisperse gold suspensions. *Nature Phys Sci* 1973, 241, 20–2.
[14] Faulk W, Taylor G. An immunocolloid method for the electron microscope. *Immunochemistry* 1971, 8, 1081–3.
[15] Hermanson GT. *Bioconjugate Techniques*. San Diego, Academic Press, 1996.
[16] Glomm WR. Functionalized gold nanoparticles for applications in bionanotechnology. *J Dispers Sci Technol* 2005, 26, 389–414.
[17] Sapsford KE, Algar WR, Berti L, Gemmill KB, Casey BJ, Oh E et al. Functionalizing nanoparticles with biological molecules: developing chemistries that facilitate nanotechnology. *Chem Rev* 2013, 113, 1904–2074.
[18] Dykman LA, Khlebtsov NG. Gold nanoparticles in biomedical applications: recent advances and perspectives. *Chem Soc Rev* 2012, 41, 2256–82.
[19] Dreaden EC, Alkilany AM, Huang X, Murphy CJ, El-Sayed MA. The golden age: gold nanoparticles for biomedicine. *Chem Soc Rev* 2012, 41, 2740–79.

[20] Khlebtsov NG, Dykman LA. Optical properties and biomedical applications of plasmonic nanoparticles. *J Quant Spectrosc Radiat Transfer* 2010, 111, 1–35.
[21] Dykman LA, Khlebtsov NG. Multifunctional gold-based nanocomposites for theranostics. *Biomaterials* 2016, 108, 13–34.
[22] Lammers T, Aime S, Hennink WE, Storm G, Kiessling F. Theranostic nanomedicine. *Acc Chem Res* 2011, 44, 1029–38.
[23] Khlebtsov NG, Bogatyrev VA, Dykman LA et al. Analytical and theranostic applications of gold nanoparticles and multifunctional nanocomposites. *Theranostics 2013*, 3, 167–80.
[24] Funkhouser J. Reinventing pharma: the theranostic revolution. *Curr Drug Discov* 2002, 2, 17–9.
[25] Picard FJ, Bergeron MG. Rapid molecular theranostics in infectious diseases. *Drug Discov Today* 2002, 7, 1092–101.
[26] Lukianova-Hleb E, Hanna EY, Hafner JH, Lapotko DO. Tunable plasmonic nanobubbles for cell theranostics. *Nanotechnology* 2010, 21, 085102.
[27] Warner S. Diagnostics + therapy = theranostics. *Scientist* 2004, 18, 38–9.
[28] Kelkar SS, Reineke TM. Theranostics: combining imaging and therapy. *Bioconjug Chem* 2011, 22, 1879–903.
[29] Leuvering JHW, Thal PJHM,van der Waart M, Schuurs AHWM. Sol particle immunoassay (SPIA). *J Immunoassay* 1980, 1, 77–91.
[30] Khlebtsov NG. Optical models for conjugates of gold and silver nanoparticles with biomacromolecules. *J Quant Spectrosc Radiat Transfer* 2004, 89, 143–52.
[31] Khlebtsov NG, Melnikov AG, Dykman LA, Bogatyrev VA. Optical properties and biomedical applications of nanostructures based on gold and silver bioconjugates. In: Videen G, Yatskiv YS, Mishchenko MI, eds. *Photopolarimetry in Remote Sensing*. Dordrecht, Kluwer Acad Publ, 2004, 265–308.
[32] Wu SH, Wu YS, Chen CH. Colorimetric sensitivity of gold nanoparticles: minimizing interparticular repulsion as a general approach. *Anal Chem* 2008, 80, 6560–6.
[33] Tsai CS, Yu TB, Chen CT. Gold nanoparticle-based competitive colorimetric assay for detection of protein-protein interactions. *Chem Commun (Camb)* 2005, 34, 4273–5.
[34] Englebienne P, van Hoonacker A, Verhas M, Khlebtsov NG. Advances in high-throughput screening: biomolecular interaction monitoring in real-time with colloidal metal nanoparticles. *Comb Chem High Throughput Screen* 2003, 6, 777–87.
[35] Zhang Y, McKelvie ID, Cattrall RW, Kolev SD. Colorimetric detection based on localised surface plasmon resonance of gold nanoparticles: merits, inherent shortcomings and future prospects. *Talanta* 2016, 152, 410–22.
[36] Leuvering JHW, Coverde BC, Thal PJHM, Schuurs AHWM. A homogeneous sol particle immunoassay for human chorionic gonadotrophin using monoclonal antibodies. *J Immunol Meth* 1983, 60, 9–23.
[37] Deelder AM, Dozy MH. Applicability of sol particle immunoassay (SPIA) for detection of *Schistosoma mansoni* circulating antigens. *Acta Leiden* 1982, 48, 17–22.
[38] Wielaard F, Denissen A, van der Veen L, Rutjes I. A sol-particle immunoassay for determination of anti-rubella antibodies. Development and clinical validation. *J Virol Meth* 1987, 17, 149–58.
[39] Zeisler R, Stone SF, Viscidi RP, Cerny EH. Sol particle immunoassays using colloidal gold and neutron activation. *J Radioanal Nucl Chem* 1993, 167, 445–52.
[40] Gasparyan VK. Hen egg immunoglobulin Y in colloidal gold agglutination assay: comparison with rabbit immunoglobulin *G. J Clin Lab Anal* 2005, 19, 124–7.
[41] Pavlov V, Xiao Y, Shlyahovsky B, Willner I. Aptamer-functionalized Au nanoparticles for the amplified optical detection of thrombin. *J Am Chem Soc* 2004, 126, 11768–9.
[42] Aslan K, Lakowicz JR, Geddes CD. Nanogold-plasmon-resonance-based glucose sensing. *Anal Biochem* 2004, 330, 145–55.

[43] Liao Y-J, Shiang Y-C, Chen L-Y, Hsu C-L, Huang C-C, Chang H-T. Detection of adenosine triphosphate through polymerization-induced aggregation of actin-conjugated gold/silver nanorods. *Nanotechnology* 2013, 24, 444003.
[44] Zhu J, Yu Z, Li J-j, Zhao J-w. Coagulation induced attenuation of plasmonic absorption of Au nanorods: Application in ultra sensitive detection of alpha-fetoprotein. *Sens Actuators B* 2013, 188, 318–25.
[45] Byun JY, Shin YB, Li T, et al. The use of an engineered single chain variable fragment in a localized surface plasmon resonance method for analysis of the C-reactive protein. *Chem Commun* 2013, 49, 9497–9.
[46] Truong PL, Choi SP, Sim SJ. Amplification of resonant Rayleigh light scattering response using immunogold colloids for detection of lysozyme. *Small* 2013, 9, 3485–92.
[47] Inoue K, Aomatsu T, Yoden A, Okuhira T, Kaji E, Tamai H. Usefulness of a novel and rapid assay system for fecal calprotectin in pediatric patients with inflammatory bowel diseases. *J Gastroenterol Hepatol* 2014, 29, 1406–12.
[48] Nekouian R, Khalife NJ, Salehi Z. Anti human fibronectin – gold nanoparticle complex, a potential nanobiosensor tool for detection of fibronectin in ECM of cultured cells. *Plasmonics* 2014, 9, 1417–23.
[49] Tanaka M, Saito Y, Misu H, et al. Development of a sol particle homogeneous immunoassay for measuring full-length selenoprotein P in human serum. *J Clin Lab Anal* 2016, 30, 114–22.
[50] Medley CD, Smith JE, Tang Z, Wu Y, Bamrungsap S, Tan W. Gold nanoparticle-based colorimetric assay for the direct detection of cancerous cells. *Anal Chem* 2008, 80, 1067–72.
[51] Zhang K, Shen X. Cancer antigen 125 detection using the plasmon resonance scattering properties of gold nanorods. *Analyst* 2013, 138, 1828–34.
[52] Chirathaworn C, Chantaramalai T, Sereemaspun A, Kongthong N, Suwancharoen D. Detection of *Leptospira* in urine using anti-*Leptospira*-coated gold nanoparticles. *Comp Immunol Microbiol Infect Dis* 2011, 34, 31–4.
[53] Lesniewski A, Los M, Jonsson-Niedziółka M, et al. Antibody modified gold nanoparticles for fast and selective, colorimetric T7 bacteriophage detection. *Bioconjug Chem* 2014, 25, 644–8.
[54] Liu Y, Zhang L, Wei W, et al. Colorimetric detection of influenza A virus using antibody-functionalized gold nanoparticles. *Analyst* 2015, 140, 3989–95.
[55] Neely A, Perry C, Varisli B, et al. Ultrasensitive and highly selective detection of Alzheimer's disease biomarker using two-photon Rayleigh scattering properties of gold nanoparticle. *ACS Nano* 2009, 3, 2834–40.
[56] Guarise C, Pasquato L, De Filippis V, Scrimin P. Gold nanoparticles-based protease assay. *Proc Natl Acad Sci USA* 2006, 103, 3978–82.
[57] Huang H, Liu F, Huang S, et al. Sensitive and simultaneous detection of different disease markers using multiplexed gold nanorods. *Anal Chim Acta* 2012, 755, 108–14.
[58] Andresen H, Mager M, Grießner M, et al. Single-step homogeneous immunoassays utilizing epitope-tagged gold nanoparticles: on the mechanism, feasibility, and limitations. *Chem Mater* 2014, 26, 4696–704.
[59] Liu H, Rong P, Jia H, et al. A wash-free homogeneous colorimetric immunoassay method. *Theranostics* 2016, 6, 54–64.
[60] Kashid SB, Tak RD, Raut RW. Antibody tagged gold nanoparticles as scattering probes for the pico molar detection of the proteins in blood serum using nanoparticle tracking analyzer. *Colloids Surf B* 2015, 133, 208–13.
[61] Yeo ELL, Chua AJS, Parthasarathy K, Yeo HY, Ng ML, Kah JCY. Understanding aggregation-based assays: nature of protein corona and number of epitopes on antigen matters. *RSC Adv* 2015, 5, 14982–93.

[62] Liu X, Dai Q, Austin L, et al. A one-step homogeneous immunoassay for cancer biomarker detection using gold nanoparticle probes coupled with dynamic light scattering. *J Am Chem Soc* 2008, 130, 2780–2.
[63] Wang X, Li Y, Wang H, et al. Gold nanorod-based localized surface plasmon resonance biosensor for sensitive detection of hepatitis B virus in buffer, blood serum and plasma. *Biosens Bioelectron* 2010, 26, 404–10.
[64] Dykman LA, Krasnov YM, Bogatyrev VA, Khlebtsov NG. Quantitative immunoassay method based on extinction spectra of colloidal gold bioconjugates. *Proc SPIE* 2001, 4241, 37–41.
[65] Khlebtsov NG, Bogatyrev VA, Khlebtsov BN, Dykman LA, Englebienne P. A multilayer model for gold nanoparticle bioconjugates: application to study of gelatin and human IgG adsorption using extinction and light scattering spectra and the dynamic light scattering method. *Colloid J* 2003, 65, 622–35.
[66] Englebienne P. Use of colloidal gold surface plasmon resonance peak shift to infer affinity constants from the interactions between protein antigens and antibodies specific for single or multiple epitopes. *Analyst* 1998, 123, 1599–603.
[67] Sakashita H, Tomita A, Umeda Y, et al. Homogeneous immunoassay using photothermal beam deflection spectroscopy. *Anal Chem* 1995, 67, 1278–82.
[68] Thanh NTK, Rees JH, Rosenzweig Z. Laser-based double beam absorption detection for aggregation immunoassays using gold nanoparticles. *Anal Bioanal Chem* 2002, 374, 1174–8.
[69] Zhang CX, Zhang Y, Wang X, Tang ZM, Lu ZH. Hyper-Rayleigh scattering of protein-modified gold nanoparticles. *Anal Biochem* 2003, 320, 136–40.
[70] Khlebtsov NG, Bogatyrev VA, Melnikov AG, Dykman LA, Khlebtsov BN, Krasnov YM. Differential light-scattering spectroscopy: a new approach to studying of colloidal gold nanosensors. *J Quant Spectrosc Radiat Transfer* 2004, 89, 133–42.
[71] Huo Q. Protein complexes/aggregates as potential cancer biomarkers revealed by a nanoparticle aggregation immunoassay. *Colloids Surf B* 2010, 78, 259–65.
[72] Kamnev AA, Dykman LA, Tarantilis PA, Polissiou MG. Spectroimmunochemistry using colloidal gold bioconjugates. *Biosci Reports* 2002, 22, 541–7.
[73] Aroca RF, Ross DJ, Domingo C. Surface-enhanced infrared spectroscopy. *Appl Spectrosc* 2004, 58, 324A–338A.
[74] López-Lorente ÁI, Mizaikoff B. Recent advances on the characterization of nanoparticles using infrared spectroscopy. *Trends Anal Chem* 2016, 84, 97–106.
[75] Porter MD, Lipert RJ, Siperko LM, Wang G, Narayanan R. SERS as a bioassay platform: fundamentals, design, and applications. *Chem Soc Rev* 2008, 37, 1001–11.
[76] Kneipp K, Kneipp H, Kneipp J. Surface-enhanced Raman scattering in local optical fields of silver and gold nanoaggregates – from single-molecule Raman spectroscopy to ultrasensitive probing in live cells. *Acc Chem Res* 2006, 39, 443–50.
[77] Ding S-Y, Yi J, Li J-F, et al. Nanostructure-based plasmon-enhanced Raman spectroscopy for surface analysis of materials. *Nat Rev Mater* 2016, 1, 16021.
[78] Khlebtsov N, Khlebtsov B. *Plasmonic SERS Substrates and Probes*. Saarbrücken, Lambert Academic Publ, 2016.
[79] Fazio B, D'Andrea C, Foti A, et al. SERS detection of biomolecules at physiological pH via aggregation of gold nanorods mediated by optical forces and plasmonic heating. *Sci Rep 2016*, 6, 26952.
[80] Stoschek CM. Protein assay sensitive at nanogram levels. *Anal Biochem* 1987, 160, 301–5.
[81] Dykman LA, Bogatyrev VA, Khlebtsov BN, Khlebtsov NG. A protein assay based on colloidal gold conjugates with trypsin. *Anal Biochem* 2005, 341, 16–21.
[82] Mirkin CA, Letsinger RL, Mucic RC, Storhoff JJ. A DNA-based method for rationally assembling nanoparticles into macroscopic materials. *Nature* 1996, 382, 607–9.

[83] Elghanian R, Storhoff JJ, Mucic RC, Letsinger RL, Mirkin CA. Selective colorimetric detection of polynucleotides based on the distance-dependent optical properties of gold nanoparticles. *Science* 1997, 277, 1078–81.
[84] Sato K, Onoguchi M, Sato Y, Hosokawa K, Maeda M. Non-cross-linking gold nanoparticle aggregation for sensitive detection of single-nucleotide polymorphisms: optimization of the particle diameter. *Anal Biochem* 2006, 350, 162–4.
[85] Baptista PV, Koziol-Montewka M, Paluch-Oles J, Doria G, Franco R. Gold-nanoparticle-probe-based assay for rapid and direct detection of Mycobacterium tuberculosis DNA in clinical samples. *Clin Chem* 2006, 52, 1433–4.
[86] Dai Q, Liu X, Coutts J, Austin L, Huo Q. A one-step highly sensitive method for DNA detection using dynamic light scattering. *J Am Chem Soc* 2008, 130, 8138–9.
[87] Zhang J, Wang L, Pan D, et al. Visual cocaine detection with gold nanoparticles and rationally engineered aptamer structures. *Small* 2008, 8, 1196–200.
[88] Wang LH, Liu XF, Hu XF, Song SP, Fan CF. Unmodified gold nanoparticles as a colorimetric probe for potassium DNA aptamers. *Chem Commun (Camb)* 2006, 36, 3780–2.
[89] Li HX, Rothberg L. Colorimetric detection of DNA sequences based on electrostatic interactions with unmodified gold nanoparticles. *Proc Natl Acad Sci USA* 2004, 101, 14036–9.
[90] He W, Huang CZ, Li YF, et al. One-step label-free optical genosensing system for sequence-specific DNA related to the human immunodeficiency virus based on the measurements of light scattering signals of gold nanorods. *Anal Chem* 2008, 80, 8424–30.
[91] Storhoff JJ, Elghanian R, Mucic RC, Mirkin CA, Letsinger RL. One-pot colorimetric differentiation of poly-nucleotides with single base imperfections using gold nano-particle probes. *J Am Chem Soc* 1998, 120, 1959–64.
[92] Witten KG, Bretschneider JC, Eckert T, Richtering W, Simon U. Assembly of DNA-functionalized gold nanoparticles studied by UV/Vis-spectroscopy and dynamic light scattering. *Phys Chem Chem Phys* 2008, 10, 1870–5.
[93] Sato K, Hosokawa K, Maeda M. Rapid aggregation of gold nanoparticles induced by non-cross-linking DNA hybridization. *J Am Chem Soc* 2003, 125, 8102–3.
[94] Doria G, Franco R, Baptista P. Nanodiagnostics: fast colorimetric method for single nucleotide polymorphism/mutation detection. *IET Nanobiotechnol* 2007, 1, 53–7.
[95] Song J, Li Z, Cheng Y, Liu C. Self-aggregation of oligonucleotide-functionalized gold nanoparticles and its applications for highly sensitive detection of DNA. *Chem Commun (Camb)* 2010, 46, 5548–50.
[96] Shawky SM, Bald D, Azzazy HME. Direct detection of unamplified hepatitis C virus RNA using unmodified gold nanoparticles. *Clin Biochem* 2010, 43, 1163–8.
[97] Xia F, Zuo X, Yang R, et al. Colorimetric detection of DNA, small molecules, proteins, and ions using unmodified gold nanoparticles and conjugated polyelectrolytes. *Proc Natl Acad Sci USA* 2010, 107, 10837–41.
[98] Ma Z, Tian L, Wang T, Wang C. Optical DNA detection based on gold nanorods aggregation. *Anal Chim Acta* 2010, 673, 179–84.
[99] Pylaev TE, Khanadeev VA, Khlebtsov BN, Dykman LA, Bogatyrev VA, Khlebtsov NG. Colorimetric and dynamic light scattering detection of DNA sequences by using positively charged gold nanospheres: a comparative study with gold nanorods. *Nanotechnology* 2011, 22, 285501.
[100] Soo PC, Horng YT, Chang KC, et al. A simple gold nanoparticle probes assay for identification of *Mycobacterium tuberculosis* and *Mycobacterium tuberculosis* complex from clinical specimens. *Mol Cell Probes* 2009, 23, 240–6.
[101] Liandris E, Gazouli M, Andreadou M, et al. Direct detection of unamplified DNA from pathogenic mycobacteria using DNA-derivatized gold nanoparticles. *J Microbiol Methods* 2009, 78, 260–4.

[102] Storhoff JJ, Marla SS, Bao P, et al. Gold nanoparticle-based detection of genomic DNA targets on microarrays using a novel optical detection system. *Biosens Bioelectron* 2004, 19, 875–83.
[103] Storhoff JJ, Lucas AD, Garimella V, Bao YP, Müller UR. Homogeneous detection of unamplified genomic DNA sequences based on colorimetric scatter of gold nanoparticle probes. *Nat Biotechnol* 2004, 22, 883–7.
[104] Parab HJ, Jung C, Lee JH, Park HG. A gold nanorod-based optical DNA biosensor for the diagnosis of pathogens. *Biosens Bioelectron* 2010, 26, 667–73.
[105] Wang X, Li Y, Wang J, et al. A broad-range method to detect genomic DNA of multiple pathogenic bacteria based on the aggregation strategy of gold nanorods. *Analyst* 2012, 137, 4267–73.
[106] Deng H, Zhang X, Kumar A, Zou G, Zhang X, Liang X-J. Long genomic DNA amplicons adsorption onto unmodified gold nanoparticles for colorimetric detection of Bacillus anthracis. *Chem Commun (Camb)* 2013, 49, 51–3.
[107] Kalidasan K, Neo JL, Uttamchandani M. Direct visual detection of Salmonella genomic DNA using gold nanoparticles. *Mol BioSyst* 2013, 9, 618–21.
[108] Khalil MAF, Azzazy HME, Attia AS, Hashem AGM. A sensitive colorimetric assay for identification of Acinetobacter baumannii using unmodified gold nanoparticles. *J Appl Microbiol* 2014, 117, 465–71.
[109] Brada D Roth J. "Golden blot"–detection of polyclonal and monoclonal antibodies bound to antigens on nitrocellulose by protein A – gold complexes. *Anal Biochem* 1984, 142, 79–83.
[110] Moeremans M, Daneles G, van Dijck A, Langanger G, De Mey J. Sensitive visualization of antigen-antibody reactions in dot and blot immune overlay assays with immunogold and immunogold/silver staining. *J Immunol Meth* 1984, 74, 353–60.
[111] Surek B, Latzko E. Visualization of antigenic proteins blotted onto nitrocellulose using the immuno-gold-staining (IGS)-method. *Biochem Biophys Res Commun* 1984, 121, 284–9.
[112] Hsu Y-H. Immunogold for detection of antigen on nitrocellulose paper. *Anal Biochem* 1984, 142, 221–5.
[113] Bio-Rad Lab. Western Blotting Detection Systems: How Do You Choose?. *Bulletin 1310*. Richmond, Bio-Rad Lab, 1987.
[114] Edwards P, Wilson T. Choose your labels. *Lab Pract* 1987, 36, 13–7.
[115] Goldman A, Harper S, Speicher DW. Detection of proteins on blot membranes. *Curr Protoc Protein Sci* 2016, 86, 10.8.1–10.8.11.
[116] Danscher G. Localization of gold in biological tissue. A photochemical method for light and electron microscopy. *Histochemistry* 1981. 71. 81–8.
[117] Ma Z, Sui S-F. Naked-eye sensitive detection of immunoglobulin G by enlargement of Au nanoparticles in vitro. *Angew Chem Int Ed* 2002, 41, 2176–9.
[118] Hou S-Y, Chen H-K, Cheng H-C, Huang, C-Y. Development of zeptomole and attomolar detection sensitivity of biotin-peptide using a dot-blot gold nanoparticle immunoassay. *Anal Chem* 2007, 79, 980–5.
[119] Blab GA, Cognet L, Berciaud S, et al. Optical readout of gold nanoparticle-based DNA microarrays without silver enhancement. *Biophys J* 2006, 90, L13–L15.
[120] Dykman LA, Bogatyrev VA. Colloidal gold in solid-phase assays. A review. *Biochemistry (Moscow)* 1997, 62, 350–6.
[121] Steffen W, Linck RW. Multiple immunoblot: a sensitive technique to stain proteins and detect multiple antigens on a single two-dimensional replica. *Electrophoresis* 1989, 10, 714–8.
[122] Poltavchenko AG, Zaitsev BN, Ersh AV, et al. The selection and optimization of the detection system for self-contained multiplexed dot-immunoassay. *J Immunoassay Immunochem* 2016, 37, 540–54.
[123] Petchclai B, Hiranras S, Potha U. Gold immunoblot analysis of IgM-specific antibody in the diagnosis of human leptospirosis. *Am J Trop Med Hyg* 1991, 45, 672–5.

[124] Scott JM, Shreffler WG, Ghalib HW, et al. A rapid and simple diagnostic test for active visceral leishmaniasis. *Am J Trop Med Hyg* 1991, 44, 272–7.
[125] Liu YS, Du WP, Wu ZX. Dot-immunogold-silver staining in the diagnosis of cysticercosis. *Int J Parasitol* 1996, 26, 127–9.
[126] Liu YS, Du WP, Wu YM, et al. Application of dot-immunogold-silver staining in the diagnosis of clonorchiasis. *J Trop Med Hyg* 1995, 98, 151–4.
[127] Thiruppathiraja C, Kamatchiammal S, Adaikkappan P, Alagar M. An advanced dual labeled gold nanoparticles probe to detect *Cryptosporidium parvum* using rapid immuno-dot blot assay. *Biosens Bioelectron* 2011, 26, 4624–7.
[128] Feodorova VA, Polyanina TI, Zaytsev SS, Laskavy VN, Ulianova OV, Dykman LA. Development of dot-ELISA for the screening rapid diagnosis of chlamydial infection in sheep. *Veterinariya* 2015, 8, 21–4 (in Russian).
[129] Chu F, Ji Q, Yan R-M. Study on using colloidal gold immuno-dot assay to detect special antibody of hemorrhagic fever renal syndrome. *Chin J Integr Tradit West Med* 2001, 21, 504–6 (in Chinese).
[130] Dar VS, Ghosh S, Broor S. Rapid detection of rotavirus by using colloidal gold particles labeled with monoclonal antibody. *J Virol Meth* 1994, 47, 51–8.
[131] Fernandez D, Valle I, Llamos R, Guerra M, Sorell L, Gavilondo J. Rapid detection of rotavirus in feces using a dipstick system with monoclonal-antibodies and colloidal gold as marker. *J Virol Meth* 1994, 48, 315–23.
[132] Yee JL, Jennings MB, Carlson JR, Lerche NW. A simple, rapid immunoassay for the detection of simian immunodeficiency virus antibodies. *Lab Anim Sci* 1991, 41, 119–22.
[133] Reboli AC. Diagnosis of invasive candidiasis by a dot immunobinding assay for candida antigen-detection. *J Clin Microbiol* 1993, 31, 518–23.
[134] Poulain D, Mackenzie DW, van Cutsem J. Monoclonal antibody-gold silver staining dot assay for the detection of antigenaemia in candidosis. *Mycoses* 1991, 34, 221–6.
[135] Vera-Cabrera L, Rendon A, Diaz-Rodriguez M, Handzel V, Laszlo A. Dot blot assay for detection of antidiacyltrehalose antibodies in tuberculous patients. *Clin Diagn Lab Immunol* 1999, 6, 686–9.
[136] Staroverov SA, Vidyasheva IV, Fomin AS, et al. Development of immunogold diagnostic systems for identification of the causative agent of tuberculosis in situ. *Russ Vet J* 2011, 2, 29–32 (in Russian).
[137] Hou D, Wang X, Huang Y. Diagnostic value of gold standard method detecting of serum anti-TB antibody on TB. *Chinese Med Factory Mine* 2001, 14, 413–4.
[138] Kunakorn M, Petchclai B, Khupulsup K, Naigowit P. Gold blot for detection of immunoglobulin M (IgM)- and IgG-specific antibodies for rapid serodiagnosis of melioidosis. *J Clin Microbiol* 1991, 29, 2065–7.
[139] Huang Q, Lan X, Tong T, et al. Dot-immunogold filtration assay as a screening test for syphilis. *J Clin Microbiol* 1996, 34, 2011–3.
[140] Zagoskina TY, Markov EY, Kalinovskiĭ AI, Golubinskiĭ EP. Use of specific antibodies, labeled with colloidal gold particles, for the detection of Brucella antigens using dot-immunoassay. *Zh Mikrobiol Epidemiol Immunobiol* 1998, 6, 64–9 (in Russian).
[141] Lazarchik VA, Titov LP, Vorobyova TN, Ermakova TS, Vrublevskaya ON, Vlasik NV. Test-system based on antibacterial antibody conjugates with colloidal gold for revelation of shigella antigens in biological liquids. *Proc Natl Acad Sci Belarus* 2005, 3, 44–7 (in Russian).
[142] Kamma S, Tang L, Leung K, Ashton E, Newman N, Suresh MR. A rapid two dot filter assay for the detection of E. coli O157 in water samples. *J Immunol Methods* 2008, 336, 159–65.
[143] Fang SB, Tseng WY, Lee HC, Tsai CK, Huang JT, Hou SY. Identification of Salmonella using colony-print and detection with antibody-coated gold nanoparticles. *J Microbiol Methods* 2009, 77, 225–8.

[144] Pandey SK, Suri CR, Chaudhry M, Tiwari RP, Rishi P. A gold nanoparticles based immunobioprobe for detection of Vi capsular polysaccharide of Salmonella enterica serovar Typhi. *Mol BioSyst* 2012, 8, 1853–60.
[145] Khadzhu A, Ivaschenko SV, Fomin AS, Scherbakov AA, Staroverov SA, Dykman LA. Usage of hyperimmune serum obtained for the DMSO-antigen of intestinal yersiniosis microbe in the indirect dot-immunoanalysis with colloidal gold conjugate. *Sci Rev* 2015, 5, 30–4 (in Russian).
[146] Noskova OA, Zagoskina TY, Subycheva EN, et al. Application of dot-immunoassay for detection of plague agent antigens in the field samples. *Prob Particul Dang Inf* 2014, 4, 69–71 (in Russian).
[147] Xu Z. Immunogold dot assay for diagnosis of early pregnancy. *J Chin Med Assoc* 1992, 72, 216–8 (in Chinese).
[148] Matsuzawa S, Kimura H, Itoh Y, Wang H, Nakagawa T. A rapid dot-blot method for species identification of bloodstains. *J Forensic Sci* 1993, 38, 448–54.
[149] Cremers AF, Jansen in de Wal N, Wiegant J, et al. Non-radioactive in situ hybridization. A comparison of several immunocytochemical detection systems using reflection-contrast and electron microscopy. *Histochemistry* 1987, 86, 609–15.
[150] Kolodkina VL, Denisevich TN, Dykman LA, Vrublevskaya ON. Preparation of gold-labeled antibody probe and its use in dot-immunogold assay for detection of diphtheria toxin. *Med J* 2009, 2, 66–9 (in Russian).
[151] Staroverov SA, Volkov AA, Fomin AS, et al. The usage of phage mini-antibodies as a means of detecting ferritin concentration in animal blood serum. *J Immunoassay Immunochem* 2015, 36, 100–10.
[152] Wang YL, Li D, Ren W, Liu ZJ, Dong SJ, Wang EK. Ultrasensitive colorimetric detection of protein by aptamer – Au nanoparticles conjugates based on a dot-blot assay. *Chem Commun* 2008, 22, 2520–2.
[153] Wang C, Liu D, Wang Z. Gold nanoparticle based dot-blot immunoassay for sensitively detecting Alzheimer's disease related β-amyloid peptide. *Chem Commun* 2012, 48, 8392–4.
[154] Tavernaro I, Hartmann S, Sommer L, et al. Synthesis of tumor-associated MUC1-glycopeptides and their multivalent presentation by functionalized gold colloids. *Org Biomol Chem* 2015, 13, 81–97.
[155] Sui J, Lin H, Xu Y, Cao L. Enhancement of dot-immunogold filtration assay (DIGFA) by activation of nitrocellulose membranes with secondary antibody. *Food Anal Methods* 2011, 4, 245–50.
[156] Guo H, Zhang J, Yang D, Xiao P, He N. Protein array for assist diagnosis of acute myocardial infarction. *Colloids Surf B* 2005, 40, 195–8.
[157] Xi D, Luo X, Ning Q, Lu Q, Yao K, Liu Z. The detection of HBV DNA with gold nanoparticle gene probes. *J Nanjing Med Univ* 2007, 21, 207–12.
[158] Starodub NF, Artyukh VP, Nazarenko VI, Kolomiets LI. Protein immunoblot and immunodot in biochemical studies. *Ukr Biokhim Zh* 1987, 59, 108–20 (in Russian).
[159] Fenoll A, Jado I, Vicioso D, Casal J. Dot blot assay for the serotyping of pneumococci. *J Clin Microbiol* 1997, 35, 764–6.
[160] Bogatyrev VA, Dykman LA, Matora LY, Schwartsburd BI. Serotyping of azospirillae using a colloidal gold solid-phase immunoassay. *Microbiology* 1991, 60, 366–70.
[161] Bogatyrev VA, Dykman LA, Matora LY, Schwartsburd BI. The serotyping of Azospirillum Spp by cell gold immunoblotting. *FEMS Microbiol Lett* 1992, 96, 115–8.
[162] Dykman LA, Bogatyrev VA. Use of the dot-immunogold assay for the rapid diagnosis of acute enteric infections. *FEMS Immunol Med Microbiol* 2000, 27, 135–7.
[163] Matveev VY, Bogatyrev VA, Dykman LA, Matora LY, Schwartsburd BI. Cell surface physicochemical properties of the R- and S-variants of Azospirillum brasilense strain. *Microbiology* 1992, 61, 454–9.

[164] Gas F, Pinto L, Baus B, Gaufres L, Monoclonal antibody against the surface of Alexandrium minutum used in a whole-cell ELISA. *Harmful Algae* 2009, 8, 538–45.
[165] Khlebtsov BN, Dykman LA, Bogatyrev VA, Zharov V, Khlebtsov NG. A solid-phase dot assay using silica/gold nanoshells. *Nanoscale Res Lett* 2007, 2, 6–11.
[166] Khlebtsov BN, Khanadeev VA, Bogatyrev VA, Dykman LA, Khlebtsov NG. Use of gold nanoshells in solid-phase immunoassay. *Nanotechnol Russ* 2008, 3, 442–55.
[167] Khlebtsov BN, Khlebtsov NG. Enhanced solid-phase immunoassay using gold nanoshells: effect of nanoparticle optical properties. *Nanotechnology* 2008, 19, 435703.
[168] Panfilova E, Shirokov A, Khlebtsov B, Matora L, Khlebtsov N. Multiplexed dot immunoassay using Ag nanocubes, Au/Ag alloy nanoparticles, and Au/Ag nanoboxes. *Nano Res* 2012, 5, 124–34.
[169] Han A, Dufva M, Belleville E, Christensen CBV. Detection of analyte binding to microarrays using gold nanoparticle labels and a desktop scanner. *Lab Chip* 2003, 3, 329–32.
[170] Duan L, Wang Y, Li SS-c, Wan Z, Zhai J. Rapid and simultaneous detection of human hepatitis B virus and hepatitis C virus antibodies based on a protein chip assay using nano-gold immunological amplification and silver staining method. *BMC Infect Dis* 2005, 5, 53.
[171] Goryacheva IY, Lenain P, De Saeger S. Nanosized labels for rapid immunotests. *Trends Analyt Chem* 2013, 46, 30–43.
[172] Yang H-W, Tsai R-Y, Chen J-P, et al. Fabrication of a nanogold-dot array for rapid and sensitive detection of vascular endothelial growth factor in human serum. *ACS Appl Mater Interfaces* 2016, 8, 30845–52.
[173] Goryacheva I, ed. Rapid Immunotests for Clinical, Food and Environmental Applications. Amsterdam, Elsevier, 2016.
[174] Peruski AH, Peruski LF. Immunological methods for detection and identification of infectious disease and biological warfare agents. *Clin Diagn Lab Immunol* 2003, 10, 506–13.
[175] Long GW, O'Brien T. Antibody-based systems for the detection of Bacillus anthracis in environmental samples. *J Appl Microbiol* 1999, 87, 214.
[176] Bird CB, Miller RL, Miller BM. Reveal for Salmonella test system. *J AOAC Int* 1999, 82, 625–33.
[177] Wu SJ, Paxton H, Hanson B, et al. Comparison of two rapid diagnostic assays for detection of immunoglobulin M antibodies to dengue virus. *Clin Diagn Lab Immunol* 2000, 7, 106–10.
[178] Engler KH, Efstratiou A, Norn D, et al. Immunochromatographic strip test for rapid detection of diphtheria toxin: description and multicenter evaluation in areas of low and high prevalence of diphtheria. *J Clin Microbiol* 2002, 40, 80–3.
[179] Shyu RH, Shyu HF, Liu HW, Tang SS. Colloidal gold-based immunochromatographic assay for detection of ricin. *Toxicon* 2002, 40, 255–8.
[180] Chanteau S, Rahalison L, Ralafiarisoa L, et al. Development and testing of a rapid diagnostic test for bubonic and pneumonic plague. *Lancet* 2003, 361, 211–6.
[181] Saidi A, Mirzaei M, Zeinali S. Using antibody coated gold nanoparticles as fluorescence quenchers for simultaneous determination of aflatoxins (B1, B2) by soft modeling method. *Chemometr Intell Lab* 2013, 127, 29–34.
[182] Grobusch MP, Schormann D, Schwenke S, Teichmann D, Klein E. Rapid immunochromatographic assay for diagnosis of tuberculosis. *J Clin Microbiol* 1998, 36, 3443.
[183] Koo HC, Park YH, Ahn J, et al. Use of rMPB70 protein and ESAT-6 peptide as antigens for comparison of the enzyme-linked immunosorbent immunochromatographic, and latex bead agglutination assays for serodiagnosis of bovine tuberculosis. *J Clin Microbiol* 2005, 43, 4498–506.
[184] Treepongkaruna S, Nopchinda S, Taweewongsounton A, et al. A rapid serologic test and immunoblotting for the detection of Helicobacter pylori infection in children. *J Trop Pediatr* 2006, 52, 267–71.

[185] Huang S-H. Gold nanoparticle-based immunochromatographic assay for the detection of Staphylococcus aureus. *Sens Actuator B* 2007, 127, 335–340.
[186] Wiriyachaiporn S, Howarth PH, Bruce KD, Dailey LA. Evaluation of a rapid lateral flow immunoassay for Staphylococcus aureus detection in respiratory samples. *Diagn Microbiol Infect Dis* 2013, 75, 28–36.
[187] Chelobanov BP, Afinogenova GN, Cheshenko IO, Sharova TV, Zyrianova AV, Veliev SN. Development of an immunochromatography tests for rapid diagnostics of viral hepatitis type B patients. *Bull SB RAMS* 2007, 5, 83–7 (in Russian).
[188] Taneja N, Nato F, Dartevelle S, et al. Dipstick test for rapid diagnosis of *Shigella dysenteriae* 1 in bacterial cultures and its potential use on stool samples. *PLoS One* 2011, 6, e24830.
[189] Duran C, Nato F, Dartevelle S, et al. Rapid diagnosis of diarrhea caused by *Shigella sonnei* using dipsticks; comparison of rectal swabs, direct stool and stool culture. *PLoS One* 2013, 8, e80267.
[190] Lyubavina IA, Valyakina TI, Grishin EV. Monoclonal antibodies labeled with colloidal gold for immunochromatographic express analysis of diphtheria toxin. *Russ J Bioorganic Chem* 2011, 37, 326–32.
[191] Joon Tam Y, Mohd Lila MA, Bahaman AR. Development of solid – based paper strips for rapid diagnosis of Pseudorabies infection. *Trop Biomed* 2004, 21, 121–34.
[192] Han S-M, Cho J-H, Cho I-H, et al. Plastic enzyme-linked immunosorbent assays (ELISA)-on-a-chip biosensor for botulinum neurotoxin A. *Anal Chim Acta* 2007, 587, 1–8.
[193] Feodorova VA, Polyanina TI, Zaytsev SS, Ulianova OV, Laskavy VN, Dykman LA. Development of immunochromatography test strip for rapid diagnosis of ovine enzootic abortion. *Veterinaria i kormlenie* 2015, 5, 16–9 (in Russian).
[194] Cui X, Huang Y, Wang J, et al. A remarkable sensitivity enhancement in a gold nanoparticle-based lateral flow immunoassay for the detection of Escherichia coli O157:H7. *RSC Adv* 2015, 5, 45092–7.
[195] Fernández-Sánchez C, McNeil CJ, Rawson K, Nilsson O, Leung HY, Gnanapragasam V. One-step immunostrip test for the simultaneous detection of free and total prostate specific antigen in serum. *J Immunol Methods* 2005, 307, 1–12.
[196] Andreeva IP, Grigorenko VG, Egorov AM, Osipov AP. Quantitative lateral flow immunoassay for total prostate specific antigen in serum. *Anal Lett* 2015, 49, 579–88.
[197] Tanaka R, Yuhi T, Nagatani N, et al. A novel enhancement assay for immunochromatographic test strips using gold nanoparticles. *Anal Bioanal Chem* 2006, 385, 1414–20.
[198] Glynou K, Ioannou PC, Christopoulos TK, Syriopoulou V. Oligonucleotide-functionalized gold nanoparticles as probes in a dry-reagent strip biosensor for DNA analysis by hybridization. *Anal Chem* 2003, 75, 4155–60.
[199] Zhou P, Lu Y, Zhu J, et al. Nanocolloidal gold-based immunoassay for the detection of the N-methylcarbamate pesticide carbofuran. *J Agric Food Chem* 2004, 52, 4355–9.
[200] Zhang C, Zhang Y, Wang S. Development of multianalyte flow-through and lateral-flow assays using gold particles and horseradish peroxidase as tracers for the rapid determination of carbaryl and endosulfan in agricultural products. *J Agric Food Chem* 2006, 54, 2502–7.
[201] Xiulan S, Xiaolian Z, Jian T, Zhou J, Chu FS. Preparation of gold-labeled antibody probe and its use in immunochromatography assay for detection of aflatoxin B1. *Int J Food Microbiol* 2005, 99, 185–94.
[202] Zhang D, Li P, Zhang Q, Zhang W. Ultrasensitive nanogold probe-based immunochromatographic assay for simultaneous detection of total aflatoxins in peanuts. *Biosens Bioelectron* 2011, 26, 2877–82.
[203] Wang S, Quan Y, Lee N, Kennedy IR. Rapid determination of fumonisin B1 in food samples by enzyme-linked immunosorbent assay and colloidal gold immunoassay. *J Agric Food Chem* 2006, 54, 2491–5.

[204] Huo T, Peng C, Xu C, Liu L. Immunochromatographic assay for determination of hexoestrol residues. *Eur Food Res Technol* 2007, 225, 743–7.
[205] Zhao Y, Zhang G, Liu Q, Teng M, Yang J, Wang J. Development of a lateral flow colloidal gold immunoassay strip for the rapid detection of enrofloxacin residues. *J Agric Food Chem* 2008, 56, 12138–42.
[206] Chen L, Wang Z, Ferreri M, Su J, Han B. Cephalexin residue detection in milk and beef by ELISA and colloidal gold based one-step strip assay. *J Agric Food Chem* 2009, 57, 4674–9.
[207] Byzova NA, Smirnova NI, Zherdev AV, et al. Rapid immunochromatographic assay for ofloxacin in animal original foodstuffs using native antisera labeled by colloidal gold. *Talanta* 2014, 119, 125–32.
[208] Cho J-H, Paek S-H. Semiquantitative, bar-code version of immunochromatographic assay system for human serum albumin as model analyte. *Biotechnol Bioengineer* 2001, 75, 725–32.
[209] Wang S, Zhang C, Wang J, Zhang Y. Development of colloidal gold-based flow-through and lateral-flow immunoassays for the rapid detection of the insecticide carbaryl. *Anal Chim Acta* 2005, 546, 161–6.
[210] Bahadır EB, Sezgintürk MK. Lateral flow assays: principles, designs and labels. *Trends Anal Chem* 2016, 82, 286–306.
[211] Gupta S, Huda S, Kilpatrick PK, Velev OD. Characterization and optimization of gold nanoparticle-based silver-enhanced immunoassays. *Anal Chem* 2007, 79, 3810–20.
[212] Venkataramasubramani M, Tang L. Development of gold nanorod lateral flow test for quantitative multi-analyte detection. *IFMBE Proc* 2009, 24, 199–202.
[213] Ren W, Huang Z, Xu Y, Li Y, Ji Y, Su B. Urchin-like gold nanoparticle-based immunochromatographic strip test for rapid detection of fumonisin B1 in grains. *Anal Bioanal Chem* 2015, 407, 7341–8.
[214] Wang L, Ma W, Chen W, et al. An aptamer-based chromatographic strip assay for sensitive toxin semi-quantitative detection. *Biosens Bioelectron* 2011, 26, 3059–62.
[215] Nangola S, Thongkum W, Saoin S, Ansari AA, Tayapiwatana C. An application of capsid-specific artificial ankyrin repeat protein produced in E. coli for immunochromatographic assay as a surrogate for antibody. *Appl Microbiol Biotechnol* 2014, 98, 6095–103.
[216] Dzantiev BB, Byzova NA, Urusov AE, Zherdev AV. Immunochromatographic methods in food analysis. *Trends Anal Chem* 2014, 55, 81–93.
[217] Quesada-González D, Merkoçi A. Nanoparticle-based lateral flow biosensors. *Biosens Bioelectron* 2015, 73, 47–63.
[218] Mak WC, Beni V, Turner APF. Lateral-flow technology: From visual to instrumental. *Trends Anal Chem* 2016, 79, 297–305.
[219] Huang X, Aguilar ZP, Xu H, Lai W, Xiong Y. Membrane-based lateral flow immunochromatographic strip with nanoparticles as reporters for detection: A review. *Biosens Bioelectron* 2016, 75, 166–80.
[220] Schalkhammer T. Metal nano clusters as transducers for bioaffinity interactions. *Chem Monthly* 1998, 129, 1067–92.
[221] Rasooly A, Herold KE, eds. *Biosensors and Biodetection*. New York, Humana Press, 2009.
[222] Li Y, Schluesener HJ, Xu S. Gold nanoparticle-based biosensors. *Gold Bull* 2010, 43, 29–41.
[223] Peng HI, Miller BL. Recent advancements in optical DNA biosensors: exploiting the plasmonic effects of metal nanoparticles. *Analyst* 2011, 136., 436–47.
[224] Musick MD, Keating CD, Lyon LA, et al. Metal films prepared by stepwise assembly. *Chem Mater* 2000, 12, 2869–81.
[225] Shipway AN, Katz E, Willner I. Nanoparticle arrays on surfaces for electronic, optical, and sensor applications. *Chemphyschem* 2000, 1, 18–52.
[226] Grabar KC, Freeman RG, Hommer MB, Natan MJ. Preparation and characterization of Au colloid monolayers. *Anal Chem* 1995, 67, 735–43.

[227] Ulman A. Formation and structure of self-assembled monolayers. *Chem Rev* 1996, 96, 1533–54.
[228] Nath N, Chilkoti A. A colorimetric gold nanoparticle sensor to interrogate biomolecular interactions in real time on a surface. *Anal Chem* 2002, 74, 504–9.
[229] Prasad BLV, Stoeva SI, Sorensen CM, Klabunde KJ. Digestive-ripening agents for gold nanoparticles: alternatives to thiols. *Chem Mater* 2003, 15, 935–43.
[230] Haynes CL, Van Duyne RP. Nanosphere lithography: a versatile nanofabrication tool for studies of size-dependent nanoparticle optics. *J Phys Chem B* 2001, 105, 5599–611.
[231] Lyon LA, Musick MD, Natan MJ. Colloidal Au-enhanced surface-plasmon resonance immunosensing. *Anal Chem* 1998, 70, 5177–83.
[232] Miller MM, Lazarides AA. Sensitivity of metal nanoparticle surface plasmon resonance to the dielectric environment. *J Phys Chem B* 2005, 109, 21556–65.
[233] Khlebtsov BN, Melnikov AG, Zharov VP, Khlebtsov NG. Absorption and scattering of light by a dimer of metal nanospheres: comparison of dipole and multipole approaches. *Nanotechnology* 2006, 17, 1437–45.
[234] Jain PK, El-Sayed MA. Plasmonic coupling in noble metal nanostructures. *Chem Phys Lett* 2010, 487, 153–64.
[235] Templeton AC, Pietron JJ, Murray RW, Mulvaney P. Solvent refractive index and core charge influences on the surface plasmon absorbance of alkanethiolate monolayer-protected gold clusters. *J Phys Chem B* 2000, 104, 564–70.
[236] Khlebtsov NG, Dykman LA, Bogatyrev VA, Khlebtsov BN. Two-layer model of colloidal gold bioconjugates and its application to the optimization of nanosensors. *Colloid J* 2003, 65, 508–17.
[237] Penn SG, He L, Natan MJ. Nanoparticles for bioanalysis. *Curr Opin Chem Biol* 2003, 7, 609–15.
[238] Schuk P. Use of surface plasmon resonance to probe the equilibrium and dynamic aspects of interactions between biological macromolecules. *Annu Rev Biophys Biomol Struct* 1997, 26, 541–66.
[239] Homola J, Yee SS, Gauglitz G. Surface plasmon resonance sensors: review. *Sens Actuators B* 1999, 54, 3–15.
[240] Mullett WM, Lai EPC, Yeung JM. Surface plasmon resonance-based immunoassays. *Methods* 2000, 22, 77–91.
[241] Niemeyer CM. Nanoparticles, proteins, and nucleic acids: biotechnology meets materials science. *Angew Chem Int Ed* 2001, 40, 4128–58.
[242] Jain KK. Nanodiagnostics: application of nanotechnology in molecular diagnostics. *Expert Rev Mol Diagn* 2003, 3, 153–61.
[243] Parak WJ, Gerion D, Pellegrino T, et al. Biological applications of colloidal nanocrystals. *Nanotechnology* 2003, 14, R15–R27.
[244] Riboh JC, Haes AJ, McFarland AD, Yonzon CR, Van Duyne RP. A nanoscale optical biosensor: real-time immunoassay in physiological buffer enabled by improved nanoparticle adhesion. *J Phys Chem B* 2003, 107, 1772–80.
[245] Rosi NL, Mirkin CA. Nanostructures in biodiagnostics. *Chem Rev* 2005, 105, 1547–62.
[246] Stewart ME, Anderton CR, Thompson LB, et al. Nanostructured plasmonic sensors. *Chem Rev* 2008, 108, 494–521.
[247] Shtykov SN, Rusanova TY. Nanomaterials and nanotechnologies in chemical and biochemical sensors: capabilities and applications. *Russ J Gen Chem* 2008, 7, 2521–31.
[248] Sepúlveda B, Angelomé PC, Lechuga LM, Liz-Marzán LM. LSPR-based nanobiosensors. *Nano Today* 2009, 4, 244–51.
[249] Daghestani HN, Day BW. Theory and applications of surface plasmon resonance, resonant mirror, resonant waveguide grating, and dual polarization interferometry biosensors. *Sensors* 2010, 10, 9630–46.

[250] Lee SE, Lee LP. Biomolecular plasmonics for quantitative biology and nanomedicine. *Curr Opin Biotechnol* 2010, 21, 489–97.
[251] Csáki A, Berg S, Jahr N, et al. Plasmonic nanoparticles – noble material for sensoric applications. In: Chow PE., ed. *Gold Nanoparticles: Properties, Characterization and Fabrication*. New York, Nova Science Publisher, 2010, 245–61.
[252] Stefan-van Staden R-I, van Staden JF, Balasoiu S-C, Vasile O-R. Micro- and nanosensors, recent developments and features: a minireview. *Anal Lett* 2010, 43, 1111–8.
[253] Abbas A, Linman MJ, Cheng Q. New trends in instrumental design for surface plasmon resonance-based biosensors. *Biosens Bioelectron* 2011, 26, 1815–24.
[254] Pérez-López B, Merkoçi A. Nanoparticles for the development of improved (bio) sensing systems. *Anal Bioanal Chem* 2011, 399, 1577–90.
[255] Mayer KM, Hafner JH. Localized surface plasmon resonance sensors. *Chem Rev* 2011, 111, 3828–57.
[256] Zhao J, Bo B, Yin Y-M. Gold nanoparticles-based biosensors for biomedical application. *Nano Life* 2012, 2, 1230008.
[257] Upadhyayula VKK. Functionalized gold nanoparticle supported sensory mechanisms applied in detection of chemical and biological threat agents: a review. *Anal Chim Acta* 2012, 715, 1–18.
[258] Saha K, Agasti SS, Kim C, Li X, Rotello VM. Gold nanoparticles in chemical and biological sensing. *Chem Rev* 2012, 112, 2739–79.
[259] Chen P-C, Roy P, Chen L-Y, Ravindranath R, Chang H-T. Gold and silver nanomaterial-based optical sensing systems. *Part Part Syst Charact* 2014, 31, 917–42.
[260] Cao J, Sun T, Grattan KTV. Gold nanorod-based localized surface plasmon resonance biosensors: A review. *Sens Actuators B* 2014, 195, 332–51.
[261] Kedem O, Vaskevich A, Rubinstein I. Critical issues in localized plasmon sensing. *J Phys Chem C* 2014, 118, 8227–44.
[262] Howes PD, Rana S, Stevens MM. Plasmonic nanomaterials for biodiagnostics. *Chem Soc Rev* 2014, 43, 3835–53.
[263] Howes PD, Chandrawati R, Stevens MM. Colloidal nanoparticles as advanced biological sensors. *Science* 2014, 346, 1247390.
[264] Szunerits S, Spadavecchia J, Boukherroub R. Surface plasmon resonance: signal amplification using colloidal gold nanoparticles for enhanced sensitivity. *Rev Anal Chem* 2014, 33, 153–64.
[265] Valcárcel M, López-Lorente ÁI, eds. Gold Nanoparticles in Analytical Chemistry. Amsterdam, Elsevier, 2014.
[266] Strobbia P, Languirand E, Cullum BM. Recent advances in plasmonic nanostructures for sensing: a review. *Opt Eng* 2015, 54, 100902.
[267] Sotnikov DV, Zherdev AV, Dzantiev BB. Detection of intermolecular interactions based on surface plasmon resonance registration. *Biochemistry (Moscow)* 2015, 80, 1820–32.
[268] Li M, Cushing SK, Wu N. Plasmon-enhanced optical sensors: a review. *Analyst* 2015, 140, 386–406.
[269] Unser S, Bruzas I, He J, Sagle L. Localized surface plasmon resonance biosensing: current challenges and approaches. *Sensors* 2015, 15, 15684–716.
[270] Johne B, Hansen K, Mørk E, Holtlund J. Colloidal gold conjugated monoclonal antibodies, studied in the BIAcore biosensor and in the Nycocard immunoassay format. *J Immunol Methods* 1995, 183, 167–74.
[271] Jason-Moller L, Murphy M, Bruno J. Overview of Biacore systems and their applications. *Curr Protoc Protein Sci* 2006, Ch. 19. Unit 19.13.
[272] Cooper MA. Label-free screening of bio-molecular interactions. *Anal Bioanal Chem* 2003, 373, 834–42.

[273] Adamczyk M, Johnson DD, Mattingly PG, Moore JA, Pan Y. Immunoassay reagents for thyroid testing. 3. Determination of the solution binding affinities of a T4 monoclonal antibody Fab fragment for a library of thyroxine analogs using surface plasmon resonance. *Bioconjug Chem* 1998, 9, 23–32.
[274] Adamczyk M, Moore JA, Yu Z. Application of surface plasmon resonance toward studies of low-molecular weight antigen-antibody binding interactions. *Methods* 2000, 20, 319–28.
[275] Seo KH, Brackett RE, Hartman NF, Campbell DP. Development of a rapid response biosensor for detection of Salmonella typhimurium. *J Food Prot* 1999, 62, 431–7.
[276] Bao P, Frutos AG, Greef C, et al. High-sensitivity detection of DNA hybridization on microarrays using resonance light scattering. *Anal Chem* 2002, 74, 1792–7.
[277] Piliarik M, Šípová H, Kvasnička P, Galler N, Krenn JR, Homola J. High-resolution biosensor based on localized surface plasmons. *Opt Express* 2012, 20, 672–80.
[278] Raschke G, Kowarik S, Franzl T, et al. Biomolecular recognition based on single gold nanoparticle light scattering. *Nano Lett* 2003, 3, 935–42.
[279] McFarland AD, Van Duyne RP. Single silver nanoparticles as real-time optical sensors with zeptomole sensitivity. *Nano Lett* 2003, 3, 1057–62.
[280] Mayer KM, Hao F, Lee S, Nordlander P, Hafner JH. A single molecule immunoassay by localized surface plasmon resonance. *Nanotechnology* 2010, 21, 255503.
[281] Deyev SM, Lebedenko EN. Modern technologies for creating synthetic antibodies for clinical application. *Acta Naturae* 2009, 1, 32–50.
[282] Wu C-S, Liu F-K, Ko F-H. Potential role of gold nanoparticles for improved analytical methods: an introduction to characterizations and applications. *Anal Bioanal Chem* 2011, 399, 103–18.
[283] Yonzon CR, Jeoung E, Zou SL, Schatz GC, Mrksich M, Van Duyne RP. A comparative analysis of localized and propagating surface plasmon resonance sensors: the binding of concanavalin a to a monosaccharide functionalized self-assembled monolayer. *J Am Chem Soc* 2004, 126, 12669–76.
[284] Svedendahl M, Chen S, Dmitriev A, Käll M. Refractometric sensing using propagating versus localized surface plasmons: a direct comparison. *Nano Lett* 2009, 9, 4428–33.
[285] Yuan Z, Hu C-C, Chang H-T, Lu C. Gold nanoparticles as sensitive optical probes. *Analyst* 2016, 141, 1611–26.
[286] Syedmoradi L, Daneshpour M, Alvandipour M, Gomez FA, Hajghassem H, Omidfar K. Point of care testing: the impact of nanotechnology. *Biosens Bioelectron* 2017, 87, 373–87.
[287] Fan MK, Andrade GFS, Brolo AG. A Review on the fabrication of substrates for surface enhanced Raman spectroscopy and their applications in analytical chemistry. *Anal Chim Acta* 2011, 693, 7–25.
[288] Baia M, Baia L, Astilean S. Gold nanostructured films deposited on polystyrene colloidal crystal templates for surface-enhanced Raman spectroscopy. *Chem Phys Lett* 2005, 404, 3–8.
[289] Wei A. Calixarene-encapsulated nanoparticles: self-assembly into functional nanomaterials. *Chem Commun* 2006, 1581–91.
[290] Doherty MD, Murphy A, McPhillips J, Pollard RJ, Dawson P. Wavelength dependence of Raman enhancement from gold nanorod arrays: quantitative experiment and modeling of a hot spot dominated system. *J Phys Chem C* 2010, 114, 19913–9.
[291] Alvarez-Puebla RA, Agarwal A, Manna P, et al. Gold nanorods 3D-supercrystals as surface enhanced Raman scattering spectroscopy substrates for the rapid detection of scrambled prions. *Proc Natl Acad Sci USA* 2011, 108, 8157–61.
[292] Khlebtsov BN, Khanadeev VA, Tsvetkov MY, Bagratashvili VN, Khlebtsov NG. Surface-enhanced Raman scattering substrates based on self-assembled PEGylated gold and gold – silver core – shell nanorods. *J Phys Chem C* 2013, 117, 23162–71.
[293] Esenturk EN, Walker ARH. Surface-enhanced Raman scattering spectroscopy via gold nanostars. *J Raman Spectrosc* 2009, 40, 86–91.

[294] Khlebtsov BN, Panfilova EV, Khanadeev VA, Khlebtsov NG. Improved size-tunable synthesis and SERS properties of Au nanostars. *J Nanopart Res* 2014, 16, 2623.
[295] Rodríguez-Lorenzo L, de la Rica R, Álvarez-Puebla RA, Liz-Marzán LM, Stevens MM. Plasmonic nanosensors with inverse sensitivity by means of enzyme-guided crystal growth. *Nat Mater* 2012, 11, 604–7.
[296] Hamon C, Postic M, Mazari E, et al. Three-dimensional self-assembling of gold nanorods with controlled macroscopic shape and local smectic B order. *ACS Nano* 2012, 6, 4137–46.
[297] Hamon C, Novikov S, Scarabelli L, Basabe-Desmonts L, Liz-Marzán LM. Hierarchical self-assembly of gold nanoparticles into patterned plasmonic nanostructures. *ACS Nano* 2014, 8, 10694–700.
[298] Zhou Y, Zhou X, Park DJ, et al. Shape-selective deposition and assembly of anisotropic nanoparticles. *Nano Lett* 2014, 14, 2157–61.
[299] Tsvetkov MY, Khlebtsov BN, Khanadeev VA, et al. SERS substrates formed by gold nanorods deposited on colloidal silica films. *Nanoscale Res Lett* 2013, 8, 250.
[300] Khanadeev VA, Khlebtsov BN, Klimova SA, et al. Large-scale high-quality 2D silica crystals: dip-drawing formation and decoration with gold nanorods and nanospheres for SERS analysis. *Nanotechnology*, 2014, 25, 405602.
[301] Khlebtsov BN, Khlebtsov NG. Surface morphology of a gold core controls the formation of hollow or bridged nanogaps in plasmonic nanomatryoshkas and their SERS responses. *J Phys Chem C* 2016, 120, 15385–94.
[302] Nam J-M, Oh J-W, Suh YD. Plasmonic nanogap-enhanced Raman scattering with nanoparticles. *Acc Chem Res* 2016, 49, 2746–55.
[303] He L, Lamont E, Veeregowda B, et al. Aptamer-based surface-enhanced Raman scattering detection of ricin in liquid foods. *Chem Sci* 2011, 2, 1579–82.
[304] Craig AP, Franca AS, Irudayaraj J. Surface-enhanced Raman spectroscopy applied to food safety. *Annu Rev Food Sci Technol* 2013, 4, 369–80.
[305] Alak AM, Vo-Dinh T. Surface-enhanced Raman spectroscopy of organo phosphorous chemical agents. *Anal Chem* 1987, 59, 2149–53.
[306] Fodjo EK, Riaz S, Li D-W, et al. Cu@Ag/β-AgVO3 as a SERS substrate for the trace level detection of carbamate pesticides. *Anal Methods* 2012, 4, 3785–91.
[307] Liu B, Han G, Zhang Z, et al. Shell thickness-dependent Raman enhancement for rapid identification and detection of pesticide residues at fruit peels. *Anal Chem* 2012, 84, 255–61.
[308] Tang X, Cai W, Yang L, Liu J. Highly uniform and optical visualization of SERS substrate for pesticide analysis based on Au nanoparticles grafted on dendritic α-Fe2O3. *Nanoscale* 2013, 5, 11193–9.
[309] Zhou X, Zhou F, Liu H, Yang L, Liu J. Assembly of polymer – gold nanostructures with high reproducibility into a monolayer film SERS substrate with 5 nm gaps for pesticide trace detection. *Analyst* 2013, 138, 5832–8.
[310] Yang J-K, Kang H, Lee H, et al. Single-step and rapid growth of silver nanoshells as SERS-active nanostructures for label-free detection of pesticides. *ACS Appl Mater Interfaces* 2014, 6, 12541–9.
[311] Shende S, Inscore F, Sengupta A, Stuart J, Farquharson S. Rapid extraction and detection of trace Chlorpyrifos-methyl in orange juice by surface-enhanced Raman spectroscopy. *Sens Instrum Food Qual Saf* 2010, 4, 101–7.
[312] Khlebtsov BN, Khanadeev VA, Panfilova EV, Bratashov DN, Khlebtsov NG. Gold nanoisland films as reproducible SERS substrates for highly sensitive detection of fungicides. *ACS Appl Mater Interfaces* 2015, 7, 6518–29.
[313] Nam J-M, Thaxton CS, Mirkin CA. Nanoparticle-based bio-bar codes for the ultrasensitive detection of proteins. *Science* 2003, 301, 1884–6.

[314] Wilson R. The use of gold nanoparticles in diagnostics and detection. *Chem Soc Rev* 2008, 37, 2028–45.
[315] Abalde-Cela S, Aldeanueva-Potel P, Mateo-Mateo C, Rodríguez-Lorenzo L, Alvarez-Puebla RA, Liz-Marzán LM. Surface-enhanced Raman scattering biomedical applications of plasmonic colloidal particles. *J R Soc Interface* 2010, 7, S435–S450.
[316] Rodríguez-Lorenzo L, Krpetic Z, Barbosa S, et al. Intracellular mapping with SERS-encoded gold nanostars. *Integr Biol* 2011, 9, 922–6.
[317] Shiohara A, Wang Y, Liz-Marzán LM. Recent approaches toward creation of hot spots for SERS detection. *J Photochem Photobiol C* 2014, 21, 2–25.

I. Y. Goryacheva

# 3 Extinction and Emission of Nanoparticles for Application in Rapid Immunotests

## 3.1 Introduction

Immunochemical rapid tests occupy leading positions in the field of rapid screening, when the result must be obtained immediately. Historically, the first tests were developed for clinical analysis (point-of-care). The quick result, without the need to send a sample to the laboratory and without services of trained personnel, allows not only to reduce costs, but also to make timely diagnose, prescribe treatment, and also to save the patient from waiting for the result of the tests. The next area of immunochemical test application is the food quality control. The speed of analysis and the possibility of its implementation in the non-laboratory environment are especially important for perishable products. When determining toxicants in food facilities, an important parameter is the sensitivity of the test methods, since it is often necessary to determine their ultra-low concentrations. The latter also concerns the control of natural objects.

The need to determine both high-molecular-weight analytes and low-molecular-weight substances led to the application of two immunoassay formats: a non-competitive sandwich format for high-molecular-weight compounds and a competitive format for low-molecular-weight substances.

The concept of the rapid tests does not involve long-term sample preparation and preconcentration, while it is often necessary to determine ultra-low concentrations. To solve this problem, there are two main approaches. The first is to improve the properties of the immunoreagents (recognition system) and optimize the method of analysis. The second approach involves the development of new labels, which are responsible for the appearance of the analytical signal, and the corresponding readers.

In the last decade, various nanoparticles are in the focus of attention. The advantages and disadvantages, the principles of generating an analytical signal, and the prospects for their application in immunoassay are the subjects of this chapter.

In the area under consideration, there are a number of reviews of different orientations. So the application of immunochromatographic strips in the clinical analysis is described in two reviews, published in 2009 [1, 2]. The use of nanolabels in optical sensor devices is considered in the review [3]. The methods of synthesis of inorganic nanosized labels and their functionalization are summarized in the review [4], which also considers approaches to increasing the sensitivity of the determination.

https://doi.org/10.1515/9783110542011-003

The optimal labels should be colloidal in water, have a uniform size and shape, be easily conjugated to biomolecules, should generate an intense analytical signal, and demonstrate resistance to aggregation during storage and analysis. Conjugation of nanoparticles with biomolecules is usually carried out with the help of amino or carboxyl groups. The main features of nanoparticles, unlike molecular labels, are photostability and resistance to degradation. The optimal size of nanolabels is 15–800 nm [1], which allows such particles without significant difficulties to move along the membrane for the realization of immunochromatographic methods.

## 3.2 Extinction of nanoparticles

### 3.2.1 Colloidal gold

Colloidal gold is the most popular label used in immunochemical test methods [3]. The first application of gold nanoparticles (GNPs) conjugated with antibodies was described in 1981 [5]. Further rapid progress in their application is associated with a set of unique physical properties of GNPs that depend on the size, shape, and distance between nanoparticles.

One of the important advantages of GNPs is the lack of toxicity of the material itself. This simplifies the biological application of these labels and eliminates the need to coat the label with an inert material. Functionalization of GNPs occurs due to the coating of their surface with substances containing various bifunctional groups, for example, amphiphilic polymers, sugars, nucleic acids, and proteins that contain an active thiol sulfur atom capable of forming a strong bond with the surface of the GNP [6].

The use of GNPs as labels in noninstrumental test methods is based on their red color caused by surface plasmon resonance (or limited [local] surface plasmon resonance). This effect is observed when the frequency of the photon incident on the nanoparticle falls into resonance with the collective vibrations of its valence electrons [3, 6]. The color of the GNPs and, correspondingly, the wavelength of the absorption maximum, essentially, depend on their size and shape. The brightness or intensity of the color of GNPs light absorption is determined by their size, which can be easily adjusted during the production process. Among the spherical GNPs, particles with a diameter of about 30 nm have the greatest brightness. The sensitivity of the analyte detection is 2–4 times higher than that of particles with a diameter of 15 nm [7]. In another paper, it has been shown that gold nanospheres with a diameter of 80 nm are much more sensitive than standard molecular luminescent labels, such as Cy-3 and Cy-5 [8]. At the same time, according to the data of [9], experimental work with GNPs greater than 30–40 nm can be difficult because of the instability of their solutions.

GNPs are now standard labels for immunochromatographic strips [10–14], applied in such areas as clinical analysis and food quality control. In recent years, immunochromatographic strips based on GNPs have also been developed to monitor the state of the environment. However, the use of spherical GNPs as labels is limited by the insufficient sensitivity of the test.

Two main approaches can be distinguished, which make it possible to increase the brightness of the label, and, consequently, to improve the sensitivity of the analysis. The first is modification. This approach does not lead to complication of the analysis procedure. The determination remains one-step procedure, without the use of any additional reagents. In the second approach, sensitivity is improved by introducing additional steps into the analysis procedure.

**Modification of GNPs** allows increasing the sensitivity of the determination without introducing additional steps into the analysis procedure. In particular, the replacement of spherical GNPs with the core–gold shell nanoparticles makes it possible to increase their brightness. Based on the theoretical estimate, it was shown that the brightness of a quartz/gold nanoparticle 1000 nm in diameter can be 1,000 times higher than a normal GNP with a diameter of 15 nm [9]. It has been shown that replacing traditional GNPs with silver/gold nanoparticles as labels allows increasing the sensitivity of the determination of aflatoxin B1 [15]. In this case, the reproducibility of the results and the stability of the tests are maintained. Similarly, the use of nanoparticles of iron oxide coated with GNPs as a mark increased the sensitivity of the determination of aflatoxin B2 [16]. Various additional steps to increase the sensitivity of the determination are usually carried out after the implementation of the standard immunoassay procedure. In this case, two methods of determination can be used: the signal is read immediately after the determination procedure, and if the sensitivity is not sufficient, the determination is repeated using signal amplification techniques [17].

**Precipitation of silver.** One of the methods of modifying the GNPs is to cover them with silver. With the addition of a solution containing silver ions, the formation of metallic silver is observed on the surface of GNPs, which can be fixed both visually and with the help of a reader device – instrumentally. This phenomenon, known as autometallography, was described in 1930 and used to amplify the signal of GNPs associated with antibodies in 1986 [18]. The role of GNPs consists in bringing electrons from the reducing agent in solution to silver ions on the surface of the nanoparticles [19]. The detection sensitivity can be increased approximately 100-fold [20]. The limitation of the approach is the complication of the analysis procedure, since very thorough washing is required to remove the chloride ions. There are a number of examples of application of silver deposition to increase the sensitivity of various immunoassay formats: a multi-channel chip for detecting human immunoglobulin G with a digital camera [21] and a model analyte with a scanner [22]. It should be noted that silver deposition can be used not only to increase the GNPs' signal,

but also to use the silver nanoparticles themselves in immunochromatographic test methods as labels [23].

**Enhancement with GNPs.** The GNPs itself can also act as signal amplifiers. Examples of such use are described for the determination of high-molecular-weight analytes. After the realization of the immunochromatographic determination, the GNPs conjugated to the primary antibodies are applied to the strip and they accumulate on the test and control lines, thus allowing the detection limit to be reduced 50-fold [24, 25]. To implement such an approach, and to avoid additional steps, preliminary separate application of two different conjugates is possible: GNPs conjugated with antibodies and blocked by bovine serum albumin (BSA) and GNPs conjugated with BSA-specific antibodies. It was shown that in this case an important role is played by the size of GNPs. The optimal combination of GNPs' sizes (using 10 and 40 nm GNPs in the first and second conjugates, respectively) made it possible to 100-fold increase the sensitivity of the tests [26]. An additional advantage of using GNPs for enhancing the immunochemical signal is the possibility of using standard readers, as well as for unmodified immunochromatographic strips.

**Enhancement with enzymes.** The use of horseradish peroxidase (HRP), which, in the presence of a suitable chromogenic substrate, produces blue-colored products, makes it possible to make the red color of the GNPs darker and more contrast and to increase sensitivity of the determination by an order of magnitude [17]. The use of catalytic properties of GNPs allows them to be used for chemiluminescence detection, in particular when using the reaction of luminol and $AgNO_3$. This approach was used to detect human immunoglobulin G [27].

A fundamentally different way of using GNPs for visual detection is based on their ability to change color depending on the distance between nanoparticles. When individual GNPs are at a small distance not exceeding their diameter multiplied by 2.5, the surface plasmon resonance of individual GNP becomes group. As a result, the color changes from red to violet and blue. This effect was first used to determine polynucleotides [28]. A similar principle was used in homogeneous immunoassay [29].

The ability of GNPs to change color depending on the distance between them was used to determine low-molecular-weight analytes containing several functional groups, such as melamine, dopamine, and ascorbic acid. Due to the presence of three amino groups, melamine molecules cause rapid aggregation of GNPs and turning the solution color into blue (violet), which allows determination of up to 0.4 ng/mL of melamine in milk in 12 minutes, including centrifugation, pH optimization, and filtration [30, 31]. A similar approach was used to determine dopamine in the presence of $Cu^{2+}$ ions, which increase the sensitivity of the reaction by forming a complex with two dopamine molecules [32]. Ascorbic acid in the presence of $Cu^{2+}$ also causes discoloration, due to the aggregation of GNPs, functionalized with azide and alkaline groups [33].

The dependence of the color of the GNPs on the distance between them was used not only when working with solutions, but also in solid-phase methods, which is more convenient for screening. The first immunochromatographic test using color change in the aggregation/disaggregation of GNPs was described in [34]. Later this approach was used for dot analysis [35] and in sensors [36].

To realize the multidetection, specific immunoreagents are applied to separate zones of the immunochromatographic strip and then the presence/intensity of red staining of the GNPs is fixed [37, 38]. Variations in the shape, size, and composition of metal nanoparticles make it possible to obtain colloids of various colors. When silver atoms are replaced by gold atoms, cubic nano-sized particles of different colors are obtained. Depending on the degree of substitution, the color of the formed colloids varies from yellow to blue. On the example of cubic silver nanoparticles with partial substitution of silver atoms for gold atoms of yellow red and blue colors, the possibility of using such particles in dot immunoanalysis was shown [39].

### 3.2.2 Colloidal carbon

The black color of carbon nanoparticles can be detected visually with a sufficiently high sensitivity. For the first time, the use of colloidal carbon as label in immunoassay was described in 1993 [40]. Synthesis, functionalization and application of carbon nanoparticles in immunochemical test methods are reviewed in [41]. Carbon nanoparticles are cheap since methods for their production in large quantities have been developed. In addition, they allow the use of "gray pixel" for detection of grayscale, having a higher sensitivity than color variants. Due to the strong absorption of light, it is possible to detect carbon nanoparticles at a very low level of 0.04 ng/mm$^2$ (0.02 atmol/mm$^2$) using a scanner and 0.2 ng/mm$^2$ (0.1 atmol/mm$^2$) with the naked eye [42]. For comparison, it can be noted that these values are comparable to the detection sensitivity of enzyme labels (alkaline phosphatase with the corresponding substrate and chemiluminescence detection can be determined in the amount of 0.02 atmol, β-galactosidase with the corresponding substrate and fluorescence detection – 0.1 atmol, HRP with an appropriate substrate and photometric detection – 5 atmol).

The sensitivity of immunochromatographic tests when used as carbon nanoparticle labels is comparable to traditional solid-phase enzyme-linked immunosorbent assay (ELISA) [43]. Using the example of a model system, the detection limits of the most frequently used labels, such as GNPs, GNP with signal enhancement by silver deposition, blue latex labels, and carbon nanoparticles, are equal to 0.1 μg/mL, 1 μg/mL, 1 mg/mL, and 0.01 μg/mL, respectively [44]. It should be noted that in other cases, the use of GNPs has proved to be more effective: for example, in immunochromatographic tests for the determination of mycotoxin sporidesmin A, the use of GNPs

allowed obtaining a detection limit of 4 ng/ml, and using colloidal carbon – 25 ng/ml [45]. At present, immunochromatographic tests based on carbon nanoparticles have been developed to determine human chorionic gonadotropin [46], immunoglobulin E [42], and other high-molecular [47–49] and low-molecular [50] weight compounds. More complex carbon nanostructures (carbon nanorods) can further improve the sensitivity of immunochromatographic tests [51, 52].

### 3.2.3 "Colloidal" dyes

Molecules of organic dyes are not bright enough to be used as labels. For creating labels on their basis, various approaches are used, which allow several individual molecules to combine into one brighter label. The use of commercial Blue colloidal dye (D-1) and Dadisperse navy blue (SP) in immunochromatographic strips is described [53–55]. As a label in immunofiltration tests, a red colloidal dye (R-3) was also proposed, the results were comparable with those for solid-phase ELISA [56]. It is shown that the use of colloidal dyes allows for both qualitative and quantitative detection. To increase the intensity of the chromophore signal, the dye molecules were bound to a polylysine of different molecular weights. The use of dyes of different colors allows the qualitative determination of several analytes, and when using a densitometer and quantitative too [57].

Another principle of creating a label is the use of nanoparticles containing a precursor of a brightly colored component. An example of such a label in an immunochromatographic test is a nanoparticle containing colorless indigo precursor 5-bromo-4-chloro-3-indolyl acetate [58]. As a result of hydrolysis of this compound, intensely colored blue 5-bromo-4-chloro-3-hydroxyindole forms, which after dissolution forms a blue precipitate of 5,5′-dibromo-4,4′-dichloroindigo. A mixture of the reagents required for hydrolysis is added after the immunochromatographic analysis is performed. A determination using a label of this type was more sensitive than using GNPs.

## 3.3 Emission of nanoparticles

Labels suggesting luminescent detection are now widely used in clinical studies since they allow achieving high sensitivity and using simultaneously for detections of different colors labels. In some cases, the sensitivity of luminescent labels is comparable to the sensitivity of enzymatic labels, while the analysis procedure is much simpler.

All luminescence emitters can be divided into two groups. The first group is luminophores, which emit photons with energy less than the absorbed photons

(down-converting), respectively; the wavelength of the emission is greater than the wavelength of the absorbed light. These are the most common processes, including fluorescence, phosphorescence, and most intermolecular energy transfer processes. There is also another group of emitters capable of emitting photons with energy greater than that of upconverting photons. Such a process is realized when two or more photons are absorbed.

### 3.3.1 Fluorescence dyes

The simplest type of luminescent labels is luminescent dyes. Historically, fluorophores, such as fluorescein, rhodamines, and cyanine dyes, are widely used as labels for fluorescence microscopy and cell biology. At present, a number of fluorescent dye series with improved fluorescence characteristics are available (high quantum yield, large Stokes shift, photo- and chemical stability) such as Alexa Fluor (Invitrogen and Molecular Probes), PromoFlor (PromoKine), DyLight Fluor (Dyomics), ATTO Dyes (ATTO-TEC), and Hilyte Fluor (AnaSpec).

Such dyes can be used as labels in rapid tests. However, it should be noted that their use is complicated by high light scattering of membranes and fluorescence of proteins (antibodies) and sample components, such as, for example, polycyclic aromatic hydrocarbons and mycotoxins. The disadvantages of fluorescent dyes in comparison with nanoparticles are low photostability, high probability of quenching of fluorescence, and more pronounced concentration quenching.

To increase the brightness of labels, several separate molecules of fluorescent dyes could be associated with one carrier, and then with immunoreagents. This allows the label–antibody ratio to increase and, accordingly, to improve the detection sensitivity. It is proposed, in particular, to incorporate fluorescent dyes in silicon oxide nanoparticles [59, 60]. Another method of increasing the brightness of the label is the use of polystyrene nanoparticles containing dye molecules. A series of such nanoparticles are commercially available, for example, FluoSpheres from Invitrogen. Such approaches make it possible to make the labels brighter, but they do not solve the problem with a wide emission band of fluorescence and a small Stokes shift, which results in overlapping of the absorption and emission bands.

In order to find the best fluorophores, several fluorescent dyes (fluorescein, rhodamine, Texas Red, Alexa Fluor 488, and Alexa Fluor 647) have been compared, and it is shown that Alexa Fluor 647 is more stable and allows obtaining the most intense fluorescent signal [61]. This dye was used as a molecular label for immunochromatographic determination of proteins in the blood [62, 63]. The absence of interfering influence of blood components was established, and it was shown that it is possible to do without sample preparation of blood, which is important for clinical analyses. A similar test, demonstrating a good correlation with more complex methods, was developed to determine albumin in urine [64]. In the field of control

of environmental objects, such labels were used to determine microcystins in surface water [61].

For visual detection, only a device containing a light source – a lamp (Cibitest's device FLORIDA) is sufficient. To obtain quantitative results with the help of such labels, both the scanners constructed in the laboratory [61] and commercial scanners (i-CHROMATM, BioditechMed, Korea) are described. Embedded Systems Engineering (Germany) has developed a miniature confocal optical sensor that can be used for a wide range of fluorescent labels.

### 3.3.2 Lanthanide chelates

As mentioned above, the membranes used in the test methods often exhibit a high level of background fluorescent signal due to the scattering of the incident light by them. The simplest way to reduce this background is to use emitters with a large Stokes shift. One of the labels that have this property is the lanthanide chelates, which are characterized by a Stokes shift of more than 150 nm. The fluorescence intensity of such chelates in aqueous media is usually small because of the high level of its quenching by water molecules. Reducing quenching allows the inclusion of these compounds in various submicron particles, allowing the concentration of a large number of luminescent chelates. For example, up to $7 \cdot 10^5$ molecules of europium chelates can be covalently bound to a silicon oxide nanoparticle [65]. Additional advantages of using such combined labels are chemical stability and ease of conjugation with bioobjects [66, 67]. Such tags are commercially available (Molecular Probes Inc., Seradyn Inc.).

For the test results evaluation, it is possible to use a digital camera and visual detection under UV irradiation. It was shown that the detection sensitivity when using terbium chelate bound to nanoparticles as a label is more than 100 times higher than using fluorescein molecules [68]. A comparison of the sensitivity of immunochromatographic tests with different labels in determining the hepatitis B surface antigen showed a 10-fold decrease in the detection limit when using silicon oxide nanoparticles associated with the europium chelate relative to the GNP labels (0.03 and 3.51 μg/L, respectively).

### 3.3.3 Quantum dots

Quantum dots (**QDs**) are a fairly new type of labels used for visual and instrumental detection of immunochemical test methods. QDs are nanocrystals of an inorganic semiconductors, the color of their luminescence depends on their size and the nature of the semiconductor. As a material for QDs, InP, InAs, GaAs, GaN, ZnS, and ZnSe can

be used. However, the most popular QDs are based on cadmium selenide because, depending on the size, the fluorescent color covers the entire visible region of the electromagnetic spectrum. For this, the radius of the CdSe cores should be in the interval 1–6 nm, that is, it is less than the radius of the Bohr exciton for cadmium selenide (6 nm). When synthesized, the diameter of the cadmium selenide core can be matched to produce different fluorescent colors.

However, CdSe nanocrystals have a low quantum yield of fluorescence and are not stable in aqueous solutions due to photodegradation and nonradiative processes occurring on the surface [69, 70]. The protection of such a core by means of a shell from a wider-gap conductor, for example, ZnS, CdS, or ZnSe, reduces the probability of nonradiative processes and increases the quantum yield.

The extinction coefficient of the QD, depending on the particle size and excitation wavelength, varies in the range of ~$10^5$–$10^6$ $M^{-1}$ $cm^{-1}$, which is much higher than for organic dyes. The quantum yield core/shell QDs is up to 40 %. Although the quantum yield of QDs' luminescence is lower than for organic luminophores (such as rhodamine 6G and fluorescein), it is compensated by a broad absorption band and a high extinction coefficient. According to the estimates of [71], each CdSe/ZnS QD is approximately 20 times brighter and has photostability 200 times higher than the rhodamine 6 G molecule.

Unlike organic fluorescent dyes, the QD luminescent spectrum is narrow and symmetrical, and the absorption band is wide, the position of the long-wave edge of which depends on the size of QDs cores. Such spectral characteristics allow one source of excitation to be used to obtain luminescence of different colors from QDs of different sizes. This makes it possible to use QDs for simultaneous detection of several analytes. In addition, the use of spectral resolution allows the determination of several analytes in one test zone [72, 73].

The disadvantages of quantum dots are their toxicity, insolubility in water, and the lack of functional groups for bioconjugation. To overcome these drawbacks, various approaches are used, for example, coating of quantum dots with silica shells [74] or with a layer of bifunctional ligands (example of the simplest ligand is mercaptopropionic acid). QDs are widely used as biolabels in molecular biology, genomics, and medical diagnostics, commercially available as labels and in the form of conjugates (Invitrogen, Evident technologies, Research Institute of Applied Acoustics). A wide excitation band and a narrow emission band make it possible to realize multianalysis and reduce the influence of the sample matrix. The latter is especially important for the analysis of blood samples. The lifetime of QDs' luminescence is 30–100 ns, which is higher than for organic dyes (1–5 ns) and background (<50 ns), although much less than for lanthanide-based luminescent materials (1 μs to 1 ms). Thus, the lifetime of QDs luminescence substantially exceeds the decay time of background fluorescence and Raman scattering for most matrices. This makes it possible to use temporal selection to reduce the background signals

[75]. Some aspects of the modification and use of QDs are described in a number of reviews: various ways of bioconjugation of QDs [76]; QDs' application for chemical and biological detection and diagnostics [77–83]; and QDs' application in automatic flow systems [84].

Core/shell CdSe/ZnS QDs were used as luminescent labels in a fluorescence-linked immunosorbent assay (FLISA) to determine analytes in various matrices, in particular sulfamethazine [85] and enrofloxacin [86] in chicken meat; chlorpyrifos in drinking water [87]; surface proteins in *Listeria monocytogenes* [88]; simultaneous detection of dexamethasone, gentamicin, clonazepam, medroxyprogesterone acetate, and ceftiofur [89]; clenbutyrol in urine [90]; and progesterone in cow's milk [91]. Comparison with solid-state ELISA showed that the use of QDs as a label can reduce the $IC_{50}$ by 4 times (0.4 and 0.1 ng/mL for zearalenone, respectively) [92]. The luminescent signal of QDs was used simultaneously with the chemiluminescent signal of the enzyme label for simultaneous detection of analytes in blood serum [93]. The introduction of QD into the composition of microspheres enhances the intensity of their luminescence and simplifies bioconjugation [94]. It is interesting to note that the use of QDs in immunoassays can be based not only on their optical properties. QD is used to amplify the electrochemical signal [95] and as a label in potentiometric sensors since CdSe QDS can be oxidized by hydrogen peroxide [96].

The use of QDs as labels for immunochromatographic analysis in the scientific literature was first described in 2010 for the determination of trichloropyridinol [97], protein markers of ceruloplasmin [98], and the antigen of syphilis [99]. Comparison of the sensitivity of immunochromatographic tests using identical immunoreagents showed that the visually detectable detection limit when using CdTe QDs (when excited by a UV lamp) was 10 times lower than when using GNPs [99, 100]. Similarly, a comparison of the sensitivity of benzo[a]pyrene determination in drinking water by a column immunofiltration test demonstrated detection limits of 5, 5, and 25 ng/L when used as QDs, HRP, and GNPs as labels, respectively [101].

### 3.3.4 Nanoparticles with infrared luminescence

The use of functionalized $Y_2O_3$:$Nd^{3+}$ nanoparticles as labels is associated with the features of their luminescence. $Nd^{3+}$, like other ions of rare earth metals, emits luminescence in the infrared (IR) region of the spectrum. In this area, the interfering effect of the background of biological objects is minimal even without the use of signal recording with time resolution. When excitation is used in the IR region (500–900 nm), excitation of components of biological systems does not occur. An attempt to use functionalized $Y_2O_3$:$Nd^{3+}$ nanoparticles as a label is described in [102] for the determination of lipoprotein in the format of solid-phase immunoassay.

### 3.3.5 Up converting phosphors

The principle of emission of phosphors, which emission wavelength is smaller than the excitation wavelength (upconverting phosphors, UCPs), is based on the combination of an absorbing and emitting ions in a submicron-sized crystal (200–400 nm in diameter). The ion (energy donor) absorbs light in the IR region (as a rule, 980 nm is used for excitation), goes into an excited state, and then, as a result of a nonradiative transition, transfers the excitation energy to the ion emitter (energy acceptor) that emits a photon in visible or near IR region (400–800 nm), depending on the nature of the ion. Such an anti-Stokes luminescence is based on the consecutive absorption of two photons with low energy.

In contrast to other two-photon absorption processes, the absorption of photons can take place with a difference in microseconds, since the lifetime of the excited states is long. This significantly increases the probability of two-photon absorption processes and, correspondingly, the intensity of the obtained signal. Since lasers used for excitation are relatively low power, photodegradation of biomolecules and the fading background effect are significantly reduced compared with other luminescent labels. Since there is no interfering background, there is no need to use time resolution.

The shift of the emission band to the anti-Stokes region simplifies the processing of the analytical signal [103, 104]. In the process of two-photon absorption, materials capable of including rare-earth metal ions are involved in the crystal structure. This process is most effective for $NaYF_4$ crystals with a hexagonal lattice. Lanthanide ions ($Ln^{3+}$) with numerous long-lived excited states are used as doping ions [105]. Various combinations of ions of rare-earth emitter–acceptors of energy (erbium, holmium, and thulium) and energy donors (ytterbium, erbium, and samarium) make it possible to obtain more than 20 different compositions [106]. The optical properties of such phosphors are not affected by the environment since energy transfer processes are carried out inside the crystal [103].

The simplest way to obtain labels based on such phosphors is to grind commercially available luminescent materials (Orasure Technologies, Inc., Phosphor Technology Ltd.) with further fractionation of the particles by precipitation or filtration. However, this method is associated with the heterogeneity of the shape and size of the resulting particles, which is not suitable for use as labels, since it causes a wide spread in the intensity of the analytical signals. To hang the homogeneity of particles in recent years, many different approaches have been proposed [105].

One of the disadvantages of these labels is low quantum yield. In addition, the submicron particle size is too large, since it is much larger than the protein, which, accordingly, affects the kinetics of the processes and enhances the nonspecific interaction [104]. The optimum label size should be less than 200 nm [106]. Like other inorganic nanoparticles, phosphors that use two-photon excitation cannot be directly

conjugated to biomolecules – they must first be functionalized [105]. One of the approaches for functionalization is the application of tetraethoxysilane to obtain a silica layer of 5–50 nm. As a result of silanization, it becomes possible to introduce functional groups for conjugation with biomolecules [103]. An alternative approach is the passivation of the particle surface with polyacrylic acid, the carboxyl groups of which are then used for bioconjugation [104].

A number of immunochromatographic tests were developed using phosphors with two-photon excitation as labels using special reading optical systems. For high-molecular-weight analytes, the tests are based on the sandwich assay principle and allow the determination of the antigen *Schistosoma* [107], *Escherichia coli* [108], *Yersinia pestis* [109], respiratory virus [110], interferon γ [111], pathogens *Streptococcus pneumonia* [112] and *Brucella* [113], hepatitis B [114], and nucleic acids [112, 115–117]. Simultaneous determination of two biomarkers in blood was realized for the diagnosis of mycbacterial infections. The results showed a good correlation with solid-phase ELISA [118]. The competitive format of the immunoassay is used to determine the drug in saliva samples [108].

To read the results from immunochromatographic strips using such labels, special UPlink readers (Orasure Technologies, Inc. Bethlehem, PA) are issued, which, depending on the conditions, can detect up to 10–100 emitting particles [108].

It was shown that the UPlink reader is capable of detecting up to 12 test lines on an immunochromatographic strip [108]. A similar test was proposed for the detection of antibodies to *Myobacterium tuberculosis* and hepatitis C viruses [118].

The determination of analytes is possible not only by increasing the intensity of the luminescence, but also by its quenching. If specific antibodies are on the phosphor surface, and the analyte competes for binding to a conjugate that includes a luminescence quencher, then the concentration of the analyte can be determined from the increase in the luminescent signal [119].

### 3.3.6 Nanoparticles with long-lived luminescence

In methods based on resolution in time, the transfer of phosphors to the excited state is realized by means of a short light pulse. The signal is recorded with a delay sufficient for the interfering short-lived signals to fade out and only the target signal of the long-lived label remains [120]. The disadvantage of this approach is a limited range of labels that have a significant lifetime of excited states. Typically, this time is >500 μs, which significantly exceeds the lifetime of background fluorescence, which usually does not exceed 50 ns. Thus, the use of labels with a long lifetime of the excited state makes it possible to completely avoid the imposition of fluorescence of the blood components and, in addition, to simplify the design of the reader, since there is no need to use high spectral resolution [121].

The most common long-lived labels are based on the use of lanthanide (more often europium) chelates, which have a high quantum yield of luminescence, a sufficient Stokes shift and, most importantly, a longer lifetime. The minimum number of labels that can be detected is $3.3 \cdot 10^7$ particles/mm$^2$ [121]. The difference in the lifetimes and the position of the emission bands makes it possible to use them to simultaneously determine several analytes in one test zone [65]. The use of such labels in immunochromatographic tests is described for the determination of eosinophils and neutrophils in blood [121] and C-reactive protein in serum [120].

Another type of radiation with a long lifetime is the phosphorescence of chelates of such metals as platinum, palladium, and ruthenium. Their lifetime is also several hundred microseconds. Ruthenium complexes emit blue luminescence and absorb in the red region (600–700 nm). Comparison of these two types of phage-luminophore types with long-lived luminescence, using the example of an immunochromatographic determination of the C-reactive protein, showed that the detection sensitivity differs insignificantly [120].

Usually, the use of long-lived luminescence requires the removal of molecular oxygen to prevent quenching of long-lived states. One way to eliminate oxygen quenching is to incorporate phosphorescent molecules into molecular oxygen-free matrices such as polyacrylonitrile, polystyrene, sephadex, and halogen-containing polymers.

## 3.4 Conclusions

Thus, progress in the development of new labels and optimization of the ways of using already developed nanoparticles lies at the intersection of the sciences of nanomaterials, biochemistry, analytical chemistry, optics, and photonics. Combining materials with different levels of organization (from atomic-molecular to macroscopic), inorganic and organic nature will create modern, effective solutions for analytical and biomedical applications.

**Acknowledgments:** The work was supported by the Russian Scientific Foundation (project 14-13-00229).

## References

[1] Posthuma-Trumpie GA, Korf J, van Amerongen A. Lateral flow (immuno)assay: its strengths, weaknesses, opportunities and threats. A literature survey. *Anal Bioanal Chem* 2009, 393, 569–82.
[2] Warsinke A. Point-of-care testing of proteins. *Anal Bioanal Chem* 2009, 393, 1393–405.

[3] Seydack M. Nanoparticle labels in immunosensing using optical detection methods. *Biosens Bioelectron* 2005, 20, 2454–69.
[4] Chafer-Pericas C, Maquieira A, Puchades R. Functionalized inorganic nanoparticles used as labels in solid-phase immunoassays. *TrAC* 2012, 31, 144–56.
[5] Leuvering JHW, Thal PJHM, Van der Waart M., Shuurs AHWM. A sol particle agglutination assay for human chorionic gonadotrophin. *J Immunol Meth* 1981, 45, 183–94.
[6] Wang Z, Ma L. Gold nanoparticle probes. *Coord Chem Rev* 2009, 253, 1607–18.
[7] Dykman LA, Bogatyrev VA. Gold nanoparticles: preparation, fictionalization and applications in biochemistry and immunochemistry, *Russ Chem Bull* 2007, 76, 181–94.
[8] Bao P, Frutos AG, Greef C, Lahiri J, Muller U, Peterson TC, Warden L, Xie X. High-sensitivity detection of DNA hybridization on microarrays using resonance light scattering. *Anal Chem* 2002, 74, 1792–7.
[9] Khlebtsov B, Khlebtsov N. Enhanced solid-phase immunoassay using gold nanoshells: effect of nanoparticle optical properties. *Nanotechnology* 2008, 19, 435703 (10pp).
[10] Nurul Najian AB, Engku Nur Syafirah EAR, Ismail N, Maizan M, Yean C. Development of multiplex loop mediated isothermal amplification (m-LAMP) label-based gold nanoparticles lateral flow dipstick biosensor for detection of pathogenic *Leptospira*. *Anal Chim Acta* 2016, 903, 142–8.
[11] Byzova NA, Zherdev AV, Zvereva EA, Dzantiev BB. Immunochromatographic assay with photometric detection for rapid determination of the herbicide atrazine and other triazines in foodstuffs. *J AOAC Int* 2010, 93, 36–43.
[12] Byzova NA, Zvereva EA, Zherdev AV, Eremin SA, Dzantiev BB. Rapid pretreatment-free immunochromatographic assay of chloramphenicol in milk. *Talanta* 2010, 81, 843–8.
[13] Rivas L, de la Escosura-Muñiz A, Serrano L, Altet L, Francino O, Sánchez A, Merkoçi A. Triple lines gold nanoparticle-based lateral flow assay for enhanced and simultaneous detection of *Leishmania* DNA and endogenous control. *Nano Research* 2015, 8, 3704–14.
[14] Chamorro-Garcia A, de la Escosura-Muñiz A, Espinoza-Castañeda M, Rodriguez-Hernandez CJ, de Torres C, Detection of parathyroid hormone-like hormone in cancer cell cultures by gold nanoparticle-based lateral flow immunoassays, Nanomedicine: *Nanotechnol Biol Med* 2016, 12, 53–61.
[15] Liao JY, Li H. Lateral flow immunodipstick for visual detection of aflatoxin B1 in food using immunonanoparticles composed of a silver core and a gold shell. *Microchim Acta* 2010, 171, 289–95.
[16] Tang D, Sauceda JC, Ott S, Basova E, Goryacheva I. Biselli S, Niessner R, Knopp D. Magnetic nanogold microspheres-based lateral flow immunodipstick for rapid detection of aflatoxin $B_2$ in food. *Biosens Bioelectron* 2009, 25, 514–8.
[17] Parolo C, De la Escosura-Muñiz A, Merkoçi A. Enhanced lateral flow immunoassay using gold nanoparticles loaded with enzymes. *Biosens Bioelectron* 2013, 40, 412–6.
[18] Scopsi L, Larsson I, Bastholm L, Nielsen MH. Silver-enhanced colloidal gold probes as markers for scanning electron-microscopy, *Histochemistry* 1986, 86, 35–41.
[19] Cho IH, Seo SM, Paek EH, Paek SH. Immunogold – silver staining-on-a-chip biosensor based on cross-flow chromatography. *J Chromatogr B* 2010, 878, 271–7.
[20] Horton JK, Swinburne S, O'Sullivan MJ. A novel, rapid, single-step immunochromatographic procedure for the detection of mouse immunoglobulin. *J Immunol Methods* 1991, 140, 131–4.
[21] Yang M, Wang C. Label-free immunosensor based on gold nanoparticle silver enhancement. *Anal Biochem* 2009, 385, 128–31.
[22] Yeh CH, Hung CY, Chang TC, Lin HP, Lin YC. An immunoassay using antibody-gold nanoparticle conjugate, silver enhancement and flatbed scanner. *Microfluid Nanofluid* 2009, 6, 85–91.
[23] Yeh CH, Chen WT, Lin HP, Chang TC, Lin YC. A newly developed immunoassay method based on optical measurement for Protein A detection. *Talanta* 2010, 83, 55–60.

[24] Nagatani N, Tanaka R, Yuhi T, Endo T, Kerman K, Takamura Y, Tamiya E. Gold nanoparticle-based novel enhancement method for the development of highly sensitive immunochromatographic test strips. *Sci Technol Adv Mat* 2006, 7, 270–5.
[25] Tanaka R, Yuhi T, Nagatani N, Endo T, Kerman K, Takamura Y, Tamiya E. A novel enhancement assay for immunochromatographic strips using gold nanoparticles. *Anal Bioanal Chem* 2006, 385, 414–20.
[26] Choi DH, Lee SK, Oh YK, Bae BW, Lee SD, Kim S, Shin YB, Kim MG. A dual gold nanoparticle conjugate-based lateral flow assay (LFA) method for the analysis of troponin I. *Biosens Bioelectron* 2010, 25, 1999–2002.
[27] Duan CF, Yu YQ, Cui H. Gold nanoparticle-based immunoassay by using non-stripping chemiluminescence detection. *Analyst* 2008, 133, 1250–5.
[28] Elghanian R, Storhoff JJ, Mucic RC, Letsinger RL, Mirkin CA. Selective colorimetric detection of polynucleotides based on the distance-dependent optical properties of gold nanoparticles. *Science* 1997, 277, 1078–81.
[29] Anfossi L, Baggiani C, Giovannoli C, Giraudi G. Homogeneous immunoassay based on gold nanoparticles and visible absorption detection. *Anal Bioanal Chem* 2009, 394, 507–12.
[30] Li L, Li B, Cheng D, Mao L. Visual detection of melamine in raw milk using gold nanoparticles as colorimetric probe. *Food Chem*. 2010, 122, 895–900.
[31] Guo L, Zhong J, Wu J, Fu FF, Chen G, Zheng X, Lin S. Visual detection of melamine in milk products by label-free gold nanoparticles, *Talanta* 2010, 82, 1654–8.
[32] Zhang Y, Li B, Chen X. Simple and sensitive detection of dopamine in the presence of high concentration of ascorbic acid using gold nanoparticles as colorimetric probes. *Microchim Acta* 2010, 168, 107–13.
[33] Zhang Y, Li B, Xu C. Visual detection of ascorbic acid via alkyne – azide click reaction using gold nanoparticles as a colorimetric probe. *Analyst* 2010, 135, 1579–84.
[34] Liu J, Mazumdar D, Lu Y. A simple and sensitive "dipstick" test in serum based on lateral flow separation of aptamer-linked nanostructures. *Angew Chem Int Ed* 2006, 45, 7955–9.
[35] Zhao W, Monsur AM, Aguirre SD, Brook MA, Li Y. Paper-based bioassays using gold nanoparticle colorimetric probes. *Anal Chem* 2008, 80, 8431–7.
[36] De la Escosura-Muñiz A, Parolo C, Merkoç A. Immunosensing using nanoparticles. *Mater Today* 2010, 13, 17–27.
[37] Shim WB, Dzantiev BB, Eremin SA, Chung DH. One-step simultaneous immunochromatographic strip test for multianalysis of ochratoxin a and zearalenone. *J Microbiol Biotechnol* 2009, 19, 83–92.
[38] Zhang C, Zhang Y, Wang S. Development of multianalyte flow-through and lateral-flow assays using gold particles and horseradish peroxidase as tracers for the rapid determination of carbaryl and endosulfan in agricultural products. *J Agric Food Chem* 2006, 54, 2502–7.
[39] Panfilova E, Shirokov A, Khlebtsov B, Matora L, Khlebtsov N. Multiplexed dot immunoassay using Ag nanocubes, Au/Ag alloy nanoparticles, and Au/Ag nanocages. *Nano Research* 2011, 5, 124–34.
[40] Van Amerongen A, Wichers JH, Berendsen LB, Timmermans AJ, Keizer GD, van Doorn AW, Bantjes A, van Gelder WM. Colloidal carbon particles of a new label for rapid immunochemical test methods: quantitative computer image analyses of results. *J Biotechnol* 1993, 30, 185–95.
[41] Posthuma-Trumpie GA, Wichers JH, Koets M, Berendsen LBJM, Van Amerongen A. Amorphous carbon nanoparticles: a versatile label for rapid diagnostic (immuno)assays. *Anal Bioanal Chem* 2012, 402, 593–600.
[42] Lonnberg M, Carlsson J. Quantitative detection in the attomole range for immunochromatographic tests by means of a flatbed scanner. *Anal Biochem* 2001, 293, 224–31.

[43] Van Dam GJ, Wichers JH, Falcao Ferreira TM, Ghati D, van Amerongen A, Deelder AM. Diagnosis of schistosomiasis by reagent strip test for detection of circulating cathodic antigen. *J Clin Microbiol* 2004, 42, 5458–61.
[44] Linares EM, Kubota LT, Michaelis J, Thalhammer S. Enhancement of the detection limit for lateral flow immunoassays: Evaluation and comparison of bioconjugates. *J Immunol Methods* 2012, 375, 264–70.
[45] Collin R, Schneider E, Briggs L, Towers N. Development of immunodiagnostic field tests for the detection of the mycotoxin, sporidesmin A. *Food Agric Immunol* 1998, 10, 91–104.
[46] Van Amerongen A, Van Loon D, Berendsen LBJM, Withers JH. Quantitative computer image analysis of a human chorionic gonadotropin colloidal carbon dipstick assay. *Clin Chim Acta* 1994, 229, 67–75.
[47] Noguera P, Posthuma-Trumpie GA, Van Tuil M, Van der Wal FJ, De Boer A, Moers APHA, van Amerongen A. Carbon nanoparticles in lateral flow methods to detect genes encoding virulence factors of Shiga toxin-producing Escherichia coli. *Anal Bioanal Chem* 2011, 399, 831–38.
[48] Bogdanovic J, Koets M, Sander I, Wouters I, Meijster T, Heederik D, van Amerongen A, Doekes G. Rapid detection of fungal a-amylase in the work environment with a lateral flow immunoassay. *J Allergy Clin Immunol* 2006, 118, 1157–63.
[49] Blazkova M, Koets M, Rauch P, van Amerongen A. Development of a nucleic acid lateral flow immunoassay for simultaneous detection of Listeria spp. and Listeria monocytogenes in food. *Eur Food Res Technol* 2009, 229, 867–74.
[50] Blazkova M, Rauch P, Fukal L. Strip-based immunoassay for rapid detection of thiabendazole *Biosens Bioelectron* 2010, 25, 2122–8.
[51] Lonnberg M, Drevin M, Carlsson J. Ultra-sensitive immunochromatographic assay for quantitative determination of erythropoietin. *J Immunol Methods* 2008, 339, 236–44.
[52] Liu C, Jia Q, Yang C, Qiao R, Jing L, Wang L, Xu C, Gao M. Lateral flow immunochromatographic assay for sensitive pesticide detection by using $Fe_3O_4$ nanoparticle aggregates as color reagents. *Anal Chem* 2011, 83, 6778–84.
[53] Wang SJ, Chang WF, Wang MY, Hsiung KP, Liu YC. Development of a disperse dye immunochromatographic test for the detection of antibodies against infectious bursal disease virus. *Vet Immunol Immunop* 2008, 125, 284–90.
[54] Zhu Y, He W, Liang Y, Xu M, Yu C, Hua W, Chao G. Development of a rapid, simple dipstick dye immunoassay for schistosomiasis diagnosis. *J Immunol Methods* 2002, 266, 1–5.
[55] Jin S, Chang ZY, Ming X, Min CL, Wei H, Sheng LY, Xiao HG. Fast dipstick dye immunoassay for detection of immunoglobulin G (IgG) and IgM antibodies of human toxoplasmosis. *Clin Diagn Lab Immunol* 2005, 12, 198–201.
[56] Xiang X, Tianping W, Zhigang T. Development of a rapid, sensitive, dye immunoassay for schistosomiasis diagnosis: a colloidal dye immunofiltration assay. *J Immunol Methods* 2003, 280, 49–57.
[57] Chang WF, Wang SJ, Lai SF, Shieh CJ, Hsiung KP, Liu YC. Evaluation on the use of reactive dye-modified polylysine as the biomarker in immunochromatographic test application. *Anal Biochem* 2011, 411, 236–40.
[58] Mak WC, Sin KK, Chan CPY, Wong LW, Renneberg R. Biofunctionalized indigo-nanoparticles as biolabels for the generation of precipitated visible signal in immunodipsticks. *Biosens Bioelectron* 2011, 26, 3148–53.
[59] Nooney RI, McCormack E, McDonagh C. Optimization of size, morphology and colloidal stability of fluorescein dye-doped silica NPs for application in immunoassays. *Anal Bioanal Chem* 2012, 404, 2807–18.
[60] Bae SW, Tan, W, Hong JI. Fluorescent dye-doped silica nanoparticles: new tools for bioapplications. *Chem Commun* 2012, 48, 2270–82.

[61] Kim YM, Oh SW, Jeong SY, Pyo DJ, Choi EY. Development of an ultrarapid one-step fluorescence immunochromatographic assay system for the quantification of microcystins. *Environ Sci Technol* 2003, 37, 1899–904.
[62] Ahn JS, Choi S, Jang SH, Chang HJ, Kim JH, Ki BN, Sang WO, Eui YC. Development of a point-of-care assay system for high-sensitivity C-reactive protein in whole blood. *Clin Chim Acta* 2003, 332, 51–9.
[63] Choi S, Choi EY, Kim DJ, Kim JH, Kim TS, Oh SW. A rapid, simple measurement of human albumin in whole blood using a fluorescence immunoassay (I). *Clin Chim Acta* 2004, 339, 147–56.
[64] Choi S, Choi EY, Kim HS, Oh SW. On-site quantification of human urinary albumin by a fluorescence immunoassay. *Clin Chem* 2004, 50, 1052–5.
[65] Song X, Knotts M. Time-resolved luminescent lateral flow assay technology. *Anal Chim Acta* 2008, 626, 186–92.
[66] Matsuya T, Tashiro S, Hoshino N, Shibata N, Nagasaki Y, Kataoka K. A core-shell-type fluorescent nanosphere possessing reactive poly(ethylene glycol) tethered chains on the surface for zeptomole detection of protein in time-resolved fluorometric immunoassay. *Anal Chem* 2003, 75, 6124–32.
[67] Huhtinen P, Kivela M, Soukka T, Tenhu H, Lövgren T, Härmä H. Preparation, characterisation and application of europium(III) chelate-dyed polystyrene – acrylic acid nanoparticle labels. *Anal Chim Acta* 2008, 630, 211–6.
[68] Xu Y, Li QG. Multiple fluorescent labeling of silica nanoparticles with lanthanide chelates for highly sensitive time-resolved immunofluorometric assays. *Clin Chem* 2007, 53, 1503–10.
[69] Chen Y, Chi YM, Wen HM, Lu ZH. Sensitized luminescent terbium nanoparticles: preparation and time-resolved fluorescence assay for DNA. *Anal Chem* 2007, 79, 960–5.
[70] Lim SJ, Chon B, Joo T, Shin SK. Synthesis and characterization of zinc-blende CdSe – based core/shell nanocrystals and their luminescence in water. *J Phys Chem C* 2008, 112, 1744–7.
[71] Yu Z, Guo L, Du H, Krauss T, Silcox J. Shell distribution on colloidal CdSe/ZnS quantum dots. *Nano Let* 2005, 5, 565.
[72] Chan WCW, Nie SM. Quantum dot bioconjugates for ultrasensitive nonisotopic detection. *Science* 1998, 281, 2016–8.
[73] Goldman ER, Clapp AR, Anderson GP, Uyeda HT, Mauro JM, Medintz IL, Mattoussi H. Multiplexed toxin analysis using four colors of quantum dot fluororeagents. *Anal Chem* 2004, 76, 684–8.
[74] Chan WC, Maxwell DJ, Gao X, Bailey RE, Han M, Nie S. Luminescent quantum dots for multiplexed biological detection and imaging. *Curr Opin Biotechnol* 2002, 13, 40–6.
[75] Bruchez M, Moronne M, Gin P, Weiss S, Alivisatos AP. Semiconductor nanocrystals as fluorescent biological labels. *Science* 1998 281, 2013–6.
[76] Chun P. Colloidal gold and other labels for lateral flow immunoassays. In: Wong RC, Tse HY., eds. *Lateral Flow Immunoassay*. New York, NY, Humana Press, 2009, 75–93.
[77] Frasco MF, Chaniotakis N. Bioconjugated quantum dots as fluorescent probes for bioanalytical applications. *Anal Bioanal Chem* 2010, 396, 229–40.
[78] Bailey RE, Smith AM, Nie S. Quantum dots in biology and medicine. *Physica E* 2004, 25, 1–12.
[79] Gill R, Zayats M, Willner I. Semiconductor quantum dots for bioanalysis. *Angew Chem Int Ed* 2008, 47, 7602–25.
[80] Jin Z, Hildebrandt N. Semiconductor quantum dots for in vitro diagnostics and cellular imaging. *Tr Biotechnol* 2012, 30, 394–403.
[81] Biju V, Mundayoor S, Omkumar RV, Anas A, Ishikawa M. Bioconjugated quantum dots for cancer research: Present status, prospects and remaining issues. *Biotechnol Advances* 2010, 28, 199–213.
[82] Kuang H, Zhao Y, Ma W, Xu L, Wang L, Xu C. Recent developments in analytical applications of quantum dots. *TrAC* 2011, 30, 1620–36.

[83] Medintz IL, Mattoussi H, Clapp AR. Potential clinical applications of quantum dots. *Int J Nanomed* 2008, 3, 151–67.
[84] Frigerio C, Ribeiro DSM, Rodrigues SSM, Abreu VLRG, Barbosa JAC, Prior JAV, Marques KL, Santos JLM. Application of quantum dots as analytical tools in automated chemical analysis: a review. *Anal Chim Acta* 2012, 735, 9–22.
[85] Ding SG, Chen JX, Jiang HY, He J, Shi WM, Zhao WS, Shen JZ. Application of quantum dot-antibody conjugates for detection of sulfamethazine residue in chicken muscle tissue. *J Agric Food Chem* 2006, 54, 6139–42.
[86] Chen JX, Fei X, Jiang, HY, Hou Y, Rao QX, Guo PG, Ding SG. A novel quantum dot-based fluoroimmunoassay method for detection of Enrofloxacin residue in chicken muscle tissue. *Food Chem* 2009, 113, 1197–201.
[87] Chen YP, Ning BA, Liu N, Feng Y, Liu Z, Liu XY, Gao ZX. A rapid and sensitive fluoroimmunoassay based on quantum dot for the detection of chlorpyrifos residue in drinking water *J Environ Sci Health B* 2010, 45, 508–15.
[88] Tully E, Hearty S, Leonard P, O'Kennedy R. The development of rapid fluorescence-based immunoassays, using quantum dot-labelled antibodies for the detection of Listeria monocytogenes cell surface proteins. *Int J of Biol Macromolecules* 2006, 39, 127–34.
[89] Peng CF, Li ZK, Zhu YY, Chen W, Yuan Y, Liu LQ, Li QS, Xu DG, Qiao RR, Wang L, Zhu SF, Jin ZG, Xu CL. Simultaneous and sensitive determination of multiplex chemical residues based on multicolor quantum dot probes. *Biosens Bioelectron* 2009, 24, 3657–62.
[90] Wang XL, Tao GH, Meng YH. A novel CdSe/CdS quantum dot-based competitive fluoroimmunoassay for the detection of clenbuterol residue in pig urine using magnetic core/shell $Fe_3O_4$/Au nanoparticles as a solid carrier. *Anal Sci* 2009, 25, 1409–13.
[91] Trapiella-Alfonso L, Costa-Fernandez JM, Pereiro R, Sanz-Medel A. Development of a quantum dot-based fluorescent immunoassay for progesterone determination in bovine milk. *Biosens Bioelectron* 2011, 26, 4753–9.
[92] Beloglazova NV, Speranskaya ES, De Saeger S, Hens Z, Abé S, Goryacheva IY. Quantum dot based rapid tests for zearalenone detection. *Anal Bioanal Chem* 2012, 403, 3013–24.
[93] Li HA, Cao ZJ, Zhang YH, Lau CW, Lu JZ. Combination of quantum dot fluorescence with enzyme chemiluminescence for multiplexed detection of lung cancer biomarkers. *Anal Methods* 2010, 2, 1236–42.
[94] Ma Q, Wang C, Su XG. Synthesis and application of quantum dot-tagged fluorescent microbeads. *J Nanosci Nanotechnol* 2008, 8, 1138–49.
[95] Pinwattana K, Wang J, Lin CT, Wu H, Du D, Lin Y, Chailapakul O. CdSe/ZnS quantum dots based electrochemical immunoassay for the detection of phosphorylated bovine serum albumin. *Biosens Bioelectron* 2010, 26, 1109–13.
[96] Thurer R, Vigassy T, Hirayama M, Wang J, Bakker E, Pretsch E. Potentiometric immunoassay with quantum dot labels. *Anal Chem* 2007, 79, 5107–10.
[97] Zou Z, Du D, Wang J, Smith JN, Timchalk C, Li Y, Lin Y. Quantum dot-based immunochromatographic fluorescent biosensor for biomonitoring trichloropyridinol, a biomarker of exposure to chlorpyrifos. *Anal Chem* 2010, 82, 5125–33.
[98] Li Z, Wang Y, Wang J, Tang Z, Pounds JG, Lin Y. Rapid and sensitive detection of protein biomarker using a portable fluorescence biosensor based on quantum dots and a lateral flow test strip. *Anal Chem* 2010, 82, 7008–14.
[99] Yang H, Li D, He R, Guo Q, Wang K, Zhang X, Huang P, Cui D. A novel quantum dots – based point of care test for syphilis. *Nanoscale Res Lett* 2010, 5, 875–81.
[100] Bai Y, Tian C, Wei X, Wang Y, Wang D, Shi X. A sensitive lateral flow test strip based on silica nanoparticle/CdTe quantum dot composite reporter probes. *RSC Advances* 2012, 2, 1778–81.

[101] Beloglazova NV, Goryacheva IY, Niessner R, Knopp D. A comparison of horseradish peroxidase, gold nanoparticles and quantum dots as labels in non-instrumental gel-based immunoassay. *Microchim Acta* 2011, 175, 361–7.
[102] Kodaira CA, Lourenco AVS, Felinto MCFC, Sanchez EMR, Rios FJO, Nunes LAO, Gidlund M, Malta OL, Brito HF. Biolabeling with nanoparticles based on Y2O3: Nd3+ and luminescence detection in the near-infrared. *J Luminescence* 2011, 131, 727–31.
[103] Hampl J, Hall M, Mufti NA, Yao YM, MacQueen DB, Wright WH, Cooper DE. Up-converting phosphor reporters in immunochromatographic assays. *Anal Biochem* 2001, 288, 176–87.
[104] Kuningas K, Rantanen T, Karhunen U, Lo1vgren T, Soukka T. Simultaneous use of time-resolved fluorescence and anti-stokes photoluminescence in a bioaffinity assay. *Anal Chem* 2005, 77, 2826–34.
[105] Soukka T, Rantanen T, Kuningas K. Photon upconversion in homogeneous fluorescence-based bioanalytical assays. *Ann NY Acad Sci* 2008, 1130, 188–200.
[106] Ouellette AL, Li JJ, Cooper DE, Ricco AJ, Kovacs GTA. Evolving point-of-care diagnostics using up-converting phosphor bioanalytical systems. *Anal Chem* 2009, 81, 3216–21.
[107] Corstjens P, van Lieshout L, Zuiderwijk M, Kornelis D, Tanke HJ, Deelder AM, van Dam GJ. Up-converting phosphor technology-based lateral flow assay for detection of Schistosoma circulating anodic antigen in serum. *J Clin Microbiol* 2008, 46, 171–6.
[108] Niedbala RS, Feindt H, Kardos K, Vail T, Burton J, Bielska B, Li S, Milunic D, Bourdelle P, Vallejo R. Detection of analytes by immunoassay using up-converting phosphor technology. *Anal Biochem* 2001, 293, 22–30.
[109] Yan Z, Zhou L, Zhao Y, Wang J, Huang L, Hu K, Liu H, Wang H, Guo Z, Song Y, Huang H, Yang R. Rapid quantitative detection of Yersinia pestis by lateral-flow immunoassay and up-converting phosphor technology-based biosensor. *Sens Actuators B Chem* 2006, 119, 656–63.
[110] Mokkapati VK, Niedbala RS, Kardos K, Perez RJ, Guo M, Tanke HJ, Corstjens PL. Evaluation of UPlink-RSV: prototype rapid antigen test for detection of respiratory syncytial virus infection. *Ann N Y Acad Sci* 2007, 1098, 476–85.
[111] Corstjens P, Zuiderwijk M, Tanke HJ, van der Ploeg-van Schip JJ, Ottenhoff TH, Geluk A. A user-friendly, highly sensitive assay to detect the IFN-gamma secretion by T cells. *Clin Biochem* 2008, 41, 440–4.
[112] Zuiderwijk M, Tanke HJ, Sam Niedbala R, Corstjens PL. An amplification-free hybridization-based DNA assay to detect Streptococcus pneumoniae utilizing the up-converting phosphor technology. *Clin Biochem* 2003, 36, 401–3.
[113] Qu Q, Zhu Z, Wang Y, Zhong Z, Zhao J, Qiao F, Du XY, Wang Z, Yang R, Huang L, Yu Y, Zhou L, Chen Z. Rapid and quantitative detection of Brucella by up-converting phosphor technology-based lateral-flow assay. *J Microbiol Methods* 2009, 79:121–3.
[114] Li LP, Zhou L, Yu Y, Zhu Z, Lin CQ, Lu CL, Yang R. Development of up-converting phosphor technology-based lateral-flow assay for rapidly quantitative detection of hepatitis B surface antibody. *Diagn. Microbiol Infect Dis* 2009, 63, 165–72.
[115] Corstjens P, Zuiderwijk M, Brink A, Li S, Feindt H, Niedbala RS, Tanke H. Use of up-converting phosphor reporters in lateral-flow assays to detect specific nucleic acid sequences: a rapid, sensitive DNA test to identify human papillomavirus type 16 infection. *Clin Chem* 2001, 47, 1885–93.
[116] Corstjens P, Zuiderwijk M, Nilsson M, Feindt H, Niedbala SR, Tanke HJ. Lateral-flow and up-converting phosphor reporters to detect single-stranded nucleic acids in a sandwich-hybridization assay. *Anal Biochem* 2003, 312, 191–200.
[117] Wang J, Chen Z, Corstjens PL, Mauk MG, Bau HH. A disposable microfluidic cassette for DNA amplification and detection. *Lab Chip* 2006, 6, 46–53.

[118] Corstjens PLAM, de Dood CJ, van der Ploeg-van Schip JJ, Wiesmeijer KC, Riuttamäki T, van Meijgaarden KE, Spencer JS, Tanke HJ, Ottenhoff THM, Geluk A. Lateral flow assay for simultaneous detection of cellular- and humoral immune responses. *Clin Biochem* 2011, 44, 1241–6.

[119] Glaspell G, Tabb JS, Shearer A, Wilkins J, Smith C, Massaro R. Utilizing upconverting phosphors for the detection of TNT. *Proc SPIE* 2010, 7664, 76641G.

[120] Song XD, Huang L, Wu B. Bright and monodispersed phosphorescent particles and their applications for biological assays. *Anal Chem* 2008, 80, 5501–7.

[121] Rundstrom G, Jonsson A, Martensson O, Mendel-Hartvig I, Venge P. Lateral flow immunoassay using Europium (III) chelate microparticles and time-resolved fluorescence for eosinophils and neutrophils in whole blood. *Clin Chem* 2007, 53 342–8.

T. Yu. Rusanova

# 4 Nanofilms as Sensitive Layers of Chemical and Biochemical Sensors

## 4.1 Introduction

One of the important directions in chemical analysis is the creation of small and inexpensive sensors for the rapid determination of chemical compounds in industrial, natural, and biological objects [1]. Prospects of their application are related to such features as minimum of sample preparation in the determination of the analyte, the fast obtaining analytical information, and the undemanding skills of the employee. Current trends in the development of sensory devices are increasingly tending to complicate their tool base, which does not always satisfy customers and consumers because of the increased cost of analytical services. An alternative direction is the use of nanotechnologies, which allows creation of a nanoscale sensitive layer with prescribed physicochemical and analytical properties and improved metrological characteristics of the sensors [2].

A wide application of nanoscale films for modifying the surface of electrodes in electrochemical, electrical, and piezoelectric sensors, as well as the surface of waveguides in optical sensors, is due to their following advantages [1, 3–8]:

- a relatively high ratio of the active surface area of molecular layers to the film volume;
- the ability to control the thickness of the film to an accuracy of a single molecule;
- a rapid diffusion of analyte molecules into the volume of the film, which causes a short response time of the sensors;
- the ability to combine layers with different analytical responses, as well as layers that have permeability only for certain ions or molecules;
- a high uniformity of the film combined with mutual orientation of the molecules and functional groups composing the film;
- the possibility of determining the optimum number of monolayers that ensures the highest analytical effect;
- a low consumption of analytical reagents and, therefore, the possibility of using expensive effective reagents (e.g., a typical mass of a self-assembled monolayer [SAM] is only $2 \cdot 10^{-7}$ g/cm$^2$).

https://doi.org/10.1515/9783110542011-004

## 4.2 Nanofilm types and techniques of their preparation

The most common methods for obtaining nanofilms used as sensitive layers of chemical and biochemical sensors include:

- SAMs of alkylthiols, alkyl sulfides, and alkyl disulfides (as well as their various derivatives) on the surface of metals (usually gold);
- layer-by-layer (LbL) technique, consisting in alternate deposition of polyelectrolytes with functional groups of different charges [9];
- Langmuir–Blodgett (LB) technology, at which monomolecular layers of amphiphilic organic molecules are transferred from the surface of the liquid subphase to a solid substrate [10].

### 4.2.1 Self-assembled monolayers

The phenomenon of the monolayers self-organization on a solid surface was discovered in the middle of the last century when it was established that molecules of alcohols with a long hydrocarbon (HC) chain can spontaneously transfer from diluted solutions to a clean glass surface, making it hydrophobic [11] and molecules of alkylamines adsorb on the platinum surface [12]. However, the formed monolayers were unstable and easily destroyed. It turned out that much more stable monolayers are formed by the interaction of alkyl chlorosilanes with the active silanol groups of the silicon surface [13], leading to formation a polysiloxane structure. However, alkyl chlorosilanes allow modifying the surface only with HC radicals. SAMs based on alkylthiols (R–SH), alkyl sulfides (R–S–R), and alkyl disulfides (R–S–S–R) on the surfaces of various metals (silver, platinum, copper, and especially gold) have become more widespread in chemical sensors [9]. Spontaneous formation of monolayers of organic disulfides on gold was discovered in 1983 [14]. At present, the mechanism of SAM formation has been well studied and described in the literature [9]. Self-assembly of monolayers is due to the formation of a bond between sulfur and metal atoms, as well as van der Waals interactions between alkyl chains. The energy of S–Au bond is 30–35 kcal/mol, while the van der Waals forces per $CH_2$ group are 0.8 kcal/mol. In many respects, the ordering of the resulting monolayers is determined by the crystallographic packing Au (1,1,1), which can be easily obtained by depositing thin gold films on polished plates of glass, silicon, and freshly mica.

To obtain a monolayer, thiols, sulfides, and disulfides are usually dissolved in ethanol (non-polar thiols) or water (alkylthiols with polar substituents). When a substrate with a gold film is immersed in this solution, in the first stage the S atoms interact with gold causing the deprotonation of thiol groups:

$$RSH + Au \rightarrow RS - Au + \bar{e} + H^+,$$

or S–S bond dissociation in disulfides. The S atom is in $sp^3$ hybridization, which also causes the ordered arrangement of HC chains with a slope angle of 20–40 degrees to the surface. In the second stage, the molecules are aligned in parallel and a crystal-like film is formed as a result of the interaction between nonpolar alkyl radicals. Figure 4.1 shows the examples of substances forming SAM on Au surface.

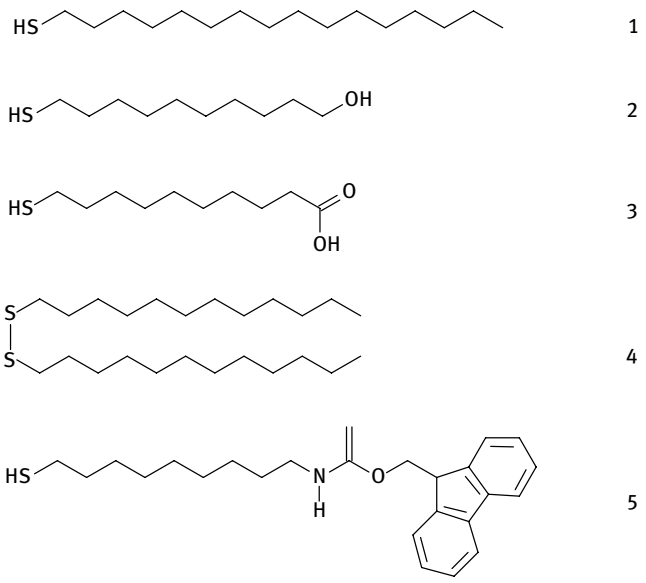


**Fig. 4.1:** Examples of substances forming SAM on Au surface: 1, n-hexadecylthiol; 2, 11-mercapto-1-undecanol; 3, 10-mercaptodecanoic acid; 4, didodecylsulfide; and 5, alkylthiol with amino group blocked by 9-fluorenylmethoxycarbonyl.

The two-step mechanism affects the kinetics of the process: a relatively fast adsorption process controlled by diffusion is followed by a slow crystallization stage. Quite dense monolayers are formed in less than an hour; however, complete crystallization sometimes takes several days. The most ordered monolayers are formed by alkylthiols with an HC chain containing 16 carbon atoms. Such monolayers are stable, resistant to the water, and acid or alkaline solutions. In addition to alkylthiols, for example, compounds such as cystamine [15] or thioctic acid [16] can be used, but the ordering of such layers has not been proven.

The possibility of modification of alkylthiols by functional groups makes them promising for obtaining monolayers with different surface properties. For example, the introduction of a hydroxyl group makes it possible to obtain a hydrophilic surface. Heterobifunctional alkylthiols can also act directly as analytical reagents. Such small functional groups (about 0.5 nm) as $NH_2$, OH practically do not affect the self-assembly. However, large functional groups (COOH, ferrocene) reduce the density and ordering of the layer.

SAMs are widely used for subsequent immobilization of biomolecules on the surface of the sensor layer [17]. It should be noted that biomolecules containing thiol groups can be directly immobilized on the surface of gold. For example, monolayers of thiolated glucose oxidase [18] and synthetic oligonucleotides [19] were obtained. Another example is the use of thiol groups of antibodies for their direct immobilization on the gold surface [20]. To increase the monolayer order and to remove weakly adsorbed oligonucleotides, the monolayer is then treated with short-chain thiols [19].

Another, more popular method of biomolecule immobilization is the modification of an already organized monolayer of alkylthiols. Biomolecules can be immobilized on a monolayer by the physical adsorption as a result of electrostatic interaction with thiols having charged groups on the other end (e.g., carboxyl groups, see Fig. 4.1), and also by covalent binding of biomolecules with different functional groups of thiols (amino, carboxy, hydroxy, ethoxy, etc.). For example, aminomodified thiols can be used for binding proteins with glutaraldehyde method [21, 22]. However, the amino group of aminoalkylthiols can also interact with the gold surface, reducing the order of the monolayer; therefore, a method of preliminary blocking this group with 9-fluorenylmethoxycarbonyl is proposed, followed by its removal by treatment with a 20 % solution of piperidine in acetonitrile [21].

Carboxyalkylthiols are often used and their binding with proteins is carried out by the carbodiimide method [23]. The use of cyanuric fluoride and pyridine is also described for the conversion of carboxyderivatives to acylfluorides having high reactivity to primary and secondary amino groups of proteins [24]. Hahn et al. [25] describe the use of SAM with aldehyde groups for the immobilization of biomolecules. Biotinylated thiols are used to produce thin streptavidin films [26]. Moreover, cross-linkers such as 4-fluoro-3-nitrophenyl azide [27], 1,4-disuccinimidyl terephthalate [28], and protein A [29] are used to bind biomolecules with a monolayer.

By combining thiols with different functional groups, sensor layer sensitive to several analytes can be obtained. Such mixed monolayers are usually formed by the exchange of molecules from an already preorganized monolayer with molecules of another thiol or disulphide from their solution [17]. The introduction into the monolayer of short-chain alkylthiols (“spacers”) reduces steric hindrance while interacting with the analyte.

Monolayers of alkylthiols are used for biomolecules’ binding not only on a flat surface of gold, but also on gold nanoparticles [30]. Immobilized biomolecules are enzymes, DNA/RNA, and their fragments, antibodies, and even living cells [31].

### 4.2.2 LbL technique

Self-assembled nanosized films can also be prepared as a result of electrostatic interaction between oppositely charged polyelectrolytes [9]. The advantage of this method is its simplicity, availability of reagents, the possibility of incorporating a

variety of analytical reagents into the film. The technique implies treatment of a charged substrate in a dilute polyelectrolyte solution, resulting in the formation of a polymer monolayer. Further, it is possible to deposit the next polymer monolayer with a charge opposite to the first [32]. Polyvinylpyridine, polyallylamine, polyethyleneimine, and amino-modified dextran are widely used from cationic polymers, polystyrene sulfonate, polyvinyl sulfate, polyacrylic acid, etc., as anionic polymers (Fig. 4.2).

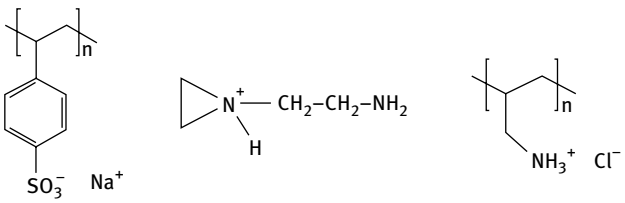


**Fig. 4.2:** Examples of polyionic molecules: 1, sodium polystyrene sulfonate; 2, polyethyleneimine; and 3, polyallylamine hydrochloride.

The adsorption of the first layer of polyionic molecules is more effective if the substrate surface has a charge opposite to the charge of the polyelectrolyte. The initial charge of the surface also can be regulated by applying the first layer of the substance, with held, for example, by hydrophobic interactions.

The following factors influence the LbL process: the concentration of polymer solutions, the nature of the solvent, the pH value, the ionic strength of the solution, temperature, mixing, times of adsorption, and washing. The conformation and thickness of the deposited layers depend on the polyelectrolyte charge and the ratio of the dimensions of the hydrophobic and hydrophilic parts. Typically, a large number of segments that directly contact and interact with the surface of a solid can be distinguished in the polymer structure. In the case of a weak polyelectrolyte, the adsorption depends on the degree of ionization of the hydrophilic groups, which is regulated by a change in the acidity of the medium and the nature of the solvent. The adsorption of both weak and strong polyelectrolytes is affected by the ionic strength of the solution. With high ionic strength, the repulsion between neighboring adsorbed segments decreases, and polyelectrolyte molecules behave as uncharged polymers, which leads to the formation of a thick layer.

In addition to polyelectrolytes, monomer charged molecules can be included in such layers, for example, aminated, carboxylated or sulfonated calixarenes or cyclodextrins [33]. For example, in [34], pillar[5]arene-based multilayer films are constructed by LbL assembly with consecutive adsorption of cationic and anionic pillar[5]arenes.

The introduction of various analytical reagents, including biomolecules, into the layers of polyelectrolytes can be accomplished either by electrostatic interaction or by covalent bonding with the functional groups of the polymer.

### 4.2.3 LB films

The Langmuir–Blodgett (LB) technology was developed in the 1930s and 1940s by Irving Langmuir and Katharina Blodgett, but its use in molecular electronics and sensors began only in the 1980s. The preparation of LB films consists of two stages: (1) the formation of an ordered monolayer of an amphiphilic substance at the interface between a liquid (usually water or aqueous solution) and gaseous (air) phases; (2) the monolayer transfer at a constant surface pressure on a solid surface [10]. The process is carried out in a special Langmuir trough equipped with Wilhelmi balance to measure the surface tension, a movable barrier to compress the monolayer, and a device providing the movement of the solid substrate through the monolayer. To form a monolayer, a solution of the amphiphilic substance is applied to the surface of the liquid subphase in a volatile inert solvent, for example chloroform.

After evaporation of the solvent, the molecules of the amphiphilic substance are initially distributed chaotically over the surface of the liquid subphase, practically not interacting with each other (Fig. 4.3a), and form the so-called "two-dimensional gas" or "gas" phase of the monolayer. When the surface area decreases with a mobile barrier, the molecules approach each other to form a liquid-expanded and further liquid-crystalline phase (Fig. 4.3b, c). Further, at a constant surface pressure corresponding to the liquid-crystalline state of the monolayer, the substrate is slowly moved (about several millimeters per minute) through the monolayer, and the first monolayer is transferred to a solid surface, then the process is repeated the required number of times. Thus, it is possible to obtain complex molecular structures with a resolution of 2–3 nm and arrangement of layers of different molecules in the required order.

The range of substances forming Langmuir monolayer is, unfortunately, limited. The substance must have surfactant properties and its solubility should not exceed $10^{-6}$ mol/L. Traditional objects of LB technology are fatty acids (e.g., stearic or arachidic) and their salts. However, with the development of organic synthesis methods, the range of substances used to produce LB films has significantly expanded. It includes various dyes with HC chain, phospholipids, phthalocyanines, cyclodextrins, calix[n]arenes, as well as unsaturated compounds capable of subsequent polymerization in the film, including derivatives of diacetylenes, etc. There are also a number of biologically active compounds such as cholesterol, chlorophyll, and various proteins that form monomolecular layers. Many compounds that do not form

monolayers by themselves easily "fit" into the structure of Langmuir monolayers of other compounds [10].

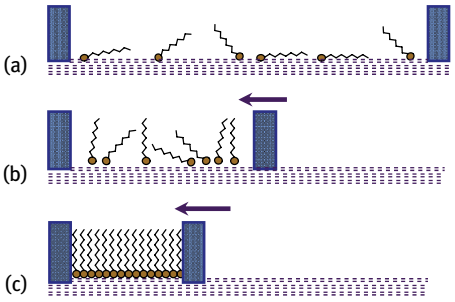


**Fig. 4.3:** Gas (a), liquid-expanded (b), and liquid-crystal (c) states of the monolayer.

## 4.3 Nanofilms' sensor application

### 4.3.1 SAM

**Enzyme sensors.** Immobilization of glucose oxidase on SAM connecting with the surface of gold nanotubes [35] allowed the creation of a highly sensitive amperometric sensor for the determination of glucose. A sensor for determining glucose based on an SAM of mercaptopropionic acid was also developed, on which the enzyme was immobilized by LbL adsorption of cationic polyelectrolyte and glucose oxidase having negatively charged groups [36]. In work [37] it was shown that the optimal system for the determination of catechol is SAM based on 2-aminoethanethiol cross-linked with enzyme laccase using glutaraldehyde. Alkene-based SAMs grafted on oxidized Pt surfaces were used as a scaffold to covalently immobilize oxidase enzymes, with the aim to develop an amperometric biosensor platform [38]. $NH_2$-terminated organic layers were functionalized with either aldehyde (CHO) or N-hydroxysuccinimide (NHS) ester-derived groups, to provide anchoring points for enzyme immobilization. To improve the efficiency of electron transfer in electrochemical sensors, mediators, for example, 1,4-diaminoanthraquinone [39], are added to the SAM. The thiol itself, modified by the corresponding groups (11-ferrocenyl-1-undecanthiol) [40], can also be a mediator. The presence of SAM between the electrode and the enzyme makes it possible to preserve its enzymatic activity [41].

*DNA sensors* are widely used in clinical diagnostics for the detection of genetic diseases, pathogenic infections, and testing of DNA colonies in molecular biology. The use of SAM to immobilize DNA allows the conformation necessary for the hybridization reaction – the specific interaction of two complementary strands of DNA, one of which is applied to the surface of the sensor, and the other is the object of determination

[42]. The hybridization reaction is recorded by a field-effect transistor [43], an electrochemical method with enzymatic amplification [44], impedance spectroscopy [45], quartz crystal microbalance [19], and surface plasmon resonance (SPR) [46]. Special DNA structures labeled with ferrocene were used to record hybridization due to conformational changes that occur, affecting the efficiency of electron transfer [47]. To reduce nonspecific DNA sorption on gold and to increase hybridization efficiency, mixed monolayers of thiolated DNA with blocking short-chain thiols are used. At the same time, by controlling the distance between DNA probes, their spatial accessibility is ensured and steric hindrances associated with the hybridization reaction are eliminated. SAM with immobilized DNA is also used to determine specific proteins [48].

**Immunosensors.** SAMs allow targeted immobilization of antibodies. Thus, SAM based on protein G, modified with 2-aminothiolane, effectively binds anti-hCG monoclonal antibodies [49], whereas for nonionized protein G the amount of bound antibodies decreases 1.6 times. Similar SAM with protein G was used to simultaneously determine the pathogenic microorganisms of *E. coli* O157:H7, *Salmonella typhimurium*, *Yersinia enterocolitica*, and *Legionella pneumophila* [50]. Immunosensors also use mixed monolayers of mercaptopropanol and 2-aminoethanethiol [51]. The immunosensor layer with optimal characteristics was obtained on the basis of a mixed monolayer of carboxy- and hydroxy-derived alkylthiols at a ratio of 1:3 [52]. Acylthiols modified with polyethylene glycol make it possible to reduce nonspecific sorption on the immunosensory coating [53]. SAMs of dithiols are usually formed faster than alkylthiols [54]. For example, N-succinimidyl-3-(2-pyridyldithiol), due to its heterobifunctionality, rapidly reacts with the amino groups of antibodies [55].

SAM based on thiol functionalized with mannose and concavalin A was used to determine *E. coli* by the quartz crystal microbalance method [56]. In this case, strong adhesion of *E. coli* to mannose and multivalent binding to concavalin A provided a detection limit of several hundred bacterial cells.

In the case of an indirect immunoassay, any analyte derivative, for example, a conjugate with a protein, is applied to the sensor surface. Thus, for example, a sensor for aflatoxin B1 was obtained [57].

Thus, SAMs of alkylthiols are used to immobilize biomolecules with a certain spatial orientation, preserve their affinity properties, reduce nonspecific sorption, and obtain multifunctional chemically sensitive layers. The technology of SAM preparation is simple and does not require special equipment. Examples of application of SAM in biosensors for the determination of various compounds are presented in Tab. 4.1.

### 4.3.2 LbL technique

Initially polyelectrolyte layers were used mainly in amperometric sensors [69] and are often combined with other methods of sensor layer preparation. This technology was further extended to other types of sensors. For example, a piezoelectric

**Tab. 4.1:** Examples of biosensors based on SAMs

| Analyte | Sensor type[a] | Sensor layer based on SAM[b] | Method of biomolecule immobilization | Linear range (LOD)[c] | Ref. |
|---|---|---|---|---|---|
| Insulin | QCM | Antibodies modified by thiol groups | Direct binding | 2.5–80 mIU/mL | [20] |
| Laccase | amper. | Laccase / cysteamine / Au | Covalent binding by glutaraldehyde | 1–400 µM | [37] |
| Methanol | amper. | Alcohol oxidase –HRP / 4,4′-dithiodibutyric acid + 11-ferrocenyl-1-undecanethiol / Au | Covalent binding by carbodiimide | 10–150 µM (10 µM) | [40] |
| *E. coli* | QCM | Thiolated mannose / Au | Binding by concanavalin A | $7.5 \cdot 10^2$ to $7.5 \cdot 10^7$ cells/mL | [56] |
| Aflatoxin B1 | QCM | MPA / conjugate of analyte with protein | Covalent binding by carbodiimide | 0.1–100 ng/mL (0.01 ng/mL) | [57] |
| Glucose | electr. | Glucose oxidase / Au nanoparticles / bilayer of 3-(tri-methoxysilyl)-propane-l-thiol / Au | Physical adsorption | $4 \cdot 10^{-10}$ to $5.3 \cdot 10^{-8}$ M ($10^{-10}$ M) | [58] |
| BSA | Impedimetric | Cysteamine- / avidin- / biotin-labeled antihuman IgG antibody | Covalent binding by glutaraldehyde | 100–900 ng/mL (100 ng/mL) (0.62 µg/mL) | [59] |
| IgG | FET | 5-Carboxy-1-pentanethiol / streptavidin / biotinylated anti-IgG antibody | Covalent binding by carbodiimide / avidin–biotin binding | 0–10 µg/mL | [60] |
| Parathion | amper. | Acetyl-cholinesterase / MPA / Au | Covalent binding by glutaraldehyde | $2 \cdot 10^{-6}$ to $15 \cdot 10^{-6}$ M (9.3 µg/L) | [61] |
| IgG | electr. | Anti-IgG antibodies / APTES / silica | Covalent binding by glutaraldehyde | (10 ng/mL) | [62] |
| Taxol | electr. | DNA / azido hexanethiol / Au | Physical adsorption | $1.2 \cdot 10^{-7}$ to $1.5 \cdot 10^{-6}$ M | [63] |
| *S. typhimurium* | SPR | Anti-*S. typhimurium* antibodies / protein G / MUA / Au | Binding by protein G | $10^{-2}$ to $10^{-9}$ CFU/mL | [64] |

**Tab. 4.1:** (continued)

| Analyte | Sensor type[a] | Sensor layer based on SAM[b] | Method of biomolecule immobilization | Linear range (LOD)[c] | Ref. |
|---|---|---|---|---|---|
| Chloramphenicol | QCM | Antibodies / MUA / Au | Covalent binding by carbodiimide | $5 \cdot 10^{-6}$ to $10^{-2}$ M | [65] |
| Anti-histamine antibodies | SPR | Histamine / MUA / Au | Covalent binding by carbodiimide | (3 ppb) | [66] |
| α-Fetoprotein | QCM | Cysteamine / polymer based on 5-[3-(4-aminophenyl) propanonylamino] -isophthalic acid / antibodies | Covalent binding by carbodiimide | 10–200 µg/mL | [67] |
| Carbaryl | QCM | Thioctic acid / conjugate of analyte with protein | Covalent binding by carbodiimide | 15–53 µg/L (11 µg/L) | [68] |

[a]amper. amperometric
electr. electrochemical
QCM quartz crystal microbalance (piezoelectric)
SPR surface plasmon resonance
FET field-effect transistor
[b]HRP horseradish peroxidase
MUA 11-mercaptoundecanoic acid
MPA 11-mercaptopropionic acid
APTES aminopropyltriethoxysilane
[c]LOD limit of detection

immunosensor for the paclitaxel determination in the concentration range 35–150 ng/mL was constructed based on three bilayers of poly(dimethyldiallylammonium chloride)/polystyrene sulfonate with covalently bound antibodies [70]. A sensitive polyaniline/titanium dioxide–based QCM sensor was fabricated for toxic gas detection [71].

The interdigital microelectrodes were covered by nanocomposite film of chemically reduced graphene oxide (RGO) and poly(diallylimethyammonium chloride) and applied as humidity sensor [72]. LbL self-assembly of the graphene films also was used for electrochemical [73], SPR [74], and impedance spectroscopy sensors creation [75]. Some LbL optical sensors were developed, for example, based on water-insoluble platinum complex for oxygen detection [76] and water-soluble fluorescent conjugated polymer for Hg (II) detection [77].

Last decade LbL assemblies with nanoparticles were intensively investigated, and a review focused on the recent advances in biosensors based on such systems was published recently [78]. Carbon nanotubes [79] and Mg–Al-layered double hydroxide nanosheets [80] also were incorporated in LbL films and applied for glucose and acephatemet detection, respectively.

### 4.3.3 LB films

LB films are used as sensitive layers in all types of chemical sensors. The greatest development at the moment has been gas sensors based on various substituted phthalocyanines (porphyrins) of metals. The central atom of these compounds is mainly the rare earth elements, as well as Cu, Zn, Sn, and Mg. Such sensors are based on the selective binding of gases ($NO_2$, $NH_3$, $Cl_2$ band, etc.) to the phthalocyanines to form complexes with charge transfer, in which the role of the donor is performed by phthalocyanine (porphyrin) rings, and the role of the acceptor is gas molecules. This leads to a significant change in a number of electrical characteristics of the films (electrical conductivity, charge, etc.), which is recorded using a system of electrodes or a field effect transistor. The detection limit of these gas sensors reaches tenth of a ppm [81], but mostly ranges from a few to tenth of ppm [82]. Moreover, bisphthalocyanines of metals, as a rule, are more sensitive than monosubstituted compounds [83].

A linear dependence of the response time of the sensors on the number of monolayers, found in a number of works, indicates the ability of gases to penetrate deeply into the film [8, 84]. The solvent that is used for LB film preparation can influence supramolecular architectures of phthalocyanines and sensor performance [85]. The selectivity of sensors based on phthalocyanines and porphyrins is regulated by the selection of substituents and by the combination of the ligand molecule and the nature of the central atom [86]. Improvement of selectivity is possible when receptor molecules, for example, calix[n]arenes, are incorporated in the film [87]. Electrochemical sensors for antioxidants [88], phenolic derivatives [89], optical sensors for

$NO_2$ [83], vapors of highly volatile organic compounds [90, 91], and vapors of nitric acid [92] have also been developed on the basis of phthalocyanine and porphyrin derivatives.

LB films of electrically conducting polymers, such as polyaniline (detection of $NH_3$ [93], $NO_2$ and $H_2S$ [94]), polythiophene ($NO_2$ and etc. [95, 96]), and polycarbazole ($NH_3$ detection [97]), are widely used. The conductive polymers can also be applied in liquid sensors, and an electric taste sensor (sweet, salty, acidic, and bitter) based on a polyaniline LB film with a Ru complex was developed [98]. This sensor recognizes these tastes below the threshold of human perception (at the level of micromolar concentrations of NaCl, HCl, quinine, and sucrose, used as model compounds) by applying the principal component analysis of data from four sensor elements, differing in the composition of the LB film. This principle was used in the development of an impedance spectroscopy sensor for the wines' classification (variety, origin, aging and storage conditions), in which LB films of various conducting polymers and lipids were applied [99].

LB films are also used in sensors for *ions determination*. Applying LB film of ionophore (e.g., valinomycin) as a membrane, a field effect transistor for measuring glial cell K + transport was obtained [100]. Films based on the amphiphilic (thiazolylazo) resorcinol can be used for visual determination of $Cd^{2+}$, $Pb^{2+}$, and $Hg^{2+}$ with detection limit of $3 \cdot 10^{-8}$ M [101, 102]. Various macrocyclic compounds are widely used for the metal detection. Thus, p-tert-butylthiacalix[4]arene was proposed for amperometric determination of the $Pb^{2+}$, $Cd^{2+}$ [103], and $Ag^{+}$ [104] with detection limits of $8 \cdot 10^{-9}$ M, $2 \cdot 10^{-8}$ M, and $3 \cdot 10^{-9}$ M, respectively. The *p-tert*-butylcalix[7]arene ethyl ester compound was synthesized, and its ability to form LB films and interact with metal ions was shown [105]. Impedance spectroscopy sensor on the basis of thiomacrocyclic ionophore ($1 \cdot 10^{-5}$ M detection limit) was proposed [106].

One of the most promising fields of ultrathin LB films application is modification of the surface of mass-sensitive sensors, based on the use of surface [107–109] and bulk acoustic waves [7, 110–115]. Such sensors have a high sensitivity to a film mass change; however, their selectivity is completely determined by the ability of the coating to selectively adsorb the analytes. For example, LB films of arachidic acid with incorporated carbon nanotubes were proposed to determine the vapors of organic compounds at the level of ppb [114] or octadecylamine films with chelating agent were used for the determination of $Ca^{2+}$ ions [110].

Application of LB films in optical sensors is not so popular. The most widespread at the moment are sensors, acting on the principle of quenching the luminescence of reagent in the presence of the analyte [116–119]. To increase the selectivity of sensors of this type, the process of energy transfer can be useful [120]. In the last decade, examples of SPR sensors [121, 122] have emerged that are highly sensitive and do not require the presence of chromophore or electrochemically active groups in the reagents. An interesting type of waveguide chemical sensors is proposed using such films as active coatings [81].

**Tab. 4.2:** The examples of sensors based on LB films

| Analyte | Sensor type | LB film nature | Linear range (LOD)[a] | Ref. |
|---|---|---|---|---|
| $Ca^{2+}$ | QCM | Octadecylamine + chelating agent | $10^{-8}$–$10^{-1}$ M ($10^{-11}$ M) | [110] |
| Chloroform, benzene, toluene, and ethyl alcohol | QCM | *N*,*N*′-dicyclohexyl-3,4:9,10-perylenebis (dicarboximide) | ($1.12 \cdot 10^4$ to $5.17 \cdot 10^4$ ppm) | [113] |
| Toluene | SAW | Carbon nanoparticles + arachidic acid | (~0.20 ppm) | [114] |
| $NO_2$, HCl, $Cl_2$ | Fluorescence quenching | Tetraphenylporphyrin + arachidic acid | 1–100 ppm | [117] |
| Amino acids, $NH_4^+$ | Fluorescence quenching | Anthroylstearate + stearate, perylene + arachidate | ~$10^{-6}$–$10^{-2}$ M | [119] |
| $Cu^{2+}$ | Fluorescence (energy transfer) | Cyan dye + dioctadecyl dithiocarbamate + eicosane amine | $10^{-7}$–$10^{-4}$ M | [120] |
| *S. typhimurium* | QCM | Phospholipid + antibodies | $10^2$–$10^8$ cells/mL | [125] |
| $NH_3$ | QCM | Poly(3,4-ethylenedioxythiophene) + stearic acid | ~10–60 ppm | [126] |
| Glucose | Optical | Glucose oxidase + poly-3-hexylthiophene | 10–50 mg/L | [127] |
| Glucose | Electrochemical | Glucose oxidase + octadecylamine | 0.1–5 mM | [128] |
| Trinitrotoluene | Fluorescence quenching | Polydiacetylene | (100 mg/L) | [129] |
| Organic and phenolic acids in wine | Voltammetric | *n*-Dodecanethiol functionalized gold nanoparticles | ($10^{-6}$ M) | [130] |
| Hg(II) | Voltammetric | ***p-tert***-butylthiacalix[4]arene | $5.0 \cdot 10^{-10}$ to $1.5 \cdot 10^{-7}$ M ($2.0 \cdot 10^{-10}$ M) | [131] |
| Catechol | Voltammetric | Dimyristoyl phosphatidic acid + lutetium bisphthalocyanine | ($3.34 \cdot 10^{-7}$ M) | [132] |
| Acetylcholine | Chemiluminescence | Acetylcholinesterase + glycolipid | ($4 \cdot 10^{-7}$ M) | [133] |
| $Ag^+$ | Voltammetric | Polyaniline + p-toluenesulfonic acid | $6.0 \cdot 10^{-10}$ to $1.0 \cdot 10^{-6}$ M ($4.0 \cdot 10^{-10}$ M) | [134] |
| Dimethyl-methyl-phosphonate | SPR | Cavitands with carboxyl groups | ppb – ppm | [135] |

[a]LOD limit of detection.

Sensors based on the light absorption have been developed. Films are prepared, for example, from the chromophore derivatives of calixarenes (determination of $NO_2$) [87]. There are examples of the use of LB films to create optical pH sensors with an adjustable probe (by changing the nature of the Langmuir film matrix) by the interval of the measured acidity [6]. The analytical parameters of some sensors [119–135] based on LB films are presented in Tab. 4.2.

LB technology can also be used to form sensitive layers of biosensors. A number of proteins, lipids, enzymes, and polysaccharides can form stable monolayers and LB films. Water-soluble biomolecules (antibodies, DNA fragments) can be included in the matrix of the film due to electrostatic and hydrophobic interactions. Thus, DNA molecules dissolved in the liquid subphase are adsorbed by a monolayer of octadecylamine [123, 124], which allows them to be transferred to the surface of the sensor and then to detect the analytes using voltammetric or other methods.

LB films with incorporated enzymes, in particular glucose oxidase, were widely used in sensors [136]. Glucose oxidase can be included in octadecylamine [128], stearic acid [137], poly-3-hexylthiophene [127], and some other monolayers. The preparation of films containing glucose oxidase is possible both from its adsorption from the aqueous subphase to the Langmuir monolayers [138] and to the application of a mixture of glucose oxidase with amphiphylic substances in chloroform on the surface of the liquid subphase [139, 140]. Moreover, the adsorption of the enzyme from solutions on the prepared LB films was shown [141, 142]. Poly(3-hexylthiophene) was utilized as a material to enhance the glucose sensing performance of glucose oxidase LB films [143].

There are examples of immobilization of other enzymes in LB films. Thus, the urease was adsorbed from the aqueous subphase onto Langmuir monolayers of dimyristoylphosphatidic acid [144], acetylcholinesterase was used in an electrochemiluminescent sensor for choline and acetylcholine [133], and the phenol derivatives were determined by a colorimetric sensor based on a LB laccase or tyrosinase film [145]. To enhance the efficiency of electron transfer to the film, conductive polymers [146], inorganic redox systems [142], and gold nanoparticles [147] are added to the film. In general, for enzyme sensors based on LB films, researchers note the high and stable catalytic activity of immobilized biomolecules [143].

There are some examples of the applying LB technology in immunosensors. LB films containing binding proteins (proteins A or G) for immunosensing were prepared [148]. A fiber optic fluorescent immunosensor for the diagnosis of cardiac diseases was described [149]. LB films based on arachidic and pyrenebutyric acids were used in a piezoelectric immunosensor for determination of pyrene in aqueous media [150].

A comparative study of the sensors based on LB films and films prepared by the conventional method (e.g., evaporation or spin-coating) [115, 151–153] showed that the use of nanotechnology increases the sensitivity of sensors, reduces response time, and improves signal stability. Moreover, a better resolution of the electrochemical peaks, reproducibility of the determination, and the sensitive layers production were noted.

At the same time, it should be noted that creation of sensors using LB technology involves certain problems. A low stability of the films seriously inhibits the development of sensors for the analysis of liquid aggressive media. The use of polymer matrices possessing thermal, mechanical, and chemical strength could be promising in this case. Another problem is related to a limited set of molecules forming stable monolayers. This problem can be solved by derivatization of functional compounds with HC chain.

## 4.4 Conclusions

Nanomaterials and nanotechnologies began to be used for chemical sensors in the 90th of the last century. In the early 2000s, the rapid development of this area began, as evidenced by an annual increase in publications of 1.5–1.8 times. This is probably due to the fact that industrial production of devices for the implementation of nanotechnology is established, they have become more accessible to a wide range of analysts, and their cost has decreased. All this led to the fact that the nanosensors moved from the field of "art" of individual experimenters and laboratories to the field of everyday practice of analyst researchers. The first commercial samples of nanosensors appeared. A new measuring technique allowed moving from the assumptions to experimental proof of the effects caused by the special properties of nanomaterials. In our opinion, the development of nanosensors will help to solve many problems of diagnostics and monitoring of the functioning of living organisms and environmental objects, especially in the cases of small concentrations of detectable substances.

The work was supported by Russian Scientific foundation (project 14-13-00229).

## References

[1] Wang W, ed. *Progresses in Chemical Sensors*. InTech, 2016. https://www.intechopen.com/books/advances-in-chemical-sensors

[2] Shtykov SN, Rusanova TY. Nanosensors. In: Vlasov YG, ed. *Problems of Analytical Chemistry*. Moscow, Nauka, 2011, 352–62 (Original source in Russian).

[3] Wang X, Wolfbeis OS. Fiber-optic chemical sensors and biosensors. *Anal Chem* 2016, 88, 203–27.

[4] Shtykov SN, Rusanova TY. Nanomaterials and nanotechnologies in chemical and biochemical sensors (review). *Russ J Gen Chem* 2008, 78(12), 2521–31.

[5] Yang M, Peng J, Wang G, Dai J. Fiber optic sensors based on nano-films. In: Matias IR, Ikezawa S, Corres J, eds. *Fiber Optic Sensors*. Springer Intern Publ Switzerland, 2017, 1–20.

[6] Shtykov SN, Korenman YI, Rusanova TY, Gorin DA, Kalach AV, Pankin KE. Langmuir-Blodgett films as effective modifiers of piezoelectric sensors. *Dokl Chemistry* 2004, 396, Pt 2, 119–21.

[7] Shtykov SN, Rusanova TY, Kalach AV, Pankin KE. Application of Langmuir Blodgett films as modifiers of piezoresonance sensors. *Sens Actuat B* 2006, 114, 497–9.

[8] Shtykov SN, Kalach AV, Pankin KE, Rusanova TY, Selemenev VF. Use of Langmuir-Blodgett films as modifiers for piezoresonance sensors. *J Anal Chem* 2007, 62, 490–3.
[9] Love JC, Estroff LA, Kriebel JK. Self-assembled monolayers of thiolates on metals as a form of nanotechnology. *Chem Rev* 2005, 105, 1103–70.
[10] Parka JY, Advincula RC. Nanostructuring polymers, colloids, and nanomaterials at the air – water interface through Langmuir and Langmuir – Blodgett techniques. *Soft Matter* 2011, 7, 9829–43.
[11] Bigelow WC, Pickett DL, Zisman WA. Oleophobic monolayers: I. Films adsorbed from solution in non-polar liquids. *J Colloid Sci* 1946, 1, 513–38.
[12] Shafrin EG, Zisman WA. Hydrophobic monolayers adsorbed from aqueous solutions. *Ibid* 1949, 4, 571–90.
[13] Sagiv J. Organized monolayers by adsorption. 1. Formation and structure of oleophobic mixed monolayers on solid surfaces. *J Am Chem Soc* 1980, 102, 92–8.
[14] Nuzzo RG, Allara DL. Adsorption of bifunctional organic disulfides on gold surfaces. *J Am Chem Soc* 1983, 105, 4481–3.
[15] Shen G, Liu M, Cai X, Lu J. A novel piezoelectric quartz crystal immunosensor based on hyperbranched polymer films for the detection of α-Fetoprotein. *Anal Chim Acta* 2008, 630, 75–81.
[16] March C, Manclus JJ, Jimenez Y. A piezoelectric immunosensor for the determination of pesticide residues and metabolites in fruit juices. *Talanta* 2009, 78, 827–33.
[17] Arya SK, Solanski PR, Datta M, Malhotra BD. Recent advances in self-assembled monolayers based biomolecular electronic devices. *Biosens Bioelectron* 2009, 24, 2810–7.
[18] McRipley MA, Linsenmeier RA. Fabrication of a mediated glucose oxidase recessed microelectrode for the amperometric determination of glucose. *J Electroanal Chem* 1996, 414, 235–46.
[19] Tombelli S, Minunni M, Santucci A, Spiriti MM, Mascini M. A DNA-based piezoelectric biosensor: strategies for coupling nucleic acids to piezoelectric devices. *Talanta* 2006, 68, 806–12.
[20] Zhang B, Jiang Y, Kuang H, et al. Development of a spiral piezoelectric immunosensor based on thiol self-assembled monolayers for the detection of insulin. *J Immunol Methods* 2008, 338, 7–13.
[21] Su X, Chew FT, Li SFG. Self-assembled monolayer-based piezoelectric crystal immunosensor for the quantification of total human immunoglobulin. *Anal Biochem* 1999, 273, 66–72.
[22] Mendes RK, Carvalhal RF, Kubota LT. Effects of different self-assembled monolayers on enzyme immobilization procedures in peroxidase-based biosensor development. *J Electroanal Chem* 2008, 612, 164–72.
[23] Scott LJN, Šípová H, Adama P, Homola J. Enhancement of affinity-based biosensors: effect of sensing chamber geometry on sensitivity. *Lab Chip* 2013, 13, 1413–21.
[24] Chi YS, Lee KB, Kim Y, Choi IS. Reactivity of acid fluoride-terminated self-assembled monolayers on gold. *Langmuir* 2007, 23, 1209–14.
[25] Hahn CD, Leitner C, Weinbrenner T. Self-assembled monolayers with latent aldehydes for protein immobilization. *Bioconjug Chem* 2007, 18, 247–53.
[26] Hou Y, Helali S, Zhang A, et al. Immobilization of rhodopsin on a self-assembled multilayer and its specific detection by electrochemical impedance spectroscopy. *Biosens Bioelectron* 2006, 21, 1393–402.
[27] Arya SK, Solanki PR, Singh SP, et al. Poly-(3-hexylthiophene) self-assembled monolayer based cholesterol biosensor using surface plasmon resonance technique. *Biosens Bioelectron* 2007, 22, 2516–24.
[28] Berdat D, Marin A, Herrera F, Gijs MAM. DNA biosensor using fluorescence microscopy and impedance spectroscopy. *Sens Actuators B* 2006, 118, 53–9.
[29] Briand E, Salmain M, Herry JM, et al. Building of an immunosensor: how can the composition and structure of the thiol attachment layer affect the immunosensor efficiency? *Biosens Bioelectron* 2006, 22, 440–8.

[30] Guo C, Boullanger P, Jiang L, Liu T. Highly sensitive gold nanoparticles biosensor chips modified with a self-assembled bilayer for detection of Con A. *Biosens Bioelectron* 2007, 22, 1830–4.
[31] Wang J, Carmon KS, Luck LA, Suni II. Electrochemical impedance biosensor for glucose detection utilizing a periplasmic E. coli receptor protein. *Electrochem Solid-State Lett* 2005, 8, H61–4.
[32] Decher G. Fuzzy Nanoassemblies: toward layered polymeric multicomposites. *Science* 1997, 277, 1232–7.
[33] Gong J, Han X, Zhu X, Guan Z. Layer-by-layer assembled multilayer films of exfoliated layered double hydroxide and carboxymethyl-β-cyclodextrin for selective capacitive sensing of acephatemet. *Biosens Bioelectron* 2014, 61, 379–85.
[34] Ogoshi T, Takashima S, Yamagishi T. Molecular recognition with microporous multilayer films prepared by layer-by-layer assembly of pillar[5]arenes. *J Am Chem Soc* 2015, 137, 10962–4.
[35] Delvaux M, Champagne SD. Immobilisation of glucose oxidase within metallic nanotubes arrays for application to enzyme biosensors. *Biosens Bioelectron* 2003, 18, 943–51.
[36] Shervedani RK, Foroushani MS. Comparative electrochemical behavior of proteins; cytochrome c, agaricus bisporus laccase, and glucose oxidase, immobilized onto gold-thiol self-assembled monolayer via electrostatic, covalent, and covalent coordinate bond methods. *Electrochim Acta* 2016,187, 646–54.
[37] Gupta G, Rajendran V, Atanassov P. Laccase biosensor on monolayer-modified gold electrode. *Electroanalysis* 2003, 15, 1577–83.
[38] Alonso JM, Bielen AAM, Olthuis W, Kengen SWM, Zuilhof H, Franssen MCR. Self-assembled monolayers of 1-alkenes on oxidized platinum surfaces as platforms for immobilized enzymes for biosensing. *Appl Surf Sci* 2016, 383, 283–93.
[39] Berchmans S, Sathyajith R, Yegnaraman V. Layer-by-layer assembly of 1,4-diaminoanthraquinone and glucose oxidase. *Mater Chem Phys* 2002, 77, 390–6.
[40] Hasunuma T, Kuwabata S, Fukusaki E, Kobayashi A. Real-time quantification of methanol in plants using a hybrid alcohol oxidase-peroxidase biosensor. *Anal Chem* 2004, 76, 1500–6.
[41] Masson JF, Kranz C, Booksh KS, Mizaikoff B. Improved sensitivity and stability of amperometric enzyme microbiosensors by covalent attachment to gold electrodes. *Biosens Bioelectron* 2007, 23, 355–61.
[42] Mehdinia A, Kazemi SH, Bathaie SZ, et al. Electrochemical studies of DNA immobilization onto the azide-terminated monolayers and its interaction with taxol. *Anal Biochem* 2008, 375, 331–8.
[43] Kalra S, Kumar MJ, Dhawan A. Dielectric-modulated field effect transistors for DNA detection: impact of DNA orientation. *IEEE Electron Device Lett* 2016, 37, 1485–8.
[44] Li ZH, Hayman RB, Walt DR. Detection of single-molecule DNA hybridization using enzymatic amplification in an array of femtoliter-sized reaction vessels. *J Am Chem Soc* 2008, 130, 12622–3.
[45] Dharuman V, Grunwald T, Nebling E, et al. Label-free impedance detection of oligonucleotide hybridisation on interdigitated ultramicroelectrodes using electrochemical redox probes. *Biosens Bioelectron* 2005, 21, 645–54.
[46] Singh A, Verma HN, Arora K. Surface plasmon resonance based label-free detection of salmonella using DNA self assembly. *Appl Biochem Biotechnol* 2015, 175, 1330–43.
[47] Fan C, Plaxco KW, Heeger AJ. Electrochemical interrogation of conformational changes as a reagentless method for the sequence-specific detection of DNA. *PNAS (Proc Nat Acad Sci)* 2003, 100, 9134–7.
[48] Gorodetsky AA, Ebrahim A, Barton JK. Electrical detection of TATA binding protein at DNA-modified microelectrodes. *J Am Chem Soc* 2008, 130, 2924–5.
[49] Fowler JM, Stuart MC, Wong DKY. Self-assembled layer of thiolated protein G as an immunosensor scaffold. *Anal Chem* 2007, 79, 350–4.

[50] Choi JW, Kim YK, Oh BK. The development of protein chip using protein G for the simultaneous detection of various pathogens. *Ultramicroscopy* 2008, 108, 1396–400.
[51] Phillips KS, Han JH, Cheng Q. Development of a "membrane cloaking" method for amperometric enzyme immunoassay and surface plasmon resonance analysis of proteins in serum samples. *Anal Chem* 2007, 79, 899–907.
[52] Ayela C, Roquet F, Valera L, et al. Antibody – antigenic peptide interactions monitored by SPR and QCM-D: a model for SPR detection of IA-2 autoantibodies in human serum. *Biosens Bioelectron* 2007, 22, 3113–19.
[53] Subramanian A, Irudayaraj J, Ryan T. A mixed self-assembled monolayer-based surface plasmon immunosensor for detection of E. coli O157:H7. *Biosens Bioelectron* 2006, 21, 998–1006.
[54] Fragoso A, Laboria N, Latta D, O'Sullivan CK. Electron permeable self-assembled monolayers of dithiolated aromatic scaffolds on gold for biosensor applications. *Anal Chem* 2008, 80, 2556–63.
[55] Lee W, Lee DB, Oh BK, et al. Nanoscale fabrication of protein A on self-assembled monolayer and its application to surface plasmon resonance immunosensor. *Enzyme Microb Tech* 2004, 35, 678–82.
[56] Shen Z, Huang M, Xiao C, et al. Nonlabeled quartz crystal microbalance biosensor for bacterial detection using carbohydrate and lectin recognitions. *Anal Chem* 2007, 79, 2312–19.
[57] Jin X, Jin X, Chen L, Jiang J, Shen G, Yu R. Piezoelectric immunosensor with gold nanoparticles enhanced competitive immunoreaction technique for quantification of aflatoxin B1. *Biosens Bioelectron* 2009, 24, 2580–5.
[58] Zhong X, Yuan R, Chai Y, Liu Y, Dai J, Tang D. Glucose biosensor based on self-assembled gold nanoparticles and double-layer 2d-network (3-mercaptopropyl)-trimethoxysilane polymer onto gold substrate. *Sens Actuat B* 2005, 104, 191–8.
[59] Ouerghi O, Diouani MF, Belkacem A, Elsanousi A, Jaffrezic-Renault N. Adjunction of avidin to a cysteamine self-assembled monolayer for impedimetric immunosensor. *J Biomat Nanobiotech* 2016, 7(1), 1–12.
[60] Minamiki T, Minami T, Kurita R, et al. A label-free immunosensor for IgG based on an extended-gate type organic field effect transistor. *Materials* 2014, 7, 6843–52.
[61] Pedrosa VA, Caetano J, Machado SAS, Bertotti M. Determination of parathion and carbaryl pesticides in water and food samples using a self assembled monolayer /acetylcholinesterase electrochemical biosensor. *Sensors* 2008, 8, 4600–10.
[62] Meskini O, Abdelghani A, Tlili A, Mgaieth R, Jaffrezic-Renault N. Porous silicon as functionalized material for immunosensor application. *Talanta* 2007, 71, 1430–3.
[63] Mehdinia A, Kazemi SH, Bathaie SZ, Alizadeh A, Shamsipur M, Mousavi MF. Electrochemical studies of DNA immobilization onto the azide-terminated monolayers and its interaction with taxol. *Anal Biochem* 2008, 375, 331–8.
[64] Oh B-K, Kim Y-K, Park KW, Lee WH, Choi J-W. Surface plasmon resonance immunosensor for the detection of *Salmonella typhimurium*. *Biosens Bioelectron* 2004, 19, 1497–504.
[65] Adányi N, Váradi M, Kim N, Szendrö I. Development of new immunosensors for determination of contaminants in food. *Curr App Phys* 2006, 6, 279–86.
[66] Li Y, Kobayashi M, Furui K, Soh N, Nakano K, Imato T. Surface plasmon resonance immunosensor for histamine based on an indirect competitive immunoreaction. *Anal Chim Acta* 2006, 576, 77–83.
[67] Shen G, Liu M, Cai X, Lu J. A novel piezoelectric quartz crystal immunosensor based on hyperbranched polymer films for the detection of α-Fetoprotein. *Anal Chim Acta* 2008, 630, 75–81.
[68] March C, Manclus JJ, Jimenez Y, Montoya A. A piezoelectric immunosensor for the determination of pesticide residues and metabolites in fruit juices. *Talanta* 2009, 78, 827–33.

[69] Hou SF, Fang HQ, Chem HY. An amperometric enzyme electrode for glucose using immobilized glucose oxidase in a ferrocene attached poly(4-vinylpyridine) multilayer film. *Anal Lett* 1997, 30, 1631–41.
[70] Pastorino L, Caneva SF, Giacomini M, Ruggiero C. Development of a piezoelectric immunosensor for the measurement of paclitaxel. *J Immunol Methods* 2006, 313, 191–8.
[71] Cui S, Wang J, Wang X. Fabrication and design of a toxic gas sensor based on polyaniline/titanium dioxide nanocomposite film by layer-by-layer self-assembly. *RSC Adv* 2015, 5, 58211–9.
[72] Zhang D, Tong J, Xia B. Humidity-sensing properties of chemically reduced graphene oxide/polymer nanocomposite film sensor based on layer-by-layer nano self-assembly. *Sens Actuat B* 2014, 197, 66–72.
[73] Chang H, Wang X, Shiu K-K, et al. Layer-by-layer assembly of graphene, Au and poly(toluidine blue O) films sensor for evaluation of oxidative stress of tumor cells elicited by hydrogen peroxide. *Biosens Bioelectron* 2013, 41, 789–94.
[74] Chung K, Ran A, Lee J-E, et al. Systematic study on the sensitivity enhancement in graphene plasmonic sensors based on layer-by-layer self-assembled graphene oxide multilayers and their reduced analogues. *ACS Appl Mater Interfaces* 2015, 7, 144–51.
[75] Andre RS, Shimizu FM, Miyazaki CM, et al. Hybrid layer-by-layer (LbL) films of polyaniline, graphene oxide and zinc oxide to detect ammonia. *Sens Actuat B* 2017, 238, 795–801.
[76] Elosua C, de Acha N, Hernaez M, Matias IR, Arregui FJ. Layer-by-Layer assembly of a water – insoluble platinum complex for optical fiber oxygen sensors. *Sens Actuat B* 2015, 207, 683–9.
[77] Li Y, Huang H, Li Y, Su X. Highly sensitive fluorescent sensor for mercury (II) ion based on layer-by-layer self-assembled films fabricated with water-soluble fluorescent conjugated polymer. *Sens Actuat B* 2013, 188, 772–7.
[78] Barsan MM, Brett CMA. Recent advances in layer-by-layer strategies for biosensors incorporating metal nanoparticles. *Trends Anal Chem* 2016, 79, 286–96.
[79] Zhao H, Guo X, Wang Y, et al. Microchip based electrochemical-piezoelectric integrated multimode sensing system for continuous glucose monitoring. *Sens Actuat B* 2016, 223, 83–8.
[80] Gong J, Han X, Zhu X, Guan Z. Layer-by-layer assembled multilayer films of exfoliated layered double hydroxide and carboxymethyl-β-cyclodextrin for selective capacitive sensing of acephatemet. *Biosens Bioelectron* 2014, 61, 379–85.
[81] Richardson TH, Dooling CM, Worsfold O, et al. Gas sensing properties of porphyrin assemblies prepared using ultra-fast LB deposition. *Coll Surf A* 2002, 198–200, 843–57.
[82] Xie D, Pan W, Jiang YD, Li YR. Erbium bis[phthalocyaninato] complex LB film gas sensor. *Mat Lett* 2003, 57, 2395–8.
[83] Xie D, Jiang YD, Ning YG, et al. Study on the characteristics and relative properties of Langmuir – Blodgett films based on substituted bis[phthalocyaninato] rare earth(III) complexes. *Mat Lett* 2001, 51, 1–6.
[84] Xie D, Jiang Y. The properties of praseodymium bis[octakis(octyloxy)-phthalocyaninato] complex Langmuir – Blodgett films for $NO_2$ sensor. *Sens Actuat B* 2003, 93, 379–83.
[85] Rubira RJG, Aoki PHB, Constantino CJL, Alessio P. Supramolecular architectures of iron phthalocyanine Langmuir-Blodgett films: the role played by the solution solvents. *Appl Surf Sci* 2017, 416, 482–91.
[86] Mukherjee D, Manjunatha R, Sampath S, Ray A. Phthalocyanines as sensitive materials for chemical sensors. In: Cesar da Paixão TRL, Reddy SM, eds. *Materials for Chemical Sensing*. Springer Intern Publ AG, 2017, 165–226.
[87] Richardson TH, Brook RA, Davis F, Hunter CA. The $NO_2$ gas sensing properties of calixarene/porphyrin mixed LB films. *Coll Surf A* 2006, 284–285, 320–5.
[88] Casillia S, De Lucaa M, Apetreia C, et al. Langmuir – Blodgett and Langmuir – Schaefer films of homoleptic and heteroleptic phthalocyanine complexes as voltammetric sensors: Applications to the study of antioxidants. *Appl Surf Sci* 2005, 246, 304–12.

[89] Olivati CA, Riul AJr, Balogh DT, et al. Detection of phenolic compounds using impedance spectroscopy measurements. *Bioprocess Biosyst Eng* 2009, 32, 41–6.
[90] Yang W, Xu J, Mao Y, Yang Y, Jiang Y. Detection of volatile organic compounds using Langmuir-Blodgett films of zinc-porphyrin and zinc-phthalocyanine. *Synth React Inorg M* 2016, 46(5), 735–740.
[91] Dunbar ADF, Richardson TH, McNaughton AJ, et al. Investigation of free base, Mg, Sn, and Zn substituted porphyrin LB films as gas sensors for organic analytes. *J Phys Chem B* 2006, 110, 16646–51.
[92] Kang ST, Ahn H. Dicyanopyrazine-linked porphyrin Langmuir – Blodgett films. *J Colloid Interface Sci* 2008, 320, 548–54.
[93] Manigandan S, Jain A, Majumder S, et al. Formation of nanorods and nanoparticles of polyaniline using Langmuir Blodgett technique: Performance study for ammonia sensor. *Sens Actuat B* 2008, 133, 187–94.
[94] Lange U, Roznyatovskaya NV, Mirsky VM. Conducting polymers in chemical sensors and arrays (review). *Anal Chim Acta* 2008, 614, 1–26.
[95] Huynh T-P, Sharma PS, Sosnowska M, D'Souza F, Kutner W. Functionalized polythiophenes: recognition materials for chemosensors and biosensors of superior sensitivity, selectivity, and detectability. *Progr Polym Sci* 2015, 47, 1–25.
[96] Naso F, Babudri F, Colangiuli D, et al. Thin film construction and characterization and gas-sensing performances of a tailored phenylene-thienylene copolymer. *J Am Chem Soc* 2003, 125, 9055–61.
[97] Saxena V, Choudhury S, Gadkari SC, et al. Room temperature operated ammonia gas sensor using polycarbazole Langmuir – Blodgett film. *Sens Actuat B* 2005, 107, 277–82.
[98] Ferreira M, Constantino CJL, Riul Jr A, et al. Preparation, characterization and taste sensing properties of Langmuir – Blodgett Films from mixtures of polyaniline and a ruthenium complex. *Polymer* 2003, 44, 4205–11.
[99] Riul AJr, de Sousa HC, Malmegrim RR, et al. Wine classification by taste sensors made from ultra-thin films and using neural networks. *Sens Actuat B* 2004, 98, 77–82.
[100] Zhu Y, Koley G, Walsh K, Galloway A, Ortinski P. Application of ion-sensitive field effect transistors for measuring glial cell K+ transport. *Sensors* 2016, 1–3.
[101] Prabhakaran D, Nanjo H, Matsunaga H. Naked eye sensor on polyvinyl chloride platform of chromo-ionophore molecular assemblies: a smart way for the colorimetric sensing of toxic metal ions. *Anal Chim Acta* 2007, 601, 108–17.
[102] Prabhakaran D, Yuehong M, Nanjo H, Matsunaga H. Naked-eye cadmium sensor: using chromoionophore arrays of Langmuir-Blodgett molecular assemblies. *Anal Chem* 2007, 79, 4056–65.
[103] Zheng H, Yan Zh, Dong H, Ye B. Simultaneous determination of lead and cadmium at a glassy carbon electrode modified with Langmuir – Blodgett film of p-tert-butylthiacalix[4]arene. *Sens Actuat B* 2007, 120, 603–9.
[104] Wang F, Liu Q, Wu Y, Ye B. Langmuir – Blodgett film of p-tert-butylthiacalix[4]arene modified glassy carbon electrode as voltammetric sensor for the determination of $Ag^+$. *J Electroanal Chem* 2009, 630, 49–54.
[105] Torrent-Burgués J, Vocanson F, Pérez-González JJ, Errachid A. Synthesis, Langmuir and Langmuir – Blodgett films of a calix[7]arene ethyl ester. *Colloids Surf A* 2012, 401, 137–47.
[106] De Oliveira IAM, Torrent-Burgues J, Pla M, et al. Nanostructuring of Langmuir-Blodgett films containing a novel thiomacrocyclic ionophore on $Si_3N_4/SiO_2/Si$ for copper ion recognition. *Anal Lett* 2006, 39, 1709–20.
[107] Ohnishi M, Ishibashi T, Aoki M, Ishimoto C. Fundamental properties and characteristics of a gas-sensitive device, made of a surface acoustic wave device and Langmuir-Blodgett film, used in a recognition system for odoriferous gases. *Jpn J Appl Phys* 1994, 33, 5987–94.

[108] Balcerzak A, Aleksiejuk M, Zhavnerko G, Agabekov V. Sensing properties of two-component Langmuir – Blodgett layer and its porous derivative in SAW sensor for vapors of methanol and ethanol. *Thin Solid Films* 2010, 518, 3402–6.
[109] Afzal A, Iqbal N, Mujahid A, Schirhagl R. Advanced vapor recognition materials for selective and fast responsive surface acoustic wave sensors: a review. *Anal Chim Acta* 2013, 787, 36–49.
[110] Kalinina MA, Golubev NV, Raitman OA, et al. A novel ultra-sensing composed Langmuir-Blodgett membrane for selective calcium determination in aqueous solutions. *Sens Actuat B* 2006, 114, 19–27.
[111] Ozmen M, Ozbek Z, Bayrakci M, Ertul S, Ersoz M, Capan R. Preparation and gas sensing properties of Langmuir – Blodgett thin films of calix[n]arenes: Investigation of cavity effect. *Sens Actuat B* 2014, 195, 156–64.
[112] Ozmen M, Ozbek Z, Buyukcelebi S, et al. Fabrication of Langmuir – Blodgett thin films of calix[4]arenes and their gas sensing properties: Investigation of upper rim para substituent effect. *Sens Actuat B* 2014, 190, 502–11.
[113] Acikbas Y, Erdogan M, Capan R, Yukruk F. Fabrication of Langmuir – Blodgett thin film for organic vapor detection using a novel N,N′-dicyclohexyl-3,4:9,10-perylenebis (dicarboximide). *Sens Actuat B* 2014, 200, 61–8.
[114] Penza M, Tagliente MA, Aversa P, et al. Single-walled carbon nanotubes nanocomposite microacoustic organic vapor sensors. *Mater Sci Eng C* 2006, 26, 1165–70.
[115] Rusanova TYu, Kalach AV, Rumyantseva SS, Shtykov SN, Ryzhkina IS. Determination of volatile organic compounds using piezosensors modified with the Langmuir – Blodgett films of calix[4]resorcinarene. *J Anal Chem* 2009, 64(12), 1270–4.
[116] Ding L, Fang Y. Chemically assembled monolayers of fluorophores as chemical sensing materials. *Chem Soc Rev* 2010, 39, 4258–73.
[117] Beswick RB, Pitt CW. Optical detection of toxic gases using fluorescent porphyrin Langmuir-Blodgett films. *J Colloid Interface Sci* 1988, 124, 146–55.
[118] Zheng Y, Orbulescu J, Ji X, Andreopoulos FM, Pham SM, Leblanc RM. Development of fluorescent film sensors for the detection of divalent copper. *J Am Chem Soc* 2003, 125, 2680–6.
[119] Aizawa M, Matsuzawa M, Shinohara H. An optical chemical sensor using a fluorophor-embedded Langmuir-Blodgett film. *Thin Solid Films* 1988, 160, 477–81.
[120] Budach W, Ahuja RC, Mobius D. Metal ion sensor based on dioctadecyldithiocarbamate-metal complex induced energy transfer. *Thin Solid Films* 1992, 210–211, 434–6.
[121] Yeh W-H, Hillier AC. Use of dispersion imaging for grating-coupled surface plasmon resonance sensing of multilayer Langmuir – Blodgett films. *Anal Chem* 2013, 85, 4080–6.
[122] James JZ, Lucas D, Koshland C. Gold nanoparticle films as sensitive and reusable elemental mercury. *Sens Environ Sci Technol* 2012, 46, 9557–62.
[123] Wang F, Zhao F, Zhang Y, Yang H, Ye B. Sensitive voltammetric determination of baicalein at DNA Langmuir – Blodgett film modified glassy carbon electrode. *Talanta* 2011, 84, 160–8.
[124] Wang F, Xu Y, Wang L, Lu K, Ye B. Immobilization of DNA on a glassy carbon electrode based on Langmuir – Blodgett technique: application to the detection of epinephrine. *J Solid State Electrochem* 2012, 16, 2127–33.
[125] Olsen EV, Pathirana ST, Samoylov AM, et al. Specific and selective biosensor for Salmonella and its detection in the environment. *J Microbiol Meth* 2003, 53, 273–85.
[126] Yang Y, Jiang Y, Xu J, Yu J. PEDOT multilayer LB films and their gas sensitivity based on quartz crystal microbalance. *Mat Sci Engineer B* 2007, 139, 251–5.
[127] Malhotra BD, Singhal R, Chaubey A, Sharma SK, Kumar A. Recent trends in biosensors. *Curr Appl Phys* 2005, 5, 92–7.
[128] Wang K-H, Syu M-J, Chang C-H, Lee Y-L. Immobilization of glucose oxidase by Langmuir – Blodgett technique for fabrication of glucose biosensors: Headgroup effects of template monolayers. *Sens Actuat B* 2012, 164, 29–36.

[129] Sabatani E, Kalisky Y, Berman A, et al. Photoluminescence of polydiacetylene membranes on porous silicon utilized for chemical sensors. *Opt Mater* 2008, 30, 1766–74.
[130] Medina-Plaza C, García-Cabezón C, García-Hernández C, et al. Analysis of organic acids and phenols of interest in the wine industry using Langmuir – Blodgett films based on functionalized nanoparticles. *Anal Chim Acta* 2015, 853, 572–8.
[131] Wang F, Wei X, Wang C, Zhang S, Ye B. Langmuir – Blodgett film of p-tert-butylthiacalix[4] arene modified glassy carbon electrode as voltammetric sensor for the determination of Hg(II). *Talanta* 2010, 80, 1198–204.
[132] Alessio P, Pavinatto FJ, Oliveira JrON, De Saja Saez JA, Constantino CJL, Rodríguez-Méndez ML. Detection of catechol using mixed Langmuir – Blodgett films of a phospholipid and phthalocyanines as voltammetric sensors. *Analyst* 2010, 135, 2591–9.
[133] Godoy S, Leca-Bouvier B, Boullanger P, et al. Electrochemiluminescent detection of acetylcholine using acetylcholinesterase immobilized in a biomimetic Langmuir – Blodgett nanostructure. *Sens Actuat B* 2005, 107, 82–7.
[134] Liu Q, Wang F, Qiao Y, Zhang Sh, Ye B. Polyaniline Langmuir – Blodgett film modified glassy carbon electrode as a voltammetric sensor for determination of $Ag^+$ ions. *Electrochim Acta*, 2010, 55, 1795–800.
[135] Daly SM, Grassi M, Shenoy DK, Ugozzoli F, Dalcanale E. Supramolecular surface plasmon resonance (SPR) sensors for organophosphorus vapor detection. *J Mater Chem* 2007, 17, 1809–18.
[136] Chen C, Xie Q, Yang D, et al. Recent advances in electrochemical glucose biosensors: a review. *RSC Adv* 2013, 3, 4473–91.
[137] Wang K-H, Syu M-J, Chang Ch-H, Lee. Headgroup effects of template monolayers on the adsorption behavior and conformation of glucose oxidase adsorbed at air/liquid interfaces. *Langmuir* 2011, 27, 7595–602.
[138] Yasuzawa M, Hashimoto M, Fujii S, Kunugi A, Nakaya T. Preparation of glucose sensors using the Langmuir – Blodgett technique. *Sens Actuat B* 2000, 65, 241–3.
[139] Singhal R, Chaubey A, Srikhirin T, Sukanya A, Pandey SS, Malhotra BD. Immobilization of glucose oxidase onto Langmuir – Blodgett films of poly-3-hexylthiophene. *Curr Appl Phys* 2003, 3, 275–9.
[140] Watanabe N, Ohnuki H, Saiki T, Endo H, Izumi M, Imakubo T. Conducting organic Langmuir – Blodgett films as chemical sensors. *Sens Actuat B* 2005, 108, 404–8.
[141] Ohnuki H, Saiki T, Kusakari A, Endo II, Ichihara M, Izumi M. Incorporation of glucose oxidase into Langmuir-Blodgett films based on Prussian blue applied to amperometric glucose biosensor. *Langmuir* 2007, 23, 4675–81.
[142] Choi J-W, Kim Y-K, Lee I-H, Min J, Lee WH. Optical organophosphorus biosensor consisting of acetylcholinesterase/viologen hetero Langmuir – Blodgett film. *Biosens Bioelectron* 2001, 16, 937–94.
[143] Wang K-H, Hsu W-P, Chen L-H, Lin W-D, Lee Y-L. Extensibility effect of poly(3-hexylthiophene) on the glucose sensing performance of mixed poly(3-hexylthiophene)/octadecylamine/glucose oxidase Langmuir-Blodgett films. *Colloids Surf B* 2017, 155, 104–10.
[144] Caseli L, SiqueiraJr JR. High enzymatic activity preservation with carbon nanotubes incorporated in urease – lipid hybrid Langmuir – Blodgett films. *Langmuir* 2012, 28, 5398–403.
[145] Cabaj J, Sołoducho J, Chyla A, Ryjak J, Zynek K. The characterization of ordered thin films built of immobilized phenoloxidases. *Sens Actuat B* 2009, 136, 425–31.
[146] Malhotra BD, Singhal R. Conducting polymer based biomolecular electronic devices. *Pramana* 2003, 61, 331–43.
[147] Matharu Z, Pandey P, Pandey MK, Gupta V, Malhotra BD. Functionalized gold nanoparticles – octadecylamine hybrid Langmuir-Blodgett film for enzyme sensor. *Electroanal* 2009, 21, 1587–96.

[148] Makaraviciute A, Ramanaviciene A. Antibody immobilization techniques for immunosensors. *Biosens Bioelectron* 2013, 50, 460–71.
[149] Choi JW, Parl JH, Lee WC, Oh BK, Min JH, Lee WH. Fluorescence immunoassay of HDL and LDL using protein A LB film. *J Microbiol Biotechnol* 2001, 11, 979–85.
[150] Rusanova TY, Taranov VA, Shtykov SN, Goryacheva IY. Piezoquartz sensor based on Langmuir-Blodgett films for pyrene detection in aqueous media. *Zavodsk Lab Diagnost Mater* 2009, 75(5), 23–7. (Original source in Russian).
[151] Casilli S, De Luca M, Apetrei C, et al. Langmuir – Blodgett and Langmuir – Schaefer films of homoleptic and heteroleptic phthalocyanine complexes as voltammetric sensors: Applications to the study of antioxidants. *J Appl Surf Sci* 2005, 246, 304–12.
[152] Wohnrath K, Pessoa CA, Dos Santos PM, Garcia JR, Batista AA, Oliveira ON. Etude de la conducivité ionique des hydrurofluorures $CaF_{2-x}H_x$. *J Progr Solid State Chem* 2005, 33, 243–52.
[153] Pereira AA, Martins GF, Antunes PA, et al. Lignin from sugar cane bagasse: extraction, fabrication of nanostructured films, and application. *Langmuir* 2007, 23, 6652–5.

T. D. Smirnova, S. N. Shtykov and E. A. Zhelobitskaya

# 5 Energy Transfer in Liquid and Solid Nanoobjects: Application in Luminescent Analysis

## 5.1 Introduction

Radiationless transfer of electronic excitation energy is a fundamental physical phenomenon playing an important role in natural processes, especially in photosynthesis, and is commonly used in photooptics, optoelectronics, biochemistry, coordination chemistry of transition metals, lanthanides, and in luminescent analysis. Energy transfer (ET) assumes a presence of a donor absorbing the light and an acceptor receiving the absorbed and transformed energy from the donor to emit it later. Excitation ET may take place within one molecule, which has two reaction centers, within metal chelates, or in between separate molecules when the donor and the acceptor collide with each other dynamically.

ET is examined in solutions, solids (crystals, films), and biological objects and is of practical significance. A lot of electronic excitation ET types are identified, for example, resonance energy transfer (RET) when the donor and acceptor are coupled by a dipole–dipole interaction within 1–10 nm, triplet–triplet (T–T) ET when the process controlled by diffusion is defined by interaction within 1–1.5 nm, and Ln(III)-specific ET when the donor and acceptor are coupled by chelate formation.

The RET in one turn can be subdivided on fluorescence (Förster) RET (FRET), bioluminescence RET (BRET), chemiluminescence RET (CRET), minor groove binder ET (MBET), and lanthanide RET (LRET) varieties of ET processes.

The use of ET in chemical analysis has two main goals:

- enhancement of luminescent signal intensity and thus increase of analyte determination sensitivity;
- improvement of determination selectivity.

Fluorescence or phosphorescence of the acceptor that occurs during ET is known as *sensitized*. The present review will consist of literature data summary as well as author's own results dedicated mostly to utilization of FRET and other ET processes in lanthanide complexes, which solubilized in liquid nanosized micelles (liquid nanoobjects) performing the role of nanoreactors and the ET between the lanthanide systems and some types of solid nanoparticles (e. g., silver, carbon, and semiconductor quantum dots (QDs)). Various approaches to promote the efficiency of ET for improvement of determination selectivity and sensitivity using liquid and solid nanoobjects will be analyzed as well.

https://doi.org/10.1515/9783110542011-005

Weissman [1] was the first who observed the ET in chelates of rare-earth elements and proposed a simple scheme of the process.

$$D^* + A \rightarrow D + A^*,$$

where D* is the donor in excited state, and A is the acceptor of excitation energy. He noticed that absorption of the UV light by $Eu^{3+}$–beta-diketonate complex causes a narrow band emission, which is typical for that lanthanide ion. In succeeding years, ET mechanism was studied more comprehensively by several researchers [2, 3]. Two mechanisms of ET are distinguished, which differed by the nature and strength of interaction: inductive-resonance ET arising from dynamic collisions between particles (FRET) and exchange resonance, observed mostly in complex metals with ligands.

The theory and mechanism of *FRET* that is realized with long-range dipole–dipole interactions are discussed in more detail by Förster and Galanin [2, 4]. Nonradiative ET was demonstrated to contain information about the molecular structure of donor–acceptor pair. The rate constant of ET may be expressed as follows [2]:

$$r = \frac{R_0}{\left(\tau_D^0/\tau_D - 1\right)^{1/6}}$$

where and $\tau_D$ are fluorescence decay times of the donor in the absence and presence of acceptor, $r$ is the distance between donor and acceptor, and $R_0$ is the characteristic distance or the Förster radius at which 50 % ET occurs.

Since the value of Förster radius ranged from 20 to 30 A, the dependence of ET on the distance makes it possible to use FRET in biochemical studies. This range fits the sizes of the most proteins and thickness of the biological membranes. Anything that can change the distance between donor and acceptor affects also the ET rate. This provides the assessment of the donor–acceptor distance changes and makes it quantified. Thus, the ET metering is used to estimate the value of a distance between binding centers or chromophoric protein groups, biomembranes, as well as the interaction between macromolecules, etc. [4, 5]. ET method allows studying the static and dynamic macromolecule's conformational changes in solutions. For instance, the examination of donor fluorescence decay time kinetics permits the distance between donor and acceptor to be measured as well as the rate of donor and acceptor diffusion relative to each other. FRET is suggested to use in analysis of structure and thermodynamical properties of lipids and its systems [6].

*Exchange-resonance* ET will be possible if emitting transitions in donor and acceptor are forbidden by the selection rules, but electronic shells of the donor–acceptor pair are overlapping. Exchange-resonance ET is going on between two organic molecules, organic molecule and rare-earth ion, different rare-earth elements [7], and transition metals [8]. The effectiveness of ET in "donor–acceptor pair" is considerably more between different substances as compared with the molecules of the same

nature [9]. The effectiveness of exchange-resonance excitation ET may be far better than FRET. It depends on many factors but nature and microenvironment of donor and acceptor are critical. The maximum of analytical signal occurs after implementation of mixed (inductive and exchange) mechanism of ET in spectroscopic system. A contribution of the inductive-resonance ET is followed by growth of medium viscosity.

Lanthanides can be a useful alternative to the common labels in the monitoring of interaction between ligands and receptors for the biochemical studies. The reason is that LRET has several advantages over common organic fluorescent dyes. Lanthanides are more readily available; the distance at which 50 % of the energy is transferred is large; the donor lifetime is single exponential and long (0.63 ms in $H_2O$), making lifetime measurements facile and highly accurate; the sensitized emission of the acceptor can be measured with little or no interfering background; lanthanides used in combination with biologically active ligands can provide more intensive luminescent signal, which may obtain by applying time-resolved fluorescence [5, 7, 10–14]. Lanthanide chelates themselves refer to energy donors that have to offer advantage over classical fluorescence probes in the measured donor–acceptor distance [15].

The ET phenomenon and sensitized fluorescence have a peculiar interest for analytics due to the high sensitivity and selectivity of fluorimetric determination the lanthanide ions themselves, organic and biomolecular substances as well. The advantages of the lanthanides complexes are well-defined fluorescence characterized by narrow and structured emission spectra, large difference between absorption and emission wavelength maximums (large Stokes shifts), long excited-states' lifetimes (micro- or milliseconds) and *antenna effect*. The sensitized lanthanides fluorescence is successfully used for detection of lanthanides and biologically active substances (BASs) in the biological, organic and nonorganic objects, herbs, medicines, and environment [16–19]. It invokes on ET in chelates from the triplet level of organic ligand (donor) to resonance emitting level of lanthanide ion (acceptor). Along with lanthanides, the solid nanoparticulates such as QDs, metal oxides, and carbon nanomaterials can be participants of ET.

## 5.2 Nanoobjects involved in ET

The ET analytical practice faced in common solvents has some limitations and drawbacks. It is not always effective to overcome ET weakness through the development of new or modification of current molecular fluorophores. For this reason, during the past 20 years, researchers tend to apply different nanoparticles or liquid nanosized objects in order to enhance the efficiency of ET.

All types of *liquid nanoobjects* formed so-called "organized media" can be tentatively subdivided into the following two large groups: media containing self-assembled (self-organized) supramolecular micellar systems, which form a proper pseudophase,

and preorganized media containing receptor supermolecules with inner cavities [20, 21]. Micellar systems are lyophilic colloid-sized assemblies of several tens of diphilic molecules or ions of micelle-forming surfactants (dispersed phase), which are distributed in the bulk of an aqueous or nonaqueous solvent (dispersion medium) [20]. Direct and reversed micelles, microemulsions (water-in-oil and oil-in-water), vesicles, liposomes, Langmuir–Blodgett films, and liquid crystals formed by diphilic surfactant molecules or ions are the examples of micellar systems. The nanophase of *direct* micelles is separated from the dispersion medium (water) by a layer containing the polar head groups of surfactants and a shell of strongly retained water molecules. This layer is often referred to as an interphase, or the Stern layer in the case of ionic surfactants and oxyethylene groups in the case of nonionic surfactants. In organic solvents the *reversed* micelles are formed and the polar groups of surfactants form the nuclei of these micelles as well as hydrocarbon radicals are oriented toward the nonaqueous solvent. The solutions of various receptor molecules (cyclodextrins [CD], calixarenes, cyclophanes, etc.), which form rigid three-dimensional cavities, belong to the *second group* of organized media.

In general, the term *organized media* is related to transparent optically isotropic solutions in which supramolecular or supermolecular nanosystems occur in the bulk of the solvent (aqueous or nonaqueous); these systems form a proper pseudonanophase. Thus, organized liquid media are homogeneous and single-phase on a macroscopic scale; however, they are microheterogeneous and two-phase on a nanoscale. If chemical reaction occurs in such a nanosized microphase rather than in the bulk of solution, this nanosized microphase is referred to as a microreactor or nanoreactor [20, 21]. The effective physicochemical parameters (local dielectric constant, micropolarity, microviscosity, and microacidity) of a medium in different parts of such nanoreactor, which are determined by spectroscopic probes, are strongly different. The solubilization of the participants of an analytical process in the different local places of this nanophase considerably affects their hydrophobic properties, hydration, rigidity, molecular conformation, and the efficiencies of intra- and intermolecular excitation ET; consequently, a number of physicochemical and spectroscopic properties are also changed. As a result, the analytical signal intensity considerably increases.

The relatively solid nanostructures such as Langmuir–Blodgett films or sol–gel materials with a thickness of 30–200 nm can also play a role of nanoreactors. These films can contain a different kind of substances with different functional groups and use for development of liquid and gas nanosensors, including sensors based on measuring sensitizing fluorescent intensity [22–24].

Other kind of *solid nanoobjects* are nanoparticles (NPs). Their significant feature is that they can themselves be participants in ET in the donor–acceptor pair. Owing to unique quantum-confined properties, they have very high molar absorption coefficients and position of their absorption and fluorescent spectra can be easily controlled by the size of the nanoparticle that is very important for construction of

donor–acceptor pair [25, 26]. The most known examples of such nanoparticles are semiconductor QDs, carbon dots, and gold and silver NPs.

Semiconductor QDs, due to their unique photophysical and spectroscopic properties, are widely used as an alternative to traditional organic fluorophores. The spectroscopic analytic signal of QDs is caused by surface plasmon resonance (SPR) phenomenon. QDs are composed of semiconductor cores (1–10 nm), which are often coated with one or more shell consisting of another semiconductor material with suitable lattice parameters and higher band-gap energy, for example, CdSe, CdSe/ZnS, or CdSe/CdS/ZnS QDs. Different QDs have found wide application in bioassay. Their use is based on various principles and concepts and allows detection of small molecules, proteins, DNA, and act as biolabels [27].

The nanoscale metal particles (Au, Ag, Au–Ag) are likely to use for optic (absorption, fluorescence, light scattering) detection of biological molecules. The detection sensitivity is increased by 200,000 times during a catalytic sedimentation of silver at the gold surface [28, 29]. The detection limit may drop down to $10^{-21}$ M when gold and magnetic nanoscale particles are combined. The absorption molar coefficients of gold nanoparticles rise to $3 \cdot 10^{11}$ L · mol · cm$^{-1}$ [28, 30].

A carbon QD and two-dimensional graphene are solid nanostructures, which form sensor-sensitive layer for the detection of different molecules. Carbon QDs were proposed as the donors of excitation energy in bioanalysis to determination of nucleus acids, proteins, and toxins in environmental objects [31–33].

## 5.3 Application of FRET in analysis

### 5.3.1 FRET in micellar solutions

The impact of surfactants on the intensity of sensitized fluorescence was considered in their ionic solutions as well as micellar ones. It has been shown using triton X-100 molecule as energy donor and the derivate of indolequinolizidine (3-acetyl-4-oxo-6,7-dihydro-12H-indolo-[2,3-a] quinolizine) as the acceptor, that ET in micellar solutions is more effective [34]. FRET between perylene and riboflavin in micellar solution of sodium dodecylsulfate (SDS) was proposed for determination of vitamin $B_2$ [35]. Fluorescence resonance ET between acridine orange and rhodamine 6G was applied for determination of vitamin $B_{12}$ using SDS micelles and flow-injection laser-induced fluorescence detection at $\lambda_{exc}$ = 454 nm with limit of detection (LOD) $1.65 \cdot 10^{-6}$ M [36]. Detection of erythromycin was described using ET from rhodamine 6G to acridine orange in the dodecyl benzene sodium sulfonate micellar solution [37]. In the presence of erythromycin, the fluorescence of acceptor is reduced; the linear dynamic range was varied from 0.75 to 15 mg/L, with LOD 0.32 mg/L.

### 5.3.2 FRET with protein participation

Lanthanide inductive resonance ET is used at the development of different FRET sensors. In the FRET pairs, the lanthanide complexes act as the excitation energy donors and fluorescent proteins as acceptors. Genetically encoded sensors enable visualization of intracellular enzyme activity, protein's interaction, and changes in protein conformations [38]. The terbium–fluorescein and terbium–green fluorescent protein (GFP) fluorescence resonance ET pairs are used for development of time-resolved FRET kinase assays [39]. ET occurs on the interaction between a terbium-labeled antibody with substrate and GFP, the efficiency of which depends on the enzyme activity [40–42].

The enzyme detection via the ubiquitin–$Tb^{3+}$–YFP (yellow fluorescent protein) pair facilitates the tumor treatment. Due to ET, the YFP lifetime increases. The enzyme affects the efficiency of ET that is used to control oncology diseases [43]. Biosensors based on lanthanide complexes, which are used as energy donors, provide estradiol [44], triiodothyronine [45], hormones [46], and serine–threonine and tyrosine kinases' enzyme activity detection [47, 48].

FRET offers an insight into red blood cells' membrane structure of patients with chronic diseases. Membrane probes can be used to diagnose myocardial infarction, cardiophyshoneurosis, and breast pang [49–51]. A high sensitivity of fluorescent analysis was demonstrated by cholinesterase inhibitor detection [52, 53]. Fluorescent detection of albumin apparent concentration in blood is based on the use of N-carboxyphenyldimethyl aminonaphthalic acid [54]. The emission intensity of that fluorescent dye in a blood serum is proportional to albumin molecule's vacant binding centers.

### 5.3.3 FRET with nanomaterials' participation

#### 5.3.3.1 Quantum dots

As a result of their discrete atom-like electronic structure, QDs have typically very narrow emission spectra with a full width at half-maximum of the luminescent emission of around 15–40 nm. QDs typically exhibit higher fluorescence quantum yields than conventional organic fluorophores, allowing for greater analytical sensitivity. QD uniqueness arises from the fact that the maximum of fluorescent emission may be adjusted through the cores size control during its synthesis or modification. Due to wide absorption spectrum and narrow emission one, the production of heterochromatic QDs is possible if only the same one excitation wavelength is being used. The photophysical properties of QDs can be controlled by their nanocrystal core sizes, the shell thickness, and the composition of the semiconductor materials of cores and shell and in some extent by their surface ligands. The final emission features of QDs can be tuned from UV to NIR to fit the desired spectral wavelength, making them

ideally suited for all kinds of fluorescent applications. QDs can have extremely high molar absorption coefficients of more than $1 \times 10^6$ $M^{-1}$ $cm^{-1}$ that is up to 10–100 times higher compared with organic dyes.

QD application helps to visualize biological processes, to eliminate or reduce an autofluorescence signal and accomplish a simultaneous identification of several BASs. QD advantages are its colloidal solubility in the wide range of solvents, including water, the stability of its luminescent intensity, high quantum yields, and resistance to photobleaching. QD ET-based nanosensors are used for detection and quantification of the peptides, low-molecular compounds, environmental contaminants, viruses, microorganisms, and toxins in immunoassay and pH sensors [55].

Fluorometric immunoassay for human serum albumin based on its inhibitory effect on the immunoaggregation of QDs with silver nanoparticle was developed [56]. The presence of albumin decreases the fluorescence induced by FRET between these two types of nanoparticles. The linear dynamic range of albumin determination is 30–600 ng/mL. Nanosensor was proposed for highly sensitive and rapid clenbuterol detection with LOD 10 μg/mL based on decrease of ET and consequently fluorescence intensity in the QD CdTe–naphthol system [57]. Aptasensor based on FRET effect for determination of adenosine in urine samples of lung cancer patients was developed [58]. The FRET takes place between QD CdS as donor and polypyrrole as acceptor. The linear dynamic range of adenosine is 23–146 nM, the detection limit is 9.3 nM.

A sensitive nanobiosensor based on FRET was developed for the detection of 22-mer oligonucleotide sequence in human papillomavirus 18 virus (HPV18) gene [59]. For this purpose, water-soluble CdTe QDs were synthesized and amino-modified 11-mer oligonucleotide to form functional QDs–DNA conjugates. The addition of the QDs–DNA (donor) and a Cyanine5 (Cy5)-labeled 11-mer oligonucleotide probe (acceptor) to the DNA target solution, the sandwiched hybrids were formed. The fluorescence intensity of Cy5 found to be linearly enhanced by increasing the DNA target concentration from 1.0 to 50.0 nM, with a detection limit of 0.2 nM. This homogeneous DNA detection method does not require excessive washing and separation steps of unhybridized DNA, due to the fact that no FRET can be observed when the probes are not ligated.

The fluorescent $Hg^{2+}$ sensor based on $Hg^{2+}$-induced conformational alteration of single-stranded DNA rich in thymin is applied in ecology. The sensor is characterized by two linear dynamic ranges of response between fluorescence intensity and $Hg^{2+}$ concentration. The limit of $Hg^{2+}$ detection is 0.18 nM. The fluorescent sensor is specific for the analyte even in the presence of high concentrations of other metal ions [60].

A new sensor system was developed for metal-ion sensing based on FRET that was carried out between coumarin (C120) as the energy donor and fluorescein (FL) as the acceptor [61]. The concentration most suitable for FRET efficiency was determined to be 0.2 μM for C120 and 20 μM for FL. It was found that the presence of $Fe^{3+}$ ions selectively inhibited ET between the two molecules mentioned, whereas the other

metal ions did not affect. The detection limit of $Fe^{3+}$ is 2.54 μM. The C120–FL system has a good potential for a sensor application in analytical systems due to its high selectivity for $Fe^{3+}$.

QD and built-in genetically encoded proteins participated in FRET are widely used in molecular composition research [27, 62–64]. The process of RET with QDs and lanthanide ions between small organic fluorophores and different fluorescent proteins was examined in [65]. Efficient intermolecular ET from carbostyril 124–sensitized $Tb^{3+}$ to $Eu^{3+}$ proceeds in aqueous solution and on cell surface that can be used to imagine the proteins in biological systems.

The excited ET between solid nanoparticles and biomolecules can be additionally enhanced by combination with liquid organized micellar media. For example, bovine serum albumin in micelles was effectively detected by an FRET-based molecular sensor using CdTe QDs as energy donors and neutral red as acceptor [66]. The FRET efficiency was enhanced by the construction of cetyltrimethylammonium (CTAB) micelles, which significantly reduced the distance between the donor and the acceptor. The results indicated that the addition of the albumin easily leads to the fluorescence quenching of CdTe–neutral red fluorescence RET due to the formation of CdTe–albumin complexes, which have weak affinity to CdTe and repel the dyes from CdTe surface. The linear range of albumin was from 0.4 to 11 mg/L with LOD 0.13 mg/L.

A comprehensive review of the development of assays, bioprobes, and biosensors using QDs as *integrated* components was published [67]. In contrast to a QD that is selectively introduced as a label, an integrated QD is one that is present in a system throughout a bioanalysis, and simultaneously has a role in transduction and as a scaffold for biorecognition. The modulation of QD luminescence provides the opportunity for the transduction of these events via FRET, BRET, charge transfer quenching, and electrochemiluminescence. The examples of their application in biological sensing include the detection of small molecules using enzyme-linked methods, or using aptamers as affinity probes; the detection of proteins via immunoassays or aptamers; nucleic acid hybridization assays; and assays for protease or nuclease activity. Strategies for multiplexed detection are highlighted among these examples.

An interesting approach based on blocking FRET between two QDs of different sizes, which causes fluorescence quenching, was suggested in publication [68]. Prebinding of glucose on the QD donor occupies the binding sites and thus blocks RET between the two QDs, protecting the fluorescence from being quenched. A glucose assay is developed based on this approach. A linear dynamic range is achieved within 0.1–2.0 mmol/L, along with a detection limit of 0.03 mmol/L and an RSD of 2.1%. Glucose of 91–105% in serum and urine samples is recovered. The glucose detection is possible in the near-infrared region using Ce/Nd Co-doped luminophores and ET in Ce/Nd Co-doped $Ca_xSr_{1-x}S$ [69].

The same determination strategy using FRET from CdSe QDs to CdTe ones was studied and used to determine the serum prostate-specific antigen (PSA) [70]. The

effective ET and intensive fluorescence occurred between CdSe and CdTe in Tris–HCl buffer solution at pH 8.0. When PSA was added, the fluorescence intensity of CdSe–CdTe system decreased, and the fluorescence was finally quenched because of the specific immunological reaction between the PSA antigen and the CdTe-labeled PSA antibody. Under optimum conditions, the linear range of PSA antigen was 2.8–10 μg/L, with LOD of 0.015 μg/L.

The detection of DNA H5N1 and nucleic acids through QD and nanotubes (NTs) in the QD (CdTe)-ssDNA/NT system has been suggested, where modified ssDNA was the donor [71]. The DNA concentration rate is 0.01–20 μM and the detection limit is 9.93 nM. The deltamethrin chemiluminescent sensor based on QD is provided [72], with the linear dynamic range of 0.053–46.5 μg/mL and LOD 0.018 μg/mL.

A novel FRET-based ratiometric sensor with the polymer nanoparticle as scaffold for detecting $Hg^{2+}$ in aqueous media was developed [73]. A fluorescent dye fluorescein isothiocyanate (served as the donor) and a spirolactam rhodamine derivative (served as mercury ion probe) were covalently attached onto polyethylenimine and polyacrylic acid, respectively; a ratiometric sensing system was then formed through the deposition of the donor- and probe-containing polyelectrolytes onto the negatively charged polymer particles via the layer-by-layer approach. It was found that the ratiometric sensor is applicable in a pH range of 4.6–7.3 in water with the detection limit of 200 nM.

The FRET between QDs emitting at 565, 605, and 655 nm as energy donors and Alexa Fluor fluorophores with absorbance maxima at 594, 633, 647, and 680 nm as energy acceptors were studied [74]. As a first step, the covalent conjugates between all three types of QDs and each of the Alexa Fluor fluorophores that could act as an energy acceptor were prepared. All of these conjugates displayed efficient RET. Then the covalent conjugates of these QDs with biotin, fluorescein, and cortisol were prepared and established that the binding of these conjugates to suitable Alexa Fluor–labeled antibodies and streptavidin can be efficiently detected by measuring the RET in homogeneous solutions. Based on these observations, competitive binding assays for these three small analytes were developed.

Along with chemical analysis, QD and FRET can be used to solve various fundamental and application problems [75, 76]. Two special types of inorganic fluorophores are lanthanide luminescent labels and semiconductor QD. The feature of it is FRET at a distance of 1–20 nm applied in optic biosensors for diagnostics and cellular imaging, which use lanthanide as donors and QDs as acceptors [77]. The advantages and disadvantages of the following systems usage are shown by the example of immunocomplex organization [78].

Lanthanide-doped QDs find their use in biomedical research as bioindicators and biolabels; they are also applied in fluorescence microscopy, magnetic resonance imaging, and medicine body processing mechanism research. The advantages of this QD type over common fluorescent materials (organic pigments, fluorescent proteins' golden nanoparticles, and luminescent transition metal complexes)

include analytical signal detection in the visible and near-infrared, resistance to photochemical degradation, tolerance to DNA/RNA systems self-radiation due to exciting light energy reduction, low cytotoxicity, and high detection sensitivity of analytes.

The several procedures of synthesis of lanthanide-doped QD nanoparticles were proposed [79]. Immunofluorescent estradiol determination performs due to ET from biotinylated europium and terbium to CdTe semiconductor NPs coated with streptavidin without preseparation at the subnanomolar level. Streptavidin was coated without spacer layer in virtue of quite short distance between a donor and an acceptor [80]. ET from benzoic acid to lanthanide ions doped into $CaF_2$:$Eu^{3+}$ and $CaF_2$:$Tb^{3+}$ nanoparticles indicates the opportunity of lanthanide sensitization that forms complexes with organic ligands [81]. Table 5.1 summarizes analytical and metrological characteristics of BAS detection using FRET phenomenon.

Microspheres exhibited large Stokes shift and long wavelength fluorescence, which allows for FRET with two dyes to be produced. It was shown that microspheres usage allows the range of fluorescent probes to be extended [91].

#### 5.3.3.2 Nanoparticles based on Au, Ag, Au–Ag, and graphene

A strong band of SPR in visible region is the noble metal nanoparticles' optical property originated under incident light action. Plasmons are the collective oscillations of conduction electrons near the metal–dielectric interface. SPR is the reason of nonlinear optical effects exhibited as the result of an increase in the absorption efficiency, luminescence, and Raman scattering of molecules around the nanoparticles. The resonance photoexcitation is more effective, so both fluorophores and nanoparticles absorb the light. Energy gained by molecule during nonresonant excitation transfers to the metal nanoparticles, which can fluoresce.

The local electric field occurring under electromagnetic waves' action on the nanoparticle's metal surface can promote fluorescence decay of fluorophores molecule localized near the nanoparticle surface [92]. There are two different mechanisms to SPR impact on fluorophore's properties, which contributes to the nanosensor development. Spectral characteristics of fluorophores would be changed, detection limit would dramatically decrease, and selectivity of analytic determination would increase by the FRET-involved metal nanostructures application in the nanosensors. The dynamics of singlet-singled and singled-triplet ET would be affected by the local surface plasmons and this aroused considerable interest of analysts to the prospects of optosensing with nanoparticles [93, 94].

**Fluorescence quenching.** Nanoparticles are effective quenchers of fluorophores emission due to high molar absorption coefficients in the visible region. Due to metal particle's electron level's interaction with adsorbed molecule, the decay process has high efficiency. The local electric field has an impact on fluorophores expressed in

**Tab. 5.1:** FRET based on usage of nanomaterials

| Nanoobject | Analyte | Sample | Linear range (LOD) | References |
|---|---|---|---|---|
| CdTe and CTAB micelles | BSA | | $0.4{\cdot}10^{-3}$–$11{\cdot}10^{-3}$ g/L | [66] |
| Cd–Se, albumin-conjugated Ag NP | BSA | | 30–600 ng/mL | [56] |
| CdS | Adenosine | Urine of lung cancer patient | 23–146 nM<br>9.3 nM | [58] |
| Cd–Te | DNA | 22-Dimension oligonucleotide sequence in HPV gen | 1.0–50.0 nM<br>0.2 nM | [59] |
| CdTe | Clenbuterol | | (10 µg/mL) | [57] |
| CaS/SrS | Glucose | | | [69] |
| CdSe–CdTe | Prostate antigen | Blood serum | 2.8–10 µg/L;<br>($1.5{\cdot}10^{-2}$ µg/L) | [70] |
| CdTe-ssDNA/ nanotubes | DNA | | 0.01–20 µM;<br>(9.39 nM) | [71] |
| CdTe | Deltamethrin | | 0.053–46.5 µg/mL;<br>(0.018 µg/mL) | [82] |
| CdTe–CTAB micelles | Hg(II) | | 20 nM | [73] |
| QD/AlexaFluor Fluorophor | Streptavidin | | | [74] |
| CdTe/lanthanide | Estradiol | | $10^{-11}$–$10^{-9}$ M | [80] |
| $CaF_2$:$Eu^{3+}$ and $CaF_2$:$Tb^{3+}$ | Benzoic acid | | | [81] |
| QD/lanthanides | DNA | Biodiagnostics, screening | | [26] |
| Au NPs | α-Protein | Blood serum of cancer patients | | [83] |
| Au NPs | Norfloxacin | Urine | $7.9{\cdot}10^{-7}$–$2{\cdot}10^{-5}$ M | [84] |
| Graphene | Thrombin | | | [85] |
| Carbon NPs | Sn (II) | – | 18.7 µM | [86] |
| Carbon nitride | Riboflavin | Milk | 0.4–10 µM<br>170 nM | [87] |
| Graphene | TNT | – | (2.2 µM) | [88] |
| Carbon dots | | Organophosphorous compounds | $5.0{\cdot}10^{-11}$–$1.0{\cdot}10^{-7}$ M | [89] |
| Carbon dots | Glyphosate | Environmental medium, water | 0.02–2.0 µM<br>(0.6 µM) | [90] |

its excited lifetime decrease, which make up the fluorophores' photostability. In the presence of metal nanoparticles, excited ET state as inverse donor–acceptor distance $R^n$, where "n" varies from 3 to 4 unlike Förster mechanisms (there $n = 6$) as was set empirically. Along with this, metal particles presence exceeds Stern–Volmer quenching constant over conventional photochemical processes [95]. FRET with anomalous high nanometal surface energy transfer (NSET) efficiency is called a "superquenching." Au and Ag nanoparticles would be used as NSET florescence probes at the matrix

surfaces and in the solvents. For example, the fluorescent routine sensor uses covalent indicator dye immobilization at the quartz glass surface, where the Ag nanoparticles have been applied [96].

The determination of methimazole in plasma is based on acridine orange desorption from Ag nanoparticle surface and the following methimazole sorption. The dye fluorescence is reducing while Ag nanoparticles are present as the result of FRET. The system being entered with antithyroid shows that fluorescent intensity increases while methimazole' concentration is in the range of $8 \cdot 10^{-9}$ to $3.75 \cdot 10^{-7}$ M, with the detection limit of $5.5 \cdot 10^{-9}$ M [97].

Metal colloid stabilizers play a particular role in analytic detection. For example, DNA-stabilized Ag NPs are used for glutathione reductase activity detection. This method is highly selective and sensitive. The activity can be determined in the range of 0.2–2.0 mIU/mL. Pepsin, lysozyme, trypsin, avidin, thrombin, and myoglobin slightly affect the fluorescent intensity of the analytical system [98]. A new explorative NSET approach to oncology has been proposed based on directly methylated DNA identification without any chemical and enzyme methods [99].

Ag nanoparticles surface modified by L-tyrosine allow for the complex formation of Co (II) and Cu (II) ions by amino- and carboxylic groups of aminoacid, which is accompanied by fluorescence decay. This phenomenon is used for these metals' determination in solutions [100]. Competitive sorption of thiols and quinolones at the Au NPs' surface applied for fluorimetric determination of the sulfur analogs of alcohols with the detection limit $4.7 \cdot 10^{-8}$ M [101]. Fluorimetric methods of fexofenadine hexachloride detection in the medicinal drugs [102] and Sudan I–IV derivatives during medical investigation were proposed [103].

Chlorophyll luminescent decay in the presence of different NPs is suggested as an analytical instrument for ecological monitoring of plant's environmental stress [104]. Captopril sensor with a detection limit of $1.6 \cdot 10^{-7}$ M was developed [105]. For this purpose, a self-assembly multilayer was designed, in which photoluminescent graphene oxide was employed as a fluorescence probe. These multilayer films can effectively recognize captopril by RET from graphite oxide to silver nanoparticles. The sensory layer containing Ag nanoparticles could be used up to 10 times. The advantages of the NSET-based sensors are low noise level, high sensitivity, and visualization capability [106, 107].

**Metal-enhanced fluorescence.** If SPR wavelength and fluorophore excited wavelength are closely matched, the metal-enhanced fluorescence (MEF) will be observed [108]. This process is based on radiationless dipole–dipole electromagnetic ET between nanoparticles and ground and exited states of the nearest molecule. A silver NP is the most common material of MEF. Gold NPs are often used as quenchers, but they may amplify fluorescence of molecules, which have longer fluorescence wavelength [109]. MEF depends on the size and form of nanoparticles, donor–acceptor distance, overlap integral of plasmon resonance spectrum, and fluorophore absorption. It has been experimentally proven that too short fluorophore–NP distance quenches

the fluorescence [110]. Nowadays, MEF has received great attention and sometimes is used for BAS determination. The colloid solutions of noble metals stabilized with sodium citrate are typically used MEF nanoparticles [111–117].

The fluorimetric method of tetracycline determination in milk based on fluorescence amplification in the presence of Ag nanoparticles was proposed [118]. The complex of $Eu^{3+}$ with tetracycline (TC) is sorbed at the surface of Ag nanoparticle. The local field of $Eu^{3+}$–TC chelate impacted by SPR allows for increases of the intensity of fluorescence by 4 times. The antibiotic's concentration linear dynamic range is 10 nM to 10 μM; detection limit is 4 nM.

It was found that silver NPs could enhance co-luminescence effect of rare-earth ions Tb(3+) and Y(3+) [119]. Based on this, a sensitive fluorescence detection method for the determination of dopamine was proposed. This is because dopamine can significantly enhance the luminescence intensity of the Tb(3+) ion by Y(3+) in the colloidal solution of the NPs, forming a new co-luminescence system. In a neutral buffer solution (pH 7.5), the luminescence intensity of the system was linear in the range of 2.0–100 nM dopamine concentration with LOD as low as 0.57 nM. The plasmon effect of silver NPs helps to enhance the fluorescence intensity of the quercetin (Q) and nucleic acid system [120]. Based on this effect, a sensitive method for the determination of nucleic acids was developed. The detection limits for the nucleic acids were reduced to the ng/mL level. The complex system of Q–Ag NPs was also successfully used for the detection of nucleic acids in agarose gel electrophoresis analysis.

The Ag nanoparticle surface modified by the β-cyclodextrins amplifies the tetracycline and chlorotetracycline (Cl–TC) intrinsic fluorescence by 3–5 times and decreases detection limit to ng/mL [121]. The linear dynamic ranges for the determination of TC and Cl–TC in aqueous solutions varied from 0.10 to 6.0 mg/L and 0.050 to 3.0 mg/L with detection limits of 0.63 and 0.19 μg/L, respectively. The method has been tested on pharmaceutical preparations. A biosensing platform using Ag@$SiO_2$-DNA-fluorophore (Cy3) nanostructure was designed for metal ions and small organic molecule detection [122]. By controlling the thickness of the silica shell on the Ag nanoparticle, the fluorescence of cyanina 3 (Cy3) could be enhanced by the SPR of Ag NP for up to 2.5 folds. This MEF sensor provided high sensitivity and selectivity for the detection of $Hg^{2+}$, $Ag^{+}$, and coralyne.

Quinolones (Qs) can form the complex with Tb(III) ion, and the intramolecular ET from Qs to Tb(III) takes place when excited [123]. When the silver nanoparticles were added to the Tb(III)–Qs system, the luminescence intensity at 545 nm greatly increased. The calibration graphs for pipemidic acid and lomefloxacin are linear in the range $2.0 \times 10^{-10}$ to $1.0 \times 10^{-5}$ and $1.0 \times 10^{-9}$ to $1.0 \times 10^{-5}$ mol/L, respectively. The method was applied to the determination of both quinolones in tablet, capsule, urine, and serum samples.

It was established that nucleic acids can greatly enhance fluorescence intensity of the kaempferol-Al(III) chelate in the presence of silver NPs. Based on this, a novel

method for the determination of nucleic acids was proposed [124]. The linear relationships between the extent of fluorescence enhancement and the concentration of nucleic acids are in the range of $5.0 \times 10^{-9}$ to $2.0 \times 10^{-6}$ g/mL for fish sperm DNA, $7.0 \times 10^{-9}$ to $2.0 \times 10^{-6}$ g/L for salmon sperm DNA, and $2.0 \times 10^{-8}$ to $3.0 \times 10^{-6}$ g/L for yeast RNA, and their detection limits are $2.5 \times 10^{-9}$, $3.2 \times 10^{-9}$, and $7.3 \times 10^{-9}$ g $L^{-1}$, respectively.

A nanocomposite based on hexagonal mesoporous silica (HMS), silver and gold NPs, and rhodamine R as a chemosensor for $Hg^{2+}$ ion determination in the aqua solutions was suggested. A comparison of the nanocomposite analytical properties with Ag and Au nanoparticles revealed that maximum fluorescence intensity amplification was observed in the Ag–HMS–rhodamine R system [125].

Ag nanoparticles are used as the carrying agents for an immobilization of the indicator dyes during FRET [98]. For example, routine determination is based on quenching of the fluorescence sensor. The Ag nanoparticles served as bridges and carriers, and covalently immobilized 3-amino-9-ethylcarbazole was developed. This allows the routine determination in the range of $2.0 \cdot 10^{-6}$ to $1.5 \cdot 10^{-4}$ M with LOD $8.0 \cdot 10^{-7}$ M [96]. The function of Ag nanoparticles is being a passive matrix in an aptamer during platelet determination based on FRET processes between Alexa Fluor 488 (Alexa), Cy3 and a Black hole quencher-2 (BHQ-2) sorbed at Ag nanoparticle surface. That system enables platelet determination in concentration ranging from 3.1 to 200 ng/mL; detection limit is 0.4 ng/mL [126].

Gold NPs can be an effective acceptor, for example, in the reaction of luminol and hydrogen peroxide, catalyzed by horseradish peroxidase. The method based on the measurement of luminol luminescence decay, as the result of immune interaction between antigen and antibody, is successfully applied to the alpha-protein determination in blood serum of cancer patients [83]. Such approach is used to determine other antibodies and biologically active agents [84].

The efficiency of FRET between donor and acceptor fragments of double spiral DNA enhances by the addition of Ag nanoparticles. The sorption at the surface of those NPs decreases the distance between the donor and acceptor centers of DNA molecule. A fluorescence intensity amplification of acceptor and donor quenching allows changing efficiency and informational value of the FRET method applied to bioanalysis [30, 127].

The analytical signal intensity of norfloxacin chemiluminescent detection with the flow-injection method based on Ce(IV)–$Na_2SO_3$ redox reaction is highly amplified at the surface of the Ag nanoparticles that promote the electron ET. This approach is used to determine the antibiotic concentration in the human urine in the range of $7.9 \cdot 10^{-7}$ to $1.9 \cdot 10^{-5}$ M; detection limit is $8.2 \cdot 10^{-8}$ M [84].

Due to the high absorption coefficients, high intensity of emission signal and photostability of the gold NPs are often used as components of FRET pairs [128]. These NPs can be both a donor and an acceptor of excitation energy. In the presence of gold NPs, the sensitivity of DNA determination increased by two orders of magnitude [129, 130].

For example, the system for atrazine pesticide detection based on Au nanoparticles was suggested [131]. QDs [132] and gold NPs are applied in express analysis based on quenching effect [132, 133].

Two reviews devoted to discussion of silver and gold application in NSET have been published [95, 134]. It was shown that the sensitized fluorescence may be applied as a spectroscopic tool for extra- and intermolecular distances between interacting components. The dependence of the ET efficiency on the distance between the donor and the acceptor can be used also for molecules bio-probing and for designing of highly sensitive chemical and biological sensors [95, 134]. The analytical signal intensity can be tuned and, therefore, the sensitivity and selectivity of target analyte determination can be amplified by varying the size, charge, and stabilization of the surface of nanoparticles and by changing the plasmon resonance spectrum. The size of nanoparticles affects the plasmon resonance band shift and the overlap integral of nanoparticles absorption spectrum with analyte fluorescence spectrum.

Relatively recent nanomaterials are carbon QD and graphene that are also used to sensitize fluorescence. They are cheap and nontoxic and they emit a bright, tunable light radiation. Carbon QDs replace the semiconductor QD in developing of chemical sensors and in biovisualization. It was shown that carbon fluorescent QD modified by PEG-200 considerably enhances the intensity of aliphatic primary amines chemiluminescence that was used for their determination in water [135]. Graphene unique properties have been applied in aptasensors for thrombin detection with sensitivity of two orders higher than that for carbon nanotube–based sensors [85]. This is explained by unique graphene structure and electron properties. The advantage of aptamer-based biosensors is a possibility of various optical detection modes (FRET fluorescence, absorption of visible light, and Raman scattering) with the use of optical nanomaterials in bioanalysis [85, 135, 136].

**Nanomaterials based on graphene are** effective and simple fluorescent sensing platform for ultrasensitive detection of 2,4,6-trinitrotoluene (TNT) in solution by FRET quenching [88]. The fluorescent graphene can specifically bind TNT species by the $\pi$–$\pi$ stacking interaction between graphene and TNT aromatic rings. As a result, TNT strongly suppresses the graphene fluorescence emission (donor) by the FRET to the irradiative TNT (acceptor) through intermolecular polar–polar interactions at spatial proximity. The limit of TNT detection was 0.495 ppm (2.2 μM), with the use of only 1 mL of graphene solution.

A novel "Turn On" fluorescence sensor platform has been developed for trace α-glucosidase inhibitor screening from natural medicines [137]. Combining with the carbon dots, cobalt oxyhydroxide (CoOOH) nanoflakes were employed to build the FRET-based sensor platform. The sensor platform was ultrasensitive to ascorbic acid with a detection limit of 5 nM, ensuring the sensitive monitoring of enzyme activity.

Ellman's test is used in the dichlorvos biosensor based on supersensitive RET, where the anion of 5-thio-2-nitrobenzoic acid is used as energy acceptor and carbon

QDs as donors [89]. The range of the concentration of a dichlorvos to be determined is $5.0 \cdot 10^{-11}$ to $1.0 \cdot 10^{-7}$ M. High sensitivity and quantum yield of fluorescing centers adapt the system to the automated control of this insecticide. ET between carbon dots and glyphosate was applied to the pesticide determination [90]. A high fluorescence of obtained inclusion complexes considerably decreases in the presence of a glyphosate. The developed method is approved for water samples with pesticide linear dynamic range determination 0.02–2.0 μM and LOD 0.6 μM. The method is recommended for environment objects screening.

An FRET biosensor for acid phosphatase (ACP) was established by attaching nile red (NR) to graphene QD (GQDs) via lecithin/β-CD complex as the linker [138]. The introduction of lecithin/β-CD brought the GQDs–NR pair close enough to making the FRET occur and thus resulting in the fluorescence quenching of GQDs (donor) and the fluorescence enhancement of NR (acceptor). The presence of ACP in the sensing system catalyzes the hydrolysis of lecithin into two parts, resulting in the GQDs–NR pair separation and decreasing of NR fluorescence owing to the inhibition of FRET process. The LOD of ACP is 28 μU/mL, which was considerably low compared to known methods of ACP detection. This biosensor was applied for in vitro imaging of human prostate cancer cells. The way of quercetin determination based on carbon nanoparticles fluorescence quenching in the concentration range from 2.87 to $31.57 \cdot 10^{-6}$ M and the detection limit ($3\sigma$) $9.88 \cdot 10^{-8}$ M was proposed [139].

## 5.4 The lanthanide chelates' ET application

### 5.4.1 Liquid micellar nanosystems

It has been shown above that ET involving lanthanide chelates' application for determination of rare earth metals, organic and bioorganic substances is a well-developed approach with number of publications more than 500. When going from homogeneous solvent to microheterogeneous micellar organized media, the ET efficiency as a rule increases owing to preconcentrating and close proximity effects [20]. Table 5.2 presents the examples of micellar media influence on the intermolecular ET in the lanthanide chelates applied to different BAS determination. One can see from the table that additional increase of fluorescence intensity in micelles is a result of ability of the lanthanide to coordinate several ligands, which enhance the antenna effect; this can lead both to a simultaneous transfer of electronic excitation energy from several donors to the metal ion and to a preliminary interligand ET. The second effect of ET and fluorescence enhancing is the presence of the second lanthanide ion (co-sensitizing effect).

The choice of the type of a liquid organized system is very important because it solves the main problem – to provide the complete solubilization and the strongest

**Tab. 5.2:** Examples of application of the intramolecular ET in lanthanide complexes for determination of BASs in organized media

| BAS | First lanthanide | Second lanthanide | Second ligand | Micelles | References |
|---|---|---|---|---|---|
| Ibuprofen and orthofen | $Tb^{3+}$ | | 1,10-Phenanthroline (Phen) | Brij-35 | [140] |
| Doxycycline (DC) | $Eu^{3+}$ | | | Triton X-100 | [141] |
| Tetracycline (TC) | $Eu^{3+}$ | | Trioctyl-phosphine oxide | Micelles | [142] |
| Bile acid | $Eu^{3+}$ | | Tetracycline | SAS micelles | [143] |
| 2-Benzoyl-indan-1,3-dione | $Eu^{3+}$, $Sm^{3+}$ | | | Cation SAS | [144] |
| Diphacinone | $Eu^{3+}$ | $Gd^{3+}$ | | Triton X-100 | [145] |
| Bromadiolone | $Tb^{3+}$ | | | Triton X-100 | [146] |
| Nucleinic acid | $Eu^{3+}$, $Tb^{3+}$ | $Gd^{3+}$ | Phen<br>$Lu^{3+}$ | | [147] |
| Ciprofloxacin, enrofloxacin | $Tb^{3+}$ | | | Sodium lauryl sulfate | [11, 148] |
| Levofloxacin | $Tb^{3+}$ | | | SDS | [149] |
| Trovafloxacin | $Tb^{3+}$ | | | SDS | [150] |
| Oxytetracycline | $Eu^{3+}$ | | | DE-β-cyclodextrin | [151] |
| Adenosine triphosphate | $Eu^{3+}$ | $Gd^{3+}$ | Thenoyltri-fluoroacetone | Brij-35 | [152] |
| Tetracycline | $Eu^{3+}$ | | Phen | Anion SAS | [17, 142] |
| Fluoroquinolones (FQ) | $Tb^{3+}$ | | Phen | Dodecylbenzene sulphonate | [153] |
| Oxytetracycline | $Eu^{3+}$ | | Phen | Dodecylbenzene sulphonate | [154] |
| Ciprofloxacin, enrofloxacin (Ef) | $Eu^{3+}$ | | Phen | Dodecylbenzene sulphonate | [155] |
| Flumequine | $Tb^{3+}$ | | Phen | Dodecylbenzene sulphonate | [156] |

binding of reactants by micelles. Therefore, the nature of surfactant molecules, which form micelles, has a major influence on fluorescence amplification. It was established that micelles of anionic surfactants offer the amplification of sensitized fluorescence intensity in most cases and give rise to widening the pH plateau of their complex formation. The protolytic properties changing of the ligands acid-base groups are caused the latter effect [20, 21].

The ET efficiency and the sensitized fluorescence intensity depend on several factors, such as the nature of the ligand, lanthanide ion, and solvent; pH of the medium; temperature; and the energy gap between the triplet level of the ligand and the fluorescent level of the lanthanide. The most important reason of ET efficiency

increase is dehydration of lanthanide ion and, therefore, a decrease of the radiationless energy loss due to its transfer to oscillatory levels of hydroxyl groups of coordinated by metal water molecules [157, 158]. The following processes cause the dehydration: a solubilization of valence-unsaturated chelates in less polar environment of micelles, and displacement of residual water molecules from the first coordination sphere of the metal ion by second ligand and in the case of SDS by surfactant anions [157, 159]. This assumption is confirmed by increased lifetime of lanthanide ion at the SAS presence [158, 160] (Tab. 5.3).

**Tab. 5.3:** $Eu^{3+}$ chelate–flumequine (Fl) photophysical properties in aqua and micellar solutions

| Chelate | $\tau$, μs | $q$* | $\varphi$, % | pH range |
|---|---|---|---|---|
| Fl–$Eu^{3+}$ | 160 | 6.4 | 2.0 | 6.5–7.5 |
| Fl–$Eu^{3+}$–SDS | 177 | 5.6 | 3.0 | 6.0–8.5 |
| Fl–$Eu^{3+}$–Phen | 178 | 5.8 | 1.8 | 6.0–9.0 |
| Fl–$Eu^{3+}$–Phen–SDS | 213 | 4.7 | 4.0 | 6.0–9.5 |

where $q$ is the number of water molecules in the local proximity of metal, which was calculated on experimental data using Horrocks method

$$q = 1.05(A_{\text{gen}} - A_r), \quad \text{where } A_{\text{gen}} = 1/\tau,$$

where $\tau$ is fluorescent decay time and $A_r$ is the radiation rate [161, 162].

The indirect evidence of microenvironment universal impact on the lanthanide hydration in the anionic micelles is provided by increase of fluorescence decay time and decrease in the number of coordinated lanthanide water molecules on mixed ligand complex formation and their solubilization in SDS micelles (see Tab. 5.3). The linear correlation between the radiationless process ($A_{nr}$) and the number of the water molecules ($q$) being entered to the europium local proximity as well as the lipophilicity of ligand confirm the above conclusion (Fig. 5.1). It was shown that mixed-ligand lanthanide chelate solubilization by micelles is accompanied by decrease of the radiationless loss of excitation energy. It confirms the data [161] about the dependence of radiationless transition rate $A_{nr}$ in $Eu^{3+}$ and $Tb^{3+}$ ions on the water molecule number in the first coordination sphere of lanthanide ion (Fig. 5.2).

It has been established that intensity amplification directly relates to aliphatic tail length in anionic surfactant molecule (Tab. 5.4). This may be also associated with enhancing of chelate micelle-binding, increasing metal dehydration, and a decreasing of radiationless processes.

Another feature associated with influence of surfactant molecule nature on the properties of mixed-ligand chelates of $Eu^{3+}$ and $Tb^{3+}$ with the antibiotics is the differentiating effect of surfactant micelles owing to different hydrophilic group charges (Tab. 5.5).

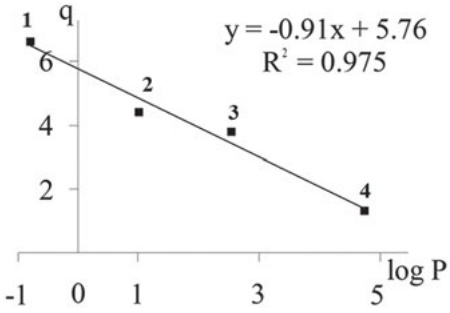


**Fig. 5.1:** Effect of ligand lipophilicity (log P) on the number of water molecules $q$ in coordination sphere of $Eu^{3+}$ chelates with fluoroquinolones solubilized in SDS micelles.

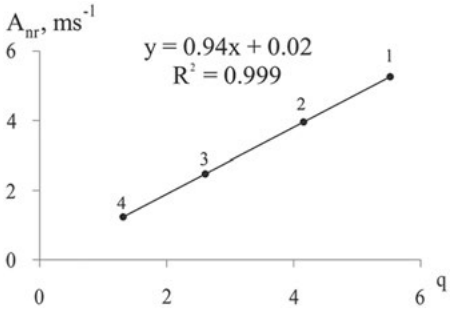


**Fig. 5.2:** Dependence of radiationless transition rate $A_{nr}$ on the number of molecules of water in the first coordination sphere of $Eu^{3+}$ chelates with enrofloxacin in the water (1), SDS micelles (2), Phen presence in the water (3), and in SDS micelles.

**Tab. 5.4:** The anionic aliphatic tail length effect on sensitized fluorescence

| Surfactant | $\Delta I$ ($Eu^{3+}$–TC –Phen) | $pH_{opt}$ | $\Delta I$ ($Ln^{3+}$–FQ–Phen) | $pH_{opt}$ |
|---|---|---|---|---|
| SDS | 1.5 | 7.5–8.5 | 1.0 | 9.0–10.0 |
| SDS | 2.5 | 7.5–8.5 | 3.0 | 10.0–11.0 |
| Sodium dodecylbenzene sulphate (DDBS) | 3.5 | 7.5–8.5 | 5.0 | 9.0–10.5 |

Thus, the anionic micelles are the fluorescence quencher of $Eu^{3+}$–doxycycline (DC)–Phen and $Tb^{3+}$–oxolinic acid–Phen chelates, while micelles of cationic CTAB enhance the sensitized fluorescence. In turn, micelles of nonionic surfactants enhance the europium chelate fluorescence with a doxycycline–Phen far more without changing the intensity of europium chelates' luminescence with enrofloxacin (Ef), nalidixic (NA), and oxolinic (OA) acids. Nonionic micelles are also more effective on solubilization of mixed-ligand $Eu^{3+}$ chelates with less hydrophobic ligands as thenoyltrifluoroacetone (TTA) and a doxycycline, because of favor solubilization of the ligands in the oxyethylene layer of the micelle.

**Tab. 5.5:** Micelles' effect on fluorescence intensity of Eu and Tb mixed-ligand chelates with antibiotics and 1.10-Phen

| SAS | $I/I_0$ | | | | | | |
|---|---|---|---|---|---|---|---|
| | $Tb^{3+}$–warfarin | $Tb^{3+}$–(OA) | $Tb^{3+}$–NA | $Eu^{3+}$–Ef | $Eu^{3+}$–DC | $Tb^{3+}$–Nf | $Tb^{3+}$–Fl |
| SDS | Quenching | Quenching | 2 | 53 | Quenching | 2.5 | 3.0 |
| DDBS | Quenching | Quenching | 1.2 | 5 | Quenching | 4 | 2.1 |
| CPC | Quenching | 1.4 | Quenching | 1 | 1 | Quenching | 2.4 |
| CTAB | Quenching | 4.2 | Quenching | 1 | 2.5 | Quenching | 1.2 |
| Triton X-100 | Quenching | 1 | 1 | 1 | 7 | Quenching | Quenching |
| Brij-35 | Quenching | 1 | 1.2 | 1 | 6 | Quenching | Quenching |
| Tween-80 | Quenching | 1 | 1 | 1 | 6 | Quenching | Quenching |

$I_0$ – initial fluorescence.

A decrease of sensitized fluorescence of some chelates in micelles of anionic surfactants may be due to the chelates destruction because of competing binding of the metal cation with anionic micelle surface. Besides, the negatively charged antibiotic ligands are weakly bound to the same-charged surface of anionic surfactant micelles, which also decreases the formation of the fluorescing chelates probability. Thus, the ion of metal and a ligand-forming chelate are spatially separated in the anionic micelles. At the same time, the positive-charged micelle surface of cationic micelles does not interfere with the chelate formation. Table 5.5 also shows that chelate solubilization in nonionic micelles caused three effects: it can have no effect, amplify, or reduce fluorescence intensity. Those effects may be due to different mechanisms of solubilization as well as and place of chelate localization in the oxyethylene layer of nonionic micelles.

The interesting fact is that differentiation is observed while Tb chelate is forming even for the same kind of ligands as shown for norfloxacin (Nf) and flumequine (Fl) comparison, which belong to one fluoroquinolone group (Tab. 5.5). It can be concluded, taking into account the different molecules structure of norfloxacin and flumequine, the variation of cation SAS micelles influence is caused by selective solubilization of the ligands. The same different influence of surfactant micelles on Tb chelates sensitized fluorescence is described in [163].

For some antibiotics the alignment between their acid ionization constants and pH-optimum range of mixed-ligand complex formation is found in which a maximum of sensitized fluorescence intensity of $Eu^{3+}$ chelates is observed (Tab. 5.6). The table shows that pH range of complex formation is enlarged to alkaline medium due to reducing ligand acid-based properties and changes the chelate microenvironment in anionic micelles.

Microemulsions (MEs) are the rarely used type of organized micellar system for observing the sensitized fluorescence. Its feature is outstanding high solubilization capacity and the ability to change solvent polarity in the microenvironment of the

**Tab. 5.6:** pK values of antibiotic aminogroup and acidity range of lanthanides complex formation in aqua and micellar solutions

| Antibiotic | pK | Acidity range in water | Acidity range in SDS micelles |
|---|---|---|---|
| $Tb^{3+}$–Nf–Phen | 8.8 | 8.5–9.0 | 8.0–9.5 |
| $Eu^{3+}$–Cf–Phen | 8.1 | 8.0–9.0 | 8.0–10.5 |
| $Tb^{3+}$–NA–Phen | 7.6 | 7.0–7.5 | 6.5–8.0 |

analytical system by inverse of "water/oil" (w/o) type of ME to "oil/water" (o/w) and vice versa. It was established that the transition of ME from SDS/n-pentanol/n-octane/water from o/w to w/o amplifies the sensitized fluorescence intensity up to 1.3 times. Besides, the ME allows for strongly hydrophobic compound usage as the second ligand no matter if they do not dissolve in micellar solutions (Fig. 5.3). It was occurred that complex formation range and ME efficiency could depend on the buffer nature of some components of which may be solubilized in the ME (Fig. 5.4).

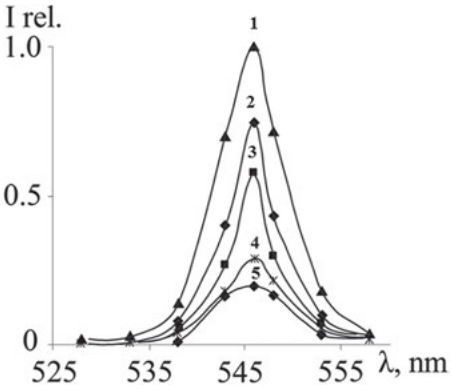


**Fig. 5.3:** A comparison of fluorescence spectra of $Tb^{3+}$–Fl (5), $Tb^{3+}$–Fl–Phen (4), $Tb^{3+}$–Fl–SDS (3), $Tb^{3+}$–Fl–Phen–SDS (2), and $Tb^{3+}$–Fl–Phen–ME (1) chelates.

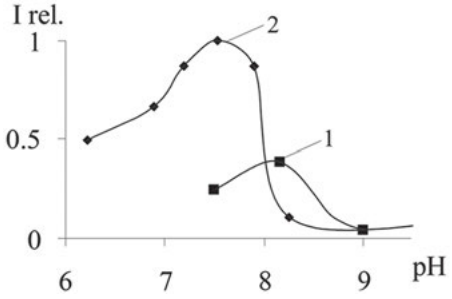


**Fig. 5.4:** Buffer and pH effect on the fluorescence intensity of Fl–$Tb^{3+}$–Phen chelate; 1 – borate; 2 – acetate-ammonium buffers.

It has been found that use of acetate-ammonium buffer enables decrease in the LOD of flumequine down to 1.5 times (Tab. 5.7).

**Tab. 5.7:** Metrological characteristics of Fl determination using $Tb^{3+}$ chelate in SDS micelles and ME ($y = ax + b$)

| Organized media | *a* | *b* | Linear range, M | LOD, M |
|---|---|---|---|---|
| 0.01 M SDS | 0.39 | 7.07 | $1.0\cdot10^{-8}$–$1.0\cdot10^{-3}$ | $6.2\cdot10^{-9}$ |
| ME | 0.45 | 5.74 | $1.0\cdot10^{-8}$–$1.0\cdot10^{-3}$ | $4.2\cdot10^{-9}$ |

Along with ME and micelles, the albumin, which globules have the ability to solubilize the chelates, also may amplify the intensity of lanthanide sensitized fluorescence. It is observed that albumin solubilization of some antibiotics and anticoagulants may amplify its intrinsic fluorescence up to 5–7 times. The reason for that could be the ET from a donor (a protein molecule) to an acceptor (a derivative of coumarin and tetracycline) and the polarity changing in fluorophore microenvironment [19, 157]. Aside from micelles, ME, and proteins, the sensitized fluorescence is described in nanofilms [164] and in polyelectrolyte layers produced by layer-by-layer method [165, 166].

### 5.4.2 ET in binuclear complexes of heteronanoparticles

The intramolecular ET efficiency amplification in micelles is observed in heterometallic 3d–4f binuclear complexes of $Nd^{3+}$, $Ho^{3+}$, $Er^{3+}$, $Tm^{3+}$, and $Yb^{3+}$ in the presence of second lanthanide as well. The intensity of sensitized fluorescence enhancement in this case is based on both inter- and intramolecular ET mechanisms in these heteronanosystems. As shown, the sensitized fluorescence intensity in $Sm^{3+}$ and $Tb^{3+}$ complexes depends on concentration and ratio of $Sm^{3+}$ and $Tb^{3+}$ concentrations in polymer film, which is the result of intermolecular ET [167].

In order to establish the relation between the size of heteronanoparticles and the intensity of sensitized fluorescence of $Eu^{3+}$–$Gd^{3+}$–TTA, binuclear complexes solubilized in different micelles were studied. Our measurements for $Eu^{3+}$–$Gd^{3+}$–TTA complex have shown that the best average size of nanoparticles in aqua solutions for highest co-luminescence is 20–50 nm. Their solubilization of the NPs in micelles enhances the fluorescence of heteronanoparticles far more. The greatest growth of fluorescence (almost on the order) is noted in the nonionic block copolymer of ethylene and propylene oxides and also oxyethylene alcohol of Brij-35. The fluorescence signal in micellar Brij-35 solutions is noted in less concentration of ligands while nanoparticles size reduces to 5–10 nm. The relative number of NPs with less size is increased to 20 % in the concentration ratio of ion $Eu^{3+}$:$Gd^{3+}$ = 1:(80–100). Thus, the synergistic

effect of co-luminescence and solubilization amplifies the intensity of $Eu^{3+}$ sensitized fluorescence up to three orders and reduces its detection limit [152] (Tab. 5.8).

**Tab. 5.8:** Effect of second ligand, lanthanide second ion, and micelles on histidine (His) and Eu LOD by sensitized fluorescence

| Lanthanide chelate | Analyte | LOD, M |
|---|---|---|
| $Eu^{3+}$–TTA–Phen | $Eu^{3+}$ | $3.9 \cdot 10^{-8}$ |
| $Eu^{3+}$–TTA–Phen–Brij-35 | | $4.0 \cdot 10^{-9}$ |
| $Eu^{3+}$–TTA–Brij-35–$Gd^{3+}$ | | $3.2 \cdot 10^{-11}$ |
| $Eu^{3+}$–TTA | His | $5.6 \cdot 10^{-6}$ |
| $Eu^{3+}$–TTA–$Gd^{3+}$ | | $1.0 \cdot 10^{-8}$ |
| $Eu^{3+}$–TTA–Brij-35–$Gd^{3+}$ | | $1.0 \cdot 10^{-9}$ |

## 5.5 Conclusions

The solubilization of fluorophore analytical systems, which influence is based on electronic excitation ET in liquid nanoobjects (micelles, microemulsions, the protein globules), their sorption on solid nanoparticles (quantum and carbon dots, silver, gold NPs), or in sol–gel nanomaterial pores, significantly reduces the distance between donor and acceptor of the excitation energy and increases the efficiency of intermolecular ET comparison to homogeneous water or nonaqueous solvents. The preconcentration and proximity effects of donor and acceptor solubilized in micellar nanoreactor allow reactions of a complex formation realizing at a lower concentration of the analyte. The compartmentalizing and bringing close together the donor and acceptor in liquid nanoreactors also increases the efficiency of intramolecular ET and reduces detection limits of many biologically active substances down to 1–3 orders. Along with that, the solubilization of lanthanide complexes in micelles increases the number of the ligands, which are coordinated by a metal ion, allows replace the maximum number of water molecules from the lanthanide coordination sphere, and increases quantum yield of its sensitized fluorescence. The additional contribution to lanthanide dehydration is made by the hydrophobic microenvironment of chelates being solubilized in the micelles. The empirical identification of the convenient donor and acceptor molecules allows selectively to excite the analyte, that is, to improve the selectivity of determination. The liquid organized solutions on the basis of micelles are often used in the analysis due to their highly sensitive determination of biologically active agents forming lanthanide chelates in such objects as blood plasma, muscular tissue, biological liquids, water, and soils.

The solid nanoparticles (silver, gold, different QDs) are intensively developed while having good prospects in the bioanalysis application due to promoting the realization of sensitized fluorescence. The luminescent method based on ET and

sensitized fluorescence with the use of various nanoobjects has considerable analytical prospects and opportunities in the analysis of food, environmental, pharmaceutical, and medicine objects.

## References

[1] Weissman SI. Intramolecular energy transfer. The fluorescence of complexes of europium. *J Chem Phys* 1942, 10, 214–7.
[2] Förster Th. Zwischenmolekulare energiewanderung und fluoreszenz. *Ann Phys* 1948, 2, 55–75.
[3] Ermolaev VL, Sveshnikova EV, Bodunov EN. Inductive-resonant mechanism of nonradiative transitions in ions and molecules in condensed phase. *Phys Usp* 1996, 39, 261–82.
[4] Agranovach VM, Galanin MD. *Electron-Excitation Energy Transfer in Condensed Media*. Moscow, Izdatel'stvo Nauka, 1978. (Original source in Russian).
[5] Huheey JE, Keiter EA, Keiter R. *Inorganic Chemistry: Principles of Structure and Reactivity,* 4th ed. New York, Harper Collins, 1993.
[6] Bünzli J-CG. Benefiting from the unique properties of lanthanide ions. *Accounts Chem Res* 2006, 39, 53–61.
[7] Pozharski E. Fluorescence resonance energy transfer-based analysis of lipoplexes. *Methods Mol Biol* 2010, 606, 393–8.
[8] Bünzli J-CG, Piguet C. Taking advantage of luminescent lanthanide ions. *Chem Soc Rev* 2005, 34, 1048–77.
[9] Eliseeva SV, Bünzli J-CG. Lanthanide luminescence for functional materials and bio-science. *Chem Soc Rev* 2010, 39, 189–227.
[10] Leif RC, Vallarino LM, Becker MC, Yang S. Review: increasing the luminescence of lanthanide complexes. *Cytometry A* 2006, 69, 767–77.
[11] Lis S. Luminescence spectroscopy of lanthanide(III) ions in solution. *J Alloys Compounds* 2002, 341, 45–50.
[12] Bünzli J-CG, Comby S, Chauvin A-S, Caroline DB. New opportunities for lanthanide luminescence. *J Rare Earths* 2007, 25, 257–74.
[13] Handl HL, Gillies RJ. Lanthanide-based luminescent assays for ligand-receptor interactions. *Life Sci* 2005, 77, 361–71.
[14] Lis S, Elbanowski M, Makowska B, Hnatejko Z. Review. Energy transfer in solution of lanthanide complexes. *J Photochem Photobiol A: Chem* 2002, 150, 233–47.
[15] Heyduk T, Heyduk E, Doisy EA. Luminescence energy transfer with lanthanide chelates: interpretation of sensitized acceptor decay amplitudes. *Anal Biochem* 2001, 289, 60–7.
[16] Shtykov CN, Smirnova TD, Molchanova YV. Synergistic effects in the europium(III)-thenoyltrifluoroacetone-1,10-phenanthroline system in micelles of block copolymers of nonionic surfactants and their analytical applications. *J Anal Chem* 2001, 56, 920–4.
[17] Shtykov SN, Smirnova TD, Bylinkin YG, Zhemerichkin DA. Fluorimetric determination of tetracyclines with the europium chelate of 1,10-phenanthroline in micellar solutions of anionic surfactants. *J Anal Chem* 2005, 60, 24–8.
[18] Shtykov CN, Smirnova TD, Kalashnikova NV, Konyukhova YuG. Complexes with energy transfer in the excited state in organized media. *Biomed Technol* 2006, 12, 4–9 (Original source in Russian).
[19] Smirnova TD, Nevryueva NV, Shtykov SN, Kochubei VI, Zhemerichkin DA. Determination of warfarin by sensitized fluorescence using organized media. *J Anal Chem* 2009, 64, 1114–9.

[20] Shtykov SN. Chemical analysis in nanoreactors: main concepts and applications. *J Anal Chem* 2002, 57, 859–68.
[21] Savvin SB, Mikhailova AV, Shtykov SN. Organic reagents in spectrophotometric methods of analysis. *Rus Chem Rev* 2006, 75, 341–9.
[22] Zhang R-J, Yang K-Z, Yu A-C, Zhao X-S. Fluorescence lifetime and energy transfer of rare earth β-diketone complexes in organized molecular films. *Thin Solid Films* 2000, 363, 275–8.
[23] Cui F, Zhang J, Cui T, Han K, Xie B, Lin Q, et al. Nanoassembly of photoluminescent films containing rare earth complex nanoparticles on planar and microspherical supports. *Colloids Surf A* 2006, 278, 39–45.
[24] Zhang R-J, Cui J-W, Lu D-M, Hou W-G. Study on high-efficiency fluorescent microcapsules doped with europium β-diketone complex by LbL self-assembly. *Chem Commun* 2007, 15, 1547–9.
[25] Baleizaõ C, Nagl S, Schaferling M, Berberan-Santos MN, Wolfbeis OS. Dual fluorescence sensor for trace oxygen and temperature with unmatched range and sensitivity. *Anal Chem* 2008, 80, 6449–57.
[26] Hildebrandt N, Löhmannsröben H-G. Quantum dot nanocrystals and supramolecular lanthanide complexes – energy transfer systems for sensitive in vitro diagnostics and high throughput screening in chemical biology. *Curr Chem Biol* 2007, 1, 167–86.
[27] Ishii H, Shimanouchi T, Umakoshi H, Walde P, Kuboi R. Analysis of the 22-NBD-cholesterol transfer between liposome membranes and its relation to the intermembrane exchange of 25-hydroxycholesterol. *Colloids. Surf B Biointerfaces* 2010, 77, 117–21.
[28] McFarland AD, Van Duyne RP. Single silver nanoparticles as real-time optical sensors with zeptomole sensitivity. *Nano Lett* 2003, 3, 1057–62.
[29] Shtykov SN, Rusanova TY. Nanomaterials and nanotechnologies in chemical and biochemical sensors: capabilities and applications. *Russ J Gen Chem* 2008, 78, 2521–31.
[30] Lakowicz JR, Kusba J, Shen Y, Malicka J, D'Auria S, Gryczynski Z, et al. Effects of metallic silver particles on resonance energy transfer between fluorophores bound to DNA. *J Fluoresc* 2003, 13, 69–77.
[31] Algar WR, Krull UJ. Quantum dots as donors in fluorescence resonance energy transfer for the bioanalysis of nucleic acids, proteins, and other biological molecules. *Anal Bioanal Chem* 2008, 391, 1609–18.
[32] Willard DM, Van Orden A. Quantum dots: resonant energy-transfer sensor. *Nat Mater* 2003, 2, 575–6.
[33] Goldman ER, Clapp AR, Anderson GP, Yueda HT, Mauro JM, Medintz IL, et al. Multiplexed toxin analysis using four colors of quantum dot fluororeagents. *Anal Chem* 2004, 76, 684–8.
[34] Das P, Mallick A, Purkayastha P, Haldar B, Chattopadhyay N. Fluorescence resonance energy transfer from TX-100 to 3-acetyl-4-oxo-6,7-dihydro-12H-indolo-[2,3-a]quinolizine in premicellar and micellar environments. *J Mol Liq* 2007, 130, 48–51.
[35] Bhattar SL, Kolekar GB, Patil SR. Fluorescence resonance energy transfer between perylene and riboflavin in micellar solution and analytical application on determination of vitamin B2. *J Lumin* 2008, 128, 306–10.
[36] Xu H, Li Y, Liu C, Wu Q, Zhao Y, Lu L, et al. Fluorescence resonance energy transfer between acridine orange and rhodamine 6G and its analytical application for vitamin $B_{12}$ with flow-injection laser-induced fluorescence detection. *Talanta* 2008, 77, 176–81.
[37] Liu B, Liu Z, Cao Z. Fluorescence resonance energy transfer between acridine orange and rhodamine 6G and analytical application in micelles of dodecyl benzene sodium sulfonate. *J Lumin* 2006, 118, 99–105.
[38] Zherdeva VV, Savitsky AP. The use of lanthanide inductive resonance energy transfer in the study of biological processes in vitro and in vivo. *Adv Biol Chem (Russia)* 2012, 52, 315–62. (Original source in Russian).

[39] Riddle SM, Vedvik KL, Hanson GT, Vogel KW. Time-resolved fluorescence resonance energy transfer kinase assays using physiological protein substrates: Applications of terbium-fluorescein and terbium-green fluorescent protein fluorescence resonance energy transfer pairs. *Anal Biochem* 2006, 356, 108–16.
[40] Robers MB, Machleidt T, Carlson CB, Bi K. Cellular LanthaScreen and beta-lactamase reporter assays for high-throughput screening of JAK2 inhibitors. *Assay Drug Dev Technol* 2008, 6, 519–29.
[41] Carlson CB, Robers MB, Vogel KW, Machleidt T. Development of LanthaScreen cellular assays for key components within the PI3K/AKT/mTOR pathway. *J Biomol Screen* 2009, 14, 121–32.
[42] Carlson CB, Mashock MJ, Bi K. BacMam-enabled LanthaScreen cellular assays for PI3K/Akt pathway compound profiling in disease-relevant cell backgrounds. *J Biomol Screen* 2010, 15, 327–34.
[43] Horton RA, Strachan EA, Vogel KW, Riddle SM. A substrate for deubiquitinating enzymes based on time-resolved fluorescence resonance energy transfer between terbium and yellow fluorescent protein. *Anal Biochem* 2007, 360, 138–13.
[44] Kokko L, Sanberg K, Lövvgren T, Soukka T. Europium(III) chelate-dyed nanoparticles as donors in a homogeneous proximity-based immunoassay for estradiol. *Anal Chim Acta* 2004, 503, 155–62.
[45] Wang G, Yuan J, Hai X, Matsumoto K. Homogeneous time-resolved fluoroimmunoassay of 3,5,3′-triiodo-l-thyronine in human serum by using europium fluorescence energy transfer. *Talanta* 2006, 70, 133–9.
[46] Prieto B, Llorente E, González-Pinto I, Alvarez FV. Plasma procalcitonin measured by time-resolved amplified cryptate emission (TRACE) in liver transplant patients. A prognosis marker of early infectious and non-infectious postoperative complications. *Clin Chem Lab Med* 2008, 46, 660–6.
[47] Degorce F, Card A, Soh S, Trinquet E, Knapik GP, Xie B. HTRF: a technology tailored for drug discovery: a review of theoretical aspects and recent applications. *Curr Chem Genomics* 2009, 3, 22–32.
[48] Xie Y, Yang X, Pua J, Zhao Y, Zhang Y, Xie G, et al. Homogeneous competitive assay of ligand affinities based on quenching fluorescence of tyrosine/tryptophan residues in a protein via Fŏrster-resonance-energy-transfer. *Spectrochim Acta, Part A* 2010, 77, 869–76.
[49] Bluma RK, Kalninia IE, Shibaeva TN. Using the DSP-6 fluorescent probe to investigate the erythrocyte membrane. *Biochem Suppl. Ser A: Membrane Cell Biol* 1990, 7, 47–9. original source in Russian
[50] Kalninia IE, Bloom RK. Application of fluorescent probes in biomedical studies. Fluorescence methods issued and clinical diagnosis. *Sat Sci Works* 1991, 1, 29–38. (Original source in Russian).
[51] Sominsky VN, Bloom RK, Kalnina IE. Binding of the fluorescent probe of the DSM probe to the erythrocyte membrane in normal and in certain diseases. *Biochem suppl. Ser A: Membrane Cell Biol* 1986, 3, 282–4 (Original source in Russian).
[52] Gainulina ET, Kljuster OB, Ryzhikov SB. An express method for the determination of cholinesterase inhibitors. *Bull Exp Biol Med* 2006, 142, 591–2 (Original source in Russian).
[53] Gainulina ET, Kondratiev KB, Ryzhikov SB. Fluorescent method for the determination of cholinesterase. *Bull Exp Biol Med* 2006, 142, 710–1 (Original source in Russian).
[54] Gryzunov Yu A, Lukicheva TI. Correctness and reproducibility of the fluorescent method for determining the mass concentration of human serum albumin. *Clin Lab Diagn* 1994, 5, 27–30. (Original source in Russian).
[55] Stanisavljevic M, Krizkova S, Vaculovicova M, Kizek R, Vojtech A, Quantum dots-fluorescence resonance energy transfer-based nanosensors and their application. *Bios Bioelectron* 2015, 74, 562–74.

[56] Marukhyan SS, Vardan K, Gasparyan G. Fluorometric immunoassay for human serum albumin based on its inhibitory effect on the immunoaggregation of quantum dots with silver nanoparticles. *Spectrochim Acta Pt A* 2017, 173, 34–7.
[57] Nguyen ND, Tung NT, Nguyen QL. Highly sensitive fluorescence resonance energy transfer (FRET)-based nanosensor for rapid detection of clenbuterol. *Adv Nat Sci Nanosci Nanotechnol* 2012, 3, 035011–7.
[58] Hashemian Z, Khayamian, T, Saraji M, Shirani MP. Aptasensor based on fluorescence resonance energy transfer for the analysis of adenosine in urine samples of lung cancer patients. *Bios Bioelectron* 2016, 79, 334–9.
[59] Shamsipur M, Nasirian V, Mansouri K, Barati A, Veisi-Rayganic A, Kashaniana S. A highly sensitive quantum dots-DNA nanobiosensor based on fluorescence resonance energy transfer for rapid detection of nanomolar amounts of human papillomavirus. *J Pharm Biomed Anal* 2017, 136, 140–6.
[60] Huang D, Niu Ch, Wang X, Li X, Zeng G. "Turn-On" fluorescent Sensor for $Hg^{2+}$ based on single-stranded DNA functionalized Mn:CdS/ZnS quantum dots and gold nanoparticles by time-gated mode. *J Anal Chem* 2013, 85, 1164–9.
[61] Bozkurt E, Arık M, Onganer Y. A novel system for $Fe^{3+}$ ion detection based on fluorescence resonance energy transfer. *Sens Actuators B* 2015, 221, 136–44.
[62] Thaler C, Koushik SV, Blank PS, Vogel SS. Quantitative multiphoton spectral imaging and its use for measuring resonance energy transfer. *Biophys J* 2005, 89, 2736–49.
[63] Gnacha A, Bednarkiewicz A. Lanthanide-doped up-converting nanoparticles: merits and challenges. *Nanotoday* 2012, 7, 532–63.
[64] Sapsford KE, Berti L, Medintz IL. Materials for fluorescence resonance energy transfer analysis: beyond traditional donor-acceptor combinations. *Angew Chem Int Ed* 2006, 45, 4562–89.
[65] Lee M, Tremblay MS, Jockusc S, Turro NJ, Sames D. Intermolecular energy transfer from $Tb^{3+}$ to $Eu^{3+}$ in aqueous aggregates on the surface of human cells. *Org Lett* 2011, 13, 2802–5.
[66] Ge S, Lu J, Yan M, Yu F, Yu J, Sun X. Fluorescence resonance energy transfer sensor between quantum dot donors and neutral red acceptors and its detection of BSA in micelles. *Dyes Pigments* 2011, 91, 304–8.
[67] Algar WR, Tavares AJ, Krull UJ. A review of the application of quantum dots as integrated components of assays, bioprobes, and biosensors utilizing optical transduction. *Anal Chim Acta* 2010, 673, 1–25.
[68] Hu B, Zhang LP, Chen ML, Wang JH. The inhibition of fluorescence resonance energy transfer between quantum dots for glucose assay. *Biosens Bioelectron* 2012, 32, 82–8.
[69] Meng JX, Wan WJ, Fan LL, Yang CT, Chen QQ, Cao LW, et al. Near infrared fluorescence and energy transfer in Ce/Nd Co-doped $Ca_xSr_{1-x}S$. *J Luminesc* 2011, 131, 134–7.
[70] Hui-Lin TAO, Shu-Huai LI, Jian-Ping LI. Fluorescence resonance energy transfer between quantum dots of CdSe and CdTe and its application for determination of serum prostate-specific antigen. *Chin J Anal Chem* 2012, 40, 224–9.
[71] Tian J, Zhao H, Liu M, Chen Y, Quan X. Detection of influenza a virus based on fluorescence resonance energy transfer from quantum dots to carbon nanotubes. *Anal Chim Acta* 2012, 723, 83–7.
[72] Ge S, Zhang C, Yu F, Yan M, Yu J. Layer-by-layer self-assembly CdTe quantum dots and molecularly imprinted polymers modified chemiluminescence sensor for deltamethrin detection. *Sens Actuators B*, 2011, 156, 222–7.
[73] Ma C, Zeng F, Wu G, Wu S. A nanoparticle-supported fluorescence resonance energy transfer system formed via layer-by-layer approach as a ratiometric sensor for mercury ions in water. *Anal Chim Acta* 2012, 734, 69–78.
[74] Nikiforov TT, Beechem JM. Development of homogeneous binding assays based on fluorescence resonance energy transfer between quantum dots and Alexa Fluor fluorophores. *Anal Biochem* 2006, 357, 68–75.

[75] Clapp AR, Medintz IL, Mattoussi H. Förster resonance energy transfer investigations using quantum-dot fluorophores. *ChemPhysChem* 2006, 7, 47–57.
[76] Algar WR, Krull UJ. Quantum dots as donors in fluorescence resonance energy transfer for the bioanalysis of nucleic acids, proteins, and other biological molecules. *Anal Bioanal Chem* 2008, 391, 160–9.
[77] Geißler D, Linden S, Liermann K, Wegner KD. Lanthanides and quantum dots as Förster resonance energy transfer agents for diagnostics and cellular imaging. *Inorg Chem* 2014, 53, 1824–38.
[78] Goryacheva OA, Beloglazova NV, Vostrikova AM, Pozharov MV, Sobolev AM, Goryacheva IYu. Lanthanide-to-quantum dot Förster resonance energy transfer (FRET): application for immunoassay. *Talanta* 2017, 164, 377–84.
[79] Lin M, Zhao Y, Wang SQ, Liu M, Duan ZF, Chen YM, et al. Recent advances in synthesis and surface modification of lanthanide-doped upconversion nanoparticles for biomedical applications. *Biotechnol Adv* 2012, 30, 1551–61.
[80] Härmä H, Soukka T, Shavel A, Gaponik N, Wellere H. Luminescent energy transfer between cadmium telluride nanoparticle and lanthanide(III) chelate in competitive bioaffinity assays of biotin and estradiol. *Anal Chim Acta* 2007, 604, 177–83.
[81] Wang J, Wang Z, Li X, Wang S, Mao H, Li Z. Energy transfer from benzoic acid to lanthanide ions in benzoic acid-functionalized lanthanide-doped $CaF_2$ nanoparticles. *Appl Surf Sci* 2011, 257, 7145–9.
[82] Gea S, Zhanga C, Yub F, Yana M, Yua J. Layer-by-layer self-assembly CdTe quantum dots and molecularly imprinted polymers modified chemiluminescence sensor for deltamethrin detection. *Sens Actuators B* 2011, 156, 222–7.
[83] Huang X, Ren J. Gold nanoparticles based chemiluminescent resonance energy transfer for immunoassay of alpha fetoprotein cancer marker. *Anal Chim Acta* 2011, 686, 115–20.
[84] Yu X, Bao J. Determination of norfloxacin using gold nanoparticles catalyzed cerium(IV)–sodium sulfite chemiluminescence. *J Luminesc* 2009, 129, 973–8.
[85] Haixin C, Longhua T, Ying W, Jinghong L. Graphene fluorescence resonance energy transfer aptasensor for the thrombin detection. *Anal Chem* 2010, 82, 2341–6.
[86] Ngu PZZ, Chia SPP, Fong JFY, Ng SM. Synthesis of carbon nanoparticles from waste rice husk used for the optical sensing of metal ions. *New Carbon Mater* 2016, 31, 135–43.
[87] Han J, Zou HY, Gao MX, Huang CZ. A graphitic carbon nitride based fluorescence resonance energy transfer detection of riboflavin. *Talanta* 2016, 148, 279–84.
[88] Fan L, Hu Y, Wang X, Zhang L, Li F, Han D, et al. Fluorescence resonance energy transfer quenching at the surface of graphene quantum dots for ultrasensitive detection of TNT. *Talanta* 2012, 101, 192–7.
[89] Hou J, Tian Z, Xie H, Tian Q, Ai S. A fluorescence resonance energy transfer sensor based on quaternized carbon dots and Ellman's test for ultrasensitive detection of dichlorvos. *Sens Actuators B* 2016, 232, 477–82.
[90] Yuan Y, Jiang J, Liu S, Yang J, Hui Z, Jingjing Y, et al. Fluorescent carbon dots for glyphosate determination based on fluorescence resonance energy transfer and logic gate operation. *Sens Actuators B* 2017, 242, 545–52.
[91] Wu WB, Wang ML, Sun YM, Huang W, Cui YiP, Xub CX. Fluorescent polystyrene microspheres with large Stokes shift by fluorescence resonance energy transfer. *J Phys Chem Solids* 2008, 69, 76–82.
[92] Krutyakov YuA, Kudrinskiy AA, Olenin AYu, Lisichkin GV. Synthesis and properties of silver nanoparticles: advances and prospects. *Rus Chem Rev* 2008, 77, 233–57.
[93] Wu M, Lakowicz JR, Geddes CD. Enhanced lanthanide luminescence using silver nanostructures: opportunities for a new class of probes with exceptional spectral characteristics. *J Fluoresc*, 2005, 15, 53–9.

[94] Lakowicz JR, Maliwal BP, Malicka J, Gryczynski Z, Gryczynski I. Effects of silver island films on the luminescent intensity and decay times of lanthanide chelates. *J Fluoresc* 2002, 12, 431–7
[95] Ghosh D, Chattopadhyay N. Gold and silver nanoparticle based superquenching of fluorescence: a review. *J Lumin* 2015, 160, 223–32.
[96] Tan SZ, Hu YJ, Gong FC, Cao Z, Xia JY, Zhang L. A novel fluorescence sensor based on covalent immobilization of 3-amino-9-ethylcarbazole by using silver nanoparticles as bridges and carriers. *Anal Chim Acta* 2009, 636, 205–9.
[97] Farzampour L, Amjadi M. Sensitive turn-on fluorescence assay of methimazole based on the fluorescence resonance energy transfer between acridine orange and silver nanoparticles. *J Lumin* 2014, 155, 226–30.
[98] Zhu S, Zhao X, Zhang W, Liu Z, Qi W, Anjum S, et al. Fluorescence detection of glutathione reductase activity based on deoxyribonucleic acid-templated silver nanoclusters. *Anal Chim Acta* 2013, 786, 111–5.
[99] Dadmehr M, Hosseini M, Hosseinkhani S, Ganjali MR, Sheikhneja R. Label free colorimetric and fluorimetric direct detection of methylated DNA based on silver nanoclusters for cancer early diagnosis. *Biosens Bioelectron* 2015, 73, 108–13.
[100] Contino A, Maccarrone G, Zimbone M, Reitano R, Musumeci P, Calcagno L, et al. Tyrosine capped silver nanoparticles: a new fluorescent sensor for the quantitative determination of copper(II) and cobalt(II) ions. *J Colloid Interface Sci* 2016, 462, 216–22.
[101] Amjadi M, Farzampour L. Fluorescence quenching of fluoroquinolones by gold nanoparticles with different sizes and its analytical application. *J Lumin* 2014, 145, 263–7.
[102] Alothman ZA, Bukhari N, Haider S, Wabaidur SM, Alwarthan AA. Spectrofluorimetric determination of fexofenadine hydrochloride in pharmaceutical preparation using silver nanoparticles. *Arab J Chem* 2010, 3, 251–5.
[103] Chen NY, Li HF, Gao ZF, Qu F, Li NB, Luo HQ. Utilizing polyethyleneimine-capped silver nanoclusters as a new fluorescence probe for Sudan I-IV sensing in ethanol based on fluorescence resonance energy transfer. *Sens Actuators, B* 2014, 193, 730–6.
[104] Falco WF, Queiroz AM, Fernandes J, Botero ER, Falcao EA, Guimaraes FEG, et al. Interaction between chlorophyll and silver nanoparticles: a close analysis of chlorophyll fluorescence quenching. *J Photochem Photobiol A* 2015, 299, 203–9.
[105] Sun X, Liu B, Li S, Li F. Reusable fluorescent sensor for captopril based on energy transfer from photoluminescent graphene oxide self-assembly multilayers to silver nanoparticles. *Spectrochim Acta, Part A* 2016, 161, 33–8.
[106] Medintz IL, Clapp AR, Mattoussi H, Goldman ER, Fisher B, Mauro JM. Self-assembled nanoscale biosensors based on quantum dot FRET donors. *Nat Mater* 2003, 9, 630–8.
[107] Bagalkot V, Zhang LF, Levy-Nissenbaum E, Jon SY, Kantoff PW, Langer R, et al. Quantum dot – aptamer conjugates for synchronous cancer imaging, therapy, and sensing of drug delivery based on bi-fluorescence resonance energy transfer. *Nano Lett* 2007, 7, 3065–70.
[108] Stranik O, Nooney R, McDonagh C, MacCraith BD. Optimization of nanoparticle size for plasmonic enhancement of fluorescence. *Plasmonics* 2007, 2, 15–22.
[109] Lakowicz JR, Ray K, Chowdhury M, Szmacinski H, Fu Y, Zhang J, et al. Plasmon-controlled fluorescence: a new paradigm in fluorescence spectroscopy. *Analyst* 2008, 133, 1308–46.
[110] Lessard-Viger M, Rioux M, Rainville L, Boudreau D. FRET enhancement in multilayer core-shell nanoparticles. *Nano Lett* 2009, 9, 3066–71.
[111] Ji XH, Song XN, Li J, Bai YB, Yang WS, Peng XG. Size control of gold nanocrystals in citrate reduction: the third role of citrate. *J Am Chem Soc* 2007, 129, 13939–48.
[112] Kimling J, Maier M, Okenve B, Kotaidis V, Ballot H, Plech A. Turkevich method for gold nanoparticle synthesis revisited. *J Phys Chem B* 2006, 110, 15700–7.
[113] Nguyen DT, Kim D-J, So MG, Kim K-S. Experimental measurements of gold nanoparticle nucleation and growth by citrate reduction of $HAuCl_4$. *Adv Powder Technol* 2010, 21, 111–8.

[114] Polte J, Ahner TT, Delissen F, Sokolov S, Emmerling F, Thünemann AF, et al. Mechanism of gold nanoparticle formation in the classical citrate synthesis method derived from coupled in situ XANES and SAXS evaluation. *J Am Chem Soc* 2010, 132, 1296–301.
[115] Pong BK, Elim HI, Chong JX, Ji W, Trout BL, Lee JY. New insights on the nanoparticle growth mechanism in the citrate reduction of gold(III) salt: formation of the Au nanowire intermediate and its nonlinear optical properties. *J Phys Chem C* 2007, 111, 6281–7.
[116] Uppal MA, Kafizas A, Ewing MB, Parkin IP. The effect of initiation method on the size, monodispersity and shape of gold nanoparticles formed by the Turkevich method. *New J Chem* 2010, 34, 2906–11.
[117] Uppal MA, Kafizas A, Lim TH, Parkin IP. The extended time evolution size decrease of gold nanoparticles formed by the Turkevich method. *New J Chem* 2010, 34, 1401–7.
[118] Tan H, Chen Y. Silver nanoparticle enhanced fluorescence of europium (III) for detection of tetracycline in milk. *Sens Actuators, B* 2012, 173, 262–7.
[119] Li H, Wu X. Silver nanoparticles-enhanced rare earth co-luminescence effect of Tb (III)–Y(III) dopamine system. *Talanta* 2015, 138, 203–8.
[120] Liu P, Zhao L, Wu X, Huang F, Wang M, Liu X. Fluorescence enhancement of quercetin complexes by silver nanoparticles and its analytical application. *Spectrochim Acta, Part A* 2014, 122, 238–45.
[121] Wang P, Wu TH, Zhang Y. Novel silver nanoparticle-enhanced fluorometric determination of trace tetracyclines in aqueous solutions. *Talanta* 2016, 146, 175–80.
[122] Sui N, Wang L, Yan T, Liu F, Sui J, Jiang Y, et al. Selective and sensitive biosensors based on metal-enhanced fluorescence. *Sens Actuators B* 2014, 202, 1148–52.
[123] Ding F, Zhao H, Jin L, Zheng D. Study of the influence of silver nanoparticles on the second-order scattering and the fluorescence of the complexes of Tb(III) with quinolones and determination of the quinolones. *Anal Chim Acta* 2006, 566, 136–44.
[124] Cao Y, Wu X, Wang M. Silver nanoparticles fluorescence enhancement effect for determination of nucleic acids with kaempferol – Al(III). *Talanta* 2011, 84, 1188–94.
[125] Cheng ZH, Li G, Liu MM. Metal-enhanced fluorescence effect of Ag and Au nanoparticles modified with rhodamine derivative in detecting $Hg^{2+}$. *Sens Actuators B* 2015, 212, 495–504.
[126] Li H, Zhao Y, Chen Z, Xu D. Silver enhanced ratiometric nanosensor based on two adjustable Fluorescence Resonance Energy Transfer modes for quantitative protein sensing. *Biosens Bioelectron* 2017, 87, 428–32.
[127] Malicka J, Gryczynski I, Fang J, Kusba J, Lakowicz JR. Increased resonance energy transfer between fluorophores bound to DNA in proximity to metallic silver particles. *Anal Biochem* 2003, 315, 160–9.
[128] Daniel MC, Astruc D. Gold nanoparticles: assembly, supramolecular chemistry, quantum-size-related properties, and applications toward biology, catalysis, and nanotechnology. *Chem Rev* 2004, 104, 293–346.
[129] Dubertret B, Calame M, Libchaber AJ. Single-mismatch detection using gold-quenched fluorescent oligonucleotides. *Nat Biotechnol* 2001, 19, 365–70.
[130] Maxwell DJ, Taylor JR, Nie SM. Self-assembled nanoparticle probes for recognition and detection of biomolecules. *J Am Chem Soc* 2002, 124, 9606–17.
[131] Seidel M, Dankbar DM, Gauglitz G. A miniaturized heterogeneous fluorescence immunoassay on gold-coated nano-titer plates. *Anal Bioanal Chem* 2004, 379, 904–12.
[132] Dyadyusha L, Yin H, Jaiswal S, Brown T, Baumberg JJ, Booy FP, et al. Quenching of CdSe quantum dot emission, a new approach for biosensing. *Chem Commun* 2005, 25, 3201–3.
[133] Gueroui Z, Libchaber A. Single-molecule measurements of gold-quenched quantum dots. *Phys Rev Lett* 2004, 93, 166108–11.
[134] Li H, Xu D. Silver nanoparticles as labels for applications in bioassays. *Trends Anal Chem* 2014, 61, 67–73.

[135] Zhou Y, Xing G, Chen H, Ogawa N, Lina J-M. Carbon nanodots sensitized chemiluminescence on peroxomonosulfate – sulfite – hydrochloric acid system and its analytical applications. *Talanta* 2012, 99, 471–7.
[136] Morales-Narváez E, Sgobbi LF, Machado SAS, Merkoçi A. Graphene-encapsulated materials: Synthesis, applications and trends. *Prog Mater Sci* 2017, 86, 1–24.
[137] Li G, Kong W, Zhao M, Lu S, Gong P, Chen G, et al. A fluorescence resonance energy transfer (FRET) based "Turn-On" nanofluorescence sensor using a nitrogen-doped carbon dot-hexagonal cobalt oxyhydroxide nanosheet architecture and application to α-glucosidase inhibitor screening. *Bios Bioelectron* 2016, 79, 728–34.
[138] Na W, Liu Q, Sui B, Hu T, Su X. Highly sensitive detection of acid phosphatase by using a graphene quantum dots-based förster resonance energy transfer. *Talanta* 2016, 161, 469–54.
[139] Xiao D, Yuan D, He H, Gao M. Microwave assisted one-step green synthesis of fluorescent carbon nanoparticles from ionic liquids and their application as novel fluorescence probe for quercetin determination. *J Lumin* 2013, 140, 120–5.
[140] Teslyuk O, Bel'tyukova S, Yegorova A, Yagodkin B. Complex compounds of terbium(III) with some nonsteroidal anti-inflammatory drugs and their analytical applications. *J Anal Chem* 2007, 62, 330–5.
[141] Jiang CQ, Zhang N. Enzyme-amplified lanthanide luminescence based on complexation reaction – a new technique for the determination of doxycycline. *J Pharm Biomed Anal* 2004, 35, 1301–6.
[142] Jee RD. Study of micellar solutions to enhance the europium-sensitized luminescence of tetracyclines. *Analyst* 1995, 120, 2867–72.
[143] Wang T, Wang X, Jiang C. Spectrofluorimetric determination of bile acid using a europium-doxycycline probe. *J Clin Lab Anal* 2007, 21, 207–82.
[144] Si ZK, Jiang W, Ding Y, Hu J. The europium/samarium-2-benzoyl-indane-1,3-dione-cetyltrimethylammonium bromide fluorescence system and its analytical application. *Fresenius' J Anal Chem* 1998, 360, 731–4.
[145] Zhu Y, Si Z-K, Zhu W-J. Study on sensitised luminescence of rare earths by fluorescence enhancement of the europium-gadolinium-diphacinone – ammonia complex system and its application. *Analyst* 1990, 115, 1139–42.
[146] Sendra B, Panadero S, Gomes-Hens A. Kinetic determination of bromadiolone based on lanthanide-sensitized luminescence. *Anal Chim Acta* 1997, 355, 145–50.
[147] Lin C, Yang J, Wu X. Study on the columinescence effect of terbium-gadolinium-nucleic acids-cetylpyridine bromide system. *J Lumin* 2003, 101, 141–6.
[148] Hernandez-Arteseros JA, Compano R, Prat MD. Application principal component regression to luminescence data for the screening of ciprofloxacin and enrofloxacin in animal tissues. *Analyst* 2000, 125, 1155–8.
[149] Ocana JA, Callejon M, Barragan FJ. Terbium-sensitized luminescence determination of lovofloxacin in tablets and human urine and serum. *Analyst* 2000, 125, 1851–4.
[150] Ocana JA, Callejon M, Barragan FJ. Determination of trovafloxacin in human serum by time resolved terbium-sensitised luminescence. *Eur J Pharm Sci* 2001, 13, 297–31.
[151] Wang H, Hou F, Jiang C. Ethyl substituted β-cyclodextrin enhanced fluorimetric method for the determination of trace amounts of oxytetracycline in urine, serum, feed of chook and milk. *J Lumin* 2005 ,113, 94–9.
[152] Shtykov SN, Smirnova TD, Bylinkin YG. Determination of adenosine triphosphoric acid by its effect on the quenching of the fluorescence of europium(III) diketonate in micelles of Brij-35. *J Anal Chem* 2004, 59, 438–41.
[153] Shtykov SN, Smirnova TD, Nevryueva NV, Zhemerychkin DA. Fluorimetric method for determining norfloxacin, based on the phenomenon of energy transfer. *Izv Univ Chem Chem Technol* 2006, 49, 27–30. original source in Russian

[154] Shtykov SN, Smirnova TD, Kalashnikova NV, Bylinkin YG, Zhemerichkin DA. Fluorescence in the system Eu(III) – oxytetracycline – co-ligand – sodium dodecylbenzene sulphonate micelles and its analytical application. *Proc SPIE* 2006, 6165, 61650Q1–6.
[155] Shtykov SN, Smirnova TD, Bylinkin YG, Kalashnikova NV, Zhemerichkin DA. Determination of ciprofloxacin and enrofloxacin by the sensitized fluorescence of europium in the presence of the second ligand and micelles of anionic surfactants. *J Anal Chem* 2007, 62, 153–7.
[156] Smirnova TD, Shtykov SN, Nevryueva NV, Zhemerichkin DA, Parashchenko II. Fluorimetric assay of flumequine using sensitized terbium fluorescence in organized media. *Pharm Chem J* 2010, 44, 635–8.
[157] Arnaud N, Georges J. Comprehensive study of the luminescent properties and lifetimes of $Eu^{(3+)}$ and $Tb^{(3+)}$ chelated with various ligands in aqueous solutions: influence of the synergic agent, the surfactant and the energy level of the ligand triplet. *Spectrochim Acta, Pt A* 2003, 59, 1829–40.
[158] Smirnova TD, Shtykov SN, Kochubei VI, Khryachkova ES. Excitation energy transfer in europium chelate with doxycycline in the presence of a second ligand in micellar solutions of nonionic surfactants. *Opt Spectrosc* 2011, 110, 60–6.
[159] Ermolaev VL, Bodunov EN, Sveshnikova EB, Shakhverdov TA. *Radiationless Transfer of Electronic Excitation Energy*. Leningrad, Nauka, 1977. (Original source in Russian).
[160] Parashchenko II, Smirnova TD, Shtykov SN, Kochubei VI, Zhukova NN. Doxycycline-sensitized solid-phase fluorescence of europium on silica in the presence of surfactants. *J Anal Chem* 2013, 68, 112–6.
[161] Horrocks W, Sidnick DR. Lanthanide ion luminescence probes of the structure of biological macromolecules. *Acc Chem Res* 1981, 14, 384–92.
[162] Horrocks WD, Sudnick DR. Lanthanide ion probes of structure in biology. Laser-induced luminescence decay constants provide a direct measure of the number of metal-coordinated water molecules. *J Am Chem Soc* 1979, 101, 334–40.
[163] Selivanova N, Vasilieva K, Galyametdinov Yu. Luminescent complexes of terbium ion for molecular recognition of ibuprofen. *J Luminesc* 2014, 29, 202–11.
[164] Lapaev DV, Nikiforov VG, Safiullin GM, Lobkov VS, Salikhov KM, Knyazev AA, et al. Laser control and temperature switching of luminescence intensity in photostable transparent film based on terbium(III) β-diketonate complex. *Optic Mater* 2014, 37, 593–9.
[165] Davydov N, Zairov R, Mustafina A, Syakayev V, Tatarinov D, Mironov V, et al. Determination off fluoroquinolone antibiotics through the fluorescent response of Eu(III) based nanoparticles fabricated by layer-by-layer technique. *Anal Chim Acta* 2013, 784, 65–71.
[166] Zairov R, Zhilkin M, Mustafina A, Nizameev I, Tatarinov D, Konovalov A. Impact of polyelectrolyte coating in fluorescent response of Eu(III)-containing nanoparticles on small chelating anions including nucleotides. *Surface Coat Technol* 2015, 271, 242–6.
[167] Jiu H, Zhang L, Liu G, Fan T. Fluorescence enhancement of samarium complex co-doped with terbium complex in a poly(methylmethacrylate) matrix. *J Lumin* 2009, 129, 317–9.

# Part III: **Application in Electroanalysis**

Kh. Brainina, N. Stozhko, M. Bukharinova and E. Vikulova

# 6 Nanomaterials: Electrochemical Properties and Application in Sensors

**Abstract:** The unique properties of nanoparticles make them an extremely valuable modifying material, being used in electrochemical sensors. The features of nanoparticles affect the kinetics and thermodynamics of electrode processes of both nanoparticles and redox reactions occurring on their surface. The paper describes theoretical background and experimental studies of these processes. During the transition from macro- to micro- and nanostructures, the analytical characteristics of sensors modify. These features of metal nanoparticles are related to their size and energy effects, which affects the analytical characteristics of developed sensors. Modification of the macroelectrode with nanoparticles and other nanomaterials reduces the detection limit and improves the degree of sensitivity and selectivity of measurements. The use of nanoparticles as transducers, catalytic constituents, parts of electrochemical sensors for antioxidant detection, adsorbents, analyte transporters, and labels in electrochemical immunosensors and signal-generating elements is described.

## 6.1 Introduction

A chemical or biochemical sensor can be defined as an analytical device that generates information about concentration of inorganic, organic, and biological substances. A sensor includes a transducer and a receptor. Biochemical sensors usually contain some biological substance (enzyme, antibodies, antigens, DNA fragments, tissues, bacteria), which serves as a receptor. The receptor responds to the presence of the determined component and takes part in generating a signal, functionally dependent on the concentration of this component. The transducer sends this signal to a measuring device [1]. In electroanalysis, the transducer is either a bulk electrode or an electrode covered with specific molecules or particles, nanoparticles in particular (modified electrode). The substance specially localized on the electrode surface (modifier) can act both as a transducer and as a receptor. Hence, there is some ambiguity in terminology: the same system can be defined as a modified electrode, a transducer or a sensor, depending on the circumstances. Further, we will not retreat from traditional terminology and will use all mentioned terms. However, we will prefer using the term “sensor” as a tool where all the components required for receiving a signal, are localized on the electrode surface.

The combined efforts and achievements of screen-printed and nanotechnologies; organic, polymer, and analytical chemistry; and electrochemistry and biochemistry

https://doi.org/10.1515/9783110542011-006

have resulted in a new generation of sensors. In recent years, the number of publications in this area has sky rocketed, as numerous reviews prove it [2–18]. The emergence and application of nanomaterials as integral part of sensors have had a visible impact on research.

Nanoparticles can be used as transducers, catalytic agents, adsorbents, transporters, and labels, for example, in immunoassay. It is not always easy to differentiate the impact of nanoparticles themselves by the mechanism of their functioning in sensors. However, in all cases, the properties of nanoparticles themselves and size effects are essential, which is manifested in the increased electrochemical activity in comparison with the corresponding bulk material [19–22]. This has led to the fact that the transition from macro- to nanoscale architectures significantly improves sensor characteristics [18, 24, 25].

Size of nanoparticles and surface excess free energy change the thermodynamics and kinetics of the oxidation of nanoparticles and processes occurring on their surface. It is reflected in voltammogram shapes. Therefore, herein after we will focus on voltammogram shapes when considering electrochemistry of nanoparticles themselves and electrochemical reactions taking place on their surface.

Chemical and biological sensors are discussed in [26], where nanoparticles and multisignal biosensors based on logically processed biochemical signals [26] are used as transducers, catalysts, or labels. The findings of the studies showed that the application of nanoscale materials in sensors is feasible and beneficial.

## 6.2 Properties of nanoparticles

Nanoparticles are known to have unique physical [27, 28], optical [29–32], catalytic [33–35], magnetic [32, 36], and sensory [23] properties that are different from the properties of their bulk analogues. At the same time, nanoparticles are characterized by quite a strong dependence of their properties on a degree of dispersion, or the so-called "size effect". For example, the constant lattice of gold nanoparticles decreases by 2–4 % in comparison with the bulk phase of the metal [37, 38]. During the transition from the bulk phase to the gold nanoparticles sized 2.5 nm, the melting temperature lowers from 1336 to 930 K [32]. The wavelength of maximum absorption in the optical spectra of gold sols with bigger particle size shifts to longer wavelengths [39]. One of the reasons for the specific behavior of nanoparticles is surface excess energy that is caused by uncompensated bonds between surface and subsurface atoms, whose proportion increases significantly with smaller particle size [32]. The other reason is quantum effects, clearly demonstrated in optics. In addition, with smaller particle size the degree of defectiveness of the crystal lattice grows [37]; therefore, there are more active reaction centers on the surface, which leads to better

adsorption properties and increased chemical activity of nanoscale structures. Size effect is observed in the electrochemistry of nanoparticles as well [40–42].

The special properties of nanoparticles offer good perspectives for creating new efficient catalysts, sensor systems, and medical drugs exhibiting high biological activity and targeted delivery. When developing new functional materials based on nanostructures, the results of experimental studies of size effects and development of these theoretical concepts, allowing us to predict the properties of newly created materials, become of great importance. Understanding thermodynamics and kinetics of electrochemical processes of nanoparticles themselves and the processes occurring on their surface can lead to selecting better conditions for more efficient and stable performance of electrochemical sensors.

## 6.3 Theoretical and experimental approaches to nanoscale material study

Despite the explosion of publications describing the use of nanoparticles in electroanalysis, theoretical and experimental investigations of the laws regulating electrochemical behavior of metal nanoparticles immobilized on the macroelectrode surface, the research is still at the initial stage [22, 43–54]. It is worth mentioning the results of microscopic and electrochemical studies of electrooxidation of silver [22, 50], gold [20, 55, 56], bismuth [21], and palladium [57] nanoparticles of different sizes immobilized on the surface of indifferent macroelectrodes. Experimental data indicate that metal particles demonstrate more intensive electrochemical activity if their size reduces, which results in the shift of the metal oxidation potential to the cathodic direction, as compared with the similar processes of bulk metal (Tab. 6.1).

There are few approaches to explaining the size effect observed in the electrochemistry of nanoparticles. Compton et al. [42, 46] proposed a mathematical model for describing electrooxidation of metal nanoparticles from the surface of the indifferent electrode. In this model, the electrochemical behavior of the nanoparticles localized on the macroelectrode surface is attributed to the transition from semi-infinite diffusion to/from the planar electrode to the radial diffusion to/from the nanoparticle. By theory, in the case of a reversible electrochemical system, there are two options: (1) when there are very few nanoparticles on the electrode surface (diffusion zones do not overlap), the peak electrooxidation potential of the particles shifts to the negative potential area with decreasing particle radius; (2) when there are larger quantities of nanoparticles on the surface (diffusion zones overlap, and the conditions for planar diffusion are satisfied), the electrooxidation potential shifts to positive values with growing metal quantity; thus, it does not depend on the particle size. Energy aspects are disregarded.

**Tab. 6.1:** The size effect of metal particles on the peak oxidation potential ($E_m$)

| Metal/ Substrate | Radius of nanoparticles, nm | $E_m$, V | Background | Reference |
|---|---|---|---|---|
| Au/ TFCCE | 10 | 0.936 | 0.1 M HCl | [20] |
| | 150 | 1.086 | | |
| | 1000 | 1.088 | | |
| Ag/ TFCCE | 35 | 0.469 | 0.1 M $KNO_3$ | [22] |
| | 270 | 0.498 | | |
| | 1000 | 0.563 | | |
| Bi/TFCCE | 53 | 0.062 | 0.1 M $HNO_3$ | [21] |
| | 150 | 0.117 | | |
| | 1000 | 0.211 | | |
| Au/ITO | 3 | 0.693 | 0.1 M $HClO_4$ + 0.01 M KBr | [55] |
| | 19 | 0.788 | | |
| | 24 | 0.851 | | |
| | 29 | 0.881 | | |
| | 116 | 0.882 | | |
| Ag/ITO | 6 | 0.275 | 0.1 M $H_2SO_4$ | [50] |
| | 8.4 | 0.291 | | |
| | 10.3 | 0.318 | | |
| | 13.3 | 0.340 | | |
| | 14 | 0.354 | | |
| | 19 | 0.371 | | |
| | 22.8 | 0.382 | | |
| Pd/GCE | 98 ± 38 (bulk) | 0.700 | 0.1M $HClO_4$ + 0.01M NaCl | [57] |
| | 3.2 ± 0.9 | 0.570 | | |
| | 1.5 ± 0.3 | 0.467 | | |
| | 1.0 ± 0.3 | 0.343 | | |

TFCCE thick film carbon containing electrode
ITO indium tin oxide
GCE glassy carbon electrode

In the irreversible electrochemical system (the second case), the electrooxidation potential of metal nanoparticles is affected by their quantity on the electrode surface and shifts to negative potentials with decreasing particle size. To validate the model, the authors investigated electrochemical dissolution of silver nanoparticles of different sizes from the surface of pyrolytic graphite electrode, by using potentiodynamic voltammetry. By interpreting the data obtained, they concluded that the peak potential of silver nanoparticles oxidation increases if the number of silver nanoparticles on the electrode surface grows and the potential rate changes. The size of the particles does not affect the potential peak. However, the authors did not consider nanoparticle aggregation that is occurred when nanoparticle concentration on the surface increases and the consequent change in the distribution of particles by size, which can be proved or disproved by microscopic studies. The comparison of the experimental data with the calculated results, applying the proposed mathematical model, showed

only qualitative similarity in the direction of shifts in the electrooxidation potential when the quantity of particles grows on the electrode. Moreover, numerical values vary greatly. It follows thence that geometric factors (the shape and size of diffusion zones) are not the only ones affecting electrochemical properties of nanoparticles. Compton's theory has been further developed in the use of the Plieth equations (see below) and the introduction of relevant amendments, which take into account the effect of surface energy of nanoparticles on the formal potential of nanoparticles oxidation [58].

The other two theoretical approaches are similar, as they introduce thermodynamic considerations when looking at electrochemical processes with nanoparticles. This allows us to take into account energy differences between ensembles with micro- and macroparticles. Thus, Ivanova and Zamborini [50, 51] explain that electrochemical activity of silver and gold nanoparticles increases with smaller size due to lower value of the standard redox potential of $M^{n+}/M$ system. According to theoretical views developed by Plieth [43, 44], the standard redox potential of metals in their nanostate shifts to the negative potential area as compared with the standard potential of bulk metal by a quantity determined by the ratio:

$$E_p^0 = E_{\text{bulk}}^0 - \frac{2\gamma V_{\text{m}}}{zFr},$$

where $E_p^0$ and $E_{bulk}^0$ are standard redox potentials of metals in their nano and bulk states, $y$ is the surface tension, $V_m$ is the molar volume, $z$ is the number of electrodes, participating in the electrode process, $F$ is Faraday's constant (96485 C/mole), and $r$ is the radius of metal nanoparticles.

On the basis of theoretical arguments put forward by Plieth, Tang et al. [52, 59] plotted the diagrams showing how the oxidation potential of the platinum nanoparticles depends on the particle radius. They also show the $E$–pH dependence for platinum particles of different sizes. In addition, it was shown that a smaller size of nanoparticles, along with the shift of the electrooxidation potential to the cathode region, causes some changes in the electrochemical process. Thus, as the graph shows, platinum nanoparticles with a diameter less than 4 nm, transfer into the solution and form $Pt^{2+}$ ions, whereas larger particles are oxidized to PtO. The correctness of the calculated data is confirmed by a good match with the experimental values. The experimentally observed electrochemical Ostwald ripening, when larger nanoparticles grow as smaller particles dissolve [60], is also explained by a decrease in the value of the standard redox potential of nanoparticles with a decrease in their radius, as Plieth predicted.

Henglein [61, 62] also predicted a negative shift of the oxidation potential with smaller metal particle size. His conclusion was based on the calculations of a standard redox potential of metal clusters, using the value of the enthalpy of sublimation. He found that with a decrease in the number of atoms in $Ag_n$ particle, the standard redox potential of silver shift to the cathode region from +0.799 $V$ ($n = \infty$) to –1.0 $V$ ($n = 3$) (the potentials are given relative to the SHE). To confirm the conclusion, it was

experimentally proven that metal clusters are able to reduce many organic molecules [62].

Some studies report the dual behavior of nanoparticles – shifts of electrooxidation potentials both to positive [54, 63–66] and negative values as compared with the equilibrium potential for $Me^{n+}/Me^0$ system or the electrooxidation potential for bulk metals. This phenomenon is explained using the third approach.

In our opinion, the third and the most general approach to describing these regularities is presented in [67] understanding of the three energy states of substances, metals in particular. This approach is illustrated as follows [67]:

| $M_I$ | $M_{II}$ | $M_{III}$ |
|---|---|---|
| $\Delta G^o < 0$ | $\Delta G^o \approx 0$ | $\Delta G^o > 0$ |

The left part describes the electrode processes involving ad-atoms (under potential deposition, UPD), while the right part describes the electrode processes involving nanoparticles [19]. In our point of view, the dual behavior of nanoparticles is explained as follows: the shift of the potential of nanoparticles electrooxidation to the negative area occurs when the substrate is inert to nanoparticles and the properties of nanoparticles themselves are displayed. The potential shifts to the positive area when metal nanoparticles interact with the substrate; this phenomenon is similar to UPD.

Brainina et al. [19] proposed a mathematical model that takes into account the processes represented by the above diagram. It describes electrooxidation processes of metal nanoparticles localized on the macroscale electrode surface. The term $(\Delta G^o/RT)$ is added in the kinetic equation of the voltammogram for metal nanoparticles electrooxidation. This enables to consider energy differences between metal nanoscale particles and a metal in its bulk state, because, as shown in [19], there is a certain correlation between the change in the free surface energy ($\Delta G°$) and the radius of the particle, which has a form of hyperbola. The position of the voltammograms of nanoparticle oxidation on the potential axis and their shape (the presence of one or two peaks), current distribution, and the difference of the current peak potentials are determined by the free surface energy and, hence, the particle radius and metal properties.

In a series of papers, a set of voltammograms, showing electrooxidation of gold [20], bismuth [21], and silver [22] nanoparticles of different sizes, was plotted experimentally and theoretically (based on the proposed mathematical model). Electrooxidation occurred on the surface of the thick-film carbon-containing electrode (TCE). It is argued that the transition from macroscale to nanoscale metallic structures affects the potential of the current oxidation peak: it shifts to the cathodic region, which indicates that electrochemical activity of nanoparticles increases as compared with bulk metal. For example, the electrooxidation potentials for gold nanoparticles with a radius of 10 and 150 nm, localized on the TCE, with 0.1 M HCl background, are lower than the oxidation potential for bulk gold (1.188 V relative to SCE) by 252 and 101 mV, respectively. The proposed theory suggests that the presence of two peaks of

electrooxidation of gold particle mixture whose radii vary considerably, on the same voltammogram can be attributed to substantial difference between the energy characteristics ($\Delta G°$) of gold particles with varying sizes. A close match between the calculated and experimental curves confirmed the relevance of the mathematical model and correctness of the calculations.

An important result of mathematical modeling of metal nanoparticle electrooxidation is an opportunity to identify the interrelationship between three factors: nanosized effects, energy effects, and the shape of experimental voltammograms for metal nanoparticles electrooxidation.

The energy state of nanoparticles, defined by their size and the Gibbs free energy $\Delta G°$, has an impact not only on the kinetics and thermodynamics of the nanoparticles themselves electrooxidation, but also on the processes occurring on the nanoparticles surface [20, 68]. Brainina et al. [69] proposed a physical-mathematical model describing electrochemical reactions of the dissolved substance, diffusing to the nanoparticle surface. These processes, along with the stage of the electron transfer, take into account possible chemical, in particular catalytic reactions, passivation of the electrode surface by the products of electrode reactions and nanoeffect manifestation. The thermodynamic approach to describing processes on nanoparticles enables to predict the shape and features of the experimental voltammograms; to obtain information about the energy properties of nanoparticles; and to identify the mechanism of the electrode process. The validity of the theoretical findings of the proposed method is confirmed by a good agreement between the calculated and experimental results concerning the electrooxidation of ascorbic acid on gold nanoparticles [68, 69].

Size effects were also observed during the oxidation of ascorbic acid on the electrodes modified with gold nanoparticles of varying sizes [70, 71]. These effects led to the shift of the voltammograms in the cathodic direction with decreasing size of nanoparticles, immobilized on the electrode.

Therefore, electrochemical methods can serve as a source of valuable information for analyzing thermodynamic and energy properties of nanomaterials, as well as for the kinetics of redox reactions of these nanoparticles, and other processes with nanoparticles involvement. On the other hand, these approaches and available data are extremely useful for predicting catalytic and sensory properties of nanoscale materials.

## 6.4 Macro- to micro- and to nanoscale transition

In electrochemical sensor systems, a signal-generating reaction undergoes at the electrode/solution boundary. In this regard, the intensity of the electrochemical response to the change of the analyte concentration is strongly dependent on the surface properties of the electrode (sensor). Therefore, the targeted modification of the structural

and material architecture of the electrode surface allows us to control selectivity and sensitivity of the sensor. Currently, the main approach to improving analytical and metrological properties of electrochemical sensors is the transition from macro- to micro- and to nanoscaled structures of the electrode surface. Developing nanomaterial-based sensors is a rapidly growing field in modern electroanalysis, which is indicated by a continuous increase in the number of publications. Of particular interest is the literature that focuses on comparative studies of sensory properties of metal macro-, micro-, and nanoscaled structures. Some examples illustrating how sensory properties are affected by a dispersed condition of the electrode surface are presented in Tab. 6.2.

**Tab. 6.2:** Examples of dependence of analytical properties of electrochemical sensors on particle size of metal modificator

| Modifier / Substrate | Particle size, nm | Analyte | LOD, µg/L (M) | *b* | Detection | Reference |
|---|---|---|---|---|---|---|
| Au/TFCCE | 50 | Cr(VI) | 5 | – | SWV | [72] |
| | bulk | | 250 | – | | |
| Bi/GCE | 270 | Pb(II) | 18 | 0.074 µC × L/µg | ASV | [73] |
| | | Cd(II) | 11 | 0.029 | | |
| | | Cr(VI) | 0.00012 | 270 | AdCSV | |
| | Bi-film | Pb(II) | 29 | 0.015 | ASV | |
| | | Cd(II) | 25 | 0.01134 | AdCSV | |
| | | Cr(VI) | 0.0374 | | | |
| Bi/TFCCE | 45.5 | Zn(II) | 0.60 | 6.14 µA × L/µg | ASV | [74] |
| | | Cd(II) | 0.09 | 21.07 | | |
| | | Pb(II) | 0.17 | 13.43 | | |
| | 90.2 | Zn(II) | 0.96 | 4.81 | | |
| | | Cd(II) | 0.21 | 15.44 | | |
| | | Pb(II) | 0.32 | 9.92 | | |
| | 282.1 | Zn(II) | 1.38 | 4.23 | | |
| | | Cd(II) | 0.48 | 11.67 | | |
| | | Pb(II) | 0.51 | 7.43 | | |
| | Bi-film | Zn(II) | 4.20 | 0.53 | | |
| | | Cd(II) | 2.54 | 3.28 | | |
| | | Pb(II) | 1.97 | 5.69 | | |
| Bi/TFCCE | 120 | Ni(II) | $7.76 \times 10^{-9}$ (M) | 6.36 µA/nM | AdCSV | [75] |
| | 380 | | $3.22 \times 10^{-9}$ (M) | 43.51 | | |
| | Bi-film (16 µm) | | $3.91 \times 10^{-9}$ (M) | 120.06 | | |
| Au/TFCCE | 26 | As(III | 0.05 | 11.03 µA × L/µg | ASV | [76] |
| | | Cu(II)) | 0.05 | 9.10 | | |
| | 122 | As(III) | 0.12 | 4.11 | | |
| | | Cu(II) | 0.12 | 4.44 | | |

**Tab. 6.2:** (continued)

| Modifier / Substrate | Particle size, nm | Analyte | LOD, µg/L (M) | *b* | Detection | Reference |
|---|---|---|---|---|---|---|
| Au/conductive substrate | 30<br>bulk | As(III) | 0.005<br>0.75 | 65.57 µA × L/µg<br>5.51 | ASV | [77] |
| Au/conductive substrate | 30<br>bulk | $I^-$ | $0.3 \times 10^{-6}$ (M)<br>$4 \times 10^{-6}$ (M) | –<br>– | CV | [78] |
| Ni/BDD | 5–690<br><br>Ni foil | Ethanol, glycerol | $1.7 \times 10^{-3}$ (M)<br>$1.03 \times 10^{-5}$<br>$6.2 \times 10^{-3}$ (M)<br>$2.2 \times 10^{-5}$ | 0.31 µA/M<br>35<br>2.42<br>279 | CV | [79] |
| Au/MPTS | 2.6<br>60 | DOPAC | $2 \times 10^{-7}$ (M)<br>$5 \times 10^{-7}$(M) | 0.020 nA/nM<br>0.1239 nA/nM | Amperometry | [82] |

| | | | |
|---|---|---|---|
| LOD | limit of detection | CV | cyclic voltammetry |
| *b* | sensitivity | BDD | boron doped diamond |
| SWV | square wave voltammetry | MPTS | (3-mercaptopropyl)trimethoxysilane |
| ASV | anodic stripping voltammetry | DOPAC | 3,4-dihydroxyphenylacetic acid |
| AdCSV | adsorptive cathodic stripping voltammetry | Other symbols: as given in Tab. 6.1 | |

As the result of complex microscopic and electrochemical studies, the relationship between the morphology of the solid electrode surface and an electrochemical response was established [23, 72–76, 80–85]. In most studies, a decreasing particle size results in higher sensitivity and selectivity of determination, an increase in the signal/noise ratio, a lower detection limit for the analyte, and shorter analytical time. The examples are the sensors, with gold [72, 76–78, 80, 82–84] or bismuth [73, 74, 81] nanoparticles as transducers. Malakhova et al. [81] obtained clear and well-separated anodic peaks for zinc, lead, and cadmium on the electrode modified with small (<100 nm) and rarely distributed bismuth particles, whereas on the electrodes modified with bismuth particles of larger size (20 and 2 µm), analytical signals either were not recorded or had a distorted wave form. Moreover, the oxidation of the detected metals on the electrodes of the first type occurred much earlier than on the electrodes with larger particles. Their anodic peaks were narrower, which resulted in improved signal resolution. Similar patterns for bismuth electrodes were obtained for stripping voltammetric determination of zinc, lead, and cadmium [73, 74]. Thus, the sensitivity of detecting cadmium on the TCE, modified with bismuth nanoparticles (45.5 nm), is seven times higher, while the detection limit is 28 times lower, compared with the same parameters on the bismuth film that can be considered as macroelectrode [74]. Analytical signals for arsenic (III) and copper (II) increase three and two times, respectively, while the size of the gold particles, located on the TCE surface, reduces from 300 to 26 nm [76].

An increase in the analytical signal of mercury (II) by 40 % when the size of gold nanoparticles decrease from 71 to 36 nm and threefold decrease of the signal when number of nanoparticles on the electrode surface [83] and their size decrease from 1000 to 100 nm [23] are observed.

The described effects are caused by the change in the surface structure during the transition from metal macro- to micro- and to nanostate on the electrode. When the particle size decreases, the relative proportion of atoms that are located on the surface, including vertices, edges, and faces, and that have a high coordination ability toward reactive substances, increases significantly [32, 35]. As a result, the area of energy-rich and electrochemically active surface expands, which leads to a better analytical performance of the electrode. For example, it was found [86] that the active surface area of the gold electrode with nano-dendritic structure is 33 times more than the surface area of the flat macroelectrode. At the same time, the signal for arsenic (III) is 40 times stronger on the nanostructured electrode. In biosensors, during the transition from macroscaled electrodes to the electrodes with nanostructured surface, a bigger area of the active surface contributes to a higher surface density of enzymes and biomolecules, and, consequently, to sensor sensitivity [87].

A manifestation of the size effect in the sensory properties of electrodes has also been associated with varying adsorption and electrochemical and electrocatalytic activity of nanostructures and their bulk analogues. Nanoparticles are characterized by a high degree of defectiveness of a crystal lattice. A large and growing with smaller particle size proportion of the surface is taken by “vertex and edge” structural elements. Adsorption properties of defects in this nanostructured surface differ from adsorption properties of the flat surface of macroelectrodes. The faces that are absent in macrocrystals can break the surface of nanoparticles. As a result, reactions that are almost impossible to occur on the macrocrystal surface can undergo on the electrodes modified with nanoparticles. In addition, the mechanism and kinetics of electrode processes are likely to change [42]. The difference in adsorption and electrocatalytic properties of nano- and microcrystals is explained by the change in the electronic state of the atom in the crystal with size [88].

Many authors study an increasing maximum current of the analyte electrochemical reaction on a nanostructured surface and the shift of its potential in the cathode region as a catalytic process. However, some recent studies have suggested that these features of the electrode process on the nanostructures are due to a bigger active surface area and increasing free energy as compared with bulk electrodes [68, 69].

The electrocatalytic activity of the electrodes modified with nanoparticles increases with decreasing particle size, whereas the size effect of the adsorption properties of nanostructured electrodes can be both positive and negative. On the one hand, the unique architecture of nanoparticles ensures the presence of many active centers on the surface, with high free energy, and, consequently, with high adsorption capacity and activity. On the other hand, the unique structure and a small size of nanoparticles may result in steric hindrances in the adsorption of large analyte

molecules and those molecules that are easily adsorbed on the polycrystalline electrode surface.

Thus, discussing electroanalytical detection of Cr(VI) traces with the use of adsorptive stripping voltammetry, Saturno et al. [73] reported that on the electrodes modified with micro- and nanoparticles of bismuth (average size is 270 nm), the signal for Cr(VI) is 50 times stronger than on the bismuth film electrode. However, in [75] where Ni(II) is detected by using adsorptive cathodic stripping voltammetry on the TFCCE, modified with particles of bismuth of different dispersions, a decrease in sensitivity is observed with decreasing particle size of the modifier. The authors attribute the reverse pattern for nickel to the fact that the distance between active centers in a large molecule of Ni–dimethylglyoxime compound exceeds the size of small Bi nanoparticles. As a result, steric hindrances preventing the adsorption of Ni compound on small Bi nanoparticles occur. Ni compound easily adsorbs on the surface of large Bi particles.

A similar effect was observed [89] in the study of electrochemical behavior of methylviologen on silver electrodes with different surface morphologies. Distinct signals for methylviologen were obtained on a silver polycrystalline electrode with a granular surface. The signal for methylviologen was not observed on the electrode modified with silver nanoparticles (<100 nm).

The negative size effect on the adsorption properties of nanostructured electrodes was also described in the study of UPD on the electrodes modified with a range of particle of different dimensions. Ad-atoms of thallium were formed on a gold polycrystalline electrode and electrodes modified with a relatively large gold nanoparticles (30–60 nm), whereas thallium did not adsorb on small gold nanoparticles (10 nm) [90]. Similar results were obtained when studying deposition of thallium [91], lead, and cadmium [92] on silver nanoparticle-modified electrodes. The authors suggest that one of the possible reasons for the established patters can be the absence of platforms with the faces ensuring the adsorption of the deposited metal atoms on the nanoscale electrode surface.

The quantity of nanoparticles localized on the electrode surface can influence on the characteristics of the analysis based on concentrating of the analyte in the form of slightly soluble compounds with the electrode material. Sudakova et al. [93] observed that $Bi_2S_3$ reduction current increased when the quantity of bismuth nanoparticles localized on the screen-printed carbon electrode grew from 0.028 to 0.7–1.4 μg. With a further increase to 2.8 μg, the analytical signal for sulfide ions weakened. The total mass of Bi particles, equal to 1.4 μg was taken as optimal, which corresponds to the formation of agglomerates of Bi nanoparticles with an average size of about 180 nm.

Electrochemical determination of most organic and biological compounds is linked to their catalytic redox transformation. Nanoscale materials, exhibiting high catalytic activity, contribute to a stronger recorded signal [88, 94]. Along with a high catalytic effect, a more stable response of the nanoscale electrodes to the concentration of the determined analyte is observed [95]. The catalytic activity of the particles correlates with their size: as a rule, the smaller the particle size, the more pronounced catalytic

effect [34, 82, 88]. For example, Li et al. [34] observed a decrease in the overvoltage of the reaction of oxygen electroreduction and an increase in its current with gold nanoparticle size reducing from 24 to 14 nm, while gold particles were immobilized on the surface of the platinum electrode. The impact of the crystallographic planes and shapes of nanoparticles on their electrocatalytic properties was also shown.

Kalimuthhu and John [82] argue that an increase in catalytic effect with decreasing size of gold particles is observed in the study of the electrocatalytic oxidation of ascorbic, uric, and 3,4-dihydroxyphenylacetic acids on electrodes modified with gold nanoparticles of varying sizes. An increase in the current peaks of the analyte oxidation and their shift to the potential cathodic is observed with decreasing size of gold particles. Thus, the oxidation potential of ascorbic acid at the transition from bulk gold electrode to the electrodes modified with gold nanoparticles with a size of 60, 40, 20, and 2.6 nm changes in the following sequence: 0.48, 0.44, 0.42, 0.38, and 0.35 V. The detection limit for 3,4-dihydroxyphenylacetic acid on the electrode modified by gold nanoparticles with a size of 2.6 nm is 200 nM, while on the electrode with gold particles sized 60 nm, the detection limit equals 500 nM. In addition, it is possible to obtain separate peaks for ascorbic and uric acids (the difference between the peak oxidation potentials is 180 mV) on the electrodes modified with gold nanostructures, which allows for their simultaneous determination in blood and urine. Moreover, only one broad peak was observed on the bulk gold electrode.

A different pattern, in which the analyte (dopamine) signal does not depend on the size and quantity of particles on the surface of the gold microelectrode, is observed in [96]. In this case, on gold nanoparticles, the peak current of dopamine oxidation shifts by 50 mV to the anodic region, and its magnitude is smaller than on the bulk gold electrode. The authors argue that this is due to the inhibitory effect of 3-aminopropyltriethoxysilane used as a linker for covalent/binding of gold nanoparticles to the electrode surface.

Composite materials with high catalytic activity hold promise to be used as electrocatalysts [88, 97, 98]. For example, the use of binary Ni–Co nanoparticles as a catalyst for direct uric acid determination enables to increase detection selectivity and sensitivity compared with individual metals [98]. The incorporation of cobalt atoms into the crystal lattice of nickel hydroxide significantly increases the number of structural defects and catalytically active centers. In addition, cobalt atoms hinder the adsorption of intermediates and reaction products on the nanocrystal surface, which facilitates electrode regeneration.

In some approximation, the combination of nanoparticles on the electrode surface can be regarded as an ensemble of nanoelectrodes that provide radial diffusion of the analyte [99–101]. In case of a planar microelectrode, the transition from semi-infinite diffusion of the analyte to the surface to radial diffusion leads to a more effective delivery of the substance to the electrode surface, a stronger signal and the increasing of signal/noise ratio. The presence of the nanoparticle excess free energy alters the kinetics of the electrode process, which is accompanied by a lower detection limit

and a broader range of determined concentrations. Table 6.2 shows that the use of nanomaterial modified electrodes in the electroanalysis enables to reduce the detection limit by one to two orders of magnitude. By accelerating the mass transfer of the analyte to a nanostructured electrode surface, the concentration time, required for obtaining a signal by stripping voltammetry, significantly reduces.

It should be noted that in some cases the use of nanomaterial-based sensors allows us not to carry out additional preparation and regeneration of the electrode surface [23, 80, 102]. As a result, detection with the use of nanostructured electrodes is simplified, and the analysis time is reduced compared with macroelectrodes.

## 6.5 Nanostructures in chemical monitoring

In the last decade, nanostructured electrodes have been successfully applied in the analytical chemistry. An array of nanomaterials – nanotubes, graphene, and metal nanoparticles – is used to modify electrodes. Metal nanoparticles can be obtained by physical methods [103], chemical synthesis [55, 104], in particular, using extracts of plants as a source of a reducing agent (green synthesis) [105, 106], and by electrochemical deposition [83, 51]. In the first two cases, nanoparticles are usually applied to the electrode surface by drop casting. With electrochemical deposition, nanoparticles are formed directly on the electrode surface.

Nanoparticles obtained by "green synthesis" exhibit excellent stability, greater biocompatibility, and lower toxicity compared with nanoparticles synthesized by using well-known physical and chemical methods. All this enables to use nanoparticles, synthesized in that way, for medical research [107].

The main areas of nanostructures usage as sensor components are:

- transducers in sensors for chemical and biochemical analysis and oxidative/antioxidant activity monitoring;
- markers and signal-generating elements for immunoassay;
- transporters in magnetic separation and in concentrating;
- catalysts in biomimetic sensors.

Various aspects of the use of nanomaterials in electroanalysis are reviewed in [13, 16, 87, 108, 109].

### 6.5.1 Nanomaterials as transducers and catalysts in electrochemical sensors

Sensory properties are determined by the nature and morphology of the electrode/solution boundary. In this regard, the use of nanoparticles as transducers becomes a fundamental issue. Some examples of using nanomaterials as transducers in the electrochemical sensors are given in Tab. 6.3.

**Tab. 6.3:** Examples of nanomaterial application as transducers and catalysts in electrochemical sensors

| Nanoparticles (size, nm) | Substrate | Method of immobilization | Analyte | Detection | Linear range (LOD), M | Sample | Reference |
|---|---|---|---|---|---|---|---|
| Au (23–49) | GCE | *In situ* (electrochemical deposition from solution) | Hg(II) | SW–ASV | $0.6 \times 10^{-9}$–$0.4 \times 10^{-6}$ ($0.4 \times 10^{-9}$) | Background solution | [83] |
| Au (13–15) | GCE/PEDOT | *Ex situ* (drop-dry) | Hg(II) | DP–ASV | $2.5 \times 10^{-9}$–$50 \times 10^{-9}$ ($0.4 \times 10^{-9}$) | Background solution | [102] |
| Au | GCE | *In situ* (electrochemical deposition from solution) | Hg(II) | ASV | ($0.5 \times 10^{-9}$) | Drinking water, plant, and pharmaceutical samples | [135] |
| Au (12) | CPE | *Ex situ* (inclusion into the paste volume with) dithiodianiline) | Fe(II) | DP–ASV | $0.1 \times 10^{-9}$–$0.1 \times 10^{-6}$ ($0.05 \times 10^{-9}$) | Lentil, wheat seed, and barley seed | [136] |
| Au (4.75–5.65) | CPE | *Ex situ* (inclusion into the paste volume together with PYTT) | Cu(II) | Potentiometry | $4 \times 10^{-9}$–$7 \times 10^{-2}$ ($1 \times 10^{-9}$) | Tap, mineral, and lake water | [115] |
| Au | CPE | *Ex situ* (inclusion into the paste volume together with MSA) | Al(III)<br>Cu(II) | Potentiometry | $4.5 \times 10^{-7}$–$1.6 \times 10^{-3}$ ($1.6 \times 10^{-7}$)<br>$4.3 \times 10^{-7}$–$1 \times 10^{-7}$ ($4 \times 10^{-7}$) | Water samples | [137] |
| Au (30) | Conductive substrate | *Ex situ* (electroless plating procedure) | As(III) | ASV | $2.6 \times 10^{-9}$–$80 \times 10^{-9}$ ($0.07 \times 10^{-9}$) | Sea water | [77] |
| Au (20–80) | GCE/poly (taurine) | *In situ* (electrochemical deposition) | As(III) | DPV | $6 \times 10^{-6}$–$28 \times 10^{-6}$ ($0.5 \times 10^{-6}$) | Tap, spring, river water | [138] |
| Au (20–30) | ITO | *In situ* (electrochemical deposition) | Cr(VI) | Amperometry | $0.5 \times 10^{-6}$–$50 \times 10^{-6}$ ($0.1 \times 10^{-6}$) | Tap, sea, river water | [139] |
| Au (30) | Conductive substrate | *Ex situ* (electroless plating) | $I^-$ | CV | $20 \times 10^{-6}$–$200 \times 10^{-6}$ ($0.3 \times 10^{-6}$) | Pharmaceutical samples, table salt | [78] |

**Tab. 6.3:** (continued)

| Nanoparticles (size, nm) | Substrate | Method of immobilization | Analyte | Detection | Linear range (LOD), M | Sample | Reference |
|---|---|---|---|---|---|---|---|
| Au (54.9) | GCE/PEDOT | *In situ* (electrochemical deposition) | NaClO | Amperometry | $1 \times 10^{-6}$–$9.32 \times 10^{-4}$ ($1 \times 10^{-6}$) | Background solution | [140] |
| Au | CPE | *In situ* (electrochemical deposition) | Morphine | DPV | $4 \times 10^{-7}$–$2 \times 10^{-4}$ ($4.2 \times 10^{-9}$) | Pharmaceutical samples, urine | [113] |
| Au | CPE | *In situ* (electrochemical deposition) | Paracetamol | DPV | $5.0 \times 10^{-8}$–$2.7 \times 10^{-4}$ ($1.46 \times 10^{-8}$) | Pharmaceutical samples, urine | [110] |
| Au | GCPE/cation exchanger resin Dowex50wx2 | *Ex situ* (inclusion into the paste volume) | Acetaminophen Tramadol | AdSSVW | $3.34 \times 10^{-8}$–$4.22 \times 10^{-5}$ ($4.7 \times 10^{-9}$) ($1.12 \times 10^{-8}$) | Pharmaceutical samples, blood serum, urine | [112] |
| Au | CPE | *Ex situ* (inclusion into the paste volume) | Acetazolamide | DPV | $0.01 \times 10^{-6}$–$80 \times 10^{-6}$ ($7.1 \times 10^{-9}$) | Blood serum, urine | [141] |
| Au (28) | GCE/L-cysteine | *Ex situ* (adsorption from sol) | Serotonin | SWV | $6 \times 10^{-8}$–$6 \times 10^{-6}$ ($2 \times 10^{-8}$) | Blood serum | [114] |
| Ag (30–50) | GCE/nafion | *In situ* (electrochemical deposition) | Cr(VI) | Amperometry | $40 \times 10^{-9}$–$4.4 \times 10^{-6}$ ($13 \times 10^{-9}$) | Waste water | [118] |
| Ag | GCE | *Ex situ* (drop-dry) | $NO_2^-$ | Amperometry | $1 \times 10^{-5}$–$1 \times 10^{-3}$ ($1.2 \times 10^{-6}$) | Food samples | [116] |
| Ag/ ibuprofen (182) | GCE | *Ex situ* (drop-dry) | Pb(II) | DPAdSV | $0.5 \times 10^{-9}$–$7.25 \times 10^{-6}$ ($0.05 \times 10^{-9}$) | Drinking, tap, river water | [142] |
| Pt(4)/DPAN | Au/4-(2-aminoethyl) benzenamine | *Ex situ* (adsorption from solution) | $NO_2^-$ | Amperometry | $10 \times 10^{-6}$–$1000 \times 10^{-3}$ ($5 \times 10^{-6}$) | Lake water | [117] |
| Au-Pt (120)/organic nanofibers ($d$ = 200, $l$ = 10,000) | GCE | *In situ* (electrochemical deposition)/ *Ex situ* (drop-dry) | Hg(II) | SW–ASV | $0$–$50 \times 10^{-9}$ ($0.04 \times 10^{-9}$) | Tap, river water | [143] |

**Tab. 6.3:** (continued)

| Nanoparticles (size, nm) | Substrate | Method of immobilization | Analyte | Detection | Linear range (LOD), M | Sample | Reference |
|---|---|---|---|---|---|---|---|
| Bi (45.5) | TFCCE | *Ex situ* (drop-dry) | Zn(II)<br>Cd(II)<br>Pb(II) | SW–ASV | $9.2 \times 10^{-9}$<br>($0.8 \times 10^{-9}$)<br>($0.8 \times 10^{-9}$) | Background solution | [74] |
| Bi (304–456) | TFCCE | *Ex situ* (drop-dry) | Ni(II) | AdCSV | $0.85 \times 10^{-8}$–$8.48 \times 10^{-8}$<br>$0.32 \times 10^{-8}$ | Background solution | [75] |
| $KAg_3[Fe(CN)_6]$ (100) | TFCCE | In situ (electrochemical deposition) | Procaine, sulfamerazine | CV | ($8.68 \times 10^{-6}$)<br>($1.0 \times 10^{-5}$) | Background solution | [144] |
| $Fe_4[Fe(CN)_6]_3$ (5–15)/ SWCNT | Pyrolytic graphite electrode | *Ex situ* (chemical deposition)/*ex situ* (drop-dry) | $NO_2^-$ | Amperometry | $0–250 \times 10^{-6}$<br>($6.26 \times 10^{-6}$) | background solution | [145] |
| $Bi_2O_3$ | Chitosan-modified gold electrode | *Ex situ* (drop-dry) | DNA | CV | $1.33 \times 10^{-10}$–$133 \times 10^{-10}$ | Background solution | [146] |
| $Bi_2O_3$ (120–127) | GCE | *Ex situ* (adsorption due to trituration) | Paracetamol | CV | $5 \times 10^{-7}$–$1.5 \times 10^{-3}$<br>($2 \times 10^{-7}$) | Blood serum | [147] |
| α-$Ni(OH)_2$ (20) | FTO | *Ex situ* (drop-dry) | Glucose | Amperometry | $10 \times 10^{-6}$–$750 \times 10^{-6}$<br>($2.5 \times 10^{-6}$) | Background solution | [120] |
| γ-$MnO_2$ (90–120) | SPGE | *Ex situ* (drop-dry) | Diazinon thiocholine | Chronoam-perometry | $5 \times 10^{-7}$–$1 \times 10^{-5}$<br>($0.6 \times 10^{-9}$)<br>($0.6 \times 10^{-7}$) | Background solution | [121] |
| (MnO, $MnO_2$, $Mn_3O_4$) (21–40) | ITO | *In situ* (electrochemical deposition) | $H_2O_2$ | DPV | $0.02 \times 10^{-3}$–$1.26 \times 10^{-3}$<br>($0.02 \times 10^{-3}$) | Lab and real samples | [119] |
| ZnO ($d$ = 100–150, $L$ = 1,000) | Au | *Ex situ* (aqueous chemical growth method onto gold glass substrate ) | Fe(III) | Potentiometry | $1 \times 10^{-5}$–$1 \times 10^{-2}$<br>($5 \times 10^{-6}$) | Background solution | [125] |

**Tab. 6.3:** (continued)

| Nanoparticles (size, nm) | Substrate | Method of immobilization | Analyte | Detection | Linear range (LOD), M | Sample | Reference |
|---|---|---|---|---|---|---|---|
| $TiO_2$ | Poly(vinyl chloride) membrane | *Ex situ* (inclusion into the mixture volume ) | Cr(III) | Potentiometry | $1 \times 10^{-5}$–$1 \times 10^{-1}$ ($8.9 \times 10^{-6}$) | Background solution | [148] |
| $TiO_2$ | CPE | *Ex situ* (inclusion into the paste volume) | Buzepide methiodide | DPV | $5 \times 10^{-8}$–$5 \times 10^{-5}$ ($8.2 \times 10^{-9}$) | Blood serum, urine | [122] |
| HRP/Au (17)/$TiO_2$ | Au | *Ex situ* (adsorption from solution)/ *ex situ* (drop-dry) | $H_2O_2$ | Amperometry | $2.3 \times 10^{-6}$–$2.4 \times 10^{-3}$ ($7 \times 10^{-7}$) | Disinfector samples | [149] |
| $IrO_2$ ($d$ = 100–120, $l$ = 1,000–3,000) | GCE/polycarbonate | *In situ* (electrochemical deposition) | Cr(III)<br>As(III) | DPV | $1 \times 10^{-6}$–$10 \times 10^{-6}$ ($0.2 \times 10^{-6}$)<br>$1 \times 10^{-6}$–$8 \times 10^{-6}$ ($0.1 \times 10^{-6}$) | Background solution | [124] |
| $ZrO_2$ | CPE | *Ex situ* (inclusion into the paste volume) | Methyl parathion | SWV | $20 \times 10^{-9}$–$11.4 \times 10^{-6}$ ($0.8 \times 10^{-9}$) | Tap, river water | [123] |
| $SiO_2$ (190) | TFCCE | *Ex situ* (inclusion into the paste volume) | Pb(II) | SW–ASV | $5 \times 10^{-6}$–$0.14 \times 10^{-3}$ ($0.5 \times 10^{-6}$) | Drinking, river, ground water | [126] |
| $LaFeO_3$ (22) | GCE | *Ex situ* (drop-dry) | Dopamine | Amperometry | $1.5 \times 10^{-7}$–$8.0 \times 10^{-4}$ ($2.22 \times 10^{-6}$) | Pharmaceutical samples | [150] |
| Graphene nanoribbons | TFCCE | *Ex situ* (drop-dry) | Dopamine<br>NADH | DPV | $5 \times 10^{-6}$–$8 \times 10^{-4}$ ($4 \times 10^{-6}$)<br>$2 \times 10^{-3}$–$7.5 \times 10^{-3}$ ($2 \times 10^{-4}$) | Background solution | [151] |
| β-CD-graphene | GCE | *Ex situ* (drop-dry) | Methyl parathion | DPV | $1 \times 10^{-9}$–$1{,}9 \times 10^{-6}$ ($0.2 \times 10^{-9}$) | Sea water | [127] |
| MWCNT ($d$ = 20–30, $l$ = 500–2,000) | GCE/poly(allyl amine hydrochloride) | *Ex situ* (drop-dry) | $SO_3^{2-}$<br>Ascorbic acid | LAV | $5 \times 10^{-6}$–$200 \times 10^{-6}$ ($3.5 \times 10^{-6}$)<br>$5 \times 10^{-6}$–$200 \times 10^{-6}$ ($3 \times 10^{-6}$) | Fruit juice | [152] |

**Tab. 6.3:** (continued)

| Nanoparticles (size, nm) | Substrate | Method of immobilization | Analyte | Detection | Linear range (LOD), M | Sample | Reference |
|---|---|---|---|---|---|---|---|
| Au (20)/MWCNT | Au/ polyaniline | *Ex situ* (adsorption from solution) | $H_2O_2$ | Amperometry | $3 \times 10^{-6}$–$600 \times 10^{-6}$ ($0.3 \times 10^{-6}$) | Milk, urine | [153] |
| Au/thionine/ GO | GCE | *Ex situ* (drop-dry) | Glucose | LCV | $0.2 \times 10^{-6}$–$22 \times 10^{-6}$ ($0.05 \times 10^{-6}$) | Background solution | [131] |
| Polyhydroxyphenol/ Au/ SWCNT ($d$ = 30–60, $l$ = 500–15,000) | GCE | *In situ* (electrochemical deposition)/*ex situ* (drop-dry) | Triazophos | CV | $2 \times 10^{-7}$–$1 \times 10^{-5}$ ($9.3 \times 10^{-8}$) | Vegetables | [154] |
| Pt (2.6)/graphene hybrid nanosheet | GCE | *Ex situ* (drop-dry) | $H_2O_2$ | Amperometry | $1 \times 10^{-6}$–$500 \times 10^{-6}$ ($0.08 \times 10^{-6}$) | Background solution | [155] |
| | | | Trinitrotoluene | ASV | 0.5–40 mg/kg (0.3 mg/kg) | | |
| SWCNT/organicnanofibers/Au–Pt (38) | GCE | *Ex situ* (drop-dry)/ *in situ* (electrochemical deposition) | Guaifenesin | DP–ASV | ($17.5 \times 10^{-9}$) | Blood serum | [156] |
| Pt–Fe(III) (70)/MWCNT ($d$ = 10–15, $l$ = 10,000–50,000) | GCE | *Ex situ* (drop-dry)/ *in situ* (electrochemical deposition) | As(III) | ASV | 0–$300 \times 10^{-9}$ ($10 \times 10^{-9}$) | Background solution | [157] |
| MWCNT ($d$ = 10–30, $l$ = 1,000–2,000)/ Ag (12) | CPE | *Ex situ* (inclusion into the paste volume) | Gabapentin | SWV | $3.1 \times 10^{-9}$–$2.9 \times 10^{-2}$ ($5.6 \times 10^{-10}$) | Blood plasma, Pharmaceutical samples | [158] |
| Pd/C (17–37) | GCE | *Ex situ* (drop-dry) | $N_2H_4$ | CV | ($8.8 \times 10^{-6}$) $5 \times 10^{-6}$–$50 \times 10^{-3}$ | Background solution | [159] |
| Pd (3–4)/ MWCNT | GCE | *Ex situ* (drop-dry) | Glucose | Amperometry | 0–$46 \times 10^{-3}$ ($2.5 \times 10^{-6}$) | Urine | [160] |

**Tab. 6.3:** (continued)

| Nanoparticles (size, nm) | Substrate | Method of immobilization | Analyte | Detection | Linear range (LOD), M | Sample | Reference |
|---|---|---|---|---|---|---|---|
| Pd (20–40)/ SWCNT | PET | *In situ* (electrochemical deposition)/ *ex situ* (adsorption from solution) | Glucose | LAV | 0–5.75 × $10^{-3}$ ($3.4 \times 10^{-6}$) | Background solution | [161] |
| Catalase/ NiO (15–20)/ MWCNT ($d$ = 20–30, $l = \leq$3,000) | GCE | *In situ* (electrochemical deposition)/*ex situ* (drop-dry) | $H_2O_2$ | Impedance | $0.019 \times 10^{-6}$–$0.170 \times 10^{-6}$ ($0.002 \times 10^{-6}$) | Milk | [162] |
| NiO (25)/ MWCNT | CPE | *Ex situ* (inclusion into the paste volume with nafion) | Metformin | Amperometry | $4 \times 10^{-6}$–$63 \times 10^{-6}$ ($0.45 \times 10^{-6}$) | Pharmaceutical samples, blood serum, urine, milk | [163] |
| HRP/$Bi_2O_3$ (50/ MWCNT ($d$ = 10–15, l = 100–10,000) | GCE | *Ex situ* (drop-dry) | $H_2O_2$ | Amperometry | $8.34 \times 10^{-3}$–$28.88 \times 10^{-3}$ | Background solution | [164] |
| $TiO_2$/Graphene | GCE | *Ex situ* (drop-dry) | Paracetamol | DPV | $1 \times 10^{-6}$–$1 \times 10^{-4}$ ($2.7 \times 10^{-7}$) | Pharmaceutical samples | [111] |
| $SnO_2$(4–5)/ Graphene | GCE | *Ex situ* (drop-dry) | Cd(II)<br>Pb(II)<br>Cu(II)<br>Hg(II) | SW–ASV | $0.3 \times 10^{-6}$–$1.2 \times 10^{-6}$<br><br>($1.02 \times 10^{-10}$)<br>($1.84 \times 10^{-10}$)<br>($2.27 \times 10^{-10}$)<br>($2.79 \times 10^{-10}$) | Drinking water | [165] |
| ZnO/MWCNT (50–200) | GCE | *Ex situ* (drop-dry)/ *in situ* (electrochemical deposition) | Glucose | Amperometry | $6.67 \times 10^{-6}$–$1.29 \times 10^{-3}$ $2.22 \times 10^{-6}$) | Background solution | [166] |

**Tab. 6.3:** (continued)

| Nanoparticles (size, nm) | Substrate | Method of immobilization | Analyte | Detection | Linear range (LOD), M | Sample | Reference |
|---|---|---|---|---|---|---|---|
| $SiO_2$/MWCNT ($d$ = 10–40, l = 1,000–25,000) | CPE | *Ex situ* (inclusion into the paste volume) | Cu(II) | Potentiometry | $1 \times 10^{-6}$–$1 \times 10^{-1}$ ($7.9 \times 10^{-7}$) | Tap water | [167] |
| $SiO_2$/MWCNT ($d$ = 10–40, l = 1,000–25,000) | CPE | *Ex situ* (inclusion into the paste volume) | Hg(II) | Potentiometry | $1 \times 10^{-7}$–$1 \times 10^{-2}$ ($1 \times 10^{-7}$) | Waste water | [168] |
| Ag (5–40)–AFS | GCE | Dropcast | $NO_2^-$ | CV | $1 \times 10^{-6}$–$1.6 \times 10^{-2}$ ($7 \times 10^{-8}$) | Spinach | [169] |
| Ag (16)/ S-graphene | GCE | Dropcast | $H_2O_2$ | Amperometry | $1 \times 10^{-4}$–$1.36 \times 10^{-1}$ ($1.4 \times 10^{-7}$) | Milk | [170] |
| $Ni_2O_3$–NiO (100)/ERG | GCE | Electrodeposition | Acetamino-phen | DPV | $4 \times 10^{-8}$–$1 \times 10^{-4}$ ($2 \times 10^{-8}$) | Pharmaceutical samples, urine | [171] |
| Cu@CuO (50) | GCE | Electrodeposition | $H_2O_2$ | DPV | $5 \times 10^{-6}$–$8 \times 10^{-3}$ ($2.3 \times 10^{-7}$) | Tap, lake water | [172] |
| CuO@$Cu_2O$–NWs /PVA | GCE | Dropcast | $H_2O_2$ | Amperometry | $1 \times 10^{-6}$–$3 \times 10^{-3}$, $3 \times 10^{-3}$–$1 \times 10^{-2}$ ($3.5 \times 10^{-7}$ | Background solution | [173] |
| Au (31–52) | CPE | *Ex situ* (inclusion into the paste volume) | Pb(II) Cd(II) Cu(II) | SW–ASV | (50–500 µg/L (9.178 µg/L) 200–700 µg/L 8(6.327 µg/L (85.373 µg/L | Background solution | [105] |
| Au (32.5 ± 0.25) | GCE | Dropcast | Pb(II) | DPV | $5 \times 10^{-9}$–$8 \times 10^{-4}$ ($7 \times 10^{-11}$) | River water | [106] |
| Au (32.06) | CPE | Dropcast | Carbendazim | Amperometry | $5 \times 10^{-8}$–$2.5 \times 10^{-5}$ ($2.9 \times 10^{-9}$) | Soil | [133] |

**Tab. 6.3:** (continued)

| Nanoparticles (size, nm) | Substrate | Method of immobilization | Analyte | Detection | Linear range (LOD), M | Sample | Reference |
|---|---|---|---|---|---|---|---|
| Au (10–30)/GO(2–4) | GCE | Dropcast | Chloramphenicol | Amperometry | $1.5 \times 10^{-6}$–$2.95 \times 10^{-6}$ ($2.5 \times 10^{-7}$) | Pharmaceutical samples (eye drops), milk, powdered milk, honey | [107] |
| Ag–Au (14)/r-GO | GCE | Dropcast | $H_2O_2$ | Amperometry | $1 \times 10^{-4}$–$5 \times 10^{-3}$ ($1 \times 10^{-6}$) | background solution | [134] |

| | | | |
|---|---|---|---|
| *in situ* | formation of a modifying layer during the determined substance precipitation | DNA | deoxyribonucleic acid |
| *ex situ* | preliminary application of the modifier of the electrode surface | FTO | fluorine doped tin oxide |
| SW–ASV | square wave anodic stripping voltammetry | SPGE | screen-printed graphite electrodes |
| DP–ASV | differential pulse anodic stripping voltammograms | HRP | horseradish peroxidase |
| PEDOT | poly(3,4-ethylenedioxythiophene) | NADH | nicotinamide adenine dinucleotide |
| CPE | carbon-paste electrode | MWCNT | multi walled carbon nanotubes |
| PYTT | 5-(pyridin-2-ylmethyleneamino)-1,3,4-thiadiazole-2-thiol | LAV | linear anodic voltammetry |
| MSA | mercaptosuccinic acid | LCV | linear cathodic voltammetry |
| DPV | differential pulse voltammetry | GO | graphene oxide |
| GCPE | glassy carbon paste electrode | PET | polyethylene terephthalate |
| AdSSWV | adsorptive stripping square wave voltammetry | AFS | aminofunctionalized silica |
| DPAdSV | differential pulse anodic stripping voltammetry | ERG | electrochemically reduced grapheme |
| DPAN | 5-[1, 2]dithiolan-3-yl-pentanoic acid [2-(naphthalene-1-ylamino)-ethyl]amide | PVA | poly(vinylalcohol) |
| SWCNT | single walled carbon nanotubes | r-GO | reduced graphene oxide |
| | | The other symbols: as given in Tabs. 6.1 and 6.2 | |

We can observe from Tab. 6.3 that gold nanoparticles have been a subject of considerable interest. This interest can be attributed to the fact that stable gold sols are easily obtained; gold nanoparticles have high electrical conductivity, catalytic activity and chemical stability, and finally, the affinity of gold surface to amine and thiol groups of biomolecules. Transducers, containing gold nanoparticles are used in sensors for determination of Hg(II), As(III), Cu(II), Cr(VI), and Al(III) in anodic stripping voltammetry [77, 83, 102, 135] and potentiometry [115, 137]. The use of these transducers ensures significantly lower detection limits for toxicants [83]. Thus, electrodeposition of gold nanoparticles with a size of 36 ± 13 nm on the surface of a glassy carbon electrode allows to obtain a very low detection limit of Hg(II) – 0.084 μg/L, which is six times lower than its maximum allowable concentration in waters used for household and amenity needs (0.5 μg/L).

Gold nanoparticles as transducers are used in the devices sensitive to biologically active substances, such as paracetamol [110, 111], tramadol [112], morphine [113], and serotonin [114]. In addition, on the electrode modified with gold nanostructures, the overpotential of paracetamol oxidation reduces by 50 mV; the oxidation current almost doubles in comparison with unmodified carbon paste electrode [110]. The detection limit for paracetamol is $1.46 \times 10^{-8}$ M. Ascorbic and uric acids and dopamine do not interfere with paracetamol detection. The sensor is used for determination of paracetamol in tablets and in human urine. Sanghavi and Srivastava [112] describe determination of paracetamol using Dowex50wx2 and gold nanoparticle modified glassy carbon paste electrode. The synergistic effect of gold nanoparticles and Dowex50wx2 makes it possible to achieve a sufficiently low limit of paracetamol detection – $4.71 \times 10^{-9}$ M. This sensor is useful when paracetamol and tramadol need to be detected with a high degree of selectivity in complex matrices such as urine, blood serum, and pharmaceutical preparations.

The use of nanomaterials as transducers in ion-selective electrodes has led to the development of a new generation of highly sensitive potentiometric sensors. Due to high surface area and conductivity of nanomaterials, their inclusion in the composition of sensitive membrane ion-selective electrodes, the number of immobilized selective ionophores can grow significantly. This enables to increase sensor sensitivity, reduce the analysis time, and to increase the duration of stable operation of the sensor. Mashhadizadeh et al. [115] propose a potentiometric sensor based on mercaptothiadiazoles and gold nanoparticle to detect Cu(II) ions in tap, lake, and mineral waters. Gold nanoparticles, added to the carbon-paste electrode, enhance the surface concentration of mercaptothiadiazole molecules that exhibit high selectivity toward Cu(II) ions, thus contributing to their concentration on the electrode surface and the reduction of the linear resistance of carbon paste. This type of a sensor ensures a wide range of measuring concentrations $-4 \times 10^{-9}$ to $7 \times 10^{-2}$ M; a low detection limit $-1 \times 10^{-9}$ M (0.06 μg/L); quick response (<5 s) and high selectivity. It can function efficiently within the pH range from 3.0 to 6.5 for 45 days.

Electrochemical sensors based on the transducers that consist of silver and platinum nanoparticles are applied for amperometric determination of $NO_2^-$ in [116, 117] and Cr(VI) [118]. Low detection limits for toxicants have been attained due to electrocatalytic activity of platinum and silver nanoparticles. For example, the detection limit for Cr(VI) with the application of a glassy carbon electrode, modified with silver nanoparticles, is 0.67 μg/L [118]. Moreover, the 100-fold excess of Cr(III) does not interfere with the detection of Cr(VI). The sensor was successfully applied to determine Cr(VI) in the wastewaters of a textile factory.

One of the most urgent tasks of stripping voltammetry for amalgamable elements is to replace toxic mercury electrodes with nontoxic ones. In this respect, the most perspective technology is application of bismuth electrodes. The use of bismuth nanoparticles as transducers is a challenging area for developing new nontoxic sensors that might be similar in terms of sensitivity and other analytical characteristics to traditionally used mercury-containing electrodes. Thus, with the application of bismuth containing sensors, detection limits for Zn(II), Cd(II), Pb(II) [74], and Ni(II) [75] are 0.60, 0.09, 0.17 μg/L, and $0.32 \times 10^{-8}$ M, respectively.

Electrodes modified with nanoparticles of metal oxides, namely $Bi_2O_3$, $MnO_2$, ZnO, $TiO_2$, $IrO_2$, silicon oxide $SiO_2$ and nickel hydroxide $Ni(OH)_2$, which play the role of catalysts, have become widely applied recently. Nanoparticles of metal oxides have high surface area, chemical stability, and photochemical stability; their synthesis does not require the use of expensive reagents. Sensors based on metal oxide nanoparticles are used in voltammetric sensors to detect $H_2O_2$ [119], glucose [120], and organic compounds [121–123]. Metal oxide nanoparticles can be included in the composition of membrane ion-selective electrodes for potentiometric determination of As(III), Cr(III) [124], and Fe(III) [125].

In its nanostate, silicon oxide $SiO_2$ has a regular 3D architecture with a pore diameter of 2–10 nm, which ensures high adsorption ability of its surface. Generally, $SiO_2$ nanoparticles are used, with organic functional groups covalently attached to the surface. These nanoparticles combine the mechanical strength of an inorganic framework with high reactivity of surface functional groups. The synthesis of $SiO_2$ nanoparticles does not require the use of expensive reagents and high temperatures. In addition, $SiO_2$ nanoparticles are biocompatible. Sanchez et al. [126] propose a mercury-free thick-film screen-printed carbon electrodes modified with functionalized $SiO_2$ nanoparticles to detect Pb(II) in non-pretreated drinking and natural waters. With the application of the developed sensor, the detection limit for Pb(II) is 0.1 mg/L with open-circuit 5-minute concentration.

Researchers draw special attention to the surface modification of electrodes with carbon nanomaterials such as carbon nanotubes, fullerenes, and graphene. Due to high surface area (e.g., for graphene it can be up to 2600 $cm^2/g$), the presence of the conjugated π-electronic system on the surface, high conductivity, and mechanical strength, carbon nanomaterials are effective sorbents and transducers.

Carbon nanomaterials are often used as a matrix for immobilization of biomolecules in biosensors, which results in a significant increase in the surface concentration of immobilized molecules and in the improved interfacial electronic conductivity [11]. The unique electronic architecture of their surface makes carbon nanomaterial promising components of electrochemical sensors that can be applied for detecting some organic compounds, for example, pesticide [127]. More widely electroanalysis uses carbon nanotubes (CNTs) (single-walled [SCNT] or multiwalled [MCNTs]), which is due to high surface area and electrocatalytic activity of defects in the graphite surface at the tube ends. Different functional groups with high analyte affinity can often be attached to the CNT surface, which enables to attain low detection limits with shorter concentration time and to conduct analysis of complex samples.

Of great interest is the application of graphene as a transducer. Graphene is a new material with unique structure and adsorption and catalytic properties. It was used in a biosensor for rotavirus infection detection [128]. Wu et al. [127] propose a highly sensitive, stable, and inexpensive grapheme-based sensor for detecting trace quantities of the pesticide methyl parathion in seawater. High adsorption capacity of graphene and strong π–π interaction of the aromatic ring of the methyl parathion molecule with graphene surface ensure effective concentration of the analyte on the electrode surface and accelerated electron transfer. The detection limit for methyl parathion with the use of the graphene-based sensor is 0.05 μg/L, which is much lower in comparison with sensors based on other sorbents. The application of carbon nanomaterials in electroanalysis is discussed in several reviews [129, 130].

Carbon nanomaterials decorated with nanoparticles of metals or oxides are often used in electrochemical sensors. The combination of unique properties of nanostructured carbon substrates and nanoparticles may enhance sensitivity, selectivity, and stability of these types of electrochemical sensors. Kong et al. [131] observed that gold nanoparticles as the composite of gold–thionine–graphene nanoparticles show higher electrocatalytic activity in glucose oxidation compared with the gold nanoparticles localized on a glassy carbon electrode surface. As part of the composite, thionine-modified graphene ensures a noticeable increase in the quantity of gold nanoparticles on the electrode surface. The electrode modified with gold–thionine–graphene nanoparticle composite shows high glucose sensitivity. The detection limit for glucose is $0.5 \times 10^{-7}$ M.

Composite hybrid materials are attracting widespread interest. Willner et al. [132] discuss the application of biomolecule – nanoparticle hybrids, supramolecular or DNA nanostructures as functional composites for sensors.

To date possible application of the nanoparticles synthesized with plant extracts in electroanalysis has remained relatively under explored. There are very few studies that have investigated the electrochemical determination of substances with the use of electrodes modified with “green synthesized” nanoparticles. Karthik et al. [107] discuss determination of chloramphenicol in milk, powdered milk, honey, and eye drops.

Several works have been published discussing the determination of heavy metals, such as Pb(II), Cd(II), and Cu(II) [105, 106] in water and low-toxicity fungicide carbendazim in soil [133]. Gnana Kumar et al. [134] proposed an amperometric hydrogen peroxide sensor based on bimetallic Au–Ag nanostructures with a detection limit of $1 \times 10^{-6}$ M.

### 6.5.2 Nanomaterials in electrochemical sensors for antioxidant detection

Antioxidants – compounds that decrease free radicals concentration or break chain oxidation processes in the body. Antioxidants include ascorbic and uric acids, caffeine, cysteine, glutathione, rutin, quercetin, bilirubin, retinol, α-tocopherol, and many others including special enzymes. Determination of their concentration enables to monitor many important processes in the human body. Disbalance in the free-radical compounds' generation versus antioxidant protection system based on antioxidant activity may lead to some dangerous pathologies. The literature describes several electrochemical methods that can be used to determine antioxidant concentration: chromatography, photometry, with the use of free radicals' generation in particular, and the electrochemical methods (coulometry [174–176], potentiometry [177–179], voltammetry [180, 181]). The literature presents the benefits of the voltammetric method in terms of sensitivity and resolution for antioxidant determination with the application of nanostructured transducers [182–188, 191–193, 195–207]. The current of oxidation is a valid signal in this case. The modification of the electrode surface with nanoparticles can reduce the overvoltage of antioxidant oxidation and increase current peaks of their oxidation, which leads to a considerably improved sensitivity and selectivity of determination. For example, Hu et al. [182] propose a sensitive electrochemical sensor based on a silver-doped poly(L-valine)-modified glassy carbon electrode for the simultaneous determination of uric acid, ascorbic acid, and dopamine in non-pretreated sample. The surface modification of the glassy carbon electrode with silver nanoparticles has resulted in a larger difference between dopamine oxidation potentials and ascorbic acid oxidation potentials – up to 238 mV, between uric acid and dopamine – up to 192 mV, which allows for their simultaneous determination. The detection limit for uric acid and dopamine is equal to $0.8 \times 10^{-7}$ M, for ascorbic acid – $3 \times 10^{-6}$ M.

Table 6.4 presents some examples of nanomaterial application as transducers in electrochemical sensors for antioxidant determination. As it can be seen from Tab. 6.4, nanoparticles of individual metals, bimetallic particles; nanoparticles of oxides and hydroxides of transition metals; and carbon nanomaterials and their composites are used as transducers. The combination of carbon nanomaterials and metallic nanoparticles contributes to a significant increase in the sensitivity of measurements, expansion of the range of the determined volumes, and lower detection limits for antioxidants (to nmol/L).

**Tab. 6.4:** Examples of nanoparticle application in electrochemical sensors for antioxidant detection

| Nanoparticles (size, nm) | Substrate (method of modification) | Antioxidant | Detection | Linear range, $\times 10^{-6}$ M (LOD, $\times 10^{-6}$ M) | Sample | Reference |
|---|---|---|---|---|---|---|
| Au–Pt | ITO | Ascorbic acid | CV | (1) | Pharmaceutical samples | [183] |
| (50) | (*in situ*) | | | 2–400 | | |
| Au–Pd | Au | | DPV | (10) | Pharmaceutical samples | [184] |
| | (*in situ*) | | | 100–500 | | |
| $TiO_2$ | CPE/BBNBH | | DPV | (0.32) | Pharmaceutical samples | [185] |
| (6.7) | (*ex situ*) | | | 4–1,400 | | |
| Pd | Pt/poly(N-methylpyrrole) | Ascorbic acid | DPV | (7) | Pharmaceutical samples, | [186] |
| | | | | 50–1,000 | urine | |
| | (*in situ*) | Uric acid | | (0.027) | | |
| | | | | 0.5–20 | | |
| Pt(80–90)/ | | Ascorbic acid | DPV | (19) | Background solution | [187] |
| MWCNT | GCE | | | 23–880 | | |
| ($d$ = 110–170, | (*in situ*) | Uric acid | | (0.032) | | |
| $l$ = 5,000–9,000) | | | | 0.046–52 | | |
| Ag | GCE/poly(L-valine) | Ascorbic acid | LAV | (3) | Urine | [182] |
| | (*in situ*) | Uric acid | | 10–1,000 | | |
| | | | | (0.08) | | |
| | | | | 0.3–10 | | |
| Au | GCE/polypyrrole | Uric acid | DPV | (0.012) | Urine | [188] |
| (80) | (*in situ*) | | | 0.05–28 | | |
| Pd | GCE/PEDOT | | DPV | (7) | Background solution | [189] |
| (4.9) | (*in situ*) | | | 7–11 | | |
| Au | GCE/cystamine | | CV | (0.6) | Model system | [190] |
| | (*in situ*) | | | 1–5,000 | | |
| Fe–C | GCE | | DPV | (0.15) | Background solution | [191] |
| | (*ex situ*) | | | 0.5–20 | | |

**Tab. 6.4:** (continued)

| Nanoparticles (size, nm) | Substrate (method of modification) | Antioxidant | Detection | Linear range, $\times 10^{-6}$ M (LOD, $\times 10^{-6}$ M) | Sample | Reference |
|---|---|---|---|---|---|---|
| Cu | GCE/polypyrrole | | DPV | (0.0008) | Urine | [192] |
| (60) | (*in situ*) | | | 0.001–10 | | |
| γ-$Zn_3Ni$ | GCE | | DPV | (0.2) | Urine | [193] |
| (12) | (*in situ*) | | | 1–400 | Serum | |
| Ni–Co | GCE | | Amperometry | (0.08) | Background solution | [98] |
| (2–4) | (*ex situ*) | | | 25–575 | | |
| MWCNT/ | GCE | | Amperometry | (0.05) | Background solution | [194] |
| $Ni_3[Fe(CN)_6]_2$ | (*ex situ*/*in situ*) | | | 0.1–18 | | |
| MWCNT | carbon-ceramic electrode | | DPV | (0.07) | Urine | [195] |
| ($d$ = 10–20, $l$ = 1,000) | | | | 0.25–100 | | |
| $TiO_2$ | CPE/BBNBH | Uric acid | DPV | (12) | Background solution | [196] |
| | | | | 200–1,500 | | |
| (6.7) | (*ex situ*) | Folic acid | | (32) | | |
| | | | | 200–2,700 | | |
| Au | Au | Caffeic acid | DPV | (0.025) | Wines | [197] |
| (10–20) | (*ex situ*) | | | 0.05–2,000 | | |
| graphene | GCE | Caffeine | DPV | (0.12) | Soft drinks | [198] |
| | (*ex situ*) | | | 0.4–600 | | |
| CNT | CPE | Gallic acid | DPV | (0.3) | Wines | [199] |
| | (*ex situ*) | | | 0.5–15 | | |
| CuO | Au | Rutin | DPV | (0.1) | Background solution | [200] |
| (10) | (*ex situ*) | | | 0.5–500 | | |
| $CeO_2$ | Au | | DPV | (0.2) | Pharmaceutical samples | [201] |
| (12) | (*ex situ*) | | | 0.5–500 | | |
| graphene | GCE/chitosan/PAMAM | | DPV | (0.0006) | Pharmaceutical samples, | [202] |
| | (*ex situ*) | | | 0.001–2 | serum | |

**Tab. 6.4:** (continued)

| Nanoparticles (size, nm) | Substrate (method of modification) | Antioxidant | Detection | Linear range, $\times 10^{-6}$ M (LOD, $\times 10^{-6}$ M) | Sample | Reference |
|---|---|---|---|---|---|---|
| $Co_3O_4$ (25) | GCE (*ex situ*) | Quercetin | LAV | (0.1) 0.5–330 | Pharmaceutical samples, urine | [203] |
| Au/BMI.$PF_6$ (11) | CPE (*ex situ*) | Fisetin | SWV | (0.05) 0.28–19.50 | Apple juice | [204] |
| Au (80)-carbon nanofiber (150) | Au (*in situ*) | Catechol hydroquinone | DPV | (0.36) 5–350 (0.86) 9–500 | Tap water | [205] |
| NiO | GCE (*ex situ*) | Glutathione | DPV | 200–6,000 | Background solution | [206] |
| $Cu(OH)_2$ (20–30) | CPE/$OPy^+PF_6^-$ (*ex situ*) | | SWV | (0.03) 1–1,800 | Plasma | [207] |
| $NaCo[Fe(CN)_6]$ (10–30) | CPE (*ex situ*) | L-Cysteine | Amperometry | (0.04) 3–37 | Urine, plasma | [208] |
| $TiO_2$ (6.7) | CPE/bis[bis(salicylidene-1, 4-phenylenediamine) molybdenum(VI)] (*ex situ*) | | DPV | (0.7) 1.5–1,200 | Plasma, pharmaceutical samples | [209] |
| $K_2Cu[Fe(CN)_6]$ (100) | pencil graphite electrode (*in situ*) | | Amperometry | (0.13) 1–13 | Urine | [210] |
| γ-$MnO_2$ (90–120) | SPGE (*ex situ*) | L-Cysteine | Chronoamperometry | (0.09) 0.5–1,000 | Background solution | [121] |
| | | Glutathione | | (0.2) 0.5–10 | | |
| RuO/ Acetaminophen | GCE (*in situ*) | N-acetyl-L-cysteine | DPV | (2.84) 0.3–14, 14–1,000 | Pharmaceutical samples | [211] |

**Tab. 6.4:** (continued)

| Nanoparticles (size, nm) | Substrate (method of modification) | Antioxidant | Detection | Linear range, $\times 10^{-6}$ M (LOD, $\times 10^{-6}$ M) | Sample | Reference |
|---|---|---|---|---|---|---|
| Au/bilirubin Oxidase (12) | Au/MPTS (*ex situ*) | Bilirubin | Amperometry | (0.0023) 1–5,000 | Plasma | [212] |
| ZnO (100–200) | Au (*ex situ*) | Uric acid | Potentiometry | (0.5) 0.5–1,500 | Background solution | [213] |
| Ag(10–30)/2-aminoethanethiol-GO | GCE (dropcast) | Morin | SWV | (0.0033) 0.001–5.0 | Grape wine | [214] |
| Au–MWCNT | GCE | Silymarin<br>Capsaicin | DPV | (0.047) 0.15–35.0<br>(0.083) 0.15–35.0 | Pharmaceutical samples, chilli peppers | [215] |
| Au(15)/MWCNT | CPE (*ex situ*) | Rutin | CV | (0.00004) 0.0004–0.01 | Medicine tablets | [216] |
| Ag(4 × 18–66)/graphene | GCE | Vanillin | SWV | (0.33) 2–100 | Biscuits | [217] |
| Au(17.8)/poly (allylamine hydrochloride) | GCE (dropcast) | Vanillin | SWV | (0.055) 0.90–15.0 | Food samples | [218] |
| AuPd(30–50)-graphene | GCE (electrodeposition) | Vanillin | AdDPV | (0.02) 0.1–7, 10–40 | Food samples | [219] |
| NiO/graphene | GCE (electrodeposition) | Ascorbic acid | DPV | (0.0167) 0.05–1,100 | Tablets | [220] |

**Tab. 6.4:** (continued)

| Nanoparticles (size, nm) | Substrate (method of modification) | Antioxidant | Detection | Linear range, $\times 10^{-6}$ M (LOD, $\times 10^{-6}$ M) | Sample | Reference |
|---|---|---|---|---|---|---|
| Au | GCE (electrodeposition) | Butylated hydroquinone | First derivative voltammetry | (0.079) 0.20–2.80 μg/mL | Edible oil | [221] |
| | | Butylated hydroxyanisole | | (0.039) 0.10–1.50 μg/mL | | |
| | | Butylated hydroxytoluene | | (0.080) 0.20–2.20 μg/mL | | |
| $CeO_2$(<25 nm)-Brij® 35 | GCE (dropcast) | Thymol | DPV | (0.20), 0.700–10.1 (0.65), 10.1–606 | Oregano | [222] |
| Au (40 ± 5)/ r-GO | GCE(dropcast) | Hydroquinone | DPV | 3–90 (0.15) | River water | [223] |
| | | Catechol | | 3–300 (0.12) | | |
| | | Resorcinol | | 15–150 0.78 | | |
| Bi(30–70) | GCE (electrodeposition) | Folic acid | SWV | 0.01–0.15 (0.0095) | Pharmaceutical samples | [224] |
| $MnO_2$(40)/ MWCNT | GCE (electrodeposition) | Ferulic acid | SWV | 0.082–220 (0.01) | Serum | [225] |
| Au–polyaniline | film application on GCE | Ascorbic acid | Amperometry | 10–12,000 (8.2) | Vitamin C tablets | [226] |
| Au(3)/graphene/ polyethyleneimine | GCE (dropcast) | Dopamine | DPV | 2–48 (0.2) | Urine | [227] |
| Au(15.8)/GO | GCE | Ascorbic acid | Amperometry | 0.11–600 (0.11) | Serum, vitamin C tablet | [228] |

**Tab. 6.4:** (continued)

| Nanoparticles (size, nm) | Substrate (method of modification) | Antioxidant | Detection | Linear range, $\times 10^{-6}$ M (LOD, $\times 10^{-6}$ M) | Sample | Reference |
|---|---|---|---|---|---|---|
| Au(3–8)-EDAS-MWCNT | GCE | Ascorbic acid | Amperometry | 0.1–9 (0.07) | Pharmaceutical samples | [229] |
| | | Dopamine | | 0.1–8 (0.08) | | |
| $IrO_x$–$RuO_x$ ($d = 50$, $h = 25$) | GCE (electrodeposition) | Caffeine | Amperometry | 0.05–5,000 | Pharmaceutical samples | [230] |
| Pd(60–75) | GCE (electrochemical synthesis) | Curcumin | SWV | 0.03–0.6 (0.022) | Spices turmeric | [231] |
| CdO($28 \pm 2$) | CPE | Curcumin | SWV | 0.2–320.0 (0.08) | Food samples | [232] |
| Cu@Au(50–100) | GCE | Eugenol | LAV | 0.05–0.80 µg/mL (0.042 µg/mL) | Food samples | [233] |
| $In_2O_3$(35) | GCPE | Luteolin | SWV | 0.00998–0.0884 (0.000199) | Thyme, serum, urine | [234] |
| $Fe_3O_4$(5)@CTAB | FTO | Citric acid | chronoamperometry | 50–2,500 (40) | Background solution | [235] |

BBNBH 2,2′-(1,2 butanediylbis(nitriloethylidyne))-bis-hydroquinone
CNT carbon nanotubes
PAMAM poly(amidoamine) dendrimers
BMI.$PF_6$ 1-butyl-3-methylimidazolium hexafluorophosphate
OPy+$PF_6$ octylpyridinum hexafluorophosphate
MPTS 3-(mercaptopropyl)-trimethoxysilane
CTAB cetyltrimethylammonium bromide
Other symbols: as in Tabs. 6.1–6.3

### 6.5.3 Nanomaterials in electrochemical immunoassay

Immunosensors are the basis of clinical analysis in medicine that allows diagnosing various pathologies, including infectious diseases, fast and with a high degree of selectively. Sensor selectivity is determined by the presence of a firmly attached layer of functional groups or molecules, able to specifically interact with a determined substance – analyte, on its surface. The possibility of creating the receptor layer has increased significantly in recent years thanks to the use of nanomaterials. It is worth noting that with regard to sensitivity and the detection limit, the electrochemical immunoassay with the application of nanomaterials is comparable (or even exceeds) to such traditional methods as enzyme-linked immunosorbent assay (ELISA) and polymerase chain reaction (PCR).

Nanomaterials, as it was mentioned above, are used as transducers, catalysts, signal-generating labels, and analyte transporters in immunoanalysis in particular. The literature [26, 87, 236–238] describes the most recent findings in this area. The examples of the nanomaterial use in electrochemical immunoassay are presented in Tab. 6.5. As can be seen from Tab. 6.5, nanoparticles of metals (gold, silver, platinum), semiconductors (CdS, ZnS, PbS), carbon nanotubes, and magnetic and composite nanoparticles (magnetite – gold, magnetite – polyaniline, gold – silver, etc.) are most commonly used in electrochemical immunosensors. The use of magnetic nanoparticles for analyte concentrating in a magnetic field significantly increases the efficiency of the process.

### 6.5.4 Nanomaterials – transducers and adsorbents in electrochemical immunosensors

The role of transducers in immunosensors is not limited to the transfer of the electrical signal from the receptor into the measuring network. Along with conductivity that enables the transducer to perform this function, it should have a high adsorption capacity, allowing immobilizing a sufficient quantity of the biological receptor material on its surface. Not least important is biocompatibility of the transducer material, which is essential for the receptor "survival" [282]. Antibodies or antigens serve as receptors. The antibodies are usually attached on the transducer surface as a result of physical adsorption or covalent linking. However, direct immobilization of antibodies on the electrode surface usually causes unwanted conformational changes in the protein structure, which ultimately leads to the loss of immune activity of immobilized antibodies. A problem often encountered with the use of covalent linkers (polymer or sol–gel films) is low reproducibility of the modified surface and complex procedure of the electrode regeneration. The application of nanomaterials as transducers for the immunoreagent immobilization often allows overcoming the above-mentioned limitations. While adsorbing on the nanoparticle surface, protein molecules are freely oriented in space, and retain their native conformation and activity. Ibii et al. [282] and Gu et al. 283] show that when hemoglobin is immobilized on the gold particles' modified electrode surface,

**Tab. 6.5:** Examples of nanoparticle application in electrochemical immunoassay

| Nanoparticles (size, nm) | Function of nanoparticles | Analyte | Method of detection | Linear range, (LOD) | Sample | Reference |
|---|---|---|---|---|---|---|
| Au | transducer | human immunoglobulin | DPV | 0.3–120 ng/mL (0.1 ng/mL) | Human serum | [239] |
| Au(13) | transducer | | CV | 0.025–1 ng/mL (0.1 ng/mL) | Background solution | [240] |
| Au/Cu(13) | label | | ASV | 2–250 ng/mL (0.5 ng/mL) | Human serum | [241] |
| Au(25) | label | | ASV | 1–50 ng/mL (0.75 ng/mL) | Background solution | [242] |
| $Fe_3O_4$(20) | transducer | | Potentiometry | 0.1–1.2 ng/mL (0.023 ng/mL) | Serum | [243] |
| $Fe_3O_4$–Au (15) | Analyte transporters/ label | | DPV | $2.5 \times 10^{-5}$–1 µg/mL | Background solution | [244] |
| $Fe_3O_4$–Au | Analyte transporters/ label | | ASV | 0.2– ng/mL (0.1 ng/mL) | Human serum | [245] |
| Au–$SiO_2$(40–50) | transducer | | Amperometry | 0.1–200 ng/mL (0.035 ng/mL) | Background solution | [246] |
| Au(13) | transducer | | Amperometry | 0.5–25 ng/mL (0.16 ng/mL) | Background solution | [247] |
| $Fe_3O_4$–Au (6.5) | Analyte transporters/ label | | DPV | (0.26 ng/mL) | Background solution | [248] |
| Au(18) | label | goat immunoglobulin | ASV | ($3 \times 10^{-12}$ M) | Background solution | [249] |
| Au/Ag | label | mouse immunoglobulin | Potentiometry | ($12.5 \times 10^{-12}$ M) | Background solution | [250] |
| γ-$Fe_2O_3$/polyaniline (80–100) | Analyte transporters/ label | Bacillus anthracis | CV | (0.01 ng/mL) | Background solution | [251] |
| $Fe_3O_4$(10) | Analyte transporters/ label | *Salmonella typhi* | AdSV | $10^3$–$10^8$ ng/mL (8.18 ng/mL) | Excrement of infected hens | [252] |
| Au/Cu(15) | Label | | ASV | 130–2600 ng/mL (98.9 ng/mL) | Human serum | [253] |

**Tab. 6.5:** (continued)

| Nanoparticles (size, nm) | Function of nanoparticles | Analyte | Method of detection | Linear range, (LOD) | Sample | Reference |
|---|---|---|---|---|---|---|
| Pt(60) | Transducer | *Escherichia coli* | Amperometry | 50–1 × $10^5$ ng/mL (20 ng/mL) | Background solution | [254] |
| $Fe_3O_4$(300) | Transducer | *Plasmodium falciparum* | Amperometry | 0.36–31.3 ng/mL (0.36 ng/mL) | Human serum | [255] |
| γ-$Fe_2O_3$/polyaniline (50–100) | Analyte transporters/ label | *Bacillus cereus*, *E. coli* O157:H7 | CV | 1–100 ng/mL (40 ng/mL) (6 ng/mL) | Background solution | [256] |
| Au (10), MWCNT ($d$ = 60–100, $l$ = 1,000–2,000) | Transducer | Staphylococcal enterotoxin B | DPV | 0.05–15 ng/mL (0.01 ng/mL) | Food | [257] |
| Au/Ag | Transducer | Diphtheria antigen | Potentiometry | 22–800 ng/mL (3.7 ng/mL) | Serum | [258] |
| $Fe_3O_4$–Au/Cu | Analyte transporters/ label | Hepatitis B surface antigen | ASV | 0.1–1500 ng/mL (0.087 ng/mL) | Human serum | [259] |
| Au(16) | Transducer | | Potentiometry | 4–960 ng/mL (1.9 ng/mL) | Background solution | [260] |
| Au(16) | Label | | CV | 0.5–650 ng/mL (0.1 ng/mL) | Human serum | [261] |
| Au(16) | Transducer | | Potentiometry | 8–1200 ng/mL (2.3 ng/mL) | Human serum | [262] |
| Au(15–20) | Transducer | Prostate-specific antigen | Amperometry | 1–80 ng/mL 0.8 ng/mL | Serum | [263] |
| Au–CNT | Transducer | α-Fetoprotein | Amperometry | 1–55 ng/mL (0.6 ng/mL) | Serum | [264] |
| Au (16)-Azure I/MWCNT | Transducer | | Amperometry | 0.1–8.0 ng/mL 8.0–250.0 ng/mL (0.04 ng/mL) | Human serum | [265] |

**Tab. 6.5:** (continued)

| Nanoparticles (size, nm) | Function of nanoparticles | Analyte | Method of detection | Linear range, (LOD) | Sample | Reference |
|---|---|---|---|---|---|---|
| Au(33) | Label | α-Enolase | SWV | 0.001–10 ng/mL (0.00238 ng/mL) | Background solution | [266] |
| Au–MWCNT (20/30) | Transducer | Testosterone | Amperometry | 0.1–10 ng/mL (0.085 ng/mL) | Human serum | [267] |
| Au | Transducer | Carcinoembryonic antigen | CV | 0.005–50 ng/mL (0.002 ng/mL) | Human serum | [268] |
| $NiFe_2O_4$ (20)–Au | Label | | Amperometry | 0.010–160 ng/mL (0.005 ng/mL) | Human serum | [269] |
| Au(100) | Transducer | Anti-transglutaminase | EIS | $10^{-6}$–$10^{-4}$ ng/mL ($5.22 \times 10^{-6}$ M) | Background solution | [270] |
| Au(12) | Transducer | NGAL | Amperometry | 50–250 ng/mL (1 ng/mL) | Blood serum, urine | [271] |
| Au (3–7)-N-MWCNT | Transducer | Microcystin-LR | DPV | 5–1000 ng/mL (2 ng/mL) | Polluted water | [272] |
| ZnS | Label | $\beta_2$-Microglobulin | SW–ASV | – | Background solution | [273] |
| CdS | | Immunoglobulin | | ($0.07 \times 10^{-9}$ M) | | |
| PbS | | Bovine serum albumin | | ($0.15 \times 10^{-9}$ M) | | |
| CuS | | C-reactive protein | | – | | |
| Au (13)/Ag | Transducer | Human immunoglobulin | ASV | (0.005 ng/mL) | Human serum | [274] |
| | | Mouse immunoglobulin | | (0.006 ng/mL) 0.01–250 ng/mL | | |
| Graphene–$Fe_3O_4$, | Transducer | Carcinoembryonic antigen | DPV | 0.01–80 ng/mL (0.001 ng/mL) | Blank calf serum | [275] |
| Au | Analyte transporters, label | α-Fetoprotein | | 0.01–200 ng/mL (0.001 ng/mL) | | |

**Tab. 6.5:** (continued)

| Nanoparticles (size, nm) | Function of nanoparticles | Analyte | Method of detection | Linear range, (LOD) | Sample | Reference |
|---|---|---|---|---|---|---|
| Au/antibodies Sandwich | Label | *Salmonella enterica* | DPV | $10^3$–$10^6$ CFU/mL (143 CFU/mL) | Skimmed milk | [276] |
| Ag@$SiO_2$/antibody | Label | *E. coli* O157:H7 | DPV | 20–8000 CFU/mL (13 CFU/mL) | Background solution | [277] |
| Antibody/Au ($d$ = 10, $l$ = 40)/FCA | Label | *E. coli* | Voltammetry | (60 CFU/mL) | Milk, yogurt | [278] |
| Au(15)/antibody | Label | *S. typhi* | Voltammetry | (98.9 CFU/mL) | Human serum | [279] |
| Au/polyaniline/ antibody | Transducer | Staphylococcal enterotoxin B | Voltammetry, EIS | 0.05–5 ng/mL (0.017 ng/mL) | Milk | [280] |
| $Fe_3O_4$/chitosan | Label | *E. coli* | Voltammetry | 10–105 CFU/mL (9.3 CFU/mL) | Model solutions, water | [281] |

AdSV adsorption stripping voltammetry
EIS electrochemical impedance spectroscopy
NGAL neutrophil gelatinase-associated lipocalin
FCA ferrocene carboxylic acid
Other symbols: as in Tabs. 6.1–6.4

the original structure of the protein has been preserved. Luo et al. [284] state that the antibodies attached to the surface of gold nanoparticles can stay stable for 100 days.

The application of nanoparticles as transducers in electrochemical immunosensors enables to accelerate the electron transfer from the protein to the electrode. This effect is attributed to a small size and high conductivity of nanoparticles. Nanoparticles, penetrating through the insulating protein layer to the redox center of biomolecules, act as bridges for electron transfer from the protein to the electrode.

Gold nanoparticles are quite often used to modify the electrode surface of immunosensors. Nevertheless, CNTs deserve to be mentioned also, as their unique structure makes them a promising material for immobilization of biological components in electrochemical immunosensors.

In the case of CNT, the immunoreagents or label enzymes can be fixed to both the external and internal surfaces, which leads to a significant increase in the surface concentration of biomolecules, and hence the sensitivity of the sensor. In addition, CNTs, like gold nanoparticles, catalyze the hydrogen peroxide reduction reaction, which is a signal-forming agent in many immunosensors containing as a label enzyme – horseradish peroxidase. The combination of catalytic activity, high conductivity, and large adsorption capacity of CNTs significantly increases the sensitivity of sensors based on them.

Modification of the electrode surface by nanoparticles increases the area of the active surface, and hence the number of binding centers for biomolecules [87]. As a result, the surface concentration of immobilized antibodies increases, and, consequently, the sensitivity of the sensor increases.

The comparison between different methods of polyclonal antibodies immobilization on the thick film graphite electrode shows that the intensity of the electrochemical response increases and its stability improves by attaching antibodies onto the graphite surface, modified with films of synthetic membrane-like didodecylammonium bromide with gold nanoparticles [285]. Physical adsorption of antibodies on nontreated surface of a graphite electrode provides for the formation of 100 nA signal, whereas after immobilization of antibodies on the transducer, consisting gold nanoparticles, the signal increases to 790 nA.

The immunosensor sensitivity increases with a decrease the size of the modifier nanoparticles. Thus, when detecting hepatitis B antigen, the signal of the potentiometric immunosensor almost doubles, with a decrease in the size of gold nanoparticles from 51 to 16 nm [260].

### 6.5.5 Nanomaterials as analyte transporters

The delivery of the analyte, conjugated with the label, to the place of signal-generating reaction is an essential stage to form an immunocomplex. This transfer is carried out either in stirring solution or using magnetic particles attached to analyte, conjugated with the label. In this case, the solution is positioned into the magnetic field.

Magnetic nanoparticles are also used for direct concentrating of the analyte on the electrode surface, when the magnet is placed behind the electrode. Magnetite nanoparticles – $Fe_3O_4$, γ-$Fe_2O_3$ and $NiFe_2O_4$ – are used as transporters [245, 251, 252, 256].

With a decrease in the size of magnetic particles, the efficiency of immunomagnetic separation increases. When separating *E. coli* O157:H7 in ground beef, Varshney et al. [286] observed an increase in the efficiency of immunomagnetic separation by 14 % while the size of the magnetic particles was decreasing from 2.8 μm to 145 nm. The use of nanoparticles as analyte transporters led to high efficiency of immunomagnetic separation (94 % and above) in a wide range of analyte concentrations without the reaction mixture stirring. The immunoreaction lasted 15 minutes. In the case of magnetic microparticles, these results were obtained during 60 minutes with continuous stirring of the sample *E. coli* O157:H7 solution. The authors [286] attributed this effect to the fact that the surface area of the nanoparticles for bacterium binding was 78-fold bigger than the area of microparticles.

### 6.5.6 Nanomaterials as labels in electrochemical immunosensors

The quantity of immunocomplexes formed during the signal forming reaction is often determined from the magnitude of the electrochemical response of the label [241, 242, 244, 248, 273]. Electroactive molecules, redox complexes, metals, or metal ions [287], including gold and silver nanoparticles [249, 250], semiconductor quantum dots, and, rarely, magnetic nanoparticles [6] serve as labels. Most often gold nanoparticles are used as labels. This is due to a simple fabrication process and high affinity of gold to amino- and sulfur groups of protein molecules, which ensures strong binding [288, 289, 290].

There are two possible approaches to obtaining a signal: (1) the dissolution of the immunocomplex containing the label, and subsequent analysis of the resulting solution with the most relevant sensitive method; (2) the record of electrochemical reaction of the label.

The first approach is implemented in [249]: gold nanoparticle labels are dissolved chemically, with toxic $Br_2$ reagent. The resulting solution is analyzed by anodic stripping voltammetry. Another option is when silver [258] or copper [253] precipitate on the gold nanoparticle surface. The benefit of using gold nanoparticles coated with a layer of silver or copper as labels is that the dissolution of these metals does not require the use of toxic reagents.

The determination of copper (II) and silver (I) by electrochemical methods is characterized by high sensitivity, which allows lowering the limit of detection of immunocomplexes. Thus, the detection limit for human IgG using gold nanoparticles covered with a layer of catalytically precipitated copper was 0.5 ng/mL [241], and the limit of hepatitis B antigen detection was 0.087 ng/mL [259].

The second case is realized in [281]. Kozitsina et al. presented a new enzyme-free *E. coli* immunosensor. The immunocomplexes between the antibodies and chitosan modified (magnetite) are formed on the surface of the planar platinum electrode. Nanoparticles of $Fe_3O_4$ served as a label. The quantity of labeled immunocomplexes is detected in the aprotic solution by using voltammetry. The electrochemical response of magnetite nanoparticles provides data about the quantity of bacteria. The designed immunosensor is highly specific and enables to detect *E. coli* in a range from 10 to 105 CFU/mL with a relative standard deviation below 10 %. The detection limit is 9.3 CFU/mL.

Advantages of nanoparticles application in immunoanalysis are demonstrated in detecting *Salmonella typhimurium* [252]. The analysis involves the following stages: localization of magnetic nanoparticles on a pathogenic cell; magnetic separation of excess $Fe_3O_4$ nanoparticles; and concentrating of pathogens conjugated with magnetic nanoparticles in the magnetic field on the substrate or the transducer (Fig. 6.1). The source of information about the pathogen concentration is either the concentration of iron ions in the solution, obtained by dissolving the immunocomplexes containing nanoparticles in a mixture of acids [252] or the current of electrochemical transformations of the electrochemically active polymer that has previously been binded to magnetic nanoparticles [252] or magnetic nanoparticles themselves [252]. The combination of magnetic separation and highly sensitive stripping voltammetry allows obtaining the detection limit of 8.18 ng/mL for bacteria and 1.51 ng/mL for bacterial gene, which agrees with the diagnostic opportunities offered by the PCR method [252].

Liu et al. [273] propose a format of an electrochemical immunoassay that enables to determine several different analytes simultaneously. To conduct multicomponent immunoassay, each analyte is labeled with nanoparticles of different metals. Metals are chosen, so that after their dissolution, no overlapping of the signals of the corresponding ions is observed. In [273], nanoparticles of semiconductors ZnS, CdS, PbS, and CuS are used as labels for simultaneous detection of four different proteins (β2-microglobulin, IgG, BSA, C-reactive protein). Semiconductor nanoparticles, conjugated with the immunocomplex, are dissolved in nitric acid, and the concentration of Zn(II), Cd(II), Pb(II) and Cu(II) ions is determined by square-wave anodic stripping voltammetry using a mercury film electrode. The difference in the anodic peak potentials for Zn(II) (–1.02 V), for Cd(II) (–0.65 V), Pb(II) (–0.50), and Cu(II) (–0.11 V) enables to simultaneously determine the concentration of the antigens.

Sharma et al. [291] described the detection of *Staphylococcal enterotoxin* B (SEB) by using a zinc sulfide (ZnS) quantum dots (QDs) based immunosensor. ZnS-QDs fluorescence and a zinc ion reduction current, obtained after the immunocomplex was dissolved in HCl, served as analytical signals. For the fluorescent detection, the detection limit for enterotoxin was 0.2 ng/mL, and for the electrochemical

detection – 0.24 ng/mL. In authors' opinion, the electrochemical detection enables to detect the analyte quickly, with low cost and regardless of the QDs' size.

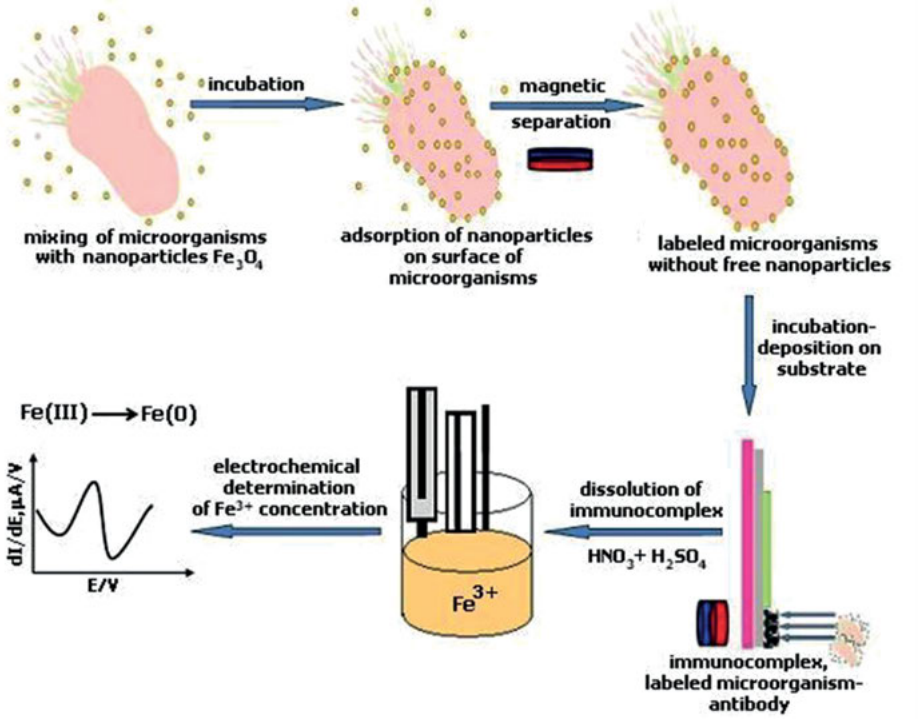


**Fig. 6.1:** Electrochemical immunoassay with the use of $Fe_3O_4$ particles as the analyte transporter and signal-generating label.

It might be possible to reduce the analysis time if we exclude the dissolving stage of the immunocomplex and the analysis of the obtained solution. For example, the use of gold nanoparticles as a signal-generating label while identifying α-enolase, a lung cancer diagnostic marker, results in obtaining a very low detection limit in the sample 2.38 pg/mL [266]. α-Enolase was detected in a "sandwich" mode. Figure 6.2 shows its main steps. Before the start of the analysis, primary monoclonal α-enolase antibodies were attached onto a polyethylene glycol modified working surface of a disposable screen-printed electrode by the adsorption method. To eliminate the impact of nonspecific interactions and adsorption, the electrode surface was treated with a casein solution. The prepared electrode then was incubated in the sample solution to generate an immunoreaction. Next, the electrode with the immobilized immunocomplex was kept in the solution containing secondary polyclonal bodies labeled by gold nanoparticles. As a result, a "sandwich" was formed. Unbound gold nanoparticles

were then washed off with a phosphate buffer solution. Gold nanoparticles were oxidized (dissolved) at +1.2 V for 2 minutes, and the signal of Au(III) was recorded at +0.35 V using the method of square wave voltammetry.

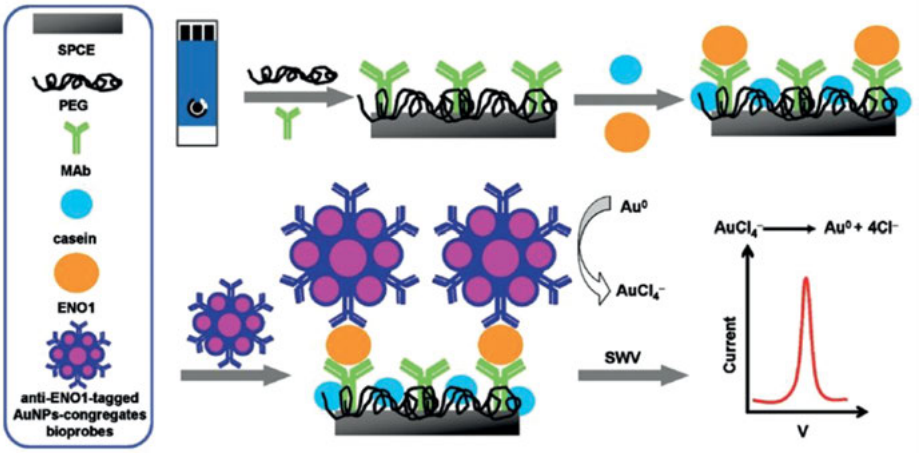


**Fig. 6.2:** Detection of α-enolase with gold nanoparticles labels. Reproduced by permission of American Chemical Society [266], Copyright 2010.

Reported in the literature are the examples of applying "sandwich" mode of immunoassay to detect tick-borne encephalitis [292], human immunoglobulin [241,242], hepatitis B antigen [259], carcinoembryonic antigen, and α-fetoprotein [275].

To obtain a signal for magnetic oxide nanoparticles, they are previously coated with some electroactive substances, for example, a layer of electroactive polymer [251].

Tang et al. [275] proposed a slightly different method for multiplexed electrochemical immunoassay involving nanoparticles. The key principle of the method implies that antibodies to two cancer markers are labeled with gold nanoparticles with encapsulated horseradish peroxidase and with two different mediators. For example, antibodies to α-fetoprotein are labeled with gold nanoparticles whose pores contained horseradish peroxidase and ferrocene, and in the case of carcinoembryonic antigen – horseradish peroxidase and thionine. The immunoassay was performed as a sandwich test. Magnetite nanoparticles localized on the surface of graphene nanorods were used for concentrating the labeled immunocomplex at the electrode surface. The current of hydrogen peroxide reduction, recorded at different potentials and in the presence of different mediators, served as an analytical signal. Thus, the difference between potential peaks for the hydrogen peroxide reduction in the presence of ferrocene and thionine was 450 mV, which allowed to simultaneously detecting α-fetoprotein and carcinoembryonic antigen in a wide range of concentrations from 0.01 to 200 ng/mL and from 0.01 to 80 ng/mL, respectively. Moreover, due to high adsorption capacity of gold

nanoparticles and the magnetic separation of immunocomplexes with magnetite nanoparticles, a low detection limit of 1 pg/mL for both cancer markers was obtained [275].

To date, composite nanoparticles architecturing magnetic core–shell gold or electroactive polymer are widely used in an electrochemical immunoassay for preconcentration and separation. The advantage of these nanoparticles is a combination of magnetic properties of the core with high chemical affinity of the gold shell to protein structures [293] or electrochemical active of the polymer coating, which allows to detect antigens avoiding the stage of chemical dissolution of nanoparticles in concentrated acids [251].

Tamer et al. [294] propose a method of synthesizing magnetic core–shell $Fe_3O_4$–Au nanoparticles with the core–shell size of 12.5 nm. These nanoparticles were used to immunomagnetic separation of *E. coli* bacteria.

Pal and Alocilja [251] show that the use of magnetic γ-$Fe_2O_3$ nanoparticles coated with polyaniline, can result in a low detection limit for *Bacillus anthracis* DNA at 0.01 ng/mL with a total analysis time of 60 minutes. Unique properties of magnetic nanoparticles (small size, large surface, high stability, electrochemical activity combined with magnetic properties, simplicity, and low cost of synthesis) ensure the presence of the stages of magnetic concentration and magnetic separation, which results in increased sensitivity of an immunosensor. These unique properties offer great perspectives for a broader application of magnetic nanoparticles in the electrochemical immunoassay.

## 6.6 Conclusions

Specific properties of nanoparticles (high adsorptive capacity, catalytic activity, excess of surface Gibbs free energy) are reflected in the kinetics and thermodynamics of the electrode processes of both the nanoparticles themselves and oxidation–reduction reactions on their surface. These features make them a very useful and promising material to be used in chemical and biochemical sensors. The development of screen printing technology, magnetic separation, polymer chemistry, fabrication, and investigation of nanostructures forms the basis for research and development of new sensors, including their application in home-clinic and telemedicine.

Nanostructures of different nature (metals, oxides, carbon), which are localized on the electrode surface, or serve as a substrate for localizing bioreceptors or labels, create a virtually unlimited choice of ways and methods of performing chemical and biochemical analysis. Reviews of relevant literature become of utmost importance. This review is just another attempt to summarize what has been researched in the field of nanomaterials and their use in sensors.

**Acknowledgments:** The research for this paper was financially supported by the Russian Foundation for Basic Research (Project no. 17-03-00679_A).

## References

[1] Будников ГК. Биосенсоры как новый тип аналитических устройств. *Соросовский Образовательный Журнал (СОЖ)* 1996, 12, 26–32 (Budnikov HC. Biosensors as a new type of analytical devices. Soros Educ J (SEJ) 1996, 12, 26–32 (original source in Russian).
[2] Hernandez-Santos D, Gonzalez-Garcia MB, Garcia AC. Metal-nanoparticles based electroanalysis. *Electroanalysis* 2002, 14(18), 1225–35.
[3] Katz E, Willner I, Wang J. Electroanalytical and bioelectroanalytical systems based on metal and semiconductor nanoparticles. *Electroanalysis* 2004, 16(1–2), 19–44.
[4] Riu J, Maroto A, Rius FX. Nanosensors in environmental analysis. *Talanta* 2006, 69(2), 288–301.
[5] Huang X-J, Choi Y-K. Chemical sensors based on nanostructured materials. *Sens Actuators B* 2007, 122(2), 659–71.
[6] Vertelov GK, Olenin AYu, Lisichkin GV. Use of nanoparticles in the electrochemical analysis of biological samples. *J Anal Chem* 2007, 62(9), 813–24.
[7] Pumera M, Sanchez S, Ichinose I, Tang J. Electrochemical nanobiosensors. *Sens Actuators B* 2007, 123(2), 1195–205.
[8] Xiao Y, Chang ML. Nanocomposites: from fabrications to electrochemical bioapplications. *Electroanalysis* 2008, 20(6), 648–62.
[9] Campbell FW, Compton RG. The use of nanoparticles in electroanalysis: an updated review. *Anal Bioanal Chem* 2010, 396(1), 241–59.
[10] Stefan-van-Staden RI, van Staden JF, Balasoiu SC, Vasile OR. Micro- and nanosensors, recent developments and features: a minireview. *Anal Lett* 2010, 43(7–8), 1111–8.
[11] Yanez-Sedeno P, Pingarron JM, Riu J, Rius FX. Electrochemical sensing based on carbon nanotubes. *TrAC-Trends Anal Chem* 2010, 29(9), 939–53.
[12] Willner I, Willner B, Tel-Vered R. Electroanalytical applications of metallic nanoparticles and supramolecular nanostructures. *Electroanalysis* 2011, 23(1), 13–28.
[13] Siangproh W, Dungchai W, Rattanarat P, Chailapakul O. Nanoparticle-based electrochemical detection in conventional and miniaturized systems and their bioanalytical applications: a review. *Anal Chim Acta* 2011, 690(1), 10–25.
[14] Aragay G, Pino F, Merkoci A. Nanomaterials for sensing and destroying pesticides. *Chem Rev* 2011, 112(10), 5317–38.
[15] Wang J. Electrochemical biosensing based on noble metal nanoparticles. *Microchim Acta* 2012, 177(3–4), 245–70.
[16] Marin S, Merkoci A. Nanomaterials based electrochemical sensing applications for safety and security. *Electroanalysis* 2012, 24(3), 459–69.
[17] Rassaei L, Marken F, Sillanpaa M, Amiri M, Cirtiu CM, Sillanpaa M. Nanoparticles in electrochemical sensors for environmental monitoring. *TrAC-Trends Anal Chem* 2011, 30(11), 1704–15.
[18] Budnikov HC, Shirokova VI. Term “Nano” in electroanalysis: a trendy prefix or a new stage of its development? *J Anal Chem* 2013, 68(8), 663–70.
[19] Brainina KZ, Galperin LG, Galperin AL. Mathematical modeling and numerical simulation of metal nanoparticles electrooxidation. *J Solid State Electrochem* 2010, 14(6), 981–8.
[20] Brainina KhZ, Galperin LG, Vikulova EV, et al. Gold nanoparticles electrooxidation: comparison of theory and experiment. *J Solid State Electrochem* 2011, 15(5), 1049–56.

[21] Brainina KZ, Galperin LG, Piankova LA, Stozhko NY, Myrzakaev AM, Timoshenkova OR. Bismuth nanoparticles electrooxidation: theory and experiment. *J Solid State Electrochem* 2011, 15(11–12), 2469–75.
[22] Brainina KhZ, Galperin LG, Kiryuhina, Galperin AL, Stozhko NYu, Murzakaev AM. Silver nanoparticles electrooxidation: Theory and experiment. *J Solid State Electrochem* 2012, 16(7), 2365–72.
[23] Stozhko NYu, Malakhova NA, Byzov IV, Brainina KhZ. Electrodes in stripping voltammetry: from a macro- to a micro- and nano-structured surface. *J Anal Chem* 2009, 64(11), 1148–57.
[24] Брайнина Х3, Викулова ЕВ, Стожко НЮ. Наноматериалы: свойства и применение в электрохимических сенсорах.: Под ред. *С.Н.Штыкова Нанообъекты и нанотехнолоГии в химическом анализе Наука. 20 т.*, Москва, 2015, 431 с. (Brainina KhZ, Vikulova EV, Stozhko NY. Nanomaterials: properties and applications in electrochemical sensors. In: Shtykov SN, ed. Nanoobjects and nanotechnologies in chemical analysis. Moscow, Russia, Nauka, 2015, 151–207, original source in Russian).
[25] Dai X, Wildgoose GG, Salter C, Crossley A, Compton RG. Electroanalysis using macro-,micro-, and nanochemical architectures on electrode surfaces. Bulk surface modification of glassy carbon microspheres with gold nanoparticles and their electrical wiring using carbon nanotubes. *Anal Chem* 2006, 78(17), 6102–8.
[26] Проблемы аналитической химии. Т. 14. Химические сенсоры. Под ред. Ю.Г. Власова. М.: Наука, 2011. 399 с. (Vlasov YuG, ed., Problems of Analytical Chemistry. V. 14. Chemical Sensors. Moscow, Russia, Nauka, 2011, original source in Russian).
[27] Qi WH, Wang MP. Size and shape dependent melting temperature of metallic nanoparticles. *Mater Chem Phys* 2004, 88(2–3), 280–4.
[28] Liu X, Atwater M, Wang J, Huo Q. Extinction coefficient of gold nanoparticles with different sizes and different capping ligands. *Colloids Surf B* 2007, 58(1), 3–7.
[29] Link S, El-Sayed MA. Size and temperature dependence of the plasmon absorption of colloidal gold nanoparticles. *J Phys Chem B* 1999, 103(21), 4212–17.
[30] Kelly KL, Coronado E, Zhao LL, Schatz GC. The optical properties of metal nanoparticles: the influence of size, shape, and dielectric environment. *J Phys Chem B* 2003, 107(3), 668–77.
[31] Lee K-C, Lin S-J, Lin C-H, Tsai C-S, Lu Y-J. Size effect of Ag nanoparticles on surface plasmon resonance. *Surf Coat Technol* 2008, 202(22–23), 5339–42.
[32] Roduner E. Size matters: why nanomaterials are different. *Chem Soc Rev* 2006, 35(7), 583–92.
[33] Hvolbaek B, Janssens TVW, Clausen BS, Falsig H, Christensen CH, Norskov JK. Catalytic activity of Au nanoparticles. *Nano Today* 2007, 2(4), 14–8.
[34] Li Y, Cox JT, Zhang B. Electrochemical responses and electrocatalysis at single Au nanoparticles. *J Am Chem Soc* 2010, 132(9), 3047–54.
[35] Bukhtiyarov VI, Slin'ko MG. Metallic nanosystems in catalysis. *Russ Chem Rev* 2001, 70(2), 179–181.
[36] Park T-J, Papaefthymiou GC, Viescas AJ, Moodenbaugh AR, Wong SS. Size-dependent magnetic properties of single-crystalline multiferroic $BiFeO_3$ nanoparticles. *Nano Lett* 2007, 7(3), 766–72.
[37] Jiang Q, Liang LH, Zhao DS. Lattice contraction and surface stress of fcc nanocrystals. *J Phys Chem B* 2001, 105(27), 6275–77.
[38] Zanchet D, Tolentino H, Alves MCM, Alves OL, Ugarte D. Inter-atomic distance contraction in thiol-passivated gold nanoparticles. *Chem Phys Lett* 2000, 323(1–2). 167–72.
[39] Jain PK, Lee KS, El-Sayed IH, El-Sayed MA Calculated absorption and scattering properties of gold nanoparticles of different size, shape, and composition: applications in biological imaging and biomedicine. *J Phys Chem B* 2006, 110(14), 7238–48.
[40] Meier J, Schiotz J, Liu P, Norskov JK, Stimming U. Nano-scale effects in electrochemistry. *Chem Phys Lett* 2004, 390(4–6), 440–4.

[41] Eftekhari A. *Nanostructured Materials in Electrochemistry*. Weinheim, John Wiley and Sons, WILEY-VCH Verlag GmbH & Co. KGaA, 2008.
[42] Belding SR, Campbell FW, Dickinson EJF, Compton RG. Nanoparticle-modified electrodes. *Phys Chem Chem Phys* 2010, 12(37), 11208–21.
[43] Plieth WJ. Electrochemical properties of small clusters of metal atoms and their role in surface enhanced Raman scattering. *J Phys Chem* 1982, 86(16), 3166–70.
[44] Plieth WJ. The work function of small metal particles and its relation to electrochemical properties. *Surf Sci* 1985, 156, 530–5.
[45] Chaki NK, Sharma J, Mandle AB, Mulla IS, Pasrichab R, Vijayamohanan K. Size dependent redox behavior of monolayer protected silver nanoparticles (2–7 nm) in aqueous medium. *Phys Chem Chem Phys* 2004, 6(6), 1304–9.
[46] Jones SEW, Campbell FW, Baron R, Xiao L, Compton RG. Particle size and surface coverage effects in the stripping voltammetry of silver nanoparticles: theory and experiment. *J Phys Chem C* 2008, 112(46), 17820–7.
[47] Cruickshank AC, Downard AJ. Electrochemical stability of citrate-capped gold nanoparticles electrostatically assembled on amine-modified glassy carbon. *Electrochim Acta* 2009, 54(23), 5566–70.
[48] Abdullin TI, Bondar OV, Nikitina II et al. Effect of size and protein environment on electrochemical properties of gold nanoparticles on carbon electrodes *Bioelectrochemistry* 2009, 77(1), 37–42.
[49] Karami H, Kafi B, Mortazavi SN. Effect of particle size on the cyclic voltammetry parameters of nanostructured lead dioxide. *Int J Electrochem Sci* 2009, 4(3), 414–24.
[50] Ivanova OS, Zamborini FP. Size-dependent electrochemical oxidation of silver nanoparticles. *J Am Chem Soc* 2010, 132(1), 70–2.
[51] Ivanova OS, Zamborini FP. Electrochemical size discrimination of gold nanoparticles attached to glass/indium-tin-oxide electrodes by oxidation in bromide-containing electrolyte. *Anal Chem* 2010, 82(13), 5844–50.
[52] Tang L, Han B, Persson K, et al. Electrochemical stability of nanometer-scale Pt particles in acidic environments. *J Am Chem Soc* 2010, 132(2), 596–600.
[53] Коршунов АВ, Превезенцева ДО, Коновчук ТВ, Миронец ЕВ. Влияние дисперсного состава золей серебра и золота на их электрохимическую активность. *Известия ТПУ*, 2010, 317(3), 6–13. (Korshunov AV, Prevezentceva DO, Konovchuk TV, Mironetc EV. The effect of the dispersed composition of silver and gold sols on their electrochemical activity. Izvestiya TPU, 2010, 317(3), 6–13, original source in Russian).
[54] Lakbub J, Pouliwe A, Kamasah A, Yang C, Sun P. Electrochemical behaviors of single gold nanoparticles. *Electroanalysis* 2011, 23(10), 2270–4.
[55] Masitas RA, Khachian IV, Bill BL, Zamborini FP. Effect of surface charge and electrode material on the size-dependent oxidation of surface-attached metal nanoparticles. *Langmuir* 2014, 30(43), 13075–84.
[56] Masitas RA, Zamborini FP. Oxidation of highly unstable <4 nm diameter gold nanoparticles 850 mV negative of the bulk oxidation potential. *J Am Chem Soc* 2012, 134(11), 5014–17.
[57] Kumar A, Buttry DA. Size-dependent anodic dissolution of water-soluble palladium nanoparticles. *J Phys Chem C* 2013, 117(50), 26783–9.
[58] Toh HS, Batchelor-McAuley C, Tschulik K, Uhlemann M, Crossley A, Compton RG. The anodic stripping voltammetry of nanoparticles: electrochemical evidence for the surface agglomeration of silver nanoparticles. *Nanoscale* 2013, 5, 4884–93.
[59] Tang L, Li X, Cammarata RC, Friesen C, Sieradzki K. Electrochemical stability of elemental metal nanoparticles. *J Am Chem Soc* 2010, 132(33), 11722–6.
[60] Redmond PL, Hallock AJ, Brus LE. Electrochemical Ostwald ripening of colloidal Ag particles on conductive substrates. *Nano Lett* 2005, 5(1), 131–5.

[61] Henglein A.Remarks on the electrochemical potential of small silver clusters in aqueous-solution. *Ber Bunsenges Phys Chem* 1990, 94(5), 600–3.
[62] Henglein A, Mulvaney P, Linnert T. Chemistry of $Ag_n$ aggregates in aqueous solution: non-metallic oligomeric clusters and metallic particles. *Faraday Discuss* 1991, 92, 31–44.
[63] Kolb DM, Ullmann R, Ziegler JC. Electrochemical nanostructuring. *Electrochim Acta* 1998, 43(19–20), 2751–60.
[64] Kolb DM, Engelmann GE, Ziegler JC. On the unusual electrochemical stability of nanofabricated copper clusters. *Angew Chem Int Ed* 2000, 39(6), 1123–25.
[65] Ng KH, Liu H, Penner RM. Subnanometer silver clusters exhibiting unexpected electrochemical metastability on graphite. *Langmuir* 2000, 16(8), 4016–23.
[66] Del Popolo MG, Leiva EPM, Mariscal M, Schmickler W. The basis for the formation of stable metal clusters on an electrode surface. *Nanotechnology* 2003, 14(9), 1009–13.
[67] Brainina KhZ, Neyman E. *V. 126. Electroanalytical Stripping Methods.* Winefordner JD, ed. New York, Wiley, 1993. p. 198.
[68] Brainina KZ, Galperin LG, Bukharinova MA, Stozhko NY. Mathematical modeling and experimental study of electrode processes. *J Solid State Electrochem* 2014, 19(2), 599–606.
[69] Brainin, KZ, Stozhko NY, Bukharinova MA, Galperin LG, Vidrevich MB, Murzakaev AM. Mathematical modeling and experimental data of the oxidation of ascorbic acid on electrodes modified by nanoparticles. *J Solid State Electrochem* 2016, 20(8), 2323–30.
[70] Cui Y, Yang C, Pu W, Oyama M, Zhang J. The influence of gold nanoparticles on simultaneous determination of uric acid and ascorbic acid. *Anal Lett* 2009, 43(1), 22–33.
[71] Kumar Jena B, Retna Raj C. Morphology dependent electrocatalytic activity of Au nanoparticles. *Electrochem Commun* 2008, 10(6), 951–4.
[72] Liu GD, Lin YY, Wu H, Lin Y. Voltammetric detection of Cr(VI) with disposable screen-printed electrode modified with gold nanoparticles. *Environ Sci Technol* 2007, 41(23), 8129–34.
[73] Saturno J, Valera D, Carrero H, Fernandez L. Electroanalytical detection of Pb, Cd and traces of Cr at micro/nano-structured bismuth film electrodes. *Sens Actuators, B* 2011, 159(1), 92–6.
[74] Lee G-J, Kim CK, Lee MK, Rhee CK. Simultaneous voltammetric determination of Zn, Cd and Pb at bismuth nanopowder electrodes with various particle size distributions. *Electroanalysis* 2010, 22(5), 530–5.
[75] Piankova LA, Malakhova NA, Stozhko NYu, Brainina KhZ, Murzakaev AM, Timoshenkova OR. Bismuth nanoparticles in adsorptive stripping voltammetry of nickel. *Electrochem Commun* 2011, 13(9), 981–4.
[76] Vikulova EV, Malakhova NA, Stozhko NYu, Kolydina LI, Brainina KhZ. Electrochemical sensor based on gold nanoparticles for determination of traces of arsenic (III) and copper (II). *Chem Sens* 2011, 1, 1–7.
[77] Mardegan A, Scopece P, Lamberti F, Meneghetti M, Moretto LM, Ugo P. Electroanalysis of trace inorganic arsenic with gold nanoelectrode ensembles. *Electroanalysis* 2012, 24(4), 798–806.
[78] Pereira FC, Moretto LM, De Leo M, Boldrin Zanoni MV, Ugo P. Gold nanoelectrode ensembles for direct trace electroanalysis of iodide. *Anal Chim Acta* 2006, 575(1), 16–24.
[79] Stradiotto NR, Toghill KE, Xiao L, Moshar A, Compton RG. The fabrication and characterization of a nickel nanoparticle modified boron doped diamond electrode for electrocatalysis of primary alcohol oxidation. *Electroanalysis* 2009, 21(24), 2627–33.
[80] Welch CM, Nekrassova O, Dai X, Hyde ME, Compton RG. Fabrication, characterisation and voltammetric studies of gold amalgam nanoparticle modified electrodes. *ChemPhysChem* 2004, 5(9), 1405–10.

[81] Malakhova NA, Stozhko NYu, Brainina KZ. Novel approach to bismuth modifying procedure for voltammetric thick film carbon containing electrodes. *Electrochem Commun* 2007, 9(2), 221–7.
[82] Kalimuthhu P, John SA. Size dependent electrocatalytic activity of gold nanoparticles immobilized onto three dimensional sol-gel network. *J Electroanal Chem* 2008, 617(2), 164–70.
[83] Hezard T, Fajerwerg K, Evrard D, Colliere V, Behra P, Gros P. Gold nanoparticles electrodeposited on glassy carbon using cyclic voltammetry: application to Hg(II) trace analysis. *J Electroanal Chem* 2012, 664, 46–52.
[84] Liu B, Lu L, Wang M, Zi Y. A study of nanostructured gold modified glassy carbon electrode for the determination of trace Cr(VI). *J Chem Sci* 2008, 120(5), 493–8.
[85] Brainina KhZ, Stozhko NYu, Shalygina ZhV. Surface microreliefs and voltage-current characteristics of gold electrodes and modified thick-film graphite-containing electrodes. *J Anal Chem* 2004, 59(8), 753–9.
[86] Huan TN, Ganesh T, Kim KS, Kim S, Han S-H, Chung H. A three-dimensional gold nanodendrite network porous structure and its application for an electrochemical sensing. *Biosens Bioelectron* 2011, 27(1), 183–6.
[87] Pierce DT, Zhao JX, eds. *Trace Analysis with Nanomaterials*. Weinheim, WILEY-VCH Verlag GmbH & Co. KGaA, 2010.
[88] Shaidarova LG, Budnikov GK. Chemically modified electrodes based on noble metals, polymer films, or their composites in organic voltammetry. *J Anal Chem* 2008, 63(10), 922–42.
[89] Zheng J, Li X, Gu R, Lu T. Comparison of the surface properties of the assembled silver nanoparticle electrode and roughened silver electrode. *J Phys Chem B* 2002, 106(5), 1019–23.
[90] Batchelor-McAuley C, Wildgoose GG, Compton RG. The contrasting behaviour of polycrystalline bulk gold and gold nanoparticle modified electrodes towards the underpotential deposition of thallium. *New J Chem* 2008, 32(6), 941–6.
[91] Campbell FW, Zhou Y-G, Compton RG. Thallium underpotential deposition on silver nanoparticles: size-dependent adsorption behavior. *New J Chem* 2010, 34(2), 187–9.
[92] Campbell FW, Compton RG. Contrasting underpotential depositions of lead and cadmium on silver macroelectrodes and silver nanoparticle electrode arrays. *Int J Electrochem Sci* 2010, 5(3), 407–13.
[93] Sudakova LA, Malakhova NA, Stozhko NY. Bismuth nanoparticles in stripping voltammetry of sulfide ions. *Electroanalysis* 2014, 26(7), 1445–8.
[94] Pal M, Ganesan V. Electrochemical determination of nitrite using silver nanoparticles modified electrode. *Analyst* 2010, *135*(10), 2711–6.
[95] Chumillas S, Busó-Rogero C, Solla-Gullón J, Vidal-Iglesias FJ, Herrero E, Feliu JM. Size and diffusion effects on the oxidation of formic acid and ethanol on platinum nanoparticles. *Electrochem Commun* 2011, 13(11), 1194–7.
[96] Huang R, Guo L-H. Lack of nano size effect on electrochemistry of dopamine at a gold nanoparticle modified indium tin oxide electrode. *Sci China: Chem* 2010, 53(8), 1778–83.
[97] Mott D, Luo J, Smith A, Njoki PN, Wang L, Zhong C-J. Nanocrystal and surface alloy properties of bimetallic gold-platinum nanoparticles. *Nanoscale Res Lett* 2007, 2(1), 12–6.
[98] Singh B, Laffir F, Dickinson C, McCormac T, Dempsey E. Carbon supported cobalt and nickel based nanomaterials for direct uric acid determination. *Electroanalysis* 2011, 23(1), 79–89.
[99] Arrigan DWM. Nanoelectrodes, nanoelectrode arrays and their applications. *Analyst* 2004, 129(12), 1157–65.
[100] De Leo M, Kuhn A, Ugo P. 3D-ensembles of gold nanowires: preparation, characterization and electroanalytical peculiarities. *Electroanalysis* 2007, 19(2–3), 227–36.
[101] Zhou Y-G, Campbell FW, Belding SR, Compton RG. Nanoparticle modified electrodes: Surface coverage effects in voltammetry showing the transition from convergent to linear diffusion.

The reduction of aqueous chromium (III) at silver nanoparticle modified electrodes. *Chem Phys Lett*, 2010, 497(4–6), 200–4.
[102] Giannetto M, Mori G, Terzi F, Zanardi C, Seeber R. Composite PEDOT/Au nanoparticles modified electrodes for determination of mercury at trace levels by anodic stripping voltammetry. *Electroanalysis* 2011, 23(2), 456–62.
[103] Malakhova NA, Mysik AA, Saraeva SYu et al. A voltammetric sensor on the basis of bismuth nanoparticles prepared by the method of gas condensation. *J Anal Chem* 2010, 65(6), 640–7.
[104] Nikolaev K, Ermakov S, Ermolenko Y, Averyaskina E, Offenhäusser A, Mourzina Y. A novel bioelectrochemical interface based on in situ synthesis of gold nanostructures on electrode surfaces and surface activation by Meerwein's salt. A bioelectrochemical sensor for glucose determination. *Bioelectrochemistry* 2015, 105, 34–43.
[105] Devnani H, Satsangee SP. Green gold nanoparticle modified anthocyanin-based carbon paste electrode for voltammetric determination of heavy metals. *Int J Environ Sci Technol* 2015, 12(4), 1269–82.
[106] Karuppiah C, Palanisamy S, Chen S-M, Emmanuel R, Muthupandi K, Prakash P. Green synthesis of gold nanoparticles and its application for the trace level determination of painter's colic. *RSC Adv* 2015, 5(21), 16284–91.
[107] Karthik R, Govindasamy M, Chen S-M, et al. Green synthesized gold nanoparticles decorated graphene oxide for sensitive determination of chloramphenicol in milk, powdered milk, honey and eye drops. *J Colloid Interface Sci* 2016, 475, 46–56.
[108] Vikesland PJ, Wigginton KR. Nanomaterial enabled biosensors for pathogen monitoring – A review. *Environ Sci Technol* 2010, 44(10), 3656–69.
[109] Aragay G, Merkoci A. Nanomaterials application in electrochemical detection of heavy metals. *Electrochim Acta* 2012, 84, 49–61.
[110] Atta NF, Galal A, Azab SM. Electrochemical determination of paracetamol using gold nanoparticles – application in tablets and human fluids. *Int J Electrochem Sci* 2011, 6(10), 5082–96.
[111] Fan Y, Liu J-H, Lu H-T, Zhang Q. Electrochemical behavior and voltammetric determination of paracetamol on Nafion/$TiO_2$-graphene modified glassy carbon electrode. *Colloids Surf B* 2011, 85(2), 289–92.
[112] Sanghavi BJ, Srivastava AK. Simultaneous voltammetric determination of acetaminophen and tramadol using Dowex50wx2 and gold nanoparticles modified glassy carbon paste electrode. *Anal Chim Acta* 2011, 706(2), 246–54.
[113] Atta NF, Galal A, Azab SM. Electrochemical morphine sensing using gold nanoparticles modified carbon paste electrode. *Int J Electrochem Sci* 2011, 6(10), 5066–81.
[114] Wei X, Wang F, Yin Y, Liu Q, Zou L, Ye B. Selective detection of neurotransmitter serotonin by a gold nanoparticle-modified glassy carbon electrode. *Analyst* 2010, 135(9), 2286–90.
[115] Mashhadizadeh MH, Khani H, Foroumadi A, Sagharichi P. Comparative studies of mercapto thiadiazoles self-assembled on gold nanoparticle as ionophores for Cu(II) carbon paste sensors. *Anal Chim Acta* 2010, 665(2), 208–14.
[116] Wang Z, Liao F, Guo T, Yang S, Zeng C. Synthesis of crystalline silver nanoplates and their application for detection of nitrite in foods. *J Electroanal Chem* 2012, 664, 135–8.
[117] Miao P, Shen M, Ning L, Chen G, Yin Y. Functionalization of platinum nanoparticles for electrochemical detection of nitrite. *Anal Bioanal Chem* 2011, 399(7), 2407–11.
[118] Xing S, Xu H, Chen J, Shi G, Jin L. Nafion stabilized silver nanoparticles modified electrode and its application to Cr(VI) detection. *J Electroanal Chem* 2011, 652(1–2), 60–5.
[119] Thiagarajan S, Tsai TH, Chen S-M. Electrochemical fabrication of nano manganese oxide modified electrode for the Detection of $H_2O_2$. *Int J Electrochem Sci* 2011, 6(6), 2235–45.
[120] Martins PR, Aparecida Rocha M, Angnes L, Eisi Toma H, Araki K. Highly sensitive amperometric glucose sensors based on nanostructured α-$Ni(OH)_2$ electrodes. *Electroanalysis* 2011, 23(11), 2541–48.

[121] Eremenko AV, Dontsova EA, Nazarov AP et al. Manganese dioxide nanostructures as a novel electrochemical mediator for thiol sensors. *Electroanalysis* 2012, 24(3), 573–80.
[122] Kalanur SS, Seetharamappa J, Prashanth SN. Voltammetric sensor for buzepide methiodide determination based on $TiO_2$ nanoparticle-modified carbon paste electrode. *Colloids Surf, B* 2010, 78(2), 217–21.
[123] Parham H, Rahbar N. Square wave voltammetric determination of methyl parathion using $ZrO_2$-nanoparticles modified carbon paste electrode. *J Hazard Mater* 2010, 177(1–3), 1077–84.
[124] Mafakheri E, Salimi A, Hallaj R, Ramazani A, Kashic MA. Synthesis of iridium oxide nanotubes by electrodeposition into polycarbonate template: fabrication of chromium(III) and arsenic(III) electrochemical sensor. *Electroanalysis* 2011, 23(10), 2429–37.
[125] Khun K, Ibupoto ZH, Ali SMU, Chey CO, Nur O, Willander M. Iron ion sensor based on functionalized ZnO nanorods. *Electroanalysis* 2012, 24(3), 521–8.
[126] Sanchez A, Morante-Zarcero S, Perez-Quintanilla D, Sierra I, Del Hierro I. Development of screen-printed carbon electrodes modified with functionalized mesoporous silica nanoparticles: application to voltammetric stripping determination of Pb(II) in non-pretreated natural waters. *Electrochim Acta* 2010, 55(23), 6983–90.
[127] Wu S, Lan X, Cui L, et al. Application of graphene for preconcentration and highly sensitive stripping voltammetric analysis of organophosphate pesticide. *Anal Chim Acta* 2011, 699(2), 170–6.
[128] Liu F, Choi KS, Park TJ, Lee SY, Seo TS. Graphene-based electrochemical biosensor for pathogenic virus detection. *BioChip J* 2011, 5(2), 123–8.
[129] Gong K, Yan Y, Zhang M, Su L, Xiong S, Mao L. Electrochemistry and electroanalytical applications of carbon nanotubes: a review. *Anal Sci* 2005, 21(12), 1383–93.
[130] Chen X, Wu G-H, Jiang Y-Q, Wang Y-R, Chen X-M. Graphene and graphene-based nanomaterials: the promising materials for bright future of electroanalytical chemistry. *Analyst* 2011, 136(22), 4631–40.
[131] Kong F-Y, Li X-R, Zhao W-W, Xu J-J, Chen H-Y. Graphene oxide-thionine-Au nanostructure composites: preparation and applications in non-enzymatic glucose sensing. *Electrochem Commun* 2012, 14(1), 59–62.
[132] Willner I, Willner B, Tel-Vered R. Electroanalytical applications of metallic nanoparticles and supramolecular nanostructures. *Electroanalysis* 2011, 23(1), 13–28.
[133] Li L, Zhang Z. Biosynthesis of gold nanoparticles using green alga Pithophora oedogonia with their electrochemical performance for determining carbendazim in soil. *Int J Electrochem Sci* 2016, 11(6), 4550–59.
[134] Gnana Kumar G, Justice Babu K, Nahm KS, Hwang YJ. A facile one-pot green synthesis of reduced graphene oxide and its composites for non-enzymatic hydrogen peroxide sensor applications. *RSCAdv* 2014, 4(16), 7944–51.
[135] Abollino O, Giacomino A, Ginepro M, Malandrino M, Zelano I. Analytical applications of a nanoparticle-based sensor for the determination of mercury. *Electroanalysis* 2012, 24(4), 727–34.
[136] Gholivand MB, Geravandi B, Parvin MH. Anodic stripping voltammetric determination of iron(II) at a carbon paste electrode modified with dithiodianiline (DTDA) and gold nanoparticles (GNP). *Electroanalysis* 2011, 23(6), 1345–51.
[137] Mashhadizadeh MH, Talemi RP. Used gold nano-particles as an on/off switch for response of a potentiometric sensor to Al(III) or Cu(II) metal ions. *Anal Chim Acta* 2011, 692(1–2), 109–15.
[138] Rajkumar M, Chiou S-C, Chen S-M, Thiagarajan S. A novel poly (taurine)/nano gold modified electrode for the determination of arsenic in various water samples. *Int J Electrochem Sci* 2011, 6(9), 3789–800.

[139] Tsai M-C, Chen P-Y. Voltammetric study and electrochemical detection of hexavalent chromium at gold nanoparticle-electrodeposited indium tinoxide (ITO) electrodes in acidic media. *Talanta* 2008, 76(3), 533–9.
[140] Tsai T-H, Lin K-C, Chen S-M. Electrochemical synthesis of poly(3,4-ethylenedioxythiophene) and gold nanocomposite and its application for hypochlorite sensor. *Int J Electrochem Sci* 2011, 6(7), 2672–87.
[141] Gholivand MB, Parvin MH. Voltammetric study of acetazolamide and its determination in human serum and urine using carbon paste electrode modified by gold nanoparticle. *J Electroanal Chem* 2011, 660(1), 163–8.
[142] Tagar ZA, Sirajuddina ZA, Memon N, et al. Selective, simple and economical lead sensor based on ibuprofen derived silver nanoparticles. *Sens Actuators, B* 2011, 157(2), 430–7.
[143] Gong J, Zhou T, Song D, Zhang L, Hu X. Stripping voltammetric detection of mercury(II) based on a bimetallic Au-Pt inorganic-organic hybrid nanocomposite modified glassy carbon electrode. *Anal Chem* 2010, 82(2), 567–73.
[144] Fenga PG, Stradiotto NR, Pividori MI. Silver nanocomposite electrode modified with hexacyanoferrate. Preparation, characterization and electrochemical behaviour towards substituted anilines. *Electroanalysis* 2011, 23(5), 1100–6.
[145] Adekunle AS, Mamba BB, Agboola BO, Ozoemena KI. Nitrite electrochemical sensor based on Prussian blue/single-walled carbon nanotubes modified pyrolytic graphite electrode. *Int J Electrochem Sci* 2011, 6(9), 4388–403.
[146] Taufik S, Yusof NA, Tee TW, Ramli I. Bismuth oxide nanoparticles/chitosan/modified electrode as biosensor for DNA hybridization. *Int J Electrochem Sci* 2011, 6(6), 1880–91.
[147] Zidan M, Tee TW, Abdullah AH, Zainal Z, Kheng GJ. Electrochemical oxidation of paracetamol mediated by nanoparticles bismuth oxide modified glassy carbon electrode. *Int J Electrochem Sci* 2011, 6(2), 279–88.
[148] Fekri MH, Khanmohammadi H, Darvishpour M. An electrochemical Cr(III)-selective sensor-based on a newly synthesized ligand and optimization of electrode with a nano particle. *Int J Electrochem Sci* 2011, 6(5), 1679–85.
[149] Zhong H, Yuan R, Chai Y, Li W, Zhang Y, Wang C. Amperometric biosensor for hydrogen peroxide based on horseradish peroxidase onto gold nanowires and $TiO_2$ nanoparticles. *Bioprocess Biosyst Eng* 2011, 34(8), 923–30.
[150] Wang G, Sun J, Zhang W, Jiao S, Fang B. Simultaneous determination of dopamine, uric acid and ascorbic acid with $LaFeO_3$ nanoparticles modified electrode. *Microchim Acta* 2009, 164(3–4), 357–62.
[151] Valentini F, Romanazzo D, Carbone M, Palleschi G. Modified screen-printed electrodes based on oxidized graphene nanoribbons for the selective electrochemical detection of several molecules. *Electroanalysis* 2012, 24(4), 872–81.
[152] Sartori ER, Fatibello-Filho O. Simultaneous voltammetric determination of ascorbic acid and sulfite in beverages employing a glassy carbon electrode modified with carbon nanotubes within a poly(allylamine hydrochloride) film. *Electroanalysis* 2012, 24(3), 627–34.
[153] Narang J, Chauhan N, Pundir CS. A non-enzymatic sensor for hydrogen peroxide based on polyaniline, multiwalled carbon nanotubes and gold nanoparticles modified Au electrode. *Analyst* 2011, 136(21), 4460–6.
[154] Li H, Xie C, Li S, Xu K. Electropolymerized molecular imprinting on gold nanoparticle-carbon nanotube modified electrode for electrochemical detection of triazophos. *Colloids Surf B* 2012, 89(1), 175–81.
[155] Guo S, Wen D, Zhai Y, Dong S, Wang E. Platinum nanoparticle ensemble-on-graphene hybrid nanosheet: one-pot, rapid synthesis, and used as new electrode material for electrochemical sensing. *ACS Nano* 2010, 4(7), 3959–68.

[156] Gholivand MB, Azadbakht A, Pashabadi A. An electrochemical sensor based on carbon nanotube bimetallic Au-Pt inorganic-organic nanofiber hybrid nanocomposite electrode applied for detection of guaifenesin. *Electroanalysis* 2011, 23(12), 2771–9.
[157] Shin S-H, Hong H-G. Anodic stripping voltammetric detection of arsenic(III) at platinum-iron(III) nanoparticle modified carbon nanotube on glassy carbon electrode. *Bull Korean Chem Soc* 2010, 31(11), 3077–83.
[158] Yari A, Papi F, Farhadi S. Voltammetric determination of trace antiepileptic gabapentin with a silver-nanoparticle modified multiwalled carbon nanotube paste electrode. *Electroanalysis* 2011, 23(12), 2949–54.
[159] Panchompoo J, Aldous L, Downing C, Crossley A, Compton RG. Facile synthesis of Pd nanoparticle modified carbon black for electroanalysis: application to the detection of hydrazine. *Electroanalysis* 2011, 23(7), 1568–78.
[160] Chen X-M, Lin Z-J, Chen D-J, et al. Nonenzymatic amperometric sensing of glucose by using palladium nanoparticles supported on functional carbon nanotubes. *Biosens Bioelectron* 2010, 25(7), 1803–8.
[161] Pham H, Bui MPN, Li CA, Han KN, Seong GH. Electrochemical patterning of palladium nanoparticles on a single-walled carbon nanotube platform and its application to glucose detection. *Electroanalysis* 2011, 23(9), 2087–93.
[162] Shamsipur M, Asgari M, Mousavi MF, Davarkhah R. A novel hydrogen peroxide sensor based on the direct electron transfer of catalase immobilized on nano-sized NiO/MWCNTs composite film. *Electroanalysis* 2012, 24(2), 357–67.
[163] Sattarahmady N, Heli H, Faramarzi F. Nickel oxide nanotubes-carbon microparticles/Nafion nanocomposite for the electrooxidation and sensitive detection of metformin. *Talanta* 2010, 82(4), 1126–35.
[164] Periasamy AP, Yang S, Chen S-M. Preparation and characterization of bismuth oxide nanoparticles-multiwalled carbon nanotube composite for the development of horseradish peroxidase based $H_2O_2$ biosensor. *Talanta* 2011, 87(1), 15–23.
[165] Wei Y, Gao C, Meng F-L et al. $SnO_2$/reduced graphene oxide nanocomposite for the simultaneous electrochemical detection of cadmium(II), lead(II), copper(II), and mercury(II): an interesting favorable mutual interference. *J Phys Chem C* 2012, 116(1), 1034–41.
[166] Hu F, Chen S, Wang C, et al. ZnO nanoparticle and multiwalled carbon nanotubes for glucose oxidase direct electron transfer and electrocatalytic activity investigation. *J Mol Catal B: Enzym* 2011, 72(3–4), 298–304.
[167] Ganjali MR, Poursaberi T, Khoobi M, et al. Copper nano-composite potentiometric sensor. *Int J Electrochem Sci* 2011, 6(3), 717–26.
[168] Ganjali MR, Alizadeh T, Azimi F, Larjani B, Faridbod F, Norouzi P. Bio-mimetic ion imprinted polymer based potentiometric mercury sensor composed of nano-materials. *Int J Electrochem Sci* 2011, 6(11), 5200–8.
[169] Sonkar PK, Ganesan V. Synthesis and characterization of silver nanoparticle-anchored amine-functionalized mesoporous silica for electrocatalytic determination of nitrite. *J Solid State Electrochem* 2015, 19(7), 2107–15.
[170] Tian Y, Liu Y, Wang W, Zhang X, Peng W. Sulfur-doped graphene-supported Ag nanoparticles for nonenzymatic hydrogen peroxide detection. *J Nanopart Res* 2015, 17(4), 193–201.
[171] Liu G-T, Chen H-F, Lin G-M, et al. One-step electrodeposition of graphene loaded nickel oxides nanoparticles for acetaminophen detection. *Biosens Bioelectron* 2014, 56, 26–32.
[172] Song H, Ni Y, Kokot S. A novel electrochemical sensor based on the copper – doped copper oxide nano – particles for the analysis of hydrogen peroxide. *Colloids Surf A* 2015, 465, 153–8.

[173] Chirizzi D, Guascito MR, Filippo E, Malitesta C, Tepore A. A novel nonenzymatic amperometric hydrogen peroxide sensor based on CuO@$Cu_2O$ nanowires embedded into poly(vinyl alcohol). *Talanta* 2016, 147, 124–31.
[174] Budnikov GK, Ziyatdinova GK, Gil'Metdinova DM. Determination of some liposoluble antioxidants by coulometry and voltammetry. *J Anal Chem* 2004, 59(7), 654–8.
[175] Ziyatdinova GK, Budnikov HC, Pogorel'tzev VI, Ganeev TS. The application of coulometry or total antioxidant capacity determination of human blood. *Talanta* 2006, 68(3), 800–5.
[176] Ziyatdinova GK, Budnikov GK, Samigullin AI, Gabdullina GT, Sofronov AV, Al'Metkina LA, et al. Electrochemical determination of synthetic antioxidants of bisdithiophosphonic acids. *J Anal Chem* 2010, 65(12), 1273–9.
[177] Shpigun LK, Arharova MA, Brainina KZ, Ivanova AV. Flow injection potentiometric determination of total antioxidant activity of plant extracts. *Anal Chim Acta* 2006, 573–574, 419–26.
[178] Brainina KhZ, Alyoshina LV, Gerasimova EL, Kazakov YaE, Ivanova AV, Beykinc YaB, et al. New electrochemical method of determining blood and blood fractions antioxidant activity. *Electroanalysis* 2009, 21(3–5), 618–24.
[179] Шарафутдинова ЕН, Иванова АВ, Матерн АИ, Брайнина Х3. Качество пищевых продуктовиантиоксидантная активность. *Аналитика и контроль* 2011, 15(3), 281–6 (Sharafutdinova EN, Ivanova AV, Matern AI, Brainina KhZ. Food quality and antioxidant activity. Anal Control 2011, 15(3), 281–6, original source in Russian).
[180] Плотников ЕВ, Короткова ЕИ, Дорожко ЕВ, Букель М, Линерт В. Исследование суммарной антиоксидантной активности сыворотки крови человека в норме и патологии алкоголизма методом вольтамперометрии. *Заводск лаб. Диагностика матер* 2009, 75(12), 14–7. (Plotnikov EV, Korotkova EI, Dorozhko EV, Bukel' M, Linert V. The study of the total antioxidant activity of human blood serum in norm and the pathology of alcoholism by the voltammetry method. Factory lab. Diagn Mater 2009, 75(12), 14–7, original source in Russian).
[181] Сажина НН, Мисин ВМ, Короткова ЕИ. Исследование антиоксидантных свойств водного экстракта мяты электрохимическими методами. *Химия растительного сырья* 2010, 4, 77–82. (Sazhina NN, Misin VM, Korotkova EI. Research of antioxidant properties of water extract of mint by electrochemical methods. Chem Plant Raw Mater 2010, 4, 77–82, original source in Russian).
[182] Hu W, Sun D, Ma W. Silver doped poly(L-valine) modified glassy carbon electrode for the simultaneous determination of uric acid, ascorbic acid and dopamine. *Electroanalysis* 2010, 22(5), 584–9.
[183] Lin Y, Hu Y, Long Y, Di J. Determination of ascorbic acid using an electrode modified with cysteine self-assembled gold-platinum nanoparticles. *Microchim Acta* 2011, 175(3–4), 259–64.
[184] Tavakkoli N, Nasrollahi S, Vatankhah G. Electrocatalytic determination of ascorbic acid using a palladium coated nanoporous gold film electrode. *Electroanalysis* 2012, 24(2), 368–75.
[185] Mazloum-Ardakani M, Sheikh-Mohseni MA, Beitollahi H, Benvidi A, Naeimi H. Electrochemical determination of vitamin C in the presence of uric acid by a novel $TiO_2$ nanoparticles modified carbon paste electrode. *Chin Chem Lett* 2010, 21(12), 1471–4.
[186] Atta NF, El-Kady MF, Galal A. Simultaneous determination of catecholamines, uric acid and ascorbic acid at physiological levels using poly(N-methylpyrrole)/Pd-nanoclusters sensor. *Anal Biochem* 2010, 400(1), 78–88.
[187] Dursun Z, Gelmez B. Simultaneous determination of ascorbic acid, dopamine and uric acid at Pt nanoparticles decorated multiwall carbon nanotubes modified GCE. *Electroanalysis* 2010, 22(10), 1106–14.
[188] Li J, Lin X-Q. Electrodeposition of gold nanoclusters on overoxidized polypyrrole film modified glassy carbon electrode and its application for the simultaneous determination of epinephrine and uric acid under coexistence of ascorbic acid. *Anal Chim Acta* 2007, 596(2), 222–30.

[189] Harish S, Mathiyarasu J, Phani KLN, Yegnaraman V. PEDOT/Palladium composite material: synthesis, characterization and application to simultaneous determination of dopamine and uric acid. *J Appl Electrochem* 2008, 38(11), 1583–8.
[190] Shaidarova LG, Chelnokova IA, Romanova EI, Gedmina AV, Budnikov GK. Joint voltammetric determination of dopamine and uric acid. *Russ J Appl Chem* 2011, 84(2), 218–24.
[191] Wang S, Xu Q, Liu G. Differential pulse voltammetric determination of uric acid on carbon-coated iron nanoparticle modified glassy carbon electrodes. *Electroanalysis* 2008, 20(10), 1116–20.
[192] Ulubay S, Dursun Z. Cu nanoparticles incorporated polypyrrole modified GCE for sensitive simultaneous determination of dopamine and uric acid. *Talanta* 2010, 80(3), 1461–66.
[193] MA Tehrani R, Ab Ghani S. Voltammetric analysis of uric acid by zinc-nickel nanoalloy coated composite graphite. *Sens Actuators B* 2010, 145(1), 20–4.
[194] Fang B, Feng Y, Wang G, Zhang C, Gu A, Liu M. A uric acid sensor based on electrodeposition of nickel hexacyanoferrate nanoparticles on an electrode modified with multi-walled carbon nanotubes. *Microchim Acta* 2011, 173(1–2), 27–32.
[195] Habibi B, Pezhhan H, Pournaghi-Azar MH. Voltammetric and amperometric determination of uric acid at a carbon-ceramic electrode modified with multi walled carbon nanotubes. *Microchim Acta* 2010, 169(3), 313–20.
[196] Ardakani MM, Mohseni MAS, Beitollahi H, Benvidi A, Naeimi H. Simultaneous determination of dopamine, uric acid, and folic acid by a modified $TiO_2$ nanoparticles carbon paste electrode *Turk J Chem* 2011, 35(4), 573–85.
[197] Curulli A, DiCarlo G, Ingo GM, Riccucci C, Zane D, Bianchini C. Chitosan stabilized gold nanoparticle-modified Au electrodes for the determination of polyphenol index in wines: a preliminary study. *Electroanalysis* 2012, 24(4), 897–904.
[198] Sun J-Y, Huang K-J, Wei S-Y, Wu Z-W, Ren F-P. A graphene-based electrochemical sensor for sensitive determination of caffeine. *Colloids Surf B* 2011, 84(2), 421–6.
[199] Souza LP, Calegari F, Zarbin AJG, Marcolino-Junior LH, Bergamini MF. Voltammetric determination of the antioxidant capacity in wine samples using a carbon nanotube modified electrode. *J Agric Food Chem* 2011, 59(14), 7620–5.
[200] Wang G, Liu M, Wang G et al. Preparation of CuO-Nanoparticle-modified electrode and its application in the determination of rutin. *Anal Lett* 2009, 42(8), 1084–93.
[201] Wei Y, Wang G, Li M, Wang C, Fang B. Determination of rutin using a $CeO_2$ nanoparticle-modified electrode. *Microchim Acta* 2007, 158(3–4), 269–74.
[202] Yin H, Zhou Y, Cui L, et al. Sensitive voltammetric determination of rutin in pharmaceuticals, human serum, and traditional Chinese medicines using a glassy carbon electrode coated with graphene nanosheets, chitosan, and a poly (amido amine) dendrimer. *Microchim Acta* 2011, 173(3–4), 337–45.
[203] Wang M, Zhang D, Tong Z, Xu X, Yang X. Voltammetric behavior and the determination of quercetin at a flowerlike $Co_3O_4$ nanoparticles modified glassy carbon electrode. *J Appl Electrochem* 2011, 41(2), 189–96.
[204] Brondani D, Vieira IC, Piovezan C et al. Sensor for fisetin based on gold nanoparticles in ionic liquid and binuclear nickel complex immobilized in silica. *Analyst* 2010, 135(5), 1015–22.
[205] Huo Z, Zhou Y, Liu Q, He X, Liang Y, Xu M. Sensitive simultaneous determination of catechol and hydroquinone using a gold electrode modified with carbon nanofibers and gold nanoparticles. *Microchim Acta* 2011, 173(1–2), 119–25.
[206] Chee SY, Flegel M, Pumera M. Regulatory peptides desmopressin and glutathione voltammetric determination on nickel oxide modified electrodes. *Electrochem Commun* 2011, 13(9), 963–5.

[207] Safavi A, Maleki N, Farjami E, Mahyari FA. Simultaneous electrochemical determination of glutathione and glutathione disulfide at a nanoscale copper hydroxide composite carbon ionic liquid electrode. *Anal Chem* 2009, 81(18), 7538–43.
[208] Sattarahmady N, Heli H. An electrocatalytic transducer for l-cysteine detection based on cobalt hexacyanoferrate nanoparticles with a core-shell structure. *Anal Biochem* 2011, 409(1), 74–80.
[209] Mazloum-Ardakani M, Beitollahi H, Taleat Z, Salavati-Niasari M. Fabrication and characterization of molybdenum(VI) complex-$TiO_2$ nanoparticles modified electrode for the electrocatalytic determination of L-cysteine. *J Serb Chem Soc* 2011, 76(4), 575–89.
[210] Majidi MR, Asadpour-Zeynali K, Hafezi B. Sensing L-cysteine in urine using a pencil graphite electrode modified with a copper hexacyanoferrate nanostructure. *Microchim Acta* 2010, 169(3), 283–8.
[211] Zare HR, Chatraei F. Preparation and electrochemical characteristics of electrodeposited acetaminophen on ruthenium oxide nanoparticles and its role as a sensor for simultaneous determination of ascorbic acid, dopamine and N-acetyl-l-cysteine. *Sens Actuators B* 2011, 160(1), 1450–7.
[212] Kannan P, Chen H, Lee VT-W, Kim D-H. Highly sensitive amperometric detection of bilirubin using enzyme and gold nanoparticles on sol-gel film modified electrode. *Talanta* 2011, 86(1), 400–7.
[213] Usman Ali SM, Ibupoto ZH, Chey CO, Nur O, Willander M. Functionalized ZnO nanotube arrays for the selective determination of uric acid with immobilized uricase. *Chem Sens* 2011, 19, 1–8.
[214] Yola ML, Gupta VK, Eren T, Şen AE, Atar N. A novel electroanalytical nanosensor based on graphene oxide/silver nanoparticles for simultaneous determination of quercetin and morin. *Electrochim Acta 2014*, 120, 204–11.
[215] Mpanza T, Sabela MI, Mathenjwa SS, Kanchi S, Bisetty K. Electrochemical determination of capsaicin and silymarin using a glassy carbon electrode modified by gold nanoparticle decorated multiwalled carbon nanotubes. *Anal Lett* 2014, 47(17), 2813–28.
[216] Zhou J, Zhang K, Liu J, Song G, Ye B. A supersensitive sensor for rutin detection based on multi-walled carbon nanotubes and gold nanoparticles modified carbon paste electrodes. *Anal Methods* 2012, 4(5), 1350–6.
[217] Huang L, Hou K, Jia X, Pan H, Du M. Preparation of novel silver nanoplates/graphene composite and their application in vanillin electrochemical detection. *Mater Sci Eng C* 2014, 38(1), 39–45.
[218] Silva TR, Brondani D, Zapp E, Vieira IC. Electrochemical sensor based on gold nanoparticles stabilized in poly(allylamine hydrochloride) for determination of vanillin. *Electroanalysis* 2015, 27(2), 465–72.
[219] Shang L, Zhao F, Zeng B. Sensitive voltammetric determination of vanillin with an AuPd nanoparticles-graphene composite modified electrode. *Food Chem* 2014, 151, 53–7.
[220] Liu B, Luo L, Ding Y, et al. Differential pulse voltammetric determination of ascorbic acid in the presence of folic acid at electro-deposited NiO/graphene composite film modified electrode. *Electrochim Acta* 2014, 142, 336–42.
[221] Lin X, Ni Y, Kokot S. Glassy carbon electrodes modified with gold nanoparticles for the simultaneous determination of three food antioxidants. *Anal Chim Acta* 2013, 765, 54–62.
[222] Ziyatdinova G, Ziganshina E, Cong PN, Budnikov HK. Voltammetric determination of thymol in oregano using $CeO_2$-modified electrode in Brij® 35 micellar medium. *Food Anal Methods* 2017, 10(1), 129–36.
[223] Palanisamy S, Karuppiah C, Chen S-M et al. Selective and simultaneous determination of dihydroxybenzene isomers based on green synthesized gold nanoparticles decorated reduced graphene oxide. *Electroanalysis* 2015, 27(5), 1144–51.

[224] Ananthi A, Kumar SS, Phani KL. Facile one-step direct electrodeposition of bismuth nanowires on glassy carbon electrode for selective determination of folic acid. *Electrochim Acta* 2015,151,584–90.
[225] Vilian ATE, Chen SM. Preparation of carbon nanotubes decorated with manganese dioxide nanoparticles for electrochemical determination of ferulic acid. *Microchim Acta* 2015, 182(5–6), 1103–11.
[226] Zhang H, Huang F, Xu S, Xia Y, Huang W, Li Z. Fabrication of nanoflower-like dendritic Au and polyaniline composite nanosheets at gas/liquid interface for electrocatalytic oxidation and sensing of ascorbic acid. *Electrochem Commun* 2013, 30, 46–50.
[227] Ponnusamy VK, Mani V, Chen SM, Huang WT, Jen JF. Rapid microwave assisted synthesis of graphene nanosheets/ polyethyleneimine/gold nanoparticle composite and its application to the selective electrochemical determination of dopamine. *Talanta* 2014, 120, 148–57.
[228] Song J, Xu L, Xing R, Li Q, Zhou C, Liu D, Song H. Synthesis of Au/graphene oxide composites for selective and sensitive electrochemical detection of ascorbic acid. *Sci Rep* 2014, 4, 1–5.
[229] Vinoth V, Wu JJ, Asiri AM, Anandan S. Simultaneous detection of dopamine and ascorbic acid using silicate network interlinked gold nanoparticles and multi-walled carbon nanotubes. *Sens Actuators, B* 2015, 210, 731–41.
[230] Shaidarova LG, Chelnokova IA, Degtev MA, et al. Amperometric detection under batch-injection analysis conditions of caffeine on an electrode modified by mixed-valence iridium and ruthenium oxides. *Pharm Chem J* 2016, 49(10), 711–4.
[231] Çakır S, Biçer E, Arslan EY. A newly developed electrocatalytic oxidation and voltammetric determination of curcumin at the surface of PdNp-graphite electrode by an aqueous solution process with $Al^{3+}$. *Croat Chem Acta* 2015, 88(2), 105–12.
[232] Cheraghi S, Taher MA, Karimi-Maleh H. Fabrication of fast and sensitive nanostructure voltammetric sensor for determination of curcumin in the presence of vitamin B9 in food samples. *Electroanalysis* 2016, 28(10), 2590–7.
[233] Lin X, Ni Y, Kokot S. Electrochemical mechanism of eugenol at a Cu doped gold nanoparticles modified glassy carbon electrode and its analytical application in food samples. *Electrochim Acta* 2014, 133, 484–91.
[234] Ibrahim H, Temerk Y. Novel sensor for sensitive electrochemical determination of luteolin based on $In_2O_3$ nanoparticles modified glassy carbon paste electrode. *Sens Actuat B* 2015, 206, 744–52.
[235] Guivar JAR, Sanches EA, Magon CJ, Fernandes EGR. Preparation and characterization of cetyltrimethylammonium bromide (CTAB)-stabilized $Fe_3O_4$ nanoparticles for electrochemistry detection of citric acid. *J Electroanal Chem* 2015, 755, 158–66.
[236] Cao X, Ye Y, Liu S. Gold nanoparticle-based signal amplification for biosensing. *Anal Biochem* 2011, 417(1), 1–16.
[237] Ravalli A, Marrazza G. Gold and magnetic nanoparticles-based electrochemical biosensors for cancer biomarker determination. *J Nanosci Nanotechnol* 2015, 15(5), 3307–19.
[238] Kumar S, Ahlawat W, Kumar R, Dilbaghi N. Graphene, carbon nanotubes, zinc oxide and gold as elite nanomaterials for fabrication of biosensors for healthcare. *Biosens Bioelectron* 2015, 70, 498–503.
[239] Huang K-J, Sun J-Y, Xu C-X, Niu D-J, Xie W-Z. A disposable immunosensor based on gold colloid modified chitosan nanoparticles-entrapped carbon paste electrode. *Microchim Acta* 2010, 168(1–2), 51–8.
[240] Zhang S, Zheng F, Wu Z, Shen G, Yu R. Highly sensitive electrochemical detection of immunospecies based on combination of Fc label and PPD film/gold nanoparticle amplification. *Biosens Bioelectron* 2008, 24(1), 129–35.

[241] Mao X, Jiang J, Luo Y, Shen G, Yu R. Copper-enhanced gold nanoparticle tags for electrochemical stripping detection of human IgG. *Talanta* 2007, 73(3), 420–24.
[242] Mao X, Jiang J, Chen J, Huang Y, Shen G, Yu R. Cyclic accumulation of nanoparticles: A new strategy for electrochemical immunoassay based on the reversible reaction between dethiobiotin and avidin. *Anal Chim Acta* 2006, 557(1–2), 159–63.
[243] Li J, Gao H. A renewable potentiometric immunosensor based on $Fe_3O_4$ nanoparticles immobilized anti-IgG. *Electroanalysis* 2008, 20(8), 881–7.
[244] de la Escosura-Muñiz A, Ambrosi A, Alegret S, Merkoçi A. Electrochemical immunosensing using micro and nanoparticles. *Methods Mol Bio* (Clifton, N.J.) 2009, 504, 145–55.
[245] Mao X, Jiang J, Huang Y, Shen G, Yu R. Gold nanoparticle accumulation using magnetic particles: a new strategy for electrochemical immunoassay based on the reversible reaction between dethiobiotin and avidin. *Sens Actuators, B* 2007, 123(1), 198–203
[246] Wang L, Jia X, Zhou Y, Xie Q, Yao S. Sandwich-type amperometric immunosensor for human immunoglobulin G using antibody-adsorbed Au/$SiO_2$ nanoparticles. *Microchim Acta* 2010, 168(3), 245–51.
[247] Zhang L, Liu Y, Chen T. Label-free amperometric immunosensor based on antibody immobilized on a positively charged gold nanoparticle/l-cysteine-modified gold electrode. *Microchim Acta* 2009, 164(1–2), 161–6.
[248] Ambrosi A, Castaneda MT, Killard AJ, Smyth MR, Alegret S, Merkoci A. Double-codified gold nanolabels for enhanced immunoanalysis. *Anal Chem* 2007, 79(14), 5232–40.
[249] Dequaire M, Degrand C, Limoges B. An electrochemical metalloimmunoassay based on a colloidal gold label. *Anal Chem* 2000, 72(22), 5521–8.
[250] Chumbimuni-Torres KY, Dai Z, Rubinova N et al. Potentiometric biosensing of proteins with ultrasensitive ion-selective microelectrodes and nanoparticle labels. *J Am Chem Soc* 2006, 128(42), 13676–7.
[251] Pal S, Alocilja EC. Electrically active magnetic nanoparticles as novel concentrator and electrochemical redox transducer in Bacillus anthracis DNA detection. *Biosens Bioelectron* 2010, 26(4), 1624–30.
[252] Brainina KZ, Kozitsina AN, Glazyrina YA. Hybrid electrochemical/magnetic assay for Salmonella typhimurium detection. *IEEE Sens J* 2010, 10(11), 1699–704.
[253] Dungchai W, Siangproh W, Chaicumpa W, Tongtawe P, Chailapakul O. Salmonella typhi determination using voltammetric amplification of nanoparticles: a highly sensitive strategy for metalloimmunoassay based on a copper-enhanced gold label. *Talanta* 2008, 77(2), 727–32.
[254] Cheng Y-X, Liu Y-J, Huang J-J, et al. Platinum nanoparticles modified electrode for rapid electrochemical detection of Escherichia coli. *Chin J Chem* 2008, 26(2), 302–6.
[255] De Souza Castilho M, Laube T, Yamanaka H, Alegret S, Pividori MI. Magneto immunoassays for plasmodium falciparum histidine-rich protein 2 related to malaria based on magnetic nanoparticles. *Anal Chem* 2011, 83(14), 5570–7.
[256] Setterington EB, Alocilja EC. Electrochemical biosensor for rapid and sensitive detection of magnetically extracted bacterial pathogens. *Biosensors* 2012, 2(1), 15–31.
[257] Tang D, Tang J, Su B, Chen G. Ultrasensitive electrochemical immunoassay of staphylococcal enterotoxin B in food using enzyme-nanosilica-doped carbon nanotubes for signal amplification. *J Agric Food Chem* 2010, 58(20), 10824–30.
[258] Tang D, Yuan R, Chai Y, Liu Y, Dai J, Zhong X. Novel potentiometric immunosensor for determination of diphtheria antigen based on compound nanoparticles and bilayer two-dimensional sol-gel as matrices. *Anal Bioanal Chem* 2005, 381(3), 674–80.
[259] Shen G, Zhang Y. Highly sensitive electrochemical stripping detection of hepatitis B surface antigen based on copper-enhanced gold nanoparticle tags and magnetic nanoparticles. *Anal Chim Acta* 2010, 674(1), 27–31.

[260] Tang D, Yuan R, Chai Y, Zhong X, Liu Y, Dai J. Electrochemical detection of hepatitis B surface antigen using colloidal gold nanoparticles modified by a sol-gel network interface. *Clinical. Biochem* 2006. 39(3), 309–14.
[261] Wu S, Zhong Z, Wang D et al. Gold nanoparticle-labeled detection antibodies for use in an enhanced electrochemical immunoassay of hepatitis B surface antigen in human serum. *Microchim Acta* 2009, 166(3–4), 269–75.
[262] Yuan R, Tang D, Chai Y, Zhong X, Liu Y, Dai J. Ultrasensitive potentiometric immunosensor based on SA and OCA techniques for immobilization of HBsAb with colloidal Au and polyvinyl butyral as matrixes. *Langmuir* 2004, 20(17), 7240–5.
[263] Lin J, He C, Pang X, Hu K. Amperometric immunosensor for prostate specific antigen based on gold nanoparticles/ionic liquid/chitosan hybrid film. *Anal Lett* 2011, 44(5), 908–21.
[264] Lin J, He C, Zhang L, Zhang S. Sensitive amperometric immunosensor for α-fetoprotein based on carbon nanotube/gold nanoparticle doped chitosan film. *Anal Biochem* 2009, 384(1), 130–5.
[265] Li N, Yuan R, Chai Y, Chen S, An H, Li W. New antibody immobilization strategy based on gold nanoparticles and Azure I/multi-walled carbon nanotube composite membranes for an amperometric enzyme immunosensor. *J Phys Chem C* 2007, 111(24), 8443–50.
[266] Ho JA, Chang H-C, Shih N-Y et al. Diagnostic detection of human lung cancer-associated antigen using a gold nanoparticle-based electrochemical immunosensor. *Anal Chem* 2010, 82(14), 5944–50.
[267] Serafin V, Eguilaz M, Agui L, Yanez-Sedeno P, Pingarron JM. An electrochemical immunosensor for testosterone using gold nanoparticles – carbon nanotubes composite electrodes. *Electroanalysis* 2011, 23(1), 169–76.
[268] Zhang Y, Xiang Y, Chai Y, et al. Gold nanolabels and enzymatic recycling dual amplification-based electrochemical immunosensor for the highly sensitive detection of carcinoembryonic antigen. *Sci. China: Chem* 2011, 54(11), 1770–6.
[269] Tang D, Yuan R, Chai Y. Ultrasensitive electrochemical immunosensor for clinical immunoassay using thionine-doped magnetic gold nanospheres as labels and horseradish peroxidase as enhancer. *Anal Chem* 2008, 80(5), 1582–8.
[270] West N, Baker PGL, Arotiba OA, et al. Overoxidized polypyrrole incorporated with gold nanoparticles as platform for impedimetric anti-transglutaminase immunosensor. *Anal Lett* 2011, 44(11), 1956–66.
[271] Kannan P, Tiong HY, Kim D-H. Highly sensitive electrochemical determination of neutrophil gelatinase-associated lipocalin for acute kidney injury. *Biosens Bioelectron* 2012, 31(1), 32–6.
[272] Zhang J, Lei J, Pan R, Leng C, Hu Z, Ju H. In situ assembly of gold nanoparticles on nitrogen-doped carbon nanotubes for sensitive immunosensing of microcystin-LR. *Chem Commun* 2011, 47(2), 668–70.
[273] Liu G, Wang J, Kim J, Jan MR, Collins GE. Electrochemical coding for multiplexed immunoassays of proteins. *Anal Chem* 2005, 76(23), 7126–30.
[274] Lai G, Yan F, Wu J, Leng C, Ju H. Ultrasensitive multiplexed immunoassay with electrochemical stripping analysis of silver nanoparticles catalytically deposited by gold nanoparticles and enzymatic reaction. *Anal Chem* 2011, 83(7), 2726–32.
[275] Tang J, Tang D, Niessner R, Chen G, Knopp D. Magneto-controlled graphene immunosensing platform for simultaneous multiplexed electrochemical immunoassay using distinguishable signal tags. *Anal Chem* 2011, 83(13), 5407–14.
[276] Afonso AS, Perez-Lopez B, Faria RC, et al. Electrochemical detection of Salmonella using gold nanoparticles. *Biosens Bioelectron* 2013, 40(1), 121–6.
[277] Chen G-Z, Yin Z-Z, Lou J-F. Electrochemical immunoassay of Escherichia coli O157:H7 using Ag@$SiO_2$ nanoparticles as labels. *J Anal Methods Chem* 2014, 2014, 231–45.

[278] Zhang X, Zhang F, Zhang H, Shen J, Han E, Dong X. Functionalized gold nanorod-based labels for amplified electrochemical immunoassay of E. coli as indicator bacteria relevant to the quality of dairy product. *Talanta* 2015, 132, 600–5.
[279] Vikesland PJ, Wigginton KR. Nanomaterial enabled biosensors for pathogen monitoring – A review. *Environ Sci Technol* 2010, 44(10), 3656–69.
[280] Wu L, Gao B, Zhang F, Sun X, Zhang Y, Li Z. A novel electrochemical immunosensor based on magnetosomes for detection of staphylococcal enterotoxin B in milk. *Talanta* 2013, 106, 360–6.
[281] Kozitsina A, Svalova T, Malysheva N, Glazyrina Y, Matern A. A new enzyme-free electrochemical immunoassay for Escherichia coli detection using magnetic nanoparticles. *Anal Lett* 2016, 49(2), 245–57.
[282] Ibii T, Kaieda M, Hatakeyama S, et al. Direct immobilization of gold-binding antibody fragments for immunosensor applications. *Anal Chem* 2010, 82(10), 4229–35.
[283] Gu H-Y, Yu A-M, Chen H-Y. Direct electron transfer and characterization of hemoglobin immobilized on a Au colloid-cysteamine-modified gold electrode. *J Electroanal Chem* 2001, 516(1–2), 119–26.
[284] Luo X, Morrin A, Killard AJ, Smyth MR. Application of nanoparticles in electrochemical sensors and biosensors. *Electroanalysis* 2006, 18(4), 319–26.
[285] Presnova GV, Rubtsova MYu, Shumyantseva VV, Bulko TV, Egorov AM. Comparative immobilization of antibodies on modified screen-printed graphite electrodes. *Moscow Univ Chem Bull (Engl transl)* 2008, 63(2), 71–4.
[286] Varshney M, Yang L, Su X-L, Li Y. Magnetic nanoparticle-antibody conjugates for the separation of Escherichia coli O157:H7 in ground beef. *J Food Prot* 2005, 68(9), 1804–11.
[287] Биосенсоры: основы и приложения. Под ред. Э. Тёрнера, И. Карубе, Дж. Уилсона. М.: Мир, 1992. 614 с. (Turner A, Karube I, Wilson G, eds. Biosensors: Fundamentals and Applications. Moscow, Mir, 1992, 614, original source in Russian).
[288] Muzyka K. Current trends in the development of the electrochemiluminescent immunosensors. *Biosens Bioelectron* 2014, 54, 393–407.
[289] Ravalli A, Marrazza G. Gold and magnetic nanoparticles-based electrochemical biosensors for cancer biomarker determination. *J Nanosci Nanotechnol*. 2015, 15(5), 3307–19.
[290] Kumar S, Ahlawat W, Kumar R, Dilbaghi N. Graphene, carbon nanotubes, zinc oxide and gold as elite nanomaterials for fabrication of biosensors for healthcare. *Biosens Bioelectron* 2015, 70, 498–503.
[291] Sharma A, Rao VK, Kamboj DV, Gaur R, Upadhyay S, Shaik M. Relative efficiency of zinc sulfide (ZnS) quantum dots (QDs) based electrochemical and fluorescence immunoassay for the detection of Staphylococcal enterotoxin B (SEB). *Biotechnol Rep 2015*, 6, 129–36.
[292] Brainina K, Kozitsina A, Beikin J. Electrochemical immunosensor for Forest-Spring encephalitis based on protein a labeled with colloidal gold. *Anal Bional Chem* 2003, 376(4), 481–5.
[293] Park H-Y, Schadt MJ, Wang L, et al. Fabrication of magnetic core @Shell Fe Oxide@ Au nanoparticles for interfacial bioactivity and bio-separation. *Langmuir* 2007, 23(17), 9050–6.
[294] Tamer U, Gundogdu Y, Boyaci IH, Pekmez K. Synthesis of magnetic core-shell $Fe_3O_4$-Au nanoparticle for biomolecule immobilization and detection. *J Nanopart Res* 2010, 12(4), 1187–96.

G. Ziyatdinova and H. Budnikov

# 7 Carbon Nanomaterials and Surfactants as Electrode Surface Modifiers in Organic Electroanalysis

## 7.1 Introduction

Electrochemical activity as response of the electrode depends on the nature of its surface. In order to improve the response parameters, chemically modified electrodes became a high grown area in the modern electroanalysis in particular voltammetry. In comparison to conventional solid electrodes, the control of the electrode characteristics and reactivity is realized by surface modification. The physicochemical properties of the modifier are transferred to the electrode surface via immobilization. The goals of electrode surface modification are acceleration of electron transfer reactions, chemical reactions at the electrode surface (e. g., preconcentration reactions by attaching ligands), changing transport properties to the electrode surface, creation of the selective membrane permeation, and decrease of the interfering effects [1, 2]. The last ones are especially important for the analysis of samples with complex matrix like foodstuff, pharmaceutical dosage forms, plant materials, and biomaterials. In general, the choice of sufficient modifier allows controlling the analytical signal, its sensitivity and selectivity, that is, the analytical characteristics of target analyte determination [3, 4].

The electrode surface modification can be realized by different approaches using chemical reagents or biomaterials. The most common ways of modification are:

a) irreversible adsorption on the electrode surface;
b) chemical interaction via spacers or linkers with covalent bond formation;
c) polymeric film coating;
d) self-organized monolayer formation;
e) inclusion of the modifier in the composite volume or graphite paste (also using screen-printed technology);
f) formation of modifier on the electrode surface using sol–gel technology;
g) coating of molecularly imprinted materials (porous polymers or other materials providing “host–guest” recognition of the analyte).

These approaches are discussed in details in [5]. Thus, the main advantages of modified electrodes are decrease of analyte oxidation/reduction potentials, increase of the determination selectivity, and sensitivity due to the decrease of so-called “chemical noise” that is important for the analysis of samples with the complex matrix. The limits of detection at almost pM level can be achieved using some types of chemically

https://doi.org/10.1515/9783110542011-007

modified electrodes, in particular under pulse modes of voltammetry in combination with preconcentration step.

Different types of nanomaterials are one of the most widely used types of modifiers applied as far as provide new properties of the electrode due to their structural and size effects. Nanostructured surface is caused by the unique properties of the nanomaterials applied and the possibility to control the morphology of the electrode interface at the nanoscale. Carbon nanomaterials as a new form of carbon became a highly investigated type of electrode surface modifier since last decades due to their unique structure, physical and chemical properties, and biocompatibility [6–8]. Carbon nanomaterial-based electrodes show important advantages in comparison with other material electrodes, in particular high surface area, a wide working potential window in both aqueous and nonaqueous media, high electrocatalytic activity toward different redox-active systems, and chemical inertness. Moreover, the surface of carbon nanomaterials can be further functionalized, that is, it can be considered as a platform for further incorporation of other modifiers enhancing the application area of the electrodes created [9, 10].

## 7.2 Carbon nanomaterial-based electrodes

Carbon nanotubes (CNTs), fullerenes, and graphene are the most commonly used carbon nanomaterials. Electrodes modified with carbon nanomaterials show enhanced electronic properties, a large-edge plane/basal plane ratio, and higher rate of electron transfer reactions [11, 12]. Thus, carbon nanomaterial-based electrodes have higher sensitivities in a low concentration or in the complex matrix, lower limits of detection, and faster electron transfer kinetics in comparison to traditional carbon electrodes. Electrode performance is strongly influenced by the type and pretreatment way of the carbon nanomaterials, their surface modification, the electrode attachment method, and the addition of electron mediators. These factors allow finding the optimal conditions of electrode response for the target analyte.

### 7.2.1 Graphene

Graphene and its derived structures (graphene oxide, graphene platelets, and graphene nanoflakes) are very popular and intensively used carbon nanomaterials in electroanalysis. It is an allotropic form of carbon and consists of single-layer two-dimensional $sp^2$-hybridized carbon. Graphene is a single-atom thick sheet of carbon atoms arrayed in a honeycomb crystal lattice. Showing outstanding characteristics such as a large specific surface area, excellent conductivity, and

strong mechanical strength, graphene is found out as an universal modifier of the electrode surface [13]. Depending on the number of the stacked layers, graphene can be classified as single-layered, few-layered (2–10 layers), and multilayered called as thin graphite [14]. Typical properties of graphene are retained for the single- or few-layer morphologies only [15]. Graphene exhibits the advantages of a large surface area (2630 $m^2/g$ for single-layer graphene) and a small size of each individual unit. In general, it can be considered as a mother of all graphitic forms (Fig. 7.1), including zero-dimensional fullerenes, one-dimensional CNT, and three-dimensional graphite [16, 17].

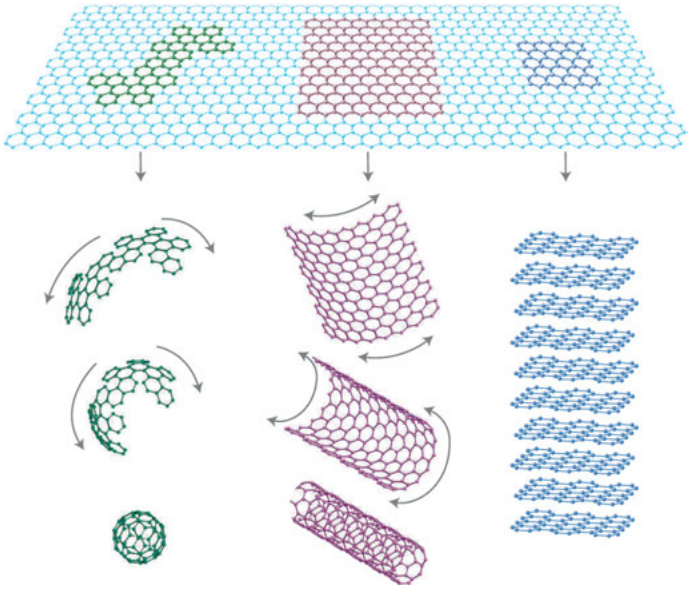

**Fig. 7.1:** Graphene is the mother of all graphitic forms. Reprinted with permission from ref. 16. Copyright 2007 Nature Publishing Group.

Graphene is an attractive material from the electroanalytical point of view due to its properties such as high conductivity, wide electrochemical potential window, and low electrical resistance in comparison to glassy carbon electrodes (GCEs), atomic thickness, and well-defined redox peaks. Peak-to-peak potential separation under conditions of cyclic voltammetry (CV) is low, suggesting rapid electron transfer kinetics, and its apparent electron transfer rate is orders of magnitude higher than that of GCE. Moreover, the electron transfer rate is surface dependent and increased significantly by the introduction of a high-density edge-plane defect sites on graphene surface providing multiple electrochemically active sites [18]. As known [19, 20], the

edges of graphene sheets possess a variety of the oxygenated species that can support efficient electrical wiring of the redox centers of molecules to the electrode and also enhance the adsorption and desorption of molecules.

Most of graphene used in electrochemistry is produced from graphene oxide (GO) by chemical/thermal or electrochemical reduction. GO structure is not fully planar due to the damage of the $sp^2$ carbon network. It contains large number of oxygen-containing groups that can facilitate further functionalization of the material. Graphene obtained by chemical/thermal reduction of GO is called chemically reduced GO (CRGO). Usually, it has abundant structural defects and functional groups, which are advantageous for electrochemical applications. Electrochemically reduced GO (ERGO) exhibits much better performance for electrochemical applications than CRGO [18].

Graphene-modified electrodes have been widely used in the electroanalysis of organic substances (Tab. 7.1).

Graphene being highly hydrophobic material is insoluble in a majority of the solvents. Therefore, it is usually functionalized through noncovalent modification without affecting its electronic structure by employing different methods such as wrapping with polyethylene glycol and other surfactants, or π–π interaction with 1-pyrene butanoic acid succinimidyl ester [41, 42] giving graphene soluble in water or dimethylformamide, respectively. The common way of the electrode surface modification is the drop-casting of graphene suspensions or dispersions in appropriate solvents. Dimethylformamide, water, and chitosan are the most frequently used media. The covalent functionalization is also effective and usually based on the derivatization of graphene with amide groups, making it soluble in organic solvents such as tetrahydrofuran, $CCl_4$, and $CH_2Cl_2$. The acid treatment of graphene with a mixture of concentrated $H_2SO_4$ and $HNO_3$ gives water-soluble graphene, which is stable for several months. Graphene can also be made soluble in $H_2O$ by sulfonation and electrostatic stabilization [17].

The important advantage of the graphene-modified electrodes is selectivity of the target analyte determination. For example, the interference effect of dopamine and ascorbic acid on the uric acid determination is fully eliminated using graphene-modified electrode [24]. Dopamine can be easily quantified in a large excess of ascorbic acid using graphene–chitosan/GCE [21]. Selective detection is realized in completely eliminating ascorbic acid, different from the methods based on the oxidation potential separations. π–π stacking interaction between dopamine and graphene surface may accelerate the electron transfer whereas weaken the ascorbic acid oxidation on this graphene-modified electrode. The phenomena were considered from the elusive two-dimensional structure and unique electronic properties of graphene. The same mixture of analytes can be successfully separated on the electrode modified with graphene dispersed in dimethylformamide using the difference in the oxidation potentials for dopamine and ascorbic acid [23]. These data confirm again the important role of the graphene synthesis and pretreatment way and their effect on the electrochemical properties of the electrode fabricated.

**Tab. 7.1:** Graphene-modified electrodes' applications in organic electroanalysis

| Electrode | Method | Analyte | Sample | LOD | Linear range | Ref. |
|---|---|---|---|---|---|---|
| Graphene–chitosan/GCE | DPV | Dopamine | Model systems | – | 5–200 μM | [21] |
| | AdDPV | Mitoxantrone | Urine | 0.2 nM | 0.6–100 nM | [22] |
| Graphene/GCE | DPV | Dopamine | Model systems | 2.64 μM | 4–100 μM | [23] |
| | CV | Uric acid | Urine | 0.6 μM | 2–120 μM | [24] |
| | DPV | Vanillin | Biscuits | 0.056 μM | 0.60–48 μM | [25] |
| | DPV | Ciprofloxacin | Drugs | 0.02 μM | 0.5–200 μM | [26] |
| | AdDPV | Hymecromone | Capsules | 0.040 μM | 0.080–6.0 μM | [27] |
| | SWV | Paracetamol | Tablets | 0.032 μM | 0.1–20 μM | [28] |
| GO/GCE | CV | Imidacloprid | Water | 0.36 μM | 0.8–10 μM | [29] |
| Irradiated RGO/GCE | SWV | Norepinephrine | Injections, human urine and serum | 50 nM | 1–200 μM | [30] |
| CRGO/GCE | Amperometry | NADH | Urine | 0.6 μM | 0–500 μM | [31] |
| PDDA–CRGO/GCE | DPV | Acetylsalicylic acid | Tablets and urine | 1.17 μM | 5–2000 μM | [32] |
| | AdDPV | Hyperin | Herb *Hypericum perforatum* | 5.0 nM | 7.0–70 nM | [33] |
| Polyethyleneimine–CRGO/GCE | AdLSV | Gallic acid | Tea | 0.07 mg $L^{-1}$ | 0.1–10 mg $L^{-1}$ | [34] |
| Nafion–CRGO/GCE | AdSDPV | Nebivolol | Tablets and human plasma | 46 nM | 0.5–24 μM | [35] |
| ERGO/GCE | Amperometry | Pyridoxine | Tablets and blood serum | 0.056 μM | 0.10–100 μM | [36] |
| | AdSSWV | Sophoridine | Spiked urine | 0.2 μM | 0.8–100 μM | [37] |
| | AdDPV | Ferulic acid | *Angelicae sinensis*, spiked urine, plasma | 20.6 nM | 0.0849–38.9 μM | [38] |
| | Amperometry | Acetaminophen | Human serum | 2.13 nM | 5–4000 nM | [39] |
| | Amperometry | Promethazine | Tablets | 0.199 μM | 1.99–1030 μM | [40] |

LOD limit of detection
DPV differential pulse voltammetry;
AdDPV adsorptive differential pulse voltammetry;
SWV square-wave voltammetry;
PDDA poly(diallyl dimethylammonium chloride);
AdLSV adsorptive linear sweep voltammetry;
AdSDPV adsorptive stripping differential pulse voltammetry;
AdSSWV adsorptive stripping square-wave voltammetry.

Recently, graphene has been considered as a platform for the immobilization of other modifiers on electrode surface. These are other carbon nanomaterials, metal, metal oxide and metal sulfide nanoparticles, inorganic materials (polyoxometalates, hexacyanoferrates, minerals), organic materials (amino acids, surfactants, organic dyes, ionic liquids, macrocycles), polymers (conventional polymers, polyelectrolytes, conducting polymers, molecularly imprinted polymers), and, finally, biomolecules including proteins and nucleic acids. Such kind of combinations provides further improvement of the electrodes' characteristics as well as the analytical application area and is discussed in detail in review [43].

### 7.2.2 Fullerenes

Fullerene consists of 20 hexagonal and 12 pentagonal rings as the basis of icosohedral symmetry closed cage structure. Each carbon atom is bonded to three others and is $sp^2$-hybridized. The buckminsterfullerene $C_{60}$ is the smallest one and the most abundant. The next stable homologue is $C_{70}$ followed by higher fullerenes $C_{74}$, $C_{76}$, $C_{78}$, $C_{80}$, $C_{82}$, $C_{84}$, and so on [44]. $C_{60}$ is not "superaromatic" due to the absence of double bonds in the pentagonal rings, resulting in poor electron delocalization. Therefore, $C_{60}$ structure behaves like an electron-deficient alkene and has been never considered as a possible electrode material due to its poor conductivity and distinct lack of edge plane-like sites/defects [45]. It was one of the reasons why fullerenes were less often applied in electroanalysis among other carbon nanomaterials. Nevertheless, further investigation has shown that fullerenes have electrocatalytic properties and thus can be considered as participants of the electron transfer reaction and as possible candidates for the electroanalytical applications.

The first effort to use $C_{60}$ as electrode surface modifier has been presented in 1992 [46]. The drop-casting technology has been applied with further Nafion coverage as protective film. Several approaches exist for the immobilization of fullerenes on the electrode surface. The easiest and most commonly applied method is drop-casting of fullerene solution in a volatile solvent [47–49]. Then, fullerene film can be obtained using electrochemical deposition [50]. More complicated approach is based on the electropolymerization where the formed fullerene units are connected by polymer side chains or via epoxide formation [51]. And, finally, the formation of self-assembled monolayer films on the electrode surface using either thiols or silane derivatives of $C_{60}$ can be applied for the modification [52]. This approach is useful for the construction of highly ordered, two- and three-dimensional structures on solid substrates.

The electrochemical activity of fullerenes has been mainly attributed to the impurities containing in the nanomaterial. The graphite impurities presented in the $C_{60}$ provide electrocatalytic effect toward cysteine oxidation [53]. The metal impurities effect has been shown on the example of nandrolone [54]. In this case, the removal of metals from fullerene shifted the peak potential of nandrolone to more positive

potentials with the peak current decrease. Thus, the untreated fullerene-modified electrode exhibited enhanced catalytic effect compared with the acid-purified and super-purified $C_{60}$ modified electrodes. Another one explanation of electrocatalytic effect of fullerenes was based on the formation of the partially reduced conductive $C_{60}$ film containing $C_{60}O_n$ [55–57]. It is important to emphasize that the claimed electrocatalysis is attributed to the $C_{60}$ film acting as the mediator, which is not associated with the electrochemistry of $C_{60}$ itself. The substrate activation through electrode pretreatment is responsible for the observed electrocatalysis likely through the introduction of surface oxygenated species [58].

The electrochemical behavior of fullerenes in solution and immobilized on the electrode as well as electroanalytical application of the fullerene-modified electrodes in nonaqueous and aqueous solutions has been discussed in detail [59]. Thus, $C_{60}$-modified electrodes have been successfully fabricated and used for the determination of methionine [60] and cysteine [61], dopamine in the presence of ascorbic acid [62], simultaneous determination of adenine and guanine [47], as well as a wide range of pharmaceutical substance [54–56, 63, 64]. In addition, fullerene $C_{60}$ is applied for the construction of electrochemical biosensors [65].

### 7.2.3 Carbon nanotubes

CNT became one of the most investigated carbon nanomaterials since their discovery in early 1990s. CNTs are cylinder-shaped macromolecules (tubes) with a radius of a few nanometers and up to 20 cm in length. CNTs are composed of a concentric arrangement of many cylinders formed by the roll-up of a graphene sheet. Two main types of CNT can be classified depending on size and structure parameters. These are multiwalled carbon nanotubes (MWNTs) comprising several concentric tubes and single-walled carbon nanotubes (SWNTs) in which only one graphite sheet is rolled up. A double-walled CNT composed of just two concentric cylinders can be considered as a special case of MWNT. The electronic properties depend on the structure of SWNT, in particular diameter and chirality. In this way, SWNT can be classified as metallic (armchair) or semiconducting (zigzag or chiral). SWNTs possess the simplest geometry and their diameters range from 0.4 to 3 nm. As to MWNT, the "hollowtube," "herringbone," or "bamboo" morphological variations exist. MWNT diameter can reach 100 nm [8, 66].

In comparison to the conventional scale materials and other types of nanomaterials, CNTs have a range of properties making them favorably usable in the electroanalysis. These are (i) the large specific area producing high sensitivity; (ii) the tubular nanostructure and the chemical stability allowing the fabrication of ultrasensitive sensors consisting of only one nanotube; (iii) the good biocompatibility that is suitable for constructing electrochemical biosensors, especially for facilitating the electron transfer of redox proteins and enzymes; (iv) the modifiable ends and sidewalls providing a chance for fabricating multifunctional electrochemical sensors via the

construction of functional nanostructures; (v) the possibility of miniaturization; and (vi) the possibility of constructing ultrasensitive nanoarrays [67].

The electrochemical properties of CNT are summarized and discussed in detail in [11, 45, 67–69]. Briefly, the electrocatalytic effect of CNT strongly depends on their structural characteristics, in particular, on the presence of the edge-like defect sites and the specific surface functional groups (especially oxygen-containing groups) that can considerably increase the rate of electron transfer. Moreover, the trace amount of iron catalyst used during CNT production can affect the electrochemical activity of target analyte [70].

CNTs are highly hydrophobic materials. Therefore, there are different ways of their immobilization on the electrode surface. The abrasive methodology based on rubbing a polished electrode on a CNT-containing paper or a CNT-ionic liquid gel did not get wide application due to the insufficient reproducibility. The inclusion of CNT in the paste allows creation of the carbon paste electrodes (CPEs) or screen-printed CPE. But the most common approach for the immobilization of CNT on the electrode surface is the drop-casting technology. In this case, the CNT dispersions or suspensions are usually obtained using sonication in appropriate solvent depending on the CNT characteristics. Among the reported solvents, N,N-dimethylformamide is the most extensively used polar solvent, but water, acetone, ethanol, and even toluene are also applicable [67]. The main disadvantage of this type of CNT preparation is the low solubility of nanomaterial and relatively low stability of the suspensions obtained. Nevertheless, the simplicity and convenience of the approach enabled its wide applicability. In order to increase the solubilization of CNT, the additives of surfactants (sodium dodecylsulfate [SDS], cetyltrimethylammonium bromide [CTAB], dihexadecyl hydrogen phosphate), and polymers (Nafion, chitosan, polyethyleneimine [PEI]) are usually used. It should be noted that the effect of dispersing additives on the electrochemical behavior of target analyte had to be taken into account. For example, Nafion forms a membrane and being an ion exchanger acts as a diffusion barrier on the surface of the electrode. Another way of solubilization improvement is the oxidative acid treatment of CNT using mixture of concentrated nitric and sulfuric acids [71]. These drastic conditions lead to the opening of the tube caps as well as the formation of holes in the sidewalls, followed by an oxidative etching along the walls with the concomitant release of carbon dioxide. The final products are nanotube fragments with lengths in the range of 100–300 nm whose ends and sidewalls are decorated with a high density of various oxygen-containing groups (mainly carboxyl groups). The presence of carboxyl groups leads to a reduction of van der Waals interactions between the CNT preventing their aggregation [66]. Carboxylated CNTs are good sites for their further functionalization and application in electroanalysis. This topic is out of the frames of this chapter.

Taking into account the mentioned above, it can be concluded that the electrochemical activity and properties of CNT are very sensitive to the synthesis and pretreatment ways of the nanomaterial. On the other hand, these factors open wide possibilities to change and control the CNT-modified electrode surface activity as well as enlarge the application of CNT in electroanalysis that is confirmed by dramatically increased number of review publications in this field [9, 11, 59, 67, 72].

The large electrocatalytic effect shown by CNT-modified electrodes has been widely used for analytical purposes. The non-enzymatic CNT-modified electrodes will be discussed in this chapter. CNT-modified electrodes have been developed for the determination of a wide range of organic compounds of different nature. The most typical examples are presented in Tab. 7.2.

**Tab. 7.2:** Analytical characteristics of biologically active compounds at CNT-modified electrodes

| Electrode | Method | Analyte | *E*/*V* | LOD | Linear range | Ref. |
|---|---|---|---|---|---|---|
| SWNT/Au | DPV | Dopamine | 0.350 | 0.79 µM | 1–10 µM | [73] |
| | CV | Uric acid | 0.451 | 1.0 µM | 4.0–700 µM | [74] |
| SWNT/CCE | DPV | Caffeine | 1.38 | 0.12 µM | 0.25–100 µM | [75] |
| | DPV | Codeine | 1.05 | 0.11 µM | 0.2–230 µM | [76] |
| | | Caffeine | 1.38 | 0.25 µM | 0.4–300 µM | |
| SWNT/EPPGE | SWV | Salbutamol | 0.600 | 4.31 ng/mL | 50–2500 ng/mL | [77] |
| SWNT–COOH/GCE | LSV | Naringenin | 0.998 | 0.02 µM | 0.08–5.0; 5.0–12 µM | [78] |
| | AdLSV | Neohesperidin dihydrochalcone | 0.666 | 0.02 µM | 0.05–8.0 µM | [79] |
| | DPV | L-Dopa | 0.220 | 0.3 µM | 0.5–2.0 µM | [80] |
| MWNT–CPE | AdCV | Quercetin | 0.320 | 0.002 µM | 0.002–0.10; 0.10–20 µM | [81] |
| | AdCV | Morin | 0.520 | 1.0 nM | 5.0–100 nM | [82] |
| $MWNT_{ox}$/GCE | LSV | Methionine | 0.800 | 0.27 mM | 0.36–2.6; 3.3–6.9 mM | [83] |
| | | Cysteine | 0.800 | 0.064 mM | 0.075–1.9 mM | |
| | | Glutathione | 0.650 | 0.043 mM | 0.076–1.8 mM | |
| | LSV | Unithiole | 0.600 | 0.041 mM | 0.18–1.4; 2.6–6.9 mM | [84] |
| | | Lipoic acid | 0.810 | 0.019 mM | 0.026–0.18; 0.21–0.78 mM | |
| | AdSSWV | Curcumin | | 5.0 nM | 10–1000 nM | [85] |
| $MWNT_{ox}$/Graphite electrode | LSV | Retinol | 0.830 | 0.04 mM | 0.05–1.50 mM | [86] |
| | | α-Tocopherol | 0.320 | 0.05 mM | 0.065–2.00 mM | |
| MWNT/GCE | AdDPV | Tartrazine | 0.930 | 0.22 µM | 1.00–7.00 µM | [87] |
| | | Sunset yellow | 0.680 | 0.12 µM | 0.55–73.00 µM | |
| | | Carmoisine | 0.600 | 0.11 µM | 0.54–5.00 µM | |
| | SWV | Ascorbic acid | 0.295 | 1.4 µM | 4.7–5000 µM | [88] |
| MWNT/GCE | CV | Hydroquinone | 0.120 | 2.9 µM | 2.9–1430 µM | [89] |
| | | Catechol | 0.150 | 1.47 µM | 3.67–1290 µM | |
| | | Pyrogallol | 0.00 | 20.0 µM | 66–1660 µM | |
| MWNT/BPPGE | AdSV | Capsaicin | 0.690 | 0.31 µM | 0.5–15; 15–60 µM | [90] |
| MWNT–COOH/GCE | Amperometry | Tetracaine hydrochloride | 0.76 | 0.036 µM | 0.1–20 µM | [91] |
| MWNT/CCE | DPV | Ascorbic acid | 0.092 | 7.71 µM | 15–800 µM | [92] |
| | | Dopamine | 297 | 0.31 µM | 0.50–100 µM | |
| | | Uric acid | 458 | 0.42 µM | 0.55–90 µM | |

LOD limit of detection
CCE carbon-ceramic electrode;
EPPGE edge-plane pyrolytic graphite electrode;
BPPGE basal plane pyrolytic graphite electrode.

As one can see, the CNT-modified electrodes allow detection of analytes at relatively low potentials that are lower than at some other electrode materials. Certain analyte are electrochemically active in the available potential window on the CNT-modified electrodes only. This phenomenon extends the number of analytes available for the electroanalysis. Neurotransmitters, ascorbic and uric acids, and different types of antioxidants and pharmaceutical substances are the most studied analytes that coincide with the common trends in analytical chemistry development. Electrode surface modification provides significant improvements in the analytical characteristics of analytes determination in comparison to bare GCE, CPE, etc. Moreover, the simultaneous determination of several analytes can be achieved without preliminary separation even in the complex matrices as biosamples or foodstuff.

Thus, the modification of electrodes with CNT opens new opportunities in the organic voltammetry. The key advantages of CNTs are their small diameter but long length, their electroactivity (good or better than for the other carbon-based electrodes) and the high surface area providing increased sensitivity of the modified electrodes. One of the limitations of CNT-modified electrodes application is the determination of structurally related compounds or isomers. This problem can be partially solved using co-modifiers. Current developments in CNT-based electrodes are focused on the CNT functionalization and their use as a platform for the immobilization of other modifiers providing further enhancement of the analytical signal as well as recognition and biorecognition of the target analyte.

## 7.3 Surfactant-modified electrodes for the organic electroanalysis

The ability of surfactants to effect on the polarization curves view is usually attributed to the changes in the double electrical layer properties. Neutral organic surfactants have been used for the suppression of polarographic maxima since the start of the polarography and voltammetry development. Aliphatic alcohols with $C_6$–$C_8$ chains gave capacitive peaks on the polarograms that were used for the development of determination methods based on the so-called depression of differential capacity [93].

Besides the suppression of polarographic maxima, the adsorption of surfactant on the electrode surface leading to the inhibition of electrochemical process steps appeared as a shift of the peak or wave potentials to higher values or as a splitting of multielectron wave on the several steps. These adsorptive effects were almost not used for the analytical purposes excluding the determination of surfactant traces in water samples. At present time, these investigations are of interest from the historical point of view.

Nevertheless, the variety of modern surfactants and their properties allows their application for the control of the analytical signal in voltammetry that is discussed in review [94].

In general, surfactants provide solubilization of organic compounds including redox active substances participating in electron transfer reactions simulating partially the processes in living systems [95–98]. As known, the application on micellar media in electrochemical reactions leads to the two effects [96]. Surfactants can stabilize ion radicals and intermediates affecting mechanism of the electrode reaction. On the other side, surfactant changes the double-layer structure and charge transfer rate constant that is confirmed by the shifts of peaks potential for the corresponding processes [98]. These effects could provide the enhancement of the target compounds' analytical characteristics in particular the increase of the system reversibility and the sensitivity of the determination [99–101].

Thus, two important properties of surfactants are advantageously used in electroanalysis, namely adsorption at the interface and self-aggregation into organized structures [97]. Therefore, surfactants are able to modify and control the properties of electrode surfaces, leading to the changes in the reaction rates and pathways. The electrode surface modification with suitable surfactants can be used for the analyte molecules preconcentration and, therefore, for decreasing the limits of determination. In these cases, the preconcentration occurs either due to the electrostatic interaction of the ionogenic groups of surfactants and the corresponding functional groups of the analyte or upon the hydrophobic interaction of hydrocarbon fragments in their structures with the hydrophobic analyte molecules [94, 102]. Thus, surfactant-modified electrodes can affect on selectivity and sensitivity of analyte determination.

The analytical signal improvement strongly depends on the concentration and nature of surfactant used. In most cases, the surfactant is added to the electrochemical cell. The CPEs are most frequently used as working electrode. The surfactant concentrations applied are usually above the critical micelle concentration in order to solubilize the analyte. In addition, the interaction of the surfactant with the electrode surface changes the electrical properties of the electrode/solution interface and causes a signal enhancement, which is due to an increase of the electrode area by partial solubilization of the agglomerant of the carbon paste [103]. On the other hand, the surfactant can be incorporated to the electrode surface during the measurement in electrolytes containing sub-micelle concentrations of surfactant giving *in situ* modified electrodes with improved analytical characteristics [104]. The important advantage of *in situ* surfactant-modified electrodes is the possibility to study a complex matrix without sample cleaning steps [105, 106]. Another way of the electrode coating with surfactant is drop-casting technique with further evaporation of the solvent. In this case, the retention of the modifier is based on the hydrophobic interaction with the carbon surface. This approach has been successfully applied in the electrochemistry of amaranth [107], bromothymol blue [108], sodium levothyroxine [109], etc.

Surfactant-modified electrodes have been widely applied in the organic electroanalysis, including food, pharmaceutical, and biosamples. The most commonly used surfactants are anionic SDS and cationic cetyltrimethylammonium or cetylpyridinium salts. Nonionic surfactants (Triton X100, Brij® 35, etc.) are used more seldom. The achievements in this field are summarized in Tab. 7.3.

The surfactant-modified electrodes allow determining several analytes without preliminary separation that is realized via the difference in their electrode reaction rates. Thus, the simultaneous determination of uric and ascorbic acids in urine has been achieved using GCE modified with chitosan and cetylpyridinium bromide film. The oxidation peak potential separation of 200 mV has been obtained under conditions of DPV (Fig. 7.2). The linear dynamic ranges are 8–1000 and 10–2000 μM for uric and ascorbic acids, respectively [132].

A simple and highly sensitive electrochemical method for the simultaneous determination of ascorbic acid and rutin on acetylene black paste electrode coated with CTAB film has been developed [133]. The electrode modification has been performed by dipping it into a $1.0 \times 10^{-2}$ M surfactant aqueous solution for 1 min. The modified electrode shows strong adsorption of ascorbic acid and rutin and significantly increased oxidation currents in comparison to bare electrode. The anodic peak potential's difference for the ascorbic acid and rutin about 350 mV allows their quantification individually and simultaneously. Under optimized conditions using a second-order derivative linear sweep voltammetry, the linear dynamic ranges are 2.0–1000 μM for ascorbic acid and 0.0060–10 μM for rutin, with the detection limits ($S/N = 3$) of 1.0 μM and 4.0 nM, respectively. The approach has been applied for the direct simultaneous determination of ascorbic acid and rutin in the pharmaceutical samples.

One of the intensively developed trends in the application of surfactant-modified electrodes is focused on the determination of catecholamines (epinephrine, norepinephrine, and dopamine) in biosamples. The voltammetric characteristics of epinephrine, norepinephrine, and related compounds (isoproterenol, metanephrine, L-dopa, methyldopa, and vanillylmandelic and homovanillic acids) have been evaluated at bare and *in situ* surfactant-modified CPE. The significant increase of the redox currents and the improvement in the reversibility of the processes have been obtained for the basic and amphoteric compounds on the CPE modified with submicellar concentrations of anionic surfactants (SDS, sodium decylsulfate, or sodium dodecylsulfonate). These effects can be explained by the electrostatic and hydrophobic interactions. On the contrary, the oxidation of acidic metabolites (vanillylmandelic and homovanillic acids) is improved at the electrodes modified *in situ* with cationic surfactant (cetyltrimethylammonium chloride), which is caused by the ability of surfactant to stabilize some of the electrochemical reaction intermediates [134].

**Tab. 7.3:** Application of surfactant-modified electrodes in the electroanalysis of foodstuff, pharmaceutical, and biomedical samples

| Electrode | Method of modification | $c_{surfactant}$, mM | Method | Analyte | Sample | LOD | Linear range | Ref. |
|---|---|---|---|---|---|---|---|---|
| SDDBS/CPE | *in situ* | 0.05 | AdDPV | Malachite green | Fish | 4.0 nM | 8.0–500 nM | [110] |
| SDS/pencil graphite electrode | *in situ* | 2.0 | SWV | Nicotin | Cigarettes | 2.0 µM | 7.6–107.5 µM | [111] |
| SDS/CPE | *in situ* | 0.05 | AdSDPV | Rifampicin | Model systems | 0.10 nM | 0.35–5.4 nM | [112] |
| | | 8.0 | CV | Dopamine | Injections | 0.05 µM | 0.5–800 µM | [113] |
| | | 3.0 | CV | Riboflavine | Multivitamin drugs | 0.02 µg/mL | 0.1–100 µg/mL | [114] |
| | | | | Ascorbic acid | | 5.0 µg/mL | 10–800 µg/mL | |
| SDS/GCE | *in situ* | 0.1 | AdDPV | Terazosin | Tablets and urine | 4.58 nM | 0.04–2.4 µM | [115] |
| | | 0.11 | CV | Retinol | Foodstuff and drugs | 15 µM | 29.4–980 µM | [116] |
| | | 10 | DPV | TBHQ | Vegetable oils | 0.23 µM | 2.02–1010 µM | [117] |
| | | | | BHA | | 0.18 µM | 2.34–1170 µM | |
| | | | | BHT | | 3.5 µM | 6.15–615 µM | |
| CPC/GCE | *in situ* | 1.0 | DPV | Ascorbic acid | Urine | 0.2 µM | 0.5–430 µM | [118] |
| DDTMAC/CPE | *in situ* | 0.05 | AdDPV | Flufenamic acid | Human serum | 0.64 nM | 0.001–50 µM | [119] |
| CTAB/HMDE | *in situ* | 0.221 | SWV | Genistein | Soy products | 0.0343 µM | 0.114–1.09 µM | [120] |
| | | 0.242 | SWV | Chlorogenic acid | Coffee, tea | 1.34 nM | 0.18–1.28 µM | [121] |
| | | | | | | | 1.23–8.5 µM | |
| CTAB/CPE | *in situ* | 0.234 | LSV | TBHQ | Soybean biodiesel | 71.1 nM | 1.05–10.15 µM | [122] |
| | | 0.06 | AdSLSV | Thyroxin | Drugs | 6.5 nM | 0.2–9.0 µM | [123] |
| DDPB/GCE | *in situ* | 1.0 | CV | α-Tocopherol | Drugs | 1.02 µM | 2–140 µM | [124] |

**Tab. 7.3:** (continued)

| Electrode | Method of modification | $c_{surfactant}$, mM | Method | Analyte | Sample | LOD | Linear range | Ref. |
|---|---|---|---|---|---|---|---|---|
| Triton X100/GCE | *in situ* | 1.0 | CV | α-Tocopherol | Drugs | 1.02 µM | 2–100 µM | [124] |
| | | 1000 | CV | Eugenol | Essential oils and spices | 3.8 µM | 15–1230 µM | [125] |
| Tween-20/HMDE | *in situ* | 8.1 | AdSSWV | Drotaverine hydrochloride | Tablets | 1.8 ng/mL | 0.8–7.2 µg/mL | [126] |
| Pluronic F-68/ GCE | *in situ* | 8.1 | DPV | BHA | Chewing gum | 0.85 µM | 1.0–10 µM<br>10–50 µM | [127] |
| Brij® 35/GCE | *in situ* | 1000 | CV | Eugenol | Model systems | 20 µM | 20–1000 µM | [128] |
| DDDMAB–-nafion/CPE | Drop-casting | 6.0 | CV | Ferulic acid | Drugs | 0.39 µM | 2.0–120 µM | [129] |
| Triton X100/CPE | Drop-casting | 0.01 | DPV | Dopamine | Injections | 0.03 µM | 0.2–500 µM | [130] |
| 3-(N,N-Dimethylpalmityl-ammonio)propane sulfonate / acetylene black paste electrode | Drop-casting | 0.05 | CV | Tetrabromobisphenol A | Water | 0.4 nM | 1–100 nM | [131] |

| | | | |
|---|---|---|---|
| LOD | limit of detection | HMDE | hanging mercury drop electrode; |
| SDDBS | sodium dodecyl benzene sulfonate | TBHQ | *tert*-butyl hydroquinone; |
| DDTMAC | dodecyl trimethylammonium chloride | BHA | butyl hydroxyanisole; |
| DDPB | N-dodecyl pyridinium bromide | BHT | butyl hydroxytoluene; |
| CPC | cetyl pyridinium chloride | AdSLSV | adsorptive stripping linear sweep voltammetry. |
| CTAB | cetyl trimethylammonium bromide | DDDMAB | didodecyl dimethylammonium bromide |

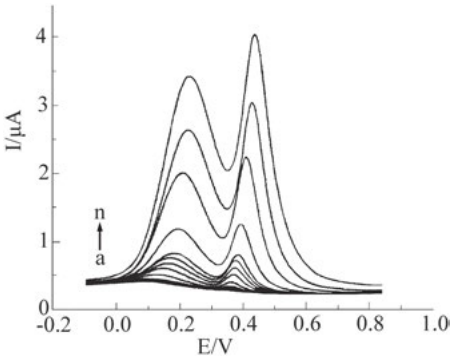


**Fig. 7.2:** Differential pulse voltammograms of 0.5–200.0 μM of uric acid and fourfold higher concentrations of ascorbic acid in 0.1 M phosphate buffer solution pH 5.0. Reprinted with permission from ref. [132]. Copyright 2010 John Wiley & Sons.

The direct determination of catecholamines in biosamples is an important problem for the medical diagnosis. Ascorbic and uric acids are the major interfering substances in these measurements. The overlapping of their oxidation potentials and the pronounced electrode fouling often results in poor selectivity and reproducibility at unmodified carbon-based electrodes. The surfactant-modified electrodes' development opened new opportunities for the application of electroanalytical methods in this field as far as providing selective determination of catecholamines in the wide dynamic ranges [135, 136]. Several examples of such types of electrodes are presented in Tab. 7.4.

The selectivity of the determination is based on the electrostatic effects of the analytes and electrode surface. In the case of anionic surfactant-modified electrodes, the determination is usually performed at pH < 8. The amine group in catecholamine molecule is electropositive, whereas the ascorbic and uric acid molecules are electronegative and the anionic surfactant layer on the electrode surface is electronegative due to its ionization. Therefore, electropositive dopamine is attracted electrostatically to the electrode surface and can be oxidized at relatively low potentials. The electronegative ascorbic and uric acids is repelled from the electrode and oxidized at other potentials [113, 148]. In the case of cationic surfactant-modified electrodes, the opposite effects are occurred.

Taking into account the mentioned above, surfactant-modified electrodes can be considered as a promising tool in the electroanalysis of organic substances providing high sensitivity and selectivity of their determination.

**Tab. 7.4:** The analytical characteristics of neurotransmitters determination using surfactant-modified electrodes

| Analyte | | Coexisting substance | Method | LOD, μM | Linear range, μM | Ref. |
|---|---|---|---|---|---|---|
| Dopamine | Ascorbic acid | 5 % SDS–CPE | DPV | 0.34 | 2.0–10 | [137] |
| | Ascorbic and uric acids | SDS micelles/ CPE | DPV | 7.71 | 10–196 | [138] |
| | | SDS/Paper/ CPE | SWV | 0.37 | 1–100 | [139] |
| | Ascorbic and uric acids Serotonin | Triton X100/ CPE | DPV | 0.03 | 0.2–500 | [130] |
| | Ascorbic acid Serotonin | TOAB/CPE | DPV | 0.019 | 0.10–2.0 | [140] |
| Dopamine | – | CPB–chitosan/GCE | DPV | – | 40–4000 | [141] |
| Ascorbic acid | | | | – | 20–2000 | |
| | – | CTAB–chitosan/GCE | DPV | – | 8.0–1000 | [142] |
| | | | | – | 10.0–2000 | |
| | L-Cysteine | DCTMAC/GCE | DPV | 6.5 | 10–1000 | [143] |
| | Glucose | | | 4.0 | 10–1000 | |
| Norepinephrine | Ascorbic and uric acids | Triton X100/УПЭ | CV | 5.0 | 50–200 | [144] |
| | Ascorbic and folic acids | SDS/CPE | CV | 1.0 | 50–400 | [145] |
| Epinephrine | Ascorbic and uric acids | SDS/CPE | DPV | 0.5 | 10–70 | [146] |
| | Ascorbic acid Serotonin | TDTMAB/CPE | DPV | 0.12 | 0.15–30 | [147] |

TOAB tetraoctyl ammonium bromide
CPB cetyl pyridinium bromide
CTAB cetyl trimethyl ammonium bromide
DCTMAC docosyl trimethyl ammonium chloride
TDTMAB tetradecyl trimethyl ammonium bromide

## 7.4 Analytical possibilities of the electrodes with co-immobilized carbon nanomaterials and surfactants

In the last decade, the combination of surfactants and carbon nanomaterials as electrode surface modifier became an attractive possibility for further improvements of the sensitivity and selectivity of the analyte quantification. The most common nanomaterial applied is CNT. The electrode surface modification can be performed using two approaches. The first one is based on the layer-by-layer coverage. On the other hand, surfactants are widely used as dispersing additives for the preparation of

carbon nanomaterial suspension and therefore the electrode becomes modified with co-immobilized nanomaterial and surfactant. The surface of the electrodes is characterized by high roughness and randomly distributed nanotubes (nanofibers, etc.) that can be strongly intertwined (Fig. 7.3). In both cases of modification, the synergetic effect of carbon nanomaterial and surfactant provides an improvement in the analytical and operational characteristics of target analyte determination caused by the high electroconductivity and electroactivity of carbon nanomaterial and electrostatic and/or hydrophobic interactions provided by surfactants.

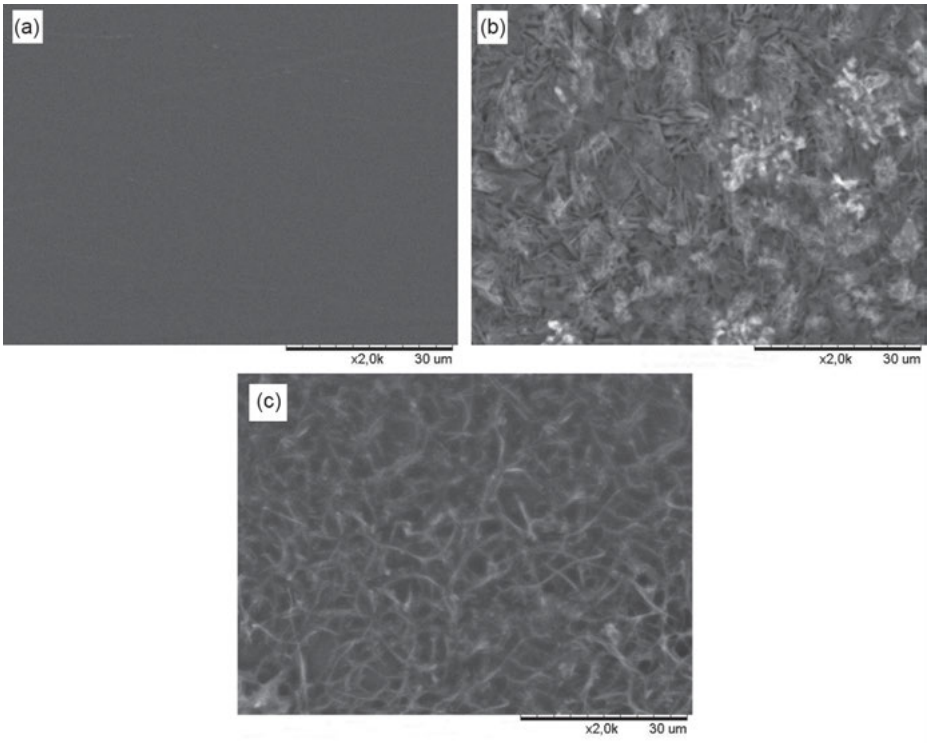


**Fig. 7.3:** SEM images of GCE (a), MWNT–SDS/GCE (b), and CPB/carbon nanofibers/GCE (c). Reprinted with permission from ref. [149, 150]. Copyright 2015 John Wiley & Sons and Copyright 2015 Springer-Verlag Wien, respectively.

Different types of analytes have been investigated using electrodes with co-immobilized carbon nanomaterials and surfactants. The most typical examples are presented in Tab. 7.5. Combination of modifiers provides lower detection limits and wider linear dynamic ranges in comparison to bare electrodes.

**Tab. 7.5:** Application of surfactant-carbon nanomaterial-modified electrodes in organic voltammetry

| Electrode | Method | Analyte | LOD | Linear range | Ref |
|---|---|---|---|---|---|
| MWNT–CTAB/GCE | CV | Epinephrine | 0.030 µM | 0.1–20; 30–100 µM | [151] |
| | | Ascorbic acid | 100 µM | 300–1000 µM | |
| | DPV | Paracetamol | 4.82 nM | 0.40–4.0 µM | [152] |
| | LSV | 6-Mercaptopurine | 8.49 nM | 0.5–3.0 µM | [153] |
| | DPV | Tripelennamine hydrochloride | 2.38 nM | 10–3000 nM | [154] |
| $MWNT_{ox}$–CTAB–CPE | AdDPV | Kaempferol | 12.7 nM | 0.02–2.0; 5.0–50 µM | [155] |
| | | Quercetin | 5.3 nM | 0.01–1.0; 2.0–20 µM | |
| $MWNT_{ox}$–SDS/GCE | DPV | Dopamine | 0.01 µM | 0.08–80 µM | [156] |
| | | Ascorbic acid | 3.0 µM | 400–3500 µM | |
| | | Uric acid | 0.04 µM | 4.0–30 µM | |
| | DPV | Terbutaline sulfate | 0.34 µM | 1.12–141 µM | [157] |
| MWNT–SDS/GCE | CV | Rutin | 0.71 µM | 1.4–28; 28–210 µM | [158] |
| | | Quercetin | 1.0 µM | 2.0–220 µM | |
| | | Taxifolin | 0.26 µM | 0.52–210 µM | |
| | DPV | Chlorogenic acid | 0.21 µM | 1.0–1060 µM | [159] |
| | | Caffeic acid | 0.0025 µM | 0.0093–5030 µM | |
| | | *p*-Coumaric acid | 0.63 µM | 5.0–1000 µM | |
| | | Ferulic acid | 0.32 µM | 5.3–530 µM | |
| | CV | Catechin | 1.2 µM | 1.7–8.5; 8.7–170 µM | [160] |
| | | Gallic acid | 5.96 µM | 9.9–99; 100–910 µM | |
| | | Tannin | 2.0 µM | 4.0–39; 40–390 µM | |
| MWNT–Brij® 35/GCE | DPV | TBHQ | 0.26 µM | 1.0–1000 µM | [161] |
| | | BHA | 0.15 µM | 0.50–7.50; 10–750 µM | |

**Tab. 7.5:** (continued)

| Electrode | Method | Analyte | LOD | Linear range | Ref |
|---|---|---|---|---|---|
| MWNT–SDDBS/paper electrode | DPV | Dopamine | 1 µM | 10–100 µM | [162] |
| SDS/pristine MWNT–CPE | Amperometry | Epinephrine | 0.045 µM | 0.1–10; 10–100 µM | [163] |
| SDS/Aligned MWNT/GCE | DPV | Dopamine | 3.75 µM | 20–200 µM | [164] |
| | | Ascorbic acid | | 200–100 µM | |
| SDS/MWNT–COOH/GCE | AdDPV | Cisplatin | 4.6 µM | 14.5–100 µM | [165] |
| CPB/Carbon nanofibers/GCE | DPV | Vanillin | 0.14 µM | 0.50–75; 75–750 µM | [150] |
| CPB/SWNT–COOH/GCE | DPV | Morin | 28.9 nM | 0.10–100; 100–750 µM | [102] |

CPB cetylpyridinium bromide
SDDBS Sodium dodecyl benzene sulfonate

Electrodes modified with surfactant and carbon nanomaterials have been successfully applied for the investigation of electrochemical properties of proteins. Thus, electrochemical activity and binding affinity of phytohemagglutinin adsorbed at the MWNT–CTAB/GCE have been evaluated using CV, DPV, and SWV. The results showed that phytohemagglutinin can act as an iron storage protein [166]. The direct electron transfer of glucose oxidase immobilized in a new film containing functionalized MWNT in dihexadecyl phosphate on the surface of GCE [167] and catalase on GCE covered by MWNT–dodecyl trimethylammonium bromide film covered with a layer of Nafion [168] has been also studied.

## 7.5 Conclusions

Carbon nanomaterials and surfactants are promising electrode surface modifier, especially in the case of their composites combining the presence of nanostructures with catalytic activity and films with accumulation properties. Nanoscaled sizes of both modifiers provide novel useful properties of the modified electrodes due to the changes in the structure of the double electric layer or interface affecting the electrochemical processes. In general, the electrode surface contains the chaos of randomly distributed nanostructures giving the electrochemical response with acceptable reproducibility. Thus, the processes occurring on the electrode surface and near-electrode layer could be considered under concept of so-called nanoreactor determining the nature of the analytical signal [169]. Application of these types of electrode surface modifiers is favored by the development of chemically modified electrodes methodology.

Further development in carbon nanomaterial-modified electrodes is focused on their functionalization in order to provide the wider spectrum of their analytical application as well as to improve the selectivity of the electrodes created toward the target analytes. In this case, the special attention has to be paid to the characterization of the functionalized material at nanoscale level. Moreover, the way of synthesis, pretreatment, and modification strongly affects on the properties of the electrodes fabricated. Therefore, these problems remain their importance in the future. In the case of surfactant, the mechanisms of their effect on the electrochemical processes need the detailed investigations and discussions. The enlargement of the surfactants applied can provide new opportunities in the organic electroanalysis. The surfactant-like ionic liquids or so-called surface active ionic liquids are of great interest from this point of view.

The future application of the chemically modified electrodes based on the carbon nanomaterials and/or surfactants could be focused on the simultaneous determination of structurally related compounds, including isomers and enantiomers, the fast screening of the sample characteristics using the portable devices with screen-printed

electrodes or the batteries of amperometric sensors with further chemometric processing of the data. Among the analytes under investigation, the biochemicals, ecotoxicants, and foodstuff active substances are of interest.

## References


[1] Wang J. *Analytical Electrochemistry*. 3rd ed. Hoboken, NJ, Wiley-VCH Pub, 2006.
[2] Stradiotto NR, Yamanaka H, Zanoni MVB. Electrochemical sensors: a powerful tool in analytical chemistry. *J Braz Chem Soc* 2003, 14, 159–73.
[3] Cavalheiro ÉTG, Brett CMA, Oliveira-Brett AM, Fatibello-Filho O. Bioelectroanalysis of pharmaceutical compounds. *Bioanal Rev* 2012, 4, 31–53.
[4] Ziyatdinova G, Budnikov H. Electroanalysis of antioxidants in pharmaceutical dosage forms: state-of-the-art and perspectives. *Monatsh Chem* 2015, 146, 741–53.
[5] Alkire RC, Kolb DM, Lipkowski J, Ross PN, eds. Advances in electrochemical science and engineering: Vol. 11. *Chemically Modified Electrodes*. Weinheim, Wiley-VCH Verlag GmbH & Co. KGaA, 2009.
[6] Agűí L, Yáñez-Sedeño P, Pingarrón JM. Role of carbon nanotubes in electroanalytical chemistry: a review. *Anal Chim Acta* 2008, 622, 11–47.
[7] Huang J, Liu Y, You T. Carbon nanofiber based electrochemical biosensors: a review. *Anal Meth* 2010, 2, 202–11.
[8] Fernández-Abedul MT, Costa-García A. Carbon nanotubes (CNTs)-based electroanalysis. *Anal Bioanal Chem* 2008, 390, 293–8.
[9] Yang NJ, Swain GM, Jiang X. Nanocarbon electrochemistry and electroanalysis: current status and future perspectives. *Electroanal* 2016, 28, 27–34.
[10] Mao XW, Rutledge GC, Hatton TA. Nanocarbon-based electrochemical systems for sensing, electrocatalysis, and energy storage. *Nano Today* 2014, 9, 405–32.
[11] Gooding JJ. Nanostructuring electrodes with carbon nanotubes: A review on electrochemistry and applications for sensing. *Electrochim Acta* 2005, 50, 3049–3060.
[12] Ziyatdinova G, Grigor'eva L, Morozov M, Gilmutdinov A, Budnikov H. Electrochemical oxidation of sulfur-containing amino acids on an electrode modified with multi-walled carbon nanotubes. *Microchim Acta* 2009, 165, 353–9.
[13] Georgakilas V, Otyepka M, Bourlinos AB, Chandra V, Kim N, Kemp KC, et al. Functionalization of graphene: covalent and non-covalent approaches, derivatives and applications. *Chem Rev* 2012, 112, 6156–214.
[14] Yang X, Tu Y, Li L, Shang S, Tao X-M. Well-dispersed chitosan/graphene oxide nanocomposites. *ACS Appl Mater Interfaces* 2010, 2, 1707–13.
[15] Ambrosi A, Sasaki T, Pumera M. Platelet graphite nanofibers for electrochemical sensing and biosensing: the influence of graphene sheet orientation. *Chem Asian J* 2010, 5, 266 –71.
[16] Geim AK, Novoselov KS. The rise of graphene. *Nature* 2007, 6, 183–91.
[17] Rao CNR, Biswas K, Subrahmanyama KS, Govindaraj A. Graphene, the new nanocarbon. *J Mater Chem* 2009, 19, 2457–69.
[18] Tiwari A, Syväjärvi M, eds. *Graphene Materials: Fundamentals and Emerging Applications*. Hoboken, NJ: John Wiley & Sons, 2015.
[19] Artiles MS, Rout CS, Fisher TS. Graphene-based hybrid materials and devices for biosensing. *Adv Drug Del Rev* 2011, 63, 1352–60.

[20] Bao H, Pan Y, Li L. Recent advances in graphene-based nanomaterials for biomedical applications. *Nano LIFE* 2012, 2, 1230001.
[21] Wang Y, Li Y, Tang L, Lu J, Li J. Application of graphene-modified electrode for selective detection of dopamine. *Electrochem Commun* 2009, 11, 889–92.
[22] Hong B, Cheng Q. Sensitive voltammetric determination of mitoxantrone by using CS-dispersed graphene modified glassy carbon electrodes. *Adv Chem Eng Sci* 2012, 2, 453–60.
[23] Kim Y-R, Bong S, Kang Y-J, et al. Electrochemical detection of dopamine in the presence of ascorbic acid using graphene modified electrodes. *Biosens Bioelectron* 2010, 25, 2366–69.
[24] Chao M, Ma X, Li X, Graphene-modified electrode for the selective determination of uric acid under coexistence of dopamine and ascorbic acid. *Int J Electrochem Sci* 2012, 7, 2201–13.
[25] Peng JY, Hou CT, Hu XY. A graphene-based electrochemical sensor for sensitive detection of vanillin. *Int J Electrochem Sci* 2012, 7, 1724–33.
[26] Xie A-J, Chen Y, Luo S-P, Tao Y-W, Jin Y-S, Li W-W. Electrochemical detection of ciprofloxacin based on graphene modified glassy carbon electrode. *Mater Technol: Adv Perform Mater* 2015, 30, 362–7.
[27] Wang L, Li Y, Li G, Xie Z, Ye B. Electrochemical characters of hymecromone at the graphene modified electrode and its analytical application. *Anal Meth* 2015, 7, 3000–5.
[28] Kang X, Wang J, Wu H, Liu J, Aksay IA, Lin Y. A graphene-based electrochemical sensor for sensitive detection of paracetamol. *Talanta* 2010, 81, 754–9.
[29] Lei W, Han Z, Si W, et al. Sensitive and selective detection of imidacloprid by graphene-oxide-modified glassy carbon electrode. *ChemElectroChem* 2014, 1, 1063–7.
[30] Rosy R, Singh F, Goyal RN. Structural and electrochemical characterization of carbon ion beam irradiated reduced graphene oxide and its application in voltammetric determination of norepinephrine. *RSC Adv* 2015, 5, 87504–11.
[31] Tabrizi MA, Zand Z. A Facile one-step method for the synthesis of reduced graphene oxide nanocomposites by NADH as reducing agent and its application in NADH sensing. *Electroanal* 2014, 26, 171–7.
[32] Zhu H. Electrochemical determination of acetylsalicylic acid in human urine samples based on poly(diallyldimethylammonium chloride) functionalized reduced graphene oxide sheets. *Int J Electrochem Sci* 2016, 11, 4007–17.
[33] Li H, Sheng K, Xie Z, Zou L, Ye B. Highly sensitive determination of hyperin on poly(diallyldimethylammonium chloride)-functionalized graphene modified electrode *J Electroanal Chem* 2016, 76, 105–13.
[34] Luo JH, Li BL, Li NB, Luo HQ. Sensitive detection of gallic acid based on polyethyleneimine-functionalized graphene modified glassy carbon electrode. *Sens Actuat B* 2013, 186, 84–9.
[35] Er E, Çelikkan H, Erk N. Highly sensitive and selective electrochemical sensor based on high-quality graphene/nafion nanocomposite for voltammetric determination of nebivolol. *Sens Actuat B* 2016, 224, 170–7.
[36] Raj MA, Gowthaman NSK, John SA. Highly sensitive interference-free electrochemical determination of pyridoxine at graphene modified electrode: importance in Parkinson and Asthma treatments. *J Colloid Interface Sci* 2016, 474, 171–8.
[37] Wang F, Wu Y, Lu K, Gao L, Ye B. A simple, rapid and green method based on pulsed potentiostatic electrodeposition of reduced graphene oxide on glass carbon electrode for sensitive voltammetric detection of sophoridine. *Electrochim Acta* 2014, 141, 82–8.
[38] Liu L, Gou Y, Gao X, et al. Electrochemically reduced graphene oxide-based electrochemical sensor for the sensitive determination of ferulic acid in A. *sinensis* and biological samples. *Mater Sci Engin C* 2014, 42, 227–33.
[39] Adhikari B-R, Govindhan M, Chen A. Sensitive detection of acetaminophen with graphene-based electrochemical sensor. *Electrochim Acta* 2015, 162, 198–204.

[40] Felix FS, Ferreira LMC, Vieira F, Trindade GM, Ferreira VSSA, Angnes L. Amperometric determination of promethazine in tablets using an electrochemically reduced graphene oxide modified electrode. *New J Chem* 2015, 39, 696–702.
[41] Subrahmanyam KS, Vivekchand SRC, Govindaraj A, Rao CNR. A study of graphenes prepared by different methods: characterization, properties and solubilization. *J Mater Chem* 2008, 18, 1517–23.
[42] Subrahmanyam KS, Ghosh A, Gomathi A, Govindaraj A, Rao CNR. Covalent and noncovalent functionalization and solubilization of graphene. *Nanosci Nanotech Lett* 2009, 1, 28–31,
[43] Xu J, Wang Y, Hu S. Nanocomposites of graphene and graphene oxides: synthesis, molecular functionalization and application in electrochemical sensors and biosensors. *A review*. *Microchim Acta* 2017, 184, 1–44.
[44] Dresselhaus MS, Dresselhaus G. Fullerenes and fullerene derived solids as electronic materials. *Annu Rev Mater Sci* 1995, 25, 487–523.
[45] Banks CE, Davies TJ, Wildgoose GG, Compton RG. Electrocatalysis at graphite and carbon nanotube modified electrodes: edge-plane sites and tube ends are the reactive sites. *Chem Commun* 2005, 7, 829–41.
[46] Compton RG, Spackman RA, Wellington RG, Green MLH, Turner J. A $C_{60}$ modified electrode: Electrochemical formation of tetra-butylammonium salts of $C_{60}$ anions. *J Electroanal Chem* 1992, 327, 337–41.
[47] Lokesh SV, Sherigara BS, Mahesh JHM, Mascarenhas RJ. Electrochemical reactivity of $C_{60}$ modified carbon paste electrode by physical vapor deposition method. *Int J Electrochem Sci* 2008, 3, 578–87.
[48] Compton RG, Spackman RA, Riley DJ, Wellington RG, Eklund JC, Fisher AC, et al. Voltammetry at $C_{60}$-modified electrodes. *J Electroanal Chem* 1993, 344, 235–47.
[49] Jehoulet C, Obeng YS, Kim YT, Zhou F, Bard AJ. Electrochemistry and Langmuir trough studies of fullerene $C_{60}$ and $C_{70}$ films. *J Am Chem Soc* 1992, 114, 4237–47.
[50] Chang C-L, Hu C-W, Tseng C-Y, Chuang C-N, Ho K-C, Leung M-K. Ambipolar freestanding triphenylamine/fullerene thin-film by electrochemical deposition and its read-writable properties by electrochemical treatments. *Electrochim Acta* 2014, 116, 69–77.
[51] Bedioui F, Devynck J, Bied-Charreton C. Immobilization of metalloporphyrins in electropolymerized films: design and applications. *Acc Chem Res* 1995, 28, 30–36.
[52] Imahori H, Azuma T, Ajavakom A, Norieda H, Yamada H, Sakata Y. An investigation of photocurrent generation by gold electrodes modified with self-assembled monolayers of $C_{60}$. *J Phys Chem B* 1999, 103, 7233–37.
[53] Kachoosangi RT, Banks CE, Compton RG. Graphite impurities cause the observed 'electrocatalysis' seen at $C_{60}$ modified glassy carbon electrodes in respect of the oxidation of L-cysteine. *Anal Chim Acta* 2006, 566, 1–4.
[54] Goyal RN, Chatteijee S, Bishnoi S. Effect of substrate and embedded metallic impurities of fullerene in the determination of nandrolone. *Anal Chim Acta* 2009, 643, 95–9.
[55] Goyal RN, Bachheti N, Tyagi A, Pandey AK. Differential pulse voltammetric determination of methylprednisolone in pharmaceuticals and human biological fluids. *Anal Chim Acta* 2007, 606, 34–40.
[56] Goyal RN, Singh SP. Voltammetric determination of atenolol at $C_{60}$-modified glassy carbon electrodes. *Talanta* 2006, 69, 932–37.
[57] Goyal RN, Gupta VK, Oyama M, Bachheti N. Voltammetric determination of adenosine and guanosine using fullerene-$C_{60}$-modified glassy carbon electrode. *Talanta* 2007, 71, 1110–7.
[58] Griese S, Kampouris DK, Kadara RO, Banks CE. The underlying electrode causes the reported 'electro-catalysis' observed at $C_{60}$-modified glassy carbon electrodes in the case of N-(4-hydroxyphenyl)ethanamide and salbutamol. *Electrochim Acta* 2008, 53, 5885–90.

[59] Sherigara BS, Kutner W, D'Souza F. Electrocatalytic properties and sensor applications of fullerenes and carbon nanotubes. *Electroanal* 2003, 15, 753–72.
[60] Tan WT, Goh JK. Electrochemical oxidation of methionine mediated by a fullerene-$C_{60}$ modified gold electrode. *Electroanal* 2008, 20, 2447–53.
[61] Tan WT, Bond AM, Ngooi SW, Lim EB, Goh JK. Electrochemical oxidation of L-cysteine mediated by a fullerene-C60-modified carbon electrode. *Anal Chim Acta* 2003, 491, 181–91.
[62] Goyal RN, Gupta VK, Bachheti N, Sharma R. Electrochemical sensor for the determination of dopamine in presence of high concentration of ascorbic acid using a Fullerene-C60 coated gold electrode. *Electroanal* 2008, 20, 757–64.
[63] Jain R, Rather JA, Dwivedi A. Highly sensitive and selective voltammetric sensor fullerene modified glassy carbon electrode for determination of cefitizoxime in solubilized system. *Electroanal* 2010, 22, 2600–6.
[64] Goyal RN, Gupta VK, Chatterjee S. Fullerene-$C_{60}$-modified edge plane pyrolytic graphite electrode for the determination of dexamethasone in pharmaceutical formulations and human biological fluids. *Biosens Bioelectron* 2009, 24, 1649–54.
[65] Pilehvar S, De Wael K. Recent advances in electrochemical biosensors based on fullerene-C60 nano-structured platforms. *Biosensors (Basil)* 2015, 5, 712–35.
[66] Balasubramanian K, Burghard M. Chemically functionalized carbon nanotubes. *Small* 2005, 1, 180–92.
[67] Hu C, Hu S. Carbon nanotube-based electrochemical sensors: principles and applications in biomedical systems. *J Sensors* 2009, 2009, Article ID 187615.
[68] Banks CE, Moore RR, Davies TJ, Compton RG. Investigation of modified basal plane pyrolytic graphite electrodes: definitive evidence for the electrocatalytic properties of the ends of carbon nanotubes. *Chem Commun* 2004, 16, 1804–05.
[69] Chou A, Bocking T, Singh NK, Gooding JJ. Demonstration of the importance of oxygenated species at the ends of carbon nanotubes for their favourable electrochemical properties. *Chem Commun* 2005, 7, 842–4.
[70] Šljukić B, Banks CE, Compton RG. Iron oxide particles are the active sites for hydrogen peroxide sensing at multiwalled carbon nanotube modified electrodes. *Nano Lett* 2006, 6, 1556–8.
[71] Chen J, Hamon MA, Hu H, et al. Solution properties of single-walled carbon nanotubes. *Science* 1998, 282, 95–8.
[72] Yáñez-Sedeño P, Riu J, Pingarrón JM, Rius FX. Electrochemical sensing based on carbon nanotubes. *Trends Anal Chem* 2010, 29, 939–53.
[73] Kurniawan F, Kiswiyah NSA, Madurani KA, Tominaga M. Single-walled carbon nanotubes-modified gold electrode for dopamine detection. *ECS J Solid State Sci Technol* 2017, 6, M3109–12.
[74] Wang J, Li M, Shi Z, Li N, Gu Z. Investigation of the electrocatalytic behavior of single-wall carbon nanotube films on an Au electrode. *Microchem J* 2002, 73, 325–33.
[75] Habibi B, Abazari M, Pournaghi-Azar MH. A carbon nanotube modified electrode for determination of caffeine by differential pulse voltammetry. *Chin J Catal* 2012, 33, 1783–90.
[76] Habibi B, Abazari M, Pournaghi-Azar MH. Simultaneous determination of codeine and caffeine using single-walled carbon nanotubes modified carbon-ceramic electrode. *Colloids Surf B* 2014, 114, 89–95.
[77] Goyal RN, Bishnoi S, Agrawal B. Single-walled-carbon-nanotube-modified pyrolytic graphite electrode used as a simple sensor for the determination of salbutamol in urine. *Int J Electrochem* 2011, 2011, Article ID 373498.
[78] Wang W, Gao J, Wang L, Ye B. Electrochemical behavior of naringenin and its sensitive determination based on a single-walled carbon nanotube modified electrode. *Anal Methods* 2015, 7, 8847–56.
[79] Yang L, Wang L, Li K, Ye B. Sensitive voltammetric determination of neohesperidin dihydrochalcone based on SWNTs modified glassy carbon electrode. *Anal Methods* 2014, 6, 9410–18.

[80] Yan X-X, Pang D-W, Lu Z-X, Lü J-Q, Tong, H. Electrochemical behavior of L-dopa at single-wall carbon nanotube-modified glassy carbon electrodes. *J Electroanal Chem* 2004, 569, 47–52.
[81] Xiao P, Zhao F, Zeng B. Voltammetric determination of quercetin at a multi-walled carbon nanotubes paste electrode. *Microchem J* 2007, 85, 244–9.
[82] Xiao P, Zhou Q, Xiao F, Zhao F, Zeng B. Sensitive voltammetric determination of morin on a multi-walled carbon nanotubes-paraffin oil paste electrode. *Int J Electrochem Sci* 2006, 1, 228–37.
[83] Ziyatdinova G, Grigor'eva L, Morozov M, Gilmutdinov A, Budnikov H. Electrochemical oxidation of sulfur-containing amino acids on an electrode modified with multi-walled carbon nanotubes. *Microchim Acta* 2009, 165, 353–9.
[84] Ziyatdinova GK, Grigor'eva LV, Budnikov GK. Electrochemical determination of unithiol and lipoic acid at electrodes modified with carbon nanotubes. *J Anal Chem* 2009, 64, 185–8.
[85] Daneshgar P, Norouzi P, Moosavi-Movahedi AA, et al. Fabrication of carbon nanotube and dysprosium nanowire-modified electrodes as a sensor for determination of curcumin. *J Appl Electrochem* 2009, 39, 1983–92.
[86] Ziyatdinova G, Budnikov H. MWNT-modified electrodes for voltammetric determination of lipophilic vitamins. *J Solid State Electrochem* 2012, 16, 2441–7.
[87] Sierra-Rosales P, Toledo-Neira C, Squella JA. Electrochemical determination of food colorants in soft drinks using MWCNT-modified GCEs. *Sens Actuat B* 2017, 240, 1257–64.
[88] Kumar S, Vicente-Beckett V. Glassy carbon electrodes modified with multiwalled carbon nanotubes for the determination of ascorbic acid by square-wave voltammetry. *Beilstein J Nanotechnol* 2012, 3, 388–96.
[89] Ziyatdinova G, Gainetdinova A, Morozov M, Budnikov H, Grazhulene S, Red'kin A. Voltammetric detection of synthetic water-soluble phenolic antioxidants using carbon nanotube based electrodes. *J Solid State Electrochem* 2012, 16, 127–34.
[90] Kachoosangi RT, Wildgoose GG, Compton RG. Carbon nanotube-based electrochemical sensors for quantifying the 'heat' of chilli peppers: the adsorptive stripping voltammetric determination of capsaicin. *Analyst* 2008, 133, 888–95.
[91] Guo W, Geng M, Zhou L, et al. Multi-walled carbon nanotube modified electrode for sensitive determination of an anesthetic drug: tetracaine hydrochloride. *Int J Electrochem Sci* 2013, 8, 5369–81.
[92] Habibi B, Pournaghi-Azar MH. Simultaneous determination of ascorbic acid, dopamine and uric acid by use of a MWCNT modified carbon-ceramic electrode and differential pulse voltammetry. *Electrochim Acta* 2010, 55, 5492–8.
[93] Heyrovský J, Kůta J. *Principles of Polarography*. New York, Academic Press, 1966.
[94] Ziyatdinova GK, Ziganshina ER, Budnikov HC. Application of surfactants in voltammetric analysis. *J Anal Chem* 2012, 67, 869–79.
[95] Franklin TC, Iwunze M. Oxidative voltammetry of organic compounds at platinum electrodes in micelle and emulsion systems. *Anal Chem* 1980, 52, 973–6.
[96] Love LJC, Habarta JG, Dorsey JG. The micelle-analytical chemistry interface. *Anal Chem* 1984, 56, 1132A–48A.
[97] Pelizzetti E, Pramauro E. Analytical applications of organized molecular assemblies. *Anal Chim Acta* 1985, 169, 1–29.
[98] Rusling JF. Molecular aspects of electron transfer at electrodes in micellar solutions. *Colloids Surf A* 1997, 123–124, 81–8.
[99] Wang L-H, Tseng S-W. Direct determination of d-panthenol and salt of pantothenic acid in cosmetic and pharmaceutical preparations by differential pulse voltammetry. *Anal Chim Acta* 2001, 432, 39–48.

[100] Acuña JA, Fuente C, Vãzquez MD, Tascón ML, Sánchez-Batanero P. Voltammetric determination of piroxicam in micellar media by using conventional and surfactant chemically modified carbon paste electrodes. *Talanta* 1993, 40, 1637–42.
[101] Posac JR, Vázquez MD, Tascón ML, et al. Determination of aceclofenac using adsorptive stripping voltammetric techniques on conventional and surfactant chemically modified carbon paste electrodes. *Talanta* 1995, 42, 293–304.
[102] Ziyatdinova G, Ziganshina E, Budnikov H. Electrooxidation of morin on glassy carbon electrode modified by carboxylated single-walled carbon nanotubes and surfactants. *Electrochim Acta* 2014, 145, 209–16.
[103] Ormonde DE, O'Neill RD. The oxidation of ascorbic acid at carbon paste electrodes: modified response following contact with surfactant, lipid and brain tissue. *J Electroanal Chem Interfacial Electrochem* 1990, 279, 109–21.
[104] Brainina KZ, Tchernyshova AV, Stozhko NY, Kalnyshevskaya LN. In situ modified electrodes in stripping voltammetry. *Analyst* 1984, 114, 173–80.
[105] Zhang S, Wu K, Hu S. Carbon paste electrode based on surface activation for trace adriamycin determination by a preconcentration and voltammetric method. *Anal Sci* 2002, 18, 1089–92.
[106] Caso García L. Voltameprometría sensibilizada por tensoactivos de metotrexato y ácido úrico en muestras biológicas, Ph.D. Thesis, University of Oviedo, 1995.
[107] Char MP, Niranjana E, Swamy BEK, Sherigara BS, Pai KV. Electrochemical studies of amaranth at surfactant modified carbon paste electrode: a cyclic voltammetry. *Int J Electrochem Sci* 2008, 3, 588–96.
[108] Chandrashekar BN, Swamy BEK, Mahesh KRV, Chandra U, Sherigara BS. Electrochemical studies of bromothymol blue at surfactant modified carbon paste electrode by using cyclic voltammetry. *Int J Electrochem Sci* 2009, 4, 471–80.
[109] Chitravathi S, Kumaraswamy BE, Niranjana E, Chandra U, Mamatha GP, Sherigara BS Electrochemical studies of sodium levothyroxine at surfactant modified carbon electrode. *Int J Electrochem Sci* 2009, 4, 223–37.
[110] Huang W, Yang C, Qu W, Zhang S. Voltammetric determination of malachite green in fish samples based on the enhancement effect of anionic surfactant. *Rus J Electrochem* 2008, 44, 946–51.
[111] Levent A, Yardim Y, Senturk Z Voltammetric behavior of nicotine at pencil graphite electrode and its enhancement determination in the presence of anionic surfactant. *Electrochim Acta* 2009, 55, 190–5.
[112] Gutiérrez-Fernández S, Blanco-López MC, Lobo-Castañón MJ, Miranda-Ordieres AJ, Tuñón-Blanco P. Adsorptive stripping voltammetry of rifamycins at unmodified and surfactant-modified carbon paste electrodes. *Electroanal* 2004, 16, 1660–6.
[113] Zheng J, Zhou X. Sodium dodecylsulfate-modified carbon paste electrodes for selective determination of dopamine in the presence of ascorbic acid. *Bioelectrochem* 2007, 70, 408–15.
[114] Jaiswal PV, Ijeri VS, Srivastava AK. Voltammetric behavior of certain vitamins and their determination in surfactant media. *Anal Sci* 2001, 17S, i741–4.
[115] Atta NF, Darwish SA, Khalli SE, Galal A. Effect of surfactants on the voltammetric response and determination of an antihypertensive drug. *Talanta* 2007, 72, 1438–45.
[116] Ziyatdinova G, Giniyatova E, Budnikov H. Cyclic voltammetry of retinol in surfactant media and its application for the analysis of real samples. *Electroanal* 2010, 22, 2708–13.
[117] Ziyatdinova GK, Ziganshina ER, Os'kina KS, Budnikov HC. Voltammetric determination of sterically hindered phenols in surfactant-based self-organized media. *J Anal Chem* 2014, 69, 750–7.
[118] Reis AP, Tarley CRT, Mello LD, Kubota LT. Simple and sensitive electroanalytical method for the determination of ascorbic acid in urine samples using measurements in an aqueous cationic micellar medium. *Anal Sci* 2008, 24, 1569–74.

[119] Amor-García I, Blanco-López MC, Lobo-Castañón MJ, Miranda-Ordieres AJ, Tuñón-Blanco P. Flufenamic acid determination in human serum by adsorptive voltammetry with in situ surfactant modified carbon paste electrodes. *Electroanal* 2005, 17, 1555–62.
[120] Fogliatto DK, Barbosa AM, Ferreira VS. Voltammetric determination of the phytoestrogen genistein in soy flours and soy based supplements using cationic surfactant cetyltrimethylammonium bromide. *Colloids Surf B* 2010, 78, 243–9.
[121] Araújo TA, Cardoso JC, Barbosa AMJ, Ferreira VS. Influence of the surfactant bromide of cetyltrimethylammonium in the determination of chlorogenic acid in instant coffee and mate tea samples. *Colloids Surf B* 2009, 73, 408–14.
[122] de Araujo TA, Barbosa AMJ, Viana LH, Ferreira VS. Voltammetric determination of tert-butylhydroquinone in biodiesel using a carbon paste electrode in the presence of surfactant. *Colloids Surf B*, 2010, 79, 409–14.
[123] Hu C, He Q, Li Q, Hu S. Enhanced reduction and determination of trace thyroxin at carbon paste electrode in presence of trace cetyltrimethylammonium bromide. *Anal Sci* 2004, 20, 1049–54.
[124] Ziyatdinova GK, Giniyatova ER, Budnikov HC. Voltammetric determination of α-tocopherol in the presence of surfactants. *J Anal Chem* 2012, 67, 467–73.
[125] Ziyatdinova G, Ziganshina E, Budnikov H. Voltammetric sensing and quantification of eugenol using nonionic surfactant self-organized media. *Anal Methods* 2013, 5, 4750–6.
[126] Jain R, Vikas R, Rather JA. Voltammetric behaviour of drotaverine hydrochloride in surfactant media and its enhancement determination in Tween-20. *Colloids Surf B* 2011, 82, 333–9.
[127] González A, Ruiz MA, Yáñez-Sedeño P, Pingarrón JM. Voltammetric determination of tert-butylhydroxyanisole in micellar and emulsified media. *Anal Chim Acta* 1994, 285, 63–71.
[128] Ziyatdinova GK, Giniyatova ER, Budnikov HC. Application of nonionic surfactants in voltammetry of eugenol in water-organic media. *Butlerov Commun* 2011, 24, 66–71.
[129] Luo L, Wang X, Li Q, Ding Y, Jia J, Deng D. Voltammetric determination of ferulic acid by didodecyldimethylammonium bromide/nafion composite film-modified carbon paste electrode. *Anal Sci* 2010, 26, 907–11.
[130] Shankar SS, Swamy BEK, Chandrashekar BN. Electrochemical selective determination of dopamine at TX-100 modified carbon paste electrode: a voltammetric study. *J Mol Liq* 2012, 168, 80–6.
[131] Wei X, Zhao Q, Wu W et al. Zwitterionic surfactant modified acetylene black paste electrode for highly facile and sensitive determination of tetrabromobisphenol A. *Sensors* 2016, 16, E1539.
[132] Zhang Y, Luo L-Q, Ding Y-P, Li Q-X, Shen X. Fabrication of cetyltrimethylammonium bromide/chitosan modified glassy carbon electrode for simultaneous determination of uric acid and ascorbic acid. *J Chinese Chem Soc* 2010, 57, 1061–66.
[133] Deng P, Xu Z, Feng Y. Highly sensitive and simultaneous determination of ascorbic acid and rutin at an acetylene black paste electrode coated with cetyltrimethylammonium bromide film. *J Electroanal Chem* 2012, 683, 47–54.
[134] Blanco-López MC, Lobo-Castañón MJ, Ordieres AJM, Tuñón-Blanco P. Electrochemical behavior of catecholamines and related compounds at in situ surfactant modified carbon paste electrodes. *Electroanal* 2007, 19, 207–13.
[135] Shankar SS, Swamy BEK, Chandra U, Manjunatha JG, Sherigara BS. Simultaneous determination of dopamine, uric acid and ascorbic acid with CTAB modified carbon paste electrode. *Int J Electrochem Sci* 2009, 4, 592–601.
[136] Vishwanath CC, Swamy BEK, Sathisha TV, Madhu GM. Electrochemical studies of dopamine at lithium zirconate/SDS modified carbon paste electrode: a cyclic voltammetric study. *Anal Bioanal Electrochem* 2013, 5, 341–51.

[137] Pătraşcu DG, David V, Bălan I, et al. Selective DPV method of dopamine determination in biological samples containing ascorbic acid. *Anal Lett* 2010, 43, 1100–10.
[138] Colín-Orozco E, Ramírez-Silva MT, Corona-Avendaño S, Romero-Romoa M, Palomar-Pardavé M. Electrochemical quantification of dopamine in the presence of ascorbic acid and uric acid using a simple carbon paste electrode modified with SDS micelles at pH 7. *Electrochim Acta* 2012, 85, 307–13.
[139] Rattanarat P, Dungchai W, Siangproh W, Chailapakul O, Henrye CS. Sodium dodecyl sulfate-modified electrochemical paper-based analytical device for determination of dopamine levels in biological samples. *Anal Chim Acta* 2012, 744, 1–7.
[140] Shankar SS, Shereema RM, Prabhu GRD, Rao TP, Swamy BEK. Electrochemical detection of dopamine in presence of serotonin and ascorbic acid at tetraoctylammonium bromide modified carbon paste electrode: a voltammetric study. *J Biosens Bioelectron* 2015, 6, 168.
[141] Xiaomei C, Luo L, Ding Y, Zou X, Bian R. Electrochemical methods for simultaneous determination of dopamine and ascorbic acid using cetylpyridine bromide/chitosan composite film-modified glassy carbon electrode. *Sens Actuat B* 2008, 129, 941–6.
[142] Zou X, Luo L, Ding Y, Wu Q. Chitosan incorporating cetyltrimethylammonium bromide modified glassy carbon electrode for simultaneous determination of ascorbic acid and dopamine. *Electroanal* 2007, 19, 1840–4.
[143] Luo L-Q, Li Q-X, Ding Y-P, Zhang Y, Shen X. Docosyltrimethylammonium chloride modified glassy carbon electrode for simultaneous determination of dopamine and ascorbic acid. *J Solid State Electrochem* 2010, 14, 1311–6.
[144] Chandrashekar BN, Swamy BEK. Simultaneous cyclic voltammetric determination of norepinephrine, ascorbic acid and uric acid using TX-100 modified carbon paste electrode. *Anal Methods* 2012, 4, 849–54.
[145] Chandrashekar BN, Swamy BEK. Electrocatalysis of SDS surfactant modified carbon paste electrode for the simultaneous determination of ascorbic acid, norepinephrine and folic acid. *Anal Bioanal Electrochem* 2016, 8, 345–57.
[146] Chandrashekar BN, Swamy BEK, Gururaj KJ, Chitravathi S, Pandurangachar M. Simultaneous electroanalysis of epinephrine, ascorbic acid and uric acid at SDS modified carbon paste electrode: a cyclic voltammetric study. *Chem Sens* 2012, 2, 5.
[147] Shankar SS, Swamy BEK. Detection of epinephrine in presence of serotonin and ascorbic acid by TTAB modified carbon paste electrode: a voltammetric study. *Int J Electrochem Sci* 2014, 9, 1321–39.
[148] Shankar SS, Swamy BEK, Chandrashekar BN, Gururaj KJ. Sodium dodecylbenzene sulfate modified carbon paste electrode as an electrochemical sensor for the simultaneous analysis of dopamine, ascorbic acid and uric acid: a voltammetric study. *J Mol Liq* 2013, 177, 32–9.
[149] Ziyatdinova G, Kozlova E, Budnikov H. Electropolymerized eugenol-MWNT-based electrode for voltammetric evaluation of wine antioxidant capacity. *Electroanal* 2015, 27, 1660–8.
[150] Ziyatdinova G, Kozlova E, Ziganshina E, Budnikov H. Surfactant/carbon nanofibers modified electrode for the determination of vanillin. *Monatsh Chem* 2016, 147, 191–200.
[151] Wang X, Li J, Yu Z. Selective determination of epinephrine in the presence of ascorbic acid on a carbon nanotubes modified electrode based on the enhancement effects of the hexadecyltrimethylammonium bromide. *Int J Electrochem Sci* 2015, 10, 93–101.
[152] Gowda JI, Gunjiganvi DG, Sunagar NB, Bhat MN, Nandibewoor ST. MWCNT-CTAB modified glassy carbon electrode as a sensor for the determination of paracetamol. *RSC Adv* 2015, 5, 49045–53.
[153] Gowda JI, Mallappa M, Nandibewoor ST. CTAB functionalized multiwalled carbon nanotube composite modified electrode for the determination of 6-mercaptopurine. *Sens BioSensing Res* 2017, 12, 1–7.

[154] Gowda JI, Nandibewoor ST. Electro-oxidation and determination of tripelennamine hydrochloride at MWCNT-CTAB modified glassy carbon electrode. *Electroanal* 2016, 28, 523–32.
[155] Liang Z, Zhai H, Chen Z, Wang S, Wang H, Wang S. A sensitive electrochemical sensor for flavonoids based on a multi-walled carbon paste electrode modified by cetyltrimethyl ammonium bromide-carboxylic multi-walled carbon nanotubes. *Sens Actuat B* 2017, 244, 897–906.
[156] Zhang J, Zhu Z, Zhu J, Li K, Hua S. Selective determination of dopamine, ascorbic acid and uric acid at SDS-MWCNTs modified glassy carbon electrode. *Int J Electrochem Sci* 2014, 9, 1264–72.
[157] Xu W, Lei R, Cao W, Guo C, Zhang X, Wang S. Voltammetric method using multi-walled carbon nanotubes modified glassy carbon electrode for the determination of terbutaline sulfate in pork sample. *J Anal Sci Meth Instrum* 2013, 3, Article ID 32352.
[158] Ziyatdinova G, Aytuganova I, Nizamova A, Morozov M, Budnikov H. Cyclic voltammetry of natural flavonoids on MWNT-modified electrode and their determination in pharmaceuticals. *Collect Czech Chem Commun* 2011, 76, 1619–31.
[159] Ziyatdinova G, Aytuganova I, Nizamova A, Budnikov H. Differential pulse voltammetric assay of coffee antioxidant capacity with MWNT-modified electrode. *Food Anal Meth* 2013, 6, 1629–38.
[160] Ziyatdinova GK, Nizamova AM, Aytuganova II, Budnikov HC. Voltammetric evaluation of the antioxidant capacity of tea on electrodes modified with multiwalled carbon nanotubes. *J Anal Chem* 2013, 68, 132–9.
[161] Ziyatdinova G, Os'kina K, Ziganshina E, Budnikov H. Simultaneous determination of TBHQ and BHA on a MWNT-Brij® 35 modified electrode in micellar media. *Anal Methods* 2015, 7, 8344–51.
[162] Aneesh K, Berchmans S. Highly selective sensing of dopamine using carbon nanotube ink doped with anionic surfactant modified disposable paper electrode. *J Solid State Electrochem* 2016, doi:10.1007/s10008-016-3482-2
[163] Thomas T, Mascarenhas RJ, D'Souza OJ, Detriche S, Mekhalif Z, Martis P. Pristine multi-walled carbon nanotubes/SDS modified carbon paste electrode as an amperometric sensor for epinephrine. *Talanta* 2014, 125, 352–60.
[164] Zheng D, Ye J, Zhang W. Some properties of sodium dodecyl sulfate functionalized multiwalled carbon nanotubes electrode and its application on detection of dopamine in the presence of ascorbic acid. *Electroanal* 2008, 20, 1811–18.
[165] Materon EM, Wong A, Klein SI, Liu JW; Sotomayor MDPT. Multi-walled carbon nanotubes modified screen-printed electrodes for cisplatin detection. *Electrochim Acta* 2015, 158, 271–6.
[166] Madrakian T, Bagheri H, Afkhami A, Rad AC. Direct electrochemical reaction of phytohemagglutinin adsorbed at the multi-walled carbon nanotubes modified glassy carbon electrode. *J Electrochem Soc* 2014, 161, G37–42.
[167] Janegitz BC, Pauliukaite R, Ghica ME, Brett CMA, Fatibello-Filho O. Direct electron transfer of glucose oxidase at glassy carbon electrode modified with functionalized carbon nanotubes within a dihexadecylphosphate film. *Sens Actuat B* 2011, 158, 411–7.
[168] Hashemnia S, Khayatzadeh S, Moosavi-Movahedi AA, Ghourchian H. Direct electrochemistry of catalase in multiwall carbon nanotube/dodecyl trimethylammonium bromide film covered with a layer of Nafion on a glassy carbon electrode. *Int J Electrochem Sci* 2011, 6, 581–95.
[169] Budnikov HC, Shirokova VI. Term "nano" in electroanalysis: a trendy prefix or a new stage of its development? *J Anal Chem* 2013, 68, 663–70.

G. Evtugyn, A. Porfireva, H. Budnikov and T. Hianik

# 8 Nanomaterials in the Assembly of Electrochemical DNA Sensors

**Abstract:** The development of electrochemical DNA sensors and aptasensors based on nanoparticles different in nature, size, shape, and preparation protocols has been considered with particular emphasis to the mechanism of their influence on signal readout and way of implementation in the biosensor assembly. Most attention is paid to application of Au nanoparticles and carbonaceous nanomaterials though the examples of other applications and hybrid nanomaterials are given. The analytical performance of DNA sensors and aptasensors utilizing nanomaterials is classified in accordance with their targets and role of nanoparticles in sensitivity and selectivity of the response. The trends of future progress in the biochemical applications of nanomaterials are discussed.

## 8.1 Introduction

There is an urgent need in the development of simple and compact analytical devices providing reliable information on the content of various samples tested. Among many other possible areas of application, chemical sensors are especially demanded in medicine in the framework of the point-of-care diagnostics concept [1, 2]. Being rather simple to operate by unqualified staff and equipped with remote control, personal medical sensors offer new opportunities in the chronic diseases medical treatment and continuous monitoring of the health status. Many medical sensors utilize conventional approaches to increase sensitivity toward particular species, for example, physical accumulation of an analyte followed by its involvement in specific reactions with an ionophore, mediator, or electrode. Nevertheless, further improvement of the biosensor performance as well as extension of the number of the analytes call for the development of new detection principles and broader application of the biochemical recognition. Such approaches assume enzymes, antibodies, or nucleic acids introduced (immobilized) in the assembly of a primary transducer (electrode, optic fiber, cantilever) and involved in an analyte recognition. Appropriate analytical devices based on specific biochemical reactions (enzyme–substrate, antigen–antibody, DNA–intercalator, etc.) are called biosensors (biochemical sensors) [3].

Starting from 1962 with first glucose sensor assembled from the oxygen electrode covered with the permeable membrane containing glucose oxidase [4], biosensors

https://doi.org/10.1515/9783110542011-008

emerged from the laboratory to a global international market covering more than $14 billion of annual sales [5]. Biosensors mostly used in medicine are intended for the detection of the metabolites (glucose, urea, and lactate analysis), the immuno- [6] and DNA assay [7, 8]. Considering further progress, the DNA sensors demonstrate maximal opportunities among other biochemical receptors due to universal targeting, prospects of miniaturization (lab-on-chip, microfluidic devices [9]), and compatibility with conventional diagnostic systems.

Nanomaterials involve those consisted of the particles sized between 1 and 100 nm in at least one dimension [11]. Their application in electrochemical sensors and biosensors is mostly directed to the increase of the sensitivity of the signal and miniaturization of the measuring devices [7–10, 12–14].

Transduction principle affects the application of the nanomaterials because of the specific requirements existed for all the transducers applied. Thus, most of the nanoparticles used in for electrochemical (bio)sensors show electroconductivity or redox activity. Small size and monolayer deposition make it possible to combine the low- and nonconductive materials with metal and carbonaceous electrodes and avoid at the same time significant worsening in electric wiring of a bioreceptor. Nevertheless, the idea of significant enhancement of the electrode surface and hence of the quantities of recognition elements dominates among other reasons to implement nanoparticles in conventional sensors. Other possible motifs involve simplification of the bioreceptor immobilization protocols, miniaturization of appropriate devices, development of new primary transducers like field effect transistors (FETs) based on a single-walled carbon nanotube (SWCNT) [15].

It should be mentioned that the variety of nanomaterials described in the assembly of electrochemical biosensors remains rather constant during the past decade and does not tend to significant increase because of the limited offers from the manufacturers and rather complex procedures of their synthesis, size-specific separation, and purification. Even for the carbon nanotubes (CNTs) with a rich story of sensor application, few researchers report about the synthesis of some specific sorts of CNTs with advantages over the commercial products, for example, alone standing forest like CNTs, especially for their application in FETs or other types of biosensors [16].

Reduced graphene oxide is mainly synthesized by oxidation of graphite by strong oxidants in acidic media followed by chemical or electrochemical reduction of the products [17, 18]. Multiwalled CNTs (MWCNTs) and SWCNTs, either as-synthesized or treated with oxidants, strong acids, biotin, and other surface modifiers, are available in Sigma-Aldrich catalog together with other carbonaceous nanoparticles [19]. Besides, silicate, ferrite, and noble metal nanoparticles are purchased, both clean and premodified with functional groups requested for the further coupling with receptors [20–22].

Other examples of nanomaterials synthesized for their further application in sensor assembly include metals obtained by controlled electrolysis from metal salts and complexes, metal oxides, and insoluble complexes that are chemically synthesized from appropriate precursors directly on the transducer surface [23–25]. They can be also obtained as suspensions in aqueous and organic media with moderate stability prior to electrode modification and casted on their surface alone or together with other components. Limited reproducibility of size distribution and rather broad range of particles' shape remain a weak point of such "home-made" protocols of nanomodification.

Owing to the importance of biosensors for medical diagnostics and potential benefits related to the application of nanomaterials in their assemblies, the number of appropriate articles has been enormously increased during the past decade. Some reviews recently published concentrated on specific targets of such biosensors or nature of nanomaterials applied [26–32]. In this chapter, we summarize the progress in the development of electrochemical DNA sensors achieved in the past 5 years with particular emphasis to the role of nanomaterials and mechanisms of their influence on the biosensor signal and its characteristics in real sample assay. The description of the DNA sensors is subdivided in accordance with the nature of recognition element and biological targets.

## 8.2 DNA sensors: Recognition elements and signal transduction

### 8.2.1 Biochemical elements applied in the DNA sensors assemblies

The DNA sensors utilize several types of biochemical receptors, either selected from natural nucleotide sequences or synthesized *de novo*, which are able to highly specific interactions with biological targets. In accordance with their nature and preparation protocol, all the DNA sensors can be classified into several groups.

**Genosensors** involve rather short single-stranded (ss-) oligonucleotide sequences (also called DNA probes) that interact with complementary strands present in the sample tested with formation of native double-stranded (ds-) DNA molecule fragment [33, 34]. The DNA primers applied in conventional genetic assay and polymerase chain reaction (PCR) are frequently used as the DNA probes in biosensor format. The interaction between the DNA probe and a target sequence called hybridization assumes the formation of stable pairs of the nucleotide bases, that is, adenine–thymine (A–T) and guanine–cytosine (C–T) via hydrogen bonds (Fig. 8.1).

The formation of a hybridization product, that is, ds-DNA piece, confirms existence of an appropriate nucleotide sequence complementary to the probe in the sample. The DNA probes can be related to the variable parts of genes, amplicons, etc.

Genosensors can be used for the direct diagnostics of the pathological microorganisms and the viruses, for the identification of genetically modified organisms (GMOs), selection of the meat origin, etc. Selectivity of agenosensor is estimated by its ability to distinguish between the fully complementary sequence and that differed from it by one, two, etc. nucleotide (so-called single, double, etc. mismatches).

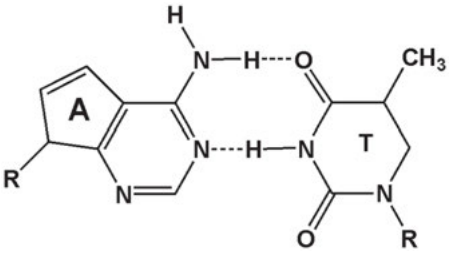


**Fig. 8.1:** Complementary interactions between nucleotides in the DNA molecule. A – adenine, T – thymine, G – guanine, and C – cytosine.

**Aptasensors** include aptamers, ss-DNA or RNA molecules with high specificity toward various analytes, for example, proteins, antibiotics, etc. [35]. They are synthesized *de novo* by selection against targets from the random DNA/RNA libraries of oligonucleotides. SELEX (**S**ystematic **E**volution of **L**igands by **EX**ponential enrichment) is the most frequently used protocol for aptamer selection [36]. The recognition of aptamer targets is often compared with antigen–antibody interaction. Contrary to the antibodies, aptamers are more stable to hydrolysis and chemical/thermal denaturation. They show in many cases efficiency of analyte binding comparable to that of specific antibodies. For this reason, aptamers are often called as "artificial antibodies." Once selected, aptamers are easily produced *quantum satis* and seem attractive as biorecognition elements from the point of view of possible commercialization. Many aptamers commercially available contain terminal amino-, carboxylic, or thiol groups or biotin residues necessary for their covalent binding to the careers or the transducers. Although the first SELEX-related patent was filed in 1989, intensive investigations are still performed to select more aptamers against various targets, stabilize their structure, and decrease cross-binding with matrix interferences. Aptamer exist in the structures that might be significantly different from those of native ds-DNA. Thus, guanine-rich areas form flat tetragons stabilized with potassium ions positioned in the center and guanine residues in the vertexes. Such $G_4$-quadruplexes can self-assemble to form stacks or reversibly switch to linear configuration after sharp changes in ionic strength or pH of microenvironment. Partially complementary aptamers form stem-loops that recognize appropriate guest molecules, including short DNA sequences complementary to the main part of the DNA probe. Such an interaction

results in disturbance of the loop and its relative position against transducer interface. The conformational changes described result in serious changes in the permeability of the aptamer layer or the accessibility of the labels implemented in their structure.

**Peptide nucleic acid (PNA) based sensors** utilize synthetic analogs of native DNA that are much more stable to hydrolysis and do not contain charged groups. Due to similar to DNA distance between the nucleic bases, the PNAs are able to hybridization with complementary DNA sequences and form DNA–PNA hybrid structures. PNAs consist of repeating N-(2-aminoethyl)-glycine units linked by amide bonds (Fig. 8.2) [37, 38].

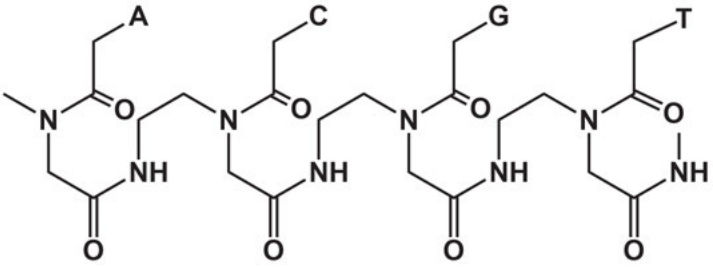


**Fig. 8.2:** Chemical structure of a PNA. The substituents marked with letters indicate nucleotide base residues.

Among other recognition elements, **native DNA** is rather rarely used in the biosensor assembly due to the large size and problems with reproducible positioning of the biomolecules on the electrode surface. Steric limitations of the DNA deposition onto the electrode surface due to rather rigid helical structure of biomolecule prevent the direct oxidation of the guanine and the adenine residues, so that electrochemical signal is mostly generated by the mediated oxidation of the above nucleotides and by changes in the surface layer permeability for the small redox probes [39, 40]. Even if native DNA is announced as a part of the biosensor assembly, it should be taken into account that manipulations with the DNA solutions (dilution, pipetting, sonication, etc.) result in fragmentation of the DNA molecules. Nevertheless, such DNA sensors have found application for the detection of the oxidative DNA damage [41] or for the determination of low-molecular compounds that are accumulated on the DNA due to intercalation or electrostatic interactions [42]. Autoimmune diseases result in formation of auto-DNA antibodies that specifically interact with ds-DNA molecules and provoke their following cleavage into the pieces. Such interactions are used for the biosensor-based diagnostics of autoimmune character of a disease [43].

**DNA nanostructures.** The progress in the nanotechnologies and investigations directed to the use of nanomaterials in biology and medicine has inspired the synthesis on various three-dimensional (3D) structures using synthetic oligonucleotides

as building blocks [8]. Variety of functional groups and reversible conformational changes controlled by the changes in the microenvironment of these synthetic constructs make them attractive as possible basis of the drug delivery systems, nanomachinery, and nanoscale sensing devices. Thus, the DNA tetrahedrons exert spatial positioning of terminal guest groups on solid support. They are compatible with conventional immobilization protocols based on self-assembling and Au–S binding, whereas the ss-DNA probe opposite to the bottom plane of the tetrahedron selectively binds a biological target [44]. Own size of a tetrahedron limits probe-to-probe spacing of neighboring 3D structures and hence their surface density (about $4.8 \times 10^{12}$ probes/$cm^2$). The DNA origami is another example of 2D and 3D nanostructures that are created using complementary interactions of specific consequences. In mostly used protocol, DNA origami assembling involves folding a long viral ss-DNA by multiple small "staple" strands [45]. Such structures can find application for the detection of the single-nucleotide polymorphism (SNP) [46]. Although the appropriate sensors utilize fluorescence signal and AFM data detection, they promise fast progress in electrochemical devices, too. The 3D structures of some DNA-related receptors applied in biosensor assembly are outlined in Fig. 8.3.

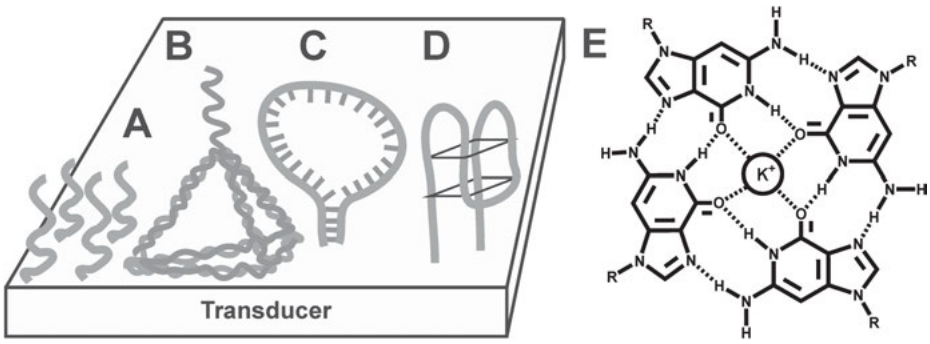


**Fig. 8.3:** Schematic outlines of DNA-related nanostructures immobilized on the transducer surface. (a) Conventional DNA probe; (b) 3D DNA tetrahedron; (c) stem loop aptamer; (d) aptamer in G4 quadruplex form; and (e) structure of the G4 quadruplex.

### 8.2.2 Measurement of the signal of electrochemical DNA sensors

Though a variety of the DNA-related species are described in the DNA sensor assembly, a limited number of universal schemes are used for generation of the signal with appropriate transducers. Owing to the domination among other electrochemical sensors, voltammetric (amperometric) and impedimetric sensors will be preferably considered. For them, the protocols of the signal measurement can be subdivided into two groups, that is, *label-free* and *label based* methods of signal quantification. The classification principles are presented in Fig. 8.4.

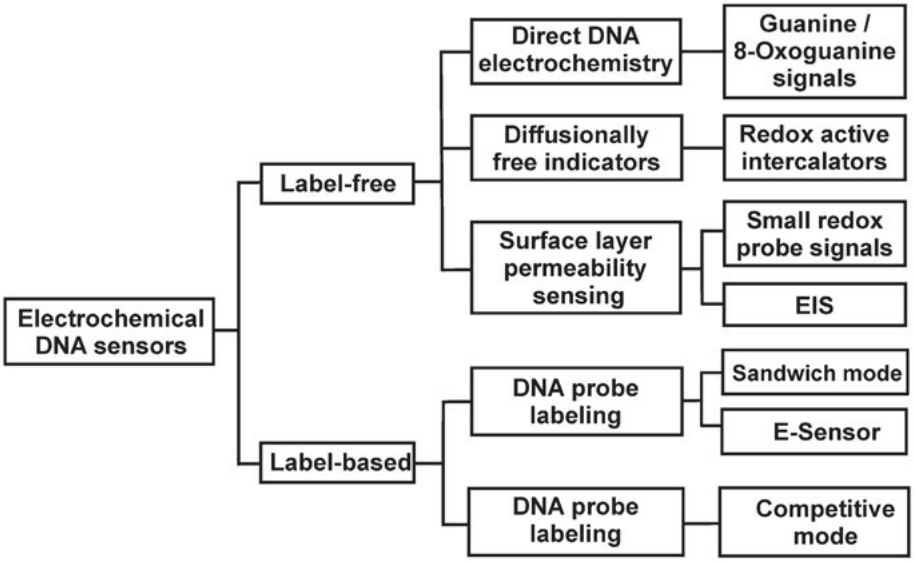


**Fig. 8.4:** Classification of the protocols for the signal determination of the DNA sensors.

**Label free** methods of signal record do not require complex manipulation with the DNA receptors except those necessary for their immobilization. Many of them are conducted in a single step or by consecutive addition of reactants to the same working solution. Taking into account that each additional step is followed by biosensor washing, this significantly reduces total measurement time and possible sources of mistakes related to wrong dilution, incomplete solution mixing, or removal of non-bonded species. On the other hand, the label-based techniques often provide lower limit of detection (LOD) and higher specificity of the response against label-free techniques.

Description of the label-free detection of a recognition event starts with the direct or mediated electrochemical oxidation of guanine residues (1).

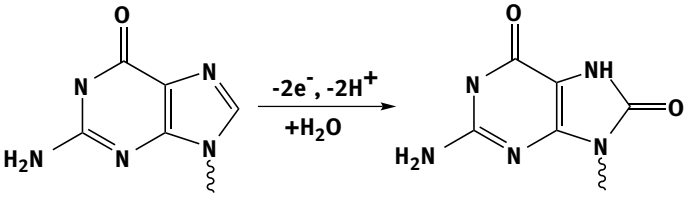


(1)

The reaction is accelerated in cases of the oxidative DNA damage and mediation with some redox probes. Also, accessibility of guanine is higher in ss-DNA sequences. The latter fact is used for the discrimination of the DNA probe and the product of hybridization with a biological target [47].

Although steric problems prevent the electron transfer from the majority of guanine units, small oxidation current appears on the electrodes covered with the

ds-DNA fragments. It can be recorded in differential pulse (DPV) or square wave voltammetry (SWV) on carbon electrodes. For better discrimination of the signals referred to ss- and ds-DNAs, the guanine residues in the DNA probe can be substituted with inosine fragments [48]. They retain its ability to form pairs with cytosine but are electrochemically inactive, so that the current generated after hybridization fully belongs to the biological target containing guanine. To a lesser extent, oxidation of adenine can be used for the same signal detection [49]. The signals of nucleotides are increased by implementation of the mediators of electron transfer, for example, bipyridine or phenanthroline complexes of Co, Ru, and Rh. The examples of mediators frequently used in the assembly of DNA sensors are presented in Fig. 8.5.

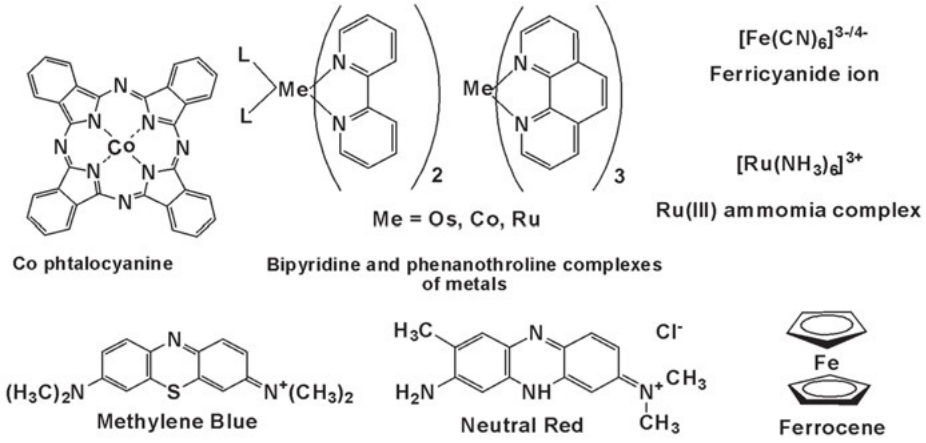


**Fig. 8.5:** Typical redox indicators and labels applied in electrochemical DNA sensors.

Another label-free technique estimates permeability of the surface layer toward small charge carriers (redox probes). In the simplest way, the charge flux is quantified by appropriate oxidation current measured in the DC mode. Ferricyanide ion $[Fe(CN)_6]^{3-}$ is mostly used in such investigations. Hybridization decreases the diffusion rate of ferricyanide and hence the current of appropriate peaks on voltammograms because of implementation of the non-conducting molecules of a biological target in the surface layer and because of the increased negative charge of phosphate groups of oligonucleotides that exert shielding effect on the transfer of negatively charged redox molecules. For aptasensors, similar effect is achieved by the reversible conformation switch of the linear form into $G_4$-quadruplex or steam-loop structure to linear one. The signal of redox probe can be recorded by electrochemical impedance spectroscopy (EIS) as a shift of the charge transfer resistance. Such a phenomenon was observed for ochratoxin A detection with impedimetric aptasensor [50].

Specific interaction of the charge carrier with ss- or ds-DNA also affects the signal. Thus, many planar heteroaromatic molecules penetrate (intercalate) the ds-DNA

helix in between pairs of complementary nucleotides and lose their redox activity [51]. Methylene blue is one of the most frequently used redox active intercalators [52]. Bipyridine and phthalocyanine ligands of metal complexes (see Fig. 8.5) partially intercalate DNA molecules and can either mediate the electron transfer from guanine residues to dissolved oxygen or to the electrode or directly participate in the electron exchange with the electrode. Appropriate changes in the currents indicate conditions of the electron transfer that indicate hybridization, oxidative DNA damage, or DNA–protein interactions. Redox active mediators are often applied as labels or together with labels in appropriate techniques.

**Labels** are rather small molecules, which are covalently bonded to the biochemical reactants and which presence (concentration) is easily quantified by appropriate sensor (transducer). For the electrochemical sensors, carbonaceous and metallic nanoparticles, phenothiazine, phthalocyanine, and ferrocene derivatives can be applied as labels [52] together with enzymes [53] and quantum dots [54].

The operation of label-based DNA sensors is often similar to that in conventional immunochemical assay. Frequently used approaches are illustrated in Fig. 8.6.

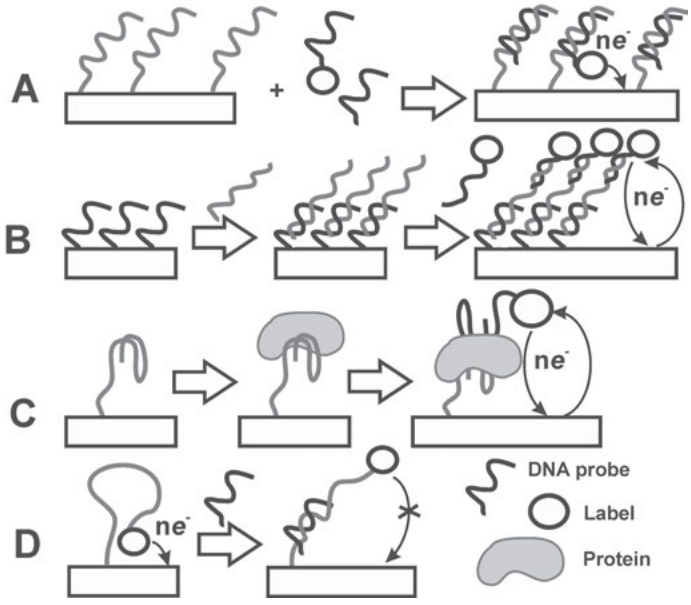


**Fig. 8.6:** The operation of label-based DNA sensors. (a) Competitive assay; (b) sandwich assay with capturing and signaling DNA probes; (c) sandwich assay with aptamers and aptamer–protein interactions; and (d) E-sensor with the labeled stem-loop DNA probe.

In **competitive assay**, a sample containing biological target is mixed with the solution of the same sequence bearing a label. Ratio of labeled and non-labeled products of

hybridization on the transducer interface yields from the ratio of their concentrations in the solution: the higher concentration of the target the lower label signal. In **sandwich assay**, two types of DNA probes are utilized. One of them (capturing probe) is attached to the electrode and interacts with a piece of a target containing complementary sequence. In this manner, the hybridization product leaves part of ss-DNA sequence free for the following interaction with a second (signaling) DNA probe that bears label. Its signal increases with the analyte concentration. Similar schemes are used for detection of species specifically interacting with the capturing DNA probe. Thus, DNA–protein interaction can be determined by aptamer specific to the binding site of the protein different from that providing its interaction with capturing aptamer/DNA probe.

Multistep protocol of the sandwich assay is one of the most obvious disadvantages of this measurement protocol because each addition of the reagents assumes time and labor consuming washing steps and increases probability of mechanical distortion of the sensing layer. For this reason, various alternatives have been elaborated to avoid these limitations. In so-called E-sensors, a stem-loop DNA probe is used. It is attached to the electrode by terminal amino or thiol group and labeled with redox active group on the opposite end. Due to partial complementarity of the fragments near both ends of the probe, label is fixed near the electrode surface to establish fast electron exchange and a high amperometric response (see Fig. 8.6d). In the presence of a target sequence, the stem-loop DNA switches to linear form with the same label withdrawn from the electrode [55]. The described mechanism of E-sensor operation is only one example of more general displacement schemes where capturing DNA probe retains their conformation due to partial hybridization with auxiliary sequence that is replaced by target DNA providing either label access or configuration necessary for wiring label to the electrode [56–58]. Thus, the displacement scheme is realized in detection of various analytes. It assumes conformational switches between $G_4$ quadruplex and linear forms of an aptamer [59]. Displacement-based DNA sensors show unusual calibration curve with a narrow linear range and a sharp rise corresponded to the conformation change initiated by ultra-small quantities of an analyte. For this reason, they are also called as "signal on-off sensors." Reversibility of the changes observed in E-sensors makes easy their regeneration after use by thermal recovery of initial conformation of the DNA probe. This prolongs the lifetime of the biosensor and decreases the measurement cost.

## 8.3 DNA sensors based on metal nanoparticles

### 8.3.1 Au nanoparticles

Au nanoparticles are easily produced by electrochemical or chemical reduction performed either in the presence of a sensor transducer or separately to form stable dispersion of nanoparticles, which can be later on casted on the electrode surface [60].

Golden electrodes are quite stable and can be cleaned prior to such modification by treating with nitric acid, hydrogen peroxide, or "piranha solution." Variety of methods and efficient control of the growth of metal nuclei provide rather narrow size distribution of the particles. Their charge is mainly determined by the synthesis conditions. In most protocols of chemical reduction, the anionic Au complexes ($Au(CN)_4^-$, $AuCl_4^-$) are used as precursors, so that the surface of the Au nanoparticles becomes negatively charged. This promotes immobilization of the DNA oligonucleotides via terminal thiol groups. Site-specific immobilization is followed by electrostatic orientation of the biomolecules orthogonally to the electrode surface and hence simplifies access of rather bulky target sequences to the probes on the hybridization stage. Together with mild conditions of immobilization and excellent electroconductive properties, this makes Au electrode and Au nanoparticles attractive for the DNA sensor assembling. Besides thiolated biomolecules, dithiols, disulfides, for example, cysteamine, and thiolated carboxylic acids can form surface monolayers modified further by carbodiimide binding (Fig. 8.7).

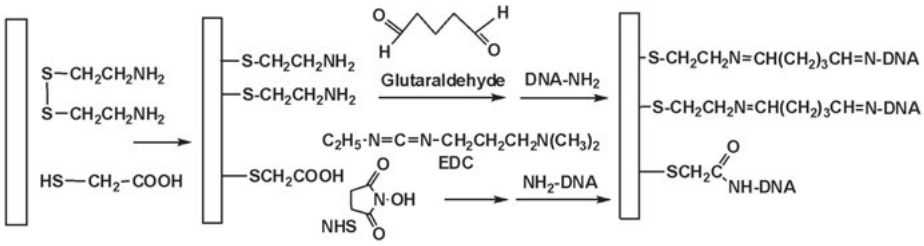


**Fig. 8.7:** Modification of Au electrode and nanoparticles with cysteamine and thioacetic acid followed by covalent binding of aminated oligonucleotides.

The surface reaction results in formation of a dense monolayer that prevents nonspecific adsorption of interferences and improves selectivity of the assay. To block undesired reactions, thiolated alcohols and physically adsorbed proteins, for example, bovine serum albumin (BSA) are commonly used for the same purpose. The appropriate treatment is mainly performed after target receptor immobilization or even after analyte binding to reach minimal background signal. The products of modification with organic thiols are called self-assembled monolayers (SAMs). They are used both with bare gold electrodes and Au nanoparticles. In all the protocols described, low thickness and regularity of the composition of the surface layer are achieved.

The Au nanoparticles are compatible with many other modifiers that mediate electron transduction, enhance working area, or promote DNA immobilization. Thus, Au nanoparticles were deposited onto electropolymerized aniline [61] followed by immobilization of thiolated DNA probes and hybridization detection by sandwich assay with alkaline phosphatase and DPV detection of naphthol as a product of enzymatic hydrolysis of α-naphthyl phosphate (2).

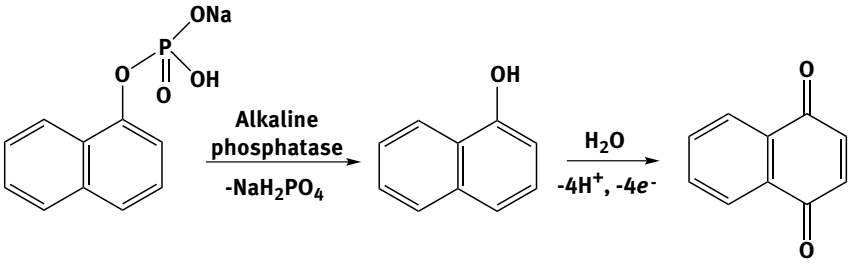


(2)

Various CNTs are frequently used as supports for the Au nanoparticles, alone or together with the stabilizing layer of chitosan [62]. Other examples of hybrid structures including the Au nanoparticles and performance of the DNA sensors based on such materials are given below in Tab. 8.1.

Reversed approach to the use of Au nanoparticles is described in [65]. Thiolated hairpin DNA probe with free terminal was first immobilized onto golden electrode and then involved in the hybridization reaction. After that, Au nanoparticles were attached to free terminal via thioglycolic acid and changes in the electroconductivity of the surface layer were quantified with EIS. Similarly, to that, Au labeling was used for detection of the homogeneous hybridization [71]. In this work, magnetic nanoparticles were first treated with the cyclodextrin and then dabcyl-modified hairpin DNA probe specific to the hepatitis B virus. The host–guest reaction resulted in liberation of the opposite terminus of the probe containing the Au nanoparticle. The product of the reaction was magnetically separated and dissolved in HCl. Anodic current of Au oxidation made it possible to detect down to 0.993 pM of a target. The steps of labeling with the Au nanoparticles and of hybridization of the complementary parts of the DNA sequences can be repeated for the amplification of the above effect. Stepwise amplification of the signal in the sandwich like assay has been described with the signaling DNA attached to the Au nanoparticles [72] (Fig. 8.8).

In this biosensor, capturing DNA probe 1 was immobilized by the Au–S bond to Au bare electrode. The reaction with a target sequence resulted in the formation of the hybridization product with free part of the sequence ready to the reaction with the signaling DNA probe 2. The amplification was achieved by use of the Au nanoparticles, which surface is modified with two types of oligonucleotides, that is, signaling probe and a shorter sequence, both with methylene blue as label. The ratio of the modifiers is determined on the stage of modification. As a result, direct coupling of a target with such a particle resulted in multiplication of the number of label molecules producing voltammetric signal. Moreover, excessive signaling probes remaining free could be then involved in similar interactions with other Au nanoparticles producing multiplicative number of labels attached.

Dual signal measurement mode has been proposed for detection of the single mutation in apolipoprotein E gene [73]. The Au nanoparticles were first electrochemically deposited onto the transparent indium-tin oxide (ITO) glass electrode.

**Tab. 8.1:** The characteristics of electrochemical DNA sensors based on Au nanoparticles

| Target | Immobilization technique | Signal measurement protocol | Linearity range/LOD | Ref. |
|---|---|---|---|---|
| | | Hybridization detection | | |
| *Staphylococcus aureus* gene | Au–S coupling on Au nanoparticles deposited onto polyaniline-covered screen-printed carbon electrode | Sandwich assay with alkaline phosphatase – streptavidin, DPV peak current of $\alpha$-naphthol oxidation | 1 fM to 10 nM / 0.33 fM | [62] |
| Gender classification of *Arowana* fish | Au–S coupling on kappa-carrageenan-polypyrrole-Au nanoparticles composite | DPV signal of diffusionally free redox active intercalator, anthraquinone-2-sulfonic acid | 5 aM to 1 pM / 5 aM | [63] |
| FLT3 gene | Aminated MWCNTs – Au nanoparticles multilayer obtained by layer-to-layer deposition on Au electrode, thiolated DNA hairpin probe | DPV signal of ferrocene, a terminal label of DNA probe, suppressed due to hybridization of a target DNA and switching conformation of a hairpin probe to linear form | 0.1–1000 pM/ 0.1 pM | [64] |
| 18-mer sequence | Thiolated hairpin DNA assembled on Au electrode | EIS signal recorded after hybridization of a target DNA followed by attachment of Au nanoparticles to free terminal of a probe modified with thioglycolic acid | 10 aM to 10 pM / 1.7 aM | [65] |
| 25-mer sequence | Rough Au covered with cathodically deposited Au nanoparticles and mixed monolayer of thiohexanol and thiolated DNA probe | Chronocoulometric and EIS measurements | Not reported, maximal surface density of DNA probe $6.5 \times 10^{-12}$ mol/cm$^2$ | [66] |
| Lung cancer–specific miRNA | 3D Origami structure with steam-loop DNA bearing ferrocene units on AU electrode covered with Au nanoparticles | DPV signal of ferrocene label | 100 pM to 1 µM / 10 pM | [67] |
| 18-mer sequence | Thiolated DNA probe attached to Au nanoparticles incorporated into 2D CuS sheet on acetyl black modified glassy carbon electrode | EIS signal with ferricyanide redox robe | 0.1 pM to 1 nM / 20 fM | [68] |
| Sequence-specific ds-DNA | Thiolated hairpin DNA probe bearing ferrocene units attached to Au nanoparticles on glassy carbon electrode | DPV signal of ferrocene units | 350 pM to 25 nM / 275 pM | [69] |
| *Lactococcus lactis* genus | Co-deposition of polypyrrole and Au nanoparticles composite followed by covalent linking of p-thiobenzoic acid and aminated DNA probe | EIS measurements of surface layer permeability with ferricyanide redox robe | 0.1 pM to 2 µM / 0.84 pM | [70] |

**Tab. 8.1:** (continued)

| Target | Immobilization technique | Signal measurement protocol | Linearity range/LOD | Ref. |
|---|---|---|---|---|
| Hepatitis B virus | Steam loop DNA probe labeled with Au nanoparticles and dabcyl interacts with target sequence and receives possibility to be attached to magnetic nanoparticles via dabcyl-β-cyclodextrin supramolecular binding | After magnetic separation, the complex is dissolved in HCl and oxidized. Then reduction of $[AuCl_4]^-$ is recorded by DPV | 1.505 pM to 0.301 nM / 0.99 pM | [71] |
| Specific point mutation in apolipoprotein E gene | Thiolated probes immobilized on Au nanoparticles synthesized on ITO glass electrode | Simultaneous measurements of surface layer permeability by EIS with ferricyanide redox probe and localized surface plasmon resonance by microfiber bundle | 500 nM to 10 µM / 512 nM | [72] |
| Gene sequences related to estrogen and progesterone receptors | Aminated 27-mer pinhole probe covalently attached to carboxylic groups of mercaptoundecanoic acid by aminated terminus and to Au nanoparticles with thiol group | Changes in electron transduction of the surface layer measured by EIS with ferricyanide redox probe | 5 fM to 500 pM / 0.3 fM | [73] |
| | Aptamer-based DNA sensors (aptasensors) | | | |
| Codeine | Au–S binding on Au-mesoporous silica nanoparticles | Changes in charge transfer resistance measured by EIS with ferricyanide redox probe | 10 pM to 100 nM / 3 pM | [74] |
| L-Histidine | Au-S binding of a pair of thiolated aptamers bearing ferrocene units on Au nanocrystals with high-index facets | SWV signal of ferrocene after cleavage of the aptamer sequence caused by DNAzyme activity of the analyte and release of the labeled sequence | 0.1 pM to 0.1 µM / 0.01 pM | [75] |
| ATP | Au electrode covered with monolayer of thiolated capture probe | ATP displacement of DNA probe from aptamer-DNA duplex followed by interaction with capture probe, saturation with thionine and DPV record of thionine signal | 0.1–50 nM/ 0.05 nM | [76] |
| $K^+$ | Au electrode covered with thiolated aptamer bearing ferrocene units | Electron transduction to DNAzyme mimicking HRP activity consisted of $G_4$ quadruplex stabilized by an analyte and hemin and mediated by ferrocene units | 5–200 µM / 1.6 µM | [77] |
| Protein tyrosine kinase | Au electrode covered with Au nanoparticles with immobilized aptamer–DNA probe complex bearing Au nanoparticles | DPV signal of methylene blue indicator, displacement mechanism | 1–100 pM / 372 fM | [78] |

This process was controlled by measurement of the localized surface plasmon resonance and showed dependence of the particle size and dense packing of their layer on the current density and electrolyte concentration. The hybridization event was recorded by EIS with the ferricyanide redox probe and simultaneous monitoring of the surface nucleation by optic part of the system.

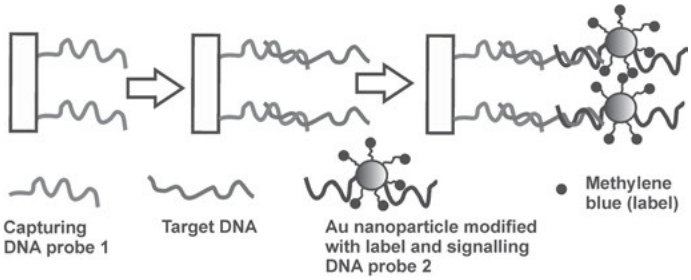


**Fig. 8.8:** Application of Au nanoparticles for multiplication of label signal in sandwich-type hybridization assay with appropriate biosensor.

Aptamers utilize the Au nanoparticles as carriers or amplifiers of the signal. Contrary to detection of hybridization effect, the relative mass and volume of the target species are often insufficient for significant changes in the permeability or conductivity of the surface layer. In some cases, this is compensated for by changes in the conformation of the aptamer. Au nanoparticles give privilege to the biosensors because of more dense and regular positioning of binding sites on the transducer interface. Thus, codeine determination showed remarkable sensitivity due to immobilization of thiolated aptamers on the nanoparticles consisting of mesoporous silica with implemented Au nanoparticles [74]. The EIS signal indicated increase of the charge transfer resistance starting from 3 pM of the target. It is interesting to note that the authors have optimized the aptamer structure and reported on the dissociation constant $K_d$ = 0.91 μM. This value contradicts with super-low LOD and can be explained by some other factors like different accessibilities of aptamers in the pores of nanoparticles and in homogeneous conditions of affinity constant determination.

Although the Au nanoparticles obtained in most common methods have rounded shape, scrupulous tuning of the conditions of their synthesis makes it possible to obtain other forms, for example, octahedrons [75]. For this purpose, a mixture of cationic surfactants was used and the periods of seedings and growth were carefully controlled. The formation of nanocrystals with high-index facets was confirmed by electron microscopy. The Au nanocrystals showed some advantages over more common shapes and resulted in ultra-low LODs of L-histidine. The measurement scheme is presented in Fig. 8.9. The analyte promotes cleavage of the aptamer molecule and dissociation of the complex existed. As a result, ferrocene-bearing aptamer attached to the Au nanocrystals becomes flexible and the current related to the ferrocene redox conversion increases with the concentration of the analyte.

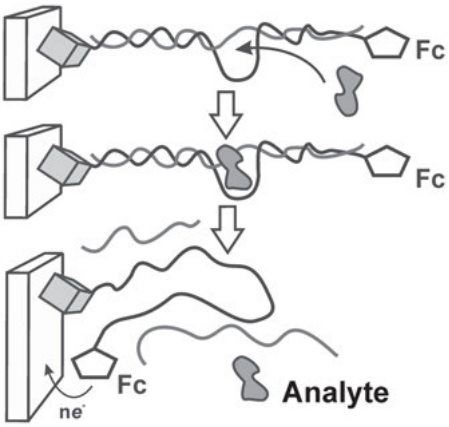


**Fig. 8.9:** Determination of histidine based on aptamers with DNAzyme activity bearing ferrocene (Fc) label and Au nanocrystals.

Displacement protocol is another approach to the detection of low-molecular compounds with appropriate aptasensor. In the work [76], aptamer toward ATP was first hybridized with the complementary DNA sequence bearing thiol group. The aptamer–DNA complex was then adsorbed on magnetic particles and incubated in the ATP solution. The reaction with aptamer resulted in release of the thiolated DNA probe, which was then involved in hybridization reaction with capturing probe on the surface of Au electrode. The resulting product was treated with the Au nanoparticles and then thionine, which redox signal was measured by DPV.

Potassium ion $K^+$ was determined with aptasensor due to its stabilization of $G_4$ quadruplex followed by hemin implementation and its redox signal measurement by DPV [77]. The sensitivity of the assay was provided by the Au nanoparticles bearing the reaction components and attaching them to the electrode surface.

In the work [78], the Au nanoparticles played the role of both aptamer carrier and signal enhancer. In this work, the aptamer was first immobilized on the surface of the Au nanoparticles on the electrode and then reacted with complementary sequence attached to other Au nanoparticles present in the solution. The product of interaction was saturated with methylene blue that was accumulated on the negatively charged phosphate residues of the sequences. In the presence of an analyte, tyrosine kinase, the aptamer–DNA probe complex was dissociated due to conversion of steam-loop structure of the aptamer binding the guest. As a result, most part of methylene blue was removed from the electrode surface and its DPV signal decreased.

In some cases, DNA plays auxiliary function in the sensing layer assembly, which is not related to specific interactions but provides the required charge of the surface or connectivity of other components. Au nanoparticles are intended to compensate for losses in electroconductivity of the layer resulted from addition of non-conductive biopolymer molecules. Many of such sensors use layer-by-layer deposition of charged species, including DNA to reach reproducibility of the properties and regularity of the content of the whole surface film. The successful examples of such an approach are given below. Polyelectrolyte layer formed by MWCNTs, poly(ethylene imine),

DNA, the Au nanoparticles, and $NAD^+$ showed remarkable electrocatalytic activity in $H_2O_2$ reduction [79]. Electropolymerization of *o*-phenylene diamine in the presence of ds-DNA and the Au nanoparticles was used for modification of the pencil graphite electrode and sensitive determination of dopamine (LOD 6 nM) [80] and Sudan II (LOD 0.3 nM) [81]. Polyaniline nanowires decorated with the Au nanoparticles have been proposed to use as universal platform for the detection of various interactions, including the DNA hybridization, glucose sensing with glucose oxidase and Lamina protein detection via its binding to specific antibody [82]. All of the receptors mentioned were just placed on the polymer net and changes in the polyaniline activity followed biochemical interactions on its surface. Additional examples of joint application of the Au nanoparticles and carbonaceous nanomaterials are given below in Section 8.3.2.

### 8.3.2 Other metal nanoparticles

Although many nanoparticles are applied in electrochemical sensors [20], their variety in the assembly of the DNA sensors is not as high as could be expected from the comparison with other electrochemical biosensors. Probably, most of the possible functions of such additives are performed with the Au and carbonaceous nanomaterials better than could be expected from other metals, which are more complicated in preparation, modification, and entrapment in the biosensor assembly. Nevertheless, some examples of the metal nanoparticles successfully applied in DNA sensors are presented below for the period of 2013–17.

In some sensors, the Au-based alloys are used to improve chemical stability of bare gold and possible influence of the Au–S interactions with biogenic thiols and proteins. The additives can also exert their own specificity in the signal generation. Thus, the Au–Pd system was applied in paper-based electrochemiluminescence DNA sensor for microfluidic detection of the cancer cells [83]. The addition of Pd accelerates the reduction of water required in luminescence generation with peroxodisulfate as precursor.

The Ag nanoparticles are mostly used in the optic biosensors based on the fluorescence quenching, but they also can substitute the Au nanoparticles in electrochemical devices though their chemical land electrochemical stabilities are lower than those of gold. Layered nanocomposite films of the polypyrrole–poly(3,4-ethylenedioxythiophene) (PEDOT)–Ag were used for immobilization of the thiolated DNA probe and following hybridization with the complementary sequence [84]. The hybridization resulted in an increase in the charge transfer resistance measured in the presence of ferricyanide as the redox probe. The formation of separate components by chemical oxidation and electrochemical deposition of the Ag nanoparticles was monitored by EIS and constant-current voltammetry. The relative shift of resistance linearly depended on the concentration of the target analyte in semi-logarithmic scale within 10 fM to 10 pM (LOD of 5.4 fM).

The Ag nanoparticles decorated with supramolecular ligands bearing dopamine groups and protecting particles from aggregation were adsorbed together with the neutral red dye on the glassy carbon electrode, pre-oxidized and "activated" by carbodiimide [85]. The ds-DNA was electrostatically accumulated onto the positively charged dye molecules. The biosensor was used for the detection of the oxidative DNA damage. The treatment of DNA with the Fenton reagent or $H_2O_2/CuSO_4$ mixture resulted in increased charge transfer resistance measured by EIS and higher peak current of neutral red reduction on voltammogram. The Ag nanoparticles amplified the signal due to better electron transduction and possible participation in the DNA damage.

The Ag and Pt nanoparticles prepared separately by chemical reduction of appropriate salts were introduced in the carbon paste to provide electrical wiring, and immobilization protocol for DNA probe related to the β-thalassemia's gene sequence. The hybridization was monitored by methylene blue current depended on the target concentration within the range 0.6–12.5 ng/μL (LOD 470 pg/μL). Both Ag and Pt showed increase in the cathodic current of the indicator measured by constant-current voltammetry but taken together as they exerted synergic effect. It is interesting to note that in this particular case the DNA probe molecules did not contain thiol groups for covalent attachment to the metals.

The Pt@Pd nanowires were used together with horseradish peroxidase (HRP) for dual amplification of the signal on the DNA sequence related to *Mycoplasma pneumoniae* [87]. The assay is performed in sandwich mode with capturing probe attached to the gold electrode covered with the Au nanoparticles and signaling probe attached together with enzyme and thionine to Pt@Pd nanowires. The latter ones were synthesized by mixing $H_2PtCl_6$ and $H_2PdCl_4$ in aqueous ethylene glycol and dimethylformamide and heating the mixture to 170°C. The current recorded after $H_2O_2$ addition was referred to the oxidized form of thionine, which is enzymatically recovered on the surface of the metal nanoparticles.

Zinc oxide (ZnO) has found increasing interest as biomolecule carrier and component of the optic and electrochemical biosensors due to high biocompatibility, no toxicity, semiconductor and photosensitizer properties [88–90]. The form and size of the ZnO particles depend on thermal conditions of its synthesis. The variety of shape offers additional opportunities to control the performance of the DNA sensors. Thus, flower-like 3D nanostructures have been obtained by mixing Zn acetate and hexamethylenetetramine at 90°C [91]. They were deposited from suspension in chitosan solution on the glassy carbon electrode and then saturated with the Au nanoparticles obtained separately by the citrate/$NaBH_4$ reduction of $HAuCl_4$ solution. Thiolated DNA probes were assembled onto the Au nanoparticles and then used for hybridization detection. Charge transfer resistance increased with the logarithm of the analyte concentration in the range from 0.1 nM to 0.01 pM (LOD 0.002 pM).

Similar flower-like ZnO particles have been obtained by thermal synthesis directly on platinized silicon [92]. The DNA probe related to *N. meningitides* was adsorbed on

the surface. The hybridization was monitored by EIS and DPV. The DNA sensors made it possible to determine from 5 to 240 ng/μL of target sequence with LOD of 5 ng/μL.

## 8.4 DNA sensors based on carbonaceous materials

### 8.4.1 Carbon nanotubes

SWCNT can be ascribed as a graphene sheet rolled up into a tube normally capped with fullerene semi-spheres. The raw products obtained mostly by chemical vapor deposition (CVD) [93] are contaminated with residues of the catalyst and amorphous carbon, which are removed prior to use by treatment with strong mineral acids and oxidants, respectively. Oxidation of MWCNTs starts from the defects on side-walls and resulted in removal of the fullerene caps. It is often used to simplify functionalization and implementation of MWCNTs in the biosensor assembly. Besides, non-covalent side-wall functionalization due to hydrophobic interactions is described [94].

The diameter of CNTs, their electroconductivity, and number of layers of MWCNTs depend on the synthesis conditions and carbon source. The diameters of SWCNTs and MWCNTs vary from 0.4 to 3 nm and from 2 to 100 nm, respectively [95]. Most of the commercially available CNTs represent a mixture of types different in the convolution of the graphene roll, and in electroconductivity they varied from metallic to dielectric. Semiconducting SWCNTs behave as hole-doped *p*-type FETs [15]. Hole-doping is commonly provided by adsorbed oxygen [96]. Other compounds able to sorption on the side-wall affect the conductivity of such SWCNTs.

There are several approaches to the development of the DNA sensors based on CNTs. First, the transducer should be modified with the CNT layer. This is made by casting the appropriate dispersions, alone or together with other reagents. The aggregation of CNTs in aqueous media prevents the formation of stable dispersion. The addition of cationic surfactants or strong mineral acids stabilizes the dispersion and improves reproducibility of the properties of the surface layer obtained by casting dispersion on the electrode.

The SWCNTs spontaneously form complexes with the partially wrapping DNAs that can be used for dispersing CNTs, their electrophoretic fractioning by size and charge [97] and for detection of the hybridization event [98]. MWCNTs are applied as components of the carbon paste and the surface layer that improve their mechanical durability and electroconductivity and increase the surface area. To some extent, the CNTs exert electrocatalytic properties and can either accelerate oxidation of the DNA or amplify the activity of other mediators implemented into the surface layer and intended for the measurement of a label signal. Contrary to SWCNTs that prefer non-covalent interaction with DNA probes, covalent immobilization of the DNA probes and auxiliary agents is typical for the MWCNTs pre-oxidized almost as often as

they are used. Oxidation provides carboxylic groups for carbodiimide binding of the aminated DNA probes and increases negative charge affecting electrostatic assembling of the biosensing layer.

The adsorption of ds-DNA onto the CNTs accelerates oxidation of nucleotides due to partial wrapping of nucleic acids and due to the electrocatalytic properties of the adduct. The adenine oxidation was observed in the layer of ionic liquid containing MWCNTs and DNA [99]. The spontaneous adsorption of the DNA from aqueous solution on the MWCNT-covered glassy carbon electrode showed independent oxidation of guanine and adenine that gave irreversible peaks at 0.70 and 0.81 V [100].

Besides adsorption, DNA and CNTs can be immobilized on the transducer surface by electrostatic self-assembling with addition of the cationic substances like polyaniline, poly(diallyldimethylammonium chloride), alkali earth metal cations, and small charged organic molecules, that is, thionine [101–103].

In Tab. 8.2, examples of the DNA sensors utilizing CNTs are given for a period from 2013 to 2017. Earlier works are summarized in [10, 13, 15, 31]. As could be seen, CNTs are rarely used alone due to obvious problems with reproducibility of the results obtained with commercial preparations. Moreover, electrocatalytic properties of the CNTs applicable for detection of oxygen, hydrogen peroxide, and antioxidants do not contribute to the improvement of the signal related to redox labels of DNA sensors, which are commonly involved in reversible redox reaction at rather low potential. The detection of enzyme activity might be an exception, but the amplification of the signal due to catalytic conversion of the substrate exceeds the positive influence of CNTs.

Besides own electrocatalytic activity, CNTs show other advantages that make them popular in the DNA sensor assembly, that is, applications for site-specific immobilization of the DNA probes and sharp increase of the real electrode surface accessible for electrochemical reactions against bare electrode. The latter parameter allows quantification by electrochemical tools because the estimation of roughness by AMF or SEM does not take into account the difference in electroconductivity of a variety of CNTs commonly present in commercial preparations. The determination of specific surface concentration of the DNA probe immobilized on the CNTs is another problem that needs optimization. It can be determined from relationships of a monolayer adsorption using redox probes or by current of $Ru(NH_3)_6^{3+}$ reduction, which is proportional to the surface concentration of the oligonucleotide [141]. In the following discussions, increase in the number of the DNA probes attached to CNTs is considered as an advantage of the immobilization protocols though steric limitations can compensate for such an improvement.

One could see, most of the CNT-based DNA sensors and aptasensors utilize additional components like metal nanoparticles and polyelectrolytes. The sequence of their deposition on the electrode varies depending on the source and nature. It should be mentioned that AFM and SEM microphotographs presented in many publications show that the size of CNTs and other nanocomponents is incomparable: CNTs are much bigger and loner. For this reason, preliminary deposition

**Tab. 8.2:** The characteristics of electrochemical DNA sensors based on CNTs

| Target | Immobilization technique | Signal measurement protocol | Linearity range / LOD | Ref. |
|---|---|---|---|---|
| | | Hybridization detection | | |
| 20-mer DNA probe | Pencil graphite electrode modified with SWCNTs/ polyaniline by electropolymerization followed by Au nanoparticle deposition and thiolated DNA probe binding | Charge transfer resistance measurements by EIS with ferricyanide ion as redox probe | 2–8 µg/mL / 2 µg/mL | [103] |
| 24-mer DNA probe | MWCNTs–PMDS composite as electrode, adsorbed DNA probe | DPV signal of methylene blue as hybridization indicator | 10–1000 nM/ 0.13 nM | [104] |
| Papilloma virus | SWCNTs obtained by CVD on silicon waver and coated with Au nanoparticles electrochemically deposited; thiolated DNA probe attached by Au–S binding | Charge transfer resistance measurements by EIS with ferricyanide ion as redox probe | 1 pM–1 aM / 1 aM | [105] |
| *TP53* gene mutation | Aligned MWCNTs covered with electrochemically deposited Au nanoparticles; thiolated DNA probe attached by Au–S binding | Charge transfer resistance measurements by EIS with ferricyanide ion as redox probe | 1 fM to 0.1 µM / 10 aM | [106] |
| *TP53* gene mutation | Pre-oxidized MWCNTs are mixed with DNA probe, then with a target sequence and placed on the electrode surface | DPV signal of methylene blue as hybridization indicator | 100–800 nM / 141 pM | [107] |
| 21-mer DNA probe | $MoS_2$/MWCNTs composite casted on glassy carbon electrode together with chitosan; then the electrode was incubated in Au nanoparticles, ss-DNA probe, and glucose oxidase | Decay in direct electron transfer from glucose oxidase was measured in the presence of glucose | 10 fM to 1 nM / 0.79 fM | [108] |
| 24-mer DNA probe | Glassy carbon electrode is physically modified with carboxylated CNTs, electropolymerized dopamine and Au nanoparticles; thiolated DNA probe is attached via Au–S binding | Chronocoulometric response of Ru hexamine complex as indicator | 1.0 nM to 1.0 fM / 3.5 fM | [109] |
| 31-merr DNA probe | MWCNTs are synthesized by CVD on Ni dots obtained by e-beam nanolithography; DNA probe covalently attached by carbodiimide binding | Microfluidic device made of PDMS, redox indicators (ferricyanide and Ru(II)) DPV signals | Micromolar range of concentrations tested | [110] |

**Tab. 8.2:** (continued)

| Target | Immobilization technique | Signal measurement protocol | Linearity range / LOD | Ref. |
|---|---|---|---|---|
| CaMV35S transgene gene sequence | Glassy carbon electrode modified with MWCNTs, electropolymerized thionine and electrodeposited $ZrO_2$, affine immobilization of DNA probe via phosphate residues | Changes in own redox activity of polythionine measured in DPV mode | 0.001–10 nM / 0.34 pM | [111] |
| Pathogenic *Aeromonas* (*aerolysin* gene) | Capturing DNA probe was immobilized on Au electrode via Au–S binding | Sandwich assay, signaling DNA probe was capped with PbS nanoparticles. After reaction, they were dissolved and $Pb^{2+}$ ions determined on glassy carbon electrode modified with Bi and MWCNTs in DPV mode | $10^6$–$10^2$ CFU/mL / LOD 102 CFU/mL or 10 fM DNA sequence | [112] |
| Amylogenin DNA | Glassy carbon electrode covered with MWCNTs either chemically or electrochemically oxidized | Charge transfer resistance measurements by EIS with ferricyanide ion as redox probe | 10 aM to 1 pM (electrochemically activated MWCNTs) 1 aM to 0.1 pM (chemically activated MWCNTs) | [113] |
| p53 gene | Biotinylated DNA probe is attached to magnetic beads bearing streptavidin | After binding with target DNA and magnetic separation it is released by alkaline treatment and oxidized on pencil graphite electrode modified with SWCNTs (DPV signal of guanine) | 0.32–0.96 µM / 0.11 µM | [114] |
| *Mycoplasma pneumoniae* | Glassy carbon electrode modified with MWCNTs and Au nanoparticles followed by thiolated DNA probe attachment via Au–S binding | Biological target bearing methylene blue, DPV signal | Selectivity ratio 3.3 (complementary/ non-complementary sequences) | [115] |
| *Mycobacterium tuberculosis* | Au electrode covered with polypyrrole wrapping on MWCNTs and PAMAM bearing ferrocene units and covalently attached to DNA probe | DPV or constant-current ferrocene signal after incubation in the solution of complementary sequence or PCR products | 1 fM to 10 pM / 0.3 fM | [116] |
| M268T Angiotensinogen A3B2 mutation | MWCNTs with pyrenebutyric acid attached by hydrophobic interactions and aminated DNA probe attached to COOH group of the acid | DPC signal of methylene blue as hybridization indicator | Normal DNA: 1.0 aM to 10 nM / 0.11 aM Mutant DNA: 1 aM to 0.1 nM / 0.24 aM | [117] |

**Tab. 8.2:** (continued)

| Target | Immobilization technique | Signal measurement protocol | Linearity range / LOD | Ref. |
|---|---|---|---|---|
| 21-mer sequence related to anthrax lethal factor | Glassy carbon electrode covered with CuO nanowires on carboxylated SWCNTs, aminated DNA probe covalently attached to carboxylic groups | DPV signal of Adriamycin as hybridization indicator | 10 fM to 10 nM / 3.5 fM | [118] |
| FLT3 gene in acute myeloid leukemia | Gold electrode alternatively covered with Au nanoparticles and aminated MWCNTs and then treated with thiolated stem-loop probe with ferrocene units | Decay in DPV signal of ferrocene unit after hybridization event | 0.1–1000 pM / 0.1 pM | [119] |
| BCR/ABL fusion gene from chronic myelogenous leukemia | Carbon paste electrode covered with $Fe_3O_4$/MWCNTs suspension and then physically adsorbed DNA probe | Charge transfer resistance measurements by EIS with ferricyanide ion as redox probe | 1 fM to 1 nM / 0.21 fM | [120] |
| Hepatitis B virus | Au electrode electrochemically covered with β-alanine and the casted MWCNTs/poly(p-phenylene-ferrocene) dispersion; aminated probe covalently attached to carboxylic groups of MWCNTs | DPV signal of ferrocene units | 1 fM to 100 pM/ 1.6 pM | [121] |
| Hepatitis B virus | Fluorine-doped tin oxide glass electrode with drop-casted nanozeolite layer and MWCNTs; electrostatic accumulation of ss-DNA probe and its saturation with methylene blue | Charge transfer resistance measurements by EIS with ferricyanide ion as redox probe | 150–$10^6$ copies/ mL of PCR product / 50 copies/mL | [122] |
| | Aptamer-based DNA sensors (aptasensors) | | | |
| Saxitoxin | Au electrode covered with SAM of octadecylthiol and hydrophobically attached MWCNTs saturated with methylene blue; aptamer covalently attached via carbodiimide binding | Decay in DPV signal of methylene blue due to binding analyte and formation of a denser non-conductive layer | 0.9–30 nM / 0.38 nM | [123] |
| Human cellular prions $PrP^C$ | Au electrode covered with polypyrrole wrapping on MWCNTs and PAMAM bearing ferrocene units and covalently attached to the aptamer | DPV or constant-current ferrocene signal | 1 pM to 10 μM / 0.5 pM | [124] |

**Tab. 8.2:** (continued)

| Target | Immobilization technique | Signal measurement protocol | Linearity range / LOD | Ref. |
|---|---|---|---|---|
| Thrombin | Glassy carbon electrode modified with PAMAM bearing reduced graphene with covalently attached aminated aptamer via carbodiimide binding | Sandwich mode with secondary thrombin binding aptamer in G4 quadruplex mode attached to mesoporous silica-MWCNTs complex with thionine, Pt nanoparticles and hemin, thionine DPV signal amplified by DNAzyme reaction mimicking peroxidase activity | 0.1 pM to 80 nM / 50 fM | [125] |
| Thrombin | Glassy carbon electrode covered with chitosan film containing MWCNTs–$TiO_2$ composite prepared by hydrothermal method and Schiff base; aptamer is adsorbed in the film by casting | Charge transfer resistance and constant-current signal of redox probe | 0.05 pM to 10 nM / 5.5 fM | [126] |
| Bisphenol A | Au electrode covered with carboxylated MWCNTs with Au nanoparticles, thiolated aptamer is attached via Au–S binding | Charge transfer resistance measurements by EIS with ferricyanide ion as redox probe | 0.1–10 nM/ 0.05 nM | [127] |
| Bisphenol A | Electrodeposition of Pt–Au nanoparticles on glassy carbon electrode modified with carboxylated MWCNTs followed by covalent attachment of acriflavine and aptamer via phosphate group | DPV signal on intrinsic redox activity of acriflavine | 0.10–1.0, 10–400 pM / 0.035 pM | [128] |
| Bisphenol A | Glassy carbon electrode casted with MWCNs-polyethylene imine and then modified with electrodeposited Pt nanoparticles. Aminated DNA probe is covalently attached via carbodiimide binding and hybridized with an aptamer | In the presence of analyte aptamer is transformed into quadruples form and increased charge transfer resistance is measured by DPV and EIS in the presence of ferricyanide redox probe | 1–400 nM / 210 pM | [129] |
| Bisphenol A | Glassy carbon electrode casted with MWCNs modified with Prussian blue and Au nanoparticles, aminated DNA probe is covalently attached via carboxylic group and hybridized with an aptamer | In the presence of analyte aptamer is transformed into quadruples form and increased charge transfer resistance is measured by EIS in the presence of ferricyanide redox probe | 0.1–1 pM, 10 pM to 10 nM / 0.045 pM | [130] |
| Hydroxylated polychlorinated biphenyl | Aminated aptamer immobilized by amide linkage to carboxylated MWCNTs on glassy carbon electrode | Charge transfer resistance measurements by EIS with ferricyanide ion as redox probe | 0.16–.5 µM / 10 nM | [131] |

**Tab. 8.2:** (continued)

| Target | Immobilization technique | Signal measurement protocol | Linearity range / LOD | Ref. |
|---|---|---|---|---|
| Cytochrome c | Screen-print electrode grafted with MWCNTs, *p*-aminobenzoic acid and then aminated aptamer by amide bond | Sandwich mode, cytochrome c bonded to aptamer is involved in reaction with biotinylated antibody and then streptavidin conjugate with Au nanoparticles, EIS measurements of charge transfer resistance | 25–100 pM / 12 pM | [132] |
| Adenosine | Glassy carbon electrode covered with Au nanoparticles, thionine and capture DNA probe, MWCNTs are modified with glucose oxidase, HRP and thiolated adenosine aptamer adsorbed on Pd–Cu alloy nanoparticles | Prior to measurement, capture DNA probe is hybridized with adenosine aptamer, in the presence of analyte, aptamer forms complex with adenosine and catalytic activity of stepwise oxidation of glucose mediated by thionine is reduced. DPV current of thionine | 10–400 nM / 2.5 nM | [133] |
| Streptomycin | Glassy carbon electrode modified with magnetic Au@MWCNTs – $Fe_3O_4$ composite and nanoporous Pt–Ti alloy in chitosan. Aptamer was immobilized onto the layer by physical adsorption | DPV signal of ferricyanide ions as redox probe | 0.05–100 ng/mL / 7.8 pg/mL | [134] |
| Dopamine | Glassy carbon electrode modified with Au nanoparticles / prussian blue / MWCNT composites by casting; aptamer immobilized by carbodiimide binding | DPV signal on intrinsic redox activity of the composite layer | 0.5–13 nM, 20–50 nM / 200 pM | [135] |
| Malathion | Fluorine-doped tin oxide glass electrode modified with chitosan – iron oxide composite and streptavidin followed by binding of biotinylated aptamer | DPV signal of ferricyanide ions as redox probe | 0.001–10 ng/mL/ 1 pg/mL | [136] |
| IgE | MWCNTs/ionic liquid/chitosan composite casted on glassy carbon electrode, aminated aptamer immobilized to carboxylic groups of MWCNTs | DPV signal of methylene blue as redox probe | 0.5–30 nM / 37 pM | [137] |
| Kanamycin | Au electrode consecutively dripped with Au nanoparticles – chitosan, Au nanoparticles – graphene and MWCNTs – Co phthalocyanine dispersions, aminated aptamer covalently bonded by carboxylic groups | Sandwich assay with biotinylated secondary aptamer and HRP–streptavidin conjugate, constant-current signal of hydroquinone as enzyme substrate | 10–150 ng/mL / 5.8 nM | [138] |

**Tab. 8.2:** (continued)

| Target | Immobilization technique | Signal measurement protocol | Linearity range / LOD | Ref. |
|---|---|---|---|---|
| Kanamycin | Glassy carbon electrode covered with MWCNTs – ionic liquid composite and then amino functionalized graphene. Aminated aptamer immobilized by carbodiimide binding | DPV registration of own activity of the surface layer | 1 nM to 100 µM / 0.87 nM | [139] |
| PDGF BB | Capture aptamer modified with magnetic beds interacted with an analyte and signaling aptamer bearing silver nanoparticles | Addition of *o*-nitrophenol and $NaBH_4$ resulted in formation of *o*-aminophenol in the presence of Ag nanoparticles, o-aminophenol was electrodeposited with MWCNTs on screen-printed carbon electrode, DPV signal of coating | 0.1–100 ng/mL / 60 pg/mL | [140] |

PDGF BB platelet-derived growth factor BB.
PDMS polydimethylsiloxane
PAMAM polyamidoamine

of CNTs on the electrode results in the formation of rather spongious net. The underlying electrode surface remains accessible for the following casting of other chemicals necessary for film formation and biosensor operation. For this reason, simultaneous casting of all the components directly added to the CNT dispersion has some advantages like one-step preparation of the surface layer, no necessity in time-consuming intermediate washing steps, etc. Layer-by-layer deposition of the components has sense if electrostatic self-assembling takes place or the chemicals are dissolved in inconsistent media. Another argument in favor of stepwise formation of biosensing layer consists of electrochemical synthesis of metal nanoparticles onto CNTs as templates. Negative charge of the CNT's shape caused by carboxylic groups promotes the formation of rather small particles, which are evenly distributed among the DNA surface. To some extent, this can be referred to the electropolymerization of pyrrole [116, 124], aniline [103], and other redox active polymers [109, 111]. Simultaneous influence of electrostatic forces and hydrophobic attraction of neutral forms of the polymers to the side-walls of CNTs results in wrapping of the CNTs with polymer wires and formation of regular structures with extended areas of redox activity [124].

In addition to rather common approaches to the signal measurement, for example, EIS control of surface layer permeability or hybridization detection via redox probe signal (Adriamycin, methylene blue), some unusual solutions can be mentioned. Thus, direct electron transfer to glucose oxidase active site was performed in [108] for hybridization detection. The enzyme was placed together with Au nanoparticles on the surface of $MoS_2$–MWCNT composite, ss-DNA probe was covalently attached to the carboxylic groups of the CNTs. The formation of ds-DNA in reaction with biological target suppressed the current recorded in the presence of enzyme substrate, glucose. The application of direct electron transfer is not typical for bioanalytical applications because it is often hindered by steric limitations of the electron transfer. In this particular case, its efficiency can be attributed to another component of the surface layer, molybdenum disulfide, which is similar to graphene in electron conductivity and some other properties.

A variety of nanomaterials have been used for the detection of *Aeromonas* bacteria related to gastroenteritis infections [112]. In sandwich assay, the complex of the capturing DNA probe with the target sequence related to *aerolysin* gene reacts with the signaling DNA probe labeled with PbS nanocrystals. After separation of the product of reaction, the PbS particles were released and dissolved. The concentration of $Pb^{2+}$ ions was determined with the electrode modified with MWCNTs and Bi. The selectivity of biosensor was confirmed by its use to detect various target DNAs from *Aeromonas* strains isolated from tap water.

In several works, the PAMAM bearing ferrocene units was used to detect hybridization event [116] and aptamer–analyte interactions (prions [124], thrombin [125]). This hyperbranched polymer has hydrophilic terminal groups suitable for functionalization and is well compatible with biomolecules. Due to the high number of

substituents typical for dendrimers of 4th generation (64 amino groups per PAMAM molecule), it provides multiplication of the signal due to the high number of redox centers participating in the electron exchange and multiple number of target molecules able to bind with specific sites available on the surface of dendrimers.

A very interesting approach has been proposed for amplification of the sensitivity of protein determination (on example of thrombin) [142]. In this work, the analyte first reacted with capturing aptamer and then with signaling aptamer attached together with HRP to the surface of MWCNTs. Sandwich complex was isolated and tetramethylbenzidine added together with $H_2O_2$. The reaction resulted in formation of insoluble product, which was then electropolymerized to form insulating film on the electrode. This increased the signal measured by EIS. The aptasensor made it possible to detect down to 0.05 pM of thrombin. In a similar manner, electrochemical postreaction with the product formed due to target interaction of the components combined in sandwich-like complex was described in [139] for platelet-derived growth factor BB (PDGF BB) detection. The only difference was that instead of enzyme, silver nanoparticles catalyzed reduction of *o*-nitrophenol to *o*-aminophenol with $NaBH_4$ followed by electrodeposition of the *o*-aminophenol with the MWCNTs on screen-printed electrode.

The development of FETs on the SWCNTs deserves special attention. The device is based on *p*-doped Si wafer where two insulated *n*-doped areas (drain and source) separated with so-called gate area. The shift of the current between the drain and the source is a measure of the charge in gate area, which is affected by external stimuli. In CNT-based FETs, the drain and the source areas are connected with the semiconducting SWCNT, which resistance depends on the charge distribution altered due to biochemical interactions. The manufacture of the CNT-based FETs employs two approaches (Fig. 8.10). In the first one, the CNTs are synthesized by CVD using metal coating of the gate area as template (catalyst) [143].

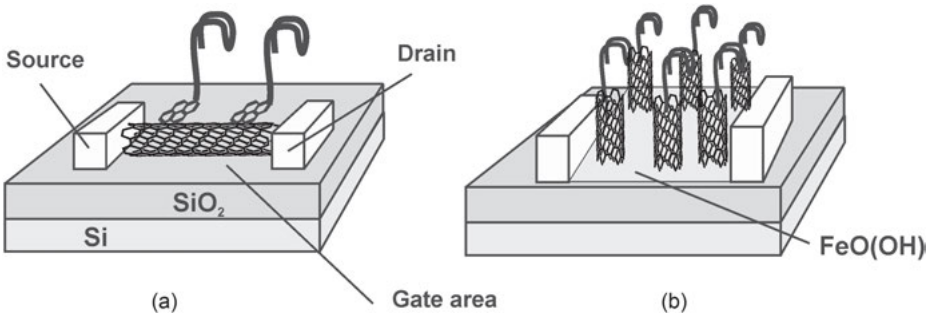


**Fig. 8.10:** CNT-based FETs. (a) SWCNT is synthesized in gate area by CVD and aptamers are attached to the side-wall due to hydrophobic interactions with pyrene unit. (b) Alone standing CNTs in gate area are modified with DNA probe or aptamer by carbodiimide binding.

The Au contacts of source and drain areas are formed by nanolithography. Second approach assumes deposition of the carboxylated SWCNTs on the iron oxide intermediate layer, so that vertically aligned SWCNTs fill the gap between the source and the drain areas. In both types of the FETs, the DNA probe or aptamer are immobilized onto the CNTs surface via hydrophobic interactions with side-walls or carbodiimide binding of aminated receptors with terminal carboxylic groups of CNTs. Contrary to many other DNA sensors, the generation of the signal does not require any labels or auxiliary reagents, for example, redox indicators.

Similar FETs have been developed for detection of immunochemical interactions and determination of specific antigens [144]. Meanwhile, the use of aptamers instead of antibodies increases the sensitivity of the analyte detection. This is explained by different sizes of the receptors. The sensitivity of the FET signal to the charge distribution changes depends on the distance from the gate to the receptor position where biochemical interaction takes place in comparison with the Debye length. This is the distance that allows screening the surplus charge of the mobile carriers present in a material [145]. If the distance from the surface of a SWCNT to receptor is bigger than Debye length, biochemical reactions do not affect mobile charges of the material. The typical size of the antibodies (~10–15 nm) is similar to the Debye length and the antigen–antibody binding finds response in the double layer near the CNT surface. The aptamer size is commonly smaller and this increases the sensitivity of the aptamer-based assay as was shown on the example of the IgE determination [146, 147].

The immobilization of several aptamers on the SWCNTs makes it possible to determine two analytes with the same FET [148]. To discriminate the signal, different amplification systems based on HRP and glucose oxidase together with appropriate mediators (ferrocene and toluidine blue) have been applied for determination of the thrombin and the PDGF. The sandwich assay was performed with the analytes first attached to capturing aptamers and then treated with labels consisted of graphene flakes bearing enzymes and mediators immobilized on the same carrier.

Similar to SWCNTs, other nanomaterials can be introduced in the FET assembly. Thus, few-layer $MoS_2$ sensing channel material with electronic structure similar to that of graphene was successfully used for this purpose [149]. The material was obtained by chemical reduction of Mo salt in the presence of $H_2S$ in Ar atmosphere followed by annealing the material to remove the oxygen residues. The $MoS_2$-based FET was tested on detection of hybridization with 10 μM ss-DNA probe and complementary targets. Other examples of bio-FETs based on graphene are given in Section 8.4.2.

### 8.4.2 Graphene-based DNA sensors

Graphene is a 2D sheet of carbon atoms linked by $sp^2$ bonds. The electric properties of graphene are related to electron transduction along the basal plane and electron exchange at the edge of the plane [150]. The relative contribution of the above mechanisms depends on the source of a raw material and production protocol.

Graphene-based nanomaterials applied in electrochemical sensors and biosensors are classified in accordance with the number of planes, their defects, production, and pretreatment protocols. Most often, reduced graphene oxide is applied that can be easily obtained by chemical oxidation of graphite followed by separation of graphene oxide and its chemical or electrochemical oxidation either in suspension or directly on the electrode interface. The formation of graphene from its oxide can be monitored by bands referred to >C = O and –C(O)OH groups in Fourier-transform infrared spectra. The surface area of graphene sheets obtained in such a manner (about 2600 $m^2/g$ [151]) exceeds that of SWCNTs (~1000 $m^2/g$ [152]). The application of the graphene nanomaterials in electrochemical sensors and biosensors was recently summarized in some reviews [153–155].

The ss-DNA probes can be simultaneously adsorbed on graphene and especially graphene oxide sheets by hydrophobic interactions. The hybridization of DNA increases the density of the negative charge and often results in desorption of biopolymers from the graphene surface. If the DNA probe is labeled with fluorescent particle or molecule, such processes result in quenching and re-establishment of the fluorescence, respectively, and can be used for homogeneous DNA assay [156]. In biosensor assembly, the DNA probe should be immobilized to exclude spontaneous leaching. The immobilization protocols are similar to those already described for other carbonaceous materials. They include carbodiimide binding via carboxylic groups of graphene defects bonded to the aminated DNA probe, electrostatic assembling of oppositely charged layers with intermediate cationic polyelectrolytes and hydrophobic binding to polyaromatic molecules, for example, 3,4,9,10-perylene tetracarboxylic acid (PTCA [156]) or 1-aminopyrene [157] covalently attached to the DNA probe or aptamer. In a similar manner, other nanomaterials can be assembled on graphene support for amplification of their electrochemical signal [158]. In comparison with the CNT-based biosensors, graphene exerts less steric hindrance for interaction of bulky molecules and forms denser layers on electrodes. In some cases, graphene layers are used to prevent undesirable sorption of the reaction components on the transducer interface instead of the use of BSA or thiolated alcohols for the glassy carbon and the Au electrodes, respectively.

In some publications summarized in Tab. 8.2, the CNT adducts are applied together with graphene [125, 138, 139]. The authors announce synergic influence of CNTs and graphene brought together in the biosensing layer though there are now direct evidences of such interactions. Moreover, analytical characteristics of such hybrid CNT–graphene biosensors do not differ dramatically from those reported for biosensors with simpler content of the biosensing layer. Most likely, the positive influence of graphene can be attributed to the higher stability of its dispersions and higher electroconductivity against commercial preparations of the CNTs. In many biosensors, graphene is casted onto the glassy carbon as a support for immobilization of the DNA probe that retains electric wiring of oligonucleotides and enhances label signal against bare glassy carbon. As CNTs, graphene is compatible with metal nanoparticles that are easily synthesized on its surface due to the accumulation of ions due to electrostatic interactions. When used in the label assembly, the graphene sheets

show higher stability in dispersion and lower aggregation and sedimentation ability than CNTs due to lesser size and rather high charge density. This simplifies the measurement protocol and improves accuracy of the signal record.

Graphene-based sensors are often used for the detection of the direct redox conversion of the low-molecular compounds like heavy metal cations [158–160], guanine and adenine [161, 162], antioxidants [163, 164], etc. This is related to the electrocatalytic properties of graphene and its charge promoting accumulation of cationic species prior to their reduction or oxidation on the electrode. The DNA can be involved in the assembly of such sensors as additional accumulation component and receptor required for selective response to certain analytes. Thus, $Ag^+$ ions form specific complexes with cytosine-rich areas of the DNA and hence can be accumulated on ss-DNA and cytosine-rich oligonucleotides for the following detection by relative increase in charge transfer resistance measured by EIS [165]. Graphene oxide – $Fe_3O_4$ composite provided platform for immobilization of DNA and site-specific immobilization of DNA sequences on its surface. LOD of 2 pM was reached together with multiple use of the biosensors based on intermediate washing with cysteine solution.

Such biospecific routes of ion recognition are especially popular for $Pb^{2+}$ and $Hg^{2+}$ ions. Thus, graphene oxide was treated with nitrogen plasma and then with a complex combining DNAzyme, substrate DNA, and binding $Hg^{2+}$ and $Pb^{2+}$ DNA [166]. Binding of the target ions results in conformational changes of the DNA and appropriate shift of the charge transfer resistance within the interval 0.01–100 nM (LOD 7.8 and 5.4 pM for $Pb^{2+}$ and $Hg^{2+}$, respectively). Graphene-based FET with aptamer immobilized in the gate area covered with graphene synthesized *in situ* by CVD showed sensitive response to $Hg^{2+}$ ions (LOD 10 pM) [167].

The $Pb^{2+}$-dependent DNAzyme was immobilized on the surface of the Au electrode [168]. In the presence of $Pb^{2+}$ ions, it was cleaved to leave ss-DNA sequence attached to the electrode and complementary to DNA probe bearing graphene nanosheets containing $MnO_2$ and hemin that exert peroxidase mimicking activity. The signal recorded in DPV mode and related to the $H_2O_2$ reduction makes it possible to determine 0.1 pM to 200 nM $Pb^{2+}$ (LOD 0.034 pM).

Another approach to the $Pb^{2+}$ detection was demonstrated in [169]. The $Pb^{2+}$-sensitive aptamer was immobilized on the Au electrode via Au–S binding. Prior to contact with an analyte, it was saturated with graphene nanosheets bearing thionine molecules hydrophobically retained on its surface. The reaction resulted in removal of graphene label together with thionine and entrapment of $Pb^{2+}$ ions into the folded $G_4$ quadruplex structure of the aptamer. Besides amplification of the signal due to the high capacity of graphene to thionine molecules, the use of this label suppresses interfering influence of $K^+$ ions competing with $Pb^{2+}$ ions for binding site of the aptamer. The aptasensor makes it possible to detect 32 pM of target ion using thionine peak current measured with DPV as a signal (concentration range from 0.16 pM to 0.16 nM). In a similar manner, $Pb^{2+}$–aptamer interaction in gate area was recorded with graphene-based FET [170].

Mercury biosensing is mainly based on its ability to form stable triple complex T–$Hg^{2+}$–T (3) with the thymine-rich areas of ss-DNA or poly(T) sequence.

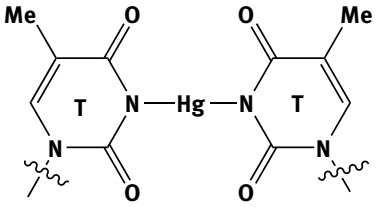


(3)

The latter one was immobilized via terminal thiol group on the Au electrode followed by incubation of the biosensor in dispersion of the graphene oxide and then in $Hg^{2+}$ solution. In the absence of the target, the current of graphene oxide reduction can be observed by constant-current voltammetry. The $Hg^{2+}$ ions are incorporated between thymine bases, so that more rigid analog of ds-DNA is formed. This results in increase of the distance between the graphene units and the electrode followed by increase of the charge transfer resistance measured with EIS and decrease in appropriate current. The biosensor makes it possible to determine 1–300 nM $Hg^{2+}$.

Nanorods of polyaniline obtained in the presence of reduced graphene oxide were used as support for immobilization of T-rich DNA and following detection of $Hg^{2+}$ that formed T–$Hg^{2+}$–T complexes on the surface [170, 171]. The EIS signal was observed from 0.01 to 100 nM (LOD 3.5 pM).

Triple-helix DNA consisted of the ss-DNA, and T-rich ds-DNA was used for silver-amplified mercury detection. In this biosensor, the addition of $Hg^{2+}$ ions removed the ds-DNA due to unwinding caused by introduction of the mercury ions and formation of T–$Hg^{2+}$–T fragments [172]. The ss-DNA is then involved in the reaction with C-rich complementary sequence that is immobilized on Au nanoparticle. The reaction results in formation of C–$Ag^{+}$–C bridges (4) to form dendrite silver nanostructures after cathodic reduction of entrapped silver ions.

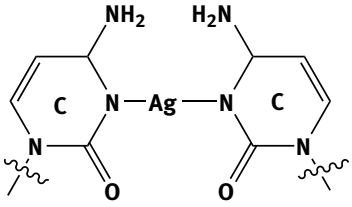


(4)

The anodic current of silver dissolution in stripping voltammetry mode is proportional to the $Hg^{2+}$ concentration in the range from 0.1 to 130 nM (LOD 0.035 nM).

The examples of application of graphene in the assembly of the DNA sensors for hybridization detection and the aptasensors are presented in Tab. 8.3 covering 2013–17.

**Tab. 8.3. The characteristics of electrochemical DNA sensors based on graphene**

| Target | Immobilization technique | Signal measurement protocol | Linearity range / LOD | Ref. |
|---|---|---|---|---|
| | | Hybridization detection | | |
| Human papilloma-virus | Capture probe immobilized on glassy carbon electrode modified with graphene / Au nanorods / polythionine | Sandwich assay with two long-range signaling probe partially complementary each other to increase ds-DNA area, DPV signal of Ru hexamine as hybridization indicator | 0.1 pM to 0.1 nM / 40 pM | [174] |
| *Staphylococcus aureus* nuc gene | $ZrO_2$/graphene nanocomposite electroreduced on carbon ionic liquid electrode, DNA probe immobilized by phosphate residue interacted with $ZrO_2$ | DPV signal of methylene blue as hybridization indicator | 0.1 pM to 1 μM / 32.3 fM | [175] |
| BCR/ABL fusion gene | Graphene sheets / polyaniline /Au nanoparticles deposited on glassy carbon electrode, thiolated stem-loop is immobilized to Au nanoparticles via Au–S binding | Capture stem-loop probe is involved in catalyzed stem-loop assembly resulted in formation of biotinylated product interacted with streptavidin–alkaline phosphatase conjugate | 10 pM to 20 nM / 1.05 pM | [176] |
| HIV1 gene | Printed graphene electrode with electrochemically reduced graphene oxide and DNA probe immobilized by hydrophobic interactions | Peak current of graphene oxide reduction | 1 pM to 0.1 μM / 0.1 pM | [177] |
| Apolipoprotein E gene associated with Alzheimer's disease | Graphene/mesoporous silica hybrid with covalently attached ferrocenocarboxylic acid, adsorbed methylene blue and DNA probe | Methylene blue current as indicator of hybridization indicator | 10 nM to 10 fM / 10 fM | [178] |
| HIV gene | $Fe_3O_4$-reduced graphene oxide composite, physically adsorbed DNA probe | Fe(II/III) signal increases in hybridization step | 10 aM to 1 nM / 2 aM | [179] |
| Fragment of PML/RARA fusion gene sequence | Graphene oxide electrochemically reduced on polyaniline modified glassy carbon electrode, physically adsorbed DNA probe | Charge transfer resistance measured by EIS in the presence of ferrocyanide ions | 1 fM to 10 nM / 0.25 fM | [180] |

**Tab. 8.3:** (continued)

| Target | Immobilization technique | Signal measurement protocol | Linearity range / LOD | Ref. |
|---|---|---|---|---|
| *Escherichia coli* O157:H7 | Graphene oxide–modified iron oxide – chitosan hybrid nanocomposite electrophoretically deposited on ITO glass electrode, physically adsorbed DNA probe | Charge transfer resistance measured by EIS in the presence of ferrocyanide ions | 10 fM to 1 µM / 10 fM | [181] |
| 18-mer DNA probe | Glassy carbon electrode modified with graphene and $Cu(phen)_2^{2+}$ complex acting as anchor for DNA probe | SWV signal of $Cu(phen)_2^{2+}$ as hybridization indicator | 1 pM to 1 µM / 0.199 pM | [182] |
| Fragment of *E. coli* DNA sequence | Glassy carbon electrode modified with graphene decorated with Au nanoparticles with immobilized thiolated capture DNA probe | Sandwich assay with signaling DNA probe modified with methylene blue, DPV signal of methylene blue | 0.1 fM to 0.1 µM / 0.035 fM | [183] |
| Breast cancer 1 (BRCA1) gene | Glassy carbon electrode modified with reduced graphene oxide – yttria and DNA probe specifically bonded to yttria with phosphate residue | Sandwich assay with signaling DNA probe labeled with Au nanoparticles, DPV signal of Au nanoparticles | 10 aM to 1 nM / 5.95 aM | [184] |
| HIV gene | Glassy carbon electrode covered with graphene – Nafion composite, DNA probe physically adsorbed | Charge transfer resistance measured by EIS in the presence of ferrocyanide ions | 0.1 pM to 0.1 nM /0.023 pM | [185] |
| | | Aptamer-based DNA sensors (aptasensors) | | |
| Platelet-derived growth factor (PDGF BB) | $MoSe_2$–graphene composite obtained by hydrothermal method, aptamer immobilized via carbodiimide binding | Aptamer reacts with complementary DNA, exonuclease digests ds-DNA releasing complementary DNA for reaction with auxiliary biotinylated DNA, the following binding with streptavidin–peroxidase conjugate provides the signal after addition of hydroquinone and $H_2O_2$, PDGF stimulates the formation of $G_4$ quadruplex and stops the above reaction | 0.1 pM to 1 nM / 20 fM | [186] |

**Tab. 8.3:** (continued)

| Target | Immobilization technique | Signal measurement protocol | Linearity range / LOD | Ref. |
|---|---|---|---|---|
| Dopamine | PEDOT doped with graphene oxide obtained by electropolymerization, aminated aptamer covalently attached via carbodiimide binding | DPV signal of dopamine | 1 pM to 160 nM / 78 fM | [187] |
| Neuropeptide Y | Aptamer covalently attached to Au nanoparticles and deposited onto the surface of graphene sheets used as electrode in flow lateral microfluidic device | Constant current signal of oxidation of tyramine residues of neuropeptide Y | 10–1000 pM / 10 pM | [188] |
| Oxytetracycline | Reduced graphene oxide was deposited on the glassy carbon electrode and Au nanoparticles were electrochemically synthesized onto its surface, aptamers were immobilized wither vis Au–S binding or specific antibodies | Sandwich assay with signaling aptamer attached to Au nanoparticles bearing peroxidase, constant current measured after addition of hydroquinine and $H_2O_2$ | 0.5 ng/L to 2 mg/L / 0.5 ng/L | [189] |

One could see covalent immobilization was applied much less against hydrophobic interactions via special labels introduced in the assembly of an aptamer or by physical adsorption of the aptamer onto the electrode surface. Contrary to graphene, reduced graphene oxide retains boundary polar groups providing the dispersion and following deposition of the suspension on the electrode surface. Electrochemical reduction is less efficient but offers new opportunities of the formation of hybrid structures due to simultaneous formation of Au nanoparticles or polyaniline (polythionine). In all such cases the function of graphene was attributed to the enhancement of electroconductivity and electric wiring of labels (redox indicators) used in measurement protocol. The simultaneous deposition of hybrid coatings provides even distribution and accessibility of the components for diffusionally free agents. This was monitored by EIS and SEM and considered as additional advantage of the modification method. The following detection of target interactions is rarely based on the intrinsic redox activity of the surface layer. In case of small species, they can be involved in redox reaction so that aptamers just concentrate the analyte molecules onto the electrode surface. In many other sensors, the activity of enzymes or redox response of labels introduced in the surface confined complex is measured by conventional methods. Contrary to the CNTs, changes in the permeability or charge distribution of the surface layer estimated by EIS are rarely applied in graphene-based biosensors. This might be referred to higher redox activity and lesser size of graphene against those of CNTs and compensation of steric hindrances appeared after binding bulky analytes. The same reason might explain higher attention to specifically biochemical approaches to the sensitivity amplification, for example, additional treatment of the sensors with exonucleases or formation of catalytic complexes for stem-loop aptamers. To some extent, such sophisticated reaction paths realized in biosensor format level their main advantage, that is, simple format and fast response, but the LOD values and dynamic range of concentrations achieved are very low and allow direct monitoring of appropriate processes *in vivo*.

## 8.5 Conclusions

The progress in the development and manufacture of novel nanomaterials for the electrochemical DNA sensors offers new opportunities of their further commercialization and application in medical diagnostics and other areas. Meanwhile the current state-of-the art also showed some problems related to the choice of nanomaterials and their role in biosensor performance.

Recently reported sensors with DNA probes and aptamers as recognition elements mostly use not one but several nanomaterials that play different role – receptor support, surface enhancer, and electric transduction improvement. This is particularly true for the combination of carbonaceous materials and Au nanoparticles that compensate for

negative effect of non-conductive additives on the electric wiring of labels or indicator redox centers. The experience of application of some nanomaterials like quantum nanodots or silver nanoparticles came from optic methods of assay where they are used as fluorophores or fluorescence quenchers. However, it should be mentioned that the size and quantities of such additives in electrochemical sensors can be significantly different from those in optic devices. Magnetic nanoparticles are used in conventional immuno- and DNA assay for separation of appropriate labeled complexes on intermediate stages of the analysis. However, their use in the assembly of biosensing layer of DNA sensors has much less substantiation excepting mechanical durability of the coating. For the same reason, semiconductors applicable in electronic devices have lesser effect in electrochemical sensors operated in aqueous electrolytes. This refers to ZnO and some metal chalcogenides that are used in DNA sensors but do not participate in electron transduction. The application of up to five different nanoparticles in the assembly of single DNA sensors also has some objections regarding the accuracy of assembling and real necessity of so many species for detection of rather simple redox reactions.

In spite of these difficulties, the application of nanomaterials in DNA sensors increases dramatically in the variety of possible analytes and mechanisms of signal transduction. Concerning nearest future, enhanced application of biochemical steps of signal amplification can be expected because many traditional opportunities of electrochemical analysis are near being exhausted. The popularity and accessibility of FET devices depend only on the offers of their manufacturers. Another possible source of the growth includes the capabilities provided by 3D printing using traditional plastics and those mixed with nanomaterials able to recognize analytes and accumulate their molecules for target interactions with DNA.

**Acknowledgments:** The work has been performed according to the Russian Government Program of Competitive Growth of Kazan Federal University. HB announces financial support of Russian Foundation for Basic Research (grant No. 15-03-03224). TH acknowledges support by the Slovak Research and Development Agency under the contract No. APVV-14-0267, by Science Grant Agency VEGA project No. 1/0152/15) and by European Union's Horizon 2020 research and innovation program under the Marie Sklodowska-Curie grant agreement No. 690898 (Formilk).

## References

[1] Kwon L, Long KD, Wan Y, Yu H, Cunningham BT. Medical diagnostics with mobile devices: comparison of intrinsic and extrinsic sensing. *Biotechnol Adv* 2016, 34, 291–304.

[2] Bahadır EB, Sezgintürk MK. Applications of commercial biosensors in clinical, food, environmental, and biothreat/biowarfare analyses. *Anal Biochem* 2015, 478, 107–20.

[3] Thévenot DR, Toth K, Durst RA, Wilson GS. Electrochemical biosensors: recommended definitions and classification (Technical Report). *Pure Appl Chem* 1999, 71, 2333–48.

[4] Clark LC, Lyons C Jr. Electrode systems for continuous monitoring in cardiovascular surgery. *Ann NY Acad Sci* 1962, 148, 133–53.
[5] Kirsch J, Siltanen C, Zhou Q, Revzin A, Simonian A. Biosensor technology: recent advances in threat agent detection and medicine. *Chem Soc Rev* 2013, 42, 8733–68.
[6] Laocharoensuk R. Development of electrochemical immunosensors towards point-of-care cancer diagnostics: clinically relevant studies. *Electroanalysis* 2016, 28, 1716–29.
[7] Kim YS, Raston NHA, Gu MB. Aptamer-based nanobiosensors. *Biosens Bioelectron* 2016, 76, 2–19.
[8] Chandrasekaran AR, Wady H, Subramanian HKK. Nucleic acid nanostructures for chemical and biological sensing. *Small* 2016, 12, 2689–700.
[9] Syedmoradi L, Daneshpour M, Alvandipour M, Gomez FA, Hajghassem H, Omidfar K. Point of care testing: the impact of nanotechnology. *Biosens Bioelectron* 2017, 87, 373–87.
[10] Wu L, Xiong E, Zhang X, Zhang X, Chen J. Nanomaterials as signal amplification elements in DNA-based electrochemical sensing. *Nano Today* 2014, 9, 197–211.
[11] Boverhof DR, Bramante CM, Butala JH, Clancy SF, Lafranconi M, West J, et al. Comparative assessment of nanomaterial definitions and safety evaluation considerations. *Regul Toxicol Pharm* 2015, 73, 137–50.
[12] Chen A, Chatterjee S. Nanomaterials based electrochemical sensors for biomedical applications. *Chem Soc Rev* 2013, 42, 5425–38.
[13] Pumera M, Sánchez S, Ichinose I, Tang J. Electrochemical nanobiosensors. *Sens Actuators B* 2007, 123, 1195–205.
[14] Jia X, Dong S, Wang E. Engineering the bioelectrochemical interface using functional nanomaterials and microchip technique toward sensitive and portable electrochemical biosensors. *Biosens Bioelectron* 2016, 76, 80–90.
[15] Tran T-T, Mulchandani A. Carbon nanotubes and graphene nano field-effect transistor-based biosensors. *Trends Anal Chem* 2016, 79, 222–32.
[16] Kharisov B, Kharissova OV, García BO, Méndeza YP, de la Fuente IG. State of the art of nanoforest structures and their applications. *RSC Adv* 2015, 5, 105507–23.
[17] Bollella P, Fusco G, Tortolini C, Sanzò G, Favero G, Gorton L, et al. Beyond graphene: Electrochemical sensors and biosensors for biomarkers detection. *Biosens Bioelectron* 2017, 89, 152–66.
[18] Martín A, Escarpa A. Graphene: the cutting-edge interaction between chemistry and electrochemistry. *Trends Anal Chem* 2014, 56, 13–26.
[19] http://www.sigmaaldrich.com
[20] Wang J. Electrochemical biosensing based on noble metal nanoparticles. *Microchim Acta* 2012, 177, 245–70.
[21] Walcarius A, Collinson MM. Analytical chemistry with silica sol-gels: traditional routes to new materials for chemical analysis. *Annu Rev Anal Chem* 2009, 2, 121–43.
[22] Urbanova V, Magro M, Gedanken A, Baratella D, Vianello F, Zboril R. Nanocrystalline iron oxides, composites, and related materials as a platform for electrochemical, magnetic, and chemical biosensors. *Chem Mater* 2014, 26, 6653–73.
[23] Liu W, Yin X-B. Metal-organic frameworks for electrochemical applications. *Trends Anal Chem* 2016, 75, 86–96
[24] Pena-Pereira F, Duarte RMBO, Duarte AC. Immobilization strategies and analytical applications for metallic and metal-oxide nanomaterials on surfaces. *Trends Anal Chem* 2012, 40, 90–105.
[25] Arduini F, Micheli L, Moscone D, Palleschi G, Piermarini S, Ricci F, et al. Electrochemical biosensors based on nanomodified screen-printed electrodes: recent applications in clinical analysis. *Trends Anal Chem* 2016, 79, 114–26.
[26] Lim M-C, Kim Y-R. Analytical applications of nanomaterials in monitoring biological and chemical contaminants in food. *J Microbiol Biotechnol* 2016, 26, 1505–16.

[27] Arduini F, Cinti S, Scognamiglio V, Moscone D. Nanomaterials in electrochemical biosensors for pesticide detection: advances and challenges in food analysis. *Microchim Acta* 2016, 183, 2063–83.
[28] Kim JE, Choi JH, Colas M, Kim DH, Lee H. Gold-based hybrid nanomaterials for biosensing and molecular diagnostic applications. *Biosens Bioelectron* 2016, 80, 543–559.
[29] Hasanzadeh M, Shadjou N. Electrochemical nanobiosensing in whole blood: recent advances. *Trends Anal Chem* 2016, 80, 167–76.
[30] Anik Ü, Timur S. Towards the electrochemical diagnosis of cancer: nanomaterial-based immunosensors and cytosensors. *RSC Adv* 2016, 6, 111831–41.
[31] Tiwari JN, Vij V, Kemp KC, Kim KS. Engineered carbon-nanomaterial-based electrochemical sensors for biomolecules. *ACS Nano* 2016, 10, 46–80.
[32] Kumar S, Ahlawat W, Kumar R, Dilbaghi N. Graphene, carbon nanotubes, zinc oxide and gold as elite nanomaterials for fabrication of biosensors for healthcare. *Biosens Bioelectron* 2015, 70, 498–503.
[33] Lucarelli F, Marrazza G, Turner APF, Mascini M. Carbon and gold electrodes as electrochemical transducers for DNA hybridisation sensors. *Biosens Bioelectron* 2004, 19, 515–30.
[34] Lucarelli F, Tombelli S, Minunni M, Marrazza G, Mascini M. Electrochemical and piezoelectric DNA biosensors for hybridisation detection. *Anal Chim Acta* 2008, 609, 139–159.
[35] Hamula CLA, Guthrie JW, Zhang H, Li H-F, Le XC. Selection and analytical applications of aptamers. *Trends Anal Chem* 2006, 25, 681–91.
[36] Tuerk C, Gold L. Systematic evolution of ligands by exponential enrichment: RNA ligands to bacteriophage T4 DNA polymerase. *Science* 1990, 249, 505–10.
[37] Bala A, Górski L. Application of nucleic acid analogues as receptor layers for biosensors. *Anal Methods* 2016, 8, 236–44.
[38] Wang J. DNA biosensors based on peptide nucleic acid (PNA) recognition layers. *A review. Biosens Bioelectron* 1998, 13, 757–62.
[39] Mascini M, Palchetti I, Marrazza G. DNA electrochemical biosensors. *Fresenius J Anal Chem* 2001, 369, 15–22.
[40] Wang C, Yuan X, Liu X, Gao Q, Qi H, Zhang C. Signal-on impedimetric electrochemical DNA sensor using dithiothreitol modified gold nanoparticle tag for highly sensitive DNA detection. *Anal Chim Acta* 2013, 799, 36–43.
[41] Imani R, Iglič A, Turner APF, Tiwari A. Electrochemical detection of DNA damage through visible-light-induced ROS using mesoporous $TiO_2$ microbeads. *Electrochem Commun* 2014, 40, 84–87.
[42] Rafique B, Khalid AM, Akhtar K, Jabbar A. Interaction of anticancer drug methotrexate with DNA analyzed by electrochemical and spectroscopic methods. *Biosens Bioelectron* 2013, 44, 21–6.
[43] Rubin R, Wall D, Konstantinov KN. Electrochemical biosensor for quantitation of anti-DNA autoantibodies in human serum. *Biosens Bioelectron* 2014, 51, 177–83.
[44] Pei H, Lu N, Wen Y, Song S, Liu Y, Yan Y, et al. A DNA nanostructure-based biomolecular probe carrier platform for electrochemical biosensing. *Adv Mater* 2010, 22, 4754–8.
[45] Rothemund PWK. Folding DNA to create nanoscale shapes and patterns. *Nature* 2006, 440, 297–302.
[46] Wang JS, Zhang DY. Simulation-guided DNA probe design for consistently ultraspecific hybridization. *Nat Chem* 2015, 7, 545–53
[47] Labuda J, Oliveira Brett AM, Evtugyn G, Fojta M, Mascini M, Ozsoz M, et al. Electrochemical nucleic acid-based biosensors: concepts, terms, and methodology (IUPAC technical report). *Pure Appl Chem* 2010, 82, 1161–87.
[48] Gokce G, Erdem A, Ceylan C, Akgöz M. Voltammetric detection of sequence-selective DNA hybridization related to Toxoplasma gondii in PCR amplicons. *Talanta* 2016,149, 244–9.

[49] Sharma VK, Jelen F, Trnkova L. Functionalized solid electrodes for electrochemical biosensing of purine nucleobases and their analogues: a review. *Sensors* 2015, 15, 1564–600.
[50] Evtugyn G, Sitdikov R, Evtugyn V, Stoikov I, Antipin I, Hianik T. Electrochemical aptasensor for the determination of ochratoxin A at the Au electrode modified with Ag nanoparticles decorated with macrocyclic ligand. *Electroanalysis* 2013, 25, 1847–54.
[51] Kerman K, Vestergaard M, Tamiya E. Electrochemical DNA biosensors: protocols for intercalator-based detection of hybridization in solution and at the surface. *Methods Mol Biol* 2009, 504, 99–113.
[52] Erdem A, Kerman K, Meric B, Ozsoz M. Methylene blue as a novel electrochemical hybridization indicator. *Electroanalysis* 2001, 13, 219–23.
[53] Gupta G, Atanassov P. Electrochemical DNA hybridization assay: enzyme-labeled detection of mutation in p53 gene. *Electroanalysis* 2011, 23,1615–22.
[54] Kokkinos C, Prodromidis M, Economou A, Petrou P, Kakabakos S. Quantum dot-based electrochemical DNA biosensor using a screen-printed graphite surface with embedded bismuth precursor. *Electrochem Commun* 2015, 60, 47–51.
[55] Lai RY, Lagally ET, Lee S-H, Soh HT, Plaxco KW, Heeger AJ. Rapid, sequence-specific detection of unpurified PCR amplicons via a reusable, electrochemical sensor. *PNAS* 2006, 103, 4017–21.
[56] Ni X, Joda H, Sedova A, Biała K, Flechsig G-U. Sequence detection of unlabeled DNA using the sandwich assay: strand-displacement, hybridization efficiency, and probe-conformation considerations for the tethered surface. *Electrochim Acta* 2016, 220, 581–6.
[57] Li F, Xu Y, Yu X, Yu Z, Ji H, Song Y, et al. Effect of the duplex length on the sensing performance of a displacement-based electrochemical nucleic acid sensor with an adjustable point mutation discrimination function. *Sens Actuators B* 2016, 234, 648–57.
[58] Wang H, Jiang W, Li W, Wang L. A bicyclo-hairpin probe mediated strand displacement amplification strategy for label-free and sensitive detection of bleomycin. *Sens Actuators B* 2017, 238, 318–24.
[59] Du Y-C, Zhu L-N, Kong D-M. Label-free thioflavin T/G-quadruplex-based real-time strand displacement amplification for biosensing applications. *Biosens Bioelectron* 2016, 86, 811–7.
[60] Castañeda MT, Alegret S, Merkoçi A. Electrochemical sensing of DNA using gold nanoparticles. *Electroanalysis* 2007, 19, 743–53.
[61] Saberi R-S, Shahrokhian S, Marrazza G. Amplified electrochemical DNA sensor based on polyaniline film and gold nanoparticles. *Electroanalysis* 2013, 25, 1373–80.
[62] Sun Y, He X, Ji J, Jia M, Wang Z, Sun X. A highly selective and sensitive electrochemical CS-MWCNTs/Au-NPs composite DNA biosensor for *Staphylococcus aureus* gene sequence detection. *Talanta* 2015, 141, 300–6.
[63] Esmaeili C, Heng LY, Chiang CP, Rashid ZA, Safitri E, et al. A DNA biosensor based on kappa-carrageenan-polypyrrole-gold nanoparticles composite for gender determination of Arowana fish (Scleropages formosus). *Sens Actuators B* 2017, 242, 616–24.
[64] Sun Y, Ren Q, Liu B, Qin Y, Zhao S. Enzyme-free and sensitive electrochemical determination of the FLT3 gene based on a dual signal amplified strategy: controlled nanomaterial multilayer and a target-catalyzed hairpin assembly. *Biosens Bioelectron* 2016, 787–13.
[65] Li S, Qiu W, Zhang X, Ni J, Gao F, Wang Q. A high-performance DNA biosensor based on the assembly of gold nanoparticles on the terminal of hairpin-structured probe DNA. *Sens Actuators B* 2016, 223, 861–7.
[66] Zhang L, Li Z, Zhou X, Yang G, Yang J, Wang H, et al. Hybridization performance of DNA/mercaptohexanol mixed monolayers on electrodeposited nano Au and rough Au surfaces. *J Electroanal Chem* 2015, 757, 203–9.
[67] Liu S, Su W, Li Z, Ding X. Electrochemical detection of lung cancer specific microRNAs using 3D DNA origami nanostructures. *Biosens Bioelectron* 2015, 71, 57–61.

[68] Xu CX, Zhai QG, Huang KJ, Lu L, Li KX. A novel electrochemical DNA biosensor construction based on layered CuS-graphene composite and Au nanoparticles. *Anal Bioanal Chem* 2014, 406, 6943–51.
[69] Miao X, Guo X, Xiao Z, Ling L. Electrochemical molecular beacon biosensor for sequence-specific recognition of double-stranded DNA. *Biosens Bioelectron* 2014, 59, 54–7.
[70] Nowicka AM, Fau M, Rapecki T, Donten M. Polypyrrole-Au nanoparticles composite as suitable platform for DNA biosensor with electrochemical impedance spectroscopy detection. *Electrochim Acta* 2014, 140, 65–71.
[71] Zheng J, Hu L, Zhang M, Xu J, He P. An electrochemical sensing strategy for the detection of the hepatitis B virus sequence with homogenous hybridization based on host-guest recognition. *RSC Adv* 2015, 5, 92025–32.
[72] Wang Z, Zhang J, Zhu C, Wu S, Mandler D, Marksacde RS, et al. Amplified detection of femtomolar DNA based on a one-to-few recognition reaction between DNA-Au conjugate and target DNA. *Nanoscale* 2014, 6, 3110–5.
[73] Cheng XR, Hau BYH, Endo T, Kerman K. Au nanoparticle-modified DNA sensor based on simultaneous electrochemical impedance spectroscopy and localized surface plasmon resonance. *Biosens Bioelectron* 2014, 53, 513–8.
[74] Huang L, Yang X, Qi C, Niu X, Zhao C, Zhao X, et al. A label-free electrochemical biosensor based on a DNA aptamer against codeine. *Anal Chim Acta* 2013, 787, 203–10.
[75] Chen Z, Guo J, Li J, Guo L. An electrochemical aptasensor based on the amplification of two kinds of gold nanocrystals for the assay of L-histidine with picomolar detection limit. *Nanotechnology* 2013, 24, 295501.
[76] Yang C, Wang Q, Xiang Y, Yuan R, Chai Y. Target-induced strand release and thionine-decorated gold nanoparticle amplification labels for sensitive electrochemical aptamer-based sensing of small molecules. *Sens Actuators B* 2014, 197, 149–54.
[77] Wang G, Chen L, Zhu Y, He X, Xu G, Zhang X. Development of an electrochemical sensor based on the catalysis of ferrocene actuated hemin/G-quadruplex enzyme for the detection of potassium ions. *Biosens Bioelectron* 2014, 61, 410–6.
[78] Miao X, Li Z, Zhu A, Feng Z, Tian J, Peng X. Ultrasensitive electrochemical detection of protein tyrosine kinase-7 by gold nanoparticles and methylene blue assisted signal amplification. *Biosens Bioelectron* 2016, 83, 39–44.
[79] Azadbakht A, Gholivand MB. Polyethyleneimine wrapped carbon nanotubes in situ formed gold nanoparticles decorated with DNA and $NAD^+$as a novel bioeletrochemical sensing platform. *Electrochim Acta* 2014, 133, 82–92.
[80] Rezaei B, Boroujeni MK, Ensafi AA. Fabrication of DNA, o-phenylenediamine, and gold nanoparticle bioimprinted polymer electrochemical sensor for the determination of dopamine. *Biosens Bioelectron* 2015, 66, 490–6.
[81] Rezaei B, Boroujeni MK, Ensafi AA. Development of Sudan II sensor based on modified treated pencil graphite electrode with DNA, o-phenylenediamine, and gold nanoparticle bioimprinted polymer. *Sens Actuators B* 2016, 222, 849–56.
[82] Chowdhury AD, Gangopadhyay R, De A. Highly sensitive electrochemical biosensor for glucose, DNA and protein using gold-polyaniline nanocomposites as a common matrix. *Sens Actuators B* 2014, 190, 348–56.
[83] Wu L, Ma C, Ge L, Kong Q, Yan M, Ge S, et al. Paper-based electrochemiluminescence origami cyto-device for multiple cancer cells detection using porous AuPd alloy as catalytically promoted nanolabels. *Biosens Bioelectron* 2015, 63, 450–7.
[84] Radhakrishnan S, Sumathi C, Umar A, Kim SJ, Wilson J, Dharuman V. Polypyrrole – poly(3,4-ethylenedioxythiophene)-Ag (PPy-PEDOT-Ag) nanocomposite films for label-free electrochemical DNA sensing. *Biosens Bioelectron* 2013, 47, 133–40.

[85] Kuzin Y, Porfireva A, Stepanova V, Evtugyn V, Stoikov I, Evtugyn G, et al. Impedimetric detection of DNA damage with the sensor based on silver nanoparticles and neutral red. *Electroanalysis* 2015, 27, 2800–8.
[86] Hamidi-Asl E, Raoof JB, Naghizadeh N, Akhavan-Niaki H, Ojania R, Banihashemi A. A bimetallic nanocomposite modified genosensor for recognition and determination of thalassemia gene. *Intern J Biol Macromol* 2016, 91, 400–8.
[87] Liu L, Xiang G, Jiang D, Du C, Liu C, Huang W, et al. Electrochemical gene sensor for Mycoplasma pneumoniae DNA using dual signal amplification via a Pt@Pd nanowire and horseradish peroxidase. *Microchim Acta* 2016, 183, 379–87.
[88] Bhat SS, Qurashi A, Khanday FA. ZnO nanostructures based biosensors for cancer and infectious disease applications: perspectives, prospects and promises. *Trends Anal Chem* 2017, 86, 1–13.
[89] Zhu P, Weng Z, Li X, Liu X, Wu S, Yeung KWK, et al. Biomedical applications of functionalized ZnO nanomaterials: from biosensors to bioimaging. *Adv Mater Interfaces* 2016, 3, 1500494.
[90] Arya SK, Saha S, Ramirez-Vick JE, Gupta V, Bhansali S, Singh SP. Recent advances in ZnO nanostructures and thin films for biosensor applications: review. *Anal Chim Acta* 2012, 737, 1–21.
[91] Fang L, Huang K, Zhang B, Liu Y, Zhang Q. A label-free electrochemistry biosensor based flower-like 3-dimensional ZnO superstructures for detection of DNA arrays. *New J Chem* 2014, 38, 5918–24.
[92] Tak M, Gupta V, Tomar M. Flower-like ZnO nanostructure based electrochemical DNA biosensor for bacterial meningitis detection. *Biosens Bioelectron* 2014, 59, 200–7.
[93] Merkoci A, Pumera M, Llopis X, Perez B, del Valle M, Alegret S. New materials for electrochemical sensing VI: carbon nanotubes. *Trends Anal Chem* 2005, 24, 826–39.
[94] Daniel S, Rao TP, Rao KS, Rani SU, Naidu GRK, Lee H, et al. A review of DNA functionalized/grafted carbon nanotubes and their characterization. *Sens Actuators B* 2007, 122, 672–82.
[95] Kim SN, Rusling JF, Papadimitrakopoulos F. Carbon nanotubes for electronic and electrochemical detection of biomolecules. *Adv Mater* 2007, 19, 3214–28.
[96] Chen RJ, Franklin NR, Kong J, Cao J, Tombler TW, Zhang Y, et al. Molecular photodesorption from carbon nanotubes. *Appl Phys Lett* 2001, 79, 2258–60.
[97] Vetcher AA, Srinivasan S, Vetcher IA, Abramov SM, Kozlov M, Baughman RH, et al. Fractionation of SWCNT/nucleic acid complexes by agarose gel electrophoresis. *Nanotechnology* 2006, 17, 4263–9.
[98] Wang J, Kawde AN, Jan MR. Carbon-nanotube-modified electrodes for amplified enzyme-based electrical detection of DNA hybridization. *Biosens Bioelectron* 2004, 20, 995–1000.
[99] Sun W, Li Y, Duan Y, Jiao K. Direct electrochemistry of guanosine on multi-walled carbon nanotubes modified carbon ionic liquid electrode. *Electrochim Acta* 2009, 54, 4105–10.
[100] Luo HX, Guo ZX, He N. Reversible electrochemistry of DNA on multi-walled carbon nanotube modified electrode. *Chinese Chem Lett*. 2007 18, 861–4.
[101] Li Q, Zhang J, Yan H, He M, Liu Z. Thionine-mediated chemistry of carbon nanotubes. *Carbon* 2004, 42, 287–91.
[102] Gutierrez F, Rubianes MD, Rivas GA. Adsorption and electrooxidation of DNA at glassy carbon electrodes modified with multiwall carbon nanotubes dispersed in glucose oxidase. *Electroanalysis* 2013, 25, 1135–42.
[103] Eksin E, Bolat G, Kuralay F, Erdem A, Abaci S. Preparation of gold nanoparticles/single-walled carbon nanotubes/polyaniline composite-coated electrode developed for DNA detection. *Polym Bull* 2015, 72, 3135–46.
[104] Hianik T, Evtugyn G. Carbon nanotubes in nucleic acids and affinity biosensors. *Horizons in DNA research, Nova Science Publishers*, 2010, 1, 1–48.

[105] Wang S, Li L, Jin H, Yang T, Bao W, Huang S, et al. Electrochemical detection of hepatitis Band papilloma virus DNAs using SWCNT array coated with gold nanoparticles. *Biosens Bioelectron* 2013, 41, 205–10.
[106] Fayazfar H, Afshar A, Dolati M, Dolati A. DNA impedance biosensor for detection of cancer, *TP53* gene mutation, based on gold nanoparticles/aligned carbon nanotubes modified electrode. *Anal Chim Acta* 2014, 836, 34–44.
[107] Li J, Lee E-C. Functionalized multi-wall carbon nanotubes as an efficient additive for electrochemical DNA sensor. *Sens Actuators B* 2017, 239, 652–9.
[108] Huang KJ, Liu Y-J, Wang H-B, Wang Y-Y, Liu Y-M. Sub-femtomolar DNA detection based on layered molybdenum disulfide/multi-walled carbon nanotube composites, Au nanoparticle and enzyme multiple signal amplification. *Biosens Bioelectron* 2014, 55, 195–202.
[109] Dong X, Lu X, Zhang K, Zhang Y. Chrono coulometric DNA biosensor based on a glassy carbon electrode modified with gold nanoparticles, poly(dopamine) and carbon nanotubes. *Microchim Acta* 2013, 180, 101–8.
[110] Kim J, Elsnab J, Gehrke C, Li J, Gale BK. Microfluidic integrated multi-walled carbon nanotube (MWCNT)sensor for electrochemical nucleic acid concentration measurement. *Sens Actuators B* 2013, 185, 370–6.
[111] Zhang N, Zhang K, Zhang L, Wang H, Shi H, Wang C. A label-free electrochemical DNA sensor based on $ZrO_2$/poly(thionine)/CNT modified electrode and its application for detecting CaMV35S transgene gene sequence. *Anal Methods* 2015, 7, 3164–8.
[112] Fernandes AM, Abdalhai MH, Ji J, Xi B-W, Xie J, Sun J, et al. Development of highly sensitive electrochemical genosensor based on multiwalled carbon nanotubes-chitosan-bismuth and lead sulfide nanoparticles for the detection of pathogenic *Aeromonas*. *Biosens Bioelectron* 2015, 63, 399–406.
[113] Benvidi A, Rajabzadeh N, Mazloum-Ardakani M, Heidari MM. Comparison of impedimetric detection of DNA hybridization on chemically and electrochemically functionalized multi-wall carbon nanotubes modified electrode. *Sens Actuators B* 2015, 207, 673–682.
[114] Congur G, Plucnara M, Erdem A, Fojta M. Detection of p53 gene by using genomagnetic assay combined with carbon nanotube modified disposable sensor technology. *Electroanalysis* 2015, 27, 1579–86.
[115] García-González R, Costa-García A, Fernández-Abedul MT. Enzymatic amplification-free nucleic acid hybridization sensing on nanostructured thick-film electrodes by using covalently attached methylene blue. *Talanta* 2015, 142, 11–9.
[116] Miodek A, Mejri N, Gomgnimbou M, Sola C, Korri-Youssoufi H. E-DNA sensor of Mycobacterium tuberculosis based on electrochemical assembly of nanomaterials (MWCNTs/PPy/PAMAM). *Anal Chem* 2015, 87, 9257–64.
[117] Mazloum-Ardakani M, Hosseinzadeh L, Heidari MM. Detection of the M268T Angiotensinogen A3B2 mutation gene based on screen-printed electrodes modified with a nanocomposite: application to human genomic samples. *Microchim Acta* 2016, 183, 219–27.
[118] Chen M, Hou C, Huo D, Yang M, Fa H. An ultrasensitive electrochemical DNA biosensor based on a copper oxide nanowires/single-walled carbon nanotubes nanocomposite. *Appl Surf Sci* 2016, 364, 703.
[119] Sun Y, Ren Q, Liu B, Qin Y, Zhao S. Enzyme-free and sensitive electrochemical determination of the FLT3 gene based on a dual signal amplified strategy: controlled nanomaterial multilayers and a target-catalyzed hairpin assembly. *Biosens Bioelectron* 2016, 78, 7–13.
[120] Zhang W. Application of $Fe_3O_4$ nanoparticles functionalized carbon nanotubes for electrochemical sensing of DNA hybridization. *J Appl Electrochem* 2016, 46, 559–66.

[121] Bizid S, Mlika R, Saïd, AH, Chemli M, Korri-Youssoufi H. Functionalization of MWCNTs with ferrocene-poly(p-phenylene) and effect on electrochemical properties: application as a sensing platform. *Electroanalysis* 2016, 28, 2533–42.
[122] Narang J, Singhal C, Malhotra N, Narang S, Krishna PNA, Gupta R, et al. Impedimetric genosensor for ultratrace detection of hepatitis B virus DNA inpatient samples assisted by zeolites and MWCNT nanocomposites. *Biosens Bioelectron* 2016, 86, 566–74.
[123] Hou L, Jiang L, Song Y, Ding Y, Zhang J, Wu X, et al. Amperometric aptasensor for saxitoxin using a gold electrode modified with carbon nanotubes on a self-assembled monolayer, and methylene blue as an electrochemical indicator probe. *Microchim Acta* 2016, 183, 1971–80.
[124] Miodek A, Castillo G, Hianik T, Korri-Youssoufi H. Electrochemical aptasensor of human cellular prion based on multiwalled carbon nanotubes modified with dendrimers: a platform for connecting redox markers and aptamers. *Anal Chem* 2013, 85, 7704–12.
[125] Zhang J, Chai Y, Yuan R, Yuan Y, Bai L, Xie S. A highly sensitive electrochemical aptasensor for thrombin detection using functionalized mesoporous silica@multiwalled carbon nanotubes as signal tags and DNAzyme signal amplification. *Analyst* 2013, 138, 6938–45.
[126] Heydari-Bafrooei E, Amini M, Ardakani MH. An electrochemical aptasensor based on $TiO_2$/MWCNT and a novel synthesized Schiff base nanocomposite for the ultra sensitive detection of thrombin. *Biosens Bioelectron* 2016, 85, 828–36.
[127] Deiminiat B, Rounaghi GH, Arbab-Zavar MH, Razavipanah I. A novel electrochemical aptasensor based on f-MWCNTs/AuNPs nanocomposite for label-free detection of bisphenol A. *Sens Actuators B* 2017, 42, 158–166.
[128] Beiranvand ZS, Abbasi AR, Dehdashtian S, Karimi Z, Azadbakht A. Aptamer-based electrochemical biosensor by using Au-Pt nanoparticles, carbon nanotubes and acriflavine platform. *Anal Biochem* 2017, 518, 35–45.
[129] Derikvandi Z, Abbasi AR, Roushani M, Derikvand Z, Azadbakht A. Design of ultrasensitive bisphenol A – aptamer based on platinum nanoparticles loading to polyethyleneimine-functionalized carbon nanotubes. *Anal Biochem* 2016, 512, 47–57.
[130] Azadbakht A, Roushani M, Abbasi AR, Derikvand Z. A novel impedimetric aptasensor, based on functionalized carbon nanotubes and prussian blue as labels. *Anal Biochem* 2016, 512, 58–69.
[131] Pilehvar S, Rather JA, Dardenn F, Robbens J, Blust R, De Wael C. Carbon nanotubes based electrochemical aptasensing platform for the detection of hydroxylated polychlorinated biphenyl in human blood serum. *Biosens Bioelectron* 2014, 54, 78–84.
[132] Ocaña C, Lukic S, del Valle M. Aptamer-antibody sandwich assay for cytochrome c employing an MWCNT platform and electrochemical impedance. *Microchim Acta* 2015, 182, 2045–53.
[133] Wu D, Ren X, Hu L, Fan D, Zheng Y, Wei Q. Electrochemical aptasensor for the detection of adenosine by using PdCu@MWCNTs-supported bienzymes as labels. *Biosens Bioelectron* 2015, 74, 391–7.
[134] Yin Y, Qin X, Wang Q, Yin Y. A novel electrochemical aptasensor for sensitive detection of streptomycin based on gold nanoparticle-functionalized magnetic multi-walled carbon nanotubes and nanoporous PtTi alloy. *RSC Adv* 2016, 6, 39401–8.
[135] Beiranvand S, Abbasi AR, Roushani M, Derikvand Z, Azadbakht A. A simple and label-free aptasensor based on amino group-functionalized gold nanocomposites-Prussian blue/carbon nanotubes as labels for signal amplification. *J Electroanal Chem* 2016, 776, 170–179.
[136] Prabhakar N, Thakur H, Bharti A, Kaur N. Chitosan-iron oxide nanocomposite based electrochemical aptasensor for determination of malathion. *Anal Chim Acta* 2016, 939, 108–16.
[137] Khezrian S, Salimi A, Teymourian H, Hallaj R. Label-free electrochemical IgE aptasensor based on covalent attachment of aptamer on to multiwalled carbon nanotubes/ionic liquid/chitosan nanocomposite modified electrode. *Biosens Bioelectron* 2013, 43, 218–25.

[138] Sun X, Li F, Shen G, Huang J, Wang H. Aptasensor based on the synergistic contributions of chitosan – gold nanoparticles, graphene-gold nanoparticles and multi-walled carbon nanotubes cobalt phthalocyanine nanocomposites for kanamycin detection. *Analyst* 2014, 139, 299–308.
[139] Qin X, Guo W, Yu H, Zhao J, Pei M. A novel electrochemical aptasensor based on MWCNTs – BMIMPF6 and amino functionalized graphene nanocomposite films for determination of kanamycin. *Anal Methods* 2015, 7, 5419–27.
[140] Song W, Niu Q, Qiang W, Li H, Xu D. Enzyme-free electrochemical aptasensor by using silver nanoparticles aggregates coupling with carbon nanotube inducing signal amplification through electrodeposition. *J Electroanal Chem* 2016, 781, 62–9.
[141] Steel AB, Herne TM, Tarlov MJ. Electrochemical quantitation of DNA immobilized on gold. *Anal Chem* 1998, 70, 4670–7.
[142] Li J, Wang J, Guo X, Zheng Q, Peng J, Tang H, et al. Carbon nanotubes labeled with aptamer and horseradish peroxidase as a probe for highly sensitive protein biosensing by post electropolymerization of insoluble precipitates on electrodes. *Anal Chem* 2015, 87, 7610–7.
[143] Kumar M, Ando Y. Chemical vapor deposition of carbon nanotubes: a review on growth mechanism and mass production. *J Nanosci Nanotechnol* 2010, 10, 3739–58.
[144] de Moraes ACM, Kubota LT. Recent trends in field-effect transistors-based immunosensors. *Chemosensors* 2016, 4, 20.
[145] Debye P. Dielectric properties of pure liquids. *Chem Rev* 1936, 9, 171–82.
[146] Maehashi K, Katsura K, Kerman K, Takamura Y, Matsumoto K, Tamiya E. Label-free protein biosensor based on aptamer-modified carbon nanotube field-effect transistors. *Anal Chem* 2007, 79, 782–7.
[147] Maehashi K, Matsumoto K, Takamura Y, Tamiya E. Aptamer-based label-free immunosensors using carbon nanotube field-effect transistors. *Electroanalysis* 2009, 21, 1285–1290.
[148] Bai L, Yuan R, Chai Y, Zhuo Y, Yuan Y, Wang Y. Simultaneous electrochemical detection of multiple analytes based on dual signal amplification of single-walled carbon nanotubes and multi-labeled graphene sheets. *Biomaterials* 2012, 33, 1090–6.
[149] Lee D-W, Lee J, Sohn IY, Kim B-Y, Son YM, et al. Field-effect transistor with a chemically synthesized $MoS_2$ sensing channel for label-free and highly sensitive electrical detection of DNA hybridization. *Nano Res* 2015, 8, 2340–50.
[150] Pumera M. Graphene-based nanomaterials and their electrochemistry. *Chem Soc Rev* 2010, 39, 4146–57.
[151] Dreyer DR, Park S, Bielawski CW, Ruoff RS. The chemistry of graphene oxide. *Chem Soc Rev* 2010, 39, 228–40.
[152] Frackowiak E, Delpeux S, Jurewicz K, Szostak K, Cazorla-Amoros D, Béguin F. Enhanced capacitance of carbon nanotubes through chemical activation. *Chem Phys Letters* 2002, 336, 35–41.
[153] Gan T, Hu S. Electrochemical sensors based on graphene materials. *Microchim Acta* 2011, 175, 1–19.
[154] Shao Y, Wang J, Wu H, Liu J, Aksay IA, Lin Y. Graphene based electrochemical sensors and biosensors: a review. *Electroanalysis* 2010, 22, 1027–36.
[155] Song Y, Luo Y, Zhu C, Li H, Du D, Lin Y. Recent advances in electrochemical biosensors based on graphene two-dimensional nanomaterials. *Biosens Bioelectron* 2016, 76, 195–212.
[156] Yuan Y, Gou X, Yuan R, Chai Y, Zhuo Y, Ye X, Gan X. Graphene-promoted 3,4,9,10-perylene tetracarboxylic acid nanocomposite as redox probe in label-free electrochemical aptasensor. *Biosens Bioelectron* 2011, 30, 123–7.
[157] Luo L, Zhang Z, Ding Y, Deng D, Zhu X, Wang Z. Label-free electrochemical impedance genosensor based on 1-aminopyrene/graphene hybrids. *Nanoscale* 2013, 5, 5833–40.
[158] Wang L, Qi W, Su R, He Z. Noncovalent functionalization of graphene by CdS nanohybrids for electrochemical applications. *Thin Solid Films* 2014, 568, 58–62.

[159] Ramnani P, Saucedo NM, Mulchandani A. Carbon nanomaterial-based electrochemical biosensors for label-free sensing of environmental pollutants. *Chemosphere* 2016, 143, 85–98.
[160] Wang Y, Hu S. Applications of carbon nanotubes and graphene for electrochemical sensing of environmental pollutants. *J Nanosci Nanotechnol* 2016, 16, 7852–72.
[161] Rezaei B, Khosropour H, Ensafi AA, Dinari M, Nabiyan A. A new electrochemical sensor for the simultaneous determination of guanine and adenine: using a NiAl-layered double hydroxide/graphene oxide – multiwall carbon nanotube modified glassy carbon electrode. *RSC Adv* 2015, 5, 75756–65.
[162] Gao D, Li M, Li H, Li C, Zhu N, Yang B. Sensitive detection of biomolecules and DNA bases based on graphene nanosheets. *J Solid State Electrochem* 2017, 21, 813–21.
[163] Ma W, Han D, Zhang N, Li F, Wu T, Dong X, et al. Bionic radical generation and antioxidant capacity sensing with photocatalytic graphene oxide – titanium dioxide composites under visible light. *Analyst* 2013, 138, 2335–42.
[164] Yang Y, Zhou J, Zhang H, Gai P, Zhang X, Chen J. Electrochemical evaluation of total antioxidant capacities in fruit juice based on the guanine/graphene nanoribbon/glassy carbon electrode. *Talanta* 2013, 106, 206–211.
[165] Yang Y, Kang M, Fang S, Wang M, He L, Feng X, et al. A feasible C-rich DNA electrochemical biosensor based on $Fe_3O_4$@3D-GO for sensitive and selective detection of $Ag^+$. *J Alloys Comp* 2015, 652, 225–33.
[166] Wang M, Zhang S, Ye Z, Peng D, He L, Yan F, et al. A gold electrode modified with amino-modified reduced graphene oxide, ion specific DNA and DNAzyme for dual electrochemical determination of Pb(II) and Hg(II). *Microchim Acta* 2015, 182, 2251–8.
[167] An JH, Park SJ, Kwon OS, Bae J, Jang J. High-performance flexible graphene aptasensor for mercury detection in mussels. *ACS Nano* 2013, 7, 10563–71.
[168] Xue S, Jing P, Xu W. Hemin on graphene nanosheets functionalized with flower-like $MnO_2$ and hollow AuPd for the electrochemical sensing lead ion based on the specific DNAzyme. *Biosens Bioelectron* 2016, 86, 958–965.
[169] Gao F, Gao C, He S, Wang Q, Wu A. Label-free electrochemical lead (II) aptasensor using thionine as the signaling molecule and graphene as signal-enhancing platform. *Biosens Bioelectron* 2016, 81, 15–22.
[170] Huan D, Mi S, Xiao-Ping W. Electrochemical lead ion aptasensor based on G-quadruplex and gate-controlled signal amplification. *Chinese J Anal Chem* 2016, 44, 888–92.
[171] Park H, Hwang S-J, Kim K. An electrochemical detection of $Hg^{2+}$ ion using graphene oxide as an electrochemically active indicator. *Electrochem Commun* 2012, 24, 100–3.
[172] Yang Y, Kang M, Fang S, Wang M, He L, Zhao J, et al. Electrochemical biosensor based on three-dimensional reduced graphene oxide and polyaniline nanocomposite for selective detection of mercury ions. *Sens Actuators B* 2015, 214, 63–9.
[173] Wang H, Zhang Y, Ma H, Ren X, Wang Y, Zhang Y, et al. Electrochemical DNA probe for $Hg^{2+}$ detection based on a triple-helix DNA and multistage signal amplification strategy. *Biosens Bioelectron* 2016, 86, 907–12.
[174] Huang H, Bai W, Dong C, Guo R, Liu Z. An ultrasensitive electrochemical DNA biosensor based on graphene/Au nanorod/polythionine for human papilloma virus DNA detection. *Biosens Bioelectron* 2015, 68, 442–6.
[175] Sun W, Wang X, Wang W, Lu Y, Xi1 J, Zheng W, et al. Electrochemical DNA sensor for *Staphylococcus aureus* nuc gene sequence with zirconia and graphene modified electrode. *J Solid State Electrochem* 2015, 19, 2431–8.
[176] Chen X, Wang L, Sheng S, Wang T, Yang J, Xie G, et al. Coupling a universal DNA circuit with graphene sheets/polyaniline/AuNPs nanocomposites for the detection of BCR/ABL fusion gene. *Anal Chim Acta* 2015, 889, 90–7.

[177] Li B, Pan G, Avent ND, Lowry RB, Madgett TE, Waines PL. Graphene electrode modified with electrochemically reduced graphene oxide for label-free DNA detection. *Biosens Bioelectron* 2015, 72, 313–9.
[178] Wu L, Ji H, Sun H, Ding C, Ren J, Qu X. Label-free ratiometric electrochemical detection of the mutated apolipoprotein E gene associated with Alzheimer's disease. *Chem Commun* 2016, 52, 12080–3.
[179] Teymourian H, Salimi A, Khezrian S. Development of a new label-free, indicator-free strategy toward ultrasensitive electrochemical DNA biosensing based on $Fe_3O_4$ nanoparticles/reduced graphene oxide composite. *Electroanalysis* 2017, 29, 409–14.
[180] Yang T, Li Q, Li X, Wang X, Du M, Jiao K. Freely switchable impedimetric detection of target gene sequence based on synergistic effect of ERGNO/PANI nanocomposites. *Biosens Bioelectron* 2013, 42, 415–8.
[181] Tiwari I, Singh M, Pandey CP, Sumana G. Electrochemical genosensor based on graphene oxide modified iron oxide-chitosan hybrid nanocomposite for pathogen detection. *Sens Actuators B* 2015, 206, 276–83.
[182] Yang L, Li X, Li X, Yan S, Ren Y, Wang M, et al. $[Cu(phen)_2]^{2+}$ acts as electrochemical indicator and anchor to immobilize probe DNA in electrochemical DNA biosensor. *Anal Biochem* 2016, 492, 56–62.
[183] Wang J, Shi Z, Fang X, Han X, Zhang Y. Ultrasensitive electrochemical super sandwich DNA biosensor using a glassy carbon electrode modified with gold particle-decorated sheets of graphene oxide. *Microchim Acta* 2014, 181, 935–40.
[184] Rasheed PA, Radhakrishnan T, Shihabudeen PK, Sandhyarani N. Reduced graphene oxide-yttria nanocomposite modified electrode for enhancing the sensitivity of electrochemical genosensor. *Biosens Bioelectron* 2016, 83, 361–7.
[185] Gong Q, Wang Y, Yang H. A sensitive impedimetric DNA biosensor for the determination of the HIV gene based on graphene-Nafion composite film. *Biosens Bioelectron* 2017, 89, 565–9.
[186] Huang K-J, Shuai H-L, Zhang J-Z. Ultrasensitive sensing platform for platelet-derived growth factor BB detection based on layered molybdenum selenide – graphene composites and Exonuclease III assisted signal amplification. *Biosens Bioelectron* 2016, 77, 69–75.
[187] Wang W, Wang W, Davis JJ, Luo X. Ultrasensitive and selective voltammetric aptasensor for dopamine based a conducting polymer nanocomposite doped with graphene oxide. *Microchim Acta* 2015, 182, 1123–9.
[188] Fernandez RE, Sanghavi BJ, Farmehini V, Chávez JL, Hagen J, Kelley-Loughnane N, et al. Aptamer-functionalized graphene-gold nanocomposites for label-free detection of dielectrophoretic-enriched neuropeptide Y. *Electrochem Commun* 2016, 72, 144–7.
[189] Liu S, Wang Y, Xu W, Leng X, Wang H, Guo Y, et al. A novel sandwich-type electrochemical aptasensor based on GR-3D Au and aptamer-AuNPs-HRP for sensitive detection of oxytetracycline. *Biosens Bioelectron* 2017, 88, 181–187.

# Part IV: **Application in Sorption and Separation Methods**

S. G. Dmitrienko and V. V. Apyari

# 9 Molecularly Imprinted Polymers: Synthesis, Properties, and Application in Analysis of Real Samples

## 9.1 Introduction

Among the broad class of nanomaterials, one can mark out nanoporous materials, which contain pores of nanometer range (1–100 nm). The term "nanoporous materials" is used to indicate that the specific material properties (sensory, adsorption, catalytic, diffusive, and others) are associated with the presence of nanopores. The concept "nanopore" combines the three pore regions: nanopores (pore size of up to 2 nm), mesopores (2–50 nm), and partially macropores (above 50 nm). Nanoporous materials include most of the known membranes, catalysts, and polymeric and inorganic sorbents.

Molecularly imprinted polymers (MIPs) represent a new generation of nanostructured polymeric sorbents, which are obtained by the method of molecular (matrix) imprints (molecular imprinting) [1]. Molecular imprinting is based on polymerization of functional and cross-linking monomers in the presence of target template molecules. After their removal, nanosized cavities (imprints), which are complementary to the template molecules, remain in the polymer. Fixation of the template molecules in the polymer skeleton during polymerization provides a particular polymer chain nanostructure, that is, appearance of its "molecular memory." Since as-prepared synthetic materials selectively interact with the molecules used as the template, one can talk about "molecular recognition." In the nature, such specificity is represented by antibodies; therefore, materials obtained by the method of molecular imprinting are often referred to as "antibody mimics." The fact that the matrix "remembers" structure of molecules that were used as molecular templates opens up new possibilities for synthesis of sorbents, catalysts, and sensor materials having improved selectivity to these molecules [2–6].

As follows from the historical overview given in [3], the concept of molecular imprinting was first proposed by M.V. Polyakov in the early 1930s. He showed that silica synthesized in the presence of various alkylbenzenes had an increased (by approximately 15 %) selectivity for the adsorption of these hydrocarbons. In the 1950–70s, the papers appeared showing that the template introduced during the synthesis affects the pore size and adsorptive properties of silica, and the activity and selectivity of metallic catalysts. However, most described by this time approaches to using molecular templates for synthesis of organized surfaces based on inorganic matrices had a common drawback: the stability of the obtained imprints was low. This situation changed dramatically with the advent of works that described methods for preparing polymeric materials with molecular imprints of various organic compounds,

https://doi.org/10.1515/9783110542011-009

first by covalent (1972) [7] and then by noncovalent (1981) [8] imprinting. In 1994, MIPs were first used in chemical analysis [9].

Currently, issues of molecular imprinting are actively studied by more than 100 academic and industrial research groups around the world. According to SciFinder (www.scifinder.cas.org) search system, from 1984 to February 2011, more than 4,000 articles and reviews devoted to MIPs were published and an exponential growth of publications on this subject was observed [10].

The growing attention from researchers working in different fields of chemistry to MIPs is associated with a number of benefits and advantages associated with these new materials. First of all, MIPs are interesting from a theoretical point of view: they can be considered as synthetic receptors, whose operation is based on the principle of molecular recognition. Molecular imprinting technology allows for the preparation of new adsorbents having high and controlled selectivity in relation to any organic compound. Unlike more complex biological receptor, MIPs are highly resistant to chemical and physical effects: they can be stored for several years without loss of memory of molecular recognition sites. These materials are distinguished by ease of preparation and relatively low cost.

The potentially high selectivity of MIPs with respect to organic compounds along with other useful properties has opened opportunities for the use of these nanomaterials in analytical chemistry. The results of many research studies have been summarized in the monograph [11] and in several general reviews [2, 12–14]. Some reviews are devoted to using MIPs in the solid phase extraction (SPE) of organic compounds [15–20]; separation of structurally similar organic compounds including enantiomers by high-performance liquid chromatography (HPLC) and capillary electrophoresis [21–23]; selective isolation and subsequent determination of analytes using electrochemical, piezoelectric, or chemical sensors [10, 24, 25]; and flow-injection [26] and biochemical analysis [6]. Data on the use of MIPs in the analysis of environmental samples [27–29], biological liquids [28, 30], drugs [28, 31], and food [28, 32–34] have been reported.

This chapter summarizes main approaches and methods used in the synthesis of MIPs; considers some questions of selective sorption of organic compounds, distinguishing them from the other sorbents; and gives examples of practical application of MIPs for SPE of organic compounds in analysis of various samples.

## 9.2 The principle of molecular imprinting

### 9.2.1 Covalent and noncovalent approach

The general approach to the synthesis of MIPs involves carrying out known polymerization reactions in the presence of the target template molecules to be "fingerprinted." MIP synthesis scheme (Fig. 9.1) involves formation of a pre-polymerization

complex between a functional monomer and template molecules in a selected solvent, their copolymerization with large amounts of a cross-linking agent, and subsequent removal of the template from the polymer. After removal of the template, highly specific binding sites (sites of molecular recognition) remain in the MIP, which are complementary in size, shape, and structure to the template molecule. The concept of complementarity includes both matching up a fingerprint and a template molecule in shape and size and the possibility of binding these molecules due to interactions between their functional groups and the imprint. Two main approaches to the synthesis of MIPs have been proposed, which differ in binding type (covalent or noncovalent) between a monomer and template molecules [2, 35]. Implementation of the first approach involves carrying out a chemical reaction between template molecules and monomers in the first stage and removing the template from the polymer by breaking covalent bonds linking these molecules to the polymer. At the secondary binding of the analyte by the polymer, the covalent bonds are re-formed.

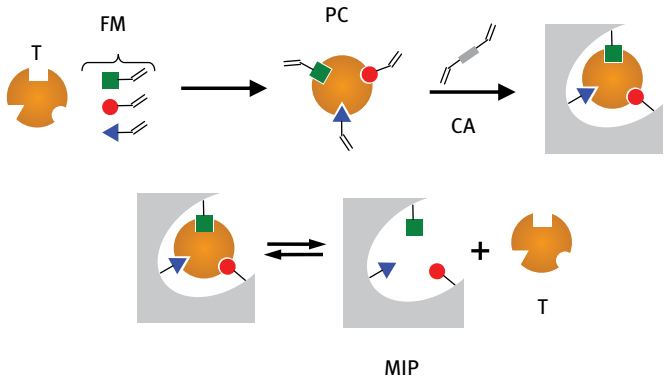


**Fig. 9.1:** Scheme of the MIP synthesis by the noncovalent imprinting (T – template, FM – functional monomers, PC – pre-polymerization complex, CA –cross-linking agent).

The more universal approach is a noncovalent one. The noncovalent method uses a very important property of polymer molecules, which is the basis of complex biological structures organization, – their ability of self-organization. The driving force behind association of a template and monomer molecules is noncovalent interactions of various types – electrostatic, ion–dipole, dipole, hydrogen bond, and hydrophobic interactions. Apparent fragility of such bonds can be compensated by multiplicity of interaction points. The method of noncovalent interactions in the molecular imprinting strongly resembles the model of recognition in the nature.

Another way – intermediate, half-covalent, wherein a template is covalently linked to a functional monomer in a polymerization process (like in the covalent approach), whereas the re-binding is realized only by noncovalent interactions.

The proposed approaches to the synthesis of MIPs have both advantages and disadvantages. A strong template–monomer interaction, which is realized through formation of chemical bonds, in the first case provides more uniform MIP binding sites. The main limitation in this case is a reduced number of monomer–template combinations having reversible formation – breaking of the covalent bonds, occurring under relatively mild conditions. The noncovalent way offers the more versatile assortment of templates; it is easier to implement in practice than the methods of covalent molecular imprinting because the binding is achieved by simply mixing a template with a functional monomer in a suitable solvent. It does not require any chemical modification. Removal of the template is carried out by repeated washing of the polymer with a solvent or solvents mixture.

The vast majority of currently known MIPs, which have found application in analytical chemistry, were obtained using the noncovalent approach, so this review focuses on consideration of the peculiarities of synthesis, properties, and applications in chemical analysis of the noncovalently imprinted polymers.

### 9.2.2 Selecting the template and the reagents

An important feature of the MIPs is that they can be synthesized using a virtually unlimited number of templates capable of reacting with a monomer molecule. Among other requirements for a template, one can note solubility in a selected solvent, stability under polymerization conditions ($t$ = 60–80°C, UV irradiation) as well as absence of functional groups that inhibit polymerization or able to participate in the polymerization reaction.

Most of the works in the field of noncovalent imprinting are dedicated to synthesis of MIPs for small organic molecules: phenols and phenolic compounds [36–39], dyes [40, 41], pesticides and herbicides [42–45], drugs [46–52], hormones [53, 54], alkaloids [55, 56]. Synthesis of molecular imprinted polymers with imprints of macromolecular compounds, such as peptides or proteins [57–59], still is a more complex and time-consuming procedure requiring careful selection of conditions and methods.

A problem that arises when using MIPs is connected with the fact that these polymers even after careful purification by solvents contain template molecules firmly associated with the polymer [2, 14]. Usually the residual content of a template is about 1% of the original quantity, but even this small amount can lead to incorrect results in isolating traces of organic compounds. This negative phenomenon is eliminated by using more effective methods of purification [14] or prevented using structural analogs of the target molecules (“template mimic”) during the MIP synthesis. Structural analogs are sometimes used in case of toxic, hard-to-get, or high-priced compounds. For example, for the synthesis of MIPs selective to melamine and cyproheptadine and mycotoxin zearalenone, one used cyromazine [60], azatadine [61], and

2,4-cyclododekanyl-hydroxybenzoate [62], respectively, as templates. For the synthesis of MIPs selective to ochratoxin A, one used N-(4-chloro-1-hydroxy-2-naphthoylamido)-(L)-phenylalanine as a template [63].

In recent years, there is evidence that MIPs, like polyclonal antibodies, can be used for selective isolation of a group of structurally related compounds. One of the compounds belonging to this group can be used as a template in the synthesis of MIPs ("fragmental imprinting"). For example, ofloxacin was used for the synthesis of MIPs selective with respect to the group of fluoroquinolone antibiotics [64, 65]. In some cases, two or more compounds are used instead of the one template in synthesis of MIPs [66].

Within the large number of commercially available functional monomers reported in reviews [2, 4, 13], methacrylic acid (MAA), 4-vinylpyridine (4-VP), and acrylamide (AA) are usually used in the synthesis of MIPs. Selection of a functional monomer (FM) for a synthesis of MIPs is paid much attention as a template is primarily responsible for the formation of molecular fingerprint in a polymer. When selecting monomer–template pairs, preference is given to such combinations, which realize the maximum number of complementary interactions providing high stability of a monomer–template associate before and during the polymerization process. To confirm the interaction between molecules of a monomer and a template and calculate the association constants, UV spectrophotometry, NMR, IR, and mass spectrometry are used [67].

Most often, the choice of FM is carried out empirically. For the synthesis of polymers with imprints of organic compounds containing basic groups, methacrylic acid is used as a functional monomer; in case of compounds with acidic groups – 4-vinylpyridine or acrylamide.

Sometimes two functional monomers are used. Particularly, the second monomer such as 2-hydroxyethyl methacrylate or glycidyl methacrylate is introduced into a reaction mixture for increasing hydrophilicity of the polymers [65, 68, 69].

An important condition for obtaining macroporous MIPs is high degree of a polymer cross-linking, providing its rigidity. Regardless of the method of synthesis (covalent, noncovalent, or semi-covalent), MIPs are prepared in the presence of large amounts of a cross-linking agent. Typically, a cross-linking agent is taken in 20-fold excess with respect to the functional monomer, and its content in a reaction mixture is 90–95 %. When selecting cross-linkers, one takes into account their good solubility in a pre-polymerization mixture. Ethylene glycol dimethacrylate (EGDMA), trimethylolpropane trimethacrylate (TRIM), p-divinylbenzene, and N,N′-bisacrylamide are often taken as cross-linking agents [2, 4]. Numerous studies have shown that the most successful cross-linking agent, both in terms of cost and MIP selectivity (specificity), is EGDMA [19]. Moreover, MIPs synthesized using it have good mechanical and thermal stability, porosity, and wettability. Chromatographic columns based on such polymers did not lose selectivity during their continuous use at the temperature of 80°C and the pressure of 6–10 MPa for several months.

The rate of radical polymerization depends on the nature and the concentration of an initiator [2, 4]. The most efficient initiator is azobisisobutyronitrile (AIBN), which is split into two isobutyronitrile radicals with the release of the nitrogen molecule upon heating the reaction mixture up to 600°C.

The porous structure of MIPs is achieved by polymerization in the presence of solvents (porogens), which readily dissolve initial monomers but do not dissolve final products. The nature, concentration, and volume of the solvent affect such structural characteristics as the specific surface area and the pore size [2]. Most often, chloroform [37, 40, 58, 63], toluene [44, 54], and acetonitrile [36, 46, 54, 56, 64] are used for the synthesis of MIPs. More polar solvents such as methanol, ethanol, or acetone are used less frequently.

## 9.3 Methods for synthesis of MIPs

### 9.3.1 Radical bulk polymerization

In the most studies on noncovalent imprinting, radical bulk polymerization method is employed for the synthesis of MIPs [19, 27–33]. The standard procedure for preparing MIPs by free radical bulk polymerization includes several stages. In the first step, a template, a functional monomer, a cross-linking agent, and a polymerization initiator are dissolved in a suitable porogen solvent. In the next step, a polymerization reaction is initiated by heating the reaction mixture up to 50–60°C or by UV irradiation. In the latter case, the MIP synthesis is carried out at low temperatures (from 15 to –20°C). Due to the fact that oxygen inhibits polymerization process, imprinting is usually preceded by oxygen removal from the pre-polymerization mixture by purging with an inert gas and/or sonication. After the polymerization, a rigid porous polymer monolith is mechanically grinded and repeatedly sieved through sieves with a certain pore diameter. Then, the particles of a desired size (typically 25–50 μm) are selected. In the final step, a template is removed from the synthesized MIP by repeated washing with organic solvents.

Along with a number of indisputable advantages of the bulk polymerization method, such as ease of the polymerization process control, relatively mild reaction conditions, absence of special requirements to the purity of the reagents, and low cost of the commercially available monomers, it also has certain drawbacks. About 30–40 % of the polymer is lost during the grinding process and its further fractionation. Irregular shape of the particles hampers their use as the stationary phases in HPLC. These drawbacks can be avoided by using macroporous monolithic MIPs, which are synthesized by the bulk polymerization directly (*in situ*) in cartridges for SPE [70–72], chromatographic columns [73, 74], or capillaries [75–77].

### 9.3.2 Synthesis of spherical microparticles

In recent years, much attention is being paid to the synthesis and properties of monodisperse spherical MIP microparticles. They can be prepared by precipitation, suspension, and seed and grafting polymerization methods [14, 19, 78, 79].

**Precipitation polymerization.** In contrast to the bulk polymerization, the precipitation polymerization is carried out in the presence of large amounts of solvent, the volume of which is 2–10 times greater than the volume of a solvent used in the conventional process for preparing MIPs. After the polymerization, precipitated polymer particles are filtered out, washed off from target template molecules, and used as selective sorbents in SPE or HPLC [80–90].

Synthesis of MIPs by the precipitation polymerization method is usually carried out in a mixture of acetonitrile and toluene [78, 80, 83–85, 90]. Pure acetonitrile [81], toluene [84, 90], and mixtures of acetonitrile with tetrahydrofuran (THF) [86] or with methanol [87, 88] are used less frequently. The size of resulting polymer particles depends on the ratio of components in a reaction mixture and polymerization conditions. For example, MIP particles with imprints of theophylline ($d$ = 5 μm), thiabendazole ($d$ = 3.5 μm), propranolol ($d$ = 3.5 μm), β-estradiol ($d$ = 3 μm), and S-nicotine [78] were obtained in a mixture of acetonitrile and toluene. By the example of MIPs with imprints of propranolol, which were synthesized using two cross-linking agents (EGDMA and TRIM), it found that the MIP particle size is decreased from 2.4 μm to 130 nm with increasing the ratio TRIM : EGDMA [80]. Replacing toluene with more polar methanol, as shown by the example of MIPs imprinted with tetracycline, causes aggregation of the spherical particles [87].

Compared with other methods of preparing MIP, the precipitation polymerization method has a number of advantages, such as exclusion of mechanical grinding procedure, uniformity of the final particles, relative ease of synthesis, high speed of analytes binding, absence of stabilizers and surfactants in the reaction mixture. This way was chosen for the synthesis of MIPs, which have found application in the analysis of real samples. Thus, for the determination of bisphenol A in biological fluids and environmental samples, an MIP with imprints of this compound was utilized [82]; for the determination of fluoroquinolone antibiotics in drinking water – an MIP with imprints of enrofloxacin [81], for the determination of benzimidazole fungicides in waters – MIPs with imprints of thiabendazole [83] and benzimidazole [84], for the determination of carbamazepine and oxcarbazepine in urine, atrazine, and tetracycline antibiotics in food – MIPs imprinted with carbamazepine [85], atrazine [86], and tetracycline [87], respectively. Precipitation polymerization was used for the synthesis of MIPs selective to a group of structurally related compounds: tetracycline antibiotics [88]; fluoroquinolone antibiotics [89]; and methyl-, ethyl-, isopropyl-, propyl-, isobutyl-, butyl-, and benzyl parabens [90].

**Suspension polymerization.** The suspension polymerization is carried out in monomer droplets dispersed in water, liquid fluorocarbons, or mineral oil [78]. In

order to form a stable emulsion of components, one uses a variety of stabilizers, which envelop the emulsion droplets, protecting them from sticking together. Depending on conditions of the emulsion formation and the amount of a stabilizer, the diameter of spherical MIP particles varies from 10 to 100 μm [19]. Such particles have much higher availability of molecular recognition sites than mechanically crushed conventional MIPs. This accelerates the mass transfer and binding of a template. The suspension polymerization method was used to prepare MIPs imprinted with penicillin [91], dicofol pesticide [92], chloramphenicol [93], indomethacin [94], enrofloxacin [95], 2,4-dichlorophenoxyacetic acid [96], and other compounds [19, 78].

**Seed polymerization.** This is mono-, di-, or multistage polymerization (multistep swelling). It is used for producing spherical polymer particles of defined and controlled size (5–50 μm) [19, 78, 91]. Unlike the above methods, the seed polymerization is more complex. According to the scheme, represented in a review [78] (Fig. 9.2), initially "seed" particles of monodisperse polystyrene latex (~1 μm) are introduced into an aqueous emulsion. The swelling is often carried out in two stages: the first one involves an activating solvent (usually dibutylphthalate), a stabilizer (sodium dodecyl sulfate), and a polymerization initiator; the second one involves functional monomers and a template. Upon reaching a certain size, the swollen particles are polymerized. This method was utilized for obtaining MIPs having found application for extraction of barbiturates [97], epigallocatechin, epicatechin gallate and epigallocatechin gallate [98], triazine herbicides [99], and metsulfurol-methyl from river and drinking waters [100]. Using phthalic acid as a template, MIP particle of 5 μm selective to domoic acid (the water-soluble neurotoxin produced by certain species of seaweed) were synthesized by seed polymerization [101].

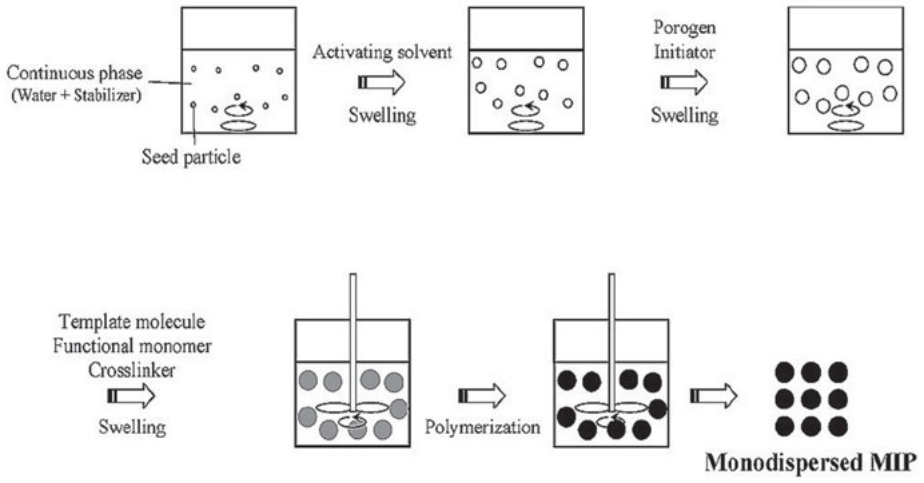


**Fig. 9.2:** The scheme for preparing monodisperse MIP particles by seed polymerization [78].

**Grafting.** A feature of this method for spherical MIP particles preparing is formation of a thin layer of an MIP on the surface of preactivated microparticles. There are two types of grafting: "grafting to" and "grafting from" [102].

In the "grafting to" method, granules of silica are premodified with groups containing double bonds, such as vinyl. The polymerization is carried out in a solution containing a template, a functional monomer, a cross-linker, and an initiator. The surface vinyl groups are involved in the polymerization process, resulting in covalent linking of the growing polymer chains to the surface. This approach has two major drawbacks – at first, formation of a polymer layer on the surface may be accompanied by uncontrolled polymerization in the bulk solution, and secondly, there are certain difficulties regarding control of thickness of the resulting MIP layer.

The "grafting from" approach is deprived of these disadvantages. Its idea is as follows. In the first step, an initiator is covalently immobilized on the surface of granules of silica or polystyrene. The compounds undergoing photolysis to form either radicals that cause slow polymerization in the solution or radicals that not capable of initiating the bulk polymerization at all are considered as the initiators, for example, sodium diethyldithiocarbamate [102–104]. Grafting with this compound can be represented by the Scheme 9.1 [103]:

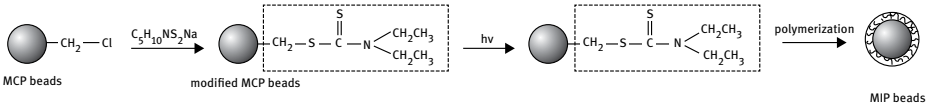


MCP - mesoporous chloromethylated polystyrene

**Scheme 9.1:** Grafting with sodium diethyldithiocarbamate.

In decomposing of grafted diethyldithiocarbamate, active methylene radicals are formed on the surface of polystyrene beads, which initiate polymerization. At the same time, less active radicals are formed in solution, which are not only incapable of initiating polymerization but, on the contrary, they cause interruption of growing polymer chains, thus forming a thin layer of MIP on the surface of a bead [104].

The method of grafting was used for the preparation of silica granules modified with imprints of lysozyme [103], hemoglobin [104], 2,4-dinitrophenol [105], and ursolic acid [106]. In the latter two cases, prospects of the prepared material using as stationary phase in chromatography were shown. In [107], sorbents for HPLC based on MIPs obtained by precipitation polymerization and "grafting from" were compared. It was found that a column packed with a sorbent prepared by grafting was significantly more efficient, but more changeable when re-used [107].

### 9.3.3 Synthesis of nanoscale imprinted materials

In recent years, considerable interest of researchers is paid to nanotechnologies and technologies of surface chemistry in the field of molecular imprinting [25, 104, 108, 109]. Nanoscale imprinted materials have a small size with an extremely high surface area-to-volume ratio, which leads to rapid sorption equilibration, higher extraction of templates, better availability of molecular recognition sites, and low mass transfer resistance [104, 108]. Because of these properties, MIP nanoparticles may be applied in capillary electrochromatography, as well as for development of electrochemical, piezoelectric, and fluorescent sensors.

The general methods for preparation of MIP nanoparticles are precipitation, seed, grafting, and miniemulsion polymerization as well as lithography [104, 108, 109]. Precipitation polymerization is probably the most simple to implement, fast and high-yield method. It is generally used for synthesis of particles of 100–500 nm [108, 109]. The size of MIP nanoparticles is influenced by the concentration of a monomer, a cross-linking agent, and the temperature. For example, increasing the concentration of a monomer or the temperature results in increasing the MIP nanoparticle size, but, at the same time, polydispersity of a material is also increased [104]. To speed up obtaining MIP nanoparticles, one proposed a procedure including a distillation step at elevated temperature. However, the as-prepared material had reduced capacity for re-binding of the template molecules and, as a result, poorer selectivity [110].

In the seed polymerization process, monodisperse latex nanoparticles are often used as seeds. To stabilize the dispersion, various surfactants are introduced. Using polymerizable surfactants allows for creating molecular imprints in a thin layer near the surface of the polymer shell. Typically the resulting nanoparticles have sizes of 50–100 nm, and their yield is as high as 98–100 % in some cases [104].

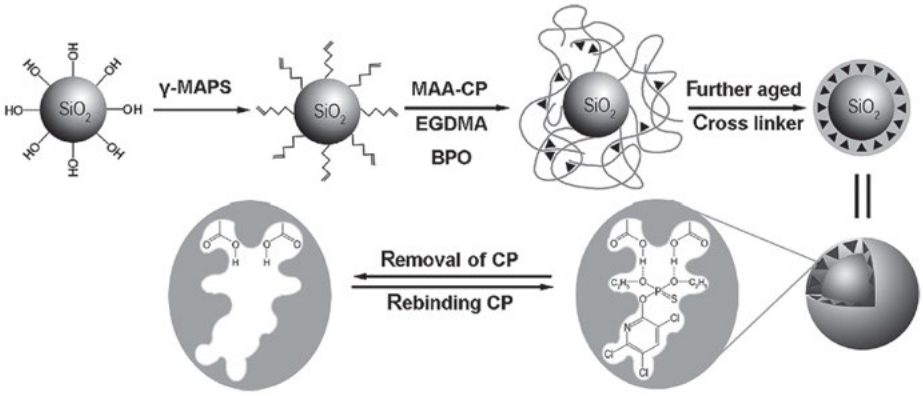


**Fig. 9.3:** The scheme of synthesis of silica nanoparticles grafted with MIP for chlorpyrifos (CP) [113]. γ-MAPS – γ-methacryloxypropyltrimethoxysilane, MAA – methacrylic acid, EGDMA – ethylene glycol dimethacrylate, BPO – benzoyl peroxide.

In the grafting approach, a layer of MIP is grafted onto the surface of nanoparticles of various materials such as magnetite [111, 112] and silica [113, 114]. The scheme of synthesis of silica nanoparticles grafted with MIP for chlorpyrifos is shown in Fig. 9.3 [113].

Silica nanoparticles with a diameter of 100–200 nm were used as a core. A layer of MIP of about 25 nm thick was formed on the surface. It was established that the density of unsaturated radicals grafting onto silica nanoparticle surface has great effect on thickness of the resulting layer. The prospects of this MIP used as a sorbent in SPE and HPLC were shown.

A similar approach was used in [114] for the synthesis of nanosized silica particles coated with an MIP layer for trinitrotoluene. It was established an important role of unsaturated radicals on the surface of the modified particles, for not only ensuring the polymerization process but also concerning a template transport through the polymer shell by formation of a charge-transfer complex.

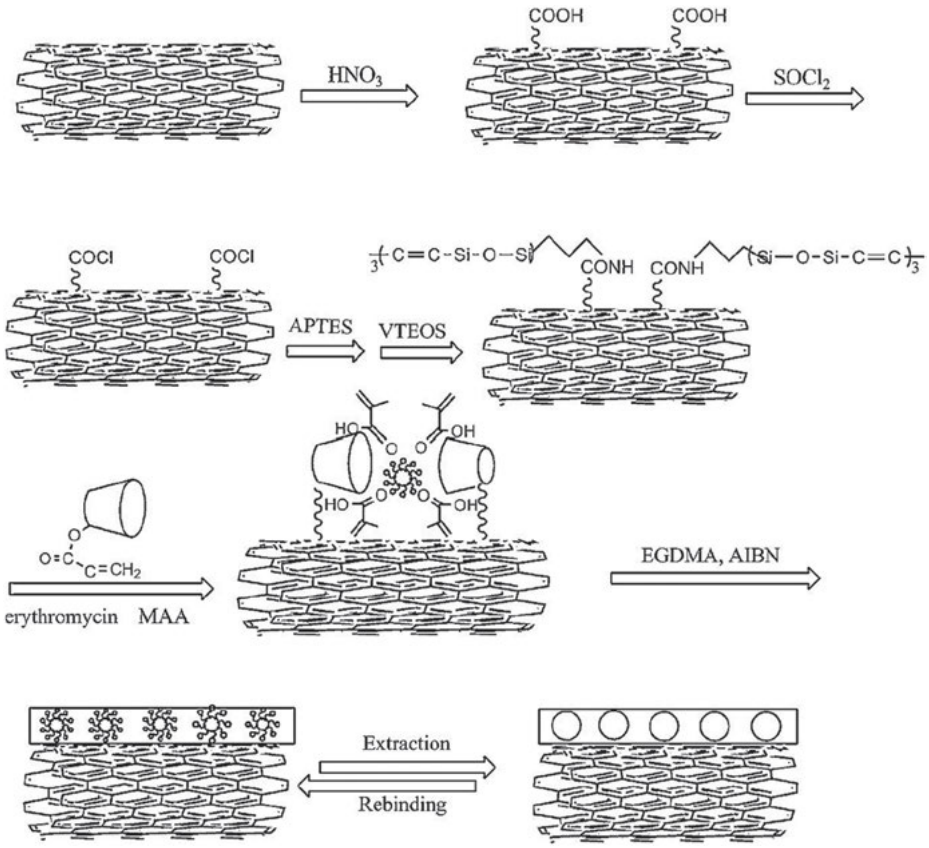


**Fig. 9.4:** Scheme for preparation of a composite material based on multiwalled carbon nanotubes and a polymer with imprints of erythromycin [116]. APTES – aminopropyltriethoxysilane, VTEOS – vinyltriethoxysilane, MAA – methacrylic acid, EGDMA – ethylene glycol dimethacrylate, AIBN – azobisisobutyronitrile.

Grafting was also used to obtain MIP layers on the surface of nanotubes [115–118]. Figure 9.4 shows a scheme for preparation of a composite material based on multiwalled carbon nanotubes with a diameter of 20–40 nm and a polymer with imprints of erythromycin [116]. Acryloyl-β-cyclodextrin and methacrylic acid were taken as the functional monomers. The carbon nanotubes were modified with carboxyl groups by treating them with nitric acid solution, then inoculated with vinyl groups, and introduced as one of the components of prepolymerization mixture. The resulting sorbent was utilized for selective extraction of erythromycin from chicken.

### 9.3.4 Other methods

Technological difficulties associated with the use of MIP particles (grinding, fractionation, centrifugation, etc.), which often lead to a significant loss of selective binding sites, can be avoided by carrying out MIP synthesis on the surface of various solid substrates (surface imprinting) [102, 119]. That is preparation of thin layers or films of MIPs on the surface of membranes, immunoassay plates, and electrodes. Synthesis of such composite materials is usually carried out by grafting. In the first step, the surface of a solid support is activated, and then immersed in a reaction mixture containing all components necessary for the MIP synthesis. After that photo- or electropolymerization is performed.

A method of *in situ* polymerization, as well as grafting of a thin MIP layer on commercially available membranes (polyethylene, nylon, and other filtration materials) was applied for preparation of porous MIP membranes, which were used in the solid-phase extraction [120–124].

Thin polymer layers on the surface of polystyrene immunoassay microtiter wells were prepared by grafting of poly-3-aminophenyl boronic acid with imprints of proper compounds [119].

Another method was also used for preparing composite materials based on silica fibers coated with MIPs for tetracycline and propranolol, which were applied for SPE of tetracyclines from egg samples [125], and β-blockers from urine and plasma [126]. Fiber surface was silylated, and then thermal polymerization was carried out at 60°C for 6 hours. It was shown that the thickness of the formed MIP coating and reproducibility of the synthesis depends on the polymerization time. Reducing the time resulted in poor reproducibility and thin films, whereas in the long-time synthesis, the fiber could not be separated from the solidified polymerization mixture. The required thickness of the homogeneous porous polymeric coating (about 20 μm) was achieved by re-polymerization on the fiber surface.

## 9.4 Sorption properties of MIPs and selectivity of processes with their participation

The most important expected property of MIPs is the ability of selective binding organic molecules, which is explained by the presence of highly specific binding sites in their composition. Difference in sorption properties of an MIP and a nonimprinted polymer (NIP), synthesized under the same conditions, but in the absence of a template, is known as "imprinting effect." To assess the imprinting effect and answer the question "What MIP is the best," different approaches have been proposed. They are based on comparison under the same conditions of chromatographic or sorption behavior of a template molecule and other tested compounds with regard to the MIP and NIP [127].

For evaluating imprinting effect in chromatographic systems, one employs the meaning of imprinting factor (IF), which is calculated as the ratio of the template retention factors on columns filled with MIP and NIP, respectively [36, 46, 58, 64, 65]. Evaluation of imprinting effect under the static equilibrium conditions is performed by comparing the extraction degrees or distribution coefficients of test compounds on MIP and NIP. This can also be done by comparing the imprinting factor values calculated as the ratio of the distribution coefficients on MIP and NIP [38, 39, 44, 50, 56]. To estimate the number of specific and nonspecific binding sites, the Scatchard method was utilized [40, 51], as well as a number of other methods, described in detail in a review [128].

Numerous studies have shown that for preparing MIPs with the high molecular recognition, it is necessary to choose properly the desired functional monomer–template combination. Among other parameters for varying MIP molecular recognition and selectivity, there are the monomer-to-template molar ratio in a reaction mixture, the nature of a solvent used both at the polymerization and at the sorption stages, and the method of polymerization [129, 130]. Below some examples are given.

A comparative analysis of the polymers synthesized from methacrylic acid, 2- and 4-vinylpyridine showed that the best ability to re-bind caffeine was achieved for the MIP based on methacrylic acid [131]. Conversely, in case of polymers molecularly imprinted with caffeic acid, the best results were obtained using 4-vinylpyridine [132]. In case of chloramphenicol, the best monomer appeared to be 2-vinylpyridine [133]. In our studies, by the example of MIP imprints of 4-hydroxybenzoic acid (4-HBA), synthesized using acrylamide (AA), 4-vinylpyridine and methacrylic acid, it was shown that 4-HBA was better recognized by AA-based polymers [38, 39]. Among the three functional monomers (methacrylic acid, 2-(dimethylamino)-ethyl methacrylate, and acrylamide) used in the preparation of MIPs with imprints of quercetin, the best one was acrylamide [52].

The important role of intermolecular hydrogen bonds between AA molecules and the hydroxybenzoic acids carboxyl is indicated by the data obtained in the study of sorption properties of MIPs with imprints of 4-hydroxybenzoic acid and

methylparaben [39]. The absence of a carboxyl in the molecule of methylparaben, which is 4-HBA ester, led to a polymer having inferior molecular recognition: IF values were decreased from 7.0 (for the MIP with imprints of 4-HBA) to 2.4 (for the MIP with imprints of methylparaben) (Tab. 9.1).

**Tab. 9.1:** Recovery efficiencies (*R*, %), distribution coefficients (*D*), and imprinting factors (IF) for 4-hydroxybenzoic acids and methylparaben regarding MIPs and NIPs for these compounds [39]

| Polymer | Template | *R*, % | *D* | IF |
|---|---|---|---|---|
| $MIP_1$ | 2-Hydroxybenzoic acid | 43 ± 2 | 219 | 2.5 |
| $NIP_1$ | – | 25 ± 1 | 86 | – |
| $MIP_2$ | 4-Hydroxybenzoic acid | 64 ± 1 | 444 | 7.1 |
| $NIP_2$ | – | 20 ± 1 | 63 | – |
| $MIP_3$ | 2,4-Dihydroxybenzoic acid | 30 ± 1 | 105 | 3.3 |
| $NIP_3$ | – | 11 ± 1 | 32 | – |
| $MIP_4$ | 3,4-Dihydroxybenzoic acid | 48 ± 1 | 221 | 7.9 |
| $NIP_4$ | – | 10 ± 1 | 28 | – |
| $MIP_5$ | Methylparaben | 41 ± 1 | 177 | 2.4 |
| $NIP_5$ | – | 22 ± 1 | 73 | – |

The important role of intermolecular hydrogen bonds in pre-polymerization complex formation was also noted in [81, 94, 134].

When choosing monomer–template couples, one should take into account not only the ability of both molecules to formation of intermolecular hydrogen bonds, but also the ability to form an intramolecular hydrogen bond in the template molecule. By the example of couples of MIPs with imprints of 2-/4-hydroxy- ($MIP_1$, $MIP_2$) and 2,4-/3,4-dihydroxybenzoic acids ($MIP_3$, $MIP_4$), we were able to trace an effect of the functional groups relative position on the MIP properties. It is well known that 2-hydroxy- and 2,4-dihydroxybenzoic acids can form an intramolecular hydrogen bond. This results in strong weakening intermolecular hydrogen bonding of these molecules with AA compared with the intermolecular hydrogen bonding of 4-hydroxy- and 3,4-dihydroxybenzoic acids with AA. Finally, it must lead to deterioration of the MIP molecular recognition. The experimental results confirmed that these polymers vary in their molecular recognition. IF varied from 7.0 ($MIP_2$) to 2.5 ($MIP_1$) and from 7.9 ($MIP_4$) to 3.3 ($MIP_3$) (Tab. 9.1).

To optimize monomer–template couples, a number of research studies systematized in reviews [135, 136] suggest applying a combinatorial approach and computational molecular modeling. According to the combinatorial approach, the optimum composition of components is selected based on simultaneous synthesis and testing from several dozen to several hundred of small batches of polymers (with the varied type of FM and the ratio of components in a reaction mixture) and creating corresponding databases.

The computational molecular modeling method is more effective. It allows for virtual implementation of a rapid search for a large number of potential functional monomers, significantly reduces the time to optimize composition of MIPs, and provides information on a possible structure of binding sites.

The combinatorial analysis of polymers synthesized from methacrylic acid, 2- and 4-vinylpyridine, and other six monomers showed that MIPs with methacrylic acid had the best ability to re-bind β-estradiol [137].

Based on a conjunction of the computational molecular modeling and the combinatorial analysis, for synthesis of MIPs with imprints of medicinal compounds, the best FMs, such as acrylamide (for methocarbamol), were chosen from 18 FM [138].

Another factor that plays a key role in the preparation of selective MIPs is the FM : template (T) ratio in a reaction mixture [2, 129]. In most of the published works, the optimal FM : T ratio is empirically found in studying the properties of several polymers prepared with adding different amounts of a template. According to the established ideas on formation of MIPs' binding sites, each individual binding site in a polymer is formed from each complex formed between a template and a functional monomer in the pre-polymerization solution. Depending on the number of functional groups capable of reacting with FM, one-, two- or multipoint binding is implemented in the template molecule during formation of such a complex. Highest affinity of the binding sites in the resulting polymer corresponds to the multiple interactions between template and functional monomer molecules. Inside the binding sites with the highest affinity for the template, there are several functional groups of the monomer that provide rebinding of the template. Increasing the number of interactions that occur with the template leads to greater "harmony" of the binding site, making it more selective.

According to Le Chatelier's principle, it can be expected that increasing the concentration of constituents of the complex in the prepolymerization mixture will increase the concentration of the pre-polymerization complex, and accordingly, the number of binding sites in the MIP. Despite the fact that increasing the concentration of the pre-polymerization complex can be achieved by increasing the amount of both components, one usually prefers to increase the amount of a template. This is due to the fact that a template does not take part in the polymerization reaction; hence, the amount of template can theoretically be increased until very high concentrations, while maintaining the optimal cross-linker–functional monomer ratio. In early studies, MIP synthesis had been carried out at the FM : T ratio of 0.25 : 1. However, it was subsequently shown that this ratio is not always optimal and can vary depending on the nature of compounds forming the pre-polymerization complex [43, 52, 132, 139–142]. By the example of couples of polymers based on acrylamide with imprints of barbital, sodium salt of 4-aminosalicylic acid, and 4-hydroxybenzoic acid as well as couples of polymers based on methacrylic acid with imprints of nicotinamide and histamine, it was found that the best recognition capabilities can be achieved by the polymers with the FM : T ratio of 1 : 1 (Fig. 9.5)

[139]. Just by changing the ratio of 2,4-D : AA in the reaction mixture from 1 : 0.25 to 1 : 1, the IF value for polymers based on AA with imprints of this compound varied from 2.9 to 34.5 [43].

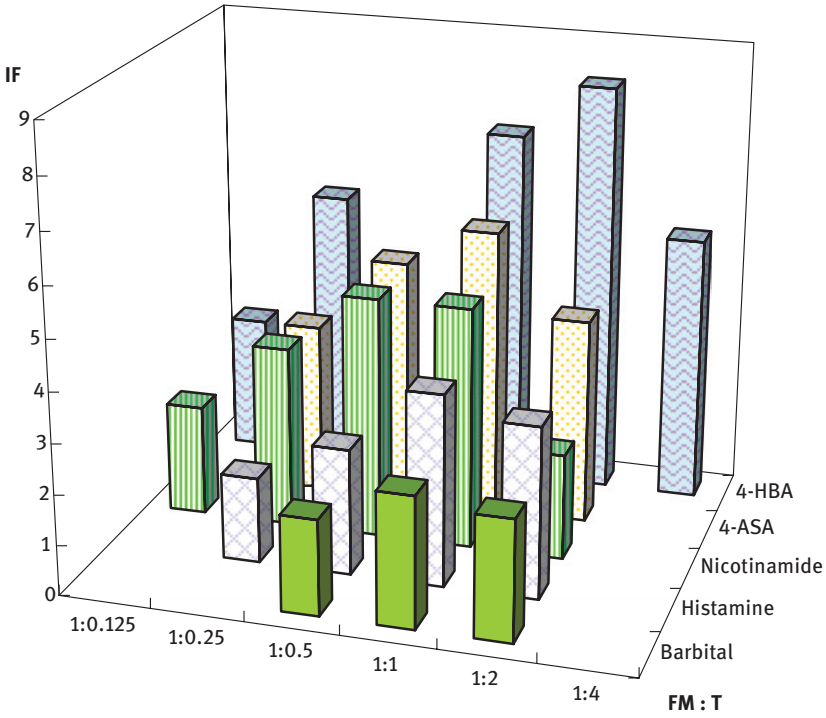


**Fig. 9.5:** The values of imprinting factor for 4-hydroxybenzoic acid, sodium salt of 4-aminosalicylic acid, and barbital (a), nicotinamide and histamine (b) on MIPs based on acrylamide (a) and methacrylic acid (b) depending on the FM : T ratio used at the synthesis [139].

Although there are hypotheses to explain formation of molecular recognition sites, the true mechanisms of formation of the binding site final structure are still unknown, because of difficulties in determining this structure during and after polymerization. Analysis of the published experimental data on the effect of the FM : T ratio allowed for the author of review [129] to suggest that the number of functional groups in an MIP-binding site does not directly depend on the composition of a prepolymerization complex and is largely determined by the polymerization process.

Selectivity and efficiency of MIPs depend on the nature of a solvent (porogen) used in their synthesis. When choosing a solvent, one primarily takes into account solubility of all components used in synthesis of polymers. Furthermore, the solvent plays an important role in formation of porous structure of MIPs, which are a subclass of macroporous polymers. Beginning of pores during polymerization is a result

of phase separation of a porogen and a polymer formed. When using porogens of low solvent power, phases are separated early, resulting in larger pore size and lower specific surface area. In contrast, when using porogens of higher solvent power, phases are separated later, resulting in materials with smaller pores and larger specific surface area. In most cases, the specific surface area of MIPs varies from 100 to 400 $m^2/g$, which conditioned by macro- (>25 nm), meso- (1–25 nm), and micro- (0.2–1 nm) pores [129]. For organic molecules, which usually have the van der Waals dimensions from 0.6 to 10 nm, the molecular recognition sites in macro- and mesopores appear to be more available.

Another important role of a solvent during MIP preparation is its influence on formation and stability of a pre-polymerization complex before, during, and after polymerization. In this respect, the most suitable solvents for molecular imprinting are those with the low dielectric constants. These solvents provide stronger monomer–template noncovalent interactions compared with polar solvents, which ultimately leads to polymers having better molecular recognition. The choice of a solvent is carried out empirically by comparing the sorption properties of MIPs synthesized in various solvents but at the same ratios of the components.

Comparing sorption properties of the methacrylic acid–based MIPs with imprints of citalopram proved that the polymer synthesized in chloroform has better recognition than those prepared in acetonitrile and THF [140]. On the contrary, caffeine is better recognized by the polymer synthesized in acetonitrile rather than chloroform [131]. Acetonitrile was the best solvent compared with toluene for synthesis of MIPs with imprints of ethylestradiol [54].

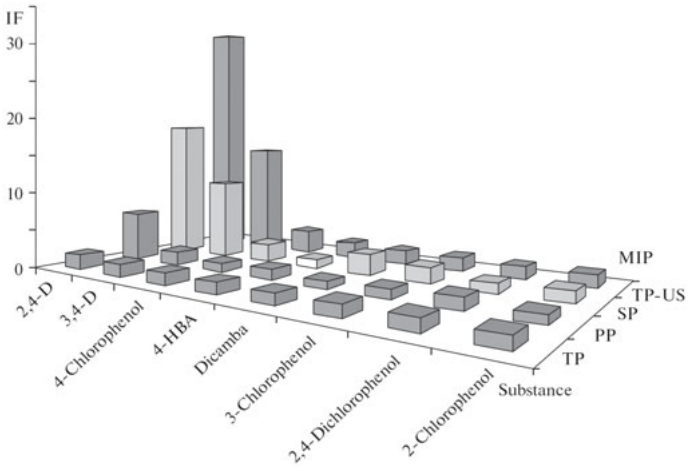


**Fig. 9.6:** The values of imprinting factors for various organic compounds on polymers with imprints of 2,4-D synthesized by thermal polymerization (TP), thermal polymerization with applying ultrasound (TP-US), photopolymerization (PP), and suspension polymerization (SP) [96].

However, in some cases, the use of traditional solvents for synthesis of MIPs is impossible due to the low solubility of templates. In this case, MIP synthesis is performed in more polar solvents: acetonitrile–methanol [142], dimethylsulfoxide (DMSO) [143, 144], and acetone [51, 52, 144].

To evaluate selectivity of MIPs, sorption by them of structurally related compounds is compared. As an example, Fig. 9.6 shows the data on evaluation of selectivity of MIPs based on acrylamide with imprints of 2,4-D, synthesized by different methods [96].

From comparison of the imprinting factors, one can see that all polymers with 2,4-D imprints better adsorb the compound which was used in their synthesis – 2,4-dichlorophenoxyacetic acid. The closest analogue – 3,4-dichlorophenoxy acetic acid is recognized a little bit worse, but other compounds are adsorbed on the MIP and the NIP nearly equally.

## 9.5 Application in the analysis of real samples

MIPs are often used as the selective sorbents in solid-phase extraction for purification and preconcentration of samples followed by determination of analytes by the conventional analytical methods [12, 14–16, 20, 28]. This combination was called molecular imprinting solid-phase extraction, MISPE.

The main prerequisites for the MIP application in SPE are high affinity and selectivity for components to be preconcentrated, in conjunction with high thermal, chemical, and mechanical resistance. Stability of MIPs in the presence of acids, bases, and organic solvents, unlike immunosorbents, allows for employing these materials in columns or cartridges, not only in offline, but also in online mode.

**Methods for implementation of SPE.** In most cases, SPE is carried out in offline mode using cartridges filled with a relatively small amount of an MIP (15–500 mg) [28, 35, 145]. SPE consists of several stages: activation and conditioning of the sorbent by washing it with a suitable solvent; passing of the sample; washing the cartridge to remove the remnant sample solution; and elution of target components. An important part of SPE optimization is a choice of solvent on each of these steps. The main function of the solvent used at the passing stage is to maximize the ability of an MIP to molecular recognition. When choosing a solvent at this stage, preference is given to solvents that were used in synthesis of an MIP, which imposes certain restrictions on sample pretreatment prior to the SPE.

Several methods for sample preparation prior to SPE on cartridges packed with MIPs have been described. The first one is based on extraction of analytes from a sample by a suitable organic solvent (chloroform, toluene, methanol, acetonitrile) followed by passing the resultant extract through a previously conditioned cartridge packed with MIP [45, 50, 146]. The second one involves successive use of two SPE cartridges [147–149]. At the first step, an analyzed microcomponent together with

impurities is isolated on a cartridge packed with "conventional" sorbent and then eluted with nonpolar organic solvent and passed through a column packed with MIP. In some cases, water samples prior to passing the cartridge are diluted with acetonitrile or methanol [89, 150, 151]. Moreover, a number of studies indicate that MIPs synthesized in acetonitrile or methanol medium can be used for extraction of target molecules from aqueous solutions [99, 152–157].

In "on-line" mode, preconcentration is performed on a small precolumn packed with ~50 mg of MIP, which often is placed in a liquid chromatograph injector loop [54, 71, 81, 83, 97, 99, 158–160]. The preconcentrated impurities are eluted with mobile phase and separated on a chromatographic column. The main problem encountered with this approach is connected with compatibility of the solvents for elution and chromatographic separation.

As it has been noted above, in recent years, MIPs are increasingly produced in the form of microsized spherical particles, which cannot always be packed in SPE cartridges. For such particles, a few new ways to implement MISPE have been proposed. The simplest one is based on carrying out sorption under static conditions: a weighed portion of MIP is placed into a polypropylene centrifuge tube, and all four conventional SPE operations are consistently carried out. Each of them is followed by the sorbent separation from the solution by centrifugation. This sample preparation method was used for selective isolation of testosterone and epitestosterone from male urine [160] and antihistamine loratadine from urine and plasma [161].

Among the other methods of MISPE, an interesting approach is based on the use of magnetic MIP particles [162]. $Fe_3O_4$ particles were treated with modifiers (ethylene glycol, polyvinyl alcohol, or oleic acid) and then dipped into a solution containing all components necessary for MIP synthesis, and then polymerization was performed. The composite materials based on $Fe_3O_4$ and MIP retain recognition of template molecules and can be easily separated from solution by applying magnetic field. They were used for selective isolation of melamine from milk [163], bisphenol A from water and milk [164, 165], triazines from foods [166], the drug tramadol [167], and catecholamines [168] from urine.

Another method of MIP-based solid-phase extraction, which is worth mentioning, is the stir bar sorptive extraction. In this method, glass magnetic stirrers coated with a thin layer of MIP are employed. The as-prepared sorption materials were used for selective extraction of $\beta_2$-agonists from pork, liver, and food [169]; 2-aminotiazolin-4-carboxylic acid – a marker of cyanide poisoning – from urine [170]; and sulfonamides from food [171].

An interesting system called "solvent extraction – molecularly imprinted solid-phase extraction (SE-MISPE)" has been proposed for selective extraction of theophylline from serum [172]. The principle is based on simultaneous extraction of the analyte from an aqueous solution in an organic solvent and re-extraction in the MIP solid phase. An apparatus for carrying out the extraction process consists of a microtube containing the MIP for theophylline, which is placed at its bottom. A small

volume of chloroform (this solvent was used in the MIP synthesis) and serum are introduced into the tube. During the extraction, theophylline is extracted into chloroform and then is sorbed onto MIP. After the extraction, the aqueous and the organic phases were removed and theophylline was desorbed using a polar solvent.

Industrial production of cartridges packed with MIPs has been mastered with a number of companies. Using the commercially available cartridges, one performed selective isolation of chloramphenicol from dairy products [173], plasma and urine [174], atrazine and its metabolites from urine [175], mycotoxin zearalenone from grains [176], and drugs from river water [177–179] (Tab. 9.2).

**Tab. 9.2:** Examples of commercially available cartridges packed with MIPs

| Cartridge | Producer | Isolated compounds | Sample | Ref. |
|---|---|---|---|---|
| MIP4SPE | MIP Technologies, Switzerland | Chloramphenicol | Dairy products | [173] |
| SupelMIP SPE chloramphenicol | MIP Technologies, Switzerland | Chloramphenicol | Urine, plasma | [174] |
| SupelIMIPTM SPE-Triazine 10 | Supelco (USA) | Atrazine and its metabolites | Urine | [175] |
| AFFINIMIPTM ZON MIP-SPE | POLYINTELL (France) | Mycotoxin zearalenone | Corn | [176] |
| MIP4SPETM – β-blockers | MIP Technologies, Switzerland | β-Blockers | River water | [177] |
| SupelMIP-NSAIDs | MIP Technologies, Switzerland | Nonsteroidal anti-inflammatory drugs, clofibric acid | River water | [178] |
| SupelMIPTM antidepressant | MIP Technologies, Switzerland | Antidepressants | River water | [179] |

According to the data represented in review [28], usually MIPs are used for preconcentration of various organic compounds from environmental objects (36 %) and body fluids (34 %), more rarely in the analysis of drugs and medicinal plants (15 %), food (12 %), and several other samples (3 %).

**Environmental samples.** The solid-phase extraction using cartridges packed with MIPs is used for selective extraction of a wide variety of toxicants from natural waters, such as 2,4-dichlorophenol [37], 2,4,6-trichlorophenol [36], Bisphenol A [70, 82, 164, 165], alkylmethylphosphonic acids [147], 2,4-dichlorophenoxyacetic acid (2,4-D) [155, 156], and some other compounds. Also, there is a growing interest in determination of pharmaceuticals in the environment.

These compounds and their metabolites, together with surfactants, hygiene agents, and other compounds related to the human daily life, enter the environmental water in a form of complex mixtures by different ways but primarily through city untreated or purified water. Table 9.3 shows the conditions for isolation of some drugs from river water.

**Tab. 9.3:** MIPs applied for isolation of drugs from river water and the conditions of SPE

| Analyte | MIP and its amount | Volume of analyzed solution, pH | Elution | Ref. |
|---|---|---|---|---|
| Diclofenac | Poly(2-vinylpyridine dimethacrylate), 100 mg | 200 mL, no pH adjustment | 3 mL of dichloromethane : acetonitrile (94 : 6 v/v) | [48] |
| Fluoroquinolone antibiotics | Poly(methacrylamide-ethyleneglycol dimethacrylate), 150 mg | 100 mL, pH 7.5 | 1 mL of methanol containing 1 % trifluoroacetic acid | [64] |
| Benzimidazoles | Poly(methacrylamide-ethyleneglycol dimethacrylate), 200 mg | 500 mL | 12 × 1 mL of methanol : acetic acid (50 : 50 v/v) | [84] |
| Antiepileptic drugs (cyclobarbital, phenobarbital, amobarbital, and phenytoin) | Poly(4-vinylpyridine-ethyleneglycol dimethacrylate) | 50 mL, no pH adjustment | 2 mM ammonia – acetate buffer : acetonitrile (60 : 40 v/v) | [97] |
| Carbamazepine | Copolymer of methacrylic acid and divinylbenzene, 200 mg | 100 mL, pH 11 | 5 mL of methanol | [157] |
| β-Blockers | Commercially available MIP4SPETM – β- blockers, 25 mg | 25 mL, pH ~7 | 2 × 1 mL of methanol containing 10 % acetic acid, 2 × 1 mL of methanol | [177] |

As it can be seen from the data shown in this table, MIPs are used for isolation of both individual compounds and groups of structurally related compounds. A recent paper [180] describes synthesis of an MIP with imprints of five drugs simultaneously: ibuprofen, naproxen, ketoprofen, diclofenac, and clofibric acid. This sorbent was used for simultaneous isolation of above compounds from lake and sewage water prior to their determination by HPLC–MS–MS.

The solid-phase extraction is often combined with subsequent determination of the isolated compounds by reversed-phase HPLC with UV or MS detection.

Use of MIPs for SPE in analysis of environmental waters allows for selective removing the target components as well as significant reducing the limit of detection (LOD). As an example, Tab. 9.4 summarizes the characteristics of methods for determination of 2,4-dichlorophenoxyacetic acid, 2,4-dichlorophenol, 2-chlorophenol, and dicamba by HPLC–UV with and without preconcentration on a microcolumn packed with, synthesized by us, acrylamide-based polymer with imprints of 2,4-D [156].

The same MIP was used for spectrophotometric determination of 2,4-D by reaction with chromotropic acid [155]. By applying the sorption preconcentration from 100 mL of a sample, the LOD of 2,4-D was reduced from 300 to 5 μg/L. The achieved LOD corresponds to 0.17 MPC for drinking water and 0.005 MPC for environmental water.

**Tab. 9.4:** Characteristics of methods for HPLC determination of 2,4-D, 2,4-dichlorophenol, 2-chlorophenol, and dicamba without (I) and with the preconcentration on a microcolumn packed with the acrylamide-based polymer with imprints of 2,4-D from 25 (II) and 100 (III) mL of aqueous solution The sorbent weight – 40 mg, eluent – 1 mL of methanol [156]

| Analyte | Linear range (μg/mL) | | | LOD (μg/mL) | | |
|---|---|---|---|---|---|---|
| | I | II | III | I | II | III |
| 2,4-D | 2–50 | 0.1–2 | 0.025–0.5 | 0.4 | 0.06 | 0.01 |
| 2,4-Dichlorophenol | 2–50 | 0.1–2 | 0.025–0.5 | 0.4 | 0.06 | 0.01 |
| 2-Chlorophenol | 2–50 | 0.1–2 | 0.025–0.5 | 0.4 | 0.10 | 0.02 |
| Dicamba | 1–50 | 0.1–2 | 0.025–0.5 | 0.2 | 0.08 | 0.01 |

LOD limit of detection.

Apart from environmental waters, MIPs are utilized for isolation of organic compounds from soil and silt [42, 45, 89, 90]. HPLC–UV analysis of nine samples of marine silt and soils from different regions of Spain has been carried out [90]. Sample preparation consisted of SPE on a cartridge packed with MIP for benzylparaben (200 mg). Most often the analyzed samples contained methyl paraben (1.6–11.5 ng/g), ethyl paraben (0.8–6.7 ng/g), and butyl paraben (0.7–2.8 ng/g).

**Biological samples.** A large number of research works are devoted to application of MIPs for selective isolation of drugs from various biological samples: urine [47, 49, 65, 85, 143, 157, 181–185], plasma [138, 143, 151, 158, 183, 186–188], serum [47, 150, 172, 185, 189], blood, saliva [188], and hair [190–193]. Using synthesized MIPs, fluoroquinolone antibiotics [65, 181], carbamazepine [85, 157], metoclopramide [47], chlorpromazine [49], sinomenin [73], methocarbamol [138], sitagliptin [143], lamotrigine [150], alfuzosin [151], bupivacaine and ropivacaine [158], theophylline [172], a marker of cancer – 1-methyladenosine [182], tramadol [183], methamphetamine and 3,4-methylenedioxymethamphetamine (ecstasy) [184], citalopram [185], β-estradiol, estrone, estriol [186], acetazolamide [187], methadone [188], methotrexate [189], benzodiazepine [190, 191], ketamine [192], and cocaine [192] were extracted from these biological samples.

Most of the works cited above employed SPE followed by the HPLC–UV determination. For example, according to [181] for extraction of nine fluoroquinolone antibiotics from urine, a water-compatible methacrylic acid–based MIP with imprints of ofloxacin was synthesized in water–methanol solution. The solid-phase extraction was carried out on a cartridge packed with 100 mg of the MIP from 10 mL of urine. The limits of detection were 0.036–0.10 μg/mL (HPLC–UV). An MIP with imprints of metoclopramide was applied for selective isolation of this drug from urine and serum ($R$,% = 90) followed by the HPLC–UV determination with detection limits of 1.2 and 3 μg/L [47]. It has been shown that application of an MIP with imprints of methocarbamol

allows extracting this compound from plasma more efficiently (91.8 %) compared with a C18 cartridge (59.0 %) [138].

**Food.** Compared with conventional sorbents, MIPs have proved more effective and selective sorbents for isolation and purification of different microcomponents from food: milk [59, 60, 71, 91, 163, 169, 171, 194–199], baby food [200], fish and seafood [40, 88, 146, 201], meat and meat products [88, 159, 202–204], fruits and vegetables [44, 86, 191, 205–207], tomato sauce [208, 209], animal feed, and grains [152, 176, 210–213].

MIPs have been used for extraction of albumin [59], penicillin [91], tetracycline [71, 88, 125, 195], fluoroquinolone [200], and cephalosporin [196] antibiotics, sulfonamides [159, 171, 197, 201], salbutamol [202], steroid hormones [198, 204], β-estradiol [199], melamine [60, 163, 194], colorants [40, 41, 146, 203, 208, 209], oleanolic acid [206], polyphenolic compounds [207], atrazine [86], fenitrothion [44, 205], sulfonylurea herbicides [152], mycotoxins [181, 201, 213], tilmicosin [211], and valnemulin [212] from these products. Let us consider some examples.

Using the precipitation polymerization method and tetracycline as a template, an MIP for selective extraction of tetracycline (IF = 7.0), chlortetracycline (IF = 7.4), doxycycline (IF = 7.7), and oxytetracycline (IF = 4.1) was synthesized [88]. By the example of seafood, honey, and egg analysis, it was demonstrated that the new sorbent extracts the tetracycline antibiotics from real samples more efficiently and selectively than the commercial cartridges C18 and Oasis HLB. The LODs were of 0.1–0.3 μg/kg (HPLC/MS).

The method for sample preparation prior to determination of the mycotoxin zearalenone in corn, based on extraction of the mycotoxin in aqueous acetonitrile solution (90:10) followed by purification of the extract on a commercial column AFFINIMIPTM ZON MIP–SPE packed with MIP has been proposed [176]. The determination was performed by HPLC with fluorescence detector. The authors note that the analytical characteristics of this column are not inferior to ZearalaTestTM column, packed with an immunoaffinity sorbent, but it is superior than the last one in cost and sustainability. To determine sulfonylurea herbicides in corn, a method was developed, based on a preliminary selective extraction of chlorsulfuron, monosulfuron, and thiophenesulfuron-methyl on a microcolumn packed with an MIP for chlorsulfuron and subsequent determination by HPLC–MS. The LODs were of 0.02, 0.75, and 1.45 μg/kg, respectively [152].

To control the content of the long-acting macrolide antibiotic tilmicosin (20-deoxy-20-(3,5-dimethylpiperidin-1-yl)desmycosin) in feed, a method was developed, which combines SPE using an MIP based on methacrylic acid with imprints of tylosin (structural analogue of tilmicosin) and HPLC determination. It has been shown that the cartridges packed with the synthesized MIP retain tilmicosin more efficiently than the C18 and Oasis HLBSPE cartridges. The LOD was 0.35 μg/g [211].

## 9.6 Conclusions

Publications in the field of molecular imprinting, whose number is increasing every year, suggest that the search for new MIPs is proceeding. This is mainly due to almost unlimited possibilities of varying the nature of the functional monomers, cross-linking agents and target template molecules, as well as the relative ease and cheapness of MIP preparation, which allows for synthesis of MIPs in scientific laboratories by researchers working in this field. Interest in MIPs is primarily owing to a rare combination of the unique properties of these materials. They are employed especially as the sorbents for SPE and HPLC, materials for membranes and sensors, a basis for artificial antibodies. Application of MIPs is not limited to research; they have already been implemented in the chemical, pharmaceutical, and biotechnology industries; they are trying to be used for water treatment [29, 214]. Several companies such as "MIP Technologies" (Sweden), "Semorex" (USA), and "POLYIntell" (France) produce and sell SPE cartridges packed with MIPs.

Despite the undoubted recent advances in molecular imprinting, there are still a number of unresolved problems. Today MIPs are usually prepared by a conventional approach – bulk thermal polymerization using commercially available functional monomers. Along with the specific binding sites, MIPs synthesized in this manner contain the nonspecific sites, the percentage of the latter being much higher, resulting in low capacity of the sorbent and high nonspecific binding. Moreover, MIPs synthesized by the "conventional" approach in nonpolar solvents have high hydrophobicity, which often makes them difficult to extract analytes from aqueous media. Besides the above-mentioned synthesis strategies, many more novel technologies have also been introduced for preparing attractive and competitive well-designed MIPs over the latest years [215].

Intensive research studies are being made for development of MIPs, which would be compatible with aqueous medium and have higher capacity and affinity. These studies aim at both development of new methods for MIP synthesis and search for new specially synthesized functional monomers "tuned" to the template molecule. In this connection, it is necessary to mention a few recent publications. Thus, in [216], by the example of a polymer with imprints of bisphenol A, a new method for synthesis of MIPs based on ring-opening metathesis polymerization has been developed. The method allows one to obtain MIPs under milder conditions and much faster. The polymerization was completed within 1 hour, whereas MIP preparation by bulk polymerization took 14–24 hours to get completed. The sorbent selectively and efficiently extracts bisphenol A from dilute aqueous solutions, urine, and milk without additional sample pretreatment and has high capacity. There is a publication [217], indicating the possibility of obtaining MIP by frontal polymerization reducing the synthesis time from 24 hours to 30 minutes. An ionic liquid vinyl-3-butylimidazolium chloride has been proposed as a new functional monomer for synthesis of an MIP with imprints of chlorsulfuron [218]. In comparison with MIP for this compound

synthesized before [152], the sorbent removes chlorsulfuron from water more efficiently (81–110 %) and faster (within 5 minutes), allowing one to implement a combination of SPE with HPLC in "online" mode. Good compatibility with aqueous medium is exhibited by MIPs synthesized by grafting with the use of silica micro- and nanoparticles [219–221] as the substrates as well as molecularly imprinted hydrogels [222]. An increasing number of works can be noted, in which the choice of components for MIP synthesis is not made empirically but utilizing different computer technologies. So the choice of components for synthesis of a water-compatible MIP with imprints of amidorone drug was performed by screening existing libraries of MIPs and NIPs [223, 224].

In the last years, great interest was paid to synthesis of MIPs with imprints of high-molecular compounds, with a molecular weight >1500 Da, such as proteins, enzymes, DNA, and cells. For the synthesis of macro-MIPs, many original approaches and techniques have been suggested. They are, in great detail, discussed in recent reviews [225, 226]. For example, for the selective binding lysozyme, one has synthesized an MIP consisting of two layers: an internal thermally sensitive layer imprinted with lysozyme and an outer layer of poly(N-isopropylacrylamide). At the temperature of 43°C, the polymer sorbs both lysozyme and other proteins, whereas at 38°C only lysozyme is essentially extracted. At 23°C, the sorption of both lysozyme and other proteins is impeded [227]. For the first time, an automated solid-phase synthesis of MIP nanoparticles with imprints of proteins was carried out [228].

Another modern trend in the field of molecular imprinting is synthesis and analytical application of new composite materials based on polymers imprinted with quantum dots [229–234]. They provide combination of high selectivity and sorption efficiency of MIPs with such properties of quantum dots as high luminescence intensity and possibility of varying position of the emission band in a wide range of wavelengths. It was used to create composite materials for selective determination of compounds based on the quantum dot fluorescence change (usually suppression) while binding an analyte. The polymers incorporating quantum dots were prepared by phase inversion of solutions of polyethylene–polyvinyl alcohol copolymer in the presence of target molecules of amylase, lipase, and lysozyme [229]. The fluorescence intensity of quantum dots at 655, 605, and 545 nm on rebinding these compounds depended on their concentration, which was the basis of determination of lysozyme in saliva samples. Synthesis of polymers with imprints of lysozyme and cytochrome was carried on the surface of denatured bovine serum albumin modified with CdTe quantum dots [230]. It was noted that bovine serum albumin serves not only as a modifier of quantum dot surface defects but also as an auxiliary monomer for creation of effective binding sites. By the example of lysozyme, the possibility of its determination with the detection limit of 6.8 nM was shown.

Evaluating the prospects of analytical applications of MIPs one can predict their increasingly intensive use not only as the selective sorbents in solid-phase extraction but also in creation of various types of sensors [25, 235–242].

## References


[1] Patek M, Drew M. Chemical synthesis in nanosized cavities. *Curr Opin Chem Biol* 2008, 12, 332–9.

[2] Chen L, Wang X, Lu W, et al. Molecular imprinting: perspectives and applications. *Chem Soc Rev* 2016, 45, 2137–211.

[3] Lisichkin GV, Krutyakov YuA. Molecularly imprinted materials: synthesis, properties, applications. *Russ Chem Rev* 2006, 75, 901–18.

[4] Dmitrienko SG, Irkha VV, Kuznetsova A Yu, Zolotov YuA. Use of molecular imprinted polymers for the separation and preconcentration of organic compounds. *J Anal Chem* 2004, 59, 808–17.

[5] Дмитриенко СГ. *Полимеры с молекулярными отпечатками. В: Золотов ЮА, Цизин ГИ, Дмитриенко СГ, Моросанова ЕИ. Сорбционное концентрирование микрокомпонентов из растворов*. Москва, Россия, Наука, 2007, 124 (Dmitrienko SG. Molecularly imprinted polymers. In: Zolotov YuA, Tsysin GI, Dmitrienko SG, Morosanova EI. Sorption Preconcentration of Microcomponents from Solutions. Moscow, Russia, Nauka, 2007, original source in Russian).

[6] Schirhagl R. Bioapplications for molecularly imprinted polymers. *Anal Chem* 2014, 86, 250–61.

[7] Wulff G, Sarhan A. The use of polymers with enzyme-analogous structures for the resolution of racemates. *Angew Chem Int Ed Engl* 1972, 11, 341–3.

[8] Arshady R, Mosbach K. Synthesis of substrate-selective polymers by host-guest polymerization. *Makromol Chem* 1981, 182, 687–92.

[9] Sellergren B. Direct drug determination by selective sample enrichment on an imprinted polymer. *Anal Chem* 1994, 66, 1578–82.

[10] Malitesta C, Mazzotta E, Picca RA, Poma A, Chianella I, Piletsky SA. MIP sensors – the electrochemical approach. *Anal Bioanal Chem* 2012, 402, 1827–46.

[11] Sellergren, B. ed. *Molecularly Imprinted Polymers. Vol. 23: Man-made Mimics of Antibodies and Their Applications in Analytical Chemistry*. Amsterdam, Netherlands, Elsevier, 2001.

[12] Wackerlig J, Schirhagl R. Applications of molecularly imprinted polymer nanoparticles and their advances toward industrial use: a review. *Anal Chem* 2016, 88, 250–61.

[13] Niu M, Pham-Huy C, He H. Core-shell nanoparticles coated with molecularly imprinted polymers: a review. *Microchim Acta* 2016, 183, 2677–26.

[14] Bui BTS, Haupt K. Molecularly imprinted polymers: synthetic receptors in bioanalysis. *Anal Bioanal Chem* 2010, 398, 2481–92.

[15] Martín-Esteban A. Molecularly-imprinted polymers as a versatile, highly selective tool in sample preparation. *Trends Anal Chem* 2013, 45, 169–81.

[16] Hu Y, Pan J, Zhang K, Lian H, Li G. Novel applications of molecularly-imprinted polymers in sample preparation. *Trends Anal Chem* 2013, 43, 37–52.

[17] Ndunda EN, Mizaikoff B. Molecularly imprinted polymers for the analysis and removal of polychlorinated aromatic compounds in the environment: a review. *Analyst* 2016, 141, 3141–56.

[18] Sarafraz-Yazdi A, Razavi N. Application of molecularly-imprinted polymers in solid-phase microextraction techniques. *Trends Anal Chem* 2015, 73, 81–90.

[19] Beltran A, Borrull F, Cormack PAG, Marce RM. Molecularly imprinted polymers: useful sorbents for selective extractions. *Trends Anal Chem* 2010, 29, 1363–75.

[20] Figueiredo L, Ernyn GL, Santos L, Alves A. Applications of molecularly imprinted polymers to the analysis and removal of personal care products: a review. *Talanta* 2016, 146, 754–65.

[21] Tiwari MP, Prasad A. Molecularly imprinted polymer based enantioselective sensing devices: a review. *Anal Chim Acta* 2015, 853, 1–18.

[22] Mu L-N, Wei Z-H, Liu Z-S. Current trends in the development of molecularly imprinted polymers in CEC. *Electrophoresis* 2015, 36, 764–72.

[23] Cheong WJ, Ali F, Choi JH, Lee JO, Sung KY. Recent applications of molecular imprinted polymers for enantio-selective recognition. *Talanta* 2013, 106, 45–59.
[24] Ермолаева ТН, Чернышова ВН, Чеснокова ЕВ, Бессонов ОИ. Пьезокварцевые сенсоры на основе полимеров с молекулярными отпечатками – формирование распознающего слоя на поверхности электрода сенсора. *Сорбц хроматогр процессы* 2015, 15, 151–67. (Ermolaeva TN, Chernyshova VN, Chesnokova EV, Bessonov OI. Piezoelectric sensors on the basis of molecularly imprinted polymers. Formation of the recognizing layers on surface of the sensors electrode. Sorbcionnye i Khromatograficheskie Processy 2015, 151–67, original source in Russian).
[25] Wackerlig J, Lieberzeit PA. Molecularly imprinted polymer nanoparticles in chemical sensing – synthesis, characterisation and application. *Sensors Actuat B* 2015, 207, 144–57.
[26] Dias ACB, Figueiredo EC, Grassi V, Zagatto EAG, Arruda MAZ. Molecularly imprinted polymer as a solid phase extractor in flow analysis. *Talanta* 2008, 76, 988–96.
[27] Caro E, Marce RM, Borrull F, Cormack PAG, Sherrington DC. Application of molecularly imprinted polymers to solid-phase extraction of compounds from environmental and biological samples. *Trends Anal Chem* 2006, 25, 143–54.
[28] He C, Long Y, Pan J, Li K, Liu F. Application of molecularly imprinted polymers to solid-phase extraction of analytes from real samples. *J Biochem Biophys Methods* 2007, 70, 133–50.
[29] Huang DL, Wang RZ, Liu YG, Zeng GM, Lai C, Xu P, et al. Application of molecularly imprinted polymers in waste water treatment: a review. *Environ Sci Pollut Res Int* 2015, 22, 963–77.
[30] Piletsky SA, Turner NW, Laitenberger P. Molecularly imprinted polymers in clinical diagnostics – Future potential and existing problems. *Med Eng Phys* 2006, 28, 971–7.
[31] Fernández-González A, Guardia L, Badía-Laíño R, Díaz-García ME. Mimicking molecular receptors for antibiotics – analytical implications. *Trends Anal Chem* 2006, 25, 949–57.
[32] Regal P, Díaz-Bao M, Barreiro R, Cepeda A, Fente C. Application of molecularly imprinted polymers in food analysis: clean-up and chromatographic improvements. *Cent Eur J Chem* 2012, 10, 766–84.
[33] Song X, Xu S, Chen L, Wei Y, Xiong H. Advances in molecularly imprinted polymers in food analysis. *J Appl Polym Sci* 2014, 131, 40766–84.
[34] Ashleya J, Shahbazia MA, Kanta K. Molecularly imprinted polymers for sample preparation and biosensing in food analysis: progress and perspectives. *Biosens Bioelectron* 2017, 91, 606–15.
[35] Jiang X, Jiang N, Zhang H, Liu M. Small organic molecular imprinted materials: their preparation and application. *Anal Bioanal Chem* 2007, 389, 355–68.
[36] Feng Q-Z, Zhao L-X, Yan W, Lin J-M, Zheng Z-X. Molecularly imprinted solid-phase extraction combined with high performance liquid chromatography for analysis of phenolic compounds from environmental water samples. *J Hazard Mater* 2009, 167, 282–8.
[37] Feng Q-Z, Zhao L-X, Yan W, Ji F, Wei Y-L, Lin J-M. Molecularly imprinted solid-phase extraction and flow-injection chemiluminescence for trace analysis of 2,4-dichlorophenol in water samples. *Anal Bioanal Chem* 2008, 391, 1073–9.
[38] Dmitrienko SG, Irkha VV, Duisebaeva TB, Mikhailik YuV, Zolotov YuA. Synthesis and study of the sorption properties of 4-hydroxybenzoic acid-imprinted polymers. *J Anal Chem* 2006, 61, 14–9.
[39] Dmitrienko SG, Irkha VV, Apyari VV, Klokova EV, Zolotov YuA. Recognition of hydroxybenzoic acids and their esters by molecularly imprinted polymers: a comparative study. *Mendeleev Commun* 2008, 18, 315–7.
[40] Li Y, Yang T, Qi X, Qiao Y, Deng A. Development of a group selective molecularly imprinted polymers based solid phase extraction of malachite green from fish water and fish feed samples. *Anal Chim Acta* 2008, 624, 317–25.
[41] Al-Degs YS, Abu-Surrah AS, Ibrahim KA. Preparation of highly selective solid-phase extractants for Cibacron reactive dyes using molecularly imprinted polymers. *Anal Bioanal Chem* 2009, 393, 1055–62.

[42] Tang J, Zhang M, Cheng G, Lu Y. Development and application of molecularly imprinted polymer as solid phase extraction of imidacloprid in environmental samples. *J Liq Chromatogr Relat Technol* 2009, 32, 59–71.
[43] Popov SA, Dmitrienko SG, Chumichkina YuA, Zolotov YuA. The sorption properties of polymers with molecular imprints of chlorine-containing pesticides. *Russ J Phys Chem A* 2009, 83, 552–7.
[44] Barros LA, Martins I, Rath S. A selective molecularly imprinted polymer-solid phase extraction for the determination of fenitrothion in tomatoes. *Anal Bioanal Chem* 2010, 397, 1355–61.
[45] Amalric L, Mouvet C, Pichon V, Bristeau S. Molecularly imprinted polymer applied to the determination of the residual mass of atrazine and metabolites within an agricultural catchment. *J Chromatogr A* 2008, 1206, 95–104.
[46] Yin J, Meng Z, Du M, Liu C, Song M, Wang H. Pseudo-template molecularly imprinted polymer for selective screening of trace β-lactam antibiotics in river and tap water. *J Chromatogr A* 2010, 1217, 5420–6.
[47] Javanbakht M, Shaabani N, Akbari-Adergani B. Novel molecularly imprinted polymers for the selective extraction and determination of metoclopramide in human serum and urine samples using high-performance liquid chromatography. *J Chromatogr B* 2009, 877, 2537–44.
[48] Sun Z, Schüssler W, Sengl M, Niessner R, Knopp D. Selective trace analysis of diclofenac in surface and wastewater samples using solid-phase extraction with a new molecularly imprinted polymer. *Anal Chim Acta* 2008, 620, 73–81.
[49] Song S, Shi X, Li R, Lin Z, Wu A, Zhang D. Extraction of chlorpromazine with a new molecularly imprinted polymer from pig urine. *Process Biochem* 2008, 43, 1209–14.
[50] Peng L, Wang Y, Zeng H, Yuan Y. Molecularly imprinted polymer for solid-phase extraction of rutin in complicated traditional Chinese medicines. *Analyst* 2011, 136, 756–63.
[51] Song X, Li J, Wang J, Chen L. Quercetin molecularly imprinted polymers: preparation, recognition characteristics and properties as sorbent for solid-phase extraction. *Talanta* 2009, 80, 694–702.
[52] Kudrinskaya VA, Dmitrienko SG, Zolotov YuA. Synthesis and study of sorption properties of molecularly imprinted polymers for quercetin. *Moscow Univ Chem Bull* 2009, 64, 124–9.
[53] Bui BS, Belmont AS, Witters H, Haupt K. Molecular recognition of endocrine disruptors by synthetic and natural 17β-estradiol receptors: a comparative study. *Anal Bioanal Chem* 2008, 390, 2081–8.
[54] Bravo JC, Garcinuño RM, Fernández P, Durand JS. Selective solid-phase extraction of ethynylestradiol from river water by molecularly imprinted polymer microcolumns. *Anal Bioanal Chem* 2009, 393, 1763–8.
[55] Zhu QH, Huang DD, Li L, Yin YG. Synthesis of molecularly imprinted polymers for the application of selective clean-up vinblastine from *Catharanthus roseus* extract. *Sci China Chem* 2010, 53, 2587–92.
[56] Lopez C, Claude B, Morin Ph, Max J-P, Pena R, Ribe J-P. Synthesis and study of a molecularly imprinted polymer for the specific extraction of indole alkaloids from *Catharanthus roseus* extracts. *Anal Chim Acta* 2011, 683, 198–205.
[57] Janiak DS, Kofinas P. Molecular imprinting of peptides and proteins in aqueous media. *Anal Bioanal Chem* 2007, 389, 399–404.
[58] Puoci F, Curcio M, Cirillo G, Iemma F, Spizzirri UG, Picci N. Molecularly imprinted solid-phase extraction for cholesterol determination in cheese products. *Food Chem* 2008, 106, 836–42.
[59] Soleimani M, Ghaderi S, Afshar M, Soleimani S. Synthesis of molecularly imprinted polymer as a sorbent for solid phase extraction of bovine albumin from whey, milk, urine and serum. *Microchem J* 2012, 100, 1–7.
[60] He L, Su Y, Zheng Y, et al. Novel cyromazine imprinted polymer applied to the solid-phase extraction of melamine from feed and milk samples. *J Chromatogr A* 2009, 1216, 6196–203.

[61] Feás X, Seijas J A, Vázquez-Tato MP, Regal P, Cepeda A, Fente C. Syntheses of molecularly imprinted polymers: molecular recognition of cyproheptadine using original print molecules and azatadine as dummy templates. *Anal Chim Acta* 2009, 631, 237–44.
[62] Gadzała-Kopciuch R, Cendrowski K, Cesarz A, Kiełbasa P, Buszewski B. Determination of zearalenone and its metabolites in endometrial cancer by coupled separation techniques. *Anal Bioanal Chem* 2011, 401, 2069–78.
[63] Vidal JC, Duato P, Bonel L, Castillo JR. Molecularly imprinted on-line solid-phase extraction coupled with fluorescence detection for the determination of ochratoxin A in wheat samples. *Anal Lett* 2012, 45, 51–62.
[64] Benito-Peña E, Urraca JL, Sellergren B, Moreno-Bondi MC. Solid-phase extraction of fluoroquinolones from aqueous samples using a water-compatible stoichiometrically imprinted polymer. *J Chromatogr A* 2008, 1208, 62–70.
[65] Benito-Peña E, Martins S, Orellana G, Moreno-Bondi MC. Water-compatible molecularly imprinted polymer for the selective recognition of fluoroquinolone antibiotics in biological samples. *Anal Bioanal Chem* 2009, 393, 235–45.
[66] Le Jeune J, Spivak DA. Analyte separation by OMNiMIPs imprinted with multiple templates. *Biosens Bioelectron* 2009, 25, 604–8.
[67] Karim K, Breton F, Rouillon R, et al. How to find effective functional monomers for effective molecularly imprinted polymers? *Adv Drug Deliver Rev* 2005, 57, 1795–808.
[68] Dźygiel P, O'Donnell E, Fraier D, Chassaing C, Cormack PAGE. Evaluation of water-compatible molecularly imprinted polymers as solid-phase extraction sorbents for the selective extraction of sildenafil and its desmethyl metabolite from plasma samples. *J Chromatogr B* 2007, 853, 346–53.
[69] Puoci F, Iemma F, Cirillo G, et al. New restricted access materials combined to molecularly imprinted polymers for selective recognition/release in water media. *Eur Polym J* 2009, 45, 1634–40.
[70] Baggiani C, Baravalle P, Giovannoli C, Anfossi L, Giraudi G. Molecularly imprinted polymer/cryogel composites for solid-phase extraction of bisphenol A from river water and wine. *Anal Bioanal Chem* 2010, 397, 815–22.
[71] Sun X, He X, Zhang Y, Chen L. Determination of tetracyclines in food samples by molecularly imprinted monolithic column coupling with high performance liquid chromatography. *Talanta* 2009, 79, 926–34.
[72] Zhang S-W, Xing J, Cai L-S, Wu CY. Molecularly imprinted monolith in-tube solid-phase microextraction coupled with HPLC/UV detection for determination of 8-hydroxy-2′-deoxyguanosine in urine. *Anal Bioanal Chem* 2009, 395, 479–87.
[73] Lin LQ, Zhang J, Fu Q, He LC, Li YC. Concentration and extraction of sinomenine from herb and plasma using a molecularly imprinted polymer as the stationary phase. *Anal Chim Acta* 2006, 561, 178–82.
[74] Liu X, Ouyang C, Zhao R, Shangguan D, Chen Y, Liu G. Monolithic molecularly imprinted polymer for sulfamethoxazole and molecular recognition properties in aqueous mobile phase. *Anal Chim Acta* 2006, 571, 235–41.
[75] Zheng C, Liu Z, Gao R, Zhang L, Zhang Y. Recognition of oxytocin by capillary electrochromatography with monolithic tetrapeptide-imprinted polymer used as the stationary phase. *Anal Bioanal Chem* 2007, 388, 1137–45.
[76] Oxelbark J, Legido-Quigley C, Aureliano CSA, et al. Chromatographic comparison of bupivacaine imprinted polymers prepared in crushed monolith, microsphere, silica-based composite and capillary monolith formats. *J Chromatogr A* 2007, 1160, 215–26.
[77] Cacho C, Schweitz L, Turiel E, Perez-Conde C. Molecularly imprinted capillary electrochromatography for selective determination of thiabendazole in citrus samples. *J Chromatogr A* 2008, 1179, 216–23.

[78] Haginaka J. Monodispersed, molecularly imprinted polymers as affinity-based chromatography media. *J Chromatogr B* 2008, 866, 3–13.
[79] Ye L, Mosbach K. Molecular imprinting: synthetic materials as substitutes for biological antibodies and receptors. *Chem Mater* 2008, 20, 859–68.
[80] Yoshimatsu K, Reimhult K, Krozer A, Mosbach K, Sode K, Ye L. Uniform molecularly imprinted microspheres and nanoparticles prepared by precipitation polymerization: the control of particle size suitable for different analytical applications. *Anal Chim Acta* 2007, 584, 112–21.
[81] Rodríguez E, Navarro-Villoslada F, Benito-Peña E, Marazuela MD, Moreno-Bondi MC. Multiresidue determination of ultratrace levels of fluoroquinolone antimicrobials in drinking and aquaculture water samples by automated online molecularly imprinted solid phase extraction and liquid chromatography. *Anal Chem* 2011, 83, 2046–55.
[82] Mei S, Wub D, Jiang M, et al. Determination of trace bisphenol A in complex samples using selective molecularly imprinted solid-phase extraction coupled with capillary electrophoresis. *Microchem J* 2011, 98, 150–5.
[83] Zamora O, Paniagua EE, Cacho C, Vera-Avila LE, Perez-Conde C. Determination of benzimidazole fungicides in water samples by on-line MISPE-HPLC. *Anal Bioanal Chem* 2009, 393, 1745–53.
[84] Cacho C, Turiel E, Perez-Conde C. Molecularly imprinted polymers: an analytical tool for the determination of benzimidazole compounds in water samples. *Talanta* 2009, 78, 1029–35.
[85] Beltran A, Marce RM, Cormack PAG, Borrull F. Synthesis by precipitation polymerisation of molecularly imprinted polymer microspheres for the selective extraction of carbamazepine and oxcarbazepine from human urine. *J Chromatogr A* 2009, 1216, 2248–53.
[86] Xu S, Li J, Chen L. Molecularly imprinted polymers by reversible addition-fragmentation chain transfer precipitation polymerization for preconcentration of atrazine in food matrices. *Talanta* 2011, 85, 282–9.
[87] Jing T, Gao X-D, Wang P, et al. Preparation of high selective molecularly imprinted polymers for tetracycline by precipitation polymerization. *Chinese Chem Lett* 2007, 18, 1535–8.
[88] Jing T, Gao X-D, Wang P, et al. Determination of trace tetracycline antibiotics in foodstuffs by liquid chromatography-tandem mass spectrometry coupled with selective molecular-imprinted solid-phase extraction. *Anal Bioanal Chem* 2009, 393, 2009–18.
[89] Turiel E, Martin-Esteban A, Tadeo JL. Molecular imprinting-based separation methods for selective analysis of fluoroquinolones in soils. *J Chromatogr A* 2007, 1172, 97–104.
[90] Núñez L, Turiel E, Martin-Esteban A, Tadeo JL. Molecularly imprinted polymer for the extraction of parabens from environmental solid samples prior to their determination by high performance liquid chromatography-ultraviolet detection. *Talanta* 2010, 80, 1782–8.
[91] Kempe H, Kempe M. Influence of salt ions on binding to molecularly imprinted polymers. *Anal Bioanal Chem* 2010, 396, 1599–606.
[92] Wang H, Yan H, Qiu M, Qiao J, Yang G. Determination of dicofol in aquatic products using molecularly imprinted solid-phase extraction coupled with GC-ECD detection. *Talanta* 2011, 85, 2100–5.
[93] Shi X, Wu A, Zheng S, Li R, Zhang D. Molecularly imprinted polymer microspheres for solid-phase extraction of chloramphenicol residues in foods. *J Chromatogr B* 2007, 850, 24–30.
[94] Yang T, Li Y-H, Wei S, Li Y, Deng A. Development of a selective molecularly imprinted polymer-based solid-phase extraction for indomethacin from water samples. *Anal Bioanal Chem* 2008, 391, 2905–14.
[95] Qu G, Wu A, Shi X, Niu Z, Xie W, Zhang D. Improvement on analyte extraction by molecularly imprinted polymer microspheres toward enrofloxacin. *Anal Lett* 2008, 41, 1443–58.
[96] Dmitrienko SG, Popov SA, Chumichkina YuA, Zolotov YuA. The sorption properties of polymers with molecular imprints of 2,4-dichlorophenoxyacetic acid synthesized by various methods. *Russ J Phys Chem A*, 2011, 85, 472–7.

[97] Hoshina K, Horiyama S, Matsunaga H, Haginaka J. Molecularly imprinted polymers for simultaneous determination of antiepileptics in river water samples by liquid chromatography-tandem mass spectrometry. *J Chromatogr A* 2009, 1216, 4957–62.
[98] Haginaka J, Tabo H, Ichitani M, Takihara T, Sugimoto A, Sambe H. Uniformly-sized, molecularly imprinted polymers for (–)-epigallocatechin gallate, -epicatechin gallate and -gallocatechin gallate by multi-step swelling and polymerization method. *J Chromatogr A* 2007, 1156, 45–50.
[99] Sambe H, Hoshina K, Haginaka J. Molecularly imprinted polymers for triazine herbicides prepared by multi-step swelling and polymerization method. Their application to the determination of methylthiotriazine herbicides in river water. *J Chromatogr A* 2007, 1152, 130–7.
[100] Liu X, Chen Z, Zhao R, Shangguan D, Liu G, Chen Y. Uniform-sized molecularly imprinted polymer for metsulfuron-methyl by one-step swelling and polymerization method. *Talanta* 2007, 71, 1205–10.
[101] Kubo T, Nomachi M, Nemoto K, et al. Chromatographic separation for domoic acid using a fragment imprinted polymer. *Anal Chim Acta* 2006, 577, 1–7.
[102] Tan CJ, Tong YW. Molecularly imprinted beads by surface imprinting. *Anal Bioanal Chem* 2007, 389, 355–68.
[103] Qin L, He X-W, Zhang W, Li W-Y, Zhang Y-K. Surface-modified polystyrene beads as photografting imprinted polymer matrix for chromatographic separation of proteins. *J Chromatogr A* 2009, 1216, 807–14.
[104] Poma A, Turner APF, Piletsky SA. Advances in the manufacture of MIP nanoparticles. *Trends Biotechnol* 2010, 28, 629–37.
[105] Luo W, Zhu L, Yu C, et al. Synthesis of surface molecularly imprinted silica micro-particles in aqueous solution and the usage for selective off-line solid-phase extraction of 2,4-dinitrophenol from water matrixes. *Anal Chim Acta* 2008, 618, 147–56.
[106] Liu H, Liu C, Yang X, Zeng S, Xiong Y, Xu W. Uniformly sized β-cyclodextrin molecularly imprinted microspheres prepared by a novel surface imprinting technique for ursolic acid. *Anal Chim Acta* 2008, 628, 87–94.
[107] Barahona F, Turiel E, Cormack PAG, Martin-Esteban A. Chromatographic performance of molecularly imprinted polymers: core-shell microspheres by precipitation polymerization and grafted MIP films via iniferter-modified silica beads. *J Polym Sci A: Polym Chem* 2010, 48, 1058–66.
[108] Tokonami S, Shiigi H, Nagaoka T. Review: micro- and nanosized molecularly imprinter polymers for high-throughput analytical applications. *Anal Chim Acta* 2009, 641, 7–13.
[109] Flavin K, Resmini M. Imprinted nanomaterials: a new class of synthetic receptors. *Anal Bioanal Chem* 2009, 393, 437–44.
[110] Yang K, Berg MM, Zhao C, Ye L. One-pot synthesis of hydrophilic molecularly imprinted nanoparticles. *Macromolecules* 2009, 42, 8739–46.
[111] Wang X, Wang L, He X, Zhang Y, Chen L. A molecularly imprinted polymer-coated nanocomposite of magnetic nanoparticles for estrone recognition. *Talanta* 2009, 78, 327–32.
[112] Li L, He X, Chen L, Zhang Y. Preparation of core-shell magnetic molecularly imprinted polymer nanoparticles for recognition of bovine hemoglobin. *Chem Asian J* 2009, 4, 286–93.
[113] Lu Q, Chen X, Nie L, et al. Tuning of the vinyl groups' spacing at surface of modified silica in preparation of high density imprinted layer-coated silica nanoparticles: a dispersive solid-phase extraction materials for chlorpyrifos. *Talanta* 2010, 81, 959–66.
[114] Gao D, Zhang Z, Wu M, Xie C, Guan G, Wang D. A surface functional monomer-directing strategy for highly dense imprinting of TNT at surface of silica nanoparticles. *J Am Chem Soc* 2007, 129, 7859–66.
[115] Dai H, Xiao D, He H, et al. Synthesis and analytical applications of molecularly imprinted polymers on the surface of carbon nanotubes: a review. *Microchim Acta* 2015, 282, 893–909.

[116] Zhang Z, Yang X, Zhang H, et al. Novel molecularly imprinted polymers based on multi-walled carbon nanotubes with binary functional monomer for the solid-phase extraction of erythromycin from chicken muscle. *J Chromatogr B* 2011, 879, 1617–24.
[117] Liu X, Zhang ZH, Zhang HB, Hu YF, Yang X, Nie LH. Solid phase extraction of ursolic acid using imprinted polymer modified multi-walled carbon nanotubes. *Chin J Anal Chem* 2011, 39, 839–45.
[118] Zhang H, Zhang Z, Hu Y, Yang X, Yao S. Synthesis of a novel composite imprinted material based on multiwalled carbon nanotubes as a selective melamine absorbent. *J Agric Food Chem* 2011, 59, 1063–71.
[119] Sergeyeva TA. Molecularly-imprinted polymers as synthetic mimics of bioreceptors. 2. Applications in modern biotechnology. *Biopolymer Cell* 2009, 25, 431–43.
[120] Boysen RI, Schwarz LJ, Nicolau DV, Hearn MTW. Molecularly imprinted polymer membranes and thin films for the separation and sensing of biomacromolecules. *J Sep Sci* 2017, 40, 314–35.
[121] Renkecz T, Ceolin G, Horváth V. Selective solid phase extraction of propranolol on multiwall membrane filter plates modified with molecularly imprinted polymer. *Analyst* 2011, 136, 2175–82.
[122] Sergeyeva TA, Gorbach LA, Slinchenko OA, et al. Towards development of colorimetric test-systems for phenols detection based on computationally-designed molecularly imprinted polymer membranes. *Mater Sci Eng* 2010, 30, 431–6.
[123] Sergeyeva TA, Gorbach LA, Piletska EV, et al. Colorimetric test-systems for creatinine detection based on composite molecularly imprinted polymer membranes. *Anal Chim Acta* 2013, 770, 161–8.
[124] Barahona F, Turiel E, Martin-Esteban A. Molecularly imprinted polymer grafted to porous polyethylene frits: a new selective solid-phase extraction format. *J Chromatogr A* 2011, 1218, 7065–70.
[125] Jing T, Niu J, Xia H, et al. Online coupling of molecularly imprinted solid-phase extraction to HPLC for determination of trace tetracycline antibiotic residues in egg samples. *J Sep Sci* 2011, 34, 1469–76.
[126] Hu X, Pan J, Hu Y, Li G. Preparation and evaluation of propranolol molecularly imprinted solid-phase microextraction fiber for trace analysis of β-blockers in urine and plasma samples. *J Chromatogr A* 2009, 1216, 190–7.
[127] Tóth B, Pap T, Horvath V, Horvai G. Which molecularly imprinted polymer is better? *Anal Chim Acta* 2007, 591, 17–21.
[128] García-Calzón JA, Díaz-García ME. Characterization of binding sites in molecularly imprinted polymers. *Sensors Actuat B* 2007, 123, 1180–94.
[129] Spivak DA. Optimization, evaluation, and characterization of molecularly imprinted polymers. *Adv Drug Deliver Rev* 2005, 57, 1779–94.
[130] Kunath S, Marchyk N, Haupt K, Feller KH. Multi-objective optimization and design of experiments as tools to tailor molecularly imprinted polymers specific for glucuronic acid. *Talanta* 2013, 105, 211–8.
[131] Farrington K, Magner E, Regan F. Predicting the performance of molecularly imprinted polymers: selective extraction of caffeine by molecularly imprinted solid phase extraction. *Anal Chim Acta* 2006, 566, 60–8.
[132] Michailof C, Manesiotis P, Panayiotou C. Synthesis of caffeic acid and p-hydroxybenzoic acid molecularly imprinted polymers and their application for the selective extraction of polyphenols from olive mill waste waters. *J Chromatogr A* 2008, 1182, 25–33.
[133] Schirmer C, Meisel H. Molecularly imprinted polymers for the selective solid-phase extraction of chloramphenicol. *Anal Bioanal Chem* 2008, 392, 223–9.

[134] Byun H-S, Youn Y-N, Yun Y-H, Yoon S-D. Selective separation of aspirin using molecularly imprinted polymers. *Sep Purif Technol* 2010, 74, 144–53.
[135] Nicholls IA, Andersson HS, Golker K, et al. Rational design of biomimetic molecularly imprinted materials: theoretical and computational strategies for guiding nanoscale structured polymer development. *Anal Bioanal Chem* 2011, 400, 1771–86.
[136] Curk T, Dobnikar J, Frenkel D. Rational design of molecularly imprinted polymers. *Soft Matter* 2016, 12, 35–44.
[137] Wei S, Jakusch M, Mizaikoff B. Investigating the mechanisms of 17β-estradiol imprinting by computational prediction and spectroscopic analysis. *Anal Bioanal Chem* 2007, 389, 423–31.
[138] Gholivand MB, Khodadadian M. Rationally designed molecularly imprinted polymers for selective extraction of methocarbamol from human plasma. *Talanta* 2011, 85, 1680–8.
[139] Dmitrienko SG, Irkha VV, Mikhailik YuV, Klokova EV. Influence of the functional monomer/template ratio in the prepolymerization mixture on the sorption properties of molecularly imprinted polymers of organic compounds. *Moscow Univ Chem Bull* 2006, 61, 54–61.
[140] Abdouss M, Asadi E, Azodi-Deilami S, Beik-Mohammadi N, Aslanzadeh SA. Development and characterization of molecularly imprinted polymers for controlled release of citalopram. *J Mater Sci: Mater Med* 2011, 22, 2273–81.
[141] Yang Y, Li J, Liu Y, Zhang J, Li B, Cai X. Optimization of polymerization parameters for the sorption of oseltamivir onto molecularly imprinted polymers. *Anal Bioanal Chem* 2011, 400, 3665–74.
[142] Song S, Wu A, Shi X, Li R, Lin Z, Zhang D. Development and application of molecularly imprinted polymers as solid-phase sorbents for erythromycin extraction. *Anal Bioanal Chem* 2008, 390, 2141–50.
[143] Rao RN, Maurya PK, Khalid S. Development of a molecularly imprinted polymer for selective extraction followed by liquid chromatographic determination of sitagliptin in rat plasma and urine. *Talanta* 2011, 85, 950–7.
[144] Кудринская ВА, Дмитриенко СГ. Влияние растворителя на сорбционные свойства полимеров с молекулярными отпечатками кверцетина. *Сорбц хроматогр процессы* 2009, 9, 824–9 (Kudrinskaya VA, Dmitrienko SG. Effect of a solvent on sorption properties of polymers with molecular imprints of quercetin. Sorbcionnye i Khromatograficheskie Processy 2009, 9, 824–9, original source in Russian).
[145] Pardo A, Mespouille L, Dubois P, Duez P, Blankert B. Targeted extraction of active compounds from natural products by molecularly imprinted polymers. *Cent Eur J Chem* 2012, 10, 751–65.
[146] Guo Z, Gai P, Hao T, Duan J, Wang S. Determination of malachite green residues in fish using a highly sensitive electrochemiluminescence method combined with molecularly imprinted solid phase extraction. *J Agric Food Chem* 2011, 59, 5257–62.
[147] Le Moullec S, Truong L, Montauban C, Begos A, Pichon V, Bellier B. Extraction of alkyl methylphosphonic acids from aqueous samples using a conventional polymeric solid-phase extraction sorbent and a molecularly imprinted polymer. *J Chromatogr A* 2007, 1139, 171–7.
[148] Figueiredo EC, Tarley CRT, Kubota LT, Rath S, Arruda MAZ. On-line molecularly imprinted solid phase extraction for the selective spectrophotometric determination of catechol. *Microchem J* 2007, 85, 290–6.
[149] Claude B, Morin P, Bayoudh S, Ceaurriz J. Interest of molecularly imprinted polymers in the fight against doping extraction of tamoxifen and its main metabolite from urine followed by high-performance liquid chromatography with UV detection. *J Chromatogr A* 2008, 1196–1197, 81–8.
[150] Mohajeri SA, Ebrahimi SA. Preparation and characterization of a lamotrigine imprinted polymer and its application for drug assay in human serum. *J Sep Sci* 2008, 31, 3595–602.

[151] Hugon-Chapuis F, Mullot JU, Tuffal G, Hennion M-C, Pichon V. Selective and automated sample pretreatment by molecularly imprinted polymer for the analysis of the basic drug alfuzosin from plasma. *J Chromatogr A* 2008, 1196–1197, 73–80.
[152] She X, Cao WQ, Shi XM, et al. Class-specific molecularly imprinted polymers for the selective extraction and determination of sulfonylurea herbicides in maize samples by high-performance liquid chromatography – tandem mass spectrometry. *J Chromatogr B* 2010, 878, 2047–53.
[153] Jégourel D, Delépée R, Breton F, Rolland A, Vidal R, Agrofoglio LA. Molecularly imprinted polymer of 5-methyluridine for solid-phase extraction of pyrimidine nucleoside cancer markers in urine. *Bioorg Med Chem* 2008, 16, 8932–9.
[154] Le Noir M, Plieva F, Hey T, Guieysse B, Mattiasson B. Macroporous molecularly imprinted polymer/cryogel composite systems for the removal of endocrine disrupting trace contaminants. *J Chromatogr A* 2007, 1154, 158–64.
[155] Попов СА, Дмитриенко СГ, Золотов ЮА. Спектрофотометрическое определение 2,4-дихлорфеноксиуксусной кислоты после сорбционного концентрирования на полимере с молекулярными отпечатками. *Заводск лабор* 2009, 75, 11–3 (Popov SA, Dmitrienko SG, Zolotov YuA. Spectrophotometric determination of 2,4-dichlorophenoxyacetic acid after sorption preconcentration on a molecularly imprinted polymer. Zavodskaya Laboratoriya 2009, 75, 11–3, original source in Russian).
[156] Popov SA, Chumichkina YuA, Shapovalova EN, Dmitrienko SG, Zolotov YuA. Preconcentration of 2,4-dichlorophenoxyacetic acid on molecularly imprinted polymers and its subsequent determination by high performance liquid chromatography. *J Anal Chem* 2011, 66, 6–10.
[157] Beltran A, Caro E, Marce RM, Cormack PAG, Sherrington DC, Borrull F. Synthesis and application of a carbamazepine-imprinted polymer for solid-phase extraction from urine and wastewater. *Anal Chim Acta* 2007, 597, 6–11.
[158] Cobb Z, Sellergren B, Andersson LI. Water-compatible molecularly imprinted polymers for efficient direct injection on-line solid-phase extraction of ropivacaine and bupivacaine from human plasma. *Analyst* 2007, 132, 1262–71.
[159] He J, Wang S, Fang G, Zhu H, Zhang Y. Molecularly imprinted polymer online solid-phase extraction coupled with high-performance liquid chromatography – UV for the determination of three sulfonamides in pork and chicken. *J Agric Food Chem* 2008, 56, 2919–25.
[160] Tse Sum Bui B, Merlier F, Haupt K. Toward the use of a molecularly imprinted polymer in doping analysis: selective preconcentration and analysis of testosterone and epitestosterone in human urine. *Anal Chem* 2010, 82, 4420–7.
[161] Ebrahimzadeh H, Molaei KK, Asgharinezhad AA, Shekari N, Dehghani Z. Molecularly imprinted nanoparticles combined with miniaturized homogenous liquid – liquid extraction for the selective extraction of loratadine in plasma and urine samples followed by high performance liquid chromatography-photo diode array detection. *Anal Chim Acta* 2013, 767, 155–62.
[162] Chen L, Li B. Application of magnetic molecularly imprinted polymers in analytical chemistry. *Anal Methods* 2012, 4, 2613–21.
[163] He D, Zhang X, Gao B, et al. Preparation of magnetic molecularly imprinted polymer for the extraction of melamine from milk followed by liquid chromatography-tandem mass spectrometry. *Food Control* 2014, 36, 36–41.
[164] Lin Z, Cheng W, Li Y, Liu Z, Chen X, Huang C. A novel superparamagnetic surface molecularly imprinted nanoparticle adopting dummy template: an efficient solid-phase extraction adsorbent for bisphenol A. *Anal Chim Acta* 2012, 720, 71–76.
[165] Hiratsuka Y, Funaya N, Matsunaga H, Haginaka J. Preparation of magnetic molecularly imprinted polymers for bisphenol A and its analogues and their application to the assay of bisphenol A in river water. *J Pharm Biomed Anal* 2013, 75, 180–5.

[166] Wang A, Lu H, Xu S. Preparation of magnetic hollow MIPs for detection of triazines in food samples. *J Agric Food Chem* 2016, 64, 5110–6.
[167] Madrakian T, Afkhami A, Mahmood-Kashani H, Ahmadi M. Superparamagnetic surface molecularly imprinted nanoparticles for sensitive solid-phase extraction of tramadol from urine samples. *Talanta* 2013, 105, 255–61.
[168] Bouri M, Lerma-García M J, Salghi R, Zougagh M, Ríos A. Selective extraction and determination of catecholamines in urine samples by using a dopamine magnetic molecularly imprinted polymer and capillary electrophoresis. *Talanta* 2012, 99, 897–903.
[169] Xu Z, Hu Y, Hu Y, Li G. Investigation of ractopamine molecularly imprinted stir bar sorptive extraction and its application for trace analysis of $\beta_2$-agonists in complex samples. *J Chromatogr A* 2010, 1217, 3612–8.
[170] Jackson R, Petrikovics I, Lai EPC, Yu JCC. Molecularly imprinted polymer stir bar sorption extraction and electrospray ionization tandem mass spectrometry for determination of 2-aminothiazoline-4-carboxylic acid as a marker for cyanide exposure in forensic urine analysis. *Anal Methods* 2010, 2, 552–7.
[171] Xu Z, Song C, Hu Y, Li G. Molecularly imprinted stir bar sorptive extraction coupled with high performance liquid chromatography for trace analysis of sulfa drugs in complex samples. *Talanta* 2011, 85, 97–103.
[172] Khorrami AR, Rashidpur A. Design of a new cartridge for selective solid phase extraction using molecularly imprinted polymers: selective extraction of theophylline from human serum samples. *Biosens Bioelectron* 2009, 25, 647–51.
[173] Mohamed R, Richoz-Payot J, Gremaud E, et al. Advantages of molecularly imprinted polymers LC-ESI-MS/MS for the selective extraction and quantification of chloramphenicol in milk-based matrixes comparison with a classical sample preparation. *Anal Chem* 2007, 79, 9557–65.
[174] Boyd B, Bjork H, Billing J, et al. Development of an improved method for trace analysis of chloramphenicol using molecularly imprinted polymers. *J Chromatogr A* 2007, 1174, 63–74.
[175] Lara FJ, Lynen F, Sandra P, García-Campană AM, Ales-Barrero F. Evaluation of a molecularly imprinted polymer as in-line concentrator in capillary electrophoresis. *Electrophoresis* 2008, 29, 3834–41.
[176] Lucci P, Derrien D, Alix F, Perollier C, Bayoudh S. Molecularly imprinted polymer solid-phase extraction for detection of zearalenone in cereal sample extracts. *Anal Chim Acta* 2010, 672, 15–1.
[177] Gros M, Pizzolato T-M, Petrovic M, Jose Lopez de Alda M, Barcelo D. Trace level determination of β-blockers in waste waters by highly selective molecularly imprinted polymers extraction followed by liquid chromatography-quadrupole-linear ion trap mass spectrometry. *J Chromatogr A* 2008, 1189, 374–84.
[178] Zorita S, Boyd B, Jonsson S, et al. Selective determination of acidic pharmaceuticals in wastewater using molecularly imprinted solid-phase extraction. *Anal Chim Acta* 2008, 626, 147–54.
[179] Demeestere K, Petrovic M, Gros M, Dewulf J, Van Langenhove H, Barcelo D. Trace analysis of antidepressants in environmental waters by molecularly imprinted polymer-based solid-phase extraction followed by ultra-performance liquid chromatography coupled to triple quadrupole mass spectrometry. *Anal Bioanal Chem* 2010, 396, 825–37.
[180] Duan YP, Dai CM, Zhang YL, Chen L. Selective trace enrichment of acidic pharmaceuticals in real water and sediment samples based on solid-phase extraction using multi-templates molecularly imprinted polymers. *Anal Chim Acta* 2013, 758, 93–100.
[181] Sun H-W, Qiao F-X. Recognition mechanism of water-compatible molecularly imprinted solid-phase extraction and determination of nine quinolones in urine by high performance liquid chromatography. *J Chromatogr A* 2008, 1212, 1–9.

[182] Scorrano S, Longo L, Vasapollo G. Molecularly imprinted polymers for solid-phase extraction of 1-methyladenosine from human urine. *Anal Chim Acta* 2010, 659, 167–71.
[183] Javanbakht M, Attaran AM, Namjumanesh MH, Esfandyari-Manesh M, Akbari-Adergani B. Solid-phase extraction of tramadol from plasma and urine samples using a novel water-compatible molecularly imprinted polymer. *J Chromatogr B* 2010, 878, 1700–6.
[184] Djozan D, Farajzadeh M A, Sorouraddin SM, Baheri T. Molecularly imprinted-solid phase extraction combined with simultaneous derivatization and dispersive liquid-liquid microextraction for selective extraction and preconcentration of methamphetamine and ecstasy from urine samples followed by gas chromatography. *J Chromatogr A* 2012, 1248, 24–31.
[185] Abdouss M, Azodi-Deilami S, Asadi E, Shariatinia Z. Synthesis of molecularly imprinted polymer as a sorbent for solid phase extraction of citalopram from human serum and urine. *J Mater Sci Mater Med* 2012, 23, 1543–52.
[186] Buszewski B, Ričanyová J, Gadzała-Kopciuch R, Szumski M. Supramolecular recognition of estrogens via molecularly imprinted polymers. *Anal Bioanal Chem* 2010, 397, 2977–86.
[187] Khodadadian M, Ahmadi F. Computer-assisted design and synthesis of molecularly imprinted polymers for selective extraction of acetazolamide from human plasma prior to its voltammetric determination. *Talanta* 2010, 81, 1446–53.
[188] Ahmadi F, Rezaei H, Tahvilian R. Computational-aided design of molecularly imprinted polymer for selective extraction of methadone from plasma and saliva and determination by gas chromatography. *J Chromatogr A* 2012, 1270, 9–19.
[189] Liu X, Liu J, Huang Y, Zhao R, Liu G, Chen Y. Determination of methotrexate in human serum by high-performance liquid chromatography combined with pseudo template molecularly imprinted polymer. *J Chromatogr A* 2009, 1216, 7533–8.
[190] Anderson RA, Ariffin MM, Cormack PAG, Miller EI. Comparison of molecularly imprinted solid-phase extraction (MISPE) with classical solid-phase extraction (SPE) for the detection of benzodiazepines in post-mortem hair samples. *Forensic Sci Int* 2008, 174, 40–6.
[191] Ariffin MM, Miller EI, Cormack PAG, Anderson RA. Molecularly imprinted solid-phase extraction of diazepam and its metabolites from hair samples. *Anal Chem* 2007, 79, 256–62.
[192] Harun N, Anderson RA, Cormack PAG. Analysis of ketamine and norketamine in hair samples using molecularly imprinted solid-phase extraction (MISPE) and liquid chromatography-tandem mass spectrometry (LC-MS/MS). *Anal Bioanal Chem* 2010, 396, 2449–59.
[193] Thibert V, Legeay P, Chapuis-Hugon F, Pichon V. Synthesis and characterization of molecularly imprinted polymers for the selective extraction of cocaine and its metabolite benzoylecgonine from hair extract before LC – MS analysis. *Talanta* 2012, 88, 412–9.
[194] Hu Y, Feng S, Gao F, Li-Chan ECY, Grant E, Lu X. Detection of melamine in milk using molecularly imprinted polymers – surface enhanced Raman spectroscopy. *Food Chem* 2015, 176, 123–9.
[195] Lv YK, Wang LM, Yang L, Zhao CX, Sun HW. Synthesis and application of molecularly imprinted poly(methacrylic acid)–silica hybrid composite material for selective solid-phase extraction and high-performance liquid chromatography determination of oxytetracycline residues in milk. *J Chromatogr A* 2012, 1227, 48–53.
[196] Quesada-Molina C, Claude B, Garcia-Campana AM, Olmo-Iruela M, Morin P. Convenient solid phase extraction of cephalosporins in milk using a molecularly imprinted polymer. *Food Chem* 2012, 135, 775–9.
[197] Chen C, Zhang X, Long Z, Zhang J, Zheng C. Molecularly imprinted dispersive solid-phase microextraction for determination of sulfamethazine by capillary electrophoresis. *Microchim Acta* 2012, 178, 293–9.
[198] Díaz-Bao M, Barreiro R, Regal P, Cepeda A, Fente C. Evaluation of molecularly imprinted polymers for the simultaneous SPE of six corticosteroids in milk. *Chromatographia* 2012, 75, 223–31.

[199] Gañán J, Gallego-Picó A, Garcinuño RM, et al. Development of a molecularly imprinted polymer-matrix solid-phase dispersion method for selective determination of β-estradiol as anabolic growth promoter in goat milk. *Anal Bioanal Chem* 2012, 403, 3025–9.
[200] Díaz-Alvarez M, Turiel E, Martín-Esteban A. Selective sample preparation for the analysis of (fluoro) quinolones in baby food: molecularly imprinted polymers versus anion-exchange resins. *Anal Bioanal Chem* 2009, 393, 899–905.
[201] Shi X, Meng Y, Liu J, et al. Group-selective molecularly imprinted polymer solid-phase extraction for the simultaneous determination of six sulfonamides in aquaculture products. *J Chromatogr B* 2011, 879, 1071–6.
[202] Yan H, Wang R, Han Y, Liu S. Screening, recognition and quantitation of salbutamol residues in ham sausages by molecularly imprinted solid phase extraction coupled with high-performance liquid chromatography – ultraviolet detection. *J Chromatogr B* 2012, 900, 18–23.
[203] Yan H, Qiao J, Pei Y, Long T, Ding W, Xie K. Molecularly imprinted solid-phase extraction coupled to liquid chromatography for determination of Sudan dyes in preserved beancurds. *Food Chem* 2012, 132, 649–54.
[204] Douéa M, Bichona E, Dervilly-Pinela G, et al. Molecularly imprinted polymer applied to the selective isolation of urinary steroid hormones: an efficient tool in the control of natural steroid hormones abuse in cattle. *J Chromatogr A* 2012, 1270, 51–61.
[205] Pereira LA, Rath S. Molecularly imprinted solid-phase extraction for the determination of fenitrothion in tomatoes. *Anal Bioanal Chem* 2009, 393, 1063–72.
[206] Chena X, Zhanga Z, Yang X, et al. Molecularly imprinted polymers based on multi-walled carbon nanotubes for selective solid-phase extraction of oleanolic acid from the roots of kiwi fruit samples. *Talanta* 2012, 99, 959–65.
[207] Euterpio MA, Pagano I, Piccinelli AL, Rastrelli L, Crescenzi C. Development and validation of a method for the determination of (E)-resveratrol and related phenolic compounds in beverages using molecularly imprinted solid phase extraction. *J Agric Food Chem* 2013, 61, 1640–5.
[208] Long C, Mai Z, Yang Y, et al. Synthesis and characterization of a novel molecularly imprinted polymer for simultaneous extraction and determination of water-soluble and fat-soluble synthetic colorants in chilli products by solid phase extraction and high performance liquid chromatography. *J Chromatogr A* 2009, 1216, 8379–85.
[209] Zhao C, Zhao T, Liu X, Zhang H. A novel molecularly imprinted polymer for simultaneous extraction and determination of sudan dyes by on-line solid phase extraction and high performance liquid chromatography. *J Chromatogr A* 2010, 1217, 6995–7002.
[210] Ali WH, Derrien D, Alix F, et al. Solid-phase extraction using molecularly imprinted polymers for selective extraction of a mycotoxin in cereals. *J Chromatogr A* 2010, 1217, 6668–73.
[211] Zheng Y, Liu Y, Guo H, Hea L, Fang B, Zeng Z. Molecularly imprinted solid-phase extraction for determination of tilmicosin in feed using high performance liquid chromatography. *Anal Chim Acta* 2011, 690, 269–74.
[212] Guo H, Liu K, Liu Y, et al. Molecularly imprinted solid-phase extraction for the selective determination of valnemulin in feeds with high performance liquid chromatography. *J Chromatogr B* 2011, 879, 181–5.
[213] Lenain P, Mavungu JD, Dubruel P, Robbens J, Saeger SD. Development of suspension polymerized molecularly imprinted beads with metergoline as template and application in a solid-phase extraction procedure toward ergot alkaloids. *Anal Chem* 2012, 84, 10411–8.
[214] Murray A, Örmeci B. Application of molecularly imprinted and non-imprinted polymers for removal of emerging contaminants in water and wastewater treatment: a review. *Environ Sci Pollut Res* 2012, 19, 3820–30.
[215] Chen L, Xu S, Li J. Recent advances in molecular imprinting technology: current status, challenges and highlighted applications. *Chem Soc Rev* 2011, 40, 2922–42.

[216] Wang X, Chen L, Xu X, Li Y. Synthesis of molecularly imprinted polymers via ring-opening metathesis polymerization for solid-phase extraction of bisphenol A. *Anal Bioanal Chem* 2011, 401, 1423–32.
[217] Zhong DD, Liu X, Pang QQ, Huang YP, Liu ZS. Rapid preparation of molecularly imprinted polymer by frontal polymerization. *Anal Bioanal Chem* 2013, 405, 3205–14.
[218] Guo L, Deng Q, Fang G, Gao W, Shuo W. Preparation and evaluation of molecularly imprinted ionic liquids polymer as sorbent for on-line solid-phase extraction of chlorsulfuron in environmental water samples. *J Chromatogr A* 2011, 1218, 6271–7.
[219] Gao R, Zhang J, He X, Chen L, Zhang Y. Selective extraction of sulfonamides from food by use of silica-coated molecularly imprinted polymer nanospheres. *Anal Bioanal Chem* 2010, 398, 451–61.
[220] Zhu G, Fan J, Gao Y, Gaoa X, Wang J. Synthesis of surface molecularly imprinted polymer and the selective solid phase extraction of imidazole from its structural analogs. *Talanta* 2011, 84, 1124–32.
[221] Zhao D, Jia J, Yu X, Sun X. Preparation and characterization of a molecularly imprinted polymer by grafting on silica supports: a selective sorbent for patulin toxin. *Anal Bioanal Chem* 2011, 401, 2259–73.
[222] Korytkowska-Wałach A. Molecularly imprinted hydrogels for application in aqueous environment. *Polym Bull* 2013, 70, 1647–57.
[223] Muhammad T, Cuia L, Jide W, Piletska EV, Guerreiro AR, Piletsky SA. Rational design and synthesis of water-compatible molecularly imprinted polymers for selective solid phase extraction of amiodarone. *Anal Chim Acta* 2012, 709, 98–104.
[224] Baggiani C, Giovannoli C, Anfossi L, Passini C, Baravalle P, Giraudi G. A connection between the binding properties of imprinted and nonimprinted polymers: a change of perspective in molecular imprinting. *J Am Chem Soc* 2012, 134, 1513–8.
[225] Kryscio DR, Peppas NA. Critical review and perspective of macromolecularly imprinted polymers. *Acta Biomaterialia* 2012, 8, 461–73.
[226] Yang K, Zhang L, Liang Z, Zhang Y. Protein-imprinted materials: rational design, application and challenges. *Anal Bioanal Chem* 2012, 403, 2173–83.
[227] Qin L, He X-W, Yuan X, Li W-Y, Zhang Y-K. Molecularly imprinted beads with double thermosensitive gates for selective recognition of proteins. *Anal Bioanal Chem* 2011, 399, 3375–85.
[228] Poma A, Guerreiro A, Whitcombe MJ, Piletska EV, Turner APF, Piletsky SA. Solid-phase synthesis of molecularly imprinted polymer nanoparticles with a reusable template – "plastic antibodies." *Adv Funct Mater* 2013, 23, 2821–7.
[229] Lee M-H, Chen Y-C, Ho M-H, Lin H-Y. Optical recognition of salivary proteins by use of molecularly imprinted poly(ethylene-co-vinyl alcohol)/quantum dot composite nanoparticles. *Anal Bioanal Chem* 2010, 397, 1457–66.
[230] Zhang W, He X-W, Chen Y, Li W-Y, Zhang Y-K. Molecularly imprinted polymer anchored on the surface of denatured bovine serum albumin modified CdTe quantum dots as fluorescent artificial receptor for recognition of target protein. *Biosens Bioelectron* 2012, 31, 84–9.
[231] Liu Y, Liu L, He Y, He Q, Ma H. Quantum-dots-encoded-microbeads based molecularly imprinted polymer. *Biosens Bioelectron* 2016, 77, 886–93.
[232] Ren X, Chen L. Quantum dots coated with molecularly imprinted polymer as fluorescence probe for detection of cyphenothrin. *Biosens Bioelectron* 2015, 64, 182–8.
[233] Ren X, Chen L. Preparation of molecularly imprinted polymer coated quantum dots to detect nicosulfuron in water samples. *Anal Bioanal Chem* 2015, 407, 8087–95.
[234] Hou J, Li H, Wang L, Zhang P, Zhou T, Ding H, et al. Rapid microwave-assisted synthesis of molecularly imprinted polymers on carbon quantum dots for fluorescent sensing of tetracycline in milk. *Talanta* 2016, 146, 34–40.

[235] Altintas Z, Guerreiro A, Piletsky SA, Tothill IE. NanoMIP-based optical sensor for pharmaceuticals monitoring. *Sensors Actuat B* 2015, 213, 305–13.
[236] Ahmad R, Griffete N, Lamouri A, Felidj N, Chehimi MM, Mangeney C. Nanocomposites of gold NPs@molecularly imprinted polymers: chemistry, processing, and applications in sensors. *Chem Mater* 2015, 27, 5464–78.
[237] Iskierko Z, Sharma PS, Bartold K, Pietrzyk-Le A, Noworyta K, Kutner W. Molecularly imprinted polymers for separating and sensing of macromolecular compounds and microorganisms. *Biotechnol Adv* 2016, 34, 30–46.
[238] Uzun L, Turner APF. Molecularly-imprinted polymer sensors: realising their potential. *Biosens Bioelectron* 2016, 76, 131–44.
[239] Fang G, Wang H, Yang Y, Liu G, Wang S. Development and application of a quartz crystal microbalance sensor based on molecularly imprinted sol-gel polymer for rapid detection of patulin in foods. *Sensors Actuat B* 2016, 237, 239–46.
[240] Karaseva N, Ermolaeva T, Mizaikoff B. Piezoelectric sensors using molecularly imprinted nanospheres for the detection of antibiotics. *Sensors Actuat B* 2016, 225, 199–208.
[241] Feng S, Hu Y, Ma L, Lu X. Development of molecularly imprinted polymers-surface-enhanced Raman spectroscopy/colorimetric dual sensor for determination of chlorpyrifos in apple juice. *Sensors Actuat B* 2017, 241, 750–7.
[242] Wang H, Yao S, Liu Y, Wei S, Su J, Hu G. Molecularly imprinted electrochemical sensor based on Au nanoparticles in carboxylated multiwalled carbon nanotubes for sensitive determination of olaquindox in food and feedstuffs. *Biosens Bioelectron* 2017, 87, 417–21.

S. Grazhulene and A. Red'kin

# 10 Sorbents Based on Carbon Nanotubes

## 10.1 Introduction

Many organic and inorganic substances are used as sorbents in analytical chemistry. In various analytical methods, they are commonly used to separate and concentrate impurities or separate matrix elements [1–5]. However, available sorbents do not always satisfy the requirements of analyses because of their insufficient selectivity, problems connected with reproducibility, sorption ability, efficiency, sorbent aggregation and blockage of columns during column filling in the dynamic regime, column regeneration, etc. This urges searching for new efficient sorbents among novel materials, including carbon allotropes. Carbon fibers, fullerenes, and carbon nanotubes (CNTs) have recently been intensively studied by many researchers as promising materials for analytical purposes, including sorbents. A large number of papers and several detailed reviews have been published [6–10]. At present, most actively studied are CNTs. They can be used both in "raw" form (as grown) and after chemical treatment (modified CNTs). The area of their analytical application is vast; they can be used as sorbents for various kinds of chromatography, as collectors for impurities concentration, as highly sensitive gaseous, bio-, electrochemical sensors and electrode materials, membranes and filters.

Among most thoroughly studied is the possibility of using CNTs for electroanalysis where their electric properties allow creating electro- and biosensors and electrode materials. The review by Trojanowicz [10] summarizes the achievements in this field and considers promising CNTs potentialities.

In this review, we consider the sorption potentialities of CNTs with the emphases on the properties which can be realized in various kinds of chromatography, solid-phase extraction (SPE), and piezosensors fabrication. Special attention is given to an increase of sorption capacity, reproducibility of results on various sorbent batches, dispersion optimization, and effectiveness of column filling, its repeated regeneration and compatibility with various methods of analysis. Finally, an emphasis is placed on the simplicity, express character, reliability, and economy of use.

Modified (chemically treated) CNTs with introduced functional groups are primarily used in practice. The functional groups are introduced to make CNTs hydrophilic, on the one hand, and as the first step of further more complicated chemical treatment, on the other hand. However, the published data on CNTs sorption capacity, oxidizability, and aptitude for further modification differ considerably, which hampers the estimation of real properties of CNTs and prospects of their use in analytic chemistry. The aim of this review was to elucidate the causes of the above differences connected, in part, with conditions of CNTs synthesis and their subsequent

https://doi.org/10.1515/9783110542011-010

modification. Moreover, the review presents the discussion of recent works on new aspects of sorption properties of CNTs revealed in several studies related to CNTs application in analytical chemistry.

## 10.2 Synthesis, properties of CNTs, and methods of their study

### 10.2.1 History of CNTs

For a long time, diamond and graphite were considered the only allotropic forms of carbon. However, after the discovery of fullerene in 1985 (awarded Nobel Prize in chemistry in 1996), new forms of carbon were discovered, for example, nanotubes, graphene, ultradispersion diamond, nanoporous carbon, nanofibres, nanorings, etc. Nanotubes presumably discovered long before the work by Iijima [11], whose priority in the discovery of CNTs is generally recognized, possess a number of unique physical and chemical properties. CNTs were first discovered in the soot at arc discharge between graphite electrodes (they were considered to be cylindrical fullerenes). However, it was soon found that CNTs are superior to the class of fullerenes by their physicochemical properties and variety of structures. These characteristics gave impetus to wide and efficient applications of CNTs in various fields of science and technology.

Further investigations led to the development of different methods of CNT preparation and radical changes in the understanding of the mechanisms of synthesis and physicochemical properties of products prepared under different experimental conditions. A unique combination of high specific surface area of CNTs and the presence of internal cavities of nanometer scale initiated fundamental studies of surface phenomena on a nanometer level and investigation of the mechanisms of capillary and sorption processes inside the tubes at sizes comparable with molecular dimensions.

Soon after the discovery of CNTs and data on their physicochemical properties and structure characteristics became available, several new areas of their application appeared in micro-, nano-, and molecular electronics. Individual CNTs can be of different types of conductivity: metallic or semiconducting depending on the geometry (chirality) of tubes, which makes them suitable for fabrication of computer devices of record-high capacity and sources of field electron emission in cold emission cathodes.

CNTs were soon discovered to be single-walled (single-layered) and multiwalled (multilayered). They are layers of graphene rolled to form a single- or multilayer (from one to ten and more layers) co-axial cylinders with a diameter from one to several tens of nanometers and several hundred micron long. Several forms of CNTs exist, e. g. achiralic (an arm–chair or a zig–zag) where two sides of each hexahedron are

oriented perpendicular or parallel, respectively, to the tube axis or chiral (spiral) with each pair of hexahedra at an angle of 0 to 30 deg. to the CNT axis. Figure 10.1 shows a schematic image of nanotubes [9].

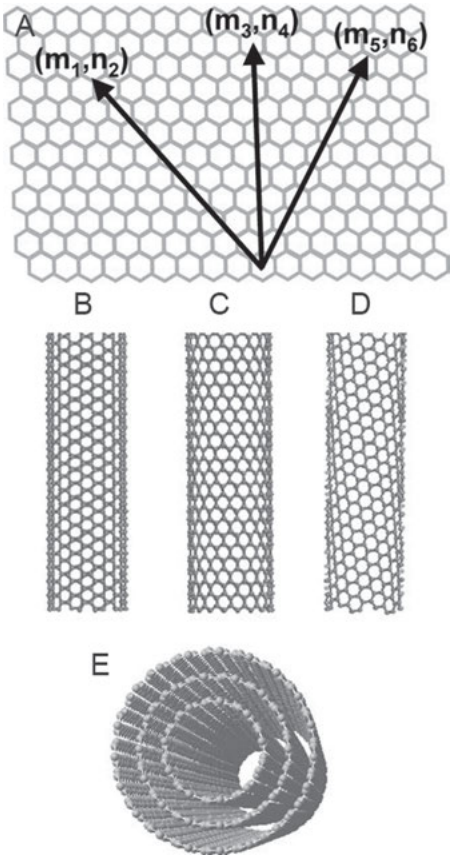


**Fig. 10.1:** Schematic of the structure of a graphene sheet (A). Singlewalled (SWCNTs ) tubes of armchair (B), zigzag (C), and chiral (D) type. The multiwalled (MWCNT) tube (E). Reprinted from ref. 9, Copyright 2005, with permission from Springer-Verlag.

Because of high length-to-diameter ratio, tubes are regarded as one-dimensional (or quasi-one dimensional) extended nanostructures. The end of CNTs is usually a semi-spherical "cap" (fullerene-like structure). The smallest tube diameter is ~0.7 nm and it sets the diameter of subsequent co-centric layers. The distance between layers in multilayered tubes is always 0.34 nm, which corresponds to the distance between layers in graphite.

The interior cavity of CNTs can be filled with various liquid, gaseous, and condensed substances due to the capillary effect and external pressure. The substances can be stored inside and protected from external physicochemical influence by the graphite surface. This property opened up large possibilities of using CNTs for storage

substances in such fields as hydrogen power technology, catalysis, medicine, etc. [12–18]. Sorption on the inner surface of CNTs and mechanisms of tube filling with substances in various aggregate states are a separate and rapidly developing field of investigation well presented in the literature and it will not be considered in detail here. Extensive and detailed information on the issue can be found in the reviews and monographs, e. g., [15–17] and references therein.

Simultaneously with physical methods of investigation, the chemistry of CNTs began to develop mainly connected with modification of the external surface of single- and multiwalled tubes using various chemical reagents. Modified CNTs were shown to possess better sorption potentialities than conventional sorbents; therefore, they found application in the analysis and purification of objects in the environment, separation, and concentration of impurities in organic and inorganic substances in combination with subsequent analysis. For more details, see part of this chapter named "Sorption properties of CNTs."

From the viewpoint of application, the cost of CNTs fabrication is still high in spite of a certain progress and updating of various methods of their synthesis. The most expensive is the synthesis and isolation of single-walled, individual, and perfect nanotubes that are essential for nanoelectronics, hydrogen power technology, medicine, biology, and other fields where the tube application implies the perfection of the inner tube surface. On the other hand, the synthesis of CNTs consisting materials for chromatography, concentration of impurities in analytical procedures, solution of various ecological problems, i. e. fields where the external surface layer and interlayer space in multilayer tubes play an important role, does not require a technology of the above high standards. Moreover, structures with defects are more appropriate because they facilitate the tube modification, increase their sorption capacity and prevent aggregation of tubes. Exact requirements to the properties of CNTs according to the purpose of their application have not been formulated yet and the progress in this direction would depend on the understanding of what correlation exists between the specific features of synthesis and quality of the product obtained.

### 10.2.2 Synthesis, functionalization, and characterization of CNTs

#### 10.2.2.1 Methods of synthesis

Many CNTs synthesis methods have been fairly well described in the literature [12–28]. The major of them are (1) electric arc synthesis under inert gas atmosphere (a time-consuming procedure giving a mixture of allotropic forms of carbon as byproduct with a large number of defects, including edge dislocations). The disorder character of thus obtained structures is connected with the nonequilibrium conditions of the arc discharge. The yield of CNTs and their morphology is strongly influenced by the basic discharge conditions (current strength, voltage between

the electrodes, plasma temperature, and time of discharge) and by parameters such as gas flow, purity and configuration of electrodes and their cooling, setup geometry, etc. Moreover, transition metal addition inside the graphite anode affects the yield and shape of tubes. (2) Laser evaporation of graphite, a most expensive and hard to control method. Its advantage is a fewer number of parameters influencing the shape and yield of CNTs than the electric arc synthesis. This probably increase the tube yield. A higher efficiency of laser ablation was achieved by addition of Ni and Co catalysts to the graphite. (3) Chemical vapor deposition (CVD) at catalytic decomposition of various carbon-containing gases is the simplest and cheap method of synthesis. The advantage of CVD is deposition of CNTs films onto different substrates such as glass, silica, metal etc., which is important in fabrication of various types of sensors. (4) Other methods of CNTs synthesis include hydrocarbons combustion in flames, electrolysis of molten salts, carbides chlorination, etc.

Materials obtained by different methods can be of various shape and morphology: solid residue, wool-like and textured structures on substrates, aggregates, ropes consisting of tube assembly cabled together and some other. Depending on the synthesis method used and/or its conditions, single- and multiwalled tubes and other carbon modifications, amorphous carbon and fullerenes, are obtained. To proceed with the discussion, it is pertinent here to consider what the term "purity of CNTs" means when used in the literature on the physical and chemical aspects of CNTs. Sometimes, it is not clear what kind of "purity" is implied and how this "purity" is determined. Evidently the term is used to denote the presence or the absence of other allotropic carbon forms. Sometimes the term refers to the content of single-walled tubes in the whole mass of carbon material. But nowhere the chemical composition of the tubes and the presence of catalyst residues and other elements are discussed. However, this issue seems important to understand the mechanism of synthesis, physicochemical properties of tubes and their application in analytical procedures, medicine, and biology. Aspects connected with the purity of CNTs will be considered in Section 10.2.2.

Each of the CNTs synthesis methods has its own advantages and disadvantages widely discussed in the literature. However, these methods are not considered in detail in this review, except for the CVD method because of its wide potentialities, promising properties from the viewpoint of simplicity, lability, and economical efficiency. First of all, it is a CVD synthesis of CNTs from ethanol vapors [19–28], so-called alcoholic catalytic CVD or AC-CVD. Its advantages are lower temperature of synthesis, simplicity, high reproducibility, and high yield. The method became of intense interest among researchers at the beginning of the 2000.

The gas-phase catalytic pyrolysis of ethanol vapors involves several chemical reactions on the catalyst; these are connected with decomposition of ethanol molecules into simpler components such as methane, carbon monoxide, and hydrogen. The major reaction to evolve carbon at the temperature below 600°C is

disproportionation of carbon monoxide. The reaction products (depending on the conditions) can be single- and multi-walled CNTs and nanofibers of various thicknesses. Moreover, AC–CVD enables the synthesis of single-walled nanotubes that are almost free of amorphous carbon, multi-walled nanotubes, and other carbon-containing admixtures. Long CNTs were prepared in [21], which were oriented along a substrate of mesoporous silica with a Mo/Co catalyst deposited onto it. The tubes were synthesized from ethanol vapors in a flow-type reactor at 850°C. The tubes were reported to grow strictly parallel to the vapor flow direction to form a two-dimensional network of oriented one-walled CNTs with interior cavity diameters in a narrow distribution range. Pure CNTs containing more than 96% single-walled nanotubes were synthesized from ethanol vapors in a similar reactor using ferrocene as a catalyst precursor [22]. By simple treatment of the CNTs in nitric acid, their purity was increased to 99 %. The comparison of various alcohols showed that ethanol gives the best results. The use of isopropanol and octanol led to a larger amount of amorphous carbon and with methanol no carbon deposition was observed. High-quality two-layered CNTs were obtained in high yield from ethanol vapors at a reduced pressure [23]. These tubes had averaged diameters of 1.55 and 0.85 nm for the first and second layers, respectively.

Synthesis of multi-walled CNTs and nanofibers by catalytic pyrolysis of ethanol vapors was the objective of a number of works. A simple and efficient method of fabrication of coatings from multi-walled tubes on quartz substrates was reported in [24]. The catalyst used was a thin (5 nm) film of iron or nickel. The synthesis was performed at atmospheric pressure in oxidizing atmosphere in the presence of $O_2$, $N_2$, and $CO_2$. Ethanol solution of ferrocene can be a source of carbon and simultaneously a catalyst in the synthesis of CNTs and nanofibers. Multi-walled CNTs with high degree of order were obtained using the above solution [25].

The effectiveness of a number of catalysts (Co, Ni, Mo, and Fe acetates, bimetallic mixtures deposited onto substrates by centrifugation) for the synthesis of single-walled CNTs from ethanol vapors was studied in [26]. The thermally oxidized silicon was used as substrate. The synthesis was performed at 500–1,000°C. The samples were analyzed using Raman spectroscopy (RS), atomic-force microscopy (AFM), scanning tunnel microscopy (STM), and transmission electron microscopy (TEM). The ratio of G and D peak intensities in the RS spectra of the samples served as a criterion to estimate the efficiency of the catalytic process. Pure nickel and cobalt were found to be highly active as catalysts, the catalytic properties of iron were weak, and molybdenum did not work as a catalyst at all. At low temperatures, binary Ni–Co catalysts were most efficient.

All known setups to synthesize CNTs by the AC-CVD method are in principle similar and can correspond to the scheme shown in Fig. 10.2 [20]. Figure 10.3 shows a typical electron-microscopy image of carbon nanomaterial prepared by AC–CVD. The material consists of multi-walled tubes and nanofibers 20–100 nm in diameter and several micrometers long. Thus, it was shown that structural, physicochemical, and

morphological properties of CNTs depend both on the method of preparation and the conditions of synthesis (temperature, catalyst, time, etc.).

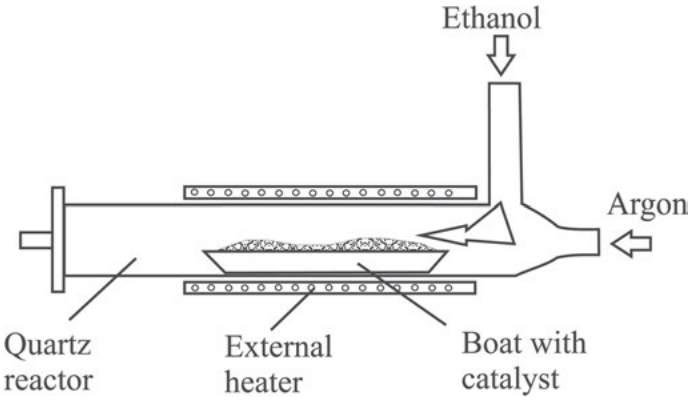


**Fig. 10.2:** The scheme of the unit for the synthesis of CNTs from ethanol vapors by the CVD method.

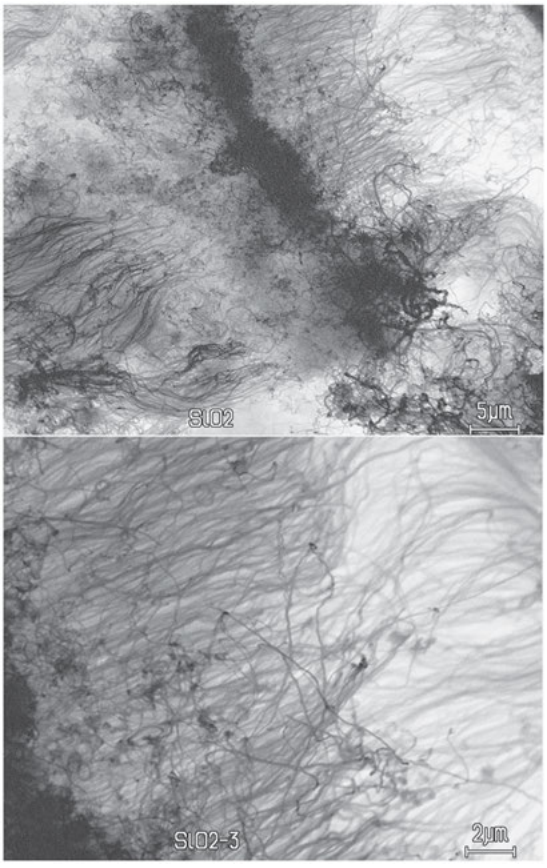


**Fig. 10.3:** Electron microscopic image of a carbon nanomaterial obtained by catalytic pyrolysis of ethanol vapors.

Regretfully, details of CNTs synthesis are not always reported in the literature, which can explain the ambiguity and discrepancy of the results concerning the CNTs properties presented in the literature.

#### 10.2.2.2 Modification and functionalization

Modification of CNTs is widely discussed in the literature devoted to the studies and application of CNTs [29–68]. Modification is believed to open ways to real application of CNTs in nanoelectronics, composite materials, as catalysts, sorbents, etc. Synthesized CNTs (by any method) are practically insoluble in water and major organic solvents. However, their use often requires them to be in a dissolved form. Their transformation into dissolved form is achieved by various methods of *modification*. The meaning of the term "modification" is rather broad. Sometimes it implies the following operations: functionalization (introduction of various functional groups to the side surfaces and tube ends), subsequent reactions involving these groups, chemical reactions inside the tubes including the filling of the tube interior with various substances, substitution of carbon atoms by other elements, purification of CNTs from catalysts, and opening the tubes during acidic treatment. Modification changing the chemical composition of the tube surface is often called *functionalization*. It can proceed by two mechanisms: covalent (chemical) and non-covalent (physical) one. The term "non-covalent functionalization" does not seem very correct, although covalent bonds are really absent. It would be more appropriate to speak about a noncovalent *interaction* or *modificatio*n in a broad sense of the word. However, the term "noncovalent functionalization" is widely used in the literature [31, 40, 47].

*Covalent functionalization* can be, in its turn, divided into direct nondestructive and that connected with surface defects [30]. Direct covalent functionalization is connected with the change in the $sp^2$ hybridization to $sp^3$ and simultaneous loss of π-conjugation of the graphene layer. This can occur during the interaction with highly reactive agents, for example, in the reactions such as ozonation, chlorination, and fluorination [31]. "Defect" functionalization presumes the formation of defects on the surface during the growth or chemical treatment of CNTs which become the sites of chemical interaction. Open ends of CNTs or irregularities of pentagons and heptagons in the graphene hexagons can serve as defects. Covalent functionalization of nanotube ends causes changes only in their electron structure and does not affect the material volume properties. Functionalization of side walls changes the properties of CNTs [31]. Oxidized centers in CNTs can also be regarded as defects. These defects are formed during oxidation with strong acids or their mixtures [32]. Defects formed by oxidants can be stabilized through combining with carboxyl and carbonyl groups, which can then become a basis for further functionalization. A step-by-step chemical treatment allows the substitution of some functional groups in CNTs by other groups, depending on the purpose of further application. The process can be regarded as a

controlled change of nanotube properties so that they suited the purposes of further application [33]. This technique enables "sewing" any groups, even complicated dendrite structures, to the surface of nanotubes so that they could make 50 % of the resulting product mass [34]. Such structures can find wide application, for example, for biomedical purposes.

*Non-covalent modification* is an alternative method of changing physicochemical properties of CNTs and is based on using weak bonds (π–π and hydrophobic interactions, hydrogen, electrostatic, and van der Waals forces). Due to van der Waals forces or other interactions, a suspension of nanotubes can form supramolecular complexes with polymers [35–41] or with surfactants [42]. This process promotes also the destruction of CNTs associates formation of individual tubes [43]. Another kind of non-covalent modification is "host–guest" interaction, which consists in sorption introduction of inorganic particles such as Ag, Au, and Pt [44] and small biomolecules, e. g. DNA [45], into the interior cavity of CNTs.

The range of fundamental and applied issues of CNT modification has been considered in a large number of publications [20–31, 41, 45, 51, 53–56]; we shall deal here with the latest works on covalent functionalization of CNTs by oxidation from the viewpoint of oxidation effect on the sorption properties related to analytical chemistry.

Covalent functionalization to oxidize the CNTs surface by introduction of oxygen-containing groups (oxidative functionalization) is the most thoroughly studied and described modification process [46, 48–51, 58–68]. Depending on the oxidant, the introduced groups can be carboxyl, carbonyl, and hydroxyl. In all cases, the number of grafted functional groups per mass unit is an important characteristic of the obtained materials. The number and kind of introduced functional groups are compared with the nature of the oxidant used, e. g. $HNO_3$, $H_2SO_4$, $KMnO_4$, $H_2O_2$, and their mixtures under various conditions: temperature, concentration, and contact time. The efficiency of the oxidation process is estimated by the concentration of introduced groups which is controlled by physical and chemical methods and compared with the nature and concentration of an oxidant, temperature, and time of treatment. A detailed comparison of the efficiency of six most frequently used oxidants was reported in [46]. The objective of investigation was commercial, multiwalled CNTs (outer diameter 15–5 nm, 5–20 μm long, 95 %). The oxidants were $HNO_3$, $KMnO_4$, $H_2SO_4/HNO_3$, $(NH_4)_2S_2O_8$, $H_2O_2$, and $O_3$. The formation of oxygen-containing groups on the CNTs surface after treatment were determined by X-ray photoelectron spectroscopy (XPS) and energy-dispersion X-ray spectroscopy; the concentration of introduced groups was determined by chemical derivation combined with XPS. It was found that different oxygen-containing groups reacted with specific derivation agents containing original chemical marks. It was also shown that the effect of oxidant concentration is much less pronounced than the oxidant type. For example, the treatment with $(NH_4)_2S_2O_8$ , $H_2O_2$, and $O_3$ mainly causes the introduction of carbonyl and hydroxyl groups whereas more aggressive oxidants ($HNO_3$, $KMnO_4$) lead to the formation of carboxyl functional groups on the surface of CNTs.

The formation and behavior of various oxygen-containing functional groups after treatment with different oxidants and subsequent treatment with a strong reductant ($NaBH_4$) was studied in [48]. It was found that the treatment with a reductant does not practically decrease the amount of oxygen on the CNTs surface but radically changes the relative content of different functional groups because of their partial reduction: the amount of carboxyl groups decreases while the content of hydroxyl groups increases.

Studies on the application of various oxidants (strong acids and their mixtures) were described several times [65–68]. Oxidation of CNTs with nitric acid under different conditions and control over the changes in such properties as mass, solubility, morphology, and order degree by Raman spectroscopy and the optical method developed in [65] was examined in order to determine CNTs solubility in concentrated water suspension. It was found that the solubility is determined not only by the functional groups on the CNTs surface but also by the functionalization of amorphous carbon formed as a result of CNTs destruction during acidic treatment. A high solubility (20–40 mg $ml^{-1}$) was obtained only after a long (24–48 h) exposition in concentrated (60 %) nitric acid. However, about 60–90 % of nanotubes are lost under such conditions. After 48 h oxidation, CNTs undergo fragmentation and become covered with amorphous carbon. Tube destruction under the effect of aggressive agents is discussed [66], and it was shown that the treatment of tubes with nitric acid under hard conditions (with refluxed nitric acid) leads to partial degradation of CNTs consisting in a considerable decrease in the tube length and the appearance of new defects. However, these defects facilitate further functionalization through the introduction oxygen-containing groups, as was shown by XPS and acid–base titration. The treatment of CNTs with alkaline agents does not cause any noticeable changes in the structure of CNTs. Similar investigation was also done in [67], showing that harsh conditions (e. g. 8 M $HNO_3$ or its mixtures with $H_2SO_4$ via sonication) radically functionalize the CNTs surface but lead to the destruction of the structure of graphite.

Under more mild treatment conditions (3 M $HNO_3$, 2 h treatment), the destruction of tubes is considerably smaller; however, the degree of their functionalization decreases as well. To prevent the decrease, the authors used additional oxidation of CNTs by $H_2O_2$ and optimized the power of sonication to obtain a higher content of oxygen-containing groups. The introduced groups were controlled by the FTIR spectroscopy. A simple procedure was also used to estimate the degree of functionalization; it consisted in visual observation of the sedimentation rate of CNTs suspension obtained by sonication in polar solvents after different techniques of functionalization. In this experiment, 5 mg of CNTs in 13 mL of ethanol were subjected to ultrasound treatment for 10 min and the time of CNTs sedimentation was determined. It was found that sedimentation of the tubes that were not subjected to acid treatment took 10 min, whereas the time of oxidized tube sedimentation depended on hardness of the treatment conditions. The functionalization at the above mild conditions gives a colloid dispersion of CNTs which is stable for several weeks. These results were in

agreement with electron microscopy data and spectroscopy data, which exhibited more intense spectral lines due to oxygen-containing groups as compared with those under different conditions.

In addition to functionalization of CNTs, oxidation of nanotubes by concentrated acids causes opening of tube ends and purification of synthesized tubes from other carbon allotropic forms and amorphous carbon.

Thus, treatment of CNTs fabricated by various synthetic methods using acidic and basic agents enables the introduction of functional groups into the side and end tube surfaces, the type and concentration of these groups depend on the oxidant and treatment conditions. Functionalization considerably increases hydrophilicity of CNTs, decreases the van der Waals interaction and, correspondingly, decreases aggregation of hydrophobic nanotubes that stabilizes the formed colloid [52]. Oxygen-containing groups substantially increase the sorption capacity of CNTs in the case of ion-exchange mechanism of sorption. These issues are considered in detail in the "10.3.1 Sorption of metals from aqueous solutions". Note that no general principles have been formulated to explain the connection between the synthetic conditions of CNTs and their ability to modification in spite of a large number of works on the effect of functionalization conditions on the type and concentration of introduced groups which change the physicochemical properties of CNTs, sorption capacity included. At the same time, the synthetic conditions that influence the morphology can affect the CNTs properties and, in the first place, their ability to modification which determines the sorption properties of obtained materials. From this point of view is of interest the discussion in [46] (one among few) which points to the discrepancy between the results obtained for various commercial samples of CNTs. To clear up the disagreement, the authors first determined the parameters of the initial commercial samples of CNTs using electron microscopy.

#### 10.2.2.3 Methods of characterization

CNTs can be characterized from different viewpoints: by the relative content of single- and multiwalled nanotubes in carbon material, presence of other allotropic carbon forms, specific surface area, dispersion, sizes (diameter and length), chirality, chemical composition. No standard parameters of characterization (neither rigorous classification of characterization methods) exist. Characterization of CNTs requires the use of several different methods. As a rule, most methods are multipurpose and are used to characterize the structure and/or morphology and chemical composition of CNTs. From the viewpoint of purpose, these methods sometimes can be divided only conventionally.

A detailed review of the methods to characterize CNTs is given by Belin and Epron [69] as well as Merkoci [9] as applied to analytical chemistry.

Characterization of the morphology and structure of CNTs is aimed at estimating their mechanical, electric, and electronic properties. Most widely used methods are

SEM, TEM, ESCA, and Raman spectroscopy [70–73]. The use in TEM of an accelerating voltage of 60–200 kV enables the resolution of several nanometers and allows the differentiation of single- and multiwalled CNTs and, roughly, the positioning of graphene planes. A high-resolution TEM (0.15–0.30 nm) with an accelerating voltage to 400 kV enables the visualization of atomic layers [74]. This method permits the determination of CNTs diameters, structure of joints and walls, and distance between graphene planes. Neutron diffraction can give information on structure features and C–C bond lengths [75, 76]. The observation of individual nanotubes by these methods requires a special preparation of samples: sonication in the medium of organic solvents often in the presence of surfactants and subsequent deposition of the obtained suspension onto an electroconducting substrate. In fact, characterized is not the initial but rather a newly obtained substance.

One of the important methods to characterize solid samples of CNTs without preliminary treatment is to determine the specific surface area and inner diameter of tubes by nitrogen adsorption at 77 K using the Brunauer–Emett–Teller (BET) method [77].

Because the use of CNTs in practice often involves their transferring into solution (real or colloidal) by functionalization or noncovalent modification, which causes changes in the CNTs properties, the characterization of introduced functional groups plays a decisive role. A detailed review of methods for chemical and structural characterization of covalently functionalized CNTs was recently published in [46, 72]. In these reviews both widely used methods (STM, TEM, XPS, IR, and RS) and some specific techniques such as chemical derivatization, acid–base titration, etc. were considered. The chemical derivatization method is based on the selective and stoichiometric reaction of a functional group with a specific derivatization agent containing a certain chemical marker. Note that derivatization in combination with various physicochemical methods of analysis is not widely used to determine functional groups in oxidized CNTs. The fact is that not all of functional groups can be derivatized, that limits the potentiality of the method. Nevertheless, the method has been successfully used by several researchers [56–60] and is worth attention.

The information on the nature of CNTs functional groups can be obtained by XPS [72, 73]. The major peak at 284.6 eV is due to the C1s atoms of carbon in graphite. The shoulder at 287.6 eV is due to carbonyl groups, that at 288.8 eV to carboxyl groups, and the shoulder at 286.3 eV appears when hydroxyl groups are present [16].

The introduced functional groups of CNTs are commonly identified by IR spectroscopy [16, 78–80]. The characteristic lines in the IR spectrum at 1614–1620, 1710–1735, 1585–1590, 1200–1205, and 1080 $cm^{-1}$ testify to the presence of carboxyl groups. The C–O–C group vibrations are observed at 1207 and 1040 $cm^{-1}$, epoxide group vibrations are seen at 1267 and 822 $cm^{-1}$, and those at 3350–3500 $cm^{-1}$ are due to $-OH^-$ groups [16]. Although a quantitative analysis by IR spectroscopy presents certain difficulties, relative changes in the –COOH group content, depending on the experimental conditions, can be determined using the intensity, for example, line at 1725 $cm^{-1}$ attributable

to the carboxyl group vibrations. The line at 1590 $cm^{-1}$ was used as a reference point because it corresponds to innerplane stretching vibrations of carbon atoms in nanotubes and does not vary with experimental conditions [78]. The line was isolated as a gaussian, and all lines in the spectrum were normalized to its integral intensity.

Raman spectra can provide information on the quality of CNTs from the viewpoint of "graphitization," i. e., the presence/absence of amorphous carbon and other allotropic forms [81–85], if use is made of the ratio of the G and D lines characterizing $sp^2$ and $sp^3$ hybridization lines, respectively [16, 46, 79]. The higher the ratio, the better is the product quality. Moreover, narrowing of the G line in the Raman spectrum suggests a stronger "graphitization" [16]. Note, however, that this conclusion mainly refers to single-walled nanotubes, because Raman spectra of multiwalled CNTs are more difficult to interpret due to the appearance of a large number of additional lines. The presence of introduced oxygen-containing groups can be inferred from the general acidity of CNTs surface employing acid–base titration [78, 86–88].

As mentioned above, considerations of CNTs purity rarely imply their chemical (impurity) composition of nanotubes themselves. In most cases, the term "purity" implies the presence of one-type structures, for example, single- or multiwalled nanotubes. Other allotropic carbon forms are also regarded as impurities. Only in 2008 Chinese researchers [89] presented a paper where they consider in detail the purity and element composition of CNTs. The impurity composition of CNTs can be determined by methods of element analysis, for example, by arc atomic-emission spectrometry (AES). By element admixture composition, the material obtained from ethanol vapors proved fairly pure [88]. The content of basic admixtures in it was at the level of graphite usually employed as an admixture collector in dc arc AES. The results of CNTs element analysis by AES depending on the method of the catalyst washing are given in Tab. 10.1. It is seen that the content of the Ni catalyst after washing decreases by approximately five times but still remains at the level of tenth parts of percent. As was expected, the contents of aluminum, silicon, and calcium decrease after washing with hydrofluoric acid.

**Tab. 10.1:** Results of dc arc atomic emission analysis of CNTs ($n$ = 3, Sr = 0,25)

| CNTs washing from the catalyst | Element, % mass | | | | | | | | | | |
|---|---|---|---|---|---|---|---|---|---|---|---|
| | Al × $10^5$ | B × $10^5$ | Cu × $10^5$ | Fe × $10^5$ | Mg × $10^4$ | Mn × $10^5$ | Si × $10^3$ | Ti × $10^5$ | Ca × $10^4$ | Mo × $10^5$ | Ni × $10^1$ |
| Without washing | 3.0 | 2.0 | <0,5 | 1.0 | 2.5 | <0,5 | 1.0 | <1 | 0,13 | <5 | 5,0 |
| $HNO_3$ | 15 | 1.5 | <0,5 | 5.0 | 2.0 | <0,5 | 1.0 | <1 | 1.6 | <5 | 1.2 |
| $HNO_3$ + HF | 0.8 | 1.0 | <5 | 7.5 | 0.1 | <5 | 0.12 | <1 | 0.10 | <5 | 1,1 |

Purification of CNTs material from other allotropic forms of carbon is especially important when single-walled nanotubes are used in biomedicine, electronics, or nanocomposites. In other cases, e. g., when CNTs are used as sorbents in SPE or in

various kinds of chromatography, the isolation and subsequent characterization of single-walled nanotubes alone makes the synthesis procedure complicated and is hardly expedient. The use of bulk material of CNTs seems more suitable for these purposes because such parameters as specific surface and/or nature of functional groups introduced during modification and sorbent dispersity play a determining role. Therefore, the effect of various parameters on the CNTs characteristics should be thoroughly studied.

## 10.3 Sorption properties of CNTs

### 10.3.1 Sorption of metals from aqueous solutions

Studies of metal ions sorption from aqueous solutions are important from the viewpoint of technology and analytical chemistry. These studies are closely related to environmental problems (e. g., sorption and determination of toxic elements). The problems of sewage disposal and treatment are closely connected with those of their analysis. As a rule, analysts deal with considerably diluted solutions (at preconcentrating trace amounts of impurities) and it may seem that the sorption capacity of CNTs is not that important as it is in technology and ecology. More significant for the results are distribution coefficients, extraction completeness, reproducibility of the results of sorption and desorption (depending on the analysis method) on various sorbent batches, and compatibility with methods of analysis. Nevertheless, some general issues such as the character of sorption isotherms, dependence on pH and initial solution concentration, etc. are equally important in analytic chemistry and technology. Therefore, the problem of element extraction from waters of various compositions is expedient for analysts. A number of works have recently appeared devoted to metal ion extraction (especially toxic metals) using CNTs prepared and oxidized by different techniques [90–109]. Some papers devoted the extraction of lead [92–98], cadmium [92, 99,101], zinc [100–103], and nickel [104–105]. The review by Rao [90] on bivalent metal ions extraction to purify waters has demonstrated considerable possibilities of CNTs to extract and concentrate heavy metals. The economic aspect of CNTs application as compared to other sorbents is considered to be essential for the solution of environmental problems.

Most of the above investigations deal with oxidized CNTs and pay much attention to the effect of oxidation conditions on the sorption properties: the type of CNTs oxidant, temperature and time of treatment, medium acidity or pH of solutions, and metal concentration. Introduced functional groups increase the negative charge on the carbon surface and, correspondingly, increase the cation-exchange capacity of CNTs [94]. It was shown that the adsorption behavior of heavy metals on CNTs can be described either by the Langmuir or the Freundlich isotherms [91] or by both [93]. The

sorption mechanism was the object of many discussions. However, there is no unified opinion on its character. It is clear that sorption involves several physical and chemical processes, which is confirmed by the absence of distinct correlation between the value of sorption capacity and specific surface area and nanotube diameter. The chemical interaction between metal ions and surface functional groups is schematically shown in Fig. 10.4 [90]. It can be explained by the ion exchange between metal ions in the aqueous phase and protons of carboxyl and phenol groups of modified CNTs [102, 105].

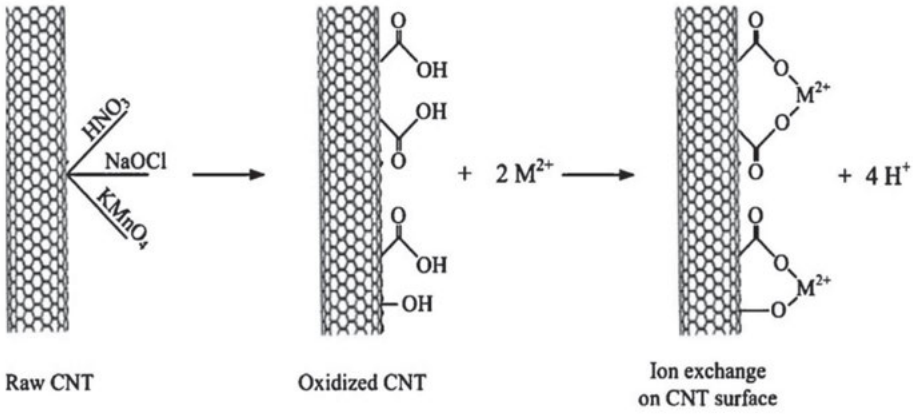


**Fig. 10.4:** Mechanism of metal ions sorption on modified CNTs. Reprinted from ref. [90], Copyright 2007, with permission from Elsevier.

It was shown that competing mechanisms of various metal ions extraction can operate depending on the sorption conditions [92]. To this end, they studied the effect of solution ionic strength (0.01, 0.05, and 0.1 M) on the sorption of $Pb^{2+}$, $Cu^{2+}$, and $Cd^{2+}$. It was shown that the adsorption interaction between the sorbent functional groups and metal cations mainly corresponds to the ion-exchange mechanism, whereas the negatively charged surface of oxidized CNTs is responsible for electrostatic interaction. The simultaneous presence of $Pb^{2+}$, $Cd^{2+}$, and $Cu^{2+}$ ions on their combined extraction in comparison with that of these individual metals [22] was performed. This influence appeared insignificant and decreasing in the following order $Pb^{2+} > Cu^{2+} > Cd^{2+}$.

It was also found [100, 102] that the contribution of electrostatic interaction increases at high pH values, which increases sorption, for example, of zinc. The effect of pH in the range 8–11 on the extraction of $Ni^{2+}$ and $Zn^{2+}$ was studied in detail [100, 105]. The behavior of various chemical species of the sorbate ($Zn^{2+}$, $Zn(OH)^{1+}$, $Zn(OH)_2$, $Zn(OH)_3^-$ and $Zn(OH)_4^{2-}$ present in the aqueous solution at various pH was considered [100]. The $Zn^{2+}$ sorption was found to dominate at pH < 8. At pH 8–11, the extraction of zinc is maximum and occurs as $Zn(OH)^+$ and $Zn(OH)_3^-$ adsorption and $Zn(OH)_2$ sedimentation. At pH 12, dominating are $Zn(OH)_3^-$ and $Zn(OH)_4^{2-}$ species; therefore, an observed decrease of zinc extraction can be partially a result of competition between

these species for the sorption places on the CNTs surface. The $Zn^{2+}$ sorption from aqueous solutions on commercial powdered activated carbon (PAC) was studied in detail [100] in comparison with the sorption by CNT [103]. It was found that the sorption capacity of CNTs is significantly higher than that of PAC.

The mechanism of $Pb^{2+}$ sorption on CNTs, as a model element, was studied [98] and by various methods of analysis showed that the contribution of functional groups to $Pb^{2+}$ sorption is 75.3 % of the total sorption capacity and the rest 24.7 % is due to the specific surface area, i. e., to physical sorption. If the latter is the case, the 21.3 % of the above 24.7 % of $Pb^{2+}$ sorption is defined by electrostatic interaction and 3.4 % is deposited as PbO, $PbCO_3$, and $Pb(OH)_2$ species. Nanotubes multitwisted in an arbitrary way form oriented spiral-like structures, which provide a considerable number of cavities of nanometer size accessible for liquids and gases from outside. In these structures, sorption occurs within the inside, outside, and intertube space via various mechanisms (Fig. 10.5) [106].

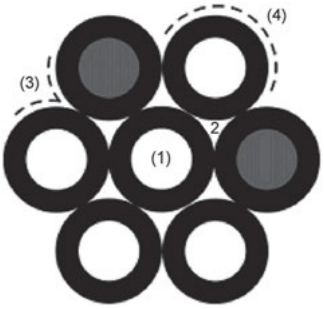


**Fig. 10.5:** Different adsorption centers of a homogeneous beam of CNTs with partially open ends: 1, internal; 2, intracanal; 3, external corner; 4, external surface. Reprinted from ref. [106], Copyright 2006, with permission from American Chemical Society.

It was found that sorption capacity depends on the concentration of introduced oxygen-containing groups. However, the order of changes in the capacity for various cations in the reported works differs. For example, in [93], this order is $Pb^{2+} > Cd^{2+} > Co^{2+} > Zn^{2+}$, which coincides with that in [78]; in the review [90] the order is $Pb^{2+} > Ni^{2+} > Zn^{2+}Cu^{2+} > Cd^{2+}$. At the same time, the maximum copper sorption was reported [91, 93, 109] and the interchange of places in the order between zinc and cobalt depending on pH was observed. Note that CNTs in [90] and [93] were fabricated by the CVD method although from different carbon-containing products and on different catalysts. Different reagents were also used for subsequent modification to oxidize the CNTs surface. The difference in the sorption capacity on the obtained materials is mainly explained by the dependence of surface acidity on the type of an oxidant used and treatment conditions, which provide the introduction of various oxygen-containing groups and their different concentrations. On the other hand, it was found that sorption capacity differs considerably when identical oxidation conditions are used [78]. For example, the ability of CNTs to accept introduced oxygen-containing functional groups (–OH, –C=O, –COOH, etc.) under otherwise equal conditions (the same oxidant, treatment time and temperature) strongly depends on the conditions of synthesis of an initial

CNTs, particularly on temperature and catalyst. The oxidative modification was estimated by comparing the intensity of –C=O and –COOH peaks in the IR spectra [84] and general acidity of modified CNT determined by back titration [86].

As was shown in [78, 107], the morphology of CNTs which determines their ability to the oxidative modification and, therefore, to sorption activity also depends on the conditions of CNTs synthesis (temperature and catalyst type). The CNTs were synthesized at 400, 450, and 550°C by ethanol CVD onto various catalysts (Ni, Co, Fe) [20]. It was found that the CNTs synthesized at the lowest used temperature (400°C) and with Ni catalyst have the maximum ability to modification and, correspondingly, the maximum capacity of the resulting materials to sorb various ions (Fig. 10.6a, b).

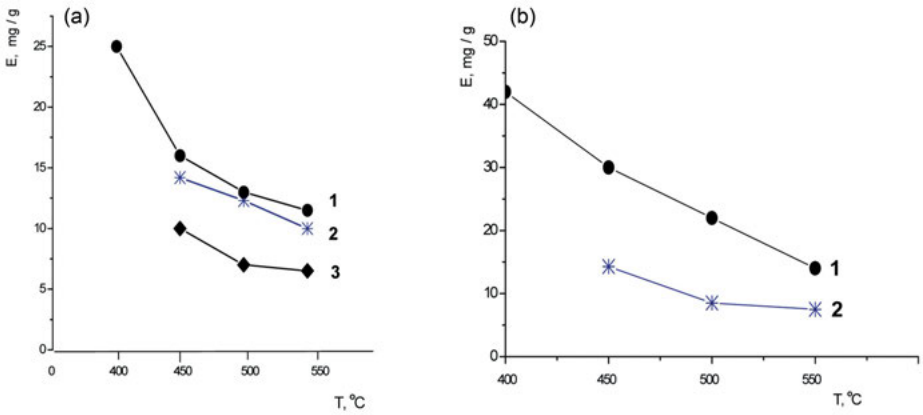


**Fig. 10.6a, b:** Sorption capacity of oxidized CNTs in relation to $Cu^{2+}$ depending on the catalyst and the temperature of CNTs synthesis: (a) static mode; (b) dynamic mode; catalysts for CNTs synthesis: 1, Ni; 2, Co; 3, Fe.

SEM studies showed that CNTs fabricated on the Ni catalyst have the form of bundles twisted with each other (Fig. 10.7a, b). Ultrasonication of such structures in water does not appreciably change the situation. Only a small part of twisted nanotubes and their fragments can be obtained in the solution as individual tubes. When the Fe is used as catalyst, the obtained material is straight individual tubes, uniformly distributed in the solution after ultrasonication (Fig. 10.8a, b).

The morphology of CNTs grown on the Co catalyst is intermediate between those of grown on Ni and Fe: both ordered and twisted components are observed (Fig. 10.9). The difference in morphology suggests various ability of CNTs to oxidative modification at the treatment with concentrated $HNO_3$. The maximum surface acidity was found in CNTs grown on the Ni catalyst whereas on the Fe catalyst it was minimal. The sorption capacity with respect to metal ions varies in the same order. The CNTs synthesized on the Co catalyst are characterized by an intermediate state by acidity and sorption capacity.

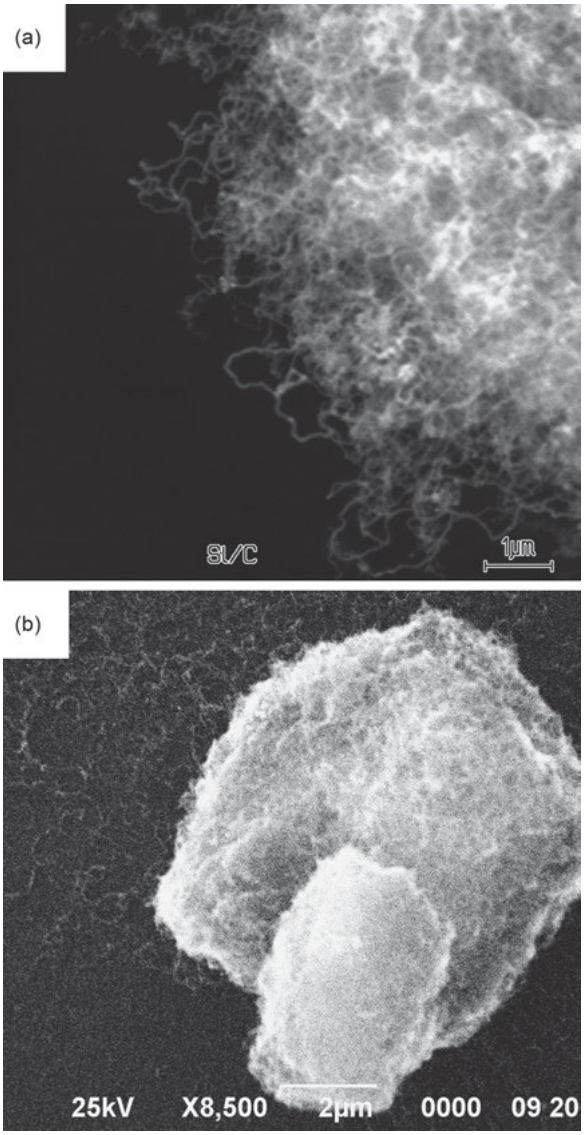


**Fig. 10.7a, b:** CNTs grown on a nickel catalyst: (a) as grown; (b) after sonication.

It is evident that CNTs synthesized on the Ni catalyst possess a much larger concentration of defects, which facilitates the introduction of oxygen-containing groups to stabilize the tube surface and prevent their subsequent aggregation. The use of Ni and Co catalysts evidently leads to the formation of more perfect structures that hamper the introduction of oxygen-containing groups as can be judged from a low surface acidity after treatment with concentrated $HNO_3$. Moreover, an increase in the solution pH to that close to neutral brings about partial dissociation of the introduced –COOH groups and increases their hydration. The hydrated CNTs form a stable colloid suspension, i. e., a sort of "solubilization" takes place.

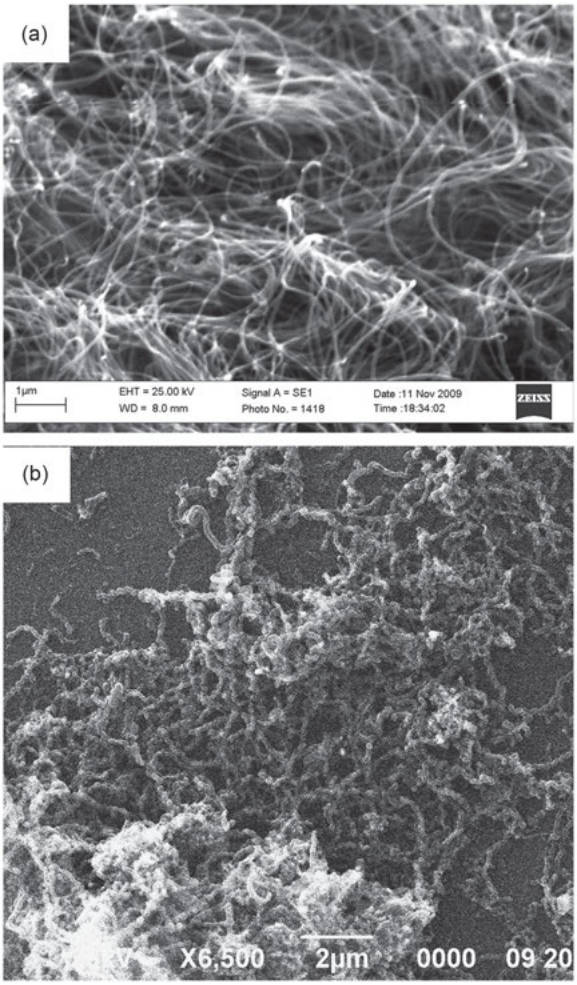


**Fig. 10.8a, b:** CNTs grown on an iron catalyst: (a) as grown; (b) after sonication.

The term "solubilization" is often used in the chemistry of CNTs to denote their transition into solution (mainly colloidal) but, in some analytical applications, it has a negative connotation. For example, in spite of CNTs attractiveness as a pseudo-stationary phase in electrokinetic chromatography, their tendency to mutual aggregation is a negative factor. This property is also of disadvantageous character in filling the chromatographic columns during separation in the dynamic mode. To avoid this effect, various methods are used, for example, coating of CNTs with surfactants [108]. The results reported in [107] suggest that CNTs in the form of twisted bundles and tubes obtained on Ni catalysts at fairly low temperatures are free of this drawback.

The dependence of various physicochemical properties of CNTs (sorption capacity, concentration of introduced functional groups by oxidative modification, size and diameter distribution of pores) upon the synthesized material morphology was studied also in detail [95]. The synthesis was carried out in horizontal and vertical

furnaces by the CVD method (similar to that in [78]) although the carbon-containing compounds were xylene (Fe catalyst, 800°C), benzene (Fe catalyst, 1150°C), propylene (Ni catalyst, 750°C), and methane (Ni catalyst, 650°C). The nanotubes were then treated with concentrated $HNO_3$ (140°C, 1 h) to remove the rest of catalysts and to introduce functional groups. The obtained nanotubes were of different morphology and different ability to oxidative modification and, hence, sorption capacity. The CNTs synthesized on a Ni catalyst at lower temperatures (those of methane and propylene decomposition) had the maximum sorption efficiency. Of minimum efficiency (by 6–8 times) were the nanotubes grown on a Fe catalyst at higher temperatures (those of xylene and benzene decomposition). The authors of [95] and [78] relate this difference in properties to different defect structures of the obtained nanotubes and note that the more perfect the structure, the worse its sorption properties are. Moreover, the nature of the initial carbon-containing compound does not play a decisive role.

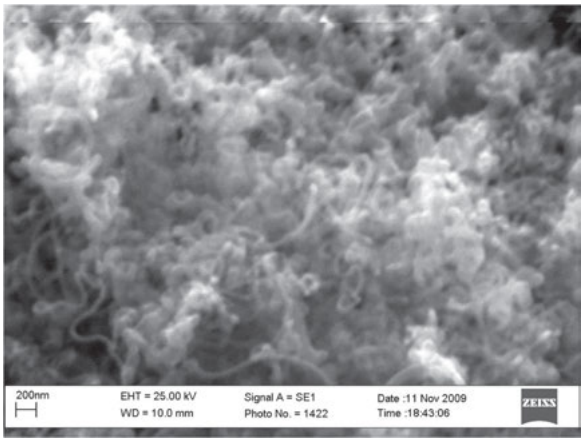


**Fig. 10.9:** CNTs grown on cobalt catalyst.

It can be concluded that the reaction ability of carbon in nanotubes is not constant and can vary depending on the synthesis conditions, catalyst nature, temperature, and other factors. CNTs with a larger number of defects would be more susceptible to the effect of strong oxidants at modification, as was shown in practice. This property is evidently the fundamental cause of substantial difference in the sorption properties of CNTs modified under similar conditions but obtained under different conditions of synthesis.

### 10.3.2 Sorption of organic substances

Extraction of organic substances from various natural and biological materials is the object of numerous papers [110–127]. A variety of organic substances that can be adsorbed on CNTs is determined by the sorption mechanism which depends on the

structure of organic compounds. Possible mechanisms of sorption are considered in the review paper of Pan and Xing [110] who came to the conclusion that this issue is not completely clear. Nevertheless, it can be stated with some degree of certainty that the mechanism of organic substances sorption from an aqueous phase consists of several processes. Several approaches, e. g. the Freindlich model [111–113], the Langmur model [114–116], BET [117], and the Polanii–Maness models [118–119], were proposed to describe this mechanism. Heterogeneous adsorption is explained by the presence of defects (high-energy adsorption centers and functional groups [120, 121]) and intermediate spaces among CNTs bundles [122]. If the dominating mechanism of sorption is the formation of hydrogen bonds, introduction of oxygen containing groups, which increase of CNTs electrophilicity, increases the sorption. In the hydrophobic mechanism, nonfunctionalized CNTs are more efficient.

In comparison with other carbon materials [122, 126], CNTs were found more effective as sorbents in SPE of chlorobenzene [111, 125], herbicides [113], fulvoacids [115], dioxine [121], dissolved natural organic substances [114], antracen [118], cyclic and polycyclic aromatic hydrocarbons [119, 126, 127]. CNTs oxidized by NaOCl appeared more effective in the sorption of benzene, toluene, ethylbenzene, and xylene from aqueous solution than CNTs treated by HCl, $H_2SO_4$, or $HNO_3$ [127]. The sorption mechanism in these compounds is due to the π–π electron donor–acceptor interaction: carboxyl oxygen atoms on the CNTs surface serves as donors and the aromatic ring serves as an electron acceptor (Fig. 10.10).

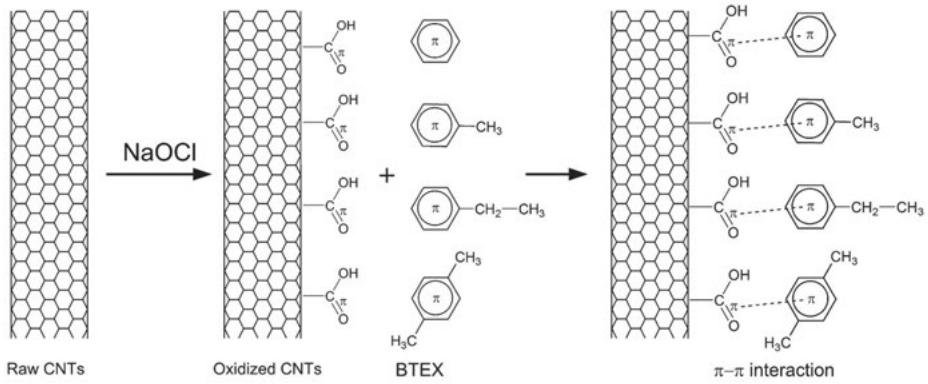


**Fig. 10.10:** The mechanism of adsorption of aromatic compounds on oxidized CNTs. Reprinted from ref. [127], Copyright 2008, with permission from Elsevier.

The ability of CNTs to adsorb aromatic hydrocarbons, especially xylene, was found to considerably exceed that of other kinds of carbon and silicon sorbents [127]. This led the authors of [127] to recommend using CNTs for purification of water from aromatic compounds.

### 10.3.3 Comparison of CNTs with other sorbents

In a number of papers [120, 123, 124], CNTs are considered as alternatives to other carbon materials for gas chromatography of volatile organic compounds. As compared with "Carbopack B" [123], CNTs are superior in separating such polar compounds as alcohols, ketones, and ethers of the same specific surface area. They are characterized by fast sorption kinetics, a stronger retention which allows the separation of low-boiling compounds, more symmetric peaks, and a smaller number of theoretic plates. One more important advantage of CNTs is the possibility of fast and complete regeneration of sorbent and the possibility of their many-times repeated use [110]. CNTs differ from other carbon structures, from activated carbon (AC) in the first place, by an ordered and well-organized surface structure with definite adsorption centers, whereas the use of AC requires knowledge on the distribution of pore diameters and sorption energy [128]. The idea was proposed in [129] that CNTs and other allotropic carbon forms can be regarded as mono- and polycrystals.

Note that comparison of characteristics of various sorbents always implies certain uncertainty because their properties crucially depend on many factors. For example, the characteristics of AC as reported in [130] radically depend on the technique of their activation. A comparison of the CNTs and AC properties modified under similar conditions requires knowledge of their genesis [78]. Note that the literature data on the AC sorption capacity are contradictory and depend on carbon specification. Therefore, an attempt was made [78] to study their sorption capacity before and after treatment (identical for CNTs treatment), using commercial charcoal (CH) and synthetic activated (SA) carbons. The subsequent comparison showed a much higher sorption efficiency of CNTs than that of carbon of the above specifications (Fig. 10.11a, b).

A comparative study on the sorption of heavy metals by various carbon sorbents and CNTs with capsulated magnetic nanoparticles (CCNTs) included was reported by Pyrzynska and Bystrzejewski in [131]. All the carbon sorbents studied were treated with conc. $HNO_3$ under similar conditions. The morphology of the sorbents was examined by SEM to reveal their difference. Raman spectroscopy enabled the estimation of the sorbents crystallinity. CNTs and CCNTs were of similar crystallinity degree, whereas AC was of low crystallinity typical of amorphous carbon materials [132]. The modified products differed slightly by the surface acidity (it was less for AC) connected with the number of introduced oxygen-containing groups. The difference in the surface charge density was essential: CCNTs > CNTs > AC. The sorption capacity on the basis of the studied model elements ($Cu^{2+}$ and $Co^{2+)}$ is approximately equal in CCNTs and CNTs, but depending on pH of solution it is 2.5–6.5 times higher than in AC although their specific surfaces are considerably larger. The observation is explained by the difference in the calculated charge density of the sorbent surfaces correlated with the degree of their "graphitization," i. e., relative content of tubes in the total mass of carbon material. An important fact found in the work is a smaller influence of

the salt composition of solution on the sorption of studied elements. The decrease in the sorption efficiency was 5–11 % for CCNTs and CNTs and 30–50 % for AC.

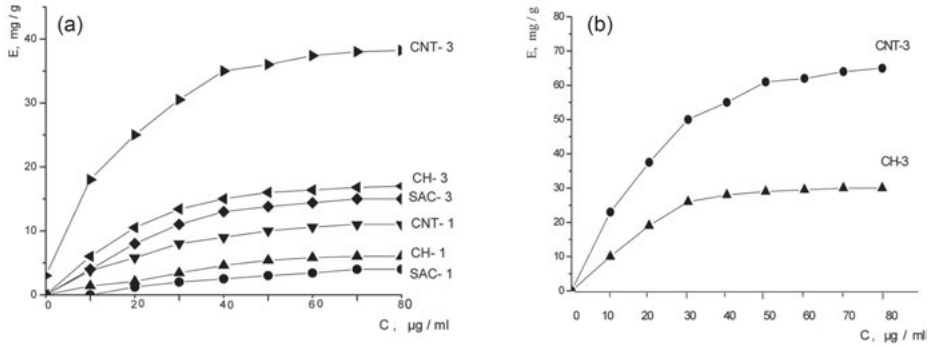


**Fig. 10.11a, b:** Isotherms of sorption of $Cu^{2+}$ (a) and $Ag^{+}$ (b) on CNTs (static mode, synthesis at 400°C in comparison with activated coals). Abbreviation of samples with the number 1 – processing of conc. $HNO_3$ at 90°C; with number 3 – treatment of conc. $HNO_3$ at 120°C.

Noteworthy is an essential advantage of CCNTs over other carbon-containing materials from the viewpoint of their lability under external magnetic field. This property enables their efficient separation from other nonmagnetic carbon phases using a simple and cheap magnet. Recently, a large number of works have appeared devoted to the use of magnetic nanoparticles, CNTs/iron oxide magnetic composites to separate various sorbates from aqueous phases [133–141].

The kinetics of Cu ions sorption on CCNTs, CNTs, and AC was studied in [134]. It was shown that the extraction of $Cu^{2+}$ by nanotubes is much faster than by AC. The sorption kinetics in nanostructured sorbents and AC differ by the involved limiting processes. The kinetics in CNTs and CCNTs is limited by the diffusion in the film, while in AC the typical stage is diffusion inside the carbon particles. The fast sorption kinetics on tubes is their important advantage in some cases, e. g., in the use of CNTs to modify the piezoelectric transducer (to be described below). A systematic comparison of $Cr^{3+}$, $Mn^{2+}$, $Pb^{2+}$, $Cu^{2+}$, $Cd^{2+}$, and $Zn^{2+}$ adsorption from aqueous solutions on oxidized and nonoxidized CNTs and AC revealed the superiority of CNTs over all the metals [132].

The adsorption properties of CNTs as compared to other sorbents with respect to organic compounds were the objective of numerous works. Noteworthy is the study of solid-SPE of pesticides, atrazine and sinazin, by CNTs as compared with AC and various silica sorbents [141]. In a number of other cases, the sorption efficiency of CNTs also proved to be higher. From the economy viewpoint, the statistic analysis in [142] on the example of $Ni^{2+}$ sorption showed that CNTs are more effective than AC because they permit repeated sorption-desorption many times with a smaller sorbent loss, which makes CNTs (in spite of their rather high cost) economically more beneficial in treatment of large water volumes.

## 10.4 CNTs for chemical analysis

### 10.4.1 Concentration and determination of metals

SPE is a well-studied and widely used method to concentrate impurities in analysis of real objects. SPE and other sorption methods are used to determine toxic substances in the environmental objects, food, geological and biological samples [1, 143]. These methods can be easily combined with modern multielement high-sensitive analytic methods, such as optical emission spectrometry with inductively coupled plasma (ICP–OES) and especially with mass-spectrometry (ICP–MS). Because instruments for the above analysis are expensive, traditional readily available and economic methods of analysis are also widely used: flame atomic absorption spectrometry (FAAS) electrothermal AAS (ETAAS) and dc arc atomic emission spectrometry (AES). The latter methods require simple and effective procedures of analyte preconcentration. Therefore, concentration by sorption makes the basis for new and modified methods of analytic control and is always in demand. The growth of works on the use of CNTs for SPE by 50 times in the period 2002 to 2010 is convincingly demonstrated by El-Sheikh and Sweileh [144]. Note that most of the papers cited in [144] deal with the analysis of organic compounds.

Table 10.2 gives the examples of CNTs application to concentrate metal ions for subsequent atomic-spectroscopy analysis. The table shows that FAAS is used to determine many metals [88, 145–153] employing oxidized CNTs without additional modification. Metals are concentrated in the dynamic mode at pH 6–9 (except gold [152]) with various concentrations of $HNO_3$ as eluent. The relative detection limits for the elements are 0.05–8.0 μg $L^{-1}$, depending on the concentration coefficient which is 12 to 150. In [153], Fe(III), Cu(II), Mn(II), and Pb(II) in the environmental objects were concentrated on CNTs at pH 9. A quantitative extraction of elements was obtained when 1 M $HNO_3$ solution in acetone was used as an eluent. The ICP–OES and ICP–MS methods enabled lower limits of detection (LOD) [156].

Concentration of impurities on CNTs columns in combination with FAAS was employed to analyze food (buckwheat), waters of various origin and river silt [88, 183]. Due to impurities preconcentration, the relative LOD for buckwheat were by an order of magnitude lower as compared to direct determination or remained the same at a smaller (by ten times) mass of the sample. These results were confirmed by the analysis of standard samples and comparison with the AES and FAAS data.

Additional modification of oxidized CNTs with various organic agents (Tab. 10.2, [158–167]) did not always give better results from the metrology viewpoint, i. e., complication of the analytic procedures hardly repays itself.

Efficient sorption of $^{243}Am(III)$ with its subsequent determination was reported in [168]. Therein the mechanism of chemisorption of americium and its analogues, actinides, and lanthanides, and prospects of this sorbent application to treat large

volumes of industrial wastes were discussed. The investigations of Myasoedova and coworkers [169, 170] were devoted to the use of CNTs (Russian sorbent "Taunit") to concentrate and separate radionuclides.

**Tab. 10.2:** Application of CNTs for preconcentration of metals

| Metal | Ligand | pH | Eluent | K | Method of analysis | LOD, μg $L^{-1}$ | References |
|---|---|---|---|---|---|---|---|
| Cu, Zn, Mg, Ag, Fe, Pb, Pd, Cd, | – | 6–7 | $HNO_3$ | 150 | FAAS | 0.02–0.98 | [88] |
| Cu(II) | – | 7 | $HNO_3$ | 60 | FAAS | 1.46 | [146] |
| Cu(II) | – | 5–8 | $HNO_3$ | 150 | FAAS | 0.42 | [147] |
| Cu(II) | – | 7–9 | $HNO_3$ | 12 | FAAS | 2.1 | [148] |
| Ag | – | 7–9 | $HNO_3$ | – | FAAS | 0.60 | [149] |
| Zn(II) | – | 8 | $HNO_3$ | – | FAAS | – | [150] |
| Cd | – | 4–6 | $HNO_3$ | 60–100 | FAAS | 0.15 | [151] |
| Au | – | 1–6 | Urea in HCl | 75 | FAAS | 0.15 | [152] |
| Fe(II), Cu(II), Mn(II), Pb(II) | – | 9.0 | $HNO_3$ + acetone | 20 | FAAS | 3.5–8.0 | [153] |
| Co(II), Mn(II), Ni(II) | – | 8.0 | $HNO_3$ | 25 | ICP-AES | 0.04–0.05 | [154] |
| Eu, Gd, Ho, La, Sm, Tb,Yb | – | 3 | $HNO_3$ | 50 | ICP-AES | 0.003–0.06 | [155] |
| Cu(II), Co(II), Pb(II) | – | 7–9 | $HNO_3$ | 50 | ICP-MS | 0.001–0.04 | [156] |
| Co(II) | – | 8.8 | $HNO_3$ | 19 | ETA-AAS | 0.01 | [157] |
| Mn(II), Au | NBHAE | 6 | $Na_2S_2O_3$ | 250 | FAAS | 0.01 | [158] |
| Rh(III) | PAN | 3.7 | DMFA | 120 | FAAS | 0.01 | [159] |
| Pd(II) | DABR | 1.0–4.5 | Thiourea | 200 | FAAS | 0.3 | [160] |
| Cd(II) | L-cysteine | 5.5–8 | HCl | 33 | FAAS | 0.28 | [161] |
| Co(II) | L-tyrosine | 9 | $HNO_3$ | 180 | FAAS | 0.05 | [162] |
| Cu(II), Cd(II), Pb(II), Zn(II), Ni(II), Co(II) | APDC | 2 | $HNO_3$ in acetone | 80 | FAAS | 0.3–0.6 | [163] |
| Co(II) | PAN | 5–8.5 | $HNO_3$ | 300 | FAAS | 0.55 | [164] |
| Cu(II), Co(II), Ni(II), Pb(II) | o-cresol-phthalein | 7 | $HNO_3$ | 40 | FAAS | 1.6–5.7 | [165] |
| Mn(II) | PAN | 8.0–9.5 | $HNO_3$ | 100 | FAAS | 0.058 | [166] |
| As(III) | CTAC | 5–6 | $HNO_3$ | 65 | AFS | 0.002 | [167] |

K Concentration factor
LOD Limit of detection
APDC Ammonium pyrrolidine dithiocarbamate
CTAC Cetyltrimethylammonium chloride
DABR 5-(4′-Dimethylaminobenzylidene-rhodanine)
DMFA *N*,*N*′-Dimethylformamide
NBHAE *N*,*N*-Bis 2-hydroxy-benzylidene)-2,2(aminophenylthio) ethane
PAN 1-(2-Pyridylazo)-2-naphtol

### 10.4.2 On-line preconcentration and speciation analysis

Injection techniques for on-line preconcentration on oxidized CNTs (without additional modification) gave impressive results. For example, a simple and effective method of Cu(II), Zn(II), Mn(II), and Pb(II) concentration in vegetable samples using a microcolumn filled with CNTs and subsequent FAAS determination was proposed by Chinese analysts in [171] (Tab. 10.3). The authors report a high sensitivity of the method, reliability of determination, high factors of concentration, and the absence of the matrix effect.

**Tab. 10.3:** On-line atomic spectroscopy methods

| Metal | pH | Eluent | K | Method of analysis | LOD, μg $L^{-1}$ | References |
|---|---|---|---|---|---|---|
| Cu(II), Zn(II), Mn(II), Pb(II) | 6,0 | $HNO_3$ | 14–20 | FAAS | 0.28–1.0 | [171] |
| Cd(II) | 4,9 | $HNO_3$ | 51 | FAAS | 0.01 | [172] |
| Cd(II) | 7,0 | $HNO_3$ | | ICP-AES | 1.03 | [173] |
| Pb(II) | | $HNO_3$ | | AFS | 0.003 | [175] |
| Pb(II) | 4,7 | $HNO_3$ | 44.2 | FAAS | 2.6 | [176] |

A successful on-line determination of nanogram content of Cd in waters, cigarettes, and standard samples of various compositions using CNTs as a sorbent for preconcentration, and FAAS analysis with thermospray was described Tarley et al. [172]. The on-line analysis enabled lowering the detection limit for Cd by 640 times as compared with traditional FAAS determination. The minimum detected concentration of Cd was 0.01 μg $L^{-1}$, which is by 1–2 orders of magnitude lower as compared to that detected with other studied sorbents (amberlite, polyurethane resins, rice husk, silica gels, fullerenes, etc.). No matrix effect and influence of foreign elements were found. The correctness of the determination was confirmed by analysis of standard biological samples. The authors emphasize the simplicity of the method, absence of complex-forming agents, and high reproducibility of the results (Sr = 6.5–2.1 for concentrations of 100 and 1000 ng $L^{-1}$, respectively).

The efficiency of oxidized CNTs for on-line SPE preconcentration of Cd in sewage waters with subsequent ICP–AES determination was confirmed in [173]. Although the reported detection limit was higher than that in [172], CNTs proved superior in high stability, ease of column regeneration, ability of many times repeated use (300 cycles of concentration) as compared to other studied sorbents.

An original method of speciation analysis of As(III) and Sb(III) in water which combines on-line preconcentration on CNTs by the SPE method with atomic-fluorescence spectroscopy and hydride generation was proposed by Wu et al. [174]. The scheme of the analysis consists in the formation and retention of pyrrolidine-dithiocarbamate complexes of As(III) and Sb(III) on the CNTs-filled column and subsequent elution and determination of As(III) and Sb(III). The total content of arsenic and antimony

was determined after the oxidation to As(V) and Sb(V) by the same scheme, and concentration was found by subtraction. The high sensitivity, reliability of determinations, simplicity of column design, ease of analytic operations make this method, by the author's opinion, a good alternative to the expensive ICP-MS method for determination of hydride-forming elements. A similar approach was used to determine Pb in waters [175] by the elution of its 0.3 M $HNO_3$ solution from a CNT-filled column with subsequent atomic absorption [176].

CNTs were also used for on-line concentration of Cd and Cu in biological samples and environmental objects at pH 4.5–6.5 and 5.0–7.5, respectively, which were then determined by FAAS [177]. Unlike other methods, elution of elements was carried out by 0.5 M HCl. The sorption kinetics was high which enabled a high flow rate of the sample (7.8 mL $min^{-1}$) for on-line microcolumn preconcentration without loss in retention efficiency. The reported detection limits were 0.30 and 0.11 μg $L^{-1}$ for Cd(II) and Cu(II), respectively (Sr = 2.1–2.4 % for Cd(II) and Cu(II), respectively, at the concentration of 10 μg $L^{-1}$).

The use of CNTs for element speciation analysis was described in a number of recent publications [174, 178–183]. Some of them deal with Cr speciation analysis in environmental objects. For example, a CNT-filled microcolumn was employed to determine the oxidation state of Cr in natural and sewage waters [179]. It was found that Cr(III) is selectively retained on the CNTs at pH 2.0–4.0 whereas Cr(VI) remains in the solution. The sorbed Cr(III) was eluted by 2.0 mL of 1.2 M $HNO_3$ and then determined by ICP-MS. The detection limit was 0.01 and 0.024 ng $mL^{-1}$ for Cr(III) and Cr(VI), respectively; $S_r$ was less than 5 % ($n$ = 9, $c$ = 1.0 ng $mL^{-1}$). CNTs were also used for on-line preconcentration of vanadium to determine its species by ET-AAS [181]. A gold electrode modified with CNTs allowed the determination of As and Bi(III) [182].

### 10.4.3 Piezosensors

A topical issue in modern analytical chemistry is the development of express methods to determine the components content on-line without laborious operations of sample selection and preparation, i. e., with the use of test-devices, sensors and sensor systems [184]. These devices are often based on high-frequency piezoelectric quartz resonators (PQR) of volume acoustic waves (VAW), which serve as transducers. The exploitation characteristics of piezosensors (PS) depend on the properties of sorbing coatings: their composition homogeneity, density, thickness, and reproducibility of the sorption surface. The most important characteristics of PS are sensitivity and selectivity relative to substances to be determined. The collection of mass signals from nonselective sensors (one of matrix response variants is "of visual prints") can enable the determination of fine differences in qualitative and quantitative composition of multi-component mixtures of gases and vapors.

Selectivity and efficiency of gas and vapor sorption can be optimized through changing the structure and composition of sensitive coatings on the PS surface [185]. One of the ways to increase sorption efficiency is to enlarge the contact area of gas and sorbent, although this possibility is limited by the mass of sorption coating. For example, for PQR of VAW type with the basic frequency of vibration of 10 MHz, the coating mass should not exceed 200 μg. Depending on the coating nature, the optimum mass is 3–4 μg. Due to high sorption capacity, CNTs are a promising material for PS and would considerably increase the measurement sensitivity.

The sorption of organic substance vapors on CNTs coatings which differ by the conditions of synthesis, deposition and treatment procedures was studied in [186] with the aim of designing efficient PS (Tab. 10.4).

**Tab. 10.4:** Synthesis conditions of CNTs with the following treatment and depositing on resonator

| CNTs, sample No. | Conditions of synthesis | | Treatment after synthesis | Coating of the resonator | |
|---|---|---|---|---|---|
| | *t*, °C | Catalyst | | Method | Mass, μg |
| I | 550 | Ni | – | Suspending | 4.1 ± 0.1 |
| II | 550 | Ni | $HNO_3$ | Suspending | 4.3 ± 0.1 |
| III | 550 | Fe | HF | Suspending | 4.2 ± 0.1 |
| IV | 450 | Ni | $HNO_3$ | Suspending | 4.2 ± 0.1 |
| V | 550 | Ni | – | Surface synthesis | 4.0 ± 0.1 |
| VI | 450 | Ni | – | Surface synthesis | 4.2 ± 0.1 |

The specific features of sorption and kinetics of interaction with analytes were studied using a gas analyzer (Voronezh, Russia) fabricated by the "electron nose" methodology as an array of eight PS. The results of measurements were registered and treated using the software ("KvadroSoft," Russia) which presents the analytic signals of sensors as graphs and tables. A special algorithm of the program allows converting them to total signal in the form of visual prints. The quantitative criteria of sorption were the maximum sensor response $\Delta F_{max}$ (Hz) and molar sensitivity $S_m$ (Hz $m^3$ $mol^{-1}$). The latter was calculated as the ratio of the maximum sensor response to the concentration of the test substance in the gas sample. The kinetics and reversibility of sorption–desorption, and wear resistance of sensor coatings were estimated from the dependence of the sensor signal ($\Delta F$, Hz) on the exposure time ($\tau$, s) and "of visual prints" of the sensor signal.

The sorption of arenas (benzene, toluene, o-xylene, ethylbenzene, cumene, and pseudo-cumene) and aliphatic alcohols ($C_2$–$C_9$) of normal and isomer composition has been studied. It was shown that the time of maximum piezosensor response ($\tau_{max}$, s) during the sorption of benzene and ethanol on CNT of any genesis is 2–6 s, which is 5–55 times faster than on standard chromatographic phases commonly used to modify PQR electrodes (Tab. 10.5).

The calculated $S_m$ of sensors with CNTs coatings to arenas and alcohols are given in Tab. 10.6.

**Tab. 10.5:** Time to achieve the maximum sorption of benzene and ethanol (τ max, s ) on CNTs in comparison to standard chromatographic phases

| ***Sorbents on quartz resonators*** | **τ max, s** | |
|---|---|---|
| | **Benzene** | **Ethanol** |
| SNTs (I–VI) | 6 | 2 |
| Polystyrene | 150 | 110 |
| Triton X-100 | 30 | 30 |
| Polyvinylpyrrolidone | 115 | 75 |
| Polyethylene glycol 2000 | 45 | 45 |
| Polyethylene glycol adipate | 45 | 60 |
| Polyethylene glycol-sebacate | 110 | 90 |
| Polyethylene glycol succinate | 60 | 45 |
| Polyethylene glycol-phthalate | 60 | 75 |
| Beeswax | 30 | 45 |

**Tab. 10.6:** The molar sensitivity of the sensors with CNTs coatings for vapor of arenes and alcohols.

| **Sensors coated by CNTs** | | **I** | **II** | **III** | **IV** | **V** | **VI** |
|---|---|---|---|---|---|---|---|
| **Arenes** | Benzene | 28,000 | 7,000 | 5,000 | 29,000 | 30,000 | 31,000 |
| | Toluene | 9,000 | 2,000 | 1,000 | 9,000 | 10,000 | 9,000 |
| | *o*-Xylene | 21,000 | 6,000 | 4,000 | 23,000 | 24,000 | 25,000 |
| | Ethylbenzene | 18,000 | 4,000 | 3,000 | 23,000 | 23,000 | 24,000 |
| | Kumol | 51000 | 20,000 | 11,000 | 53,000 | 56,000 | 62,000 |
| | Pseudokumol | 52,000 | 20,000 | 17,000 | 58,000 | 63,000 | 63,000 |
| **Alcohols** | Ethanol | 398 | 129 | 64 | 411 | 427 | 456 |
| | *n*-Propanol | 933 | 302 | 151 | 939 | 1,001 | 1,070 |
| | Isopropanol | 411 | 171 | 85 | 417 | 566 | 605 |
| | *n*-Butanol | 2,850 | 954 | 477 | 2,917 | 3,167 | 3,384 |
| | *deut*-Butanol | 824 | 364 | 182 | 883 | 1,206 | 1,289 |
| | Isobutanol | 466 | 215 | 108 | 516 | 715 | 764 |
| | *tert*-Butanol | 1,532 | 683 | 341 | 1,658 | 2,266 | 2,421 |
| | *n*-Pentanol | 11,031 | 3,666 | 1,833 | 11,109 | 12,164 | 12,997 |
| | Isopentanol | 7,068 | 3,063 | 1,532 | 7,289 | 10,164 | 10,860 |
| | *n*-Hexanol | 18,403 | 6,601 | 3,301 | 19,667 | 21,904 | 23,404 |
| | *n*-Heptanol | 56,043 | 19,426 | 9,713 | 57,876 | 64,458 | 68,873 |
| | *n*-Nonanol | 112,811 | 39,733 | 19,866 | 117,393 | 131,841 | 140,871 |

It is seen that the coatings of sensors I, IV, V, and VI possess the maximum $S_m$ with respect to arenas and alcohols. The results presented Tab. 10.6 allow the conclusion that the sorption efficiency depends on the genesis of CNTs, namely synthesis

conditions (temperature and catalysts) and subsequent treatment. This conclusion agrees with the data [71,107] on the ability of CNTs to undergo modification depending on the synthesis conditions. For example, sample III with the lowest molar sensitivity was prepared of an iron catalyst (Tab. 10.4). Its morphological properties hamper the introduction of carboxyl groups during its treatment with $HNO_3$ [107], which lead to the formation of CNTs aggregates at sonication and decrease its sorption capacity. The comparison of samples II and IV prepared on an Ni catalyst and then treated under similar conditions (conc. $HNO_3$ for 2 h at 110°C) revealed a considerable difference in the piezosensor sensitivity caused by different temperatures of synthesis. Sample IV obtained at 450°C is easier to modify and, therefore, has a larger concentration of introduced carboxyl groups than the sample synthesized at 550°C. The introduced functional groups stabilize CNTs and prevent their aggregation during sonication, thus increasing the sorption capacity of IV as compared with that of sample II. The comparison of samples I and IV also points to the effect of the synthesis temperature on the CNTs properties. A similar picture is typical of samples V and VI; sensitivity increases with the synthesis temperature lowering, i. e., at an increase in defect character of the CNTs surface. To estimate the PS sensitivity, also account should be taken of sorbates chemical nature which mechanisms of sorption contribute to its total value.

Another advantage of CNTs is stability of the zero signal, one of the important characteristics a sensor should have. It was found that the zero line drift in sensors with CNTs is by 4–15 times smaller than in sensors with other coatings. This means that the use of CNTs to form sorption coatings decreases the error of detection and lowers the detection limit.

However, the application of CNT-based sensor coatings is drastically limited by nonselective sorption. To improve the selectivity, some procedures were developed to identify vapors of organic substances by the signals of a multisensor system [186]. Specifically, a relative coefficient of sorption efficiency ($k$) calculated as the ratio of signals from two sensors in the massif was used to determine fine differences in the sorption kinetics and, thus, to increase the selectivity of detection.

Noteworthy is the use of CNT-based sensors to detect changes in the parameters of electron properties caused by molecule sorption on their surface. A large number of papers report the creation and studies of analytic potentialities of CNTs as gas sensors to detect $O_2$, $N_2$, CO, $H_2O$, $NH_3$, $NO_2$, and $SO_2$ at very low detection limits. To increase the selectivity of determinations, the CNTs modified usually with various organic substances. A review of such investigations and comparison with the potentialities of other gas sensors based on changes in their electron properties can be found in the paper by analysts from Spain [187].

### 10.4.4 Other applications of CNTs

Several promising, although less studied and less popular, directions of CNTs application are worth considering, e. g., CNTs as a material to obtain a new generation of stationary phases in liquid chromatography and capillary electrophoresis. In part,

of interest are monolith column sorbents in liquid high-resolution chromatography and electrochromatography, which are a good alternative to granulated sorbents [188]. In this case, CNTs are introduced into an organic polymer monolith containing divinylbenzene chloride and ethylenedimethacrylate. A comparison of chromatographic characteristics of initial monolith organic stationary phases with those containing CNTs revealed a better resolution of chromatographic peaks and a higher efficiency of separation of the studied peptides on the monolith CNTs-modified organic phases.

The presence of CNTs in the dc arc AES was found to increase the volatility of a number of elements during their evaporation from the crater of arc. This observation allowed effectively using CNTs as a spectral additive [189]. The influence of CNTs concentration (2, 5, 10, and 15 mass%) on the character of evaporation and intensity of spectral lines of hard volatile elements to be detected in the graphite powder was studied to determine the optimum additive content which is 5 %. Figure 10.12 displays the curves of Al, Ba, Bi, and Hf evaporation from a graphite powder in the presence of 5 % CNTs and without the additive. For comparison, the figure shows the curves of the same elements' evaporation in the presence of the known additive carrier $Ga_2O_3$. It is seen that the effectiveness of CNTs as an additive is higher than that of $Ga_2O_3$. This observation shows that the introduction of CNTs promotes an increase in evaporation rate of determined elements and creation of favorable conditions for their excitation in the dc arc plasma.

It is known that the optimum temperature ($t_{opt}$) of plasma to excite atomic spectral lines of elements depends on the potentials of their ionization and excitation. For elements with ionization potentials of 7–8 eV and potentials of line excitation 4–5 eV, the optimum plasma temperature is 5,600–6,000°C. The values of $t_{opt}$ to excite ionic lines used in AES are much higher than for atomic lines (≥7,000°C). The dc arc plasma temperature is determined by the ionization potential of the major component in an analyzed sample. For pure carbon arc (ionization potential of carbon is 11.3 eV), the temperature is (6,000 ± 100)°C. Introduction of CNTs additive into an analyzed graphite powder, i. e., the same carbon, does not change the plasma temperature and it remains close to $t_{opt}$ for the excitation of analytic lines of most elements to be determined. The addition of $Ga_2O_3$ (its ionization potential is 6 eV) lowers the arc plasma temperature to (5,500 ± 100)°C and, hence, would impair the detection limits for elements. Table 10.7 presents the LOD ($C_{lim}$) for several elements in graphite as estimated by the lowest point in the calibrated plot [190].

It is seen that CNTs improve the detection limits for impurities in graphite by three times as compared to the procedure without using CNTs. This can be explained as due to an increase of the evaporation rate of studied elements from the electrode crater because of their co-evaporation with the additive and a creation of favorable conditions for atomic and ionic analytic lines to be excited in the arc plasma

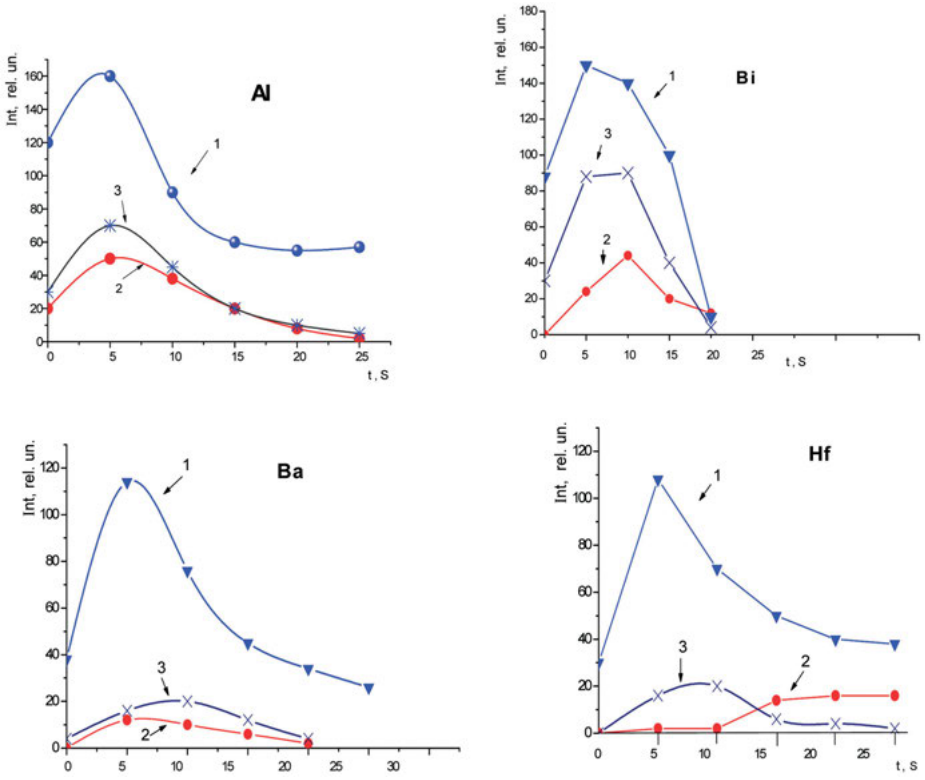


**Fig. 10.12:** Evaporation curves of elements Al, Ba, Bi and Hf from the d.c. arc crater: 1, with 5 % CNTs; 2, no additives; 3, with 5 % $Ga_2O_3$.

**Tab. 10.7:** The LOD of elements in graphite at the presence of 5 % CNT additives and without additives and relative standard deviation ($S_r$) of elements in the presence of additives ($n = 10$, $p = 0.95$).

| Element | LOD % mass | | $S_r$ |
|---|---|---|---|
| | Without additives | With additives | |
| Al | $2 \times 10^{-4}$ | $5 \times 10^{-5}$ | 0.18 |
| Ba | $1 \times 10^{-3}$ | $2 \times 10^{-4}$ | 0.15 |
| Bi | $1 \times 10^{-4}$ | $5 \times 10^{-5}$ | 0.15 |
| Ca | $2 \times 10^{-4}$ | $1 \times 10^{-4}$ | 0.18 |
| Cd | $2 \times 10^{-4}$ | $5 \times 10^{-5}$ | 0.12 |
| Cr | $2 \times 10^{-4}$ | $1 \times 10^{-4}$ | 0.15 |
| Hf | $1 \times 10^{-3}$ | $2 \times 10^{-4}$ | 0.18 |
| Nb | $1 \times 10^{-3}$ | $3 \times 10^{-4}$ | 0.17 |
| Zr | $5 \times 10^{-3}$ | $1 \times 10^{-3}$ | 0.17 |

## 10.5 Conclusions

As sorbents in analytical chemistry, CNTs proved highly promising material for extraction and preconcentration of metal ions, radioisotopes, and organic substances owing to high sorption capacity, completeness of analyte extraction–reextraction stages, and easily lend themselves to modification. A comparison of CNTs sorption parameters with other sorbents revealed their priority in sorption efficiency almost in all the cases. The mechanisms of CNTs interaction with a sorbate play an important role and should be taken into account. In the case of ion-exchange mechanism (sorption of metals from aqueous solutions), the use of covalently modified CNTs is more effective than other sorbents. In this case, a simple oxidative functionalization to introduce oxygen-containing groups is often sufficient to avoid additional modification with complex organic fragments. Attention should also be given to another important factor: the dependence of CNTs properties both on the reagent nature (in the case of functionalization) and on the synthesis conditions. For example, synthesis of multiwalled nanotubes by catalytic decomposition of ethanol vapors on an Ni catalyst at lower temperatures gives a material of chaotic morphology which sorption and dispersion properties suit best for application in chromatography. For the noncovalent mechanism of CNTs interaction with a sorbate, a nonmodified material grown as films on quartz substrates by synthesis from the gas phase was found preferable. In view of extremely high rate of sorption–desorption processes, this property can be used to create piezosensors. A much higher sorption capacity and resolution in chromatography was found for sorption of some toxic aromatic organic substances as compared with traditional sorbents (carbons of various origins and carbopack).

This review covers the papers on CNTs as sorbents published to 2012. In recent years, including the year of 2016, interest in CNTs has not diminished, as evidenced by the large number of published reviews and original papers covering various aspects of their synthesis, modification, properties, and sorption characteristics in relation to different classes of substances [191–216]. As is noted in the review, the CVD technique remains one of the preferred methods of CNT synthesis. It has been untiredly employed by researchers to produce CNTs of various crystallographic configurations. It should be noted that in recent years more attention has been paid to the structure and morphology of CNTs depending on the CVD synthesis conditions (carbon source, temperature, and catalyst) which is reflected in the review of Shah and Tali [191]. The role of these parameters in synthesis of CNTs is explained keeping the up-to-date literature in view. Recent understandings with regard to preferential growth of CNTs are also discussed. This literature review showed that carbon diffusibility and carbon solubility of any catalyst are two important factors in determining the CNTs nucleation and growth.

The review by Pyrzynska [192] presents recent applications of carbon-based nanomaterials in sample-preparation procedures for sample clean-up and preconcentration of the analytes. Solid-phase extraction (SPE), microextraction (MSPE), and filtration techniques reported are reviewed and discussed.

The review by Liang et al. [193] is focussed on the detailed description of different CNTs-based extraction modes such as SPE and MSPE (including fiber SPME, electrosorption-enhanced SPME, stir bar sorptive extraction, etc.) Compared with other new sorbents, CNTs have found a growing application field in SPE procedures, but few applications of CNTs were commercialized. The reasons are that CNTs are not fabricated at a large scale, and their characterization is not standardized. CNT-based SPE and SMPE techniques are promising for various sample pretreatments. Further development of SPE technologies for sample pretresatment as seen by the authors of the review is in increasing the selectivity of functionalized CNTs, especially for the extraction of organic compounds, as well as in the improvement and optimization of other extraction modes, for example on-line, for automation and miniaturization of separation processes. Another important motivation for further research related to the expanding use of CNTs and their release into the environment, is, according to the authors, the control over the content of CNTs in various environmental objects. As a nanomaterial, CNTs long-term impact on health and environment should be studied. Therefore, sensitive analytical methods in which CNTs would will become the target analyte must be developed. The importance of this aspect, connected with the methods of characterization of CNTs themselves, is also discussed in the review by Herrero-Latorre et al. [194]. There, the authors draw attention to the fact that the determination of CNTs in environmental and biological samples in different environmental phases, along with their mobility, biotransformation, and degradation, persistence and hazardous effects, need to be studied because this area has not been investigated to date. In principle, CNTs in various samples of the environment (water, soil, air), as well as in food and biological materials, can be determined by the same methods that are used to characterize them: TEM, SEM, AFM, ICP-MS, NAA, UV-vis-NIR, and photoluminescence spectroscopy. However, the issue of determination of CNTs differs from that of their characterization. In the case of developing the methods to determine CNTs, the issues of sampling and sample preparation of increasing selectivity, sensitivity, and reliability of determinations play a primary role. A serious obstacle in the development of quantitative methods to determine CNTs is also the absence of standard samples characterized by purity, morphology, chirality, etc. In the last years, a number of interesting studies were published [194–200] that are focussed on CNTs as analytical targets in real samples. The need for further research on possible toxicity of CNTs and CNTs-related materials is mentioned in the review by Srivastava [201]. The review presents the sorption data published in a large number of studies, and shows that the sorption capacities of metal ions to different CNTs roughly follow the order: $Pb^{2+} > Ni^{2+} > Zn^{2+} > Cu^{2+} > Cd^{2+}$.

Quite number of works pertains to the study of the sorption properties of CNTs and the factors that affect these properties with respect to various classes of organic and inorganic substances [202–210]. Among them are the articles by Mubarak et al. [209–210] dealing with the kinetics of sorption processes involving CNTs. These studies are of interest because they corroborate to the known notions that one of the advantages of CNTs is the rapid sorption kinetics.

Recent applications of CNTs (from 2010 to early 2014) as sorbents in analytical chemistry are also considered in the review by Socas-Rodríguez et al. [211]. In this review, the advantages and disadvantages of CNTs as sorbents in various types of chromatography (conventional SPE, SPME, matrix solid-phase dispersion (MSPD), membrane-based microextractions, etc.) are detailed and discussed. Note is taken of large number of positive results obtained when CNTs fibers are used SPMe. Over the past few years, the use of porous polymer membranes in combination with CNTs has also increased significantly. On the contrary, the applications of CNTs in MSPD and SBSE are few.

The review pays considerable attention to the prospects of using CNTs composites with magnetic particles. Note that the above approach has been developing quite intensively in recent years, judging by the number of original works and reviews [211–216]. The essence of the method consists in the sorption of an analyte on a magnetic sorbent, followed by phase separation with the help of a permanent magnet. This technology significantly simplifies the separation process, allowing one to avoid abandon long filtering and centrifugation operations. Although magnetic particles, mainly magnetite, stabilized and modified in various ways, have been used for a long time in the separation processes, recent decades have seen a surge in work in this direction. It should be noted that there is a certain terminological feature associated with the synthesis and modification of these particles. In some papers, emphasis is placed on the modification of magnetite by various sorbents, including functionalized CNTs [211], while in other articles modifications of CNTs by magnetite are also considered. Since the nature of the particles interaction is the same in both cases, mainly by noncovalent interaction, apparently it is more correct to regard it as the synthesis of composites containing magnetic particles as sorbents. Further studies are also needed to determine the contribution of magnetic particles to the overall sorption efficiency. Therefore, the contribution of magnetic particles to the overal sorption efficiency requires further investigation. For example, Masotti and Caporali [211] reported a significant sorption contribution of magnetic particles, while Herrera-Herrera et al. [216] observed a decrease in the sorption efficiency (in the latter case) when comparing magnetic and nonmagnetic CNTs in DSPE.

Because studies on various aspects of CNTs are often related to different fields of science, it is important to formulate general principles of their fundamental and applied investigation. The absence of generally accepted normative, terminological, and metrological requirements to CNTs parameters, as well as the absence of reference samples of CNTs often hampers the understanding of the subject and makes it difficult to quantify them in different objects. For example, there is no distinct definition of the term “purity” relatively to CNTs. The knowledge on the sorption mechanisms in the inner space of nanotubes also expects its adaptation to analytical chemistry.

Since the fields of application of CNTs are constantly expanding, unpredictable applications of their sorption properties can be expected in the near future.

## References


[1] Zolotov Y, Tsysin G, Dmitrienko S, Morosanova E. Sorption preconcentration of microcomponents from solutions. *Application in Chemical Analysis*. Moscow, Russia, Nauka, 2007. (Original source in Russian).

[2] Fontanals N, Marcé R, Borrull F. Overview of the novel sorbents available in solid-phase extraction to improve the capacity and selectivity of analytical determinations. *Trends Anal Chem* 2005, 24, N3, 394–406.

[3] Poole C. New trends in solid-phase extraction. *Trends Anal Chem* 2003, 22, 362–73.

[4] Zolotov Y, Tsysin G, Morosanova E, Dmitrienko S. Sorption preconcentration of microcomponents for chemical analysis. *Russ Chem Rev*. 2005, 74, N1, 37–60.

[5] Thurman E, Mills M. *Solid Phase Extraction – Principles and Practice*. New York, Wiley-Interscience, 1998.

[6] Valcarcel M, Simonet BM, Cardenas S, Suarez B. Present and future applications of carbon nanotubes to analytical science. *Anal Bioanal Chem* 2005, 382, 1783–90.

[7] Valcarcel M, Cardenas S, Simonet BM. Role of carbon nanotubes in analytical science *Anal Chem* 2007, 79, 4788–94.

[8] Valcárcel M, Cárdenas S, Simonet B, Moliner-Martínez Y, Lucena R. Carbon nanostructures as sorbent materials in analytical processes. *Trends Anal Chem* 2008, 27, 34–43.

[9] Merkoci A. Carbon nanotubes in analytical sciences. *Microchim Acta* 2006, 152, 157–72.

[10] Trojanowicz M, Analytical applications of carbon nanotubes. *Trends Anal Chem* 2006, 25, 480–89.

[11] Iijima SY. Helical microtubules of graphite carbon. *Nature* 1991, 354, 56–58.

[12] Ebbesen T. *Carbon Nanotubes. Preparation and Properties*. New York, USA, CRC Press, 1996.

[13] Dresselhaus M, Eklund P. *Science of Fullerenes and Carbon Nanotubes*. San Diego, CA, USA, Academic Press, 1996.

[14] Harris PJF. *Carbon Nanotubes and Related Structures. New Materials Twenty-first Century*. Cambridge, University Press, 1999.

[15] Yeletsky AV. Sorption properties of carbon nanostructures. *Physics-Uspekhi* 2004, 174, №11, 1191–231.

[16] Rakov E. *Nanotubes and Fullerenes*. Moscow, Russia, Logos, 2006. (Original source in Russian).

[17] Rakov E. The chemistry and application of carbon nanotubes. *Russ Chem Rev* 2001, 70, N10, 827–63.

[18] Rakov E. Methods for preparation of carbon nanotubes. *Russ Chem Rev* 2000, 69, 35–52.

[19] Maruyama S, Kojima R, Miyauchi Y, Chiashi S, Kohno M. Low-temperature synthesis of high-purity single-walled carbon nanotubes from alcohol. *Chem Phys Lett* 2002, 360, 229–34.

[20] Ped'kin A, Kipin V, Malyarevich L. Synthesis of fibrous carbon nanomaterials from ethanol vapor on a nickel catalyst. *Inorg Mater* 2005, 42, N3, 242–45.

[21] Huang L, Cui X, White B, O`Brien S. Long and oriented single-walled carbon nanotubes grown by ethanol chemical vapor deposition. *J Phys Chem B* 2004, 108, 16451–56.

[22] Li Y, Zhang L, Zhong X, Windle A. Synthesis of high purity single-walled carbon nanotubes from ethanol by catalytic gas flow CVD reactions. *Nanotechnology* 2007, 18, 225604.

[23] Gruneis A, Rummeli M, Kramberger C, et al. High quality double wall carbon nanotubes with a defined diameter distribution by chemical vapor deposition from alcohol. *Carbon* 2006, 44, 3177–82.

[24] Wienecke M, Bunescu M-C, Deistung K, Fedtke P, Borchartd E. MWCNT coatings obtained by thermal CVD using ethanol decomposition. *Carbon* 2006, 44, 718–23.

[25] Xu B, Li T, Liu X, Lin X, Li J. Growth of well-aligned carbon nanotubes in a plasma system using ferrocene solution in ethanol. *Thin Solid Films* 2007, 515, 6726–29.

[26] Ansaldo A, Haluska M, Cech J, et al. A study of the effect of different catalysts for the efficient CVD growth of carbon nanotubes on silicon substrates. *Phys E* 2007, 37, 6–10.
[27] Wasthi K, Srivastava A, Srivastava O. Synthesis of carbon nanotubes. *J Nanosci Nanotechnol* 2005, 5, 1616–36.
[28] Meyyappan M. Carbon nanotube growth by chemical vapor deposition. In: *Encyclopedia of Nanoscience and Nanotechnology*, ed. Nalwa H, NY, USA, American Science Publishers 2004, 1, 581–8.
[29] Kim H, Sigmund W. Modification of carbon nanotubes. In: *Encyclopedia ofNanoscience and Nanotechnology* ed. Nalwa H, NY, USA, American Science Publishers 2004, 5, 619–29.
[30] Ma P-C, Siddiqui N, Marom G, Kim J-K. Dispersion and functionalization of carbon nanotubes for polymer-based nanocomposites. *Compos Part A* 2010, 41, 1345–67.
[31] Khabashesku E. Covalent functionalization of carbon nanotubes: synthesis, properties and applications of fluorinated derivatives. *Adv Chem* 2011, 80, 739–60.
[32] Esumi K, Ishigami M, Nakajima A, Sawada K, Honda H. Chemical treatment of carbon nanotubes. *Carbon* 1996, 34, 279–81.
[33] Banerjee S, Hemraj-Benny T, Wong S. Covalent surface chemistry of single-walled carbon nanotubes. *Adv Mater* 2005, 17, 17–29.
[34] Pan B, Cui D, Gao F, He R. Growth of multi-amine terminated poly(amidoamine) dendrimers on the surface of carbon nanotubes. *Nanotechnology* 2006, 17, 2483–9.
[35] Hill D, Lin Y, Rao A, Allard L, Sun Y. Functionalization of carbon nanotubes with polystyrene. *Macromolecules* 2002, 35, 9466–71.
[36] Grossiord N, Loos J, Regev O, Koning C. Toolbox for dispersing carbon nanotubes into polymers to get conductive nanocomposites. *Chem Mater* 2006, 18, 1089–99.
[37] Vaisman L, Marom G, Wagner H. Dispersions of surface modified carbon nanotubes in water-soluble and water insoluble polymers. *Adv Funct Mater* 2006, 6, 357–363.
[38] O'Connell M, Boul P, Ericson L, et al. Reversible water-solubilization of single-walled carbon nanotubes by polymer wrapping. *Chem Phys Lett* 2001, 342, 265–71.
[39] Dalton A, Stephan C, Coleman J, et al. Selective interaction of a semiconjugated organic polymer with single-wall nanotubes. *J Phys Chem B* 2000, 104, 10012–16.
[40] Carrillo A, Swartz J, Gamba J, et al. Noncovalent functionalization of graphite and carbon nanotubes with polymer multilayers and gold nanoparticles. *Nano Lett* 2003, 3, 1437–40.
[41] Mittal V. *Advances in Surface Functionalization of Carbon Nanotubes in Polymer Nanocomposites*. New York, USA, Nova Science Hauppauge, 2009.
[42] Vaisman L, Wagner H, Marom G. The role of surfactants in dispersion of carbon nanotubes. *Adv Colloid Interface Sci* 2006, 128, 37–46.
[43] Hirsch A. Functionalization of single-walled carbon nanotubes. *Angew Chem Int Ed* 2002, 41, 1853–59.
[44] Georgakilas V, Gournis D, Tzitzios V, Pasquato L, Guldi D, Prato M. Decorating carbon nanotubes with metal or semiconductor nanoparticles. *J Mater Chem* 2007, 17, 2679–94.
[45] Nepal D, Geckeler K. Interactions of carbon nanotubes with biomolecules advances and challenges. In: *Advanced Nanomaterials,* eds. Geckeler K, Nishide H. Weinheim, Germany, Wiley-VCH, 2010, 715–30.
[46] Wepasnick K, Smith B, Schrote H, Diegelmann S, Fairbrother D. Surface and structural characterization of multi-walled carbon nanotubes following different oxidative treatments. *Carbon* 2011, 49, 24–36.
[47] Chen R, Zhang Y, Wang D, Dai H. Noncovalent sidewall functionalization of single-walled carbon nanotubes for protein immobilization. *J Am Chem Soc* 2001, 123, 3838–39.
[48] Langley L, Fairbrother D. Effect of wet chemical treatments on the distribution of surface oxides on carbonaceous materials. *Carbon* 2007, 45, 47–54.
[49] Tasis D, Tagmatarchis N, Bianco A, Prato M. Chemistry of carbon nanotubes. *Chem Rev* 2006, 106, 1105–36.

[50] Bahr J, Tour J. Covalent chemistry of single-wall carbon nanotubes. *J Mater Chem* 2002, 12, 1952–58.
[51] Krueger A, Monthioux M. *Strained Hydrocarbon*. ed. Dodziuk H. Weinheim, Germany, Wiley-VCH, 2009.
[52] Smith B, Wepasnick K, Schrote K, Cho H, Ball W, Fairbrother D. Influence of surface oxides on the colloidal stability of multi-walled carbon nanotubes: a structure–property relationship. *Langmuir* 2009, 25, 9767–76.
[53] Zhang Y, Bai Y, Yan B. Functionalized carbon nanotubes for potential medicinal applications. *Drug Discov Today* 2010, 15, 428–35.
[54] Vazquez E, Plato M. Functionalization of carbon nanotubes for applications in materials science and nanomedicine. *Pure Appl Chem* 2010, 82, 853–61.
[55] Meng L, Fu C, Lu Q. Advanced technology for functionalization of carbon nanotubes. *Prog Nat Sci* 2009, 19, 801–61.
[56] Langley L, Villanueva D, Fairbrother D. Quantification of surface oxides on carbonaceous materials. *Chem Mater* 2006, 18, 169–79.
[57] Povstugar V, Mikhailova S, Shakov A. Chemical derivatization techniques in the determination of functional groups by x-ray photoelectron spectroscopy. *J Anal Chem* 2000, 55, 455–67.
[58] Dementev N, Feng X, Borguet E. Fluorescence labeling and quantification of oxygen-containing functionalities on the surface of single-walled carbon nanotubes. *Langmuir* 2009, 25, N13, 7573–7.
[59] Masheter A, Xiao L, Wildgoose G, Crossley A, Jones J, Compton R. Voltammetric and x-ray photoelectron spectroscopic fingerprinting of carboxylic acid groups on the surface of carbon nanotubes via derivatisation with arylnitro labels. *J Mater Chem* 2007, 17, 3515–24.
[60] Singh S, Kruse P. Carbon nanotube surface science. *Int J Nanotechnol* 2008, 5, 900–29.
[61] Herrero M, Plato M. Recent advances in the covalent functionalization of carbon nanotubes. *Mol Cryst Liq Cryst* 2008, 483, 21–32.
[62] Lynam C, Minett A, Habas S, Gambhir S, Officer D, Wallace G. Functionalizing carbon nanotubes. *Int J Nanotechnol* 2008, 5, 331–51.
[63] Kharisov B, Kharissova O, Gutierrez H, Mendez U. Recent advances on the soluble carbon nanotubes. *Ind Eng Chem Res* 2009, 48, 572–90.
[64] Mercuri F, Sgamellotti A. Theoretical investigations on the functionalization of carbon nanotubes. *Inorg Chim Acta* 2007, 360, 785–93.
[65] Rosca I, Watari F, Uo M, Akasaka T. Oxidation of multiwalled carbon nanotubes by nitric acid. *Carbon* 2005, 43, 3124–31.
[66] Datsyuk V, Kalyva M, Papagelis K, et al. Chemical oxidation of multiwalled carbon nanotubes. *Carbon* 2008, 46, 833–40.
[67] Avile S F, Cauich-Rodri guez J, Moo-Tah L, May-Pat A, Vargas-Coronado R. Evaluation of mild acid oxidation treatments for mwcnt functionalization. *Carbon* 2009, 47, 2970–5.
[68] Shieh Y, Liu G, Wu H, Lee C. Effects of polarity and ph on the solubility of acid-treated carbon nanotubes in different media. *Carbon* 2007, 45, 1880–90.
[69] Belin T, Epron F. Characterization methods of carbon nanotubes: a review. *Mater Sci Eng B* 2005, 119, 105–18.
[70] Sattler K. Scanning tunneling microscopy of carbon nanotubes and nanocones. *Carbon* 1995, 33, 915–20.
[71] Puchý V, Tatarko P, Dusza J, Morgie J, Bast Z, Mihály J. Characterization of carbon nanofibers by sem, tem, esca and raman spectroscopy. *Kovove Mater* 2010, 48, 379–86.
[72] Wepasnick K, Smith B, Bitter J, Fairbrother D. Chemical and structural characterization of carbon nanotube surfaces. *Anal Bioanal Chem* 2010, 396, 1003–14.
[73] Gommes C, Blacher S, Dupont-Pavlovsky N, et al. Comparison of different methods for characterizing multi-walled carbon nanotubes. *Colloids Surf A Phys Eng Aspects* 2004, 241, 155–64.

[74] Branca C, Frusteri F, Magazu V, Mangione A. Characterization of carbon nanotubes by tem and infrared spectroscopy. *J Phys Chem B* 2004, 108, 3469–73.
[75] Burian A, Koloczk J, Dore J, Hannon A, Nagy J, Fonseca A. Radial distribution function analysis of spatial atomic correlations in carbon nanotubes. *Diam Relat Mater* 2004, 13, 1261–65.
[76] Cao A, Xu C, Liang J, Wu D, Wei B. X-ray diffraction characterization on the alignment degree of carbon nanotubes. *Chem Phys Lett* 2001, 344, 13–17.
[77] Kingston C, Simard B. Fabrication of carbon nanotubes. *Anal Lett* 2003, 36, 3119–45.
[78] Grazhulene S, Red'kin N, Telegin G, Bazhenov A, Fursova T. Adsorption properties of carbon nanotubes depending on the temperature of their synthesis and subsequent treatment. *J Anal Chem* 2010, 65, 682–9.
[79] Arepalli S, Nikolaev P, Gorelik O, et al. Protocol for the characterization of single-wall carbon nanotube material quality. *Carbon* 2004, 42, 1783–91.
[80] Dai H. Nanotube growth and characterization. *Appl Phys* 2001, 80, 29–53.
[81] Hadjiev V, Iliev M, Arepalli S, Nikolaev P, Files B. Raman scattering test of single-wall carbon nanotube composites. *Appl Phys Lett* 2001, 78, 3193–6.
[82] Osswald S, Havel M, Gogotsi Y. Monitoring oxidation of multiwalled carbon nanotubes by raman spectroscopy. *J Raman Spectrosc* 2007, 38, 728–36.
[83] Yangjun X, Dementev N, Borguet E. Chemical labeling for quantitative characterization of surface chemistry. *Solid State Mater Sci* 2007, 11, 86–91.
[84] Bazhenov A, Fursova T, Grazhulene S, Red'kin A, Telegin G. Sorption of metal ions on multi-walled carbon nanotubes. *Fuller Nanotub Carbon Nanostruct* 2010, 18, 564–8.
[85] Mawhinney D, Naumenko V, Kuznetsova A, Yates JrJ, Liu J, Smalley R. Surface defect site density on single walled carbon nanotubes. *Chem Phys Lett* 2000, 324, 213–6.
[86] Boehm HP. Surface oxides on carbon and their analysis a critical assessment. *Carbon* 2002, 40, 145–9.
[87] Hu H, Bhowmik P, Zhao B, Hamon M, Itkis M, Haddon R. Determination of the acidic sites of purified single-walled carbon nanotubes by acid–base titration. *Chem Phys Lett* 2001, 345, 25–8.
[88] Grazhulene S, Red'kin A, Telegin G, Zolotareva N. Study of carbon nanomaterials as potential sorbents to concentrate admixtures in the atomic spectroscopy analysis methods. *Inorg Mater* 2009, 45, 1559–63.
[89] Hou P, Liu C, Cheng H. Purification of carbon nanotubes. *Carbon* 2008, 46, 2003–25.
[90] Rao G, Lu C, Su F. Sorption of divalent metal ions from aqueous solution by carbon nanotubes. *Sep Purif Technol* 2007, 58, 224–31.
[91] Stafiej A, Pyrzynska K. Adsorption of heavy metal ions with carbon nanotubes. *Sep Purif Technol* 2007, 58, 49–52.
[92] Li Y, Ding J, Luan Z, et al. Competitive adsorption of pb, cu and cd ions from aqueous solutions by multiwalled carbon nanotubes. *Carbon* 2003, 41, 2787–92.
[93] Tofighy M, Mohammadi T. Adsorption of divalent heavy metal ions from water using carbon nanotube sheets. *J Hazard Mater* 2011, 185, 140–7.
[94] Li Y, Wang S, Wei J, et al. Lead adsorption on carbon nanotubes. *Chem Phys Lett* 2002, 357, 263–6.
[95] Li Y, Zhu Y, Zhao Y, Wu D, Luan Z. Different morphologies of carbon nanotubes effect on the lead removal from aqueous solution. *Diamond Relat Mater* 2006, 15, 90–4.
[96] Li Y, Di Z, Ding J, Wu D, Luan Z, Zhu Y. Adsorption thermodynamic, kinetic and desorption studies of $Pb^{2+}$ on carbon nanotubes. *Water Res* 2005, 39, 605–14.
[97] Shao D, Ren X, Hu J, Chen Y, Wang X. Preconcentration of $Pb^{2+}$ from aqueous solution using poly(acrylamide) and poly(n,n-dimethylacrylamide) grafted multiwalled carbon nanotubes. *Colloids Surf A* 2010, 360, 74–84.
[98] Wang H, Zhou A, Peng F, Yu H, Yang J. Mechanism study on adsorption of acidified multiwalled carbon nanotubes to Pb(II). *J Colloid Interface Sci* 2007, 316, 277–83.

[99] Li Y, Wang S, Luan Z, Ding J, Xu C, Wu D. Adsorption of Cadmium(II) from aqueous solution by surface oxidized carbon nanotubes. *Carbon* 2003, 41, 1057–62.
[100] Lu C, Chiu H. Adsorption of Zinc(II) from water with purified carbon nanotubes. *Chem Eng Sci* 2006, 61, 1138–45.
[101] Cho H, Wepasnick K, Smith B, Bangash F, Fairbrother D, Ball W. Sorption of aqueous Zn(II) and Cd(II) by multiwalled carbon nanotubes the relative roles of oxygen-containing functional groups and graphenic carbon. *Langmuir* 2010, 26, 967–81.
[102] Lu C, Chiu H, Liu C. Removal of Zinc(II) from aqueous solution by purified carbon nanotubes: kinetics and equilibrium studies. *Ind Eng Chem Res* 2006, 45, 2850–5.
[103] Leyva R, Bernal J, Mendoza B, Fuentes R, Guerrero C. Adsorption of Zinc(II) from an aqueous solution onto activated carbon. *J Hazard Mater* 2002, B90, 27–38.
[104] Chen C, Wang X. Adsorption of Ni(II) from aqueous solution using oxidized multiwall carbon nanotubes. *Ind Eng Chem Res* 2006, 45, 9144–9.
[105] Lu C, Liu C. Removal of Nickel(II) from aqueous solution by carbon nanotubes. *J Chem Technol Biotechnol* 2006, 81, 1932–40.
[106] Agnihotri S, Mota J, Rostam-Abadi M, Rood M. Theoretical and experimental investigation of morphology and temperature effects on adsorption of organic vapors in single-walled carbon nanotubes. *J Phys Chem B* 2006, 110, 7640–7.
[107] Grazhulene S, Red'kin A, Telegin G. Study of correlations between the physico-chemical properties of carbon nanotubes and the type of catalyst used for their synthesis. *J Anal Chem* 2012, 67, 423–8.
[108] Suarez B, Simonet BM, Gardenas S, Valcarcel M. Surfactant-coated single-walled carbon nanotubes as a novel pseudostationary phase in capillary EKC. *Electrophoresis* 2007, 28, 1714–22.
[109] Stafiej A, Pyrzynska K. Solid phase extraction of metal ions using carbon nanotubes. *Microchem J* 2008, 89, 29–33.
[110] Pan B, Xing B. Adsorption mechanisms of organic chemicals on carbon nanotubes. *Environ Sci Technol* 2008, 42, 9005–13.
[111] Liu G, Wang J, Zhu Y, Zhang X. Application of multiwalled carbon nanotubes as a solid-phase extraction sorbent for chlorobenzenes. *Anal Lett* 2004, 37, 3085–3104.
[112] Agnihotri S, Rood M, Rostam-Abadi M. Adsorption equilibrium of organic vapors on single-walled carbon nanotubes. *Carbon* 2005, 43, 2379–88.
[113] Pyrzynska K, Stafiej A, Biesaga M. Sorption behavior of acidic herbicides on carbon nanotubes. *Microchim Acta* 2007, 159, 293–8.
[114] Su F, Lu C. Adsorption kinetics, thermodynamics and desorption of natural dissolved organic matter by multiwalled carbon nanotubes. *J Environ Sci Health Part A* 2007, 42, 1543–52.
[115] Wang S, Liu X, Gong W, Nie W, Gao B, Yue Q. Adsorption of fulvic acids from aqueous solutions by carbon nanotubes. *J Chem Technol Biotechnol* 2007, 82, 698–704.
[116] Lu C, Chung Y, Chang K. Adsorption thermodynamic and kinetic studies oftrihalomethanes on multiwalled carbon nanotubes. *J Hazard Mater* 2006, 138, 304–10.
[117] Hilding J, Grulke E, Sinnott S, Qian D, Andrews R, Jagtoyen M. Sorption of butane on carbon multiwall nanotubes at room temperature. *Langmuir* 2001,17, 7540–4.
[118] Yan X, Shi B, Lu J, Feng C, Wang D, Tang H. Adsorption and desorption of atrazine on carbon nanotubes. *J Colloid Interface Sci* 2008, 321, 30–8.
[119] Yang K, Zhu L, Xing B. Adsorption of polycyclic aromatic hydrocarbons by carbon nanomaterials. *Environ Sci Technol* 2006, 40, 1855–61.
[120] Shih Yang-hsin, Li Mei-syue. Adsorption of selected volatile organic vapors on multiwall carbon nanotubes. *J Hazard Mater* 2008, 154, 21–8.
[121] Long R, Yang R. Carbon nanotubes as superior sorbent for dioxin removal. *J Am Chem Soc* 2001, 123, 2058–9.

[122] Pyrzynska K. Carbon nanotubes as a new solid-phase extraction material for removal and enrichment of organic pollutants in water. *Sep Purif Rev* 2008, 37, 375–92.
[123] Li Q,Yuan D-X. Evaluation of multi-walled carbon nanotubes as gas chromatographic column packing. *J Chromatogr A* 2003, 1003, 203–9.
[124] Li Q, Yuan D-X, Lin Q-M. Evaluation of multi-walled carbon nanotubes as an adsorbent for trapping volatile organic compounds from environmental samples. *J Chromatogr A* 2004, 1026, 283–8.
[125] Peng X, Li Y, Luan Z, et al. Adsorption of 1,2 dichlorobenzene from water to carbon nanotubes. *Chem Phys Lett* 2003, 376, 154–8.
[126] Liang G, Kee L. Development of multiwalled carbon nanotubes based micro-solid-phase extraction for the determination of trace levels of sixteen polycyclic aromatic hydrocarbons in environmental water samples. *J Chromatog A* 2011, 1218, 9321–7.
[127] Lu C, Su F, Hu S. Surface modification of carbon nanotubes for enhancing BTEX adsorption from aqueous solutions. *Appl Surf Sci* 2008, 254, 7035–41.
[128] Ren X, Chen C, Nagatsu M, Wang X. Carbon nanotubes as adsorbents in environmental pollution management: a review. *Chem Eng J* 2011, 170, 395–410.
[129] Kondratyuk P, Yates JT Jr. Molecular views of physical adsorption inside and outside of single-wall carbon manotubes. *Acc Chem Res* 2007, 40, 995–1004.
[130] Vidic R, Tessmer C, Uranowski L. Impact of surface properties of activated carbon on oxidative coupling of phenolic compounds. *Carbon* 1997, 35, 1349–59.
[131] Pyrzynska K, Bystrzejewski M. Comparative study of heavy metal ions sorption onto activated carbon, carbon nanotubes, and carbon-encapsulated magnetic nanoparticle. *J Colloid Surf A* 2010, 362, 102–9.
[132] El-Sheikh A. Effect of oxidation of activated carbon on its enrichment efficiency of metal ions: comparison with oxidized and non-oxidized multi-walled carbon nanotubes. *Talanta* 2008, 75, 127–34.
[133] Bystrzejewski M, Pyrzynska K, Huczko A, Lange H. Carbon-encapsulated magnetic nanoparticles as separable and mobile sorbents of heavy metal ions from aqueous solutions. *Carbon* 2009, 47, 1189–1206.
[134] Bystrzejewski M, Pyrzynska K. Kinetics of Copper ions sorption onto activated carbon, carbon nanotubes and carbon-encapsulated magnetic nanoparticles. *J Colloid Surf A* 2011, 377, 402–8.
[135] Chen C, Hu J, Shao D, Li J, Wang X. Adsorption behavior of multiwall carbon nanotube/iron oxide magnetic composites for Ni(II) and Sr(II). *J Hazard Mater* 2009, 164, 923–8.
[136] Velickovica Z, Vukovic G, Marinkovic A, Moldovan M, Peric-Grujic A, Uskokovic P, et al. Adsorption of arsenate on Iron(III) oxide coated ethylenediamine functionalized multiwall carbon nanotubes. *Chem Eng J* 2012, 181–182, 174–81.
[137] Gupta V, Agarwal Sh, Saleh T. Synthesis and characterization of alumina-coated carbon nanotubes and their application for lead removal. *J Hazard Mater* 2011, 185, 17–23.
[138] Kuang Q, Li S, Xie Z-X, et al. Controllable fabrication of $SnO_2$-coated multiwalled carbon nanotubes by chemical vapor deposition. *Carbon* 2006, 44, 1166–72.
[139] Huang Sh, Rapid removal of heavy metal cations and anions from aqueous solutions by an amino-functionalized magnetic nano-adsorbent. *J Hazard Mater* 2009, 163, 174–9.
[140] Chen C, Wang X, Nagatsu M. Europium adsorption on multiwall carbon nanotube/iron oxide magnetic composite in the presence of polyacrylic acid. *Environ Sci Technol* 2009, 43, 2362–7.
[141] Zhou Q., Wang W, Xiao J, et al. Comparison of the enrichment efficiency of multiwalled carbon nanotubes, $C_{18}$ silica, and activated carbon as the adsorbents for the solid phase extraction of atrazine and simazine in water samples. *J Microchim Acta* 2006, 152, 215–24.
[142] Lu C, Liu C, Rao G. Comparisons of sorbent cost for the removal of $Ni^{2+}$ from aqueous solution by carbon nanotubes and granular activated carbon. *J Hazard Mater* 2008, 151, 239–46.

[143] Panteleev G, Tsyzin G, Formanovskiy A, Starshinova N, Sedykh E, Kuzmin N. Sorption-atomic-emission (inductively coupled plasma) determination of metals in highly mineralized natural waters. *J Anal Chem* 1991, 46, 355–60.
[144] El-Sheikh A, Sweileh J. Recent applications of carbon nanotubes in solid phase extraction and preconcentration: a review. *Jordan J Chem* 2011, 6, 1–16.
[145] Pyrzynska K. Carbon nanostructures for separation, preconcentration and speciation of metal ions. *Trends Anal Chem* 2010, 29, 718–27.
[146] Soylak M, Ercan O. Selective separation and preconcentration of Copper(II) in environmental samples by the solid phase extraction on multi-walled carbon nanotubes. *J Hazard Mater* 2009, 168, 1527–31.
[147] Liang P, Ding Q, Song F. Application of multiwalled carbon nanotubes as solid phase extraction sorbent for preconcentration of trace copper in water samples. *J Sep Sci* 2005, 28, 2339–43.
[148] Stafiej A, Pyrzynska K. Solid phase extraction of metal ions using carbon nanotubes. *Microchem J* 2008, 9, 29–33.
[149] Ding Q, Liang P, Song F, Xiang A. Separation and preconcentration of silver ion using multiwalled carbon nanotubes as solid phase extraction sorbent. *Sep Sci Tech* 2006, 41, 2723–32.
[150] Lu C, Chiu H. Adsorption of Zinc (II) from water with purified carbon nanotubes. *Chem Eng Sci* 2006, 61, 1138–45.
[151] Xiao J, Zhou Q, Bai H. Application of multiwalled carbon nanotubes treated by potassium permanganate for determination of trace cadmium prior to flame atomic absorption spectrometry. *J Environ Sci* 2007, 19, 1266–71.
[152] Liang P, Zhao E, Ding Q, Du D. Multiwalled carbon nanotubes microcolumn preconcentration and determination of gold in geological and water samples by flame atomic absorption spectrometry. *Spectrochim Acta B* 2008, 63, 714–7.
[153] Ozcan S, Satirogla N, Soylak M. Column solid phase extraction of Iron(III), Copper(II), Manganese(II) and Lead(II)ions food and water samples on multi-walled carbon nanotubes. *Food Chem Toxicol* 2010, 48, 2401–6.
[154] Liang P, Liu V, Guo L, Zeng J, Lu H. Multiwalled carbon nanotubes as solid-phase extraction adsorbent for the preconcentration of trace metal ions and heir determination by inductively coupled plasma atomic emission spectrometry. *J Anal Atom Spectrom* 2004, 19, 1489–92.
[155] Liang P, Liu Y, Guo L. Determination of trace rare earth elements by inductively coupled plasma atomic emission spectrometry after preconcentration with multiwalled carbon nanotubes. *Spectrochim Acta B* 2005, 60, 125–9.
[156] Chen S, Liu C, Yang M, Lu D, Zhu L, Wang Z. Solid-phase extraction of Cu, Co and Pb on oxidized single-walled carbon nanotubes and their determination by inductively coupled plasma mass spectrometry. *J Hazard Mater* 2009, 170, 247–251.
[157] Souza J, Tarley C. Sorbent separation and enrichment method for cobalt ions determination by graphite furnace atomic absorption spectrometry in water and urine samples using multiwall carbon. *Int J Environ Anal Chem* 2009, 89, 489–502.
[158] Shamspur T, Mostafavi A. Application of modified multiwalled carbon nanotubes as a sorbent for simultaneous separation and preconcentration trace amounts of Au(III) and Mn(II). *J Hazard Mater* 2009, 168, 1548–53.
[159] Ghaseminezhad S, Afzali D, Taher M. Flame atomic absorption spectrometry for the determination of trace amount of rhodium after separation and preconcentration onto modified multiwalled carbon nanotubes as a new solid sorbent. *Talanta* 2009, 80, 168–72.
[160] Afzali D, Jamshidi R, Ghaseminezhad S, Afzali Z. Preconcentration procedure trace amounts of palladium using modified multiwalled carbon nanotubes sorbent prior to flame atomic absorption spectrometry. *Arab J Chem* 2012, 5, 461–6.

[161] Liu Y, Li Y, Yan X. Preparation, characterization, and application of L-cysteine functionalized multiwalled carbon nanotubes as a selective sorbent for separation and preconcentration of heavy metals. *Adv Funct Mater* 2008, 18, 1536–43.
[162] Pacheco P, Smichowski P, Polla G, Martinez L. Solid phase extraction of Co ions using L-tyrosine immobilized on multiwall carbon nanotubes. *Talanta* 2009, 79, 249–53.
[163] Tuzen M, Saygi K, Soylak M. Solid phase extraction of heavy metal ions in environmental samples on multiwalled carbon nanotubes. *J Hazard Mater* 2008, 152, 632–9.
[164] Afzali D, Mostafavi A. Potential of modified multiwalled carbon nanotubes with 1-(2-Pyridylazo)-2-naphtol as a new solid sorbent for the preconcentration of trace amounts of Cobalt(II) ion. *Anal Sci* 2008, 24, 1135–9.
[165] Duran A, Tuzen M, Soylak M. Preconcentration of some trace elements via using ultiwalled carbonnanotubes as solid phase extraction adsorbent. *J Hazard Mater* 2009, 169, 466–71.
[166] Afzali D, Mostafavi A, Etemadi F, Ghazizadeh A. Application of modified multiwalled carbon nanotubes as solid sorbent for separation and preconcentration of trace amounts of manganese ions. *Arab J Chem* 2012, 5, 187–191.
[167] Li L, Huang Y, Wang Y, Wang W. Hemimicelle capped functionalized carbon nanotubes-based nanosized solid-phase extraction of arsenic from environmental water samples. *Anal Chim Acta* 2009, 631, 182–8.
[168] Wang X, Cheng C, Hu W, Ding A, Xu D, Zhou X. Sorption of $^{243}$Am(III) to multiwalled carbon nanotubes. *Environ Sci Technol* 2005, 39, 2856–60.
[169] Myasoedova G, Molochnikova N, Tkachev A, Tugolukov E, Mischenko S, Myasoedov B. Sorption preconcentration of radionuclides carbon nanostructured material "Taunit." *Radiochemistry* 2009, 51, 138–9.
[170] Kulyako Yu, Perevalov S, Malikov D, Vinokurov S, Myasoedov B. Sorption of plutonium in various oxidation states from aqueous solutions to carbon nanomaterial. *Radiochemistry* 2010, 52, 234–7.
[171] Zhao X, Song N, Jia Q, Zhou W. Determination of Cu, Zn, Mn, and Pb by microcolumn packed with multiwalled carbon nanotubes on-line coupled with flame atomic absorption spectrometry. *Microchim Acta* 2009, 166, 329–35.
[172] Tarley C, Barbosa A, Segatelli M, Figueiredo E, Luccas P. Highly improved sensitivity of TS-FF-AAS for Cd(II) determination at ng $L^{-1}$ levels using a simple flow injection minicolumn preconcentration system with multiwall carbon nanotubes. *J Anal Atom Spectrosc* 2006, 21, 1305–13.
[173] Parodi B, Savio M, Martinez L, Gil R, Smichowski P. Study of carbon nanotubes and functionalized-carbon nanotubes as substrates for flow injection solid phase extraction associated to inductively coupled plasma with ultrasonic nebulization. Application to Cd monitoring in solid environmental samples. *Microchem J* 2011, 98, 225–30.
[174] Wu H, Wang X, Liu B, et al. Simultaneous speciation of inorganic arsenic and antimony in water samples by hydride generation-double channel atomic fluorescence spectrometry with on-line solid- phase extraction using single-walled carbon nanotubes micro-column. *Spectrochim Acta B* 2011, 66, 74–80.
[175] Wu H, Wen H, Han B, Du B, Lu J, Tian J. Simple micro-column with multi-walled carbon nanotubes for on-line preconcentration and determination of lead in natural water by hydride generation atomic fluorescence spectrometry. *Microchim Acta* 2009, 166, 41–6.
[176] Barbosa A, Segatelli M, Pereira A, et at. Solid-phase extraction system for Pb(II) ions enrichment based on multiwall carbon nanotubes coupled on-line to flame atomic absorption spectrometry. *Talanta* 2007, 71, 1512–9.
[177] Liang H, Ha D. Multi-walled carbon nanotubes as sorbent for flow injection on-line microcolumn preconcentration coupled with flame atomic absorption spectrometry for determination of cadmium and copper. *Anal Lett* 2006, 39, 2285–95.

[178] Tuzen M, Soylak M. Multiwalled carbon nanotubes for speciation of chromium in environmental samples. *J Hazard Mater* 2007, 147, 219–25.
[179] Chen S, Zhu L, Lu D, Chen X, Zhou X. Separation and chromium speciation by single-wall carbon nanotubes microcolumn and inductively coupled plasma mass spectrometry. *Microchim. Acta* 2010, 169, 123–8.
[180] Hu J, Chen C, Zhu X, Wang X. Removal of chromium from aqueous solution by using oxidized multiwalled carbon nanotubes. *J Hazard Mater* 2009, 162, 1542–50.
[181] Gil R, Goyanes S, Polla G, Smichowski P, Olsinaab R, Martinez L. Application of multi-walled carbon nanotubes as substrate for the on-line preconcentration, speciation and determination of vanadium by ETAAS. *J Anal Atom Spectrom* 2007, 22, 1290–5.
[182] Profumo A, Fagnoni M, Merli D, Quartarone E, Protti S, Dondi D, et al. Multiwalled carbon nanotube chemically modified gold electrode for inorganic As speciation and Bi(III) determination. *Anal Chem* 2006, 78, 4194–8.
[183] Grazhulene S, Zolotareva N, Telegin G, Red'kin A. Atomic spectroscopic methods of analysis of environmental objects using carbon nanotubes for the sorption preconcentration of microimpurities. *Zavodsk Lab Diagnostics Mater* 2012, 78(8), 16–19. (Original source in Russian).
[184] Ermolaeva T, Kalmykova E. *Piezoquartz Immunosensors. Analytical Opportunities and Prospects*. Lipetsk, Russia, Lipetsk State Technical University, 2007. (Original source in Russian)
[185] Kuchmenko T. *Application of the Piezoquartz Micro-weighting Method in Analytical Chemistry*, Voronezh, Russia, Publishing house Voronezh State Technol Acad, 2001. (Original source in Russian)
[186] Shogenov Yu, Kuchmenko T, Grazhulene S, Red'kin A. Quartz crystal microbalance determination of vapors of volatile organic compounds on carbon nanotubes under batch conditions. *J Anal Chem*, 2012, 67, 21–27.
[187] Cadena G, Riu J, Rius F. Gas sensors based on nanostructured materials. *Analyst* 2007, 132, 1083–99.
[188] Li Y, Chen Y, Xiang R, et al. Incorporation of single-wall carbon nanotubes into an organic polymer monolithic stationary phase for HPLC and capillary electrochromatography. *J Anal Chem* 2005, 77, 1398–406.
[189] Zolotareva N, Grazhulene S. The use of carbon nanotubes in dc arc atomic emission analysis as a spectroscopic additives. *Zavodsk Lab Diagnostics Mater* 2013, 79(2), 23–5 (Original source in Russian)
[190] Experiandova L, Belikov K, Himchenko S, Blank T. Once again on the limits of detection and determination. *J Anal Chem* 2010, 65, 229–234.
[191] Shah K, Tali B. Synthesis of carbon nanotubes by catalytic chemical vapour deposition. A review on carbonsources, catalysts and substrates. *Mater Sci Semicond Process* 2016, 41, 67–82.
[192] Pyrzynska K. Use of nanomaterials in sample preparation. *Trends Anal Chem* 2013, 43, 100–8.
[193] Liang X, Liu S, Wang S, Guo Y, Jiang S. Carbon-based sorbents: Carbon nanotubes. *J Chromatogr A* 2014, 1357, 53–67.
[194] Herrero-Latorre C, Álvarez-Méndez J, Barciela-García J, García-Martín S, Peña-Crecente R. Characterization of carbon nanotubes and analytical methods for their determination in environmental and biological samples. *Anal Chim Acta* 2015, 853, 77–94.
[195] López-Lorente A, Simonet B, Valcárcel M. Determination of carboxilic swcnts in river water by microextraction in ionic liquid and determination by raman spectroscopy. *Talanta* 2013, 105, 75–9.
[196] Irin F, Shrestha B, Cañas J, Saed M, Green M. Detection of carbon nanotubes in biological samples through microwave induced-heating. *Carbon* 2012, 50, 4441–9.
[197] Li S, Irin F, Atore F, Green M, Cañas-Carrell J. Determination of multi-walled carbon nanotube bioaccumulation in earthworms measured by microwave-based detection technique. *Sci Total Environ* 2013, 445–446, 9–13.

[198] Doudrik K, Herckes P, Westerhoff P. Detection of carbon nanotubes in environmental matrices using programmed thermal analysis. *Environ Sci Technol* 2012, 46, 2246–53.
[199] Jeong K, Kim K, Jeong S, An K, Lee S, Lee Y. Optical absorption spectroscopy for determining carbon nanotube concentration in solution. *Synth Met* 2007, 157, 570–4.
[200] Plata D, Reddy CM, Gschwend P. Thermogravimetry-mass spectrometry for carbon nanotube detection in complex mixtures. *Environ Sci Technol* 2012, 46, 12254–61.
[201] Srivastava S. Sorption of divalent metal ions from aqueous solution by oxidized carbon nanotubes and nanocages: a review. *Adv Mat Lett* 2013, 4, 2–8.
[202] Wei Y, Li Y, Duan J, Jing C. Sorption of organophosphate esters by carbon nanotubes. *J Hazard Mater* 2014, 273, 53–60.
[203] Tiany, Gao B, Morales V L, Chen H, Wangy, Li H. Removal of sulfamethoxazole and sulfapyridine by carbon nanotubes in fixed-bed columns. *Chemosphere* 2013, 90, 2597–2605.
[204] Takada T, Kurosaki R, KonnoY, Abe S. Interaction of multi-walled carbon nanotubes with water-soluble proteins: effect of sidewall carboxylation. *J Nanosci Nanotechnol* 2014, 14, 3216–20.
[205] Li M, Liu X, Dong F, et al. Simultaneous determination of cyflumetofen and its main metabolite residues in samples of plant and animal origin using multi-walled carbon nanotubes in dispersive solid-phase extraction and ultrahigh performance liquid chromatography-tandem mass spectrometry. *J Chromatogr* 2013, 1300, 95–103.
[206] Tehrani M, Azar P, Namin P, Dehaghi S. Removal of lead ions from wastewater using functionalized multiwalled carbon nanotubes with tris(2-aminoethyl)amine. *J Environ Prot Sci* 2013, 4, 529–36.
[207] Song X-Y, Shi Y-P, Chen J. Carbon nanotubes reinforced hollow fiber solid phase microextraction for determination of strychnine and brucine inurine. *Talanta* 2013, 116, 188–94.
[208] Mubarak N, Sahu J, Abdullah E, Jayakumar N. Microwave assisted mulltiwall carbon nanotubes enhancing Cd(II) adsorption capacity in aqueous media. *Sep Purif Technol* 2014, 43 311–42.
[209] Mubarak N, Alicia R, Abdullah E, Sahu J, Haslija A, Tan J. Statistical optimization and kinetic studies on removal of $Zn^{2+}$ using functionalized carbon nanotubes and magnetic biochar. *J Environ Eng* 2013, 1, 486–95.
[210] Mubarak N, Ruthiraan M, Sahu J, et al. Adsorption and kinetic study on $Sn^{2+}$ removal using modified carbon nanotube and magnetic c-biochar. *Int J Nanosci* 2014, 1350044.
[211] Socas-Rodrígueza B, Herrera-Herrerab AV, Asensio-Ramosc M, Hernández-borges J. recent applications of carbon nanotube sorbents in analytical chemistry. *J Chromatogr* 2014, 1357, 110–46.
[212] Xie L, Jiang R, Zhu F, Liu H, Ouyang G. Application of functionalized magnetic nanoparticles in sample preparation. *Anal Bioanal Chem* 2014, 406, 377–99.
[213] Masotti A, Caporali A. Preparation of magnetic carbon nanotubes (Mag-CNTs) for biomedical and biotechnological applications. A review. *Int J Mol Sci* 2013, 14, 24619–42.
[214] Giakisikli G, Anthemidis A. Magnetic materials as sorbents for metal/metalloid preconcentration and/or separation. A review. *Anal Chim Acta* 2013, 789, 1–16.
[215] Gao L, Chen L. Preparation of magnetic carbon nanotubes for separation of pyrethroids from tea samples. *Microchim Acta* 2013, 180, 423–30.
[216] Herrera-Herrera A, Hernández-Borges J, Afonso M, Palenzuela J, Rodríguez-Delgado M. Comparison between magnetic and non magnetic multi-walled carbon nanotubes-dispersive solid-phase extraction combined with ultra-high performance liquid chromatography for the determination of sulfonamide antibiotics in water samples. *Talanta* 2013, 116, 695–703.

A. V. Pirogov

# 11 Application of Microemulsions for Extraction and Preconcentration of Hydrophobic Target Compounds

## 11.1 Introduction

In modern analytical chemistry, a problem of the rapid and simultaneous determination of substances significantly differing in polarity and hydrophobicity is very important. Another problem is the determination of trace amounts of various compounds in the objects with complex multicomponent matrix, and their quantitative extraction from that matrix. In most cases, the application of mass-selective detectors is proposed, which allows one to avoid sample preparation. Another option is to conduct preliminary chromatographic separation on the column with unique stationary phase specially designed for the particular set of compounds. The drawbacks of both approaches are obvious: they are very specific and require expensive instrumentation and consumables. In the beginning of 1990s, the application of microemulsions as mobile phases for liquid chromatography was proposed [1, 2]. Microemulsions are often used in capillary electrokinetic chromatography [3, 4], but a method of microemulsion liquid chromatography (MELC) has not been properly developed yet. Several reviews devoted to MELC have been recently proposed in order to give an insight to the readers [1–3].

In this chapter the examples of microemulsions application as media for extraction and preconcentration of target compounds from various matrices are summarized. The main parameters influencing recovery as well as advantages and disadvantages of the method are considered.

The author of this chapter did not try to cover all features of microemulsion extraction and to thoroughly consider structure, properties of microemulsions and ways of their preparation and decomposition. The purpose was to give an overview of microemulsions as representatives of nanostructured media and to demonstrate the ways of controlling selectivity and efficiency of extraction in the determination of particular classes of compounds.

## 11.2 Microemulsions: structure and classification

For the first time microemulsions were mentioned in the work of Hore and Schulman in 1943, where spontaneous formation of microemulsion consisting of water and oil after adding a surfactant was described [4]. In 1959, Schulman introduced the term “microemulsion” for indicating a transparent solution consisting of four

https://doi.org/10.1515/9783110542011-011

components, namely water, hydrocarbon, surfactant, and co-surfactant (alcohol) [5]. Schulman was titrating multiphase sample with alcohol and obtained an isotropic solution of microemulsion. In 1981, more detailed definition appeared stating that microemulsion is a system composed of water, oil, and surfactant, which is a uniform optically isotropic and thermodynamically stable solution [6]. A few years later, the term "microemulsion" was used for indicating optically transparent complex system with a droplet size of 20–25 nm [7]. Four years later, the term "microemulsion" was assigned to a different category and described as a layered liquid crystal structure in water phase with a particle size below 200 nm [8]. Since that moment, several other definitions of "microemulsions" were proposed. For example, Tadros et al. [9] used that term for all kinetically stable emulsions with a droplet size from 50 to 200 nm.

For determining a droplet size and other parameters and properties of microemulsions, various physical and physicochemical methods are used [10–12]. Microemulsions are mixtures of water, other liquid immiscible with water (further indicated as oil), and surfactant, which are homogeneous at the macroscopic level, while at the microscopic level they consist of separate domains of water and oil divided by a monolayer of surfactant. In this case, any organic substance having limited solubility in water can be defined as "oil."

The first classification was introduced by Winsor in 1948 [13]. Schematic representation of such classification is shown in Fig. 11.1. Strictly speaking, only Winsor IV can be considered as "classical" microemulsion.

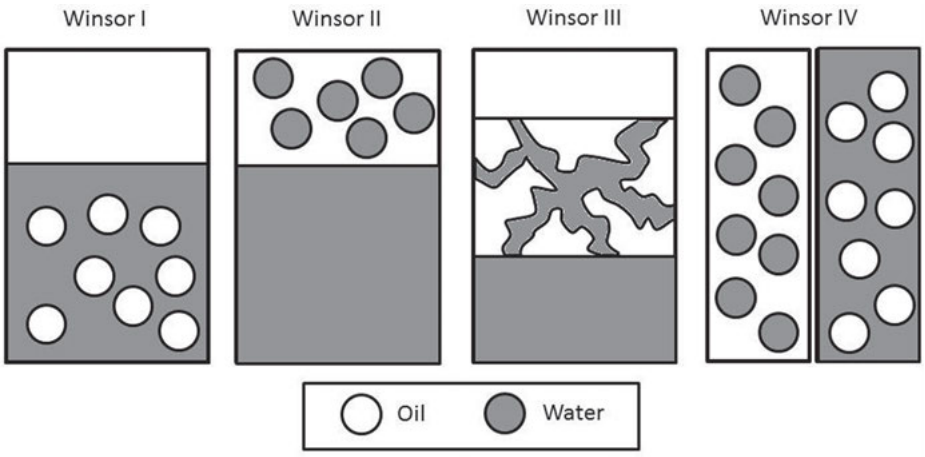


**Fig. 11.1:** Classification of microemulsions by Winsor. W I – excess of water, W II – excess of oil, W III – bicontinuous microemulsion (as spaghetti), W IV – homogeneous (pure) microemulsions "o/w" or "w/o."

Microemulsions cannot be considered as emulsions with droplets of a very small size (only few dozens of nanometers). Micro- and macroemulsions have several fundamental differences. Although macroemulsions (emulsions) are unstable systems, in which droplets will inevitably coalesce, microemulsions are thermodynamically stable [14] and have intensive internal structure dynamics [15]. In contrast to macroemulsions, microemulsions have high surface area (about 200 $m^2\ g^{-1}$). Due to a smaller droplet size, microemulsion solutions are optically transparent. Since the formation of thermodynamically stable phase is based on the principles of self-organization of surfactants, microemulsions are in many ways similar to other organized surfactant systems such as micellar solutions and liquid crystal phases. Being macroscopically homogeneous and microscopically heterogeneous, microemulsion organized media are considered as intermediate between the traditional single-phase and double-phase systems containing reagents of interphase transfer. If a chemical reaction proceeds in such nanosized microphase rather than in the whole volume of solution, the former one is referred to as a "nanoreactor" or a "microreactor" [16–18]. The main difference of microheterogeneous organized media from the common homogeneous solutions (aqueous, nonaqueous, or water-organic) is that the key role in them is played by local effect. It means that changes in the properties of the substances solubilized in organized media are caused by the change of medium conditions only in their microenvironment rather than in the whole solution volume. Several main features of organized media (systems) can be emphasized [19]:

- the ability to solubilize (dissolve) substances, which are insoluble in a solvent forming dispersion medium;
- the ability to bring together and concentrate components of analytical reaction in the micro phase of organized medium, even if they have completely different hydrophobicity;
- multicenter and multifunctional interactions (electrostatic, donor–acceptor, van der Waals, hydrophobic) of components or parts of microphase with a solubilized substrate, where hydrophobic interactions are dominating.

Effective physicochemical parameters of a medium in various parts of the organized system will be significantly different. Thus, local dielectric permittivity ($\varepsilon_{eff}$) in the micro surrounding of a solubilized reagent can change from 78 to 5–6 with its transfer from aqueous to micellar medium. Such a sharp gradient of that parameter, together with a possibility to change the reagent localization, allows one to influence the properties of each component of chemical reaction directly. Solubilization of substances in micro phase of the organized system significantly changes their hydrophobic properties, hydration, "hardness," and conformation of molecules and, as a result, the whole set of physicochemical, spectroscopic, electrochemical, and adsorption properties.

The examples of such properties are character of charge distribution in the molecule, efficiency of intra- and intermolecular transfer of excitation energy and

electrons, interphase particle distribution, solubility, rate, direction, and equilibrium of analytical reaction. The mechanism of a physicochemical action of organized media on both the reactant properties and target substances separation processes is based on the emphasized features. As a result, analytical signal intensity increases considerably, which results in the sensitivity growth and selectivity improvement for the analytical determination [20].

Depending on the liquid forming micro phase, three types of microemulsions can be distinguished:

1) "Oil-in-water" (further used without quotation marks), where oil droplets are suspended in aqueous phase;
2) "Water-in-oil" (further used without quotation marks), where organic liquid represents macro phase;
3) Bicontinual microemulsion, which is characterized by interpenetration of aqueous and organic phases and formation of a specific three-dimensional net, in which separate domains of water and oil cannot be allocated. This type of microemulsions possesses dynamic, constantly changing structure and relatively high viscosity [12]. The properties of such phase (conductivity, viscosity, transport properties) mainly depend on the quantity of aqueous phase. Bicontinual microemulsions are not used as mobile phases in chromatography. In practice, such systems are not always simple. In several papers [21, 22], big variety of possible types of emulsions macro phase is demonstrated (Fig. 11.2).

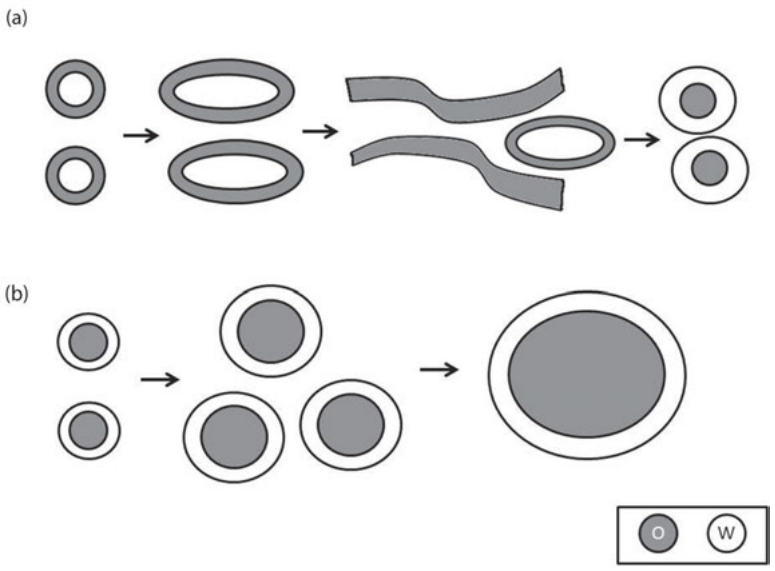


**Fig. 11.2:** A scheme of microemulsion formation. A – phase inversion, B – mechanical dispergation.

Very often double microemulsions such as oil-in-water-in-oil or water-in-oil-in-water are formed [23–25]. Such systems are often used in pharmacology and medicine for highly effective encapsulation and target delivery of substances.

Not only hydrophilic–lipophilic balance, but also geometry of surfactant molecule is a key factor determining the choice of surfactant for obtaining microemulsion possessing required composition and properties. The most popular approach for evaluating surfactant geometry is based on the use of critical packing parameter concept. Geometry evaluation results in the conclusion that surfactants with moderately long aliphatic hydrocarbon substitutes are the most suitable ones for obtaining microemulsions of oil-in-water type, while surfactants having bulky hydrophobic groups in the structure are more suitable for forming bicontinual emulsions.

Microemulsion can be formed without adding a surfactant [22–26] and in the mixtures of an individual surfactant, oil, and water [23, 27], but in many cases their formation requires adding the second surfactant called co-surfactant such as alcohol with hydrophobic substitute of an average size [28]. It decreases surface tension on the phase border between two liquids forming microemulsion. In some cases, the introduction of salt [29] or organic modifiers [30] is required for the formation of microemulsion in the system.

Sometimes, when there are some other compounds present (either as microemulsion or as individual compounds) in the solution besides those forming microemulsion, they are distributed between macro phase and microemulsion droplets in a particular way. It should be noted that penetrating the droplet, they can behave as co-surfactants, thus changing the structure and properties of either individual droplets or even microemulsion itself.

## 11.3 Preparation and decomposition of microemulsions

The most simplified thermodynamic theory of microemulsion formation is based on the equation of free Gibbs energy, where free energy of microemulsion depends on how much a surfactant decreases surface tension on the phase border in microemulsion and changes system entropy. Free energy ($\Delta G_f$) of microemulsion formation is described by the following equation:

$$\Delta G_f = \gamma \Delta H - T\Delta S,$$

where γ is a surface tension of microemulsion, $\Delta H$ is a change of surface area, $\Delta S$ is a change of entropy in the system, and $T$ is temperature.

When microemulsion is formed, the change in phase border surface area ($\Delta H$) is very significant due to the appearance of numerous oil droplets of a very small

diameter. The contribution of entropy is also very significant due to the same reason, and it is connected with dynamic processes. Therefore, negative value of free Gibbs energy is achieved by a significant decrease of surface tension, which, in turn, is accompanied by a drastic change of system entropy. The process of microemulsion formation is spontaneous, and the obtained disperse medium is thermodynamically stable.

Since the addition of a surfactant and a co-surfactant decreases surface tension on the phase border of two liquids to very low values, microemulsions are formed spontaneously. Very slight stirring is sufficient for the arrangement of surfactant molecules. Nevertheless, this process can be difficult to realize because of some kinetic complications, and the period of stable microemulsion formation can take up to several days in some cases [14]. Therefore, for accelerating the process external disturbances are applied such as heating, intensive stirring, and ultrasonication. The latter option is the most wide-spread, but even in that case microemulsion formation takes 30 minutes on average.

There is a way of obtaining microemulsions by temperature inversion of the phases [31–33]. The idea of the method is as follows: the initial microemulsion is prepared by mixing all components (surfactant, co-surfactant, water, and oil) using either ultrasonic bath or mechanical stirring for 10 minutes at 11000 rpm. The obtained solution is heated up to the temperature higher than the phase inversion point, which is about 50–60°C on average for various microemulsions, and then drastically cooled to the initial temperature. At elevated temperature, microemulsion of water-in-oil type is formed (temperature should be higher than critical temperature of inversion point), with particle size and surface tension achieving their minimum. With a temperature decrease those particles are decomposing, the phase transition occurs, and stable oil-in-water microemulsion with regular spherical shape of the particles is formed. The second option is preferable, because the droplets of the formed microemulsion are smaller than in case of mechanical dispersion. A method of temperature phase inversion is mostly often used for obtaining microemulsions based on nonionic surfactants.

The main drawback of the described approach is a very narrow interval of concentrations of components forming the initial microemulsion. Not all types of microemulsions can be obtained in that way. Such approach is rather seldom used in analytical chemistry, where there is a necessity to obtain various microemulsions in different constituents concentration range. Basically, this is a technological process of preparing pharmaceutical preparations based on microemulsions.

Apparently, it is more convenient to use a method of subsequent mixing of the reagents during the ultrasonication of solution [34].

Phase separation of various surfactants solutions is known to depend on several factors, namely temperature, concentration of surfactant, various inorganic and organic salting-out agents, pH, etc. Water solutions of nonionic surfactants are very sensitive to the temperature changes and decompose into two separate phases

above the certain temperature point. Such phase separation is called a "cloud point extraction" (CPE) [35]. This method is based on the separation of the homogeneous surfactant solution into two isotropic phases. The first one enriched with surfactant contains the substances (of hydrophobic character) distributed throughout the whole volume before the phase separation; the second one is water phase containing surfactants in the concentration below the CMC and residual amounts of substances that were not extracted (Fig. 11.3).

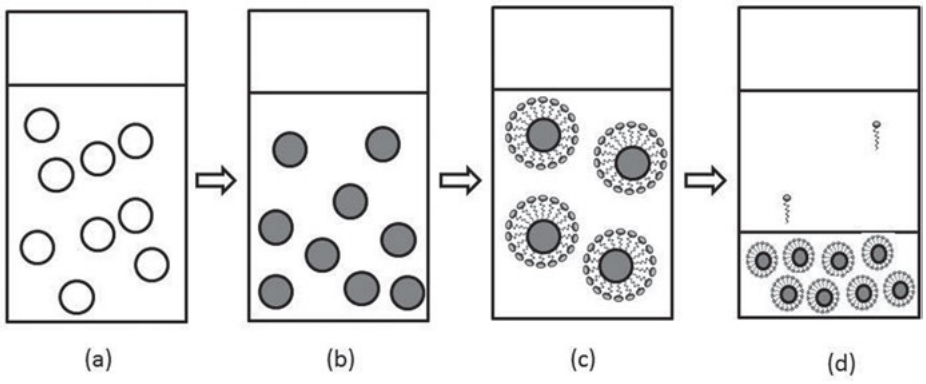


**Fig. 11.3:** Cloud point extraction of metals [84]: a – solution of ions of metal with low concentration; b – chelates of metals formed by addition of a complex-forming reagent in the solution; c – preconcentration of ions of metals in micelles of surfactant; d – separation of micelle-saturated phase after heating and centrifugation.

The same effect is observed for zwitterionic surfactants [36], and it can also appear with the changes in pH [37] and ionic strength of solutions. This can be conveniently used as a first concentration step for the analysis and extraction of organic or inorganic (e. g., metal ions) substances from diluted water solutions. Such way of preconcentration and separation of the target components is characterized by high concentration coefficients in the small sample volumes, possibility of determining compounds of different nature (hydrophobic and hydrophilic) in the complex matrices, simplicity and efficiency of the approach, low toxicity of surfactants applied in comparison with other organic solvents used as extractants.

When detergentless microemulsions are used, there is sometimes a possibility just to dilute a microemulsion solution [38, 39]. It results in going beyond the boundaries of microemulsion existence range and in microemulsion splitting. Very often such method does not work, when there are own surfactants in the sample or when microemulsion containing high amount of ionogenic micelle forming surfactants is used [40]. Then target compounds are partly solubilized by micelles and quantitative extraction into organic phase cannot be achieved. While working with anionic

surfactants (e. g., sodium dodecylsulfate), the authors of ref. [41] proposed the addition of calcium chloride for precipitating slightly soluble calcium dodecylsulfate and splitting a microemulsion. Such method was used for the preconcentration and further chromatographic determination of alkylphthalates [41] and polycyclic aromatic hydrocarbons (PAHs) [42].

## 11.4 Application of micellar and microemulsion media for extraction of target compounds

Due to their unique properties, microemulsions found their extensive application in sample preparation.

### 11.4.1 Extraction and preconcentration of organic substances

Microemulsions of water-in-oil type are used for liquid–liquid extraction of proteins, and protein polymers can be easily isolated and extracted again [43]. Protein extraction with oil-in-water-type microemulsion was, for the first time, considered in ref. [44]. Cytochrome c protein was used as a model sample. Maximum recovery of protein in microemulsion phase composed of poly(ethyleneoxymonoleate)-block poly(D,L-lactide) (MOPEO-PLA) /methanol /chloroform was observed at pH 10.1, which is equal to Cytochrome c isoelectric point. The main drawback of such microemulsion system is its dependence on the parameters that can influence the hydrophobicity of surfactant chain such as pH, temperature, and buffer concentration, which can lead to the decrease in complexe formation between determined Cytochrome c protein and MOPEO-PLA surfactant.

Selective extraction of haemoglobin from blood sample with reversed microemulsion composed of water/AOT/1-butyl-3-methylimidazole hexafluorophosphate (6/50/5) was proposed [45] with recovery about 96 %. Haemoglobin can exist in microemulsion either in the volume of ionic liquid or in “aqueous phase” of microemulsion. Electrostatic interactions are a main driving force causing haemoglobin transfer from water to microemulsion phase. Iron ions contained in haemoglobin form coordination bonds with cations of ionic liquid, which leads to the distribution in ionic liquid volume.

The way of separating peptide hydrolyzate from heme using Winsor microemulsion system III, which is known to be unstable and to decompose quickly, is proposed [46]. Microemulsion system was composed of tetraethyleneglycoldecyl ether (C10E4)/*n*-octane/1 % peptide hydrolyzate of bull haemoglobin. Such surfactant can form three-component microemulsion at room temperature without addition of co-surfactants or other surfactants. Moreover, ionic nature of surfactant results in the

transformation of Winsor system I into Winsor system III with the increase in its concentration and temperature from 20 to 30°C, which is often used for increasing recovery of peptide hydrolyzate and its selective separation from heme. Using common organic solvents results in the formation of strong intermolecular interactions between heme and proteins, which leads to better solubility of heme in water and thus, significantly decreases separation selectivity. Using the surfactants decreases surface tension on the border of water and organic phases, which is a good condition for extracting heme into organic phase.

Microemulsions are suitable extractants for peptides, amino acids, and nucleic acids, since such biological compounds are not soluble in water and often denature or lose their properties in organic solvents. Therefore, in microemulsions of water-in-oil type, peptide occurs in water droplets protected from organic solvent by a surfactant layer.

A composition of microemulsion for the determination of licopene (carotenoid pigment determining the color of some fruits) in tomatoes was varied [47]. Different types of surfactants (Span 20, Twin 20, Twin 60, Twin 80, saponin, sarcosemonopalmitate, and lecithin) and co-surfactants (glycerol, propyleneglycol, 1-propanol, and ethanol) were considered. The disadvantage of using microemulsions is low extraction efficiency, which can be increased by ultrasonic and fermentative sample preparation.

A comparison of microemulsion extraction of quercetin from guava leaves with classical liquid phase extraction is conducted [48]. It is shown that even though extraction with microemulsions was not quantitative (72%), recovery was higher than when using common solvents.

Microemulsion system composed of rapeseed oil/lecithin/propanol/water was considered for extraction of food oils [49]. Natural lecithin is one of the most promising and useful agents in food analysis and medicine, since it is a natural surfactant, which is nontoxic, biocompatible, and can accelerate transportation of substances through the skin. However, for forming stable lecithin-water-oil systems the introduction of an additional component, namely co-surfactant is required. The drawback of such microemulsions is a presence of toxic aliphatic alcohols as co-surfactants.

The application of reverse microemulsions for extraction of organic compounds of average polarity from tea leaves is considered [50]. It is shown that microemulsions increase solubilization of ferrulic acid. The drawback of such approach is incomplete extraction of target compounds and interference of fat-soluble components, which are well extracted from tea leaves with microemulsions.

A method of CPE is widely used for the extraction from water solutions and/or preconcentration of some organic substances. The possibility of removing tannic acids from water solutions by extraction in a cloud point is studied. Two nonionic surfactants, namely Lutensol ON 30 and Triton X-114 were used, and recovery under the optimized conditions was 87 and 95%, respectively.

### 11.4.2 Extraction and preconcentration of metals

Microemulsion systems are widely used in sample preparation for extraction and concentration of various metal ions, mainly from water and oil solutions. In recent years, such approaches as metal isolation by CPE, formation of ion pairs with metal followed by its simultaneous transfer into organic phase of microemulsion as a complex, and leaching with further re-extraction of metals from solid ores with microemulsions have gained significant development and wide application. The advantage of such techniques is sample preparation simplicity, use of less toxic solvents, possibility of varying microemulsion composition for increasing selectivity of extraction and sensitivity of determination.

Recently, two- and three-phase microemulsions composed of coconut oil, 1-butanol, and kerosene have been used for removing chromium(III) from water samples [51]. The optimal composition of microemulsion was chosen, which provided recovery of 96 %. Microemulsion of the same composition was used for the simultaneous extraction of chromium, copper, iron, manganese, nickel, and lead from water [52]. For all metals, recovery was higher than 98 %.

Microemulsion based on cyclohexanol, hexanol, hydrochloric acid solution, and ionic liquid of 1-*n*-tetradecyl-3-methylimidazole was used for the extraction of gold(III) ions [53, 54]. In that case, due to its diphilic structure, ionic liquid played the role of surfactant and extractant participating in anion exchange with gold ions. The proposed approach provided high selectivity in the presence of other metal ions in the system. In other works, microemulsions based on cetyltrimethylammonium bromide (CTAB), cetylpyridinium bromide [55], and tetradecyldimethylbenzylammonium chloride (TDMBAC) [56] as surfactants were used for extraction of gold ions. The formation of gold complexes with such surfactants allows one to achieve selective extraction in the presence of other metals in the system.

Introduction of the reagents forming hydrophobic complexes with metals with their further solubilization into surfactant micelles in the system can significantly increase efficiency of microemulsion extraction. In turn, a chelating agent can be either water insoluble and localized in the surfactant micelles or water soluble and having ionized donor centers, which can bind metal ions. In the latter case, coordination of metal ions should decrease the charge, and thus, increase the affinity of the formed complex for nonionic surfactant micelles.

A novel approach for mercury extraction from gasoline by microemulsion destruction was offered by a group of scientists from Brazil [57]. Propanol and aqueous hydrochloric acid solution were added to gasoline samples, which resulted in the formation of optically transparent stable microemulsion. Further addition of deionized water caused splitting of microemulsion into two layers, with the upper one containing the residuals of gasoline and the lower one (water–alcohol) containing mercury. Mercury recovery was in the range from 88 to 109 %.

The same approach with microemulsion splitting was applied in several other works. For example, microemulsion based on Triton X-114 with its further decomposition by adding deionized water was used for extracting of zink ions [58] and several metal ions simultaneously (copper, manganese, nickel) from diesel oil [59], for the determination of copper, iron, and manganese in lubricating oil [60], and for the determination of chromium and magnesium in food oils [61]. A little later, the same group of scientists proposed microemulsion based on Triton X-100 with further system splitting by heating up to 90°C for the simultaneous determination of calcium, magnesium, and cobalt in diesel fuel samples [62]. Recovery was in the range from 88 to 106 %. That approach is rather simple and does not require additional reagents, but it cannot be applied for the determination of thermosensitive compounds, because it requires heating the system.

For the first time, Chinese scientists used microemulsion of water-in-oil type based on such ionic liquid as 1-methyl-3-[tri-(methylsiloxy)]silane propyl-imidazole chloride ([Si4mim]Cl) for selective extraction of palladium(II) ions [63]. The stability of such microemulsion was studied, and extraction conditions were chosen (ionic strength, concentration of [Si4mim]Cl, time, microemulsion, and water phase ratio, influence of sodium chloride and hydrochloric acid as additives), which resulted in 98 % palladium (II) recovery from water in the presence of other metal ions (Cu(II), Co(II), Ni(II), Fe(III), Al(III), Zn(II), Ce(III), Li(I), Mg(II), and Sn(IV)).

A method of isolating and extracting trace amounts of copper (II) from drinking water and blood of the patients with hepatitis C is proposed [64]. The method is based on liquid extraction of copper (II) ions with microemulsion composed of such ionic liquid as 1-butyl-3-methylimidazole hexafluorophosphate ($[C_4mim][PF_6]$) and nonionic surfactant Triton X-100 with further concentration based on a cloud point approach. The proposed approach provides a low detection limit of 0.132 μg/kg and high concentration coefficient equal to 70.

Microemulsion composed of oleic acid/*n*-butanol/sodium carbonate solution (5/5/4, weight %) was used for extracting nickel (II) ions with 99 % recovery [65]. Some other microemulsion systems composed of water/isopropanol/Brij 30/pine oil and water/Brij 30/ethylacetate were also used for nickel extraction. The factors influencing recovery (the ratio between microemulsion and water phases, the type of oil, the concentration and the type of co-surfactant) were studied [66]. Recovery of nickel in the concentration of up to 1000 mg/L was 85 %.

The way for selective extraction of cobalt (II) ions from hydrochloric acid solution in the presence of nickel is presented [67]. The proposed approach includes an application of microemulsion composed of hexadecyltrimethylammonium chloride (HDTAC)/*n*-pentanol/*n*-heptane/hydrochloric acid solution/tertiary amine. In that case, tertiary amine increased the stability of microemulsion and increased cobalt recovery, which was 92 %, while nickel recovery was below 6.7 %. Another example of microemulsion for extracting cobalt ions is described [68]. Microemulsion consisting of 2-ethylhexylphosphoric acid, mono-2-ethylhexyl ether, and kerosene was

used. With a small amount of mono-2-ethylhexyl ether (6 %) at pH 2 and 6 minutes extraction time recovery was above 90 %. Such approach provided good efficiency and low consumption of organic solvents.

Russian scientists proposed the use of structured systems (microemulsions and micellar solutions) for extracting metals from solid-phase particles (microemulsion leaching) [69]. Metal extraction was conducted using microemulsion based on sodium di-(2-ethylhexyl)phosphate with the following metal re-extraction and microemulsion decomposition by adding an excess of aqueous acid solution and intensive stirring for 1 minute. For completing the process of re-extraction and splitting the phases, the system was kept for 24 hours.

A method of microemulsion leaching implies the extraction of metals from technogenic raw materials (concentrates, sludge, ash, dust, etc.) by their contact with extractant-containing microemulsion, which allows one to combine leaching and extraction in one process. Such microemulsions can find their application for extracting metals that are easily extracted by di-(2-ethylhexyl)phosphoric acid, namely rare earth elements, zirconium, hafnium, vanadium, etc. For example, such approach was used for extracting copper as copper di-(2-ethylhexyl)phosphate from copper (II) oxide, the samples of copper-containing galvanic sludge and copper ore [70]. The method included grinding raw materials and leaching copper with microemulsion, which had water phase consisting of sodium hydroxide water solution and organic phase composed of sodium di-(2-ethylhexyl)phosphate in kerosene. Extraction of copper as copper di-(2-ethylhexyl)phosphate with microemulsion was conducted in the closed vessel at constant temperature and stirring. Copper was re-extracted from microemulsion by active stirring for 1 minute with triple (by volume) amount of 10 % sulfuric acid solution. For completing the process of re-extraction and splitting the phases, the samples were kept for 24 hours at room temperature. Then, copper content in the re-extract was determined by photometry with cuprizone. After leaching with direct microemulsion within several days, copper recovery from ore sample and galvanic sludge was 13 and 80 %, respectively.

Selective extraction and separation of rhenium(VII) and molybdenum(VI) using microemulsion composed of Triton X-100/trialkylamine/iso-amyl alcohol/*n*-heptane/sodium chloride solution was proposed [71]. Rhenium recovery was 80 %, while molybdenum recovery was below 20 %. A possibility of europium extraction by water-in-oil microemulsion composed of sodium oleate/pentanol/heptane/chloride aqueous solution is considered [72]. Under optimal extraction conditions, recovery was higher than 99 %.

Another example of microemulsion for the extraction of metal ions is devoted to the determination of aluminum in tea samples [73]. The method is based on the formation of stable aluminum(III) complexes with 8-hydroxyquinoline and their following extraction by the microemulsion composed of Triton X-100/*n*-pentanol/*n*-hexane. Aluminum recovery was within the range of 96.8–103.5 %. Some examples of using microemulsion for metal extraction are shown in Tab. 11.1.

**Tab. 11.1:** Examples of application of ME for the metals extraction

| Metal | ME composition | Recovery, % | Ref. |
|---|---|---|---|
| Co(II) | AOT / *n*-pentanol / *n*-heptane / water solution of NaCl | 95 | [86] |
| Ge(IV) | AOT/*n*-butanol/*n*-heptane/$Na_2SO_4$/N235 | 99 | [87] |
| Co(II), Cd(II), Cu(II), Pb(II), Zn(II), Eu(III), La(III), and Sr(II) | AOT / perfluoropolyetherphosphate | 90 | [88] |
| Sm(III) | Sodium oleate (0.24 M) / *n*-pentanol (20 % vol.) | 100 | [89] |
| Nd(III) | OP-4 [polyoxyrthylene(4)nonylphenol] or OP-7 [polyoxyethylene (7) nonylphenol] / benzyl alcohol / 2-(2-ethylhexylphosphonic acid) / petroleum / water solution of HCl | 95,3 | [90] |
| Co(II) | CTAB 0.10 M / *n*-pentanol (30 % vol) / *n*-heptane / water solution of HCl (4 % mass) | 93 | [91] |
| Ur(VI) | *N*,*N*-dimethyldodecylamine / *n*-hexanol / *n*-heptane / trialkylphosphonic acid / 4.0 M water solution of $HNO_3$ | 95 | [92] |
| Eu(III) | AOT / *N*,*N*-dioctyl-*N*,*N*-dimethyl-2-(30-oxapentadecyl)propane-1,3-diamide / *n*-hexane | – | [93] |

An effective way of extraction and preconcentration of metal ions from water solutions is CPE. A method of uranium extraction in a cloud point as a complex of uranium(IV) with pyrocatechol violet was developed on the base of micellar solutions of TX100 and CTAB [74]. However, a big disadvantage of using the listed chelating agents is that effective lanthanide extraction can be observed only in neutral and weakly alkaline media, while, at pH 2–3, recovery is less than 1 %. One of the ways of expanding pH range of micellar extraction using temperature-induced phase separation is to apply pH-independent chelating agents with good solubility in water solutions of nonionic surfactants.

The use of 2-(5-bromo-2-pyridylazo)-5-(diethylamino)phenol (5-Br-PADAP) as a complexing agent and Triton X-114 as nonionic surfactant for extraction and preconcentration of vanadium from natural water samples is proposed [75]. Such approach provides high recovery and is suitable for determining trace amounts of vanadium. A method of extracting lanthanides with micellar solutions of Triton X-100 and calix[4]resorcinarene phosphonic acid as a chelating agent is described [76]. It allows one to extract gadolinium ions in acidic medium (recovery is 30 % at pH 2) rather effectively, but such lanthanides as Yb and Lu cannot be quantitatively extracted, since they form precipitates, while lanthanum is not extracted under those conditions at all.

### 11.4.3 Extraction and preconcentration of PAHs

Modern methods of determining PAHs in environmental samples are usually high-performance liquid chromotograhy (HPLC) with fluorimetric and spectrophotometric detection or on GC-MS. A drawback of many proposed techniques of PAH determination is long sample preparation, usually including several steps, which increases the total analysis time and the error in determining target compounds. Moreover, sometimes the organic solvents do not extract all determined PAHs simultaneously.

Special attention was paid to the studies of PAH solubilization by various surfactants and their mixtures. The influence of length of hydrocarbon groups and of hydrophilic groups on PAH solubilization on pyrene, naphthalene, and anthracene solubilization is studied [77]. One-, two-, and three-component systems composed of surfactants with dodecyl (C12) and hexadecyl (C16) hydrocarbon chains having cationic and nonionic polar groups were used. It was found that surfactant with C12 hydrocarbon chain possessed lower solubility than the one with C18. While comparing two-component mixtures of surfactants, it was found that solubility was higher in the mixture of cationic and nonionic surfactant as compared with cationic–cationic surfactant mixture or individual cationic surfactant. However, three-component mixture composed of two cationic and one nonionic surfactant possesses lower solubilization than two-component mixture of cationic and nonionic surfactant.

Solubilization of PAHs was studied both individually and in the mixtures with some nonionic surfactants, namely Twin 20, Twin 80, Triton X-100, Brij 35, and Brij 58 [78]. It was supposed that there are additional interactions of PAHs with each other and with surfactant molecules in the mixture of PAHs, which results in the change in the shape and size of micellar droplet and changes solubility. Thus, for single-component system, solubilization changes from 84 to 95 %, while for two- and three-component systems it changes from 76 to 88 % and from 75 to 83 %, respectively.

It was found that solubilization of naphthalene, acenaphthene, anthracene, phenanthrene, and pyrene in micellar surfactant solutions with concentrations exceeding CMC decreases in the following row: Triton X-100 > Brij 35 > Triton X-305 > sodium dodecyl sulfate (SDS) [79]. Other examples of studying PAH solubilization from soil using surfactants are presented in Tab. 11.2.

Microemulsions and micellar solutions are used for the extraction of PAHs from different objects followed by their chromatographic and spectrophotometric determination. The efficiencies for phenanthrene and pyrene extraction from soil using dichloromethane and sodium dodecylbenzenesulfonate (SDBS) solution as extractants followed by HPLC analysis with UV- and fluorimetric detection were compared [80]. It was shown that PAH recovery with SDBS depends on the soil type and its value is in the range from 75 to 93 %, which is slightly lower than that for dichloromethane as an extractant. A group of scientists studied the dependence

of efficiency of phenanthrene and pyrene extraction from different types of soils using SDBS micellar solution on extraction time [81]. SDBS as a surfactant did not provide quantitative PAH recovery (<95 %); however, using a surfactant increases precision and reproducibility due to lower volatility of SDBS in comparison with dichloromethane.

**Tab. 11.2:** Examples of PAHs solubilization from soils by ME

| Surfactants | PAH concentration | Soil (g) / solution (mL) | t°C | PAHs solubilization, % | Ref. |
|---|---|---|---|---|---|
| Twin 40, Twin 80, Brij 30, Brij 35 | 2 g/L | 50/500 | – | 84 (phenanthrene) | [94] |
| SDS | 2 % | 135/1800 | – | 90 (phenanthrene) | [95] |
| Triton X-100, Twin 20 | 3 % | 1/ 7,5 | 25 | 47 (phenanthrene) и 51 (anthracene) | [96] |
| Twin 80, Brij 35, Twin 20, Tiloxapol, Tergitol NP10 | 10 g/L | 2,5/ 50 | 30 | 89,8 (fluoranthene), 50,2 (pyrene), 86,5 (benz(a) anthracene) | [97] |

Phenanthrene solubilization and recovery from soil using microemulsions based on sulfonated castor oil and pure castor oil with different surfactants (synthetic surfactants, Triton X-100, Twin 80, Brij 35, SDBS, and SDS) were studied [82].

Application of surfactants and microemulsions for pyrene and phenanthrene extraction from soil was studied using various techniques (ultrasonic extraction, microwave extraction, and accelerated extraction with solvent) [83]. It was shown that using microemulsion system composed of 0.5 M SDS/1-butanol/1:1 (v/v) hexane:acetone (90:7:3, vol.%) resulted in recovery of 97 % and 80 % for phenanthrene and pyrene, respectively. It was also noted that using nonionic surfactants (Triton X-100) results in lower recovery compared with anionic surfactants (SDS) that form less viscous systems.

The technique of CPE using anionic surfactants was applied for the first time for preconcentration of PAHs and other organic substances (vitamins, steroid hormones) with further HPLC analysis [84]. It was noted that micellar solutions of anionic surfactants such as SDS, SDBS, and sodium dodecylsulfosuccinate split into two phases in acidic media. The proposed approach is characterized by high recovery and concentration coefficients for all studied PAHs in soil and water analysis. Ionogenic character and the absence of aromatic groups in the most abundant anionic surfactants make them applicable for polar analytes preconcentration; moreover, such approach is applicable for the analysis of thermostable compounds. A little later the factors

influencing the splitting of anionic surfactant micellar solutions were considered in detail [85]. Such approach does not allow the determination of substances that are sensitive to pH of the medium. Such approach was used for extraction and following chromatographic determination of 10 PAHs and dialkylphthalates from soils [41, 42]. It was noted that using microemulsion consisting of 3 % SDS, 0.8 % benzene, 6 % *n*-butanol, and 90.2 % water the highest concentration degree is achieved for benz(a) pyrene in organic phase after microemulsion splitting; therefore, microemulsion with such composition was used in further experiments. For extracting 10 PAHs three types of soil were chosen, namely sand, clay, and peat. The results showed that microemulsion composed of 3 % SDS, 0.8 % benzene, 6 % *n*-butanol, and 90.2 % water is a good extractant for all 10 considered PAHs in three types of soil. Recoveries are in the range from 90 to 105 %, and they only slightly depend on the soil type.

Adding 10-fold excess of dry calcium chloride to SDS-based microemulsion causes its splitting and formation of two immiscible phases, namely water and oil. Due to their high hydrophobicity ($\log P \geq 3.36$) (Tab. 11.3), all 10 PAHs are concentrated in organic phase after microemulsion splitting.

Figure 11.4 represents the chromatograms of standard mixtures of 10 PAHs in microemulsion without splitting and in organic layer formed after splitting.

**Tab. 11.3:** Coefficients of the preconcentration of 10 PAHs in oil phase after the ME decomposition

| Compound | Coefficients of preconcentration |
|---|---|
| Naphthalene | 6.5 |
| Acenaphthylene | 5.9 |
| Fluorene | 5.2 |
| Fluoranthene | 5.8 |
| Pyrene | 6.1 |
| Benz[a]anthracene | 5.8 |
| Chrysene | 5.7 |
| Benzo[b]fluoranthene | 5.7 |
| Benzo[k]fluoranthene | 5.8 |
| Benzo(a)pyrene | 5.8 |

Concentration coefficients are in the range from 5.2 to 6.5, and they almost do not depend on log *P* (in the log *P* range from 3.4 to 6.6). The obtained detection limits are considerably lower than maximum permissible concentrations stated by Environmental Protection Agencies of Canada and Netherlands and lower than maximum permissible concentration stated for benz(a)pyrene in soil in Russia.

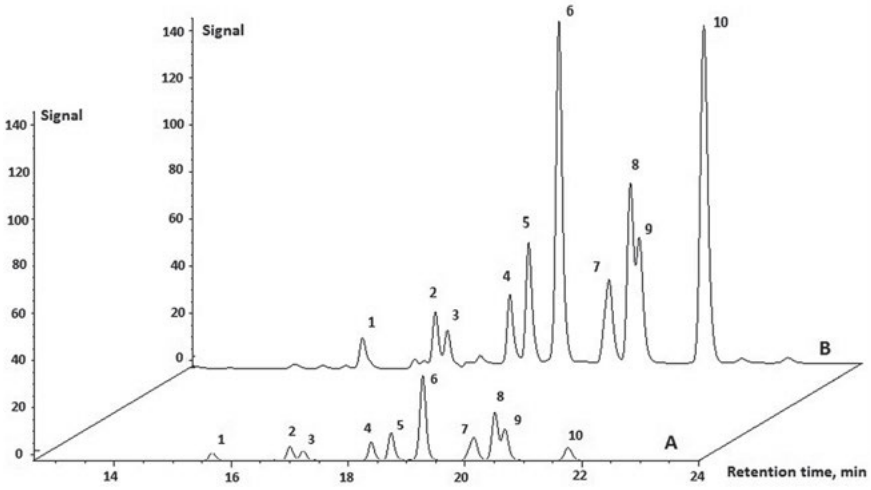


**Fig. 11.4:** Chromatograms of model mixture of 10 PAHs in microemulsion without decomposition (chromatogram A), in organic layer (oil) formed after decomposition of the microemulsion (chromatogram B). HPLC-FLD method. Column *Luna* C18 (2) (250 mm × 4.6 mm, 5 µm), mobile phase: acetonitrile – water, gradient elution, flow rate of the eluent: 1 mL/min. Injection volume: 20 µL. Column temperature: 30°C. Peaks: 1 – Naphthalene, 2 – Acenaphthylene, 3 – Fluorene, 4 – Fluoranthene, 5 – Pyrene, 6 – Benz[*a*]anthracene, 7 – Chrysene, 8 – Benzo[*b*]fluoranthene, 9 – Benzo[*k*]fluoranthene, 10 – Benzo(a)pyrene.

## 11.5 Conclusions

Thus, due to their unique properties, microemulsions can be used as promising extractants of hydrophobic target compounds from various food, pharmaceutical, ecological, and other objects. At the same time, it is convenient to conduct the procedures of subsequent microemulsion splitting and concentration of target compounds in organic phase with following HPLC analysis. The proposed approach is characterized by low detection limits, significantly simplifies sample preparation by decreasing total analysis time, and decreases total number of steps, which results in lower errors of the determination.

**Acknowledgements:** The author's papers and research mentioned in the text were funded by the Russian Foundation for Basic Research (RFBR) for the financial support under grant no. 16-03-00257A and Russian Science Foundation (RSF) grant no. 16-13-10079.

## References


[1] Gao HS, Li YN, Wang LY, Gao CK, Li N. Establishment of quantitative retention-activity model by optimized microemulsion liquid chromatography. *J Chromatogr A* 2016, 1478, 10–18.

[2] Xu LY, Li LX, Huang JD, Yu SN, Wang J, Li N. Determination of the lipophilicity (log P-o/w) of organic compounds by microemulsion liquid chromatography. *J Pharm Biomed Anal* 2015, 102, 409–16.

[3] Ryan R, Donegan S, Power J, McEvoy E, Altria K. Microemulsion HPLC. *LC-GC Europe* 2008, 21, 502–10.

[4] Hoar TP, Schulman JH. Transparent water-in-oil dispersions the oleopathic hydro-micelle. *Nature* 1943, 152, 102–03.

[5] Schulman JH, Stoeckenius W, Prince LM. Mechanism of formation and structure of micro emulsions by electron microscopy. *J Phys Chem* 1959, 63, 1677–80.

[6] Danielsson I, Lindman B. The definition of micro-emulsion. *Colloids Surf* 1981, 3, 391–92.

[7] Shaw JM, Futch WS, Schook LB. Induction of macrophage antitumor-activity by acetylated low-density lipoprotein containing lipophilic muramyl tripeptide. *Proc Natl Acad Sci USA* 1988, 85, 6112–16.

[8] Weder H, Mutsch M. Process for the production of a nanoemulsion of oil particles in an aqueous phase: Patent: USA. 1990, CA2019710 A1.

[9] Tadros T, Izquierdo R, Esquena J, Solans C. Formation and stability of nano-emulsions. *Adv Colloid Interface Sci* 2004, 108, 303–18.

[10] Weber A, Stuhn B. Structure and phase behavior of polymer loaded non-ionic and anionic microemulsions. *J Chem Phys* 2016, 144, 1–9.

[11] Vettegren VI, Mamalimov RI, Lozhkin VN, Morozov VA, Lozhkina OV, Pimenov YA. IR spectroscopic investigation of the structure of water-fuel microemulsion for diesel engines. *Techn Phys* 2016, 61, 1433–35.

[12] Hickey RJ, Gillard TM, Irwin MT, Lodge TP, Bates FS. Structure, viscoelasticity, and interfacial dynamics of a model polymeric bicontinuous microemulsion. *Soft Matter* 2016, 12, 53–66.

[13] Winsor PA. Hydrotropy, solubilisation and related emulsification processes. Part 1. *Trans Faraday Soc* 1948, 44, 376–98.

[14] Kartsev VN, Shtykov SN, Bogomolova IV, Ryzhov IP. Thermodynamic stability of microemulsion based on sodium dodecyl sulfate. *J Molec Liq* 2009, 145, 173–76.

[15] Kartsev VN, Shtykov SN, Sineva AV, Tsepulin VV, Shtykova LS. Volumetric and transport properties of water-n-octane-sodium dodecyl sulfate-n-pentanol microemulsions. *Colloid J* 2003, 65, 394–97.

[16] Holmberg K. Organic and bioorganic reactions in microemulsions. *Adv Colloid Interface Sci* 1994, 51, 137–74.

[17] Kometani N, Toyoda Y, Asami K, Yonezawa Y. An application of the water/supercritical $CO_2$ microemulsion to a novel "microreactor." *Chem Lett* 2000, 6, 682–83.

[18] Garti N, Lichtenberg D, Silberstein T. The hydrolysis of phosphatidylcholine by phospholipase A(2) in microemulsion as microreactor. *J Dispers Sci Technol* 1999, 20, 357–74.

[19] Shtykov SN. Chemical analysis in nanoreactors: main concepts and applications. *J Anal Chem* 2002, 57, 859–68.

[20] Kargin ID, Sokolova LS, Pirogov AV, Shpigun OA. The determination of tetracycline antibiotics in milk by HPLC with post-column reaction and fluorimetric detection. *Zavodsk Lab (in Russian)* 2015, 81, 5–9.

[21] Rodriguez-Abreu C, Shrestha RG, Shrestha LK, Harush E, Regev O. Worm-like soft nanostructures in nonionic systems: principles, properties and application as templates. *J Nanosci Nanotechnol* 2013, 13, 4497–4520.
[22] Klossek ML, Touraud D, Zemb T, Kunz W. Structure and solubility in surfactant-free microemulsions. *Chemphyschem* 2012, 13, 4116–19.
[23] Cabos C, Delord P, Marignan J. Local lamellar structure in dense microemulsions. *Phys Rev B Condens Matter* 1988, 37, 9796–99.
[24] Tyowua AT, Yiase SG, Binks BP. Double oil-in-oil-in-oil emulsions stabilised solely by particles. *J Colloid Interface Sci* 2017, 488, 127–34.
[25] Qi X, Wang L, Zhu J. Water-in-oil-in-water double emulsions: an excellent delivery system for improving the oral bioavailability of pidotimod in rats. *J Pharm Sci* 2011, 100, 2203–11.
[26] Fischer V, Marcus J, Touraud D, Diat O, Kunz W. Toward surfactant-free and water-free microemulsions. *J Colloid Interface Sci* 2015, 453, 186–93.
[27] Xu Z, Jin J, Zheng M, Zheng Y, Xu X, Liu Y, Wang X. Co-surfactant free microemulsions: preparation, characterization and stability evaluation for food application. *Food Chem* 2016, 204, 194–200.
[28] Mendonca CR, Silva YP, Bockel WJ, Simo-Alfonso EF, Ramis-Ramos G, Piatnicki CM, Bica CI. Role of the co-surfactant nature in soybean w/o microemulsions. *J Colloid Interface Sci* 2009, 337, 579–85.
[29] Mitra RK, Paul BK. Effect of temperature and salt on the phase behavior of nonionic and mixed nonionic-ionic microemulsions with fish-tail diagrams. *J Colloid Interface Sci* 2005, 291, 2, 550–59.
[30] Tchakalova V, Testard F, Wong K, Parker A, Benczedi D, Zemb T. Solubilization and interfacial curvature in microemulsions. II. Surfactant efficiency and PIT. *Colloids Surf Physicochem Eng Asp* 2008, 331, 40–47.
[31] Papapanagiotou PA, Quinn H, Molitor JP, Nienow AW, Hewitt CJ. The use of phase inversion temperature (PIT) microemulsion technology to enhance oil utilisation during Streptomyces rimosus fed-batch fermentations to produce oxytetracycline. *Biotechnol Lett* 2005, 27, 1579–85.
[32] Gu YX, Huang YH, Liao B, Cong GM, Xu M. Studies on the characterization of phase inversion during emulsification process and the particle sizes of water-borne microemulsion of poly(phenylene oxide) ionomer. *J Appl Polym Sci* 2000, 76, 690–94.
[33] Jeirani Z, Jan BM, Ali BS, Noor IM, Hwa SC, Saphanuchart W. Prediction of phase-inversion temperature of a triglyceride microemulsion using design of experiments. *Ind Eng Chem Res* 2013, 52, 744–50.
[34] Svidritskii EP, Pashkova EB, Pirogov AV, Shpigun OA. Simultaneous determination of fat- and water-soluble vitamins by microemulsion electrokinetic chromatography. *J Anal Chem* 2010, 65, 287–92.
[35] Wang L, Jiang GB, Cai YQ, He B, Wang YW, Shen DZ. Cloud point extraction coupled with HPLC-UV for the determination of phthalate esters in environmental water samples. *J Environ Sci (China)* 2007, 19, 874–78.
[36] Materna K, Schaadt A, Bart HJ, Szymanowski J. Dynamics of surfactant-rich phase separation from solutions containing non-ionic and zwitterionic surfactants. *Colloids Surf Physicochem Eng Asp* 2005, 254, 223–29.
[37] Stalikas CD. Micelle-mediated extraction as a tool for separation and preconcentration in metal analysis. *Trends Anal Chem* 2002, 21, 343–55.
[38] Pons R, Carrera I, Caelles J, Rouch J, Panizza P. Formation and properties of miniemulsions formed by microemulsions dilution. *Adv Colloid Interface Sci* 2003, 106, 129–46.
[39] Trotta M, Gasco MR, Morel S. Behavior of oil-water microemulsions upon dilution with water. *J Dispers Sci Technol* 1991, 12, 239–55.

[40] Sole I, Solans C, Maestro A, Gonzalez C, Gutierrez JM. Study of nano-emulsion formation by dilution of microemulsions. *J Colloid Interface Sci* 2012, 376, 133–39.
[41] Pirogov AV, Tolmacheva NG., Shpigun OA. Use of microemulsion for the extraction of dialkylphthalates from soils with following decomposition of microemulsions, preconcentration, and GC determination of target compounds. (rus.). *Moscow Univ Chem Bull* 2017, 58, 83–88. (in Russian)
[42] Mongjoo J. Tolmacheva NG., Pirogov AV, Popik MV, Shpigun OA. Use of microemulsions for the extraction, preconcentration, and determination of 10 PAHs from different types of soils. *J Anal Chem* 2017, 72, 515–20. (in Russian)
[43] Shen CW, Yu T. Protein separation and enrichment by counter-current chromatography using reverse micelle solvent systems. *J Chromatogr A* 2007, 1151, 164–68.
[44] Nishino S, Kishida A, Yoshizawa H, Shiomori K. A protein extraction system with a water/oil microemulsion formed by a biodegradable polymer surfactant. *Solv Extr Res Develop (Japan)* 2014, 21, 47–54.
[45] Shu Y, Cheng DH, Chen XW, Wang JH. A reverse microemulsion of water/AOT/1-butyl-3-methylimidazolium hexafluorophosphate for selective extraction of hemoglobin. *Separ Purif Technol* 2008, 64, 154–59.
[46] Ontiveros JF, Froidevaux R, Dhulster P, Salager JL, Pierlot C. Haem extraction from peptidic hydrolysates of bovine haemoglobin using temperature sensitive C10E4/O/W microemulsion system. *Colloids Surf Physicochem Eng Asp* 2014, 454, 135–43.
[47] Amiri-Rigi A, Abbasi S. Microemulsion-based lycopene extraction: Effect of surfactants, co-surfactants and pretreatments. *Food Chem* 2016, 197, 1002–07.
[48] Lu RX, Lu,WB. Study on extraction of quercetin in guava leaf by microemulsion. *J Chin med mater* 2009, 32, 608–10.
[49] Radi M, Abbasi S, Hamidi Z, Azizi MH. Development of a new method for extraction of canola oil using lecithin based microemulsion systems. *Agro Food Industry Hi-Tech* 2013, 24, 70–72.
[50] Gao J, Yi H, Yang H, Ren YF. Extraction of Angelica sinensis by using O/W microemulsion. *Chin J New Drugs* 2011, 20, 503–07.
[51] Melo KRO, Dantas TNC, Moura MCPA, Neto AAD, Oliveira MR, Neto ELB. Chromium extraction by microemulsions in two- and three-phase systems. *Brazil J Chem Eng* 2015, 32, 949–56.
[52] Dantas TNC, Neto AAD, Moura MCPA, Neto ELB, Forte KR, Leite RHL. Heavy metals extraction by microemulsions. Water *Res* 2003, 37, 2709–17.
[53] Tong Y, Han L, Yang YZ. Microemulsion extraction of gold(III) from hydrochloric acid medium using ionic liquid as surfactant and extractant. *Ind Eng Chem Res* 2012, 51, 16438–43.
[54] Lu WJ, Lu YM, Liu F, Shang K, Wang W, Yang YZ. Extraction of gold(III) from hydrochloric acid solutions by CTAB/n-heptane/iso-amyl alcohol/$Na_2SO_3$ microemulsion. *J Hazard Mater* 2011, 186, 2166–70.
[55] Yang XJ, Li XL, Huang K, Wei QY, Huang ZJ, Chen J, Xie QY. Solvent extraction of gold(I) from alkaline cyanide solutions by the cetylpyridinium bromide/tributylphosphate system. *Minerals Eng* 2009, 22, 1068–72.
[56] Jiang JZ, Wang XY, Zhou WJ, Gao HC, Wu JG. Extraction of gold from alkaline cyanide solution by the tetradecyldimethylbenzylammonium chloride/tri-n-butyl phosphate/n-heptane system based on a microemulsion mechanism. *PhysChem ChemPhys* 2002, 18, 4489–94.
[57] Vicentino PO, Cassella RJ. Novel extraction induced by microemulsion breaking: a model study for Hg extraction from Brazilian gasoline. *Talanta* 2017, 162, 249–55.
[58] Cassella RJ, Brum DM, Lima CF, Caldas LFS, de Paula CER. Multivariate optimization of the determination of zinc in diesel oil employing a novel extraction strategy based on emulsion breaking. *Anal Chim Acta* 2011, 690, 79–85.

[59] Cassella RJ, Brum DM, de Paula CER, Lima CF. Extraction induced by emulsion breaking: a novel strategy for the trace metals determination in diesel oil samples by electrothermal atomic absorption spectrometry. *J Anal Atom Spectrom* 2010, 25, 1704–11.
[60] Caldas LFS, Brum DM, de Paula CER, Cassella RJ. Application of the extraction induced by emulsion breaking for the determination of Cu, Fe and Mn in used lubricating oils by flame atomic absorption spectrometry. *Talanta* 2013, 110, 21–27.
[61] Robaina NF, Brum DM, Cassella RJ. Application of the extraction induced by emulsion breaking for the determination of chromium and manganese in edible oils by electrothermal atomic absorption spectrometry. *Talanta* 2012, 99, 104–12.
[62] Pereira FM, Brum DM, Lepri FG, Cassella RJ. Extraction induced by emulsion breaking as a tool for Ca and Mg determination in biodiesel by fast sequential flame atomic absorption spectrometry (FS-FAAS) using Co as internal standard. *Microchem J* 2014, 117, 172–77.
[63] Zheng Y, Fang LY, Yan Y, Lin SJ, Liu ZH, Yang YZ. Extraction of palladium (II) by a silicone ionic liquid-based microemulsion system from chloride medium. *Separ Purif Technol* 2016, 169, 289–95.
[64] Arain SA, Kazi TG, Afridi HL, Arain MS, Panhwar AH, Khan N, Baig JA, Shah F. A new dispersive liquid-liquid microextraction using ionic liquid based microemulsion coupled with cloud point extraction for determination of copper in serum and water samples. *Ecotoxicol Environ Safety* 2016, 126, 186–92.
[65] Chen J, Liang R, Wang X. Extraction of Ni by Microemulsion. *Mo Kexue Yu Jishu* 2006, 26, 44–47.
[66] Mihaly M, Comanescu AF, Rogozea EA, Meghea A. Nonionic microemulsion extraction of Ni(II) from wastewater. *Molec Cryst Liq Cryst* 2010, 523, 63–72.
[67] Shang K, Yang YZ, Guo JX, Lu WJ, Liu F, Wang W. Separation of cobalt and nickel from concentrated HCl solutions by Winsor II microemulsion system with N235 as carrier. *Asian J Chem* 2012, 24, 546–50.
[68] Huang TC, Tsai TH. Separation of cobalt and nickel ions in sulfate-solutions by liquid-liquid-extraction and supported liquid membrane with di(2-ethylhexyl) phosphoric-acid dissolved in kerosene. *J Chem Eng Jap* 1991, 24, 126–32.
[69] Levchishin SYu, Murashova NM, Yurtov EV. Extragent-containing microemulsion of sodium di-(2-ethylhexyl)phosphate. *Uspehi Khimii I Khim Technol*. 2008, 22, 37–39. (in Russian)
[70] Levchishin SYu, Murashova NM, Yurtov EV. Microemulsion with di-(2-ethylhexyl)phosponic acid for extraction of transition metals from slimes. *Khim Technol*. 2011, 7, 405–10. (in Russian)
[71] Lou ZN, Guo CF, Feng XD, Zhang SQ, Xing ZQ, Shan WJ, Xiong Y. Selective extraction and separation of Re(VII) from Mo(VI) by TritonX-100/N235/iso-amyl alcohol/n-heptane/NaCl microemulsion system. *Hydrometallurgy* 2015, 157, 199–206.
[72] Wang W, Yang YZ, Zhao H, Guo QW, Lu WJ, Lu YM. Extraction of europium by sodium oleate/pentanol/heptane/NaCl microemulsion system. *J Radioanal Nucl Chem* 2012, 292, 1093–98.
[73] Lu JS, Tian JY, Guo N, Wang Y., Pan YC. Microemulsion extraction separation and determination of aluminium species by spectrofluorimetry. *J Hazardous Materials* 2011, 185, 1107–14.
[74] Madrakian T, Afkhami A, Mousavi A. Spectrophotometric determination of trace amounts of uranium(VI) in water samples after mixed micelle-mediated extraction. *Talanta* 2007, 71, 610–14.
[75] Souza VS, Teixeira LSG, Bezerra MA. Application of multivariate designs in the development of a method for vanadium determination in natural waters by HR-CS GF AAS after cloud-point extraction. *Microchem J* 2016, 129, 318–24.
[76] Mustafina A, Elistratova J, Burilov A, Knyazeva I, Zairov R, Amirov R, Solovieva S, Konovalov A. Cloud point extraction of lanthanide(III) ions via use of Triton X-100 without and with water-soluble calixarenes as added chelating agents. *Talanta* 2006, 68, 863–68.
[77] Dar AA, Rather GM, Das AR. Mixed micelle formation and solubilization behavior toward polycyclic aromatic hydrocarbons of binary and ternary cationic-nonionic surfactant mixtures. *J Phys Chem B* 2007, 111, 3122–32.

[78] Prak DJL, Pritchard PH. Solubilization of polycyclic aromatic hydrocarbon mixtures in micellar nonionic surfactant solutions. *Water Res* 2002, 36, 3463–72.
[79] Zhu LZ, Feng SL. Synergistic solubilization of polycyclic aromatic hydrocarbons by mixed anionic-nomonic surfactants. *Chemosphere* 2003, 53, 459–67.
[80] Zhao Q, Weise L, Li PJ, Yang K, Zhang YQ, Dong DB, Li P, Li XJ. Ageing behavior of phenanthrene and pyrene in soils: a study using sodium dodecylbenzenesulfonate extraction. *J Hazard Mater* 2010, 183, 881–87.
[81] Zhao Q, Xing BS, Tai PD, Yang K, Li H, Zhang LZ, Lin G, Li PJ. Effect of freeze-thawing cycles on aging behavior of phenanthrene, pyrene and their mixture in soil. *Sci Total Environ* 2013, 452, 246–52.
[82] Zhao BW, Zhu LZ, Gao YZ. A novel solubilization of phenanthrene using Winsor I microemulsion-based sodium castor oil sulfate. *J Hazard Mater* 2005, 119, 205–11.
[83] Song GQ, Lu C, Lin JM. Application of surfactants and microemulsions to the extraction of pyrene and phenanthrene from soil with three different extraction methods. *Anal Chim Acta* 2007, 596, 312–18.
[84] Casero I, Sicilia D, Rubio S, Perez-Bendito D. An acid-induced phase cloud point separation approach using anionic surfactants for the extraction and preconcentration of organic compounds. *Anal Chem* 1999, 71, 4519–26.
[85] Goryacheva IY, Shtykov SN, Loginov AS, Panteleeva IV. Preconcentration and fluorimetric determination of polycyclic aromatic hydrocarbons based on the acid-induced cloud-point extraction with sodium dodecylsulfate. *Anal Bioanal Chem* 2005, 382,1413–18.
[86] Shang K., Yang YZ, Guo JX, Lu WJ, Liu F, Wang W. Extraction of cobalt by the AOT microemulsion system. *J Radioanal Nucl Chem* 2012, 291, 629–33.
[87] Liu F, Yang YZ, Lu YM, Shang K, Lu WJ, Zhao XD. Extraction of germanium by the AOT microemulsion with N235 system. *Ind Eng Chem Res* 2010, 49, 10005–08.
[88] Wang JS, Chiu K. Metal extraction from solid matrices using a two-surfactant microemulsion in neat supercritical carbon dioxide. *Microchim Acta* 2009, 167, 61–65.
[89] Chuan-Bo X, Yan-Zhao Y, Xue-Mei X, Song-Xian W. Extraction of rare earth metal samarium by microemulsion. *J Radioanal Nucl Chem* 2008, 275, 535–40.
[90] Gong F, Ma P, Luo Y, Liu L, Zhang L. Solubilization and phase behavior of nonionic water-in-oil microemulsion and its application to extraction of $Nd^{3+}$ in hollow fiber modules. *Huagong Xuebao/J Chem Ind Eng (China)* 2006, 57, 590–95.
[91] Tao Z, Zhao YY, Yu LZ, Bo XC, Mei XX. Extraction of cobalt by CTMAB-pentanol-heptane-HCl Winsor II microemulsion systems. *J Radioanal Nucl Chem* 2006, 267, 401–06.
[92] Zeng S, Yang YZ, Zhu T, Han J, Luo CH. Uranium(VI) extraction by Winsor II microemulsion systems using trialkyl phosphine oxide. *J Radioanal Nucl Chem* 2005, 265, 419–21.
[93] Suzuki H, Naganawa H, Tachimori S. Extraction of europium(III) into W/O microemulsion containing aerosol OT and a bulky diamide. *I. Cooperative effect. Solv Extr Ion Exchange* 2003, 21, 527–46.
[94] Ahn CK, Kim YM, Woo SH, Park JM. Soil washing using various nonionic surfactants and their recovery by selective adsorption with activated carbon. *J Hazard Mater* 2008, 154, 153–160.
[95] Lopez-Vizcaino R, Saez C, Canizares P, Rodrigo MA. The use of a combined process of surfactant-aided soil washing and coagulation for PAH-contaminated soils treatment. *Separ Purif Technol* 2012, 88, 46–51.
[96] Paterson IF, Chowdhry BZ, Leharne SA. Polycyclic aromatic hydrocarbon extraction from a coal tar-contaminated soil using aqueous solutions of nonionic surfactants. *Chemosphere* 1999, 38, 3095–3107.
[97] Alcantara MT, Gomez J, Pazos M, Sanroman MA. PAHs soil decontamination in two steps: desorption and electrochemical treatment. *J Hazard Mater* 2009, 166, 462–68.

E. G. Sumina

# 12 Surfactant Micelles in Liquid Chromatography

## 12.1 Introduction

Liquid chromatography has always used homogeneous solvents or mixtures thereof, sometimes with an addition of inorganic ions, as mobile phases (MPs). The components of the mixture to be separated had to dissolve in the mobile phase, so polar and nonpolar MPs allowed dissolving and separating polar and nonpolar substances, respectively. However, complex natural and man-made mixtures of substances needed to be separated often contain both polar (hydrophilic) and nonpolar (hydrophobic) ones. The appearance of micellar liquid chromatography (MLC) made it possible to solve the problem of the *joint solubility* of both polar and nonpolar substances in a nontrivial way, namely, by the use of micellar surfactant solutions, homogeneous at the macroscopic level but heterogeneous at the nanoscopic one, as mobile phases [1].

Micellar solutions have a peculiarity: in a homogeneous aqueous or nonaqueous dispersion medium, the diphilic surfactant molecules at a certain concentration, called the critical micelle concentration (CMC), spontaneously form nanoscale (3–5 nm) dynamic dispersed aggregates of several tens of surfactant ions or molecules, called micelles. The number of micelles forming a new "pseudophase" in the main solvent is enormous and calculated by dividing the total surfactant concentration in the solution by the aggregation number of surfactant ions (molecules) in a micelle; however, the micelles volume fraction relative to the main solvent is small since the CMC values are in the range of $10^{-4}$–$10^{-2}$ M. The presence of nanoscale micelles in the main solvent is the basis for *concentrating* of the substances to be separated, which, depending on their hydrophobicity, are solubilized (dissolve) either on the surface of the micelle or inside it.

The main feature of micelles is that the medium inside these aggregates formed by alkyl radicals ($C_{10}$–$C_{16}$) is opposite, in polarity, to water as the main solvent of the mobile phase, which allows dissolving both polar (in the aqueous macrophase) and nonpolar (in the nanoscale micelles) substances in a micellar solution. Surfactant micelles are often called biomimetic systems, resembling, by structure and properties, the liposomes and vesicles of living organisms.

A second feature of micelles is the microheterogeneity of the medium inside the micelle, that is, a rapid change in polarity in the direction from the micelle surface to the center. For example, in an aqueous solution, the effective dielectric constant of the medium varies along the micelle's radius from that of water (81) to that characteristic of benzene or dioxane [2, 3]. This allows different (by properties) substances to be localized in different parts of the micelle and to have different binding constants with it. Therefore, the compounds separated in the chromatographic system

https://doi.org/10.1515/9783110542011-012

participate not only in the stationary phase (SP)–MP equilibrium, but also in additional solvent–micelle equilibrium within the MP itself, which affects the selectivity of chromatographic separation.

Another factor influencing separation in MLC is that, when the micellar MP is moving along the sorbent, either single ions (molecules) of the surfactant are sorbed on the surface forming a monolayer (bilayer), or semi-micelles (admicells) are formed, depending on the surfactant concentration in the solution. This dynamically changes the nature of the SP, and, hence, the character of the adsorption equilibrium and distribution of the sorbate in the SP–solvent–MP system as well.

For the first time, surfactant micelles were applied as the main components of aqueous mobile phases in gel chromatography by Armstrong and Fendler [4] in 1977. To date, more than 1,000 publications have described their use in high-performance liquid, thin-layer, ionic, supercritical fluid, extraction, and micellar electrokinetic chromatography (MEKC). Surfactant micelles, due to the efficiency of their modifying effect on the chromatographic process in the whole, are most widely used in high-performance liquid chromatography (HPLC), thin-layer chromatography (TLC), and MEKC. Liquid chromatography (LC) based on the use of micellar surfactant solutions as mobile phases was first referred to as pseudo-phase LC [5, 6] and then MLC [7, 8], and such mobile phases containing surfactant micelles were named micellar mobile phases (MMP) [9, 10]. As the surfactant concentration in MP exceeds its CMC, the main carriers of the substances to be separated are normal (in aqueous media) or reversed (in nonaqueous media) surfactant micelles selectively solubilizing hydrophobic or hydrophilic substances, respectively.

Micellar mobile phases in TLC were proposed by D. Armstrong in 1979 [10]. The following year this author applied MMP in reversed-phase liquid column chromatography (RP HPLC) [11]. This new type of mobile phases has made it possible to significantly expand the capabilities of liquid chromatography and, in some cases, to effectively separate mixtures of hydrophobic and hydrophilic (neutral and charged) organic compounds. Surfactants are shown to modify both MP and SP, as a result of which these phases acquire qualitatively new properties, and the LC method gets novel analytical capabilities.

For more than 30 years, the development of micellar liquid chromatography has progressed in several directions: studying of the chromatographic properties of surfactant-modified stationary phases, studying of the properties and characteristics of MMP; the development of retention models in MLC; evaluation of the efficiency, selectivity, and optimization of the separation of substances in MLC; the use of MLC for separation and analysis of the components of real environmental, pharmaceutical, biological, and food objects. The results of such comprehensive studies and application of the main options of MLC are summarized in a number of reviews dealing with micellar HPLC variants [12–21, 115], TLC [22–25, 115], and a monograph on micellar

HPLC [26]. However, no joint consideration of the micellar options of HPLC and TLC has been carried out.

In this connection, the purpose of this review chapter is to consider the capabilities and limitations of micellar liquid chromatography in the whole, as well as features of both variants in comparison with the classical LC with water–organic mobile phases.

## 12.2 General characteristics of the method

Micellar HPLC, like the classical LC variant, can be performed in isocratic and gradient elution modes with pre-column and post-column derivatization of the analytes, at room or elevated (up to 40°C) temperatures, usually on hydrophobic nonpolar sorbents. Micellar TLC is commonly conducted in isocratic mode at room temperature on ordinary or high-efficiency plates with a normal or reversed phase. In spite of similar methods of implementing the chromatographic process, both MLC options have a number of advantages over classical chromatography based on the use of nonaqueous and water-organic MPs (Fig. 12.1).

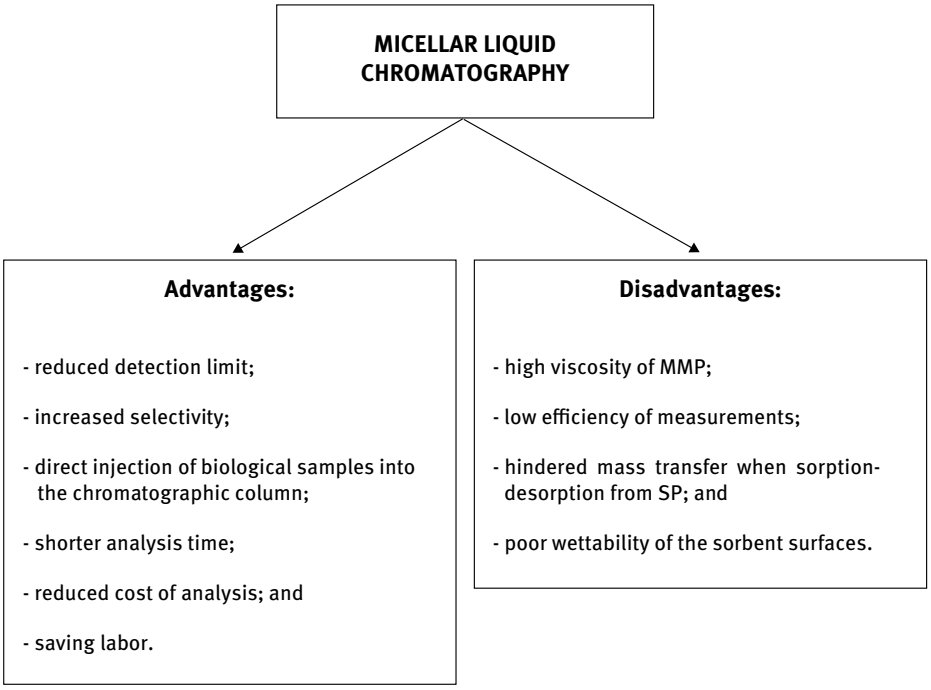
MICELLAR LIQUID CHROMATOGRAPHY
Advantages:
- reduced detection limit;
- increased selectivity;
- direct injection of biological samples into the chromatographic column;
- shorter analysis time;
- reduced cost of analysis; and
- saving labor.
Disadvantages:
- high viscosity of MMP;
- low efficiency of measurements;
- hindered mass transfer when sorption-desorption from SP; and
- poor wettability of the sorbent surfaces.

**Fig. 12.1:** Advantages and disadvantages of micellar liquid chromatography in comparison with liquid chromatography with water-organic mobile phases.

For example, aqueous MMPs lack a number of disadvantages of organic solvents traditionally used in LC, such as acrid odor, volatility, flammability, chemical aggressiveness, and toxicity. In this regard, they are recommended not only for production and research laboratories, but also for educational laboratories and even for lecture demonstrations [27]. Another merit of MMPs is their low cost and good biodegradability [9]. One more advantage of MLC is the possibility of achieving lower detection limits than in traditional liquid chromatography. This is especially true when using fluorescent or phosphorescent detectors, since the analytical signal intensity increases upon solubilization of compounds in micelles due to changes in the micropolarity and microviscosity of the medium in the local environment of the luminophor, as well as the effect of concentration in surfactant micelles. In addition, the use of MMP simplifies sample preparation and decreases the time analysis of complex objects, for example, biological fluids, allowing them to be directly injected into the chromatographic column due to solubilizing proteins in surfactant micelles.

The retention mechanism in micellar liquid chromatography is based on the following properties of surfactant micelles, determining a number of specific features of the technique [3]:

- the ability to solubilize (dissolve and bind) and concentrate substances in nanoscale micelles, which are insoluble in the solvent forming the dispersion medium of the micellar solution;
- the selective nature of solubilization due to a combination of electrostatic, donor–acceptor, and hydrophobic interactions, which underlies differentiation and separation of compounds with different binding constants of the analytes with surfactant micelles;
- the appearance of a new equilibrium ("micelle–solvent") in the mobile phase with the participation of the analyte, complementing the MP–SP equilibrium; and
- the ability of individual surfactant ions and molecules to be sorbed on the sorbent surface and to dynamically change the properties of the stationary phase.

The listed properties of micellar solutions serve as a basis for increasing the separation selectivity of substances in LC compared with water–organic eluents.

The efficiency of binding of a substance with micelles is determined by both the characteristics of the surfactant micelles themselves and the nature of the analyte. Normal and reversed micelles are known to bind, as a rule, hydrophobic and hydrophilic compounds, respectively. A more fine differentiation of substances (and, therefore, a higher selectivity) is due to the following factors: the micelle–analyte charge ratio, for example, anionic surfactant micelles mainly bind cationic analytes; the presence of functional groups in the molecules of surfactants and analytes; the presence of aromatic rings and unsaturated bonds in the hydrocarbon radical; the hydrophilic–lipophilic balance of the surfactant and analyte molecule as a whole,

and changes in the counter ion nature of ionic surfactants. Additional opportunities for improving the separation selectivity in MLC can be achieved by modifying the properties of the micelles themselves, for example, by adjusting the charge density and/or surface potential, and also by varying the hydration degree and micelle size or the viscosity of the micellar mobile phase by adding electrolytes, organic solvents, or co-surfactants [2, 3]. In light of these advantages, MMPs have become an important addition, and, in some cases, an alternative to simple mobile phases containing organic solvents.

Comparison with classical water–organic MP reveals few disadvantages of MMP. One of them is associated with the higher viscosity of MMP compared with organic solvents, which increases the duration of analysis. Such a viscosity is due to high surfactant concentrations in the mobile phase, sometimes even exceeding $CMC_2$, at which the micelles are no longer spherical, but cylindrical and have very high aggregation numbers [1, 3]. In the case of lower surfactant concentrations (corresponding to spherical micelles), the separation time is comparable or shorter than when using MP based on organic solvents.

Another significant demerit of MMP is the lower separation efficiency of compounds in MLC compared with water–organic MPs, which is a consequence of poor mass transfer during the sorption/desorption of substance to/from the stationary phase. The causes are the poor wettability of the surface of hydrophobic sorbents and surfactant adsorption on their surface, which increases the thickness and microviscosity of the surface layer, especially in the case of the reversed phase. To improve the wettability and mass transfer, it is recommended to add alcohols to MP, which would partially displace the surfactant from the surface of the sorbent. Another way to improve mass transfer may be using elevated temperatures. The efficacy is significantly improved and becomes comparable with the classical LC version, when inverse surfactant micelles are used as MMP. This technique is mainly used in TLC [24].

## 12.3 Features of mobile and stationary phases in MLC

### 12.3.1 Mobile phases

Low CMC values and small aggregation numbers of surfactant micelles are common requirements to select micellar eluents. The size of micelles should not exceed 6–8 nm, and the CMC should not exceed 0.01 M. Such micellar characteristics provide the formation of not very viscous eluents and a decreased pressure in the chromatographic column, as well as a depressed effect of light scattering by surfactant micelles in the operating ranges of UV and spectrophotometric detectors [20].

Aqueous micellar solutions of all surfactant types (cationic, anionic, and nonionic) that meet this condition are used as mobile phases in micellar HPLC. Of the cationic surfactants (CS), cetyltrimethylammonium bromide and chloride (CTAB and CTAC), dodecyltrimethylammonium bromide (DDTAB) are most often used, of the anionic ones – sodium dodecyl sulfate (SDDS, or simply SDS), sodium tetradecylsulfate, and sodium dodecylsulfonate. Brij-35, Tween-20, Tween-80, Triton X-100, and Triton X-114 are the main representatives of nonionic surfactants (NS) used as components of MMP. In most works, SDS is preferred with its concentration in the MMP within 0.02–0.08 M [28–41].

The situation is almost the same in micellar TLC (MTLC). It has been established that the effects needed in MTLC are mainly inherent in ionic surfactants [22, 24]. This is especially true for polar silica gel, with the surface of which cationic surfactants bind more strongly due to not only hydrophobic, but also electrostatic interactions with dissociated silanol groups. Of this surfactant group, CTAB and CTAC are most often used, and more rarely – other salts of alkyltrimethylammonium and alkylpyridinium. Of anionic surfactants, alkylsulfates and alkylsulfonates are used. In separate studies, the MMP also included micelles of nonionic surfactants: Tween-80 and Triton X-100, SPAN-20. Mixtures of surfactants are sometimes used: SDS and TX-100, CTAB (CTAC) and Brij-35, CTAB and Tween-80. However, SDS is preferred of all types of surfactants [42–49].

Besides normal micelles formed in water, reversed micelles are also used in MTLC, for example, Aerosol OT (AOT) in cyclohexane [9, 10, 27]. The recommended surfactant concentrations in micellar mobile phases are very various: from 1.5–5 $CMC_1$ to 10–50 $CMC_1$ [22, 24].

The optimum micelle concentration in MMP can be calculated by the equation [50]

$$pM_{opt} \approx \lg K_{XM} - \frac{1}{2} \lg \frac{K_X^{/}}{K_1^{/}}, \tag{1}$$

$$pM_{opt} = -\lg[M], \tag{2}$$

where $M_{opt}$ is the optimum concentration of micelles, $M$;
$K_{XM}$ the sorbate–micelle binding constant;
$K_X^{/}$ the limiting value of the sorbate retention factor; and
$K_1^{/}$ the sorbate retention factor at a surfactant concentration equal to 1 M.

This equation was used to calculate the $pM_{opt}$ values for SDS, CTAB, or Brij-35 for chromatography of a wide range of sorbed substances [14]. The properties of mobile phases containing surfactant micelles can be influenced by various factors, which may substantially change the chromatographic pattern of separation. It is therefore necessary to consider them in more detail.

**Organic modifier effect.** The micellar mobile phases containing an organic modifier, in addition to surfactants, are proposed to be called *the hybrid or modified* MMP [20]. The following substances are used as organic MMP modifiers: aliphatic alcohols, generally of normal structure with the number of carbon atoms from $C_1$ to $C_5$ [51–56], sometimes their mixtures (e. g., 1-butanol and 1-pentanol) [57], acetonitrile [29, 47], and tetrahydrofuran [20]. Branched isomers of aliphatic alcohols are taken less often [54, 58]. Aliphatic carboxylic acids (acetic, propionic, butyric, valeric, and hexanoic) were proposed for the first time as MMP modifiers, as well as two fluorine-substituted acetic acids (monoacetic and trifluoroacetic) [45].

Such organic modifiers have been established [1, 3, 20, 59, 60, 104] to be able to modify both the micellar properties of surfactants themselves (CMC values, aggregation numbers) and the eluent strength of surfactant-containing mobile phases, and, therefore, the solubilization conditions of the analytes in micelles, their retention, and the selectivity of separation.

The effect of alcohols on the CMC of sodium dodecylsulfate has been studied most thoroughly [20, 58, 61]. It was shown methanol to be the only representative of aliphatic alcohols whose introduction increases the CMC of SDS [62]. By measuring the surface tension in SDS solutions, it was found that at 25°C the CMC was $2.3 \cdot 10^{-2}$, $3 \cdot 10^{-2}$, and $3.8 \cdot 10^{-2}$ M at the $CH_3OH$ concentration of 0 %, 5 %, and 20 %, respectively. Other alcohols, on the contrary, reduce the value of CMC and the stronger, the higher the alcohol concentration and the longer its hydrocarbon radical [20]. For example, an equal decrease in CMC is observed when 15 % propanol, 5 % butanol, or 1 % pentanol is added to an aqueous DDS solution. High (exceeding 20 vol.%) alcohol concentrations, vice versa, suppress micelle formation, for example, no micelles are formed in water–alcohol solutions containing above 23 % 1-propanol or 27.5 % 1-butanol. Hexanol, octanol, and decanol are not used to modify MMP due to their low solubility in water and emulsion formation. It has been established [45] that aliphatic carboxylic acids, like their corresponding alcohols, reduce CMC and stabilize SDS micelles.

Solvents of another chemical nature (acetonitrile and tetrahydrofuran) act in different ways. Acetonitrile, similar to methanol in polarity, also increases the CMC of SDS. The effect of tetrahydrofuran depends on its concentration, namely: a change in the solvent volume fraction from 0 % to 5 % causes a slight decrease in the CMC, with its further increase.

Studies of the effect of solvents on the chromatographic properties of sorbates have established the following features of hybrid MMPs:

- dependence of their properties on the nature and hydrophobicity of the organic solvent modifier;
- dependence of the eluent strength of the MMP on the concentrations of the solvent and surfactant; and
- dependence of sorbate retention on the hydrophobicity of the substances to be separated.

For example, Ruiz-Angel et al. [63], when chromatographing benzene and 2-ethylanthraquinone, found that solvents of similar polarity but belonging to different types according to Snyder's classification (methanol, tetrahydrofuran, and acetonitrile) caused smaller changes in the retention factors ($k'$) than one-type solvents, for example, monohydric alcohols, differing in hydrophobicity. For alcohols, the values of $k'$ of the sorbates studied decrease in the row: methanol > ethanol > propanol > butanol > pentanol > hexanol, that is, with an increase in the alcohol hydrocarbon radical length. The observed selectivity row of alcohols correlates with their ability to adsorb on the hydrophobic surface of the reversed-phase sorbent $C_{18}$, which suppresses the sorption and retention of the analytes, and thereby enhances their transport by normal SDS micelles.

The effect of aliphatic carboxylic acids with different hydrocarbon radical lengths on the retention and selectivity of separation of amino acid derivatives was studied [45]. It has been shown that *the more hydrophobic the acid is, the lower concentration is necessary for complete separation of the components* of the mixture under analysis. The authors explain the less pronounced effect of acetic acid by its lower hydrophobicity in comparison with other acids and, consequently, the poorer possibility to act as a co-surfactant in the modification of micelles. Aliphatic carboxylic acids are recommended by these authors to separate substances of an acidic nature. In contrast to alcohols, acids in MMP perform two functions, namely stabilization of the pH value of the mobile phase, which avoids the additional use of buffer solutions, and modification of the surfactant micelles.

To select the most suitable organic modifier for a certain micellar mobile phase, it was suggested to use data on the hydrophobicity of separated compounds in accordance with the values of their distribution coefficients in the octanol–water system ($P_{o/w}$) [20]. Propanol is recommended for use to separate such hydrophilic compounds, which lg $P_{o/w}$ values fall within the range of –1 to 2 (amino acids, proteins [64], sulfonamides, and phenolic antioxidants [65]), butanol – for less hydrophilic substances: $1 < \lg P_{o/w} < 3$ (e. g., β-blockers [66]). Pentanol (<6 %) is suitable for separation of sufficiently hydrophobic compounds, when $\lg P_{o/w} > 3$ (corticosteroids, barbiturates, diuretics, stimulants, and polyaromatic hydrocarbons [67, 68]).

It is known [69, 70] that in RP HPLC, the eluent strength of water–organic MP is calculated by the equation

$$\lg k' = \lg k_0 - S\varphi, \tag{3}$$

where $k_0$ is the sorbate retention factor in the absence of an organic solvent;
$k'$ the sorbate retention factor in the presence of an organic solvent;
$S$ the eluent strength; and
$\varphi$ the solvent volume fraction in MP.

A similar equation was proposed for hybrid micellar mobile phases [60]:

$$\lg k' = \lg k_0 - S_{hyb}\varphi, \tag{4}$$

where $k_0$ *is* the sorbate retention factor in MMP in the absence of any organic solvent;
$k'$ the sorbate retention factor in MMP in the presence of an organic solvent;
$S_{hyb}$ the eluent strength parameter of the hybrid micellar eluent; and
$\varphi$ the solvent volume fraction in MMP.

Eqs (3) and (4) show that with increasing $S$ and $S_{\text{hyb}}$, the sorbate retention should decrease. However, in classical RP LC, the eluent strength depends on the solvent concentration in the mobile phase only, while in MLC it depends on the concentrations of both components (the surfactant and organic solvent). It was shown that the influence of the surfactant concentration in MMP is stronger than that of the solvent concentration in the mobile phase [26]. Detailed studies of the effect of organic modifiers in MMP were also carried out in few papers [29, 58, 71–74].

**pH effect of the mobile phase.** The necessary pH values of the MMP in column and planar chromatography are usually maintained by acetate-ammonia or phosphate buffer solutions, which are usable in weakly acidic, neutral and slightly alkaline media. The MMP acidity mostly affects the chromatography of ionizable substances. In this case, a small change in pH may significantly change the chromatographic pattern, especially if this value is close to p$K_{\text{a}}$ of acids or p$K_{\text{b}}$ of bases [75]. In HPLC, such studies are mainly known for reversed-phase sorbents [26, 75], while in TLC – for sorbents with normal and reversed phases [22, 24].

The pH effect in TLC is described for organic reagents of the series of fluorescein, sulfophthaleins, and dicarboxylic acids [43, 76–78]. Studies have shown that the optimum separation condition for the reagent classes studied is an alkaline (fluoresceins, sulfophthaleins) or slightly alkaline (phenol carboxylic acids) medium, irrespective of the stationary phase nature (Silufol or Plasmachrom). Under these conditions, they are all in the same $R^{2-}$-ionized form [79], which makes it possible to compare their chromatographic behavior in MMP.

**Effect of the ionic strength of solution.** Strong electrolytes, like organic solvents, primarily affect the micelle formation of ionic surfactants and, as a result, the modifying properties of ionic micelles [1, 3, 22, 24, 26, 60, 75, 105, 106]. Due to adsorption of the salt counter ions on the micelle, some of its ionic charge (for various surfactants and according to different authors: from 60 % to 90 %) is screened. It is noted [1] that at a thickness of the Stern layer of 0.7 nm, the local concentration of counter ions therein could reach 3–5 M, that is could exceed their concentration in the solvent by 2–3 orders of magnitude. The remaining counter ions are located in the diffuse Gouy–Chapman layer. According to the general approach [60, 80], the potential ζ of

the Stern layer should depend on the activity of the potential-determining surfactant ions in the bulk of solution, for example:

$$\zeta = \zeta_0 + \left(2.303 \cdot \frac{RT}{F}\right) \cdot \lg a_{csurf^+} \tag{5}$$

An increased activity of counter ions in the aqueous phase enhances the neutralization of the micelle's charge. The $\zeta$ value in the presence of salts therefore decreases and the critical micelle concentration decreases as well. An additional effect of salts is expressed in the dehydration of the micelles and separated substances solubilized therein (the salting-out effect), which changes their binding and, consequently, the chromatographic characteristics. Therefore, the salt effects in micellar solutions should be determined by the effect of the adsorbed salts on the Stern layer potential, and, as a consequence, on the micelle formation of surfactants, the solubilization of organic compounds, and also on the distribution processes occurring in this medium. However, these questions have so far been studied little and do not allow predicting the effect of an electrolyte in every particular case.

The review [20] notes that the effect of all the above parameters can be optimized by using the mathematical apparatus and computer programs, which will allow the researcher to select directly the optimum separation conditions in MMP [81–87]. Unlike HPLC, electrolytes have virtually no effect on the chromatographic behavior of sorbates in TLC. This is perhaps due to the presence of a double solvent front on the sorbent surface in MTLC [42], which determines the simultaneous existence of two separation mechanisms (micellar and ion-pair). Electrolytes differently affect the solubilization process in micelles and the formation of ion pairs with the participation of surfactants [1, 12], so their influence on the SP surface in TLC is difficult to predict.

### 12.3.2 Stationary phases

Micellar HPLC commonly uses *reversed-phase sorbents* produced by few firms, namely: Separon $C_{18}$, Nucleosil $C_{18}$, Hypersyl ODS, μ-Bondapak $C_{18}$, Ultrasphere ODS, Spherisorb ODS-2, etc. Unlike RP HPLC, according to some authors [20, 88–90], the brand of reversed-phase sorbents has little effect on the results of separation. To test columns, a new approach to comparing the selectivity of stationary phases was developed [90], based on the use of a test mixture of sorbates chromatographed by different mechanisms. A classification of stationary phases is proposed to make it possible to reveal interchangeable columns, which greatly simplifies and accelerates the practical application of methods for analyzing various objects in the MLC conditions. This is a feature of the reversed stationary phase in micellar HPLC.

In micellar TLC, mixtures of compounds are separated on normal SP (Silufol and Sorbfil plates, alumina, cellulose) and reversed SP (silica gel with a grafted $C_3$ phase

(Plasmachrom plates), silica gel with a grafted $C_{18}$ phase), as well as on silica gel mixed with a polymeric material and on polyamide-6 or polyamide-11 [22, 24]. According to [24] and some previous studies, polyamide is the best sorbent for the micellar mobile phase in TLC. The good separating ability of polyamide plates is attributed to the relatively weak adsorption of the surfactant and, as a result, the relatively constant concentration of surfactant micelles in MP as it moves along the sorbent's surface, which leads to good reproducibility of analysis. Good separation in micellar TLC was also achieved on polar Silufol and Sorbfil plates [22, 24].

It has been established that the chemical stability of SP on the TLC plate is affected by the nature of the surfactants that form MMP. For instance, when silica gel plates coated with chemically bound octadecylsilane (KC18F) are used, CTAC less destroys the stationary phase than SDS. Effective separation on KC18F is achieved when using 0.4 M CTAC solution or a mixture of 0.2 M CTAC + 0.2 M sodium chloride as MP. In the case of SDS, it is recommended to add high concentrations of strong electrolytes to prevent destruction of the reversed nonpolar phases in MMP. The total concentration of the surfactant and electrolyte in MP should be constant; it can reach 0.4–0.6 M [91].

When the surfactant-containing mobile phase moves along the sorbent layer in the chromatographic column or on the surface of the chromatographic plate due to adsorption of hydrophobic ions or surfactant molecules, its surface is *dynamically modified* [42, 120]. This is another feature of the stationary phase in MLC. The consequence of such dynamic modification of SP is a radical change in its properties and the corresponding chromatographic regime. This is a third feature of the stationary phase in MLC. Let us dwell on its characteristics.

Anionic surfactants mainly adsorb on the hydrophobic surface of the sorbent by the hydrophobic mechanism (hydrophobic adsorption). The driving force of this process is the hydrophobic interactions between the hydrocarbon radicals of the grafted sorbent layer and the surfactant. As a result, the sorbent's surface which negatively charged hydrophilic groups of the anionic surfactant appear on becomes hydrophilic and acquires the ability to cation exchange with the ions in the mobile phase. Therefore, the *reversed-phase chromatography regime changes to the normal-phase one* and the analyte elution order is also reversed [24, 75].

If cationic surfactants adsorb on a hydrophobic surface, two types of interaction are possible, namely hydrophobic and electrostatic [75]. The first one, just as in the case of anionic surfactants, is accomplished through hydrophobic interactions. The second one is due to interactions between the unmodified dissociated silanol groups of the silica gel surface and the cationic groups of the surfactant. A combination of both mechanisms is possible. The final result depends on the surface modification degree, that is, the ratio between the alkylated and nonalkylated surface silanol groups. Depending on this, the chromatography mechanism may change or remain unchanged.

In the case of weakly hydrophobic reversed phases RP-3 or RP-2 and ionic surfactant of different types, the elution order usually does not change in comparison with

the normal phase. In contrast to reversed phases, ionic surfactant adsorption on the normal phase (unmodified or hydrophilically modified silica gel) results in hydrophobization of the sorbent, which acquires the reversed-phase properties. The result is a switch from *the normal-phase chromatography mode to the reversed-phase one*. The elution order of substances changes accordingly [43, 76, 92, 93].

Such changes were described for normal-phase TLC during the chromatography of fluorescein derivatives [43, 76, 77], phenol carboxylic acids [78], sulfophthaleins [77], Cu (II), Co (II), Ni (II) diketonates on Silufol plates [94] and for reversed-phase TLC when separation of amino acids on KC18 layers [22, 24, 75]. It should be noted that there are still no rules to predict the elution order. A comparison of the chromatographic behavior of substances with their distribution coefficients in the octanol–water system could probably be a good criterion. The modification nature becomes more predictable if the sorption mechanism of various surfactants on the normal and reversed phases is clear. An important research in this direction was carried out by Berthod and García–Álvarez–Coque [26].

Ionic surfactants are most often used to *modify* SP, whereas nonionic surfactants are used rarely. This is due to some peculiarities of their adsorption on a solid surface. Unlike ionic surfactants adsorbed vertically oriented, the oxyethylated chains of nonionic surfactants are located horizontally to the surface and modify the stationary phase to a lesser degree [95].

Regardless of the sorbent nature, temperature, the nature and structure of the surfactant, the pH and ionic strength of the aqueous solution, the simultaneous presence of several surfactants in solution and the presence of an organic solvent strongly influence the surface modification and the shape of the adsorption isotherms of the surfactant [102].

**Molecular structure of surfactants.** It has been established [95] that within a homologous series, an increased length of the hydrocarbon chain of the surfactant leads to an increased adsorption $\Gamma_{max}$ on both polar and nonpolar sorbents. An increased size of the polar (head) group in ionic surfactants or the oxyethylated chain length in nonionic ones, on the contrary, reduces the value of $\Gamma_{max}$. For example, when the oxyethylated chain length of a nonionic surfactant >44, no adsorption of oxyethylated tetramethylbutylphenols on silica gel is possible, since the hydration energy of the oxyethylated chain exceeds the adsorption energy [96]. With a low surfactant content in solution ($C$ « 0.1 $CMC_1$), the adsorption grows insignificantly with concentration, and for concentrations ≥0.1 $CMC_1$ it sharply increases. This may be due to changes in the orientation of surfactant molecules on the surface: from horizontal (in very dilute solutions) to vertical (around $CMC_1$) [95].

***The acidity of solution*** affects the adsorption properties, especially those of ionic surfactants, especially in the case of unmodified polar silica gel, for which the adsorption of cationic surfactants increases with pH, while that of anionic surfactant decreases [97–99]. For nonionic surfactants, the acidity effect is weaker, however, on

polar sorbents containing *carboxyl* groups, when pH > 5.2 the adsorption is small but increases by an order of magnitude with decreasing pH. This increase is associated with the formation of hydrogen bonds between the undissociated carboxylic groups of the sorbent and the ester groups of the surfactant.

***Electrolytes*** that cause salting out of surfactants from an aqueous solution due to their own hydration increase their adsorption. At the same time, some inorganic salts themselves can be adsorbed on polar surfaces and actually displace surfactants. An example is the hydrated lanthanum ion [95]. Finally, electrolyte ions, sorbing on a solid surface, change the surface charge, and, as a consequence, modify the surfactant adsorption. This adsorption can also be influenced by nonelectrolytes, which high concentrations could change the solvent structure or the sorbent surface nature.

***Joint adsorption*** of various surfactant types on the stationary phase has not yet been studied sufficiently. However, it has been established that the adsorption isotherm of nonionic surfactants in the presence of anionic ones varies insignificantly. On the contrary, nonionic surfactants significantly affect the adsorption of anionic ones, causing an adsorption peak to appear on the isotherm [100]. Similar changes in the isotherm are characteristic for joint adsorption of nonionic and cationic surfactants [101]. It is believed that when the concentration exceeds $CMC_1$, due to the formation of mixed micelles, the relative concentrations of surfactant molecules or ions in solution vary. Moreover, in the mixed system of CS–NS, the surfactant cation diffuses to the surface faster than the NS molecule, but after adsorption the ionic surfactant is gradually replaced by the nonionic one.

The ***organic solvent*** present in the solution not only alters the CMC of the surfactant, but can also be sorbed on the surface of the solid phase, reducing the surfactant concentration thereon, so the stationary phase undergoes further changes [95]. Although the mechanism of action of the solvent when combined with a surfactant is not well studied, it can be assumed that the resultant effect depends on the nature of all the three components: the surfactant, the surface, and the organic additive, as well as on the concentration of the organic additive and surfactant.

Together, the listed factors underlie the modification of the properties of the stationary phase in the presence of a surfactant.

## 12.4 Retention models in MLC

The model by Armstrong and Nome [107] is the most common one describing the equilibrium processes in the column and on the sorbent surface in micellar liquid chromatography. According to this model, the sorbate is distributed not only between the stationary and mobile phases, but also inside the mobile phase itself, that is between water and surfactant micelles (Fig. 12.2).

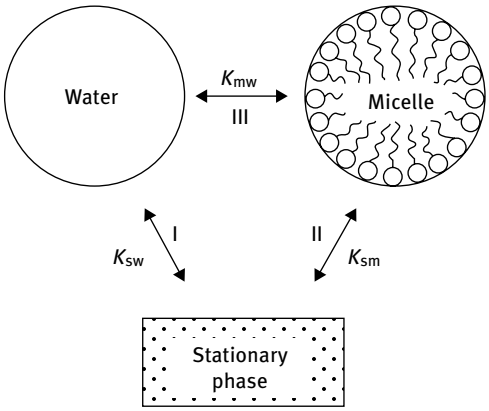


**Fig. 12.2:** The chromatographic behavior of the sorbate in the micellar mobile phase.

The chromatographic behavior of the sorbate in the micellar mobile phase is determined by three distribution coefficients, namely:

$K_{sw}$ – the distribution coefficient between the stationary phase and water;
$K_{sm}$ – the distribution coefficient between the stationary phase and the micelle; and
$K_{mw}$ – the distribution coefficient between the micelle and water.

The existence of this second equilibrium distinguishes MLC from liquid chromatography with water–organic eluents.

In accordance with this model, all compounds can be divided into four groups [108]. The first one includes substances bound by micelles, their mobility increases with the surfactant concentration in the mobile phase ($K_{mw} > 0$). The second group consists of substances not bound by micelles, their mobility does not change with the surfactant concentration ($K_{mw} = 0$). The third one includes so-called anti-bound substances, whose mobility decreases with increasing surfactant concentration in the mobile phase ($K_{mw} < 0$). The fourth option includes high-molecular-weight compounds with an abnormally strong binding, which more than one surfactant micelle is involved in.

It is obvious that the electrostatic repulsion of like-charged surfactant micelles and substrate particles is the factor determining the anti-binding behavior of the substrate. However, this rule is not always observed; for example, there are many compounds carrying a positive charge and bound by cationic micelles – and negatively charged ones interacting with anionic micelles. In the case of the anti-binding effect due to electrostatic interactions, the $K_{mw}$ value should be influenced by strong electrolyte additives (the salt effect). For most compounds, the values of $K_{mw}$ increase with the salt concentration in the mobile phase. Often, when a salt is added, the substrate switches from anti-binding to binding.

There are other developed models that summarized in a number of reviews, for example [14, 20]. Modern variants of modeling processes in MLC are discussed in few papers [82, 85, 109–113].

For column chromatography, Armstrong and Nome [102] have proposed the following equation:

$$\frac{V_S}{V_l - V_0} = \frac{\nu\,(K_{mw} - 1)}{K_{sw}} C_m + \frac{1}{K_{sw}}, \tag{6}$$

where $V_s$ is the volume of the stationary phase;
$V_l$ the volume of the mobile phase;
$V_0$ the column dead volume;
$\nu$ the partial specific volume of the surfactant (mL/g) (0.862 mL/g for DDS); and
$C_m$ the micelle concentration in the mobile phase, $C_m = (C - \mathrm{CMC})$, $C$ being the total surfactant concentration in the mobile phase, and CMC is the critical micelle concentration (g/mL).

A similar equation was proposed by Armstrong and Stein for micellar thin-layer chromatography [114]:

$$\frac{R_f}{1 - R_f} = \frac{V_m}{V_s} \cdot \left( \frac{\nu\,(K_{mw} - 1)}{K_{sw}} \right) \cdot C_m + \frac{V_m}{V_s} \cdot \frac{1}{K_{sw}}, \tag{7}$$

where $R_f$ is the sorbate mobility;
$V_s$ the volume of the stationary phase;
$V_m$ the volume of the mobile phase;
$\nu$ the partial specific volume of the surfactant (mL/g);
$C_m$ the micelle concentration in the mobile phase, $C_m = (C - \mathrm{CMC})$, where $C$ is the total surfactant concentration in the mobile phase, CMC is the critical micelle concentration (g/mL); and $V_m/V_s$ the phase-volume ratio.

According to the above equations, the $V_s/(V_l - V_0)$ *vs.* $C_m$ and $R_f/(1 - R_f)$ *vs.* $C_m$ dependences are linear, which makes it possible to calculate the constants of equilibrium processes from graphical data.

Let us consider a graphical version of the algorithm with micellar TLC as an example. The equation describing the dependence of retention ($R_f$) in TLC on the surfactant micelle concentration $R_f/(1 - R_f) = f(C_m)$ is a straight line equation $y = ax + b$, where the coefficients are:

$$a = \frac{V_m}{V_s} \times \left[ \frac{(K_{mw} - 1)\nu}{K_{sw}} \right], \tag{8}$$

$$b = \frac{V_m}{V_s} \times \frac{1}{K_{sw}}, \tag{9}$$

Transition to the $a/b$ ratio, that is, to the ratio of the slope of this line (coefficient $a$) to the segment cutoff on the ordinate axis (coefficient $b$) reduces ($V_m/V_s$) and $K_{sw}$ in the equation to obtain the dependence

$$\frac{a}{b} = \frac{V_m \times (K_{mw} - 1)v \times K_{sw} \times V_s}{V_s \times K_{sw} \times V_m} = (K_{mw} - 1)v, \tag{10}$$

Then, by measuring the value of $R_f$ and plotting $R_f/(1 - R_f) = f(C_m)$, the sorbate distribution coefficients between the aqueous (dispersion medium) and micellar phases can be calculated by the formula

$$K_{mw} = \frac{a}{bv} + 1, \tag{11}$$

The distribution coefficient $K_{sw}$ can be calculated from Eq. (9), and the coefficient $K_{sm}$ is obtained as the ratio of the two previous coefficients

$$K_{sm} = \frac{K_{sw}}{K_{mw}}, \tag{12}$$

It has been shown [2, 3, 7, 22–24] that the solubilization of a substance into micelles is determined by the surfactant charge, the nature of its counter ion, and the nature of the solubilizate, regardless of whether the particles of the compounds to be separated are charged or neutral. The hydrocarbon radical length of the surfactant also influences the distribution coefficient $K_{mw}$. This is consistent with the results of determining $K_{mw}$ by other methods and is well revealed with a significant contribution of hydrophobic interactions to the solubilization of substances [1–3]. The nature of the sorbate bound by micelles is a more significant factor, also caused by hydrophobic interactions. This conclusion can be arrived at by analysis of the data in Tab. 12.1, which shows the results of calculating $K_{mw}$ and $K_{sw}$ for several compounds of the xanthene and triphenylmethane series (TLC). It can be seen that the presence of bromine (eosin) and iodine (erythrosine) atoms in the molecules of the fluorescein reagents significantly increases the binding constant of the indicator anions with anionic surfactant micelles. A similar dependence is also observed for sulfophthalein derivatives (phenol red and its derivatives), but the growth of the binding constant is not so great. The joint presence of halogen atoms and alkyl substituents enhances the binding of the anionic forms of reagents with SDS micelles, the longer the hydrocarbon radical of the substituent in the reagent molecule is, the stronger the binding [43, 47].

**Tab. 12.1:** Coefficients $a$ and $b$ in the equation $R_f/(1 - R_f) = aC_m + b$ and the distribution coefficients of substances from water into SDS micelles $K_{mw}$ and on the sorbent surface $K_{sw}$ (297 K)

| Substance | $a$ | $b$ | $K_{mw}$ | $K_{sw}$ |
|---|---|---|---|---|
| Fluorescein | 42.6 | 4.07 | 13.1 | 0.30 |
| Eosin | 29.1 | 0.33 | 105 | 3.6 |
| Erythrosin | 37.4 | 0.10 | 431 | 11.7 |
| Phenol red | 59.3 | 2.14 | 33.2 | 0.50 |
| Bromophenol red | 56.5 | 1.39 | 48.1 | 0.80 |
| Bromophenol blue | 35.5 | 0.38 | 108 | 3.1 |
| Cresol red | 46.2 | 0.45 | 119 | 2.6 |
| Thymol blue | 37.1 | 0.060 | 681 | 18.6 |
| Bromothymol blue | 38.9 | 0.060 | 710 | 18.5 |

## 12.5 Application of MLC in analysis

Micelles have found much wider application in LC than surfactants in their ionic state involved in the implementation of ion-pair chromatography, which selectivity is also due to the appearance of a second equilibrium in the mobile phase. This is related, as shown above, to much greater capabilities that arise in connection with the appearance of a nanoscale pseudophase in solution, which include varying the properties of the medium in the microenvironment of analytes solubilized in micelles, expanding their solubility range, the effects of concentrating the components of the mixture to be separated, changing the sorbent surface, and other above-mentioned factors, which, as a rule, act simultaneously and allow optimizing the separation conditions of the components of complex objects [21, 115, 116]. The objects of analysis in MLC are diverse: biological fluids (urine, serum, and blood plasma), placenta, medicines, food products, cosmetics, environmental objects, forensic objects, etc. The analytes are diverse as well (Fig. 12.3).

MLC is most widely used in analysis of medicinal products, in the quality control of medicinal substances and ready-made dosage forms, as well as in analysis of medicines in biological fluids, studying metabolic processes, the stability, destruction kinetics, toxicity, and therapeutic effects of medicines in the human body. MLC is also used to study the retention mechanism on the normal and reversed phases and to establish the relationship between retention and the hydrophobicity of the analytes [14, 20, 22–25]. The use of surfactant micelles is promising for extraction, separation, and concentration of biological substrates, especially proteins, in combination with high-performance liquid chromatography [117–120]. Application examples of the micellar options of TLC and HPLC in practice are presented in Tabs. 12.2 and 12.3.

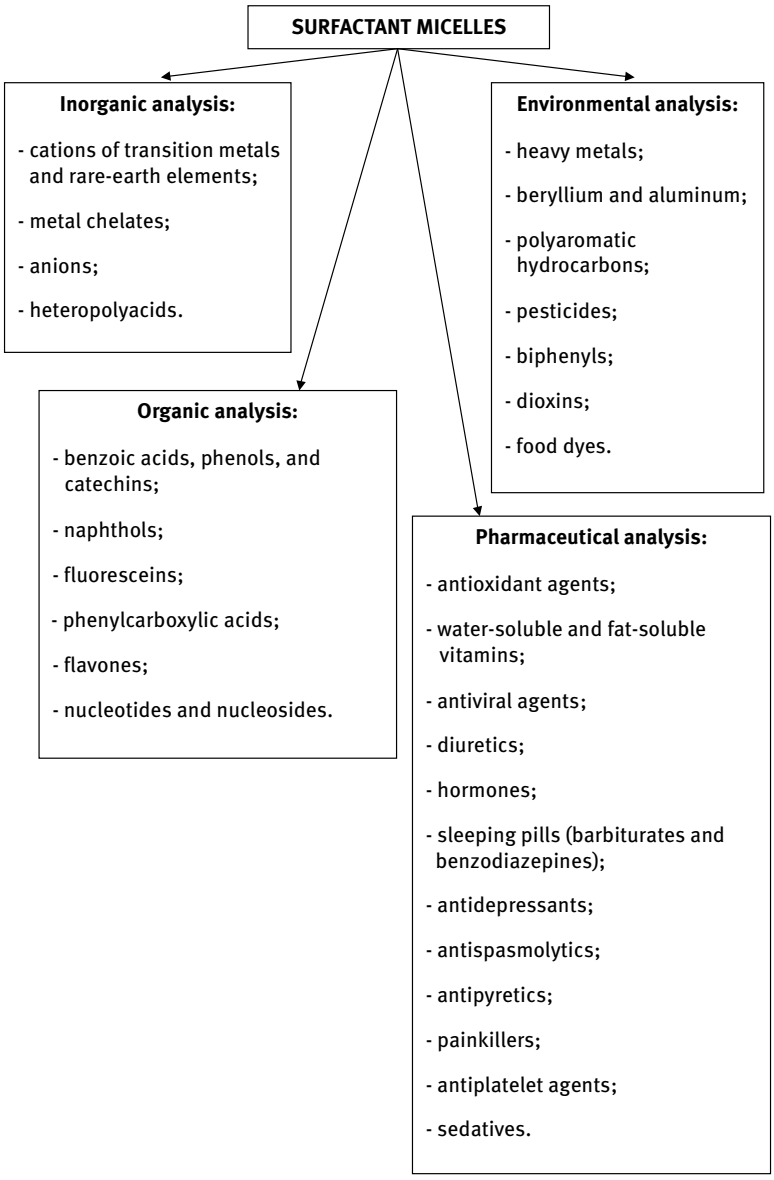


**Fig. 12.3:** Examples of analytical applications of surfactant micelles in liquid chromatography.

The main advantage of micellar mobile phases in comparison with water–organic eluents, as noted above, is the improved metrological characteristics of the analytical techniques (Tabs. 12.4 and 12.5), which have enabled many of them to be included in the Pharmacopoeia of the world's leading countries [121, 122].

**Tab. 12.2:** Basic chromatographic parameters of separation of organic substances by micellar TLC [123]

| Compounds to be separated | Stationary phase | Mobile phase | Detection |
|---|---|---|---|
| o-, m-, p-Aminophenols | Whatman $KC_{18F}$ plates impregnated by SDS and CTA in the presence of NaCl | 0.1 M CTAC + 0.3 M NaCl; 0.2 M SDS + 0.2 M NaCl | |
| p-Nitrophenol | Polyamide-6 $UV_{254}$ | DDTA; ATMA salts ($C_{10}$, $C_{12}$, $C_{14}$, $C_{16}$) | UV 254 nm; |
| p, m-Nitrophenol | Surfactant-impregnated polyamide-6 $UV_{254}$ | CTAB; CTAC; SDS | UV 218 nm – SDS, 226 nm – CTAB, CTAC |
| p-Nitroaniline | Polyamide-6 $UV_{254}$ | CTAB; CTAC; SDS; ATMA salts ($C_{10}$, $C_{12}$, $C_{14}$, $C_{16}$) | UV 254 nm |
| Benzoic acids (o-, m-bromo-, o-amino, p-hydroxy-) | Polyamide-6 $UV_{254}$ | CTAB, SDS; α-cyclodextrin | UV 254 nm |
| 19 amino acids | Whatman $KC_{18}$ | 0.015 M SDS + 0.5 M NaCl CTAB–$H_2O$ (1:19 v/v) + 0.5 M NaCl 1.3 M DOSS in the cyclohexane–water system (50:4 v/v) (reversed micelles) | Visual, 0.2 % ninhydrin solution |
| 20 amino acids | Polyamide-6 $UV_{254}$ silanized silica gel $F_{254}$ | 1.3 M DOSS in cyclohexane (reversed micelles) | 0.1 % ninhydrin solution |
| Alkaloids | | CTAC and DDS in the presence of NaCl | UV 254 nm |
| Nucleosides | Silanized silica gel-60 $F_{254}$ | 1.5 M DOSS solution in cyclohexane (reversed micelles) | UV 254 nm |
| Pesticides | Polyamide-6 $UV_{254}$, $Al_2O_3$ $F_{254}$, Silica Gel 60 $F_{254}$ | SDS, CTAB or Igepal-CO-710 | UV 254 nm |
| Polycyclic aromatic compounds | Polyamide-6 $UV_{254}$ Silanized silica gel | SDS | |

**Tab. 12.2:** (continued)

| Compounds to be separated | Stationary phase | Mobile phase | Detection |
|---|---|---|---|
| 33 medicines | Polyamide | Aqueous micellar solutions of cationic and anionic surfactants | |
| Vitamins $K_1$, $K_5$ | Polyamide-6 $UV_{254}$ | 0.4 M SDS, 0.2 M CTAB, 0.1 M α-cyclodextrins | |
| Bromophenol blue, bromo-cresol green | | CTAC and DDS in the presence of NaCl | UV 254 nm |
| Anthraquinone, 1,4-naphthoquinone | Polyamide-6 $UV_{254}$ | 0.4 M SDS, 0.3 M CTAB, 0.1 M α-cyclodextrin | |
| Acid indicators | SDS and CTAC-impregnated Whatman $KC_{18}F$ in static conditions in the presence of NaCl | 0.1 M CTAC + 0.3 M NaCl 0.2 M SDS + 0.2 M NaCl | |
| Metal cations (Au, Cu, Ag) | Silica gel | 0.01 M DDS + 0.01 M *i*-tryptophan (*i*-histidine) (1:9) | Visual (dithizone, dimethylglyoxime, aluminon) |

ATMA alkyltetramethylammonium chloride.
DOSS sodium dioctylsulfosuccinate.

**Tab. 12.3:** Basic chromatographic parameters of separation of inorganic and organic substances by micellar liquid chromatography

| Substances separated | Stationary phase | Mobile phase | Detection |
|---|---|---|---|
| Bolasterone, cortisone, methyltestosterone, progesterone, testosterone, and testosterone acetate | C18 | 0.1 M SDS – 20 % acetonitrile – 0.01 M $Tb(NO_3)_3$ | Fl 254/547 nm |
| 6-Mercaptopurine, 6-thioguanine, 6-mercaptopurine riboside, 6-thioguanine riboside, and 6-thioxanthine | LiChrosorb 100 RP-18 | 0.08 M SDS in 0.01 M phosphate buffer solution, pH 3.0 | UV 320 nm |
| Amyloride, bendroflumethiazide, piretanide, triamterene, acebutolol, atenolol, labetalol, metoprolol, nadolol, and propranolol | Spherisorb ODS-2 | 0.11 M SDS – 8 % 1-propanol | Fl 230/440 |
| Amyloride, bendroflumethiazide, bumetanide, hydrofluethiazide, piretanide, and triamterene | Spherisorb ODS-2 | 0.055 M SDS – 8 % 1-propanol | Fl 270/430 nm |
| Amiphenazole, amiloride, amphetamine, cloestabol, ephedrine, phenylpropanolamine, methandienone, methoxyphenamine, nandrolone, and spironolactone | Spheri-5 RP-18 | 0.2 M SDS – 3 % 1-pentanol | UV 260 nm |
| Codeine, morphine, propranolol, quinidine, and quinine | μ-Bondapak C18 and Supelcosil LC-CN | 0.02–0.05 M SDS – 10 % 1-propanol | Fl 215/300 nm |
| Hydroxycorticosterone, corticosterone, norhisterone, testosterone, medroxyprogesterone acetate, and progesterone | Spheri-5 RP-18 | 0.05 M SDS – 9 % 1-butanol | UV 245 nm |
| Lidocaine hydrochloride and tolperisone | C18 | 0.075 M SDS – 7.5 % isopropanol | UV 210 nm |
| Chlorazepam, diazepam, and diltiazem (capsules, dragees, suspensions) | Spherisorb ODS-2 | 0.1M SDS – 3 % 1-butanol | UV 230 nm |
| Hydroxytestosterone, ketotestosterone, boldenone, testosterone, androstenolone, bolasterone, epitestosterone, cortisone, cortisol, corticosterone, hydroxyprogesterone, deoxycorticosterone, dehydroepiandrosterone, and methyltestosterone | Hypersil ODS | 0.04M SDS – 5 % 1-propanol | UV 254 nm |

**Tab. 12.3:** (continued)

| Substances separated | Stationary phase | Mobile phase | Detection |
|---|---|---|---|
| Arsenic compounds: dimethylarsenic acid, monomethylarsenic acid, As (III) and As (V) | Hamilton PRP-1 | 0.05 M CTAB – 10 % 1-propanol in 0.02 M borate buffer solution, pH 10.2 | ICP-MS |
| Copper, lead, cadmium, nickel, cobalt, molybdenum, selenium (IV), mercury, thallium, and chromium (VI) | Nucleosil 100-5 C18 | Methanol–acetonitrile–water–diisopropyl ether (42:20:31:7) with 1 % SDS. Derivatization with *bis*(ethoxyethyl)-dithiocarbamate | UV 254 nm |
| Barbital, diallylbarbiturate, aprobarbital, bromobarbital, phenobarbital, hexobarbital, butabarbital, butetal, butalbital, mefobarbital, secobarbital, amobarbital, and pentobarbital | Spherisorb ODS-2 | 0.15 M SDS in 0.05 M phosphate buffer solution, pH 3.5 or 0.02 M Brij-35 in 0.05 M phosphate buffer solution, pH 7.4 or 0.05 M CTAB in 0.05 M phosphate buffer solution, pH 3.5 | UV 254 nm |
| Furosemide and its metabolites (tablets, capsules, injections, drops) | ODS-2 | 0.04 M SDS – 2 % 1-propanol in 0.05 M phosphate buffer solution, pH 3.0 | UV 274 nm |
| Amitriptylin, clomipramine, doxepin, maprotillin, nortriptyline, and trimipramine | Zorbax Eclipse XDB C8 | 0.075 M SDS – 6 % 1-pentanol in 0.05 M phosphate buffer solution, pH 3.0 | UV 254 nm |
| Bromoazepan, diazepam, flunitrazepam, galazepam, medazepam, nitrazepam, oxazepam, and tetrazepam | Zorbax Eclipse XDB C8 | 0.06 M SDS – % 1-butanol in 0.05 M phosphate buffer solution, pH 7.0 | UV 230 nm |
| Atenolol, pratolol, sotalol, cardiolol, nadolol, pindolol, ayebutolol, celiprolol, esmolol, metoprolol, timolol, bisoprolol, labetalol, oxprenalol, propranolol, and alprenolol | Spherisorb ODS-2 | 0.10 M SDS – 15 % 1-propanol | UV 225 nm |
| Iron, cadmium, zinc, copper, manganese, cobalt, and nickel | Inertsil ODS-2 | 0.0945 M SDS in 0.0684 M tartrate buffer solution, pH 4.2 | UV 540 nm |

**Tab. 12.3:** (continued)

| Substances separated | Stationary phase | Mobile phase | Detection |
|---|---|---|---|
| Carbamazepine, bentazepam, galazepam, oxazepam, pinazepam, and tetrazepam (tablets, capsules) | ODS-2 | 0.10 M SDS – 3 % 1-butanol – 0.1 % triethylamine – 0.01 M phosphate buffer solution, pH 3.0 | UV 230 nm |
| Sulfonamides: sulfacetamide, sulfadiazine, sulfamerazine, sulfathiazole, sulfamethazine, sulfamethoxypyridazine, sulfonyl pyridazine, sulfonamethoxyne, sulfabenzamide, sulfadimethoxin, sulfaquinoxaline, and sulfisomidine | ODS | 0.07 M SDS – 6.0 % 1-propanol | UV 254 nm |
| Sulfonamides: sulfadiazine, sulfaguanidine, sulfamethizole, sulfamethoxazole, and sulfathiazole | Spherisorb ODS-2 | 0.05 M SDS – 2.4 % 1-pentanol | 550 nm |
| Caffeine and its metabolites, theophylline, and theobromine | Spherisorb ODS-2 | 0.075 M SDS – 1.5 % 1-propanol | UV 273 nm |
| Cephalosporins: cephmenoxime hemihydrochloride, and cephotami-dihydrochloride | Nucleosil C18 | 0.08 M SDS – 8.0 % 2-propanol in 0.05 M phosphate buffer solution with pH 3.0 | UV 260 nm |
| Theophylline | μ-Bondapakphenyl | 0.001 M $C_{12}$ DAPS – 3 % 1-propanol | UV 273 nm |
| Hydrochlorothiazide | Hypersil C18 | 0.02 M Brij-35 – 0.004 M SDS in 0.01 M phosphate buffer solution pH 6.5 | UV 271 nm |
| Amyloride, bendroflumethiazide, bumetanide, chlorthalidone, ethacrynic acid, furosemide, spironolactone, triamterene, xypamide, and probenecid | Spherisorb ODS-2 | 0.042 M SDS – 4 % 1-propanol in 0.01 M phosphate buffer solution, pH 4.5 | UV 254 nm |

**Tab. 12.4:** Separation of several mycotoxins by TLC with organic and micellar mobile phases

| Characteristics | Mobile phase | | |
|---|---|---|---|
| | Ethyl acetate:toluene (3:1) | | $5 \cdot 10^{-3}$ M CPC and $5 \cdot 10^{-3}$ M Tween-80, pH 9 (phosphate buffer) |
| Difference in $R_f$ for neighboring spots | | | |
| Zearalenone–E-2 toxin | 0.02 | | 0.07 |
| E-2 toxin–NT-2 toxin | 0.27 | | 0.29 |
| NT-2 toxin–T-2 tetraol | 0.14 | | 0.39 |
| Toxicity (TLV, mg/m$^3$) | Ethyl acetate 0.2 M (highly hazardous) | Toluene 0.5 M (a precursor, moderately hazardous) | All components are nontoxic |
| Chamber saturation time, min | 90 | | No saturation |
| Chromatography duration, min | 20 | | 10 |

**Tab. 12.5:** Fluorescent detection limits of polyaromatic hydrocarbons (ng/ml) by HPLC with water–methanol and water–micellar MPs

| Compound | RP-HPLC MeOH: $H_2O$ (40:60) | MLC, 0.024 M SDS | Compound | RP-HPLC MeOH: $H_2O$ (30:70) | MLC, 0.035 M SDS |
|---|---|---|---|---|---|
| Pyrene | 2.6 | 0.25 | Pyrene | 17.4 | 1.7 |
| Naphthalene | 1.2 | 0.3 | 1,2-Benzanthracene | 2.0 | 0.5 |
| Biphenyl | 0.7 | 0.2 | Acenaphthylene | 270 | 100 |
| Fluoranthene | 0.8 | 2.5 | Benzo[a]fluorene | 480 | 270 |
| Benzo[e]pyrene | 0.5 | 0.2 | | | |
| Anthracene | 0.2 | 0.2 | | | |

## 12.6 Conclusions

Our analysis of the literature and comparison of the surfactant micelle modification of both mobile and stationary phases in HPLC and TLC allow the following conclusions to be drawn:

– The use of nanoheterogeneous micellar MPs has not only widened the capabilities of liquid chromatography, allowing simultaneous separation of the polar and nonpolar components of mixtures, but also excluded or significantly reduced the use of toxic and carcinogenic organic solvents.

- Water–micellar eluents allow the researcher to dynamically modify the normal and reversed stationary phases, as well as medium-polarity sorbents (polyamide, cyanopropyl, and diol sorbents); ionic surfactants are most frequently used for the SP modification.
- In micellar MPs, in comparison with water–organic ones, it is easier to optimize the separation conditions and to improve the metrological characteristics of the techniques using LC.
- The separation efficiency in MMP is worse and selectivity is better than when using classical nonaqueous or water–organic MPs; the efficiency and selectivity depending significantly on the surfactant concentration and the introduction of an additional organic modifier.
- In micellar HPLC, nonpolar sorbents are effective in most cases.

## References

[1] Savvin SB, Chernova RK, Shtykov SN. *Surfactants (Analytical reagents)*. Moscow, USSR, Nauka, 1991, original source in Russian.
[2] Shtykov SN. Surfactants in analysis: progress and development trends. *J Anal Chem* 2000, 55, 608–14.
[3] Shtykov SN. Chemical analysis in nanoreactors: main concepts and applications. *J Anal Chem* 2002, 57, 859–68.
[4] Armstrong DW, Fendler JH. Differential partitioning of tRNAs between micellar and aqueous phases: a convenient gel filtration method for separation of tRNAs. *Biochim Biophys Acta* 1977, 478, 75–80.
[5] Armstrong DW. Pseudophase liquid chromatography: applications to TCL. *J Liquid Chromatogr*, 1980, 3, 895–900.
[6] Armstrong DW. Use of micellar and cyclodextrin solutions in liquid chromatographic separations. In: Mittal KL, Fendler EJ, eds. *Solution Behavior of Surfactants. Theoretical and Applied Aspects*. Vol. 2. NY, London, Plenum Press, 1982, 1273–82.
[7] Pelizzetti E, Pramauro E. Analytical applications of organized molecular assemblies. *Anal Chim Acta* 1985, 169, 1–29.
[8] Berthod A, Dorsey JG. Les Phases mobiles micellaires. *Analusis* 1988, 16, 75–89.
[9] Armstrong DW, Terrill RQ. Thin layer separation of pesticides, decachlorobiphenyl and nucleosides with micellar solutions. *Anal Chem* 1979, 51, 2160–3.
[10] Armstrong DW, McNeely M. Use of micelles in TLC separation of polynuclear aromatic compounds and amino acids. *Anal Lett* 1979, 12, 1285–91.
[11] Armstrong DW, Henry SJ. Use of an aqueous micellar mobile phase for separation of phenols and polynuclear aromatic hydrocarbon via HPLC. *J Liquid Chromatogr* 1980, 3, 657–62.
[12] Pelizzetti E, Pramauro E, Minero C. Ordered ensembles in chemical separation and analysis. *Russian Chem J* 1995, 39, 129–38, original source in Russian.
[13] Khaledi MG. Micelles as separation media in high-performance liquid chromatography and high-performance capillary electrophoresis: overview and perspective. *J Chromatogr A* 1997, 780, 3–40.

[14] Basova EM, Ivanov VM, Shpigun OA. Micellar liquid chromatography. *Russ Chem Rev* 1999, 68, 1083–101, original source in Russian.
[15] Dorsey JG. Micellar liquid chromatography. *Adv Chromatogr* 1987, 7, 167–214.
[16] Koenigbauer MJ. Application of micellar mobile phases for the assay of drugs in biological fluids. *J Chromatogr* 1990, 531, 79–99.
[17] Jiménez O, Marina ML. Retention modeling in micellar liquid chromatography. *J Chromatogr A* 1997, 780, 149–63.
[18] Okado T. Micellar chromatography of inorganic compounds. *J Chromatogr A* 1997, 780, 343–60.
[19] García-Alvarez-Coque MC, Carda-Broch S. Direct injection of physiological fluids in micellar liquid chromatography. *J Chromatogr B* 1999, 736, 1–18.
[20] Kulikov AYu, Loginova LP, Samokhina LV. Micellar chromatography in pharmaceutical analysis and other fields of analysis. *Farmacom* 2004, 4, 22–52, original source in Russian.
[21] Ruiz-Ángel MJ, García-Álvarez-Coque MC, Berthod A. New insights and recent developments in micellar liquid chromatography. *Separ Purif Rev* 2009, 38, 45–96.
[22] Sumina EG, Shtykov SN, Tyurina NV. Surfactants in thin-layer chromatography. *J Anal Chem* 2003, 58, 720–30.
[23] Sumina EG, Shtykov SN, Tyurina NV. Physicochemical aspects of thin-layer micellar chromatography. *Russ J Phys Chem* 2002, 76, 1538–43.
[24] Shtykov SN, Sumina EG, Tyurina NV. Micellar thin-layer chromatography: features and analytical capabilities. *Rus Chem J* 2003, 47, 119–26, original source in Russian.
[25] Sumina EG. Organized nanosystems in thin-layer chromatography. *Sorption Chromatogr Processes* 2010, 10, 150–60, original source in Russian.
[26] Berthod A, García-Álvarez-Coque C. *Micellar Liquid Chromatography*. NY, USA, CRC Press, 2000.
[27] Armstrong DW, Bui KH, Barry RM. Use of pseudophase TLC in teaching laboratories. *J Chem Educ* 1984, 61, 457–8.
[28] Detroyer A, Vander Heyden Y, Cambré I, Massart DL. Chemometric comparison of recent chromatographic and electrophoretic methods in a quantitative structure-retention and retention-activity relationship context. *J Chromatogr A* 2003, 986, 227–38.
[29] Carda-Broch S, Torres-Lapasió JR, Esteve-Romero JS, García-Alvarez-Coque MC. Use of a three-factor interpretive optimisation strategy in the development of an isocratic chromatographic procedure for the screening of diuretics in urine samples using micellar mobile phases. *J Chromatogr A* 2000, 893, 321–37.
[30] Ruiz-Angel MJ, Carda-Broch S, Torres-Lapasió JR, Simó-Alfonso EF, García-Alvarez-Coque MC. Micellar-organic versus aqueous-organic mobile phases for the screening of β-blockers. *Anal Chim Acta* 2002, 454, 109–23.
[31] Gil-Agustí M, Monferrer-Pons L, García-Alvarez-Coque MC, Esteve-Romero J. Determination of active ingredients in cough-cold preparations by micellar liquid chromatography. *Talanta* 2001, 54, 621–30.
[32] Gonzalo-Lumbreras R, Izquierdo-Hornillos R. Conventional and micellar liquid chromatography method development for danazol and validation in capsules. *J Pharm Biomed Anal* 2003, 32, 433–9.
[33] Youngvises N, Liawruangrath B, Liawruangrath S. Simultaneous micellar LC determination of lidocaine and tolperisone. *J Pharm Biomed Anal* 2003, 31, 629–38.
[34] Monferrer-Pons L, Capella-Peiró ME, Gil-Agustí M, Esteve-Romero J. Micellar liquid chromatography determination of B vitamins with direct injection and ultraviolet absorbance detection. *J Chromatogr A* 2003, 984, 223–31.
[35] Ruiz-Angel MJ, Carda-Broch S, Simó-Alfonso EF, García-Alvarez-Coque MC. Optimised procedures for the reversed-phase liquid chromatographic analysis of formulations containing tricyclic antidepressants. *J Pharm Biomed Anal* 2003, 32, 71–84.

[36] Capella-Peiró ME, Bose D, Martinavarro-Domínguez A, Gil-Agustí M, Esteve-Romero JS. Direct injection micellar liquid chromatographic determination of benzodiazepines in serum. *J Chromatogr B* 2003, 780, 241–9.
[37] Caballero RD, Torres-Lapasió JR, García-Álvarez-Coque MC, Ramis-Ramos G. Rapid liquid chromatographic determination of tetracyclines in animal feeds using a surfactant solution as mobile phase. *Anal Lett* 2002, 35, 687–705.
[38] Gil-Agustí M, Carda-Broch S, García-Álvarez-Coque MC, Esteve-Romero J. Micellar liquid chromatography determination of anti-convulsant drugs in pills and capsules. *J Liquid Chromatogr Relat Technol* 2000, 23, 1387–401.
[39] Gil-Agustí M, Carda-Broch S, García-Álvarez-Coque MC, Esteve-Romero J. Use of micellar mobile phases for the chromatographic determination of clorazepate, diazepam, and diltiazem in pharmaceuticals. *J Chromatogr Sci* 2000, 38, 521–7.
[40] Noguera-Orti JF, Villanueva-Camanas RM, Romis-Ramos G. Determination of parabens in cosmetics without previous extraction by micellar liquid chromatography. *J Chromatogr Sci* 1999, 37, 83–7.
[41] Gonzalo-Lumbreras R, Izquierdo-Hornillos R. Optimization and validation of conventional and micellar LC methods for the analysis of methyltestosterone in sugar-coated pills. *J Pharm Biomed Anal* 2003, 31, 201–8.
[42] Armstrong DW, Bui KH. Use of aqueous micellar mobile phases in reverse phase TLC. *J Liquid Chromatogr* 1982, 5, 1043–50.
[43] Sumina EG, Shtykov SN, Parshina EV, Lopukhova SS. Use of micellar mobile phases for separating fluorescein derivatives by means of thin layer chromatography. *J Anal Chem* 1995, 50, 684–8, original source in Russian.
[44] Shtykov SN, Sumina EG. Analytical capabilities of micellar mobile phases in the thin-layer chromatography of metal 1,3-diketonates. *J Anal Chem* 1998, 53, 446–50, original source in Russian.
[45] Boichenko AP, Kulikov AYu, Loginova LP. Aliphatic carboxylic acids as new modifiers for separation of 2,4-dinitrophenyl derivatives of amino acids by micellar liquid chromatography. *Kharkov Univ Bull Chem Ser* 2006, 14(37), 101–11, original source in Russian.
[46] Kartsova LA, Koroleva OA. Simultaneous determination of water- and fat-soluble vitamins by high-performance thin-layer chromatography using an aqueous micellar mobile phase. *J Anal Chem* 2007, 62, 255–9.
[47] Kartsova LA, Khmelnitsky IK, Pechenko TV, Alekseeva AV, Berezkin VG. Simultaneous determination of water- and fat-soluble vitamins in different modes of high-performance thin-layer chromatography. *Sorption and Chromatogr Processes* 2007, 7, 909–17, original source in Russian.
[48] Kartsova LA, Strel'nikova EG. Separation of exogenous and endogenous steroid hormones by micellar high-performance thin-layer chromatography. *J Anal Chem* 2007, 62, 872–4.
[49] Kartsova LA, Strel'nikova EG. Effect of organized media on the chromatographic and electrophoretic determination of pharmaceutical preparations in biological samples. *J Anal Chem* 2009, 64, 156–63.
[50] Foley JP. Critical compilation of solute-micelle binding constants and related parameters from micellar liquid chromatographic measurements. *Anal Chim Acta* 1990, 231, 237–47.
[51] Yedamenko DV, Loginova LP, Pugach AI, Trufanov OV. Application of micellar solutions of surfactant as eluents at TLC-determination of micotoxines in grain. *Kharkov Univ Bull Chem Ser* 2007, 15(38), 147–54, original source in Russian.
[52] Le Cong H, Boichenko AP, Drobot AV, Loginova LP. The quantitative determination of 4-aminobutyric acid impurity in drug substance sodium alendronate by micellar thin-layer chromatography. *Methods Objects Chem Anal* 2009, 4, 130–8, original source in Russian.

[53] Loginova LP, Yedamenko DV, Kulikov AU, Lavrenenko AN. Control of content of *p*-hydroxybenzoic acid and parabens in cosmetic products by micellar thin layer chromatography. *Kharkov Univ Bull Chem Ser* 2006, 127, 127–34, original source in Russian.
[54] Loginova LP, Galat MN, Yakovleva EYu. The influence of some aliphatic alcohols and acids on micellar properties of sodium dodecyl sulphate. *Kharkov Univ Bull Chem Ser* 2007, 15(38), 109–18, original source in Russian.
[55] Boichenko AI, Kulikov AU, Loginova LP, Iwashchenko AL. Aliphatic carboxylic acids as new modifiers for separation of 2,4-dinitrophenyl amino acids by micellar liquid chromatography. *J Chromatogr A* 2007, 1157, 252–9.
[56] Loginova LP, Yakovleva EY, Galat MN, Boichenko AP. Effect of aliphatic alcohols and aliphatic carboxylic acids on the critical micelle concentration and counter-ion binding degree of sodium dodecylsulfate. *J Molec Liq* 2009, 145, 177–81.
[57] Iwashchenko AL, Boichenko AP, Loginova LP. The first communication on the opportunity of simultaneous isocratic separation of water- and fat-soluble vitamins by HPLC. *Kharkov Univ Bull Chem Ser* 2007, 15(38), 82–9, original source in Russian.
[58] Kulikov AU, Loginova LP, Samokhina LV. Influence of various factors on the chromatographic behavior of cytostatic antibiotics of rubomicin derivatives in micellar liquid chromatography. *Chromatographia* 2003, 57, 463–9.
[59] Loginova LP, Boichenko AP, Kulikov AY. Modification of the Murakami retention model in reversed-phase high-performance liquid chromatography for micellar chromatographic separations. *Russ J Phys Chem A* 2008, 82, 1470–4.
[60] Rusanov AI. *Micelle Formation in Surfactant Solutions*. Saint Petersburg, Khimiya, 1992, original source in Russian.
[61] Loginova LP, Samokhina LV, Mchedlov-Petrossyan NO, Alekseeva VI, Savvina LP. Modification of the properties of NaDS micellar solutions by adding electrolytes and non-electrolytes: investigations with decyl eosin as a $pK_a$-probe. *Colloids Surf A* 2001, 193, 207–19.
[62] Abramson AA, Gaevoy GM, eds. *Surfactants. Reference Book*. Leningrad, Khimiya, 1979, original source in Russian.
[63] Ruiz-Angel MJ, Caballero RD, Simó-Alfonso EF, Garcí a-Alvarez-Coque MC. Micellar liquid chromatography: suitable technique for screening analysis. *J Chromatogr A* 2002, 947, 31–45.
[64] López-Grío S, Torres-Lapasió JR, Baeza-Baeza JJ, García-Alvarez-Coque MC. Micellar liquid chromatographic separation of amino acids using pre- and post-column *o*-phthalaldehyde/*N*-acetylcysteine derivatization. *Anal Chim Acta* 2000, 418, 153–65.
[65] Noguera-Ortí JF, Villanuena-Camañas RM, Ramis-Ramos G. Determination of phenolic antioxidants in vegetal and animal fats without previous extraction by dilution with *n*-propanol and micellar liquid chromatography. *Anal Chim Acta* 1999, 402, 81–6.
[66] López-Grío SJ, Vivó-Truyols G, Torres-Lapasió JR, García-Alvarez-Coque MC. Resolution assessment and performance of several organic modifiers in hybrid micellar liquid chromatography. *Anal Chim Acta* 2001, 433, 187–98.
[67] Capella-Pieró M-E, Gil-Agustí M, Monferrer-Pons L, Esteve-Romero J. Direct injection micellar liquid chromatographic method for the analysis of corticosteroids in creams, ointments and other pharmaceuticals. *Anal Chim Acta* 2002, 454, 125–35.
[68] Khaledi MG, Peuler E, Ngeh-Ngwainbi J. Retention behavior of homologous series in reversed-phase liquid chromatography using micellar, hydro-organic, and hybrid mobile phases. *Anal Chem* 1987, 59, 2738–47.
[69] Shchatz V D, Sakhartova OV. *High-Performance Liquid Chromatography*. Riga, Zinatne, 1988, original source in Russian.
[70] Rudakov OB, Vostrov IA, Fedorov SV, Filippov AA, Selemenev VF, Pridantsev AA. *A Companion to the Chromatographist. Methods of Liquid Chromatography*. Voronezh, Vodoley Publishing House, 2004, original source in Russian.

[71] Torres-Lapasió JR, García-Alvarez-Coque MC, Rosés M, Bosch E. Prediction of the retention in reversed-phase liquid chromatography using solute – mobile phase – stationary phase polarity parameters. *J Chromatogr A* 2002, 955, 19–34.
[72] Carda-Broch S, Esteve-Romero J, García-Alvarez-Coque MC. Furosemide assay in pharmaceuticals by micellar liquid chromatography: study of the stability of the drug. *J Pharm Biomed Anal* 2000, 23, 803–17.
[73] Gil-Agustí M, García-Alvarez-Coque MC, Esteve-Romero J. Correlation between hydrophobicity and retention data of several antihistamines in reversed-phase liquid chromatography with aqueous-organic and micellar-organic mobile phases. *Anal Chim Acta* 2000, 421, 45–55.
[74] Grushka E, Grinberg N, eds. *Advances in Chromatography,* Vol. 44. Boca Raton, CRC Press, 2005.
[75] Sumina EG, Shtykov SN, Tyurina NV. Basics of the Modifying Action of Surfactants in Liquid Chromatography. *A Textbook*. Saratov, Saratov Univ Press, 2006, original source in Russian.
[76] Shtykov SN, Sumina EG, Smushkina EV, Tyurina NV. Thin layer chromatography of fluorescein derivatives on direct and reversed stationary phases with aqueous micellar solutions. *J Planar Chromatogr Modern TLC* 1999, 12, 129–34.
[77] Tyurina NV. Surfactants as Modifiers of the Mobile and Stationary Phases in Thin-layer Chromatography. PhD thesis. Saratov, Russian Federation, Saratov State Univ, 2002, original source in Russian.
[78] Sumina EG, Shtykov SN, Tyurina NV. Hydrophobic TLC of phenolcarboxylic acids of the triphenylmethane series in surfactant micelles. *Bulletin Univ Chem Chem Technol* 2001, 44(4), 10–13, original source in Russian.
[79] Mchedlov-Petrossyan NO, Plichko AV, Schumakher AS. Acidity of microheterogeneous systems: effect of nonionic admixtures on acid-base equilibria of dyes bound to micelles of ionogenic surfactants. *Russ J Phys Chem B* 1996, 15, 1661–78.
[80] Friedrichsberg DA. *A Course of Colloid Chemistry*. Saint Petersburg, Russian Federation, Khimiya, 1995, original source in Russian.
[81] Ghorbani AR, Momenbeik F, Khorasani JH, Amini MK. Simultaneous micellar liquid chromatographic analysis of seven water-soluble vitamins: optimization using super-modified simplex. *Anal Bioanal Chem* 2004, 379, 439–44.
[82] García-Álvarez-Coque MC, Torres-Lapasió JR, Baeza-Baeza JJ. Models and objective functions for the optimisation of selectivity in reversed-phase liquid chromatography. *Anal Chim Acta* 2006, 579, 125–45.
[83] Torres-Lapasió JR, García-Álvarez-Coque MC. Levels in the interpretive optimisation of selectivity in high-performance liquid chromatography: a magical mystery tour. *J Chromatogr A* 2006, 1120, 308–21.
[84] Torres-Lapasió JR, Villanueva-Camañas RM, Sanchis-Mallols JM, Medina-Hernándes MJ, García-Alvarez-Coque MC. Interpretive strategy for optimization of surfactant and alcohol concentration in micellar liquid chromatography. *J Chromatogr A* 1994, 677, 239–53.
[85] Boichenko AP, Loginova LP, Kulikov AU. Micellar liquid chromatography (Review). Part 1. Fundamentals, retention models and optimization of separation. *Methods Objects Chem Anal* 2007, 2(2), 92–116.
[86] Kulikov AU, Galat MN, Boichenko AP. Optimization of micellar LC conditions for the flavonoid separation. *Chromatographia* 2009, 70, 371–9.
[87] Kulikov AYu, Galat MN, Boichenko AP. Optimization of the separating of flavonoids with the use of micellar liquid chromatography. *Farmacom* 2009, 1, 20–9, original source in Russian.
[88] Lesellier E, West C. Description and comparison of chromatographic tests and chemometric methods for packed column classification. *J Chromatogr A* 2007, 1158, 329–60.
[89] Kulikov AU, Galat MN. Comparison of C18 silica bonded phases selectivity in micellar liquid chromatography. *J Sep Sci* 2009, 32, 1340–50.

[90] Galat MN. Analogous Alkyl-Grafted Stationary Phases in Micellar and Reversed-Phase Liquid Chromatography. PhD thesis. Kharkov, Ukraine, Kharkov Univ, 2010, original source in Russian.
[91] Sherma J, Sleckman BP, Armstrong DW. Chromatography of amino acids on reversed phase thin layer plates. *J Liquid Chromatogr* 1983, 6, 95–108.
[92] Shtykov SN, Sumina EG, Smushkina EV, Tyurina NV. Dynamic and static modifications of stationary phases with surfactants in TLC: a comparative study. *J Planar Chromatogr Modern TLC* 2000, 13, 182–6.
[93] Sumina EG, Smushkina EV, Shtykov SN, Tyurina NV. Application of micellar mobile phases to evaluate the purity of xylenol orange preparations. *Zavodsk Lab. Mater Diagn* 2001, 67(10), 13–15, original source in Russian.
[94] Shtykov SN, Sumina EG, Tyurina NV. Micellar mobile phases in TLC separation of some transition metal ions and their 1,3-diketonates. *J Planar Chromatogr Modern TLC* 2000, 13, 264–8.
[95] Parfitt GD, Rochester CH, eds. *Adsorption from Solution at the Solid/Liquid Interface*. St Louis, Missouri, Acad Press, 1983.
[96] Koganovskiy AM, Klimenko NA, Levchenko TM, Roda NG. *Adsorption of Organic Substances from Water*. Leningrad, Russian Federation, Khimiya, 1992, original source in Russian.
[97] Muller VM, Sergeeva IP, Churaev NV. Adsorption of ionogenic surfactants on a charged surface: two models. *Colloid J* 1995, 57, 368–71, original source in Russian.
[98] Sergeeva IP, Muller VM, Zakharova MA, Sobolev VD, Churaev NV. Adsorption of CTAB from aqueous solutions on fused quartz. *Colloid J* 1995, 57, 400–6, original source in Russian.
[99] Golub TP, Sidorova MP. Influence of the ionic surfactant adsorption on the surface charge and the stability of Aerosil. *Colloid J* 1992, 56, 17–20, original source in Russian.
[100] Schwuger MJ, Smolka HG. Mixed adsorption of ionic and nonionic surfactants on active carbon. *Coll Polym Sci* 1977, 255, 589–94.
[101] Romanova NE, Golub TP, Sidorova MP, Kabirova NA. The surface charge and the stability of Aerosil in the aqueous solutions of oxyethylated alkyl phenol and polyacrylamide. *Colloid J* 1993, 55, 114–9, original source in Russian.
[102] Ageyev AA, Volkov VA. *Adsorption of Surfactants*. Moscow, Russian Federation, MSTU Press, 2015, original source in Russian.
[103] Mudzhikova GV, Brodskaya EN. An AOT reverse micelle in a medium of supercritical carbon dioxide. *Colloid J* 2015, 77, 306–11.
[104] Mirgorodskaya AB, Yackevich EI, Valeeva FG, Pankratov VA, Zakharova LY. Solubilizing and catalytic properties of supramolecular systems based on gemini surfactants. *Russ Chem Bull* 2014, 63, 82–7.
[105] Ismagilov IF, Kuryashov DA, Vagapov BR, Bashkirtseva NY. Influence of an electrolyte on micelle formation and rheological properties of aqueous solutions of sodium oleylmethyltaurate. *Kazan Technol Univ Bull* 2014, 17(18), 46–50, original source in Russian.
[106] Vasilieva EA, Zakharov SV, Kuryashov DA, Valeeva FG, Ibragimova AR, Bashkirtseva NYu, Zakharova LYa. Supramolecular systems based on cationic surfactants: an influence of hydrotropic salts and oppositely charged polyelectrolytes. *Russ Chem Bull* 2015, 64, 1901–5.
[107] Armstrong DW, Nome F. Partitioning behavior of solutes eluted with micellar mobile phases in liquid chromatography. *Anal Chem* 1981, 53, 1662–6.
[108] Armstrong DW, Stine GY. Selectivity in pseudophase liquid chromatography. *Anal Chem* 1983, 55, 2317–20.
[109] Loginova LP, Kulikov AU, Yakovleva EY, Boichenko AP. MLC determination of preservatives in cranberry foodstuffs. *Chromatographia* 2008, 67, 615–20.
[110] Boichenko AP, Loginova LP, Iwashchenko AL, Kulikov AU. New approach to modeling in micellar liquid chromatography. *Res J Chem Environ* 2006, 10, 53–62.

[111] Boichenko AP, Iwashchenko AL, Loginova LP, Kulikov AU. Heteroscedasticity of retention factor and adequate modeling in micellar liquid chromatography. *Anal Chim Acta* 2006, 576, 229–38.
[112] Ryazanov VV. Simulation of micelles conductance using stochastic model of storage. *Mathematical modeling* 2016, 28, 47–64, original source in Russian.
[113] Vanin AA, Brodskaya EN. Computer simulation of the surface layer of an ionic micelle with explicit allowance of water. *Colloid J* 2015, 77, 409–17.
[114] Armstrong DW, Stine GY. Evaluation of partition coefficients to micelles and cyclodextrins via planar chromatography. *J Amer Chem Soc* 1983, 105, 2962–4.
[115] Dhote SS, Deshmukh L, Paliwal L. Micellar thin layer chromatography of various heavy metal cations using non ionic surfactant. *Int J Chem Tech Res* 2014, 6, 366–74.
[116] Carda-Broch S, Ruiz-Ángel MJ, García-Álvarez-Coque MC. High submicellar liquid chromatography. *Separ Purif Rev* 2014, 43, 124–54.
[117] Starova VS., Kulichenko SA. Preconcentration of proteins using modified micellar phases of sodium dodecyl sulfate. *J Anal Chem* 2010, 65, 1215–20.
[118] Kulichenko SA, Doroschuk VO, Lelyushok SO. The cloud point extraction of copper (II) with monocarboxylic acids into non-ionic surfactant phase. *Talanta* 2003, 59, 767–73.
[119] Garrido M, Di Nezio MS, Lista AG, Palomeque M, Fernández BS. Band. Cloud-point extraction/preconcentration on-line flow injection method for mercury determination. *Anal Chim Acta* 2004, 502, 173–7.
[120] Carabias-Martínez R, Rodríguez-Gonzalo E, Moreno-Cordero B, Pérez-Pavón JL, García-Pinto C, Fernández-Laespada E. Surfactant cloud point extraction and preconcentration of organic compounds prior to chromatography and capillary electrophoresis. *J Chromatogr A* 2000, 902, 251–65.
[121] *European Pharmacopoeia*. 3rd ed. 1997. (Supplement 4.7), 2003.
[122] *United States Pharmacopoeia*, 24th ed. The United States Pharmacopoeia Convention Inc. Rockville, MD, 2000, 2570p.
[123] Sumina EG. Hydrophobic and Salt Effects in Surfactant Solutions in Spectrophotometric Analysis and Liquid Chromatography. Doctorate thesis. Saratov, Russian Federation, Saratov Univ, 2004, original source in Russian.

# Index


2,4-D 324
$\beta_2$-agonists 321
β-Blockers 323

affinity of the binding 317
aminosalicylic acid 318
analysis 343
analytical chemistry 304
antenna effect 133
Antidepressants 322
Antiepileptic drugs 323
Application 320
aptamers 256
aptasensor 253, 256, 260, 266, 268, 272, 275, 280, 283, 284, 286
Ascorbic and uric acids 237
Atrazine 322

barbiturates 310
biosensor 57, 66–68, 253–255, 257–259, 262, 264, 267, 269–271, 279, 282–284, 288, 327

carbon nanomaterial 188, 224, 239, 242
– carbon nanotubes 224, 229
– fullerenes 224, 228
– graphene 224, 225, 226
Carbon Nanotubes 343
cartridges 320
catecholamines 234, 237
chelating agents 401
chemical analysis 366
– (FAAS) 366
– (AES) 366
– (ETAAS) 366
– (ICP–MS) 366
– (ICP–OES) 366
– AFS 367
– chromatography 373
– CNTs 353, 365
– for element speciation analysis 369
– ICP–AES 368
– polycyclic aromatic hydrocarbons 396
– sensor 372
– Piezosensors 369
Chemical and biological sensors 166
chloramphenicol 310
chromatography 311, 343
cloud point extraction (CPE) 395
CNTs 353, 361, 365
– determination 376
– functionalization 350, 354
– modification 343, 344, 346, 350, 351, 353, 354, 358, 359, 361, 362, 377
– morphology 353, 359
– multi-walled 348
– oxidized 354, 366
– single 348
– structure 353
– surface area 357
colloid chemistry 8
colloidal gold 55
colorants 325
column packed with MIP 321
combinatorial approach 316
commercially available cartridges 322
composite 321
computational molecular modeling 317
computer technologies 327
Covalent 304
cross-linking agent 305
cross-linking 307

definition of nanoobject 14
DNA origami 258
DNA probe 255, 256, 261, 262, 264–266, 268–275, 277, 279, 281, 286, 288
– capture 262, 264, 274, 277, 279, 286
– stem-loop 261, 262, 266
DNA sensor 253–255, 258, 260–263, 269, 270, 271, 272, 288, 289
DNA 327
– hairpin 264
– signaling 262, 264, 274, 279
DNAzyme 283
drugs 323

electroanalysis 188
electrochemical sensor 165, 187, 189
– electrochemical activity 167
– mathematical model 167
– shift of the electrooxidation potential 169
electrode surface modification 223, 226, 232, 233, 238
electron microscopy 4
– (TEM, SEM) 4

energy effects 171
Energy transfer (ET) 131, 132, 133, 147, 152
– (RET) 131
– FRET 131
– BRET 131, 138
– CRET 131
– MBET 131
– LRET 131, 133
– inductive-resonance 132, 133
– exchange resonance 132
– FRET 132, 135, 136, 137, 138, 144
– donor–acceptor pair 132, 134
– NSET 141
– metal-enhanced fluorescence (MEF) 142
– co-sensitizing effect 146
enrofloxacin 310
epigallocatechin 310
estrone 324
ET 131–133, 147, 152
Extraction and preconcentration 396
– PAHs 402, 404
– Protein extraction 396
– haemoglobin 396
– peptide 396
– metal ions 398
– PHAs 402, 404
– dialkylphthalates 404
– pyrene and phenanthrene 403
– dialkylphthalates 404
extraction 400

fish 325
Fluorescence 131, 135, 140
– sensitized 131, 133
– quenching 140
fluoroquinolone antibiotics 309, 323
frontal polymerization 326
functional groups 318
functional monomer 305, 307
functionalization 346

general approach to the synthesis of MIPs 304
gold nanoparticles 56, 87–89
gold nanostructures 176
– catalytic activity 176
Grafting 311
grinding 308

hemoglobin 311
histamine 318
historical overview 303
HPLC–UV 324
hydrogen bonds 315
Hydroxybenzoic acid 316

imprinting factor 315
immunoassay 137
Immunochemical rapid tests 87
immunochemical test 87
immunochromatographic assay 64, 65
immunodot 61, 62
ionic micelles
– Stern layer 420
*in situ* polymerization 314
intercalator 253, 261, 265
issues of molecular imprinting 304

LbL technique 110
lanthanide 133, 139, 146, 148, 152
layer of MIP 313
LC 414
Liquid chromatography (LC) 412
– high-performance liquid chromatography (HPLC) 412
– stationary phases 420
– thin-layer chromatography (TLC) 412
Liquid nanoobjects 15, 19, 20, 133
– calixarenes 15
– cyclodextrins 15
– micelles 15, 149, 147, 141
– micellar solutions 135
– micellar systems 16, 150
– microemulsions 15
– multicenter and multifunctional interactions 391
– Oil-in-water 392
– receptor molecules 15, 16
– specific features 17
– surfactant, co-surfactant 394
– thermodynamic theory 393
– vesicles 15
– β-cyclodextrins 143
lysozyme 311

magnetic MIP particles 321
magnetite 313
main approaches to the synthesis of MIPs 305
meat 325
membranes 314
metal nanoparticles 170

methacrylic acid–based MIPs 319
methylene blue 261, 264, 266, 268, 270, 273–275, 277, 279, 285, 286
methylparaben 316
MLC 412, 424, 427
– a nanoscale pseudophase 427
– dynamic modification 421
– hybrid MMPs 417
– micellar mobile phase 424, 428
– micellar mobile phases (MMP) 412
– micellar TLC 416, 420
– MMP modifiers 417
– MMP 415, 416, 419
– MMPs 414
– normal-phase TLC 422
– organic modifier 418
– retention factor 419
– retention mechanism 414
– reversed-phase TLC 422
– sorbate retention factor 416
– stationary phase (SP) 412
– thin-layer chromatography 425
– TLC 425
micellar liquid chromatography (MLC) 411
– Micellar HPLC 413
micellar liquid chromatography 412–414, 423, 431
– Micellar TLC 413
micellar solutions 416
– critical micelle concentration (CMC) 411
– salt effects 420
– CMC 417
micelles 134, 411, 412, 424, 426
– biomimetic systems 411
– direct 134
– effective dielectric constant 411
– inverse 415
– microenvironment 427
– microheterogeneity of the medium 411
– Normal 414
– reversed 134, 414
– salt effect 424
– Surfactants 412, 423
micellar liquid chromatography (MLC) 413
– Micellar HPLC 413
microemulsion liquid chromatography (MELC) 389
microemulsions 389, 397
– Bicontinual 392
– Free energy (ΔGf) 393
– Water-in-oil 392
– Winsor system I 397
– Winsor system III 397
– classification 390
– co-surfactant 390, 393
– definition 390
– detergentless 395
– droplets 394
– geometry of surfactant molecule 393
– ionic liquid 399
– multicenter and multifunctional interactions 391
– Oil-in-water 392
– surfactant, co-surfactant 394
– thermodynamic theory 393
milk 325
MIP on the surface 311
molecular recognition 315
Molecularly imprinted polymers 303

nanoanalysis
– Local surface and interface analysis 32
– scanning electrochemical microscopy 34
– (ICP-MS) 34
– (SP-ICP-MS) 34
– (CE-SP-ICP-MS) 35
– Field-flow fractionation (FFF) 35
nanoanalytics 10–12, 15, 26, 27, 29
– analysis of single NPs 32
– analysis of the nanopowder 32
– local analysis 32
– nanometrology 31
– theranostics 31
– tools 15
– Nanoanalysis 31
– Nanometrology 37
Nanoobject 3–5, 13, 14, 23–25, 133, 141
– external energy 14
– biological colloid particle 9
– bionanosystems 37
– carbon nanotubes 6
– electrostatic potentials 29
– fullerenes 6, 224
– gold NPs 8, 10
– Graphene 188
– internal energy 14
– micelles 9, 15
– Nanodimension 5
– nanoparticles 6, 88–94, 96, 97, 99, 134, 135, 142–144, 152, 165, 168, 186, 189, 203, 204, 206
– nanosheets 7

– nanosized state 15
– Nanotube 5
– One-dimensional 23
– quantum dots 6
– self-assembly 4
– self-organization 4
– semiconductor quantum dots 10
– size effects 4, 166, 167, 174
– superparamagnetism 4
– surface plasmon resonance 4
– Three-dimensional 24
– Two-dimensional 24
– Zero-dimensional 23
Nanocomposite 5
Nanofilms 107
– LB films 112, 117
– Self-assembled nanosized films 110
– Self-assembled monolayers 108
nanomaterial-based sensors 172, 177
– transducers 177
– catalyst 177
– immunosensors 196
– electrochemical immunosensors 201
Nanomaterial 5, 6, 177, 186, 196, 224
Nanomedicine 37
Nanometrology 5, 7, 11
Nanoparticle 87–97, 99, 142, 166, 312
nanoparticles of metal oxides 187
nanoreactor 17, 134, 391
nanoscale imprinted materials 312
Nanoscale materials 175
Nanoscience 3, 5
Nanosensor 5, 137, 139
nanosized effects 171
Nanostructure 5, 14, 15, 177, 206
– green synthesis 177
– Nanopores 5
nanostructured electrodes 175
nanostructured media 389
nanostructured object 14
nanosystem 14, 17
nanotechnology 3, 5, 9
– (AFM) 3
– (SEM) 3
– (STM) 3
– (TEM) 3
– dynamic light scattering 29
– electron energy-loss spectroscopy (EELS) 29
– electron microscope 9
– energy-filtering TEM 33
– fast-acting scanning tunnel microscope 10
– Langmuir–Blodgett 24
– Langmuir–Schaefer technique 24
– layer-by-layer 30
– lithography 30
– molecular-beam and gas epitaxy 30
– NEMS 29
– optical ultramicroscope 9
– scanning electrochemical microscopy 34
– scanning TEM 33
– scanning tunnel microscope 9
– self-assembling monolayers 30
– shell-isolated NP-enhanced Raman spectroscopy (SHINERS) 33
– silver photography 8
– Sol-gel 30
– surface-enhanced Raman spectroscopy (SERS) 33
– tip-enhanced Raman spectroscopy (TERS) 33
– transmission electron microscope 10
nanotubes 314
natural waters 322
nicotinamide 318
noncovalent approach 304
noncovalent imprinting 306

on-line 321
organized media 133, 134
oxidative DNA damage 259
– nanoparticles as transducers 173
particle size 173, 174
plasma 322, 324
porogens 319
pre-polymerization complex 317
Precipitation polymerization 309
proteins 327
purification 306

Quantum dots 94, 327

Radical bulk polymerization 308
Raman spectroscopy 354
reaction is initiated by heating 308
ring-opening metathesis 326
role of a solvent 319

sample preparation 320
scanning probe microscopy 4
– AFM 4
– STM 4
Seed polymerization 310
selective MIPs 317

self-assembled monolayers 263
SEM, TEM, ESCA 354
sensor 107, 137, 139, 145, 206, 327
– biosensors 188
– Enzyme sensors 113
– Immunosensors 114, 196
– transducers 186
silica fibers 314
silica 313
size of MIP nanoparticles 312
soil 324
Sol particle immunoassay 58, 59
solid nanoobjects 15, 21, 22, 134
– carbon QD 135, 145
– Carbon dots 141
– graphene 10, 24, 145, 188, 224, 141
– graphene fluoride 24
– graphene oxide 24
– magnetic nanoparticles 202, 203
– magnetic oxide nanoparticles 205
– nanobelts 24
– nanodiamonds 36
– nanofibers 24
– nanoparticles 134, 135, 140, 143, 144, 152, 165, 168, 174, 186, 189, 201, 203, 204, 206
– nanorods 24
– nanotubes 24
– nanowires 24
– QDs 135, 136, 139
– solid-phase extraction 320, 399
– superparamagnetic iron oxides (SPIONs) 36
– whiskers 24
– solid-phase immunoassays 60
solvents (porogens) 308
sorbent 343, 346
– carbon 343, 344, 346, 347, 352
– carbon nanotubes 343
– CNTs 344, 346–374, 376, 377
– determination 376
– functionalization 346, 350, 354
– iron oxide magnetic composites 365
– modification 343, 344, 346, 350, 351, 353, 354, 358, 359, 361, 362, 377
– morphology 353, 359
– multi-walled CNTs 348
– on CCNTs, CNTs, and AC 365
– oxidized 354, 366
– single 348
– structure 353
– surface area 357
sorption 343, 344, 351, 353, 356–359, 362–365, 371, 377
– capacity 357, 358, 362, 364
– efficiency 362, 365
– Isotherms 365
– kinetics 365
– mechanism 362, 363
– on-line preconcentration 368
– organic substances 362
– SPE 366, 368
Sorption properties 315
Sorption 346, 356, 362
spherical microparticles 309
structurally related compounds 320
sulfonamides 325
surface imprinting 314
surface plasmon resonance 66, 135
surface-enhanced Raman spectroscopy 58
surfactant-modified electrodes 232–234, 237, 238
– in situ 233, 234
– drop-casting 233
surfactants 230, 233, 238, 242
– cetylpyridinium bromide 234
– cetyltrimethylammonium bromide 230
– cetyltrimethylammonium chloride 234
– sodium decylsulfate 234
– sodium dodecylsulfate 230
– sodium dodecylsulfonate 234
suspension polymerization 309, 319

template and the reagents 306
tools of nanoanalytics
– nanoobjects 31
– nanotechnologies 31
template 305
The Langmuir–Blodgett (LB) technology 112
theranostics 36, 57
trinitrotoluene 313

ultrasound 319
uniformity of the final particles 309
urine 324